

Molybdenum Enzymes, Cofactors, and Model Systems

Edward I. Stiefel, EDITOR

Exxon Research and Engineering Company

Dimitri Coucouvanis, EDITOR

University of Michigan

William E. Newton, EDITOR

Virginia Polytechnic Institute and State University

Developed from a symposium sponsored
by the Division of Inorganic Chemistry
at the 204th National Meeting
of the American Chemical Society,
Washington, DC,
August 23–28, 1992





Library of Congress Cataloging-in-Publication Data

Molybdenum enzymes, cofactors, and model systems: developed from a symposium sponsored by the Division of Inorganic Chemistry at the 204th National Meeting of the American Chemical Society, Washington, DC, August 23–28, 1992 / Edward I. Stiefel, Dimitri Coucouvanis, William E. Newton [editors].

p. cm.—(ACS symposium series, ISSN 0097–6156; 535)


Includes bibliographical references and index.

ISBN 0–8412–2708–X

1. Molybdenum enzymes—Congresses. I. Stiefel, Edward I., 1942–
. II. Coucouvanis, Dimitri, 1940– . III. Newton, William E.
(William Edward), 1938– . IV. American Chemical Society.
Division of Inorganic Chemistry. V. American Chemical Society.
Meeting (204th: 1992: Washington, D.C.) VI. Series.

QP601.75.M64M65 1993
574.19'25—dc20

93–22876
CIP

The paper used in this publication meets the minimum requirements of American National Standard for Information Sciences—Permanence of Paper for Printed Library Materials, ANSI Z39.48–1984. 

Copyright © 1993

American Chemical Society

All Rights Reserved. The appearance of the code at the bottom of the first page of each chapter in this volume indicates the copyright owner's consent that reprographic copies of the chapter may be made for personal or internal use or for the personal or internal use of specific clients. This consent is given on the condition, however, that the copier pay the stated per-copy fee through the Copyright Clearance Center, Inc., 27 Congress Street, Salem, MA 01970, for copying beyond that permitted by Sections 107 or 108 of the U.S. Copyright Law. This consent does not extend to copying or transmission by any means—graphic or electronic—for any other purpose, such as for general distribution, for advertising or promotional purposes, for creating a new collective work, for resale, or for information storage and retrieval systems. The copying fee for each chapter is indicated in the code at the bottom of the first page of the chapter.

The citation of trade names and/or names of manufacturers in this publication is not to be construed as an endorsement or as approval by ACS of the commercial products or services referenced herein; nor should the mere reference herein to any drawing, specification, chemical process, or other data be regarded as a license or as a conveyance of any right or permission to the holder, reader, or any other person or corporation, to manufacture, reproduce, use, or sell any patented invention or copyrighted work that may in any way be related thereto. Registered names, trademarks, etc., used in this publication, even without specific indication thereof, are not to be considered unprotected by law.

PRINTED IN THE UNITED STATES OF AMERICA

American Chemical
Society Library
1155 16th St. N. W.
Washington, D. C. 20036

1993 Advisory Board

ACS Symposium Series

M. Joan Comstock, *Series Editor*

V. Dean Adams
University of Nevada—
Reno

Robert J. Alaimo
Procter & Gamble
Pharmaceuticals, Inc.

Mark Arnold
University of Iowa

David Baker
University of Tennessee

Arindam Bose
Pfizer Central Research

Robert F. Brady, Jr.
Naval Research Laboratory

Margaret A. Cavanaugh
National Science Foundation

Dennis W. Hess
Lehigh University

Hiroshi Ito
IBM Almaden Research Center

Madeleine M. Joullie
University of Pennsylvania

Gretchen S. Kohl
Dow-Corning Corporation

Bonnie Lawlor
Institute for Scientific Information

Douglas R. Lloyd
The University of Texas at Austin

Robert McGorin
Kraft General Foods

Julius J. Menn
Plant Sciences Institute,
U.S. Department of Agriculture

Vincent Pecoraro
University of Michigan

Marshall Phillips
Delmont Laboratories

George W. Roberts
North Carolina State University

A. Truman Schwartz
Macalaster College

John R. Shapley
University of Illinois
at Urbana—Champaign

L. Somasundaram
DuPont

Peter Willett
University of Sheffield (England)

Foreword

THE ACS SYMPOSIUM SERIES was first published in 1974 to provide a mechanism for publishing symposia quickly in book form. The purpose of this series is to publish comprehensive books developed from symposia, which are usually “snapshots in time” of the current research being done on a topic, plus some review material on the topic. For this reason, it is necessary that the papers be published as quickly as possible.

Before a symposium-based book is put under contract, the proposed table of contents is reviewed for appropriateness to the topic and for comprehensiveness of the collection. Some papers are excluded at this point, and others are added to round out the scope of the volume. In addition, a draft of each paper is peer-reviewed prior to final acceptance or rejection. This anonymous review process is supervised by the organizer(s) of the symposium, who become the editor(s) of the book. The authors then revise their papers according to the recommendations of both the reviewers and the editors, prepare camera-ready copy, and submit the final papers to the editors, who check that all necessary revisions have been made.

As a rule, only original research papers and original review papers are included in the volumes. Verbatim reproductions of previously published papers are not accepted.

M. Joan Comstock
Series Editor

Preface

MOLYBDOENZYMES ARE PRESENT IN MICROORGANISMS, plants, and animals, where they catalyze a variety of inorganic and organic reactions. These transformations affect the organisms themselves, as well as global biogeochemical cycles. Molybdoenzyme-catalyzed reactions are prominently associated with the nitrogen cycle, in which the fixation of nitrogen (reduction of dinitrogen to ammonia by molybdenum nitrogenase) and the reduction of nitrate to nitrite (by nitrate reductase) are critical steps. However, molybdoenzymes are also associated with key steps in the sulfur and carbon cycles and are of crucial importance in a number of human physiological, pathological, and pharmacological contexts.

The element molybdenum is the only member of the second transition series that has an essential biological function: Molybdenum is present at the active sites of more than 30 enzymes. In each of these enzymes, the molybdenum is part of a biosynthesized cofactor that contains additional organic and inorganic components. These cofactors fall into two distinct categories, Moco (in most molybdenum enzymes) and FeMoco (in nitrogenase). The enzymes, cofactors, and model systems for each class of enzymes have received growing attention in recent years as a result of several developments.

The first X-ray crystallographic determination of the structure of the molybdenum–iron protein, the component of the nitrogenase enzyme that contains the substrate-reducing site, was a major breakthrough. This structural definition (described in Chapters 11 and 12) reveals for the first time the three-dimensional structure of the iron–molybdenum cofactor (FeMoco), the unique eight-iron P-clusters, and the polypeptide conformation in this protein. The spectacular power of molecular genetic analysis and state-of-the-art spectroscopic studies, which were already being brought to bear on this enzyme, can now be combined with the crystallographic results to greatly accelerate work in the field.

All other molybdenum enzymes contain Moco, the molybdenum cofactor, the full organic structure of which has now been elucidated (Chapter 3). This information, coupled with spectroscopic, mechanistic, and model studies of mononuclear molybdenum sites, has accelerated the pace of research on these enzymes.

This book describes the recent advances in the study of both classes of molybdenum enzymes and their model systems. The interdisciplinary nature of these studies is evidenced by the variety of subjects addressed in the book: genetics, enzymology, biochemistry, biophysics, spectroscopy, bioorganic chemistry, and bioinorganic model chemistry. The key features responsible for the chemical behavior and evolutionary choice of molybdenum in enzymatic systems are addressed. We feel that the comparison of work on the different enzymes and model systems will further stimulate this and related fields.

We hope that the structure and reactivity of molybdenum enzymes discussed in this book can shed light on the choice of molybdenum in various technologies. In industrial systems, molybdenum has been chosen as the active site of numerous catalytic systems, including hydrotreating, hydrodesulfurization, and hydrodenitrogenation of petroleum fractions; partial oxidation (propylene \rightarrow acrolein and methanol \rightarrow formaldehyde) and ammoxidation (propylene \rightarrow acrylonitrile) in commercial operations; and metathesis, metathesis polymerization, CO and H₂ conversion to alcohols, epoxidation, and allylic rearrangements, which are in smaller scale use or under active research and development. The molybdenum centers of industrial and enzymatic systems have many features in common, including oxygen atom transfer, two-electron redox processes, multi-electron redox processes, internal redox processes, binding of hard and soft substrates, and formation and breaking of sulfur–sulfur bonds. As this book shows, some aspects of this chemistry are better understood in the enzymes or enzyme models than in the corresponding industrial catalytic systems. We believe that the insight from the enzyme and bioinorganic model studies may be brought to bear on these technological systems.

This book is intended to introduce researchers to the field of molybdenum enzymes and models and to provide an up-to-date picture of work in the various subfields. Four overview chapters (1, 5, 10, and 20) introduce various aspects of the field and prepare those less familiar with the area for the state-of-the-art chapters that follow. This book should, therefore, provide a broad overview of molybdenum enzymes and models as well as a picture of the status and future directions of research in this burgeoning field.

ACKNOWLEDGMENTS

We are grateful for the assistance of Joni Phillips in the organization of the symposium and in the handling of many secretarial and administrative details. Support was provided by the Donors of the Petroleum Research Fund (administered by the American Chemical Society), Exxon Research

and Engineering Company, Mallinckrodt Medical, and Monsanto Company. We are grateful to Anne Wilson of ACS Books for her assistance and good cheer during the assembly and production of this volume.

EDWARD I. STIEFEL
Exxon Research and Engineering Company
Annandale, NJ 08801–0998

DIMITRI COUCOUVANIS
University of Michigan
Ann Arbor, MI 48109

WILLIAM E. NEWTON
Virginia Polytechnic Institute
and State University
Blacksburg, VA 24061–0308

April 12, 1993

Chapter 1

Molybdenum Enzymes, Cofactors, and Chemistry

An Introductory Survey

Edward I. Stiefel

Exxon Research and Engineering Company, Clinton Township,
Route 22 East, Annandale, NJ 08801

Molybdenum enzymes, which are present in plants, animals, and microorganisms, play key roles in the biogeochemical cycles of nitrogen, sulfur, and carbon. A variety of molybdenum enzymes contain the molybdenum cofactor, Moco, which consists of a pterin-enedithiolate organic ligand (molybdopterin) and a single Mo atom. These enzymes include nitrate reductase, xanthine oxidase, sulfite oxidase, and DMSO reductase. Their Mo active sites engage in oxygen atom and/or proton-electron transfer reactions. The second main class of Mo enzymes consists of the molybdenum nitrogenases which are responsible for dinitrogen reduction to ammonia. The nitrogenase FeMo proteins contain Fe_3S_3 (P cluster) centers and iron-molybdenum cofactor (FeMoco) centers, the latter consisting of a Fe_7MoS_8 cluster and the homocitrate ligand. P clusters and FeMoco have unique structures, which have yet to be achieved synthetically. Nitrogenase model systems include structural mimics of the metal-sulfur clusters, reactivity analogs for dihydrogen, dinitrogen and reduced intermediates, and simple (chemical) dinitrogen reducing systems. Studies on tungsten enzymes from thermophilic organisms promise a rich comparative biochemistry with molybdenum.

Molybdenum is not one of the more abundant elements in the universe, nor in the earth as a whole, nor in the earth's crust (1). However, in the oceans, where life likely arose and still thrives, molybdenum is the most abundant of the redox-active transition metals (2). Therefore, it is not surprising that living systems from the simplest bacteria to higher plants and animals use molybdenum at the active centers of their redox-active enzymes.

Molybdenum enzymes are ubiquitous in the biosphere. They are present in anaerobic and aerobic organisms and play prominent roles in the metabolism of microorganisms, plants, and animals. The molybdenum enzymes are classified into two categories according to the type of molybdenum site that is present. The first category includes a variety of enzymes that contain the molybdenum cofactor, whose structure involves a mononuclear (monometallic) Mo atom and a unique pterin-dithiolene ligand called molybdopterin (3). The second category contains the molybdenum nitrogenases, which possess the iron-molybdenum cofactor (FeMo-co) whose structure comprises an iron-molybdenum-sulfur cluster of unusual nature (4).

Both cofactors remain with their proteins during all biochemical manipulations and are considered to be nondissociable under physiologically relevant conditions. On the other hand, the cofactors are removable from their proteins under denaturing or partly denaturing conditions (5), which has significantly aided our ability to fully characterize them.

Table 1 displays a list of Mo enzymes. Although not comprehensive, we have tried to list at least one example for each physiological reaction known to be catalyzed by a molybdenum enzyme.

Molybdenum in Biogeochemical Cycles

Molybdenum enzymes play crucial roles in biogeochemical cycles due to their ability to transform small inorganic and organic molecules and ions.

Molybdenum Acquisition. Organisms have evolved the capacity to take up molybdenum via active transport systems, and, at least in some cases, appear to have elaborated proteins that store molybdenum for use in biosynthesis (6,7). In most natural environments the form of molybdenum is the soluble anionic molybdate ion, MoO_4^{2-} . This tetrahedral oxyanion resembles sulfate, SO_4^{2-} , in size, shape and charge and, indeed, the molybdate transport system bears much in common with the sulfate transport system (8).

Molybdenum Copper Antagonism. In terrestrial environments it is known that excess copper in soils can lead to molybdenum deficiency while excess molybdenum in soils can lead to copper deficiency, which is a more serious condition (9). The effect is seen in ruminant animals and requires the presence of sulfate in the soil. This so-called copper-molybdenum antagonism is now understood in the following manner (10). In the anaerobic rumen of sheep and cattle, sulfate is reduced to sulfide by sulfate-reducing bacteria. Sulfide converts the molybdate present into tetrathiomolybdate, MoS_4^{2-} , which complexes and precipitates the Cu. When excess Mo is present, all of the copper is precipitated and made unavailable to the organism. Similarly, when excess copper is present all of the molybdenum is precipitated and hence unavailable for uptake.

The Nitrogen Cycle. The role of molybdenum appears most strikingly in the nitrogen cycle (38). This cycle is shown in schematic form in Figure 1. The reservoirs of nitrogen are soil, where the nitrogen is largely organic, water, where nitrogen is mostly in the form of NO_3^- and NO_2^- , and air, where nitrogen is in its elemental diatomic form, N_2 . For nitrogen to be assimilated into metabolic pathways it must be present in its most reduced form, i.e., at the ammonia level (39). To achieve this level of reduction requires decomposition of the organonitrogen compounds in the soil, reduction of aqueous nitrate, and/or reduction of atmospheric dinitrogen. In each case Mo enzymes are critically involved.

In the metabolism of organonitrogen compounds the Mo enzymes xanthine oxidase, pyrimidine oxidase (aldehyde oxidase), picolinic acid dehydrogenase, and quinoline oxidase each catalyze hydroxylation of an organonitrogen compound, which allows further metabolic deconstruction (hydrolytic and/or oxidative) to free reduced nitrogen for biosynthesis.

In the case of nitrate the first step in the reduction pathway is catalyzed by nitrate reductase, which generates nitrite. Some organisms reduce the nitrite obtained to ammonia as part of their nitrogen acquisition pathway (termed nitrate assimilation). Other nitrate-reducing organisms utilize nitrate as their terminal electron acceptor, which constitutes the first step of the dinitrification pathway (termed nitrate dissimilation or nitrate respiration). All known nitrate reductases, whether assimilatory or dissimilatory, use molybdenum at their active sites. Recently, a nitrite oxidase, which catalyzes the reverse reaction, has also been shown to be a molybdenum enzyme (40).

Table 1. Composition of Molybdoenzymes

<u>Enzymes</u>	<u>Source</u>	<u>Mol. Wt.(subunits)</u>	<u>Prosthetic Groups</u>	<u>ref.</u>
Nitrogen Metabolism				
Xanthine oxidase	cow's milk, mammalian liver, kidney	275,000 (σ_2)	2 Moco, 4 Fe ₂ S ₂ , 2 FAD	(11)
Xanthine dehydrogenase	chicken liver, bacteria	300,000 (σ_2)	2 Moco, 4 Fe ₂ S ₂ , 2 FAD	(11)
Pyrimidine oxidase	rabbit liver	280,000 (σ_2)	2 Moco	(12)
Pyridoxal oxidase				(13,14)
Nicotinamide hydroxylase				(15)
Quinoline oxidoreductase	bacteria	300,000	1.6 Moco, FeS, 1.6 FAD	(16,17)
Picolinic acid dehydrogenase	bacteria	130,000-230,000		(18,19)
Nitrate reductase	plants, fungi, algae, bacteria	228,000	2 Moco, 2 FAD, 2 cyt b 2 Moco, 2 FAD, 2 cyt b Moco, FeS	(20)
Trimethylamine N-oxide reductase	bacteria			(21)
Nitrogenase				(22)
Fe Protein		65,000 (σ_2)	Fe ₄ S ₄	(23,24)
Fe-Mo Protein		225,000 ($\sigma_2\beta_2$)	2 FeMoco, 2 FeS8	
Sulfur Metabolism				
Sulfite oxidase	mammalian liver, bacteria	110,000 (σ_2)	2 Moco, 2 cyt b	(25)
DMSO reductase	bacteria	82,000		(26,27)
Biotin sulfonoxide reductase	bacteria			(28,29)
Tenathionite reductase	bacteria			(30)

Continued on next page.

Table 1. *Continued*

Enzymes	Source	Mol. Wt.(subunits)	Prosthetic Groups	ref.
Carbon Metabolism				
Aldehyde oxidase	mammalian liver	280,000-300,000 (α_2)	2 Moco, 4 Fe ₂ S ₂ , 2 FAD	(11)
Formate dehydrogenase	fungi, yeast, bacteria, plants	105,000 - 263,000		(20)
Carbon monoxide oxidoreductase	bacteria	230,000 - 300,000	2 Moco, 4 Fe ₂ S ₂ , 2 FAD, 2 Se	(31,32)
Formylmethanofuran dehydrogenase	bacteria	400,000	Moco, FeS	(33,34,35)
Miscellaneous				
Arsenite oxidase	bacteria	85,000	Moco, FeS	(36)
Chlorate reductase	bacteria	135,000-183,000		(37)

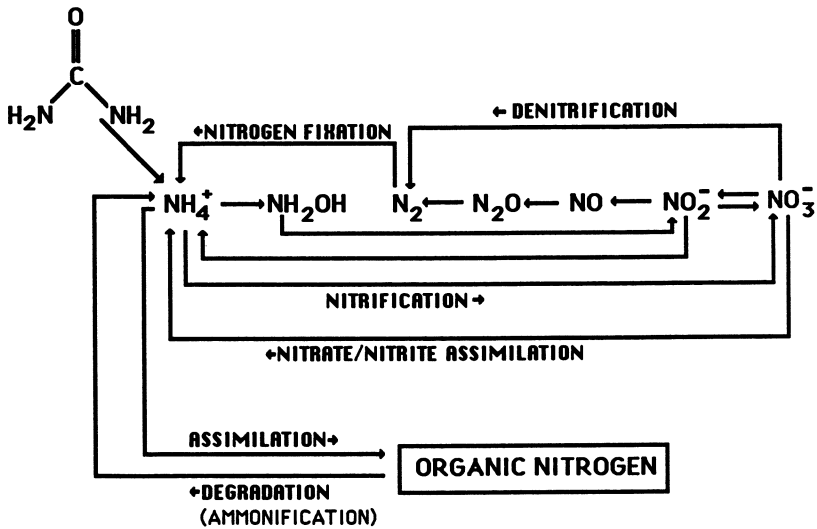
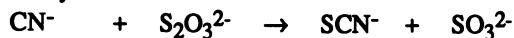


Figure 1. A Schematic Representation of the Biological Nitrogen Cycle. The Enzymes Nitrate Reductase (NO_3^- to NO_2^-), Nitrite Oxidase (NO_2^- to NO_3^-), and Nitrogenase (N_2 to NH_3) are Molybdenum Enzymes.

For nitrogenase, the reaction catalyzed is the reduction of atmospheric dinitrogen to ammonia. This enzyme is found solely in prokaryotic organisms (both eubacteria and archaeobacteria), some of which live symbiotically with plants or animals. The nitrogenase reaction does not, under ordinary conditions, produce any free intermediates between dinitrogen and ammonia (41). As in the industrially prominent Haber-Bosch process (42), the sole nitrogen-containing product is ammonia. The nitrogenase enzyme is extremely air sensitive (43), and although some nitrogen-fixing organisms are aerobes, elaborate metabolic and/or structural contrivances have been developed to limit the access of the nitrogenase enzyme to dioxygen *in vivo* (44).

Sulfur Metabolism. As in nitrogen metabolism both organic and inorganic sulfur chemistry are effected by Mo enzymes. Perhaps the best studied enzyme in this set is sulfite oxidase whose distribution ranges from microorganisms to humans. In higher organisms sulfite is formed in the detoxification pathway of cyanide. The enzyme rhodanese (45) catalyzes the conversion:



Thiocyanate is readily eliminated through the kidneys but sulfite is toxic and must be oxidized to sulfate by the Mo enzyme, sulfite oxidase. The conversion of sulfite, SO_3^{2-} to sulfate, SO_4^{2-} , involves a formal oxygen-atom transfer as do many of the reactions of molybdenum enzymes. Mechanistically, the reactions may or may not be so simple.

The Mo enzyme that is coming under increasing study is dimethyl sulfoxide (DMSO) reductase, which catalyzes the deoxygenation of dimethyl sulfoxide to form dimethyl sulfide. The oxidation of the volatile dimethyl sulfide to methylsulfonic acid has been implicated in cloud formation (46), especially above oceans, which has been postulated as a key part of the bioregulation of temperature on earth in the Gaia hypothesis (47). The DMSO reductase is a rich object of biochemical and biophysical study insofar as, to date, it is the only Mo enzyme devoid of additional prosthetic groups. Since these prosthetic groups are highly chromophoric, the DMSO reductase offers the opportunity to observe the molybdenum center without spectroscopic interference from other chromophores.

The enzyme biotin sulfoxide reductase catalyzes a similar sulfur deoxygenation to produce biotin, which is an important growth factor for microorganism as well as higher organisms. Tetrathionate reductase catalyzes the reduction of tetrathionate ($\text{S}_4\text{O}_6^{2-}$) to thiosulfate ($\text{S}_2\text{O}_3^{2-}$) in a reaction that solely involves the net transfer of two electrons.

Carbon Metabolism. In anaerobic methanogenic organisms the reductive fixation of CO_2 leads to a formylmethanofuran intermediate. The reductase that is responsible for this process is the molybdoenzyme, formylmethanofuran dehydrogenase. The reaction is:



In other anaerobic or facultative organisms (such as *Escherichia coli*) the enzyme formate dehydrogenase catalyzes the dehydrogenation of formate to CO_2 . This reaction may serve the function of a CO_2 reductase in autotrophic organisms and thus, again, a Mo enzyme stands at the entry point of a simple inorganic substrate into a major metabolic cycle. In carboxydo bacteria the enzyme that oxidizes CO to CO_2 is the molybdoenzyme carbon monoxide oxidoreductase. In various manifestations, aldehyde oxidation is also catalyzed by Mo enzymes. Examples include the aldehyde oxidases (pyrimidine oxidases) from mammalian systems and pyridoxal oxidase, which catalyzes the oxidation of pyridoxal to pyridoxoic acid.

Other Mo enzymes have been reported to be involved in the oxidation of highly toxic arsenite to less toxic arsenate and of chlorate to chlorite.

Molybdenum Cofactor Enzymes

All of the Mo enzymes in Table 1, with the exception of the nitrogenases, contain the molybdenum cofactor, which is discussed below and in Chapters 3 and 4 of this volume. This cofactor has a single molybdenum atom and the organic ligand called molybdopterin, which together constitute Moco. Except for DMSO reductase, all of the Moco enzymes also contain other prosthetic groups in addition to Moco. These include hemes (in, for example, nitrate reductase and sulfite oxidase), flavins (in, for example, xanthine oxidase, aldehyde oxidase, and nitrate reductase), and iron-sulfur centers (in, for example, xanthine oxidase, formate dehydrogenase, and carbon monoxide oxidoreductase).

Electrochemical Organization The other prosthetic groups in Moco enzymes serve to complete electron transfer chains, which allow electrons to selectively flow from the reductant to the oxidant during the redox reaction that the enzyme catalyzes (48,49). For xanthine oxidase, as shown in Figure 2, the oxidation of xanthine occurs at the Moco site wherein Mo is initially in the hexavalent state. As xanthine is oxidized by two electrons, Mo(VI) is reduced to Mo(IV). The Mo(IV) site is then reoxidized by internal electron transfer involving the flavin and iron-sulfide centers. The oxidant, usually dioxygen, removes electrons from the enzyme at either the flavin or iron sulfide sites to form superoxide or hydrogen peroxide, in a one- or two-electron process, respectively. In this and, probably, all other Mo enzymes there is no direct transfer of electrons (or more complex redox processes occurring) between the substrate and its redox partner. In a sense the enzyme is engineered as an electrochemical cell in which one half reaction occurs at one prosthetic group (e. g., Mo-co, the 'anode' in this case) and the other half reaction occurs at another prosthetic group (e. g., flavin, the 'cathode'). The enzyme provides the electrical connection between the 'electrodes'. In all cases, whether the substrate reaction is an oxidation, as in xanthine oxidase, or a reduction, as in nitrate reductase, the substrate reaction occurs at the Moco site.

The Moco Site The Moco site has been extensively probed by combined spectroscopic and fast-reaction techniques (48,49). Electron paramagnetic resonance (EPR), X-ray absorption edge (XANES or NEXAFS) and X-ray absorption fine structure spectroscopy (EXAFS), and resonance Raman spectroscopy have proven useful, especially when coupled with freeze-quench experiments on the millisecond time scale. These experiments have established that in most Moco enzymes the molybdenum shuttles between the limiting oxidation states IV and VI during turnover. The intermediate Mo(V) site is detectable by EPR spectroscopy in many cases.

The combined EXAFS and EPR studies implicate a sulfur-containing oxo or oxo/sulfido coordination sphere for most Mo enzymes (50). Specifically, the Mo(VI) state of sulfite oxidase is assigned a dioxo structure, with additional sulfur ligation presumably supplied by the dithiolene-containing side chain of the molybdopterin (see Chapter 3). In the Mo(IV) state the Mo site appears to have a monooxo structure. Xanthine oxidase has a monooxo, monosulfido coordination of molybdenum in the Mo(VI) state and a monooxo Mo(IV) state. Additional sulfur, presumably from molybdopterin and from sulfhydryl in the Mo(IV) state, complete the xanthine oxidase Mo coordination sphere.

Reaction Mechanisms. Two major mechanistic schemes have been proposed as limiting cases for the reactions of Mo enzymes (48). We use the enzyme sulfite oxidase

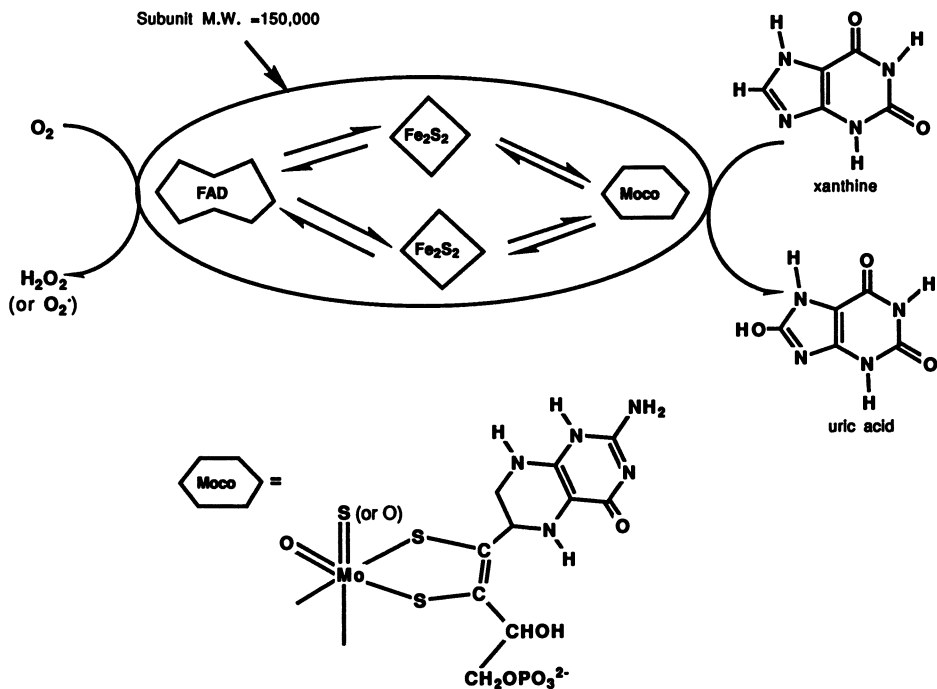


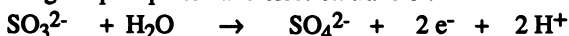
Figure 2. A Schematic Representation of the Functioning of a Subunit of Xanthine Oxidase Illustrating Prosthetic Groups, Substrate Xanthine, Oxidation, Internal Electron Transfer, and Electron Acceptance by Dioxygen. [The molybdenum cofactor is shown in its tetrahydropterin form although its state of oxidation in this enzyme and in many states of other Mo enzymes is not firmly established. The oxo-sulfido coordination of Mo shown is characteristic of the Mo(VI) state of the enzyme. The dioxo form is characteristic of both the inactive (desulfo) form of xanthine oxidase and the active Mo(VI) state of other Mo enzymes such as sulfite oxidase. No spatial arrangement is implied for either the Mo site of the prosthetic groups. Remaining ligands in the Mo coordination sphere are not established but assumed to be present.]

to illustrate these schemes. Many of the Mo enzymes effect reactions in which the product differs from the reactant by an oxo group. In the sulfite oxidase example the reaction can be written:



Many Mo(VI) dioxo complexes containing the MoO_2^{2+} core are known (51) to undergo oxygen atom transfer to yield Mo monooxo complexes containing the MoO^{2+} core (52). It is therefore tempting to postulate that this and other Moco enzymes proceed mechanistically by simple oxygen atom transfer chemistry.

On the other hand, it is also possible to formulate the reaction of sulfite oxidase as a process involving coupled proton and electron transfer:



It is also well known in molybdenum chemistry that the higher oxidation states tend to have deprotonated ligands, such as oxido, sulfido, and amido groups (52). Lower oxidation states more likely have hydroxo or aquo, hydrosulfido or dihydrosulfido, or amino coordination (52). This difference in ligation is a manifestation of the effect of oxidation state on the pKa of coordinated ligands. In high oxidation states the pKa values for coordinated ligands are low and at physiological pH the ligands tend to be deprotonated. In low oxidation states the ligands have high pKa values and tend to be protonated. Therefore, as electrons are transferred to a Mo site, the basicity of ligands at that site increases and proton transfer to a Mo-coordinated ligand is favored. Proton transfer is thereby coupled to electron transfer (53).

For sulfite oxidase EXAFS provides strong indication that the change in the Mo coordination sphere involves transformation of a dioxo to a monooxo Mo site (54). While this is consistent with a simple oxygen atom transfer, it is also consistent with a reaction in which two electrons and one or two protons are added to the Mo site. The electrons change the oxidation state of the molybdenum and the protons attach to the oxo ligand, transforming it into a hydroxo or aquo ligand, which (at the resultant longer Mo-O distance) is no longer detected as an oxo in the EXAFS experiment. More detailed study is required to allow choice between or elaboration upon the limiting mechanisms for this reaction.

In the case of xanthine oxidase EXAFS studies have identified an oxo, sulfido Mo(VI) state as the oxidant, which appears to transform into an oxo, sulfhydryl Mo(IV) state upon reduction by substrate (50). Clearly, simple oxygen atom transfer does not appear to be present but labeling studies have shown that labeled enzyme does transfer oxygen of some kind to the substrate (55). The elegant work of Hille in the mechanistic elucidation of this enzyme is described in Chapter 2.

Moco Model Systems. Moco enzyme model systems are of four general types. First are structural models that aim to reproduce the general features of the Mo coordination sphere. These models have been useful in calibrating the spectroscopic techniques (56) and in establishing the Mo coordination in the limiting and intermediate states of the enzymes. In particular, the models have helped to establish the terminal oxo and sulfur ligands identified on Mo in the various Moco enzymes (57).

A second class of Moco enzyme models are reactivity analogs that aim to reproduce the oxygen atom or proton-electron reactivity of Mo sites. The oxo transfer aspects of Mo and other metal complexes have been extensively reviewed by Holm (58). The ability of model complexes to effect simple oxygen atom transfer from N-, P-, and S-bound oxo groups confirm this pathway as a viable mechanistic possibility for enzymes such as DMSO reductase and trimethylamine N-oxide reductase. On the other hand, to understand the redox interconversion of all three oxidation states of Mo,

and to develop sites that mimic other Mo enzymes in various states of turnover, requires consideration of protonated states of oxo and sulfido molybdenum complexes. These aspects of Mo coordination chemistry are discussed in the overview article by Young and Wedd (Chapter 5, this volume).

A third type of model study involves synthetic constructions that aim to reproduce all or part of the pterin-ene-dithiolate ligand (molybdopterin) and its molybdenum complex, Moco (52). These studies have as their ultimate goal the total synthesis of Moco in a biologically active form. This approach is described in detail by Pilato et al. and by Garner et al. in Chapters 6 and 7, respectively.

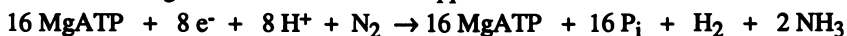
Finally, additional work on model systems seeks to understand the redox relationship between molybdenum and pterins (59) or between molybdenum and other redox-active prosthetic groups such as heme (60). These redox models are discussed by Burgmayer et al., and by Enemark et al. in Chapters 8 and 9, respectively.

Nitrogenase, P Clusters, FeMoco, and Model Systems

The nitrogenase enzyme system contains two separately isolated component proteins as described in the detailed overview by Burgess in Chapter 10 of this volume. Crystallographic studies have recently yielded significant breakthroughs on both proteins (61-64), as discussed in Chapters 11 and 12 by Rees et al. and Bolin et al., respectively. Chapters 10 through 19 of this volume should be consulted for additional details on nitrogenase genetics, spectroscopy, structure, and function.

Here we compare and contrast aspects of the nitrogenase system with the other Mo enzymes. Similarly to the Moco enzymes, nitrogenases have multiple redox centers and have an electron transfer system to bring reducing equivalents to dinitrogen and other substrates (65,66). The two proteins that constitute the nitrogenase system are the Fe protein and the FeMo protein, which are shown schematically in Figure 3. Only when both proteins, reductant, ATP and Mg^{2+} are present does enzyme turnover take place (67). During turnover ATP is hydrolyzed to ADP and inorganic phosphate at a minimal ratio of four equivalents of ATP hydrolyzed per pair of electrons transferred (68). None of the Moco enzymes require ATP (or for that matter any added cofactor) for their activity.

In the absence of dinitrogen the nitrogenase enzyme continues to turn over at the same rate with all reducing equivalents going to form dihydrogen. Even in the presence of N_2 an apparently stoichiometric amount of H_2 is evolved (69). The net minimal reaction for nitrogenase turnover therefore appears to be:



The manner in which the component proteins interact to effect this ATP-driven reduction of N_2 is discussed in Chapters 10, 18, and 19.

The iron protein of nitrogenase contains a single Fe_4S_4 cluster and a nucleotide binding site (70). The FeMo protein contains two rather remarkable clusters, the P clusters and the iron-molybdenum cofactor (71). [Recent studies have revealed the existence of an alternative nitrogen fixing system that contains vanadium in place of molybdenum (72). A third nitrogenase system, which contains only iron, is apparently found in some organisms (73).]

The P Cluster. The P cluster, as discussed further in Chapters 10-12, 16, and 17 is an Fe_8S_8 center consisting of two subclusters, each of which have, approximately, the Fe_4S_4 thio cubane structure (see Figure 3). The two thio cubanes are connected by two cysteine thiolate ligands, which bridge Fe atoms and, remarkably, by what may be a disulfide (S_2^{2-}) linkage, which forms a corner to corner link between the two subclusters (64, 74, 75).

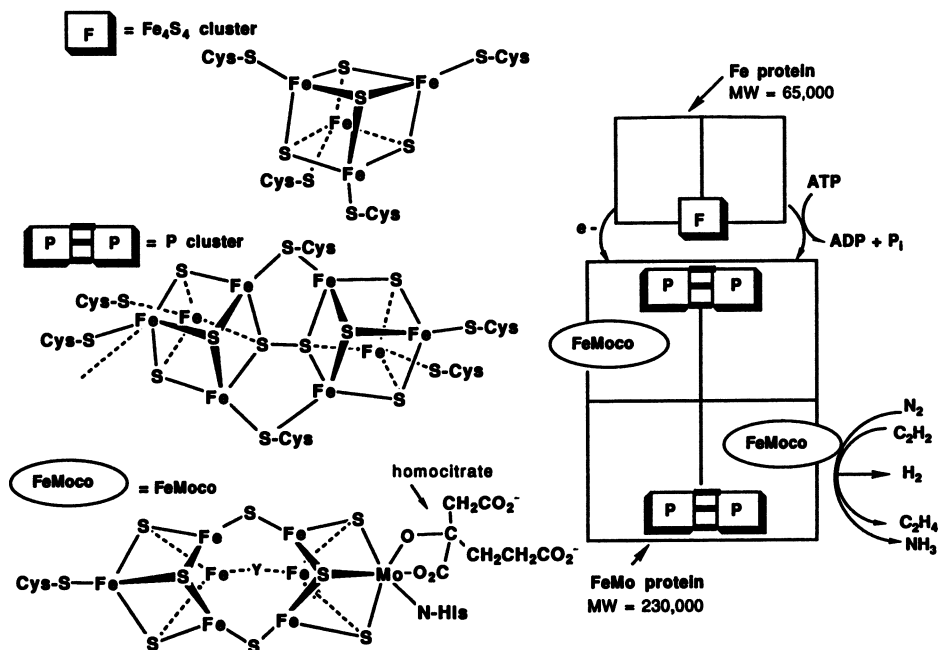
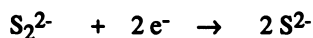


Figure 3. A Schematic Drawing of the Iron and Iron-Molybdenum Proteins of Nitrogenase Indicating the Prosthetic Groups, the Direction of Electron Flow, and the Overall Reaction of the Enzyme. [The three prosthetic groups displayed here are discussed in greater detail in Chapters 11 and 12 of this volume. These reports should be consulted for metrical and spatial details which are only approximated here. The dotted bond to the leftmost iron of the P cluster is a possible serine residue coordinating to iron.]

The disulfide linkage adds an intriguing redox center to this already unusual cluster. Specifically, it would appear possible for the P center to store additional redox equivalents in a two-electron reduced form, which would contain two sulfide ions in place of the disulfide bridge. Even in its all ferrous state (See Orme-Johnson, this volume, chapter 17), the P cluster could still accept electrons into the S-S bond according to:



Reformation of the disulfide bridge (the reverse reaction) would allow the P cluster to deliver two redox equivalents (76, 77) in addition to those delivered through changes in iron oxidation state.

The presence of redox-active sulfur atoms also raises the possibility of induced internal electron transfer during nitrogenase turnover. This type of reactivity can lead to seemingly paradoxical redox behavior in which added oxidant elicits reduction of the metal, or added reductant leads to the formation of metal in a higher oxidation state (76). The reactions are quite explicable when the sulfide/disulfide two-electron redox couple is taken into account (see below under Transition Metal Sulfur Complexes). The ability to deliver electrons in multielectron redox proteins has been suggested as a possible role for the sulfide/disulfide redox couple in nitrogenase (77).

The Iron-Molybdenum Cofactor (FeMoco). Overwhelming evidence points to the iron-molybdenum cofactor, FeMoco, as the site of hydrogen evolution and substrate reduction in nitrogenase (68). FeMoco is an Fe_7S_8Mo inorganic unit that contains a nonprotein organic component, a homocitrate ion (see Ludden et al., Chapter 13), which binds exclusively to the molybdenum atom (63, 64, 74, 75). The cofactor appears to be covalently bound to the protein by two amino-acid ligands, a cysteine to Fe and a histidine to Mo. Single changes in the amino-acid residues near FeMoco change both the substrate specificity and the EPR spectroscopic properties of the cofactor. Mutants of the type *nifV*⁻, which do not produce homocitrate, have a defective cofactor whose altered substrate specificity is transferable to an inactive FeMo protein from a cofactor deficient mutant (*nifB*⁻). Aspects of FeMoco structure within the protein are considered in Chapters 11, 12, 14, and 15. The cofactor is extractable into organic solvents as described by Ludden et al. (Chapter 13) and Watt et al. (Chapter 16). The iron-molybdenum cofactor is clearly genetically, biochemically, and chemically distinct from the molybdenum cofactor. Figure 4 shows schematically that FeMoco and Moco do not cross react in the reconstitution of proteins from mutant organisms that lack enzymic activities associated with the respective cofactors.

The proposed structure of FeMoco (Figure 3) as determined by X-ray crystallography involves two subclusters (74, 75). One subcluster has the Fe_4S_3 structure of a thiocubane missing one sulfur vertex. The second subcluster has a structurally similar $MoFe_3S_3$ thiocubane fragment with homocitrate ion bound to the molybdenum. The two subclusters are joined by eclipsing their Fe_3 faces and are bridged by two (74), or three (75), sulfide ions. The model with two sulfide bridges allows a third bridge to be formed by a putatively lower z element, possibly nitrogen, which suggests a binding site for dinitrogen or reduced intermediates. Alternatively, all six of the interior iron atoms of the cofactor are potentially coordinatively unsaturated suggesting a multiiron binding site for N_2 or its reduction products.

Models for Nitrogenase and FeMoco. Models for biological nitrogen fixation involve: transition metal sulfide clusters that seek to mimic the P clusters or FeMoco center of nitrogenase; transition metal sulfur chemistry that seeks to understand the binding and activation of dihydrogen, dinitrogen, and reduced intermediates; and the

binding and reduction of dinitrogen in transition metal complexes and heterogeneous catalytic systems.

Iron and Iron-Molybdenum Sulfide Clusters. The study of iron sulfide clusters followed closely the elucidation of Fe_4S_4 and Fe_2S_2 centers in ferredoxins (78). The coupling of two of the Fe_4S_4 clusters into a P cluster analog has yet to be effected but, as detailed by Coucouvanis in Chapter 20, progress is being made. The study of iron-molybdenum sulfide clusters was inspired by early Mo EXAFS experiments, which identified Mo-Fe distances characteristic of Mo-Fe-S clusters in nitrogenase and FeMoco (79). Many clusters were prepared, some of which capture key structural aspects of the FeMoco subclusters. However, no clusters yet come close to approaching the newly revealed structures of the P cluster and FeMoco center. The progress that has been made and the challenges that remain are reviewed in Chapter 20 by Coucouvanis.

Transition Metal Sulfur Complexes. The study of transition metal sulfur complexes has revealed some of the possible ways in which dihydrogen, dinitrogen, and reduced nitrogenous intermediates can be bound, activated or stabilized at transition metal sulfur sites. Novel modes of redox activity are also suggested by recent work on multisulfur transition metal sites (76). It is now known that transition metal complexes bind and activate H_2 in a variety of ways that involve the formation of H_2 complexes (80), hydride complexes (81), sulfhydryl complexes (82), and mixed sulfhydryl/hydride complexes (83). These modes of hydrogen activation are illustrated in Figure 5. Once activated the resultant site should be able to deliver the activated components, electrons and protons, to an appropriately activated substrate as required in nitrogenase catalysis.

Insofar as substrate activation and binding are concerned, again, as in the consideration of redox reactions, the normal metal-centered way of thinking may not be adequate (77, 84). In Chapter 21, Sellmann shows how diimide, N_2H_2 , can be bound and stabilized by iron-sulfur complexes. Specifically, nitrogen lone pairs bind to Fe while N-H groups hydrogen bond to sulfur that is coordinated to Fe to further stabilize the complex. Other studies (84, 85) reveal that certain nitrogenase substrates, such as acetylenes, can bind to the sulfur ligands in transition metal sulfide complexes. Clearly, delocalized sites that involve multiple metal and sulfur centers must be considered as strong candidates for the binding and activation of substrate, and/or the stabilization of key intermediates.

The redox reactions of transition metal sulfide compounds have been intensively studied. An example (86) of the unusual chemistry involves the tetrathiomolybdate ion, MoS_4^{2-} , which has molybdenum in the VI oxidation state. Addition of oxidants, such as organic disulfides, RSSR (R = aryl group), leads to the formation of the dinuclear Mo(V) complex $\text{Mo}_2\text{S}_8^{2-}$ according to:



How can the addition of an oxidant lead to the reduction of the metal center? The answer lies in the formation of disulfido ligands, which are found in the structure of $\text{Mo}_2\text{S}_8^{2-}$ shown in Figure 6. The formation of the two disulfide ligands involves the four-electron oxidation of four sulfide ions. The four electrons released are able to reduce the external organic disulfide oxidant by two electrons and, by internal redox, both molybdenum atoms from Mo(VI) to Mo(V). This type of reaction, called induced internal electron transfer, is common in the chemistry of transition metal chalcogenide systems (76). Clearly, this type of redox behavior is possible in both FeMoco and P clusters of nitrogenase.

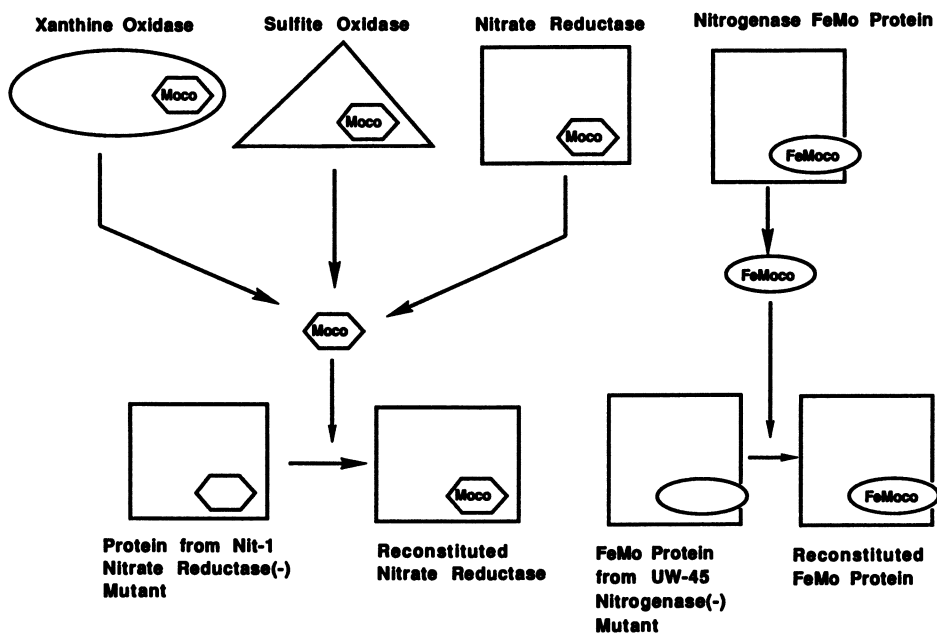


Figure 4. A Schematic Drawing Illustrating the Nonidentity of the Cofactors from the Two Classes of Molybdenum Enzymes. The Nit-1 (Nitrate Reductase-) Mutant Apoprotein Is Only Reconstituted by Moco and the UW-45 (Nitrogenase-) Mutant Apoprotein Is Only Reconstituted by FeMoco.

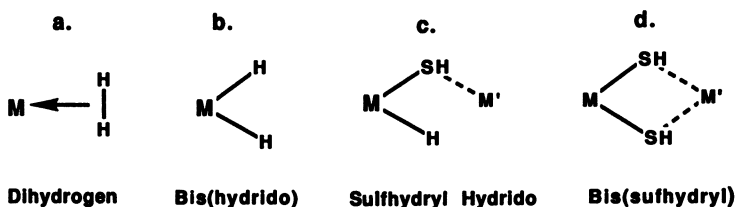


Figure 5. The Various Modes of Hydrogen Activation on Transition Metal Sulfur Active Sites. a. Dihydrogen Complex, b. Dihydride Complex, c. Hydride/Sulfhydryl Complex, and d. Bis(sulfhydryl) Complex.

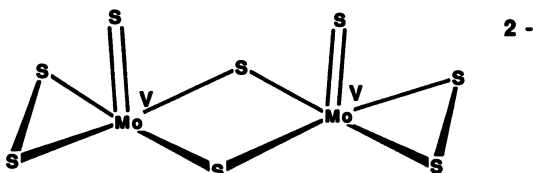
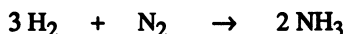


Figure 6 The Structure of $\text{Mo}_2\text{S}_8^{2-}$ Illustrating the Presence of Disulfide Ligands Formed in the Oxidation of MoS_4^{2-} in an Internal Redox Process.

Nitrogen Fixing Systems. A final category of models are systems that reduce N_2 but do not chemically resemble the nitrogenase active site. These reactivity analogs are discussed in Chapters 22 and 23 by Hidai et al. and George et al., respectively. Their studies shows how bound dinitrogen is converted to reduced nitrogen products. A key enabling feature of the conversions seems to be the formation of multiple bonds between the nitrogen and the metal center to stabilize the complex as the dinitrogen bond is broken. The breaking of the N-N triple bond clearly proceeds in concert with the making of metal-nitrogen multiple bonds to facilitate the process.

Interestingly, the industrial Haber-Bosch process (42) can be viewed in similar terms. The Haber-Bosch process is the central reaction of the nitrogenous fertilizer business. This reaction:



produces ammonia, which may be converted to other fertilizers, such as urea, ammonium nitrate, ammonium phosphate, etc. The reaction requires temperatures of 350-500°C to proceed at effective rates and pressures of 200-400 atm to give acceptable yields. The common Haber-Bosch catalyst consists of metallic iron promoted by potassium and supported on alumina to prevent sintering at the high temperature of the reaction (87). The formation of several bonds between the nitrogen atoms of the reactant and the Fe atoms of the catalyst seems to be a key feature of the reaction (88). As in the simple chemical systems, the breaking of the N-N triple bond is accompanied by the formation of several metal-nitrogen bonds, in this case to different metal atoms. It is interesting to speculate that nitrogenase is also designed to allow multiple M-N bonds (again Fe-N bonds!) to be formed to compensate for breaking the N-N multiple bond.

Molybdenum versus Tungsten

The prevalence of molybdenum in microorganisms has recently been highlighted by the finding that certain thermophilic and extremely thermophilic organisms (hyperthermophiles) use tungsten (W) apparently in place of molybdenum (89,90). Many of these organisms have been isolated from deep-sea or shallow hydrothermal vents. The best characterized W-dependent enzyme is an aldehyde oxidoreductase (91), which appears to play a role in aldehyde oxidation that is akin to that played by the Mo-containing aldehyde oxidases in mesophilic organisms. Significantly, the tungsten seems to be associated with a pterin that may be identical to the molybdopterin of molybdenum enzymes (92). Why do the thermophilic organisms use tungsten rather than molybdenum?

A plausible explanation lies in the comparative electrochemistry of W and Mo compounds. Specifically, the redox potentials for W complexes are known to be more negative than those of the corresponding molybdenum complexes (93). Such a low potential W site could more effectively reduce Fe-S sites within the protein and in the electron-accepting ferredoxin, which, in turn, delivers electrons to hydrogenase for the production of dihydrogen. Thus, the use of W may be preferred to allow the organism to more effectively deliver redox equivalents for dihydrogen evolution.

However, despite the attractiveness of this hypothesis, there is potentially a simpler explanation. Specifically, the deep sea vents, for example, have been reported to have no detectable molybdenum and significant tungsten in their effluent waters. This finding is consistent with the greater affinity of Mo for sulfide in the vent effluent leading to the precipitation of MoS_3 and MoS_2 and consequent unavailability of molybdenum. If this finding is confirmed for deep-sea vents and extended to shallow hydrothermal vents, then organisms would have no choice but to use W over Mo, if they are to occupy the ecological niche provided by the hydrothermal vents.

It has been suggested that deep-sea hydrothermal vents are prime candidate sites for the origins of life on early earth (93). If this is so then W enzymes may actually have preceded Mo enzymes in an evolutionary sense. Molybdenum enzymes may have been developed in response to the greater availability of Mo to mesophilic organisms in low sulfide environments. Clearly, continued study of the family of W and Mo enzymes could teach us much about the acquisition of trace element specificity and its evolutionary implications.

Conclusion

The molybdenum enzymes are under intense study due to their inherent scientific interest and their potential relevance to agricultural, environmental, and biomedical biotechnology. In the case of the Moco enzymes much progress has been made in the elucidation of the structure of the cofactor and in the detailed reaction mechanism at the Mo site. Model systems are closely approaching the structures and beginning to display features of the reactivity of the enzyme sites. The total synthesis of Moco would seem to be an accomplishable goal. For nitrogenase the recent breakthroughs in crystallography of the component proteins have revealed the level of our ignorance of intimate catalytic mechanisms. The novel structural entities, the P cluster and FeMoco, serve as tantalizing synthetic targets. The structure of the protein complex should allow us to fathom the role of ATP and the intimate mechanism of the reduction of N_2 as effected by this remarkable enzyme.

Literature Cited

1. Cox, P. A. *The Elements*; Oxford University Press: New York, NY, 1989; pp 8-21.
2. Cox, P. A. *The Elements*; Oxford University Press: New York, NY, 1989; pp 151-156.
3. Rajagopalan, K. V. In *Biochemistry of the Elements*; Frieden, E., Ed.; Plenum Press, New York, NY, 1984; pp 149-171.
4. Burgess, B. K. *Chem. Rev.* **1990**, *90*, 1377.
5. Pienkos, P. T.; Shah, V. K.; Brill, W. J. *Proc. Natl. Acad. Sci. USA* **1977**, *74*, 5468.
6. Elliot, B. B.; Mortenson, L. E. *J. Bacteriol.* **1975**, *124*, 1295.
7. Pienkos, P. T.; Brill, W. J. *J. Bacteriol.* **1981**, *145*, 743.
8. Johann, S.; Hinton, S. M. *J. Bacteriol.* **1987**, *169*, 1911.
9. Weber, K. M.; Boston, R. C. *Austr. J. Agric. Res.* **1983**, *34*, 295.
10. Mason, J. *Toxicology* **1986**, *42*, 99.
11. Coughlan, M. P. In *Molybdenum and Molybdenum-Containing Enzymes*; Coughlan, M. P., Ed.; Pergamon Press, New York, NY 1980, pp 119-185.
12. Rajagopalan, K. V.; Handler, P.; Palmer, G.; Beinert, H. *J. Biol. Chem.* **1968**, *143*, 3784.
13. Hanly, E. W. *Mol. Gen. Genet.* **1980**, *180*, 455.
14. Courtright, J. B. *Adv. Genet.* **1976**, *18*, 249.
15. Dilworth, G. L. *Arch. Biochem. Biophys.* **1983**, *221*, 565.
16. Bauder, R.; Tshisuaka, B.; Lingens, F. *Biol. Chem. Hoppe-Seyler* **1990**, *371*, 1137.
17. Schwarz, G.; Bauder, R.; Speer, M.; Rommel, T. O.; Lingens, F. *Biol. Chem. Hoppe-Seyler* **1989**, *370*, 1183.
18. Tate, R. L.; Ensign, J. C. *Can. J. Microbiol.* **1974**, *20*, 695.
19. Siegmund, I.; Koenig, K.; Andreesen, J. R. *FEMS Microbiol. Lett.* **1990**, *67*, 281.

20. Adams, M. W. W.; Mortenson, L. E. In *Molybdenum Enzymes*, Spiro, T. G., Ed.; John Wiley & Sons, New York, NY 1985; pp 519-594.
21. Shimokawa, O.; Ishimoto, M. *J. Biochem.* **1979**, *86*, 1709.
22. Chen, J.-S.; Multani, J. S.; Mortenson, L. E. *Biochim. Biophys. Acta* **1973**, *310*, 51.
23. Eady, R. R.; Smith, B. E.; Cook, K. A.; Postgate, J. R. *Biochem. J.* **1972**, *128*, 655.
24. Ludden, P. W.; Burris, R. H. *Biochem. J.* **1978**, *175*, 251.
25. Rajagopalan, K. V. In *Molybdenum and Molybdenum-Containing Enzymes*, Coughlan, M. P., Ed.; Pergamon Press, New York, NY 1980, pp 241-272.
26. Satoh, K.; Kurihara, F. N. *J. Biochem. Tokyo* **1987**, *102*, 191.
27. McEwan, A. G.; Ferguson, S. J.; Jackson, J. B. *Biochem. J.* **1991**, *174*, 305.
28. Del Campillo-Campbell, A.; Dykhuizen, D.; Cleary, P. P. In *Methods in Enzymology*, Academic Press, New York, NY, 1979, pp 379-385.
29. Del Campillo-Campbell, A.; Campbell, A. *J. Bacteriol.* **1982**, *149*, 469.
30. Oltmann, L. F.; Claassen, V. P.; Kastelein, P.; Reijnders, W. N. M.; Stouthamer, A. H. *FEBS Lett.* **1979**, *106*, 43.
31. Bell, J. M.; Colby, J.; Williams, E. *Biochem. J.* **1988**, *250*, 605.
32. Meyer, O. *J. Biol. Chem.* **1982**, *257*, 1333.
33. Schwoerer, B.; Thauer, R. K. *Arch. Microbiol.* **1991**, *155*, 459.
34. Karrasch, M.; Boerner, G.; Enssle, M.; Thauer, R. K. *Eur. J. Biochem.* **1990**, *194*, 367.
35. Jablonski, P. E.; DiMarco, A. A.; Robik, T. A.; Cabell, M. C.; Ferry, J. G. *J. Bacteriol.* **1990**, *172*, 1271.
36. Anderson, G.; Williams, J. Hille, R. *J. Biol. Chem.* **1992**, *267*, 23674.
37. Oltmann, L. F.; Reijnders, W. N. M.; Stouthamer, A. H. *Arch. Microbiol.* **1976**, *111*, 25.
38. Kroneck, P. M. H.; Beuerle, J.; Schumacher, W. In *Metal Ions in Biological Systems*, Sigel, H.; Sigel, A., Eds.; Marcel Dekker, New York, NY, Vol. 3, pp 455-505
39. Rawn, J. D. *Biochemistry*; Neil Paterson Publishers, Burlington, NC, 1989, pp 582-593.
40. Meincke, M.; Bock, E.; Kastrau, D.; Kroneck, P. M. H. *Arch. Microbiol.* **1992**, *158*, 127.
41. Thorneley R. N. F.; Lowe, D. J. In *Molybdenum Enzymes*, Spiro, T. G., Ed.; John Wiley & Sons, New York, NY 1985; pp 221-284.
42. Haber, L. F. *Endeavour* **1968**, *27*, 151.
43. Wang, Z.-C.; Burns, A.; Watt, G. D. *Biochemistry* **1985**, *24*, 214.
44. Fay, P. *Microbiol. Rev.* **1992**, *56*, 340.
45. Ploegman, J. H.; Drent, G.; Kalk, K. H.; Hol, W. G. J. *J. Mol. Biol.* **1978**, *123*, 557.
46. Bates, T. S.; Charlson, R. J.; Gammon, R. H. *Nature* **1987**, *329*, 319.
47. Lovelock, J. *The Ages of Gaia*, W. W. Norton, New York, NY, pp 141-148.
48. Pilato, R. S.; Stiefel, E. I. In *Bioinorganic Catalysis*; Reedijk, J., Ed.; Marcel Dekker, New York, NY, 1993; pp 131-188.
49. Bray, R. C. *Q. Rev. Biophys.* **1988**, *21*, 299.
50. Garner, C. D.; Bristow, S. In *Molybdenum Enzymes*; Spiro, T. G., Ed.; John Wiley & Sons, New York, NY 1985; pp 343-410.
51. Stiefel, E. I. In *Comprehensive Inorganic Chemistry*; Wilkinson, G.; Gillard, R. D.; McCleverty, J. A.; Eds.; Pergamon Press, New York, NY, 1987 Vol. 3 pp 1375-1420.
52. Stiefel, E. I. *Prog. Inorg. Chem.* **1977**, *22*, 1.
53. Stiefel, E. I. *Proc. Natl. Acad. Sci. USA* **1973**, *70*, 988.

54. Cramer, S. P.; Wahl, R.; Rajagopalan, K. P. *J. Am. Chem. Soc.* **1981**, *103*, 7721.
55. Hille, R.; Sprecher, H. *J. Biol. Chem.* **1987**, *262*, 10914.
56. Cramer, S. P. In *Advances in Inorganic and Bioinorganic Mechanisms*; Sykes, A. G., Ed.; Academic, London, 1983 pp 259-316.
57. Young, C. G.; Wedd, A. G. Chapter, 5, This Volume.
58. Holm, R. H. *Chem. Rev.* **1987**, *87*, 1401.
59. Burgmayer, S. J. N.; Everett, K.; Bostick, L. Chapter 8, This Volume.
60. LaBarre, M. J.; Ratsimiring, A.; Enemark, J. H. Chapter 9, This Volume.
61. Bolin, J. T.; et al. In *Nitrogen Fixation: Achievements and Objectives*, Gresshoff, P. M.; Roth, L.E.; Stacey, G.; Newton, W. E., Eds.; Chapman & Hall, New York, NY, 1990, pp 117-124.
62. Georgiadis, M. M.; Komiya, H.; Chakrabarti, P.; Woo, D.; Rees, D. C. *Science*, **1992**, *257*, 1653.
63. Kim, J.; Rees, D. C. *Science*, **1992**, *257*, 1677.
64. Kim, J.; Rees, D. C. *Nature*, **1992**, *360*, 553.
65. Orme-Johnson, W. H. *Annu. Rev. Biophys. Biophys. Chem.* **1985**, *14*, 419.
66. Mortenson, L. E.; Thorneley, R. N. F. *Annu. Rev. Biochem.* **1979**, *48*, 387.
67. Evans, D. J.; Henderson, R. J.; Smith, B. E. In *Bioinorganic Catalysis*; Reedijk, J., Ed.; Marcel Dekker, New York, NY, 1993; pp 89-130.
68. Stephens, P. J. In *Molybdenum Enzymes*, Spiro, T. G., Ed.; John Wiley & Sons, New York, NY 1985; pp 117-160.
69. Simpson, F. B.; Burris, R. *Science*, **1984**, *224*, 1095.
70. Wolle, D.; Dean, D. R.; Howard, J. B. *Science*, **1992**, *258*, 992
71. Smith, B. E.; Eady, R. R. *Eur. J. Biochem.* **1992**, *205*, 1.
72. Eady, R. R. in *Vanadium in Biological Systems*, Chasteen, D., Ed.; Kluwer Academic Publishers, Dordrecht, Netherlands, 1990; p99.
73. Robson, R. L. In *Biology and Biochemistry of Nitrogen Fixation*; Dilworth, M. J.; Glenn, A. R., Eds.; Elsevier, Amsterdam, 1991, pp 142-161.
74. Rees, D. C. et al., Chapter 11, This Volume.
75. Bolin, J. T. et al., Chapter 12, This Volume.
76. Harmer, M. A.; Halbert, T. R.; Pan, W.-H.; Coyle, C. L.; Stiefel, E. I. *Polyhedron* **1986**, *5*, 341.
77. Stiefel, E. I.; Chianelli, R. R. In *Nitrogen Fixation: The Chemical-Biochemical-Genetic Interface* Müller, A.; Newton, W. E., Eds.; Plenum, NY, 1983; p 341.
78. Berg, J. M.; Holm, R. H. In *Iron-Sulfur Proteins*; Spiro, T. G., Ed.; John Wiley & Sons, New York, NY 1982; p 1.
79. Cramer, S. P.; Hodgson, W. O.; Gillum, W. O.; Mortenson, L. E. *J. Am. Chem. Soc.* **1978**, *100*, 3398.
80. Kubas, G. J.; Ryan, R. R.; Swanson, B. I.; Vergamini, P. J.; Wasserman, H. *J. Am. Chem. Soc.* **1986**, *108*, 1000.
81. Cotton, F. A.; Wilkinson, G. *Advanced Inorganic Chemistry*; John Wiley & Sons, New York, NY, 1988, 5th Ed., pp 1097-1121.
82. Rakowski DuBois, M.; VanDerveer, M. C.; DuBois, D. L.; Haltiwanger, R. C.; Miller, W. K. *J. Am. Chem. Soc.* **1980**, *102*, 7456.
83. Bianchini, C.; Mealli, C.; Meli, A.; Sabat, M. *Inorg. Chem.* **1986**, *25*, 4617.
84. Stiefel, E. I.; Thomann, H.; Jin, H.; Bare, R. E.; Morgan, T. V.; Burgmayer, S. J. N.; Coyle, C. L. In *Metal Clusters in Proteins*, Que, L., Ed.; ACS Symposium Series, No. 372, American Chemical Society, Washington, DC, 1988, pp 372-389.
85. Halbert, T. R.; Pan, W.-H.; Stiefel, E. I. *J. Am. Chem. Soc.* **1983**, *105*, 476.

86. Coyle, C. L.; Harmer, M. A.; George, G. N.; Daage, M.; Stiefel, E. I. *Inorg. Chem.* **1990**, *29*, 14.
87. Emmet, P. H. *Heterogeneous Catalysis: Selected American Histories*, Davis, B. H.; Hettinger, W. P. Eds.; ACS Symposium Series, No.222, American Chemical Society, Washington, DC, 1983, pp 195-216.
88. Mahdi, W.; Schütze, J.; Weinberg, G.; Schoonmaker, R.; Schlögl, R.; Ertl, G.; *Catal. Lett.* **1991**, *11*, 19.
89. Yamamoto, I.; Saiki, T.; Liu, S.-L.; Ljungdahl, L. *J. Biol. Chem.* **1983**, *258*, 1826.
90. Makund, S.; Adams, M. W. W. *J. Biol. Chem.* **1990**, *265*, 11516.
91. George, G. N.; Prince, R. C.; Makund, S.; Adams, M. W. W. *J. Am. Chem. Soc.* **1992**, *114*, 3521.
92. Makund, S.; Adams, M. W. W. *J. Biol. Chem.* **1991**, *266*, 14208.
93. Tunncliffe, V. *Am. Sci.* **1992**, *80*, 336.

RECEIVED April 20, 1993

Chapter 2

The Reaction Mechanism of Xanthine Oxidase

Russ Hille

Department of Medical Biochemistry, Ohio State University,
Columbus, OH 43210

The reaction of xanthine oxidase with 2-hydroxy-6-methylpurine, 1-methylxanthine and xanthine has been reexamined using rapid kinetic techniques. Reaction of enzyme with substoichiometric concentrations of 2-hydroxy-6-methylpurine at pH 10.0 exhibits two reaction intermediates having difference absorbance maxima at 470 nm and 540 nm relative to oxidized enzyme. Comparison of the kinetics of the reaction as monitored by UV/visible absorption and electron paramagnetic resonance spectrometry indicates that these spectral intermediates arise from the molybdenum center of the enzyme in the Mo^{IV} and Mo^V valence states, respectively, with the latter species exhibiting the well-known "very rapid" Mo^V EPR signal. Similar results are obtained with xanthine as substrate. Under single-turnover conditions, none of the Mo^V EPR signals designated "rapid" appears transiently in these experiments. Additional work indicates that this species is not a *bona fide* catalytic intermediate in the reaction mechanism of xanthine oxidase. The mechanistic implications of these results are discussed.

Of the biological systems capable of catalyzing the hydroxylation of inorganic, aliphatic or aromatic substrates, the molybdenum-containing hydroxylases are unique in two regards. Systems possessing heme or non-heme iron, flavin or pterin prosthetic groups utilize O₂ as the source of the oxygen atom to be incorporated into substrate and externally supplied reducing equivalents to reduce the other oxygen atom of O₂ to water. The thermodynamic driving force derived from water formation is used to generate highly reactive intermediates – heme ferryl oxides (1,2) or flavin/pterin 4a peroxides (3) – which act as the proximal oxygen donors to substrate in their respective reaction mechanisms. The molybdenum-containing hydroxylases, by contrast, use water as the ultimate source of the oxygen atom incorporated into substrate, and generate rather than consume reducing equivalents. As a consequence of these two mechanistic features, these enzymes represent a unique solution to the problem of oxygen activation.

Because it is easily isolated in quantity from a convenient source, milk xanthine oxidase has become the paradigm for the molybdenum-containing hydroxylases (4-7). The enzyme is a homodimer of 300,000 molecular weight and catalyzes the hydroxylation of xanthine to uric acid, reducing molecular oxygen to

either peroxide or superoxide (depending on the pH and level of enzyme reduction). A wide variety of other aromatic heterocycles, even simple aldehydes, are substrates for xanthine oxidase. In addition to its molybdenum center, xanthine oxidase contains two iron-sulfur centers of the spinach ferredoxin variety and flavin adenine dinucleotide. The reductive half-reaction (involving xanthine hydroxylation) occurs at the molybdenum center of the enzyme (8) while the oxidative half-reaction (involving O₂ reduction) takes place at the flavin center (9). It is in fact a general feature of the molybdenum hydroxylases that they contain at least one redox-active site in addition to the molybdenum center, and that the molybdenum center participates directly in only one of the two half-reactions of the catalytic cycle. On the basis of the close agreement between k_{lim} for the reductive half-reaction (17.5 s⁻¹ at pH 8.5, 25 °C) and k_{cat} (15 s⁻¹ under the same conditions), the rate-limiting step in overall catalysis is thought to reside in the reductive half-reaction (10).

The Structure of the Molybdenum Center

Consensus structures for the molybdenum center in oxidized and reduced xanthine oxidase, as elucidated by x-ray absorption spectroscopy (11-16), are shown in Figure 1. In the oxidized enzyme, the Mo^{VI} coordination sphere is dominated by a single oxo group (Mo=O, 1.68 Å) and a sulfido group (Mo=S, 2.15 Å); at least two and perhaps three thiolate ligands (Mo-SR, 2.45 Å) are also present. In addition, there is evidence for O/N at a distance of ~ 2 Å, although the improvement in fit to the x-ray fine structure data by including this distance is not great (16). On the basis of the Mo=O distance, the formal bond order of the bond is estimated to be almost three (17). Reduction of the enzyme molybdenum to the (IV) valence state results in the protonation of the Mo=S group to form Mo-SH, manifested in the x-ray absorption data as the loss of the short Mo=S bond and the appearance of an additional long Mo-S bond in the molybdenum coordination sphere (13). This behavior is consistent with the chemistry of dioxomolybdenum complexes (18,19), which are known to be effective in simultaneously taking up both electrons and protons.

The Mo=S group of oxidized xanthine oxidase can be removed by reaction with cyanide to give thiocyanate and an inactive desulfo form of the enzyme that contains a second Mo=O group in place of Mo=S (with the oxygen atom derived from water (13)). The substitution of a second oxo group for the sulfido group of the molybdenum coordination sphere lowers the molybdenum midpoint potential by approximately 45 mV at pH 8.3 (20), but does not seriously compromise the thermodynamic ability of the enzyme to oxidize xanthine. The loss of catalytic activity cannot be accounted for on the basis of thermodynamics alone, and any proposed mechanism for xanthine oxidase must adequately account for the loss of activity on formation of the desulfo enzyme.

In addition to the catalytically essential sulfido group, the molybdenum center of xanthine oxidase also requires a pterin cofactor for activity (21). On the basis of mass spectral, proton NMR and energy dispersive x-ray analysis, the structure shown in Figure 2 appears to be the correct assignment for the oxidized form of the cofactor obtained after covalent modification with iodoacetamide. On the basis of the known presence of thiols in the molybdenum coordination sphere of xanthine oxidase (11), the cofactor is thought to coordinate directly to the molybdenum in the active site (Figure 2). This is consistent with the observation that the isolated cofactor forms a discrete complex with molybdenum (V) which is detectable by EPR (22), and the observation of vibrational modes attributable to a dithiolene complex in the resonance Raman spectrum of the enzyme DMSO reductase (23). The role of the cofactor in catalysis is uncertain at present. It is extremely unlikely that the pterin ring undergoes a change in oxidation state in the course of catalysis, since the molybdenum, FAD and iron-sulfur centers of the enzyme plus a reversibly reducible disulfide account for the stoichiometry of reducing equivalents taken up by the enzyme on reduction by either xanthine or sodium dithionite (24). It has been suggested that the cofactor acts as the proximal donor to substrate in the hydroxylation reaction, accepting an oxo oxygen from the molybdenum center to form a 4a hydroxy species prior to hydroxylation of substrate (21). While

there is precedent for a pterin 4a hydroxide in the catalytic mechanism of phenylalanine hydroxylase (25,26), for example, this species is formed from the corresponding 4a peroxide. The 4a peroxide is itself generated by reaction of the dihydropterin with molecular oxygen, and is thought to be the oxygenating species in the catalytic reaction (26). For the molybdenum-containing hydroxylases, formation of a pterin 4a hydroxide via oxo transfer from a molybdenum center, even a reduced one, is unlikely to be thermodynamically favorable. The cofactor may instead serve primarily to modulate the reduction potential of the molybdenum center so as to optimize the overall thermodynamic favorability of catalysis. One possible mechanism whereby this may occur is illustrated in the complex $\text{MoO}_2[\text{SC}(\text{CH}_3)_2\text{CH}_2\text{NH}(\text{CH}_3)]_2$, which possesses a pair of *cis* thiolate ligands in the molybdenum coordination sphere (27). The sulfur atoms in this nominally Mo^{VI} complex are more approximately 1 Å closer than van der Waals contact, indicating at least partial formation of a disulfide bond. To the extent that disulfide bond formation occurs (with concomitant reduction of the molybdenum to Mo^{IV}) the formal reduction potential of the complex is expected to decrease. In the enzymes, such an interaction could account for the >300 mV lower reduction potential of the dioxomolybdenum center of desulfo xanthine oxidase relative to that of sulfite oxidase. The biochemistry of the pterin cofactor and its possible role in the reaction mechanism of xanthine oxidase and other enzymes is discussed in greater detail in Chapter 3 of this volume.

EPR Studies of the Reaction of Xanthine Oxidase with Substrate

A number of kinetic studies utilizing pseudo-first order concentrations of substrate have been reported aimed at elucidating the chemical sequence of events taking place in the reductive half-reaction of xanthine oxidase (10, 28-30). The principal tool for studying the molybdenum center has been electron paramagnetic resonance EPR spectroscopy, which probes the Mo^{V} valence state. Three distinct Mo^{V} EPR signals are observed in the course of the reaction of enzyme with a stoichiometric excess of substrate, and have been designated "very rapid", "rapid" and "slow" on the basis of the time scales over which they appear and disappear (Figure 3) (31). The "slow" signal has been shown to arise from the catalytically nonfunctional desulfo form of the enzyme and exhibits kinetics too slow to be catalytically competent (5,10,30,32). The "very rapid" and "rapid" signals, on the other hand, are both viable catalytic intermediates on the basis of their kinetics. The "very rapid" signal is markedly anisotropic ($g_{1,2,3} = 2.0252, 1.9550, 1.9494$), has no proton superhyperfine coupling and, when 8- ^{13}C -labeled substrate is used, exhibits coupling to the labeled carbon with $a_{\text{ave}} = 3.2 \text{ G}$ (33,34). Formation of the signal-giving species is favored at high pH (29). Among the many substrates of xanthine oxidase that have been examined, xanthine, 1-methylxanthine, 6-methylpurine, 2-hydroxy-6-methyl-purine, 8-hydroxy-6-methylpurine, lumazine, 2-amino-4-hydroxy-6-formylpteridine and formamide have been found to give rise to a "very rapid" EPR signal to varying extents. Oxidation of the inhibitory complex of reduced xanthine oxidase with alloxanthine also gives rise to a "very rapid" EPR signal which exhibits weak coupling to N_8 of the pyrazolopyrimidine nucleus (35). Two distinct types of "rapid" signal have been observed, differing principally in their proton superhyperfine patterns. The "rapid Type 1" signal (seen, e.g., with xanthine or 1-methylxanthine; 36,37) exhibits coupling to two inequivalent protons ($a_{\text{ave}} = 13 \text{ G}$ and 3 G), whereas the "rapid Type 2" signal (seen with moderate concentrations of xanthine (38) or with the complex of partially reduced enzyme with the substrate analog 8-bromoxanthine (39) exhibits coupling to two approximately equivalent protons ($a_{\text{ave}} = 10 \text{ G}$). All these protons exchange rapidly with solvent, although the strongly coupled proton of the "rapid Type 1" signal is initially derived from the C_8 position of substrate when the signal is generated with a stoichiometric excess of substrate (36). Under most experimental conditions, the "rapid Type 1" signal is predominant, appearing at a rate comparable to that for the decay of the "very rapid" signal (30). While the species giving rise to the "rapid Type 2" signal has been attributed to a dead-end complex of partially reduced enzyme with misoriented substrate in the active site (38), the species

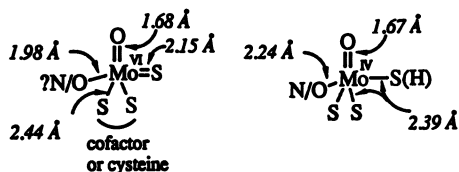


Figure 1. Consensus structures for the molybdenum center of oxidized (left) and reduced (right) xanthine oxidase.

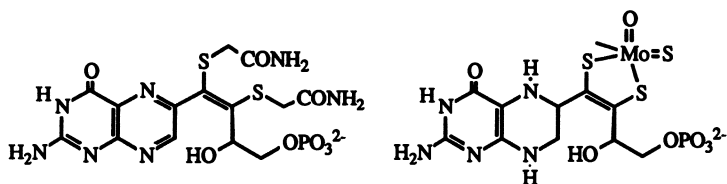


Figure 2. Proposed structures for the iodoacetamide-alkylated form of the pterin cofactor as isolated (left) and its complex with molybdenum in the active site of xanthine oxidase (right).

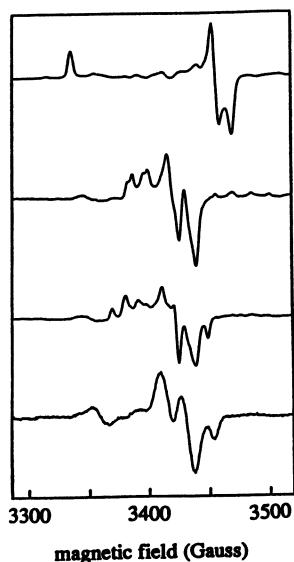


Figure 3. Mo(V) EPR signals seen in the course of the reaction of xanthine oxidase with excess xanthine. From top to bottom: the "very rapid", "rapid Type 1", "rapid Type 2" and "slow" signals. The experimental conditions were 9.47 GHz microwave frequency, 5 G field modulation, 10 mW microwave power and 150 K.

giving rise to the "rapid Type 1" signal has long been considered to be a legitimate catalytic intermediate lying downstream in the reaction mechanism from the species giving rise to the "very rapid" signal (5,10,37). Despite the difference of a strongly coupled proton between the "rapid Type 1" and "very rapid" signals, it has been shown that the signal-giving species do not constitute a conjugate acid/base pair (40).

UV/vis and Resonance Raman Studies of the Reductive Half-Reaction

The observation of UV/visible spectral changes associated with the molybdenum center of xanthine oxidase in the course of the reaction of enzyme with substrate is complicated by the large changes associated with reduction of the FAD and iron-sulfur centers of the enzyme. In the case of the reaction of enzyme with the substrate lumazine (2,6-dihydroxypteridine), however, two long-wavelength absorbing species attributable to the molybdenum center have been identified as intermediates in the reaction (41,42). These correspond to $E_{ox}S$ (i.e., Mo^{VI} -lumazine) and $E_{red}P$ (Mo^{IV} -violapterin); the latter intermediate is readily formed by anaerobic addition of violapterin (2,6,7-trihydroxypteridine, the product of enzyme action on lumazine) to dithionite-reduced enzyme. Formation of both of these long-wavelength absorbing species requires the functional form of the molybdenum center possessing a catalytically essential Mo=S group, and the wavelength dependence of the kinetics indicates that both are intermediates in the reaction of enzyme with lumazine (42). On the basis of their long-wavelength absorbance, the absorption bands have been assigned to charge-transfer transitions between the reduced molybdenum center (donor) and pterin ring (acceptor) in the active site of the enzyme (42). In the case of the reduced enzyme-violapterin complex this assignment has been corroborated in recent resonance Raman experiments (43). This latter study utilized the well-separated long-wavelength absorption of the reduced molybdenum center in complex with violapterin, using laser excitation at 676.4 nm. Several internal vibrational modes of violapterin were found to be resonance enhanced, as were a number of bands in the 250-1100 cm^{-1} range, presumably arising from vibrational modes of the molybdenum coordination sphere. A set of three bands at 1553, 1562 and 1584 cm^{-1} were also seen, possibly arising from vibrational modes within the dithiol-coordinated pterin portion of the molybdenum cofactor. Upon substitution of ^{18}O for ^{16}O in the molybdenum coordination sphere (accomplished *in situ* by multiple turnover of enzyme in $H_2^{18}O$), bands at 1469, 853, 517, 325 and 276 cm^{-1} exhibited shifts of 5-12 cm^{-1} to lower energy. By analogy to previous vibrational studies of Mo-O-Mo and Mo-O-R model compounds (44), the 853, 517 and 276 cm^{-1} frequencies were judged consistent with a labeled Mo-O-R linkage of the complexed violapterin. The relatively small frequency shifts observed in these and other vibrations upon incorporation of ^{18}O were also very similar to those observed for ^{18}O -labeled phenol and metal-phenolate complexes (45) that model iron-tyrosinate proteins. The resonance Raman data are thus consistent with direct coordination of violapterin to molybdenum via its C7-hydroxyl group (43). No oxygen isotope-sensitive bands were observed in the 900-1100 cm^{-1} region where Mo=O stretching modes are expected to occur, presumably due to poor resonance enhancement of the vibrational mode with 676.4 nm excitation. This is consistent with the assignment of the electronic transition to a Mo violapterin charge-transfer transition, since such a transition is most likely to be in the x-y plane of the molybdenum coordination sphere (the z axis being defined by the Mo=O bond). Application of resonance Raman spectroscopy to the molybdenum center of xanthine oxidase should prove extremely useful in future studies of the molybdenum center in xanthine oxidase and other oxomolybdenum enzymes.

Reaction of Enzyme with Substoichiometric Concentrations of Substrate

Most previous kinetic studies of the reaction mechanism of xanthine oxidase have been complicated by the routine use of substrate concentrations in pseudo-first order excess over that of enzyme. Because six reducing equivalents are required to fully reduce the

enzyme under anaerobic conditions with substrate (two at the molybdenum center, one at each of the two iron-sulfur centers and two at the FAD; 24), under conditions of excess substrate each enzyme molecule reacts sequentially with three substrate molecules (each of which donates two reducing equivalents to the enzyme). This constitutes a substantial kinetic complication that can be avoided by utilizing single-turnover conditions (*i.e.*, substoichiometric rather than pseudo first-order excess concentrations of substrate).

The Reaction of Enzyme with Substoichiometric Concentrations of 2-Hydroxy-6-Methylpurine. The reaction of xanthine oxidase with substrate under single-turnover conditions is most straightforward in the case of 2-hydroxy-6-methylpurine, a slow substrate for the enzyme that is hydroxylated with a k_{cat} of 0.1 s^{-1} at pH 8.5, $25 \text{ }^{\circ}\text{C}$ (34,46). Because the reaction is so slow, the experiment can be carried out aerobically, with the advantage that the flavin and iron-sulfur centers of the enzyme remain fully oxidized throughout the course of the reaction ($k_{\text{ox}} = 8 \text{ s}^{-1}$ under the experimental conditions used in the study). As a result, these centers do not contribute to any spectral change that may be observed, permitting small changes taking place transiently at the molybdenum center to be more conveniently monitored. The spectral changes observed in the reaction of xanthine oxidase with limiting concentrations of 2-hydroxy-6-methylpurine at pH 10 provide clear evidence for two intermediates: the first exhibiting an absorption difference maximum (relative to oxidized enzyme) at 470 nm, and the second a difference maximum at 540 nm (Figure 4). The formation and decay of the second intermediate correlate very well with that of the "very rapid" EPR signal under the same experimental conditions. Because of the good agreement between the amount of "very rapid" EPR signal observed in these experiments (~80% of the functional molybdenum at maximum) with that expected on the basis of rate constants for the formation and decay of the signal-giving species (1.3 and 0.11 s^{-1} , respectively, giving a theoretical yield of 76%), it can be concluded that the species giving rise to the "very rapid" Mo^{V} EPR signal is an obligatory catalytic intermediate with 2-hydroxy-6-methylpurine at pH 10. Interestingly, when the kinetics of the "very rapid" EPR signal are followed in D_2O , both the formation and decay of the signal-giving species exhibit isotope effects of approximately three (Figure 5). Given that deprotonation of solvent-exchangeable sites must occur in the course of the reaction of enzyme with substrate (see below), the magnitude of the solvent isotope effect is not surprising. These results emphasize the kinetic as well as thermodynamic significance of protonation/deprotonation events in the oxidation-reduction chemistry of oxomolybdenum centers.

Because the reaction of xanthine oxidase with 2-hydroxy-6-methylpurine is so slow, the transfer of reducing equivalents from enzyme to oxygen (forming two equivalents of superoxide) is limited by the transfer of electrons out of the molybdenum center to the other redox-active sites of the enzyme. When the reduction of cytochrome *c* by the O_2^- thus formed is followed at 550 nm, a biphasic timecourse is observed with rate constants consistent with the formation and decay of the species giving rise to the "very rapid" EPR signal (46). In addition, the extent of the observed absorbance change in each the two kinetic phases accounts for approximately 1.0 (0.8 ± 0.2) reducing equivalent per 2-hydroxy-6-methylpurine in the reaction mix. These results demonstrate unequivocally that the "very rapid" Mo^{V} species is formed by the oxidation of a Mo^{IV} species (corresponding to the species exhibiting the difference maximum relative to oxidized enzyme at 470 nm), and not the direct one-electron reduction of the molybdenum center by xanthine (to give Mo^{V} and a xanthyl radical) as has been recently suggested (47). In 0.1 M CAPS buffer (3-(cyclohexylamino)-1-propanesulfonic acid), pH 10, $25 \text{ }^{\circ}\text{C}$, the minimal kinetic scheme suggested by the above data is the following (with the rate constant for each step indicated):

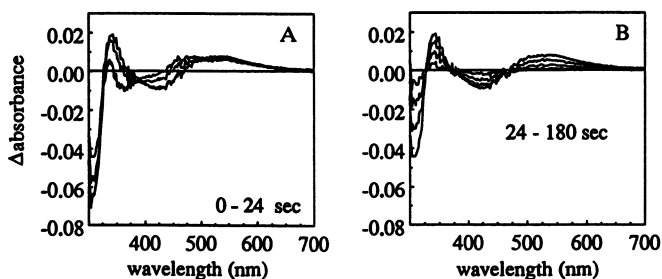


Figure 4. The reaction of xanthine oxidase with substoichiometric 2-hydroxy-6-methylpurine under aerobic conditions. The reaction was carried out in aerobic 0.1 M CAPS, 0.1 KCl, 0.3 mM EDTA, pH 10.0, 10°C. Spectra were recorded at regular intervals after the addition of substrate. The spectra shown were obtained at the following times: *Panel A*, immediately after the addition to 23.8 sec. *Panel B*, 23.8 sec to 180.6 sec. All absorbance changes are given relative to oxidized enzyme. The rate constants obtained for the conversion of the 470 nm-absorbing species to that absorbing at 540 nm, and the decay of the latter to oxidized enzyme were 0.24 s⁻¹ and 0.012 s⁻¹, respectively for the reaction carried out at 10°C.

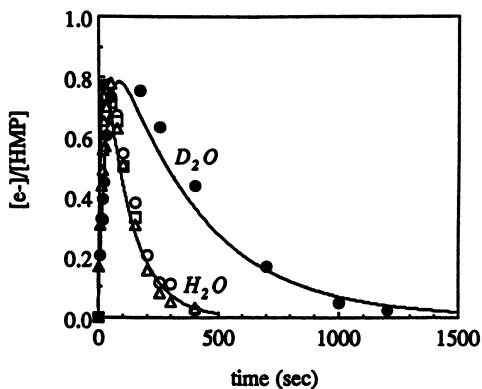
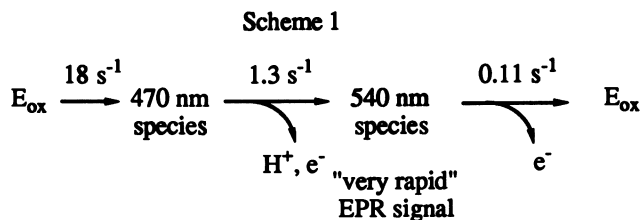


Figure 5. The appearance and disappearance of the "very rapid" E^- signal in the course of the reaction of xanthine oxidase with limiting 2-hydroxy-6-methylpurine. Reaction conditions were identical to those given in the legend to Figure 4, with the exception that the temperature was 2°C. The timecourses shown are for enzyme in H₂O and D₂O. The solid lines in each case represent fits to the data using rate constants for the formation and decay of the signal-giving species of 0.10 and 0.009 s⁻¹, respectively, in H₂O, and 0.03 and 0.0027 s⁻¹, respectively, in D₂O.



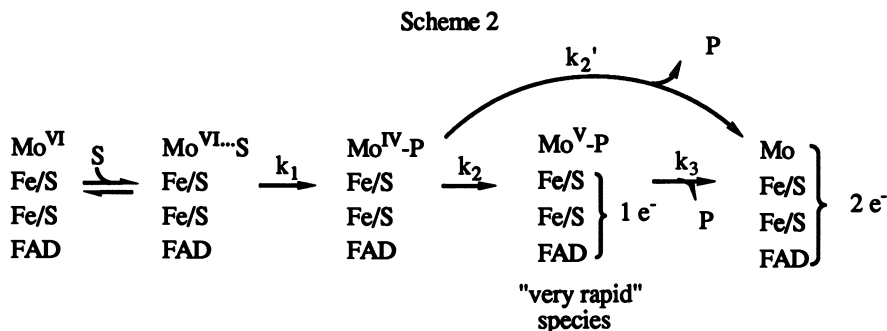
In an acid quench experiment, it has been demonstrated that 2,8-dihydroxy-6-methylpurine has formed by the time the 470 nm-absorbing species has been generated, indicating that C8-O bond formation precedes the formation of this intermediate. These results are consistent with similar studies using xanthine as substrate, where it is found that product uric acid is generated in the dead-time of the reaction (48).

The Reaction of Enzyme with Substoichiometric Concentrations of Xanthine and 1-Methylxanthine. In light of the above results with 2-hydroxy-6-methylpurine as substrate, the reaction of enzyme with substoichiometric concentrations of xanthine and 1-methylxanthine has been reinvestigated. In the case of the reaction with xanthine, timecourses observed at longer wavelengths (>600 nm) exhibit a small initial increase on a time-scale of 100 ms, followed by an exponential decrease in absorbance. This behavior is consistent with the formation of a spectral intermediate. Figure 6 shows the wavelength dependence of the faster phase of the reaction, as determined from two-exponential fits of the kinetic transients at various wavelengths. This kinetic difference spectrum is virtually identical to the difference spectrum observed on addition of uric acid to reduced enzyme (39). This transient absorbance increase is not due to accumulation of the neutral flavin semiquinone, as the deflavo form of xanthine oxidase exhibits kinetic behavior indistinguishable from that of native enzyme.

Whereas the observed rate constant for the reaction with 2-hydroxy-6-methylpurine is independent of the reactant present in excess (46), the rate of reaction of xanthine oxidase with limiting xanthine is found to be dependent on enzyme concentration (following the reaction at 450 nm). At pH 10, k_{cat} and K_d , as determined from a plot of $1/k_{obs}$ vs. $1/[xanthine\ oxidase]$ are 5.0 s^{-1} and $85\text{ }\mu\text{M}$, respectively (49). A small temperature-dependence for K_d accounts for the apparent discrepancy compared with the value of $260\text{ }\mu\text{M}$ obtained at $25\text{ }^\circ\text{C}$. When the kinetics of the "very rapid" EPR signal are followed in a freeze-quench experiment, rate constants for formation and decay of the signal at this temperature of 46 s^{-1} and 2.3 s^{-1} , respectively, are obtained (at 5°C ; 49). The slower rate constant is in very good agreement with that for the decay of the spectral intermediate seen in stopped-flow experiments carried out at the same temperature and concentration. At pH 8.5 the kinetic pattern for the reaction of xanthine oxidase with xanthine is similar to that observed at pH 10 except that the reaction is considerably faster; values for k_{cat} and K_d are 2.2 s^{-1} and $2.5\text{ }\mu\text{M}$, respectively. As with the data at pH 10, the K_d value determined at pH 8.5 and 5°C is approximately threefold lower than the value obtained at $25\text{ }^\circ\text{C}$. Evidence for the formation of an intermediate having absorbance in the 470 nm region is also found at pH 8.5, albeit to a smaller extent than at pH 10. At present it is difficult to determine whether the transient absorbance increase seen in the reaction of xanthine oxidase with xanthine is due to $\text{Mo}^{\text{IV}}\text{-P}$ or $\text{Mo}^{\text{V}}\text{-P}$. The similarity of the kinetic difference spectrum to the spectral change observed on addition of uric acid to reduced enzyme argues for the former species, while the decrease in magnitude of the absorbance increase on going from pH 10 to 8.5 argues for the latter. Most likely, both intermediates contribute to the kinetic difference spectrum seen in Figure 6. Experiments with 1-methylxanthine gave rate constants for the reaction of xanthine oxidase with limiting 1-methylxanthine, as determined by stopped-flow kinetic experiments at $5\text{ }^\circ\text{C}$, are 0.4 s^{-1} and 3.5 s^{-1} at pH 10 and pH 8.5, respectively (46). With this substrate, however, no obvious spectral

intermediate is observed at either pH 10 or 8.5, and all kinetic transients are well-behaved single exponentials.

The amount of "very rapid" EPR signal observed at maximum varies considerably with substrate and pH, from ~80% with 2-hydroxy-6-methylpurine at pH 10 to essentially 0% with 1-methylxanthine at pH 8.5. Assuming a common reaction mechanism for the hydroxylation of all three purines, the most likely explanation, as previously proposed (34,50), invokes a bifurcation in the reaction mechanism with Mo^{IV}-P breaking down by either one-electron transfer to other sites in the enzyme to give the "very rapid" Mo^V-P species with rate constant k_2 , or by dissociation of product with rate constant k_2' (followed by very fast transfer of both reducing equivalents to other sites in the enzyme (10,51), as shown in Scheme 2:



In such a bifurcated mechanism, differences in the amount of "very rapid" EPR signal observed as a function of substrate or reaction conditions are accounted for by the relative magnitudes of k_2 , k_2' and k_3 . Scheme 2 is consistent with the recent kinetic isotope effect study of D'Ardenne and Edmondson (48), which demonstrated that while the intrinsic deuterium kinetic isotope effect at position 8 of xanthine is large for the isotope-sensitive step $k_H/k_D=7.4\pm 0.7$, the rate constant associated with this step is several-fold greater than that for the rate limiting step of catalysis (product dissociation, either from Mo^{IV} or Mo^V), i.e., $k_1 \gg k_2, k_3$.

The Species Giving Rise to the "Rapid Type 1" Mo^V EPR Signal and the Kinetic Mechanism of Xanthine Oxidase

In none of the reactions described above with limiting concentrations of substrate are any of the Mo^V EPR signals designated "rapid" (31) observed. This is especially surprising in the case of 1-methylxanthine, which is known to form substantial amounts of "rapid Type 1" EPR signal under conditions of excess substrate. As illustrated in Figure 7, large amounts of "rapid" signal can be generated by addition of xanthine, 1-methylxanthine, 2-hydroxy-6-methylpurine or 8-bromoxanthine to partially reduced enzyme. In agreement with the literature, 1-methylxanthine gives an essentially pure "rapid Type 1" EPR spectrum (36) and 8-bromoxanthine an essentially pure "rapid Type 2" (39) while xanthine gives a mixture of the Type 1 and Type 2 forms of the "rapid" signal (36); 2-hydroxy-6-methylpurine also gives a "rapid Type 1" EPR signal in good yield, indicating that this substrate is able to generate this EPR signal under the appropriate conditions. The EPR signals generated by the addition of substrate to partially reduced deflavo xanthine oxidase are indistinguishable from those observed transiently in the course of the reaction of enzyme with that substrate.

In the case of 2-hydroxy-6-methylpurine, it is significant that the time between addition of substrate to the partially reduced deflavo enzyme and freezing the sample (~10 sec) in the above experiments does not permit significant turnover ($k_{cat} = 0.0085 \text{ s}^{-1}$ at 4°C; 44). Even in a rapid quench experiment mixing partially reduced enzyme with this substrate, substantial amounts of "rapid Type 1" EPR signal are observed at

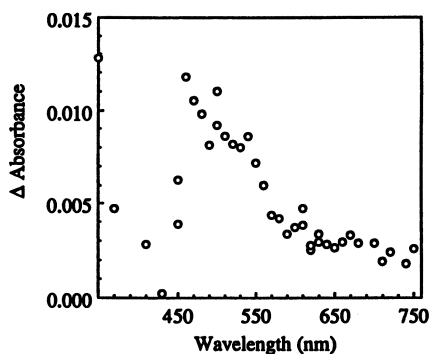


Figure 6. Wavelength dependence of the initial absorbance increase observed in the course of the reaction of deflavo xanthine oxidase with limiting xanthine at pH 10. The initial absorbance increase was calculated from stopped-flow kinetic transients, obtained at 5 °C, using the amplitude for the fast phase of a two-exponential fit to the data.

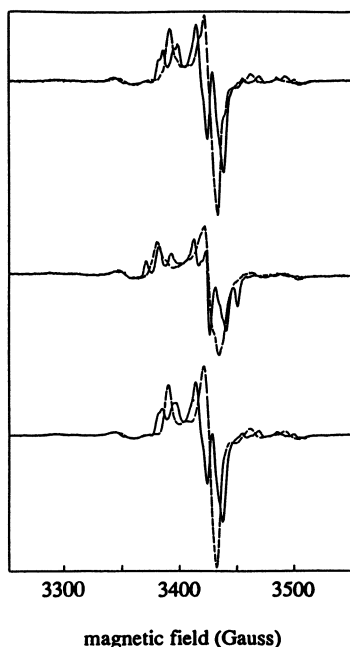
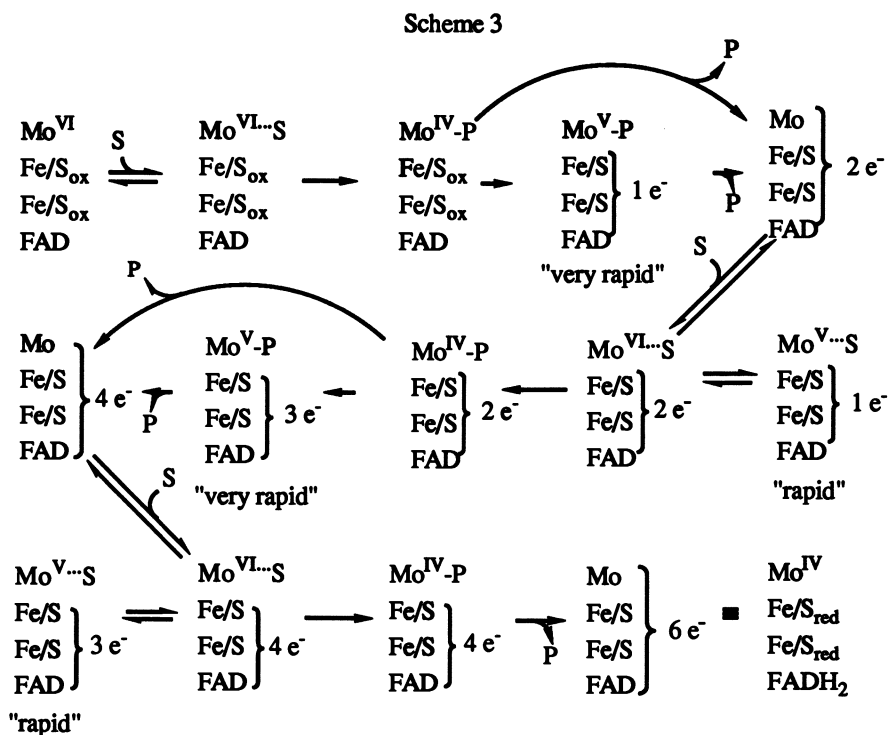


Figure 7. EPR signals seen on addition of purines to deflavo xanthine oxidase partially reduced by prior reaction with sodium dithionite. From top to bottom: partially reduced deflavo xanthine plus 1.0 mM 1-methylxanthine, enzyme plus 1.0 mM 8-bromoxanthine and enzyme plus 1.0 mM 2-hydroxy-6-methylpurine. Solid lines, H₂O; dashed lines, D₂O.

the shortest time (22 ms). This contrasts with the kinetic studies described above using limiting concentrations of 2-hydroxy-6-methylpurine in which no "rapid" EPR signal is observed in the course of the reaction, even at very long times (> 400 sec). Furthermore, partial reduction of the enzyme prior to reaction with 2-hydroxy-6-methylpurine reverses the order of appearance of the "very rapid" and "rapid" signals. These experiments demonstrate that the species giving rise to the "rapid Type 1" Mo^V EPR signal of xanthine oxidase can be generated in the absence of enzyme turnover simply by the addition of substrate to partially reduced enzyme, and that under at least some circumstances formation of the species giving rise to the "rapid Type 1" signal is much too fast to be accounted for by catalytic formation of an intermediate lying downstream from the species giving rise to the "very rapid" EPR signal. The most likely explanation for the above results is that the "rapid" signal is formed only when substrate is able to encounter partially reduced enzyme (*i.e.*, enzyme which has already reacted with at least one prior substrate molecule or, alternatively, enzyme that has been partially reduced by prior reaction with dithionite) in forming the Michaelis complex. Under single turnover conditions, with enzyme in stoichiometric excess over substrate, all substrate molecules will react with fully oxidized enzyme and the species giving rise to the "rapid" signal will thus not form. The species giving rise to the "rapid Type 1" EPR signal is thus most appropriately thought of as a Mo^V analog of the Mo^{VI}-substrate Michaelis complex. Mechanistically, the species is a dead-end complex unable to proceed in the catalytic sequence until the molybdenum center is reoxidized to Mo^{VI} rather than a *bona fide* catalytic intermediate.

A comprehensive kinetic mechanism for the reaction of oxidized enzyme with a stoichiometric excess of substrate is illustrated in Scheme 3. In this scheme, the species giving rise to the "rapid" and "very rapid" EPR signals are indicated, and in the case of the "rapid" species only those possible distributions of reducing equivalents among the several redox-active sites at a given level of reduction giving Mo^V are represented. The "rapid" species lies "upstream" rather than "downstream" from the "very rapid" species *in the oxidation of a given substrate molecule*, and the "rapid Type 1" species is only observed in the second and third reaction sequences (only these sequences begin with partially reduced enzyme). Such an assignment for the "rapid" species contrasts with conclusions of recent work in which the "rapid" species is placed downstream from the species giving the "very rapid" EPR signal in a given catalytic sequence (5,34,50), but is in agreement with earlier work in which it was concluded that the "rapid" species was a Mo^V...substrate complex (37,38). The "very rapid" species is shown in Scheme 3 as an obligatory reaction intermediate, as has been demonstrated to be the case with 2-hydroxy-6-methylpurine as substrate (46), but is partially circumvented in the cases of xanthine and 1-methylxanthine by direct dissociation of product from the Mo^{IV}-P complex (Scheme 3, dashed arrows). It is to be noted that just as the first catalytic sequence cannot form the "rapid" species, so the final catalytic sequence cannot form the "very rapid" species, since the flavin and iron-sulfur centers are fully reduced at this stage and unable to accept a reducing equivalent from Mo^{IV}-P to form Mo^V-P. Scheme 3 also provides a clear explanation as to why the "very rapid" and "rapid Type 1" do not constitute a conjugate acid/base pair (40): on the basis of a variety of evidence the former species contains a Mo-OR group (34,43,52,53), while the latter simply has substrate bound at the active site (but not necessarily coordinated to the molybdenum itself). In particular, the Cg-O bond of product has not been formed in the "rapid Type 1" species. Olson *et al.* (10) have demonstrated that a kinetic mechanism similar to that depicted in Scheme 3 is able to adequately account for the kinetics of the appearance and disappearance of the "rapid" EPR signal observed in the course of the reaction of xanthine oxidase with excess xanthine, although these workers assumed that the "rapid" signal arose principally from uncomplexed rather than substrate-complexed forms of partially reduced enzyme (a conclusion that is not consistent with subsequent work clearly demonstrating that the form of the "rapid" signal observed is substrate-dependent; 35). Scheme 3 appropriately emphasizes that the species giving rise to the "rapid" EPR signal is not a



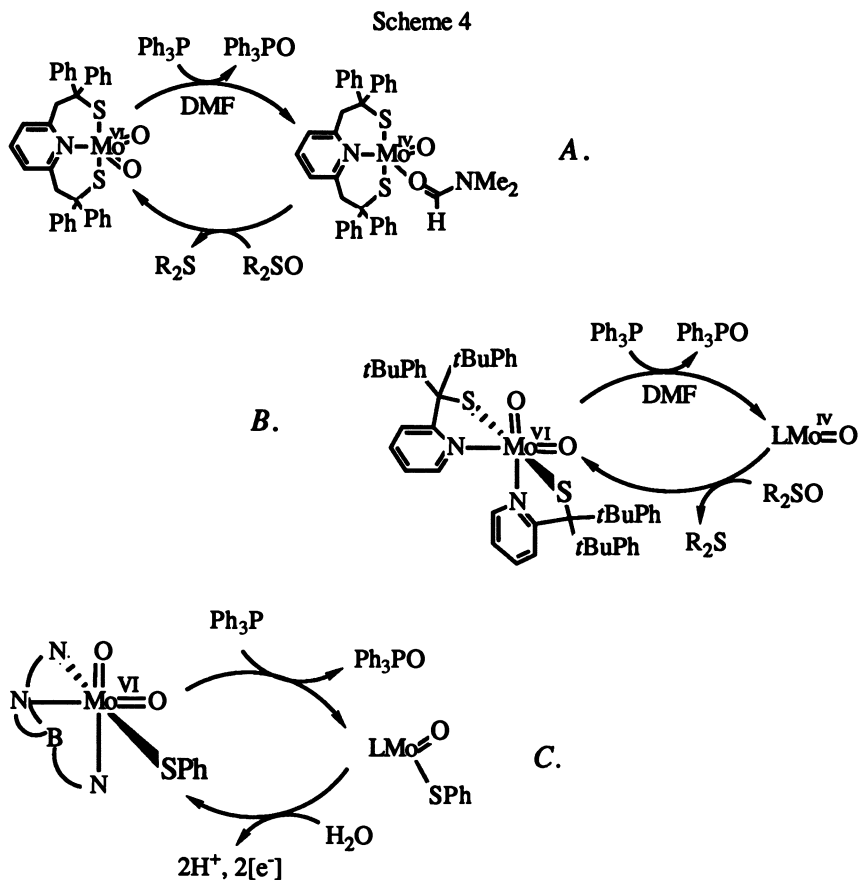
reaction intermediate *per se*, but rather a dead-end complex, unable to proceed with the catalytic sequence until the molybdenum center becomes fully oxidized by transfer of a reducing equivalent to one of the other redox-active centers of the enzyme.

The ability to generate relatively large amounts of kinetically stable "rapid" EPR signal in the absence of contaminating FADH[•] signal has also permitted a reexamination of the magnetic interaction between Mo^V and the C₈-H of substrate. The failure to observe any detectable difference between the "rapid" signal generated by addition of the C₈-¹H and C₈-²H forms of 2-hydroxy-6-methylpurine (again on a time scale too short for catalysis to have taken place) indicates that the C₈-H is only very weakly coupled at best in the Mo^V-S complex. It is well-known, however, that the strongly coupled proton seen in "rapid" signal generated under conditions of excess substrate is derived from the C₈ position of substrate (35). This indicates that it is only after substrate has been oxidized and the C₈ proton transferred from the purine ring that the proton becomes strongly coupled, and that proton abstraction has not yet occurred on the timescale that the sample was prepared. This is in agreement with the earlier conclusion that both magnetically coupled protons seen in the "rapid Type 1" EPR signal reside on the enzyme rather than substrate (36).

The Chemical Mechanism of Molybdenum-Based Hydroxylation

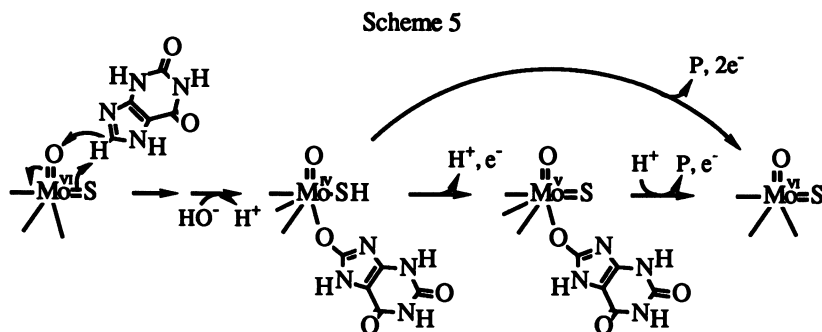
Studies of the chemical mechanism of the molybdenum hydroxylases has been given considerable impetus by the elaboration of the chemistry of two oxomolybdenum complexes by Holm and coworkers that are likely mechanistic models for the active sites of these enzymes (52-54). These complexes are of the general formula LMoO₂ and are sterically blocked from dimerizing. Both have been shown to be capable of cleanly catalyzing the transfer of an oxygen atom from a suitable donor to an acceptor according to the chemistry shown in Scheme 4, A and B. Despite the known strength of the

Mo=O bond (with an enthalpy of formation on the order of -45 kcal/mol; 55), it is clear from the chemistry shown in Scheme 4 that it is sufficiently labile in solution to permit the removal of the oxygen with its transient replacement by a solvent ligand. A variety of oxo donors and acceptors have been examined, and the suitability of a given pair for turnover has been adequately accounted for on thermodynamic grounds (55). A similar dioxomolybdenum model LMoO_2X (L=hydrotris(3,5-dimethyl-1-pyrazolyl)borate, $\text{X}=\text{PhS}^-$, NCS^-) has recently been developed by Enemark and coworkers (56,57). Especially significant from the standpoint of the enzyme-catalyzed reaction is the ability of this complex, in its reduced LMoOX form, to react with water in the presence of a suitable oxidant to return to the oxidized LMoO_2X parent compound (Scheme 4C). The second oxo group is thus regenerated from water in a manner similar to the manner likely to be used by the enzyme.



Similar oxo-transfer chemistry is likely taking place in the reaction of xanthine oxidase with substrate (58). When enzyme is labeled with ^{18}O by extensive turnover in H_2^{18}O , then taken up in H_2^{16}O and reacted with substoichiometric xanthine (so that no enzyme molecule had the opportunity to react more than once with substrate), 92% of the uric acid recovered from the reaction mix contains ^{18}O at the 8 position as determined by mass spectral analysis of the product. When the converse experiment is done with ^{16}O -labeled enzyme in H_2^{18}O , the uric acid is found to contain predominantly ^{16}O at the 8 position. Control experiments have demonstrated that label incorporated

into neither enzyme nor uric acid exchanged with solvent on the time scale of the experiment, and that the silylation reaction necessary to volatilize the uric acid for the mass spectral analysis did not displace label. Xanthine oxidase thus acts in such a way that oxygen is transferred from a catalytically labile site in the enzyme, most likely the Mo=O group (see below), to substrate with each catalytic cycle. In order to account for the well-established observation that solvent is the ultimate source of the oxygen incorporated into product, it is assumed that the catalytically labile site is regenerated from solvent in the course of each catalytic cycle. On the basis of the above labeling experiments, the chemical sequence shown in Scheme 5 has been proposed for the reductive half-reaction of xanthine oxidase (58).



The above chemical sequence is consistent with an intermediate of the form Mo^{IV}-OR in the reaction of enzyme with substrate, and with the subsequent EXAFS work indicating that both Mo^{IV}-P and Mo^V-alloxanthine complexes possess Mo=O groups. While not addressed in the mechanism as originally proposed, it is now clear that the Mo=O group must be immediately regenerated, since such a group is observed in the EXAFS analysis of reduced enzyme in complex with violapterin (corresponding to the first intermediate shown in Scheme 5). The oxo group may be regenerated by hydroxide from solvent or, alternatively, by deprotonation of hydroxide already present in the molybdenum coordination sphere (A.G. Wedd, personal communication). In either case a conformational change or a HO-Mo=O/O=Mo-OH proton transfer must occur in order to return the molybdenum center to its original stereochemical configuration. The presence of a Mo-OR group is also consistent with the resonance Raman study of the Mo^{IV}-violapterin complex of xanthine oxidase, and with recent EPR studies comparing the ¹⁷O and ³³S coupling of molybdenum model compounds and the Mo^V EPR signals of the enzyme (see below). The mechanism shown in Scheme 5 is consistent with the known acidity of the C₈ proton of xanthine (it is, for example, sufficiently acidic to exchange with solvent under relatively mild conditions; 30), and the fact that upon reduction of the enzyme molybdenum the Mo=S group protonates to form a thiol. The greater basicity of Mo=S relative to Mo=O makes the former group the more likely proton acceptor, and also provides a rationale for the catalytic requirement for this group in those enzymes catalyzing hydroxylations that involve C-H bond cleavage.

The evidence indicating that the catalytically labile oxygen site is in fact the Mo=O group of oxidized enzyme comes from EPR studies using ¹⁷O-labeled enzyme (59,60). Exchange of ¹⁷O into the molybdenum coordination sphere is slow (1-2 hr) for the enzyme alone, but quite rapid (seconds) during turnover. When the "rapid Type 1" signal is generated with formamide clear evidence is found for a single strongly and anisotropically coupled ¹⁷O superhyperfine interaction (60), and this has been interpreted as arising from a Mo=O group. The "very rapid" signal, generated by reaction of enzyme with excess xanthine, exhibits a strong but nearly isotropic superhyperfine interaction, consistent with the formation of a Mo-O-R group, with the (now oxidized) purine moiety covalently bound at the molybdenum center (59). Recent

EPR work by Wedd and coworkers with a homologous series of ^{33}S - and ^{17}O -labeled molybdenum (V) complexes indicate that at least in six-coordinate complexes $\text{Mo}-^{17}\text{OH}$ is strongly coupled whereas $\text{Mo}=\text{O}$ is only weakly coupled to the electron spin, consistent with the $\text{Mo}-\text{OR}$ assignment for the "very rapid" species (61,62), but inconsistent with $\text{Mo}=\text{O}$ being the strongly coupled oxygen in the "rapid Type 1" species. These workers ascribed the strongly coupled oxygen to a $\text{Mo}-\text{O}-\text{R}$ species, similar to that proposed for the "very rapid" species but possessing strongly coupled protons as well. It follows from Scheme 3, however, that neither removal of the C_8 proton of substrate nor formation of the C_8-O bond of product has taken place at the point in the reaction mechanism that the "rapid" species is formed for a given substrate molecule. A $\text{Mo}-\text{OR}$ formulation for the "rapid" species is thus unlikely. It is possible that the strongly coupled oxygen in the "rapid Type 1" EPR signal arises from hydroxide coordinated to molybdenum, a possibility given the evidence from x-ray absorption studies for $\text{Mo}-\text{OH}$ in the reduced enzyme (16). It remains for future work to confirm the presence of a hydroxyl in the active site of oxidized enzyme and its catalytic role (if any).

Acknowledgments

The author would like to thank A.G. Wedd for helpful discussion and communication of data prior to publication. Work in the author's laboratory is supported by grants AR38917 and RR06706 from the National Institutes of Health, and DMB 9108417 from the National Science Foundation.

Literature Cited

1. Wikstrom, M. *Proc. Natl. Acad. Sci. U.S.A.* **1981**, *78*, 4051-4053.
2. Varotsis, C.; Babcock, G.T. *Biochemistry* **1990**, *29*, 7357-7362.
3. Entsch, B.; Ballou, D.P.; Massey, V. *J. Biol. Chem.* **1976**, *251*, 2550-2563.
4. Bray, R.C. In *The Enzymes*; Boyer, P. D., Ed.; Academic Press: New York, NY, **1975**, vol. 12, pp. 299-419.
5. Bray, R.C. *Quart. Rev. Biophys.* **1988**, *21*, 299-329.
6. Hille, R.; Massey, V. In *Molybdenum Enzymes*; Spiro, T. G., Ed.; John Wiley and Sons: New York, **1985**; pp. 443-518.
7. Hille, R. In *Chemistry and Biochemistry of Flavoenzymes*; F. Müller, Ed.; CRC Press: Boca Raton, FL, **1991**, Vol. 3; pp. 21-68.
8. Bray, R.C.; Palmer, G.; Beinert, H. *J. Biol. Chem.* **1964**, *239*, 2667-2676.
9. Komai, H.; Massey, V.; Palmer, G. *J. Biol. Chem.* **1969**, *244*, 1692-1700.
10. Olson, J.S.; Ballou, D.P.; Palmer, G.; Massey, V. *J. Biol. Chem.* **1974**, *249*, 4363-382.
11. Tullius, T.D.; Kurtz, D.M., Jr.; Conradson, S.D.; Hodgson, K.O. *J. Am. Chem. Soc.* **1979**, *101*, 2776-2779.
12. Bordas, J.; Bray, R.C.; Garner, C.D.; Gutteridge, S.; Hasnain, S.S. *Biochem. J.* **1980**, *191*, 499-508.
13. Cramer, S.P.; Wahl, R.; Rajagopalan, K.V. *J. Am. Chem. Soc.* **1981**, *103*, 7721-7727.
14. Cramer, S.P.; Hille, R. *J. Am. Chem. Soc.* **1985**, *107*, 8164-8169.
15. Hille, R.; George, G.N.; Eidsness, M.K.; Cramer, S.P. *Inorg. Chem.* **1989**, *28*, 4018-4022.
16. Turner, N.A.; Bray, R.C.; Diakun, G.P. *Biochem. J.* **1989**, *260*, 563-571.
17. Cotton, F.A.; Wing, R.M. *Inorg. Chem.* **1965**, *4*, 867-874.
18. Stiefel, E.I. *Prog. Inorg. Chem.* **1977**, *21*, 1-221.
19. Stiefel, E.I. *Proc. Natl. Acad. Sci.* **1973**, *70*, 988-992.
20. Porras, A.G.; Palmer, G. *J. Biol. Chem.* **1982**, *257*, 11617-11626.
21. Rajagopalan, K.V. *Adv. Enzymol.*, **1991**, *64*, 215-290.

22. Hawkes, T.R.; Bray, R.C. *Biochem. J.* **1984**, *222*, 587-590.
23. Gruber, S.; Kilpatrick, L.; Bastian, N.R.; Rajagopalan, K.V.; Spiro, T.G. *J. Am. Chem. Soc.* **1990**, *112*, 8179-8180.
24. Hille, R.; Massey, V. *J. Biol. Chem.* **1982**, *257*, 8898-8901.
25. Lazarus, R.A.; Dietrich, R.F.; Wallick, D.E.; Benkovic, S.J. *Biochemistry* **1981**, *20*, 6834-6841.
26. Dix, T.A.; Bollag, G.E.; Domanico, P.L.; Benkovic, S.J. *Biochemistry*, **1985**, *24*, 2955-2962.
27. Stiefel, E.I.; Miller, K.F.; Bruce, A.E.; Corbin, J.L.; Berg, J.M.; Hodgson, K.O. *J. Am. Chem. Soc.* **1980**, *102*, 3624-3627.
28. Bray, R.C. *Biochem. J.* **1961**, *81*, 196-199.
29. Palmer, G.; Bray, R.C.; Beinert, H. *J. Biol. Chem.* **1964**, *239*, 2657-2666.
30. Edmondson, D.E.; Ballou, D.P.; van Heuvelen, A.; Palmer, G.; Massey, V. *J. Biol. Chem.* **1973**, *248*, 6135-6144.
31. Bray, R.C.; Vanngard, T. *Biochem. J.* **1969**, *114*, 725-734.
32. McGartoll, M.A.; Pick, F.M.; Swann, J.; Bray, R.C. *Biochim. Biophys. Acta* **1970**, *212*, 523-526.
33. Tanner, S.; Bray, R.; Bergmann, F. *Biochem. Soc. Trans.* **1978**, *6*, 1328-1330.
34. Bray, R.C.; George, G.N. *Biochem. Soc. Trans.* **1985**, *13*, 560-567.
35. Hawkes, T.R.; George, G.N.; Bray, R.C. *Biochem. J.* **1984**, *218*, 961-968.
36. Bray, R.C.; Barber, M.J.; Lowe, D.J. *Biochem. J.* **1978**, *171*, 653-658.
37. Gutteridge, S.; Tanner, S.J.; Bray, R.C. *Biochem. J.* **1978**, *175*, 869-878.
38. Pick, F.M.; Bray, R.C. *Biochem. J.*, **1969**, *114*, 735-742.
39. Hille, R.; Stewart, R.C. *J. Biol. Chem.* **1984**, *259*, 1570-1576.
40. Tsopanakis, A.D.; Tanner, S.J.; Bray, R.C. *Biochem. J.* **1978**, *175*, 879-885.
41. Davis, M.D.; Olson, J.S.; Palmer, G. *J. Biol. Chem.* **1982**, *257*, 14730-14737.
42. Davis, M.D.; Olson, J.S.; Palmer, G. *J. Biol. Chem.* **1984**, *259*, 3526-3533.
43. Oertling, T.A.; Hille, R. *J. Biol. Chem.* **1990**, *265*, 17446-17450.
44. Pinchas, S.; Sadeh, D.; Samuel, D. *J. Phys. Chem.* **1965**, *69*, 2259-2264.
45. Pysz, W.J.; Roe, L.A.; Stern, L.J.; Que, L.J., Jr. *J. Am. Chem. Soc.* **1985**, *107*, 614-620.
46. McWhirter, R. B.; Hille, R. *J. Biol. Chem.* **1991**, *266*, 23724-23731.
47. Symons, M.; Taiwo, F.A.; Peterson, R.L. *J. Chem. Soc. Faraday Trans. 1* **1989**, *85*, 4063-4074.
48. D'Ardenne, S.C.; Edmondson, D.E. *Biochem.* **1990**, *29*, 9046-9052.
49. Kim, J.H.; Hille, R. *J. Biol. Chem.* **1993**, *268*, 44-51.
50. Bray, R.C.; Gutteridge, S.; Stotter, D.A.; Tanner, S.J. *Biochem. J.* **1979**, *177*, 357-360.
51. Hille, R.; Anderson, R.F. *J. Biol. Chem.* **1991**, *266*, 5608-5615.
52. Berg, J.M.; Holm, R.H. *J. Am. Chem. Soc.* **1984**, *106*, 3035-3036.
53. Berg, J.M.; Holm, R.H. *J. Am. Chem. Soc.* **1985**, *107*, 917-924.
54. Gheller, S.F.; Schultz, B.E.; Scott, M.J.; Holm, R.H. *J. Am. Chem. Soc.* **1992**, *114*, 6934-6935.
55. Holm, R.H. *Coord. Chem. Rev.* **1990**, *100*, 183-221.
56. Roberts, S.A.; Young, C.G.; Kipke, C.A.; Cleland, W.E., Jr.; Yamanouchi, K.; Carducci, M.D.; Enemark, J.H. *Inorg. Chem.* **1990**, *29*, 3650-3656.
57. Xiao, Z.; Young, C.G.; Enemark, J.H.; Wedd, A.G. *J. Am. Chem. Soc.* **1992**, *114*, 9194-9195.
58. Hille, R.; Sprecher, H. *J. Biol. Chem.* **1987**, *262*, 10914-10917.
59. Gutteridge, S.; Bray, R.C. *Biochem. J.* **1980**, *189*, 615-623.
60. Bray, R.C.; Gutteridge, S. *Biochemistry* **1982**, *21*, 5992-5999.
61. Dowerah, D.; Spence, J.T.; Singh, R.; Wedd, A.G.; Wilson, G.; Farchione, F.; Enemark, J.H.; Kristofski, J.; Bruck, M. *J. Am. Chem. Soc.* **1987**, *109*, 5655-5665.
62. Wilson, G.L.; Greenwood, R.J.; Pilbrow, J.R.; Spence, J.T.; Wedd, A.G. *J. Am. Chem. Soc.* **1991**, *113*, 6803-6812.

Chapter 3

Biochemistry of the Molybdenum Cofactors

K. V. Rajagopalan

Department of Biochemistry, Duke University Medical Center,
Durham, NC 27710

Studies on the chemical nature of the molybdenum cofactor of liver sulfite oxidase led to the discovery of molybdopterin, a 6-alkyl pterin containing a dithiolene moiety and a phosphomonoester in the 4-carbon side chain. Subsequently, the cofactor in *Rhodobacter sphaeroides* DMSO reductase was found to contain molybdopterin linked to guanosine monophosphate by pyrophosphate linkage. Other dinucleotide variants with cytosine, adenine or hypoxanthine as the nucleotide base have also been discovered in bacteria. In contrast only molybdopterin was associated with four tungsten-containing enzymes from hyperthermophilic organisms. Magnetic circular dichroism spectra of DMSO reductase support the proposed ligation of Mo to the dithiolene sulfur atoms of molybdopterin. A discussion of the genetics and biochemistry of molybdopterin biosynthesis in *Escherichia coli* and in humans is presented.

Molybdenum is an essential component of a number of enzymes from diverse sources. All of the molybdoenzymes other than nitrogenase carry out either oxidative hydroxylation or reductive dehydroxylation at C, N or S atoms. Most of the well-characterized enzymes contain, in addition to Mo, other prosthetic groups, such as heme, FAD, Fe/S or Se, or combinations of these. The molybdoenzymes xanthine oxidase, aldehyde oxidase and sulfite oxidase, all from animal sources, have been studied extensively by electron paramagnetic resonance (EPR) spectroscopy. The shapes of the Mo(V) signal in these enzymes suggested coordination of the metal to sulfur ligands. More recently, the technique of extended X-ray absorbance fine structure analysis (EXAFS) has provided definitive evidence for the presence of thiolate ligands in the coordination field of Mo in these enzymes. These techniques, however, provided no information on the sources of the thiolate sulfur atoms and did not indicate the possible presence of a non-protein moiety in association with the Mo in these proteins. Evidence for the existence of a prosthetic molecule, termed molybdenum cofactor, at the Mo centers of molybdoenzymes emerged, not from physicochemical approaches, but from genetic studies with *Aspergillus nidulans* (1) and *Neurospora crassa* (2). These early studies, while providing evidence for the transferability of the cofactor from any purified molybdoprotein to the apoprotein of nitrate reductase in extracts of the *nit-1* mutant of *N. crassa*, indicated that the free cofactor was extremely labile.

The Molybdopterin Family

Studies carried out in our laboratory on the nature of association of Mo to the protein of liver sulfite oxidase culminated in the discovery and structural characterization of a unique organic metallophore termed molybdopterin (Figure 1). Two notable features of molybdopterin are the pterin ring and the dithiolene group on the 6-alkyl side chain. Active molybdenum cofactor was proposed to contain Mo liganded to the S atoms of the dithiolene group. A comprehensive review of the evidence supporting the proposed structure of the cofactor has been published (3).

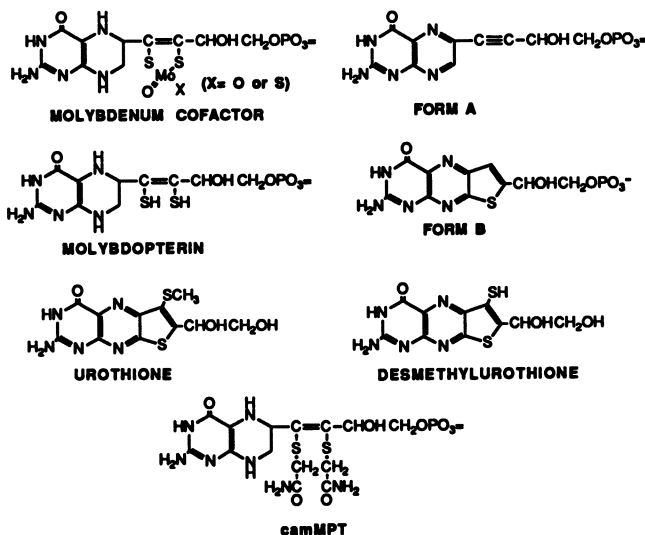


Figure 1. Structures of the molybdenum cofactor and derivatives. The pterin ring is shown in the tetrahydro state in molybdopterin, molybdenum cofactor and camMPT.

Unlike most of the other known cofactors the molybdenum cofactor is extremely unstable and does not retain its activity in the free state. The proposed structure of the cofactor was in fact deduced from the established structures of two degradation products, Form A and Form B, obtained from purified molybdoenzymes, and of urothione, the metabolic excretion product of the cofactor in animals. Isolation and structural characterization of an inactive alkylated derivative of the pterin, dicarboxamidomethylmolybdopterin (camMPT), allowed experimental verification of the structural features of the pterin (4). More recently, desmethylurothione has also been obtained from sulfite oxidase (5). The structures of the various derivatives of the cofactor are shown in Figure 1. Similar studies on milk xanthine oxidase, chicken liver xanthine dehydrogenase and rabbit liver aldehyde oxidase showed that all of the animal enzymes contain the same cofactor.

The molybdenum cofactor can be released from molybdoenzymes by treatment with denaturing reagents. The released cofactor is stable under rigorously anaerobic conditions in the presence of stabilizing reagents such as dithionite, ascorbate or dithiothreitol. Addition of iodoacetamide to anaerobically denatured molybdoenzymes leads to the alkylation of the dithiolene thiols. Arsenite, a reagent known to form a stable complex with *cis* dithiols, but does not react with any protein side chain residues including individual thiols, completely blocks the alkylation reaction (6),

providing strong evidence for the presence of dithiols and for the proposed *cis* configuration of the dithiolene in the released pterin.

In the course of their studies on the enzyme CO dehydrogenase from *Pseudomonas carboxydoflava*, Meyer and coworkers (7,8) obtained presumptive evidence for the existence of a larger form of cofactor, containing two phosphate groups. In our laboratory failure to obtain camMPT from *Rhodobacter sphaeroides* DMSO reductase led to the discovery and structural characterization of molybdopterin guanine dinucleotide (MGD) in the Mo cofactor of that enzyme (9). Shortly thereafter the Mo cofactor of CO dehydrogenase was found to contain molybdopterin cytosine dinucleotide (MCD) (10). Since then other dinucleotide variants of molybdopterin containing adenine (MAD) or hypoxanthine (MHD) as the nucleotide component have been identified (11). These dinucleotide structures are shown in Figure 2. The distribution of molybdopterin variants in a number of enzymes is shown in Table 1. While dinucleotides have not yet been reported in higher organisms, it is to be noted that molybdopterin itself is present in some bacterial enzymes.

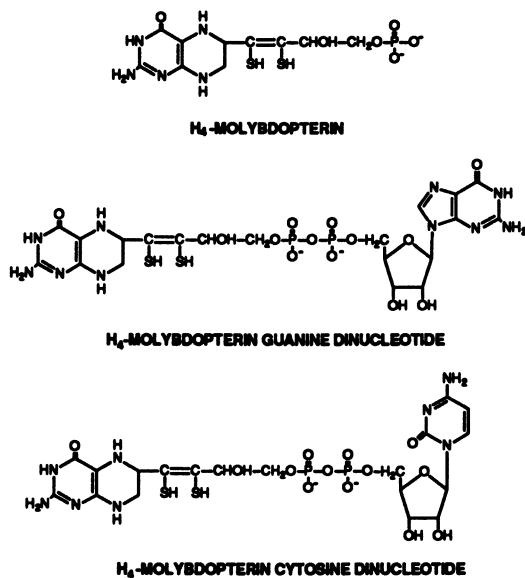


Figure 2. Structures of molybdopterin (MPT), molybdopterin guanine dinucleotide (MGD) and molybdopterin cytosine dinucleotide (MCD). Dinucleotides containing the purine bases adenine (MAD) and hypoxanthine (MHD) are not shown.

A highly interesting recent development has been the discovery by Mukund and Adams (12) of a group of tungsten-containing enzymes in hyperthermophilic organisms catalyzing reactions analogous to those catalyzed by molybdoenzymes in mesophilic organisms. We have examined four different tungsten enzymes for the presence of molybdopterin using established procedures for the preparation of Form A and of camMPT (13). Form A was indeed obtained from *P. furiosus* aldehyde oxidoreductase, demonstrating the presence of the molybdopterin moiety. Preparation of the carboxamidomethyl derivative and analysis by HPLC showed that the enzyme contained molybdopterin, not one of the dinucleotides. Analogous data were obtained from all of the tungsten enzymes examined. In view of the proposal that

hyperthermophilic bacteria and archaea are likely to have been the earliest forms of life, these findings lead to the conclusion that the molybdopterin structure has remained unchanged during the entire evolutionary history.

Table 1. Distribution of molybdenum cofactor variant forms

<i>Pterin</i>	<i>Enzyme</i>	<i>Source</i>	<i>Other cofactors</i>	
MPT	sulfite oxidase	animals	heme	
	xanthine dehydrogenase	animals	FAD, Fe/S	
	nitrate reductase	corn	heme, FAD	
	nitrate reductase	<i>Chlorella vulgaris</i>	heme, FAD	
	xanthine dehydrogenase	<i>Pseudomonas aeruginosa</i>	FAD, Fe/S	
	xanthine dehydrogenase	<i>Pseudomonas putida</i>		
	aldehyde ferredoxin oxidoreductase	<i>Pyrococcus furiosus</i>	Fe/S	
	formaldehyde ferredoxin oxidoreductase	<i>Thermococcus litoralis</i>	Fe/S	
	MGD	DMSO reductase	<i>Rhodobacter sphaeroides</i>	none
		nitrate reductase	<i>Rhodobacter sphaeroides</i>	none
nitrate reductase		<i>Escherichia coli</i>	Fe/S, Se	
nitrate reductase		<i>Pseudomonas carboxydoflava</i>	-	
formate dehydrogenase		<i>Escherichia coli</i>	Fe/S, Se	
formate dehydrogenase		<i>Methanobacterium formicicum</i>	Fe/S, Se	
formylmethanofuran dehydrogenase		<i>Methanosarcina barkeri</i>	-	
formylmethanofuran dehydrogenase		<i>Methanobacterium thermoautotrophicum</i>	-	
MCD	CO dehydrogenase	<i>Pseudomonas carboxydoflava</i>	FAD, Fe/S	
	quinoline oxidoreductase	<i>Pseudomonas putida</i>	-	
	quinoline oxidoreductase	<i>Rhodococcus spec. B1</i>	-	
MAD	formylmethanofuran dehydrogenase	<i>Methanobacterium thermoautotrophicum</i>	-	
	MHD	formylmethanofuran dehydrogenase	<i>Methanobacterium thermoautotrophicum</i>	-

Structure Spectra Correlations

The uniqueness of molybdopterin may be attributed to the combination of three structural features--the phosphate group, the dithiolene moiety and the pterin ring. These features are common to all the variant forms of molybdopterin and presumably are essential for the catalytic function of the molybdenum cofactors. A reasonable role for the phosphate group is in the binding of the molybdenum cofactor to apoproteins. Indeed there is presumptive evidence for this (6). The logical role for the dithiolene sulfur atoms is as ligands for Mo. Such a role is supported by the ability of synthetic Mo-dithiolene complexes to carry out reductive dehydroxylation of nitrate and sulfoxides. Laser Raman Spectroscopy has provided evidence for the ligation of Mo to dithiolene in DMSO reduction (14).

Magnetic circular dichroism (MCD) spectroscopy on the Mo(V) form of DMSO reductase also provides support for the existence of Mo-dithiolene charge transfer in DMSO reductase (15). The temperature-dependent MCD spectrum, shown in Figure 3 (left), displays six bands with alternating negative and positive features, all arising from

an $S=1/2$ ground state. These bands may logically be assigned to dithiolene- π to Mo(V) charge transfer. The probable transitions giving rise to the MCD bands are presented in Figure 3 (right). The combined evidence from resonance Raman and MCD spectroscopy of DMSO reductase suggest that the dithiolene-Mo bonding is retained in the Mo(VI), Mo(V) and Mo(IV) states of the enzyme.

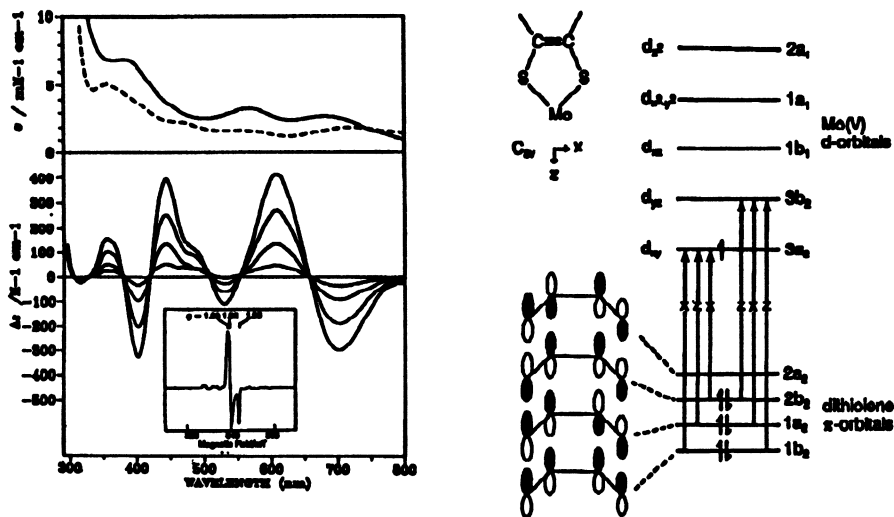


Figure 3. *Left: top panel*, Absorption spectra of Mo(V) (solid line) and Mo(VI) (dashed line) forms of DMSO reductase. *Left lower panel*, Temperature-dependent MCD spectra in the Mo(V) state. The four spectra, in order of decreasing intensities, were obtained with a magnetic field of 4.5 T at temperatures of 1.61, 4.22, 9.6, and 27.3 K. Inset shows the EPR spectrum of the sample used for MCD. *Right*, The probable dithiolene- π to Mo(V) transitions yielding the MCD spectrum.

The most intriguing aspect of the structure of the molybdenum cofactor is the presence of the pterin ring. The fact that, despite its ephemerality in the free state, molybdopterin has survived the pressures of evolutionary adaptation means that the pterin ring may play a significant role in the overall catalytic efficiency of the molybdenum cofactor.

The electrochemical properties of the molybdenum centers of several enzymes have been examined. The oxidation-reduction potentials span a remarkably wide range of about 600 mV (16). Since the pterin ring can exist in several isomeric dihydro forms as well as the tetrahydro state, it is conceivable that different enzymes can stabilize one or another of the reduced forms of the pterin, accounting, at least in part, for the differences in oxidation reduction potentials. Another possible role for the pterin ring is the facilitation of electron transfer between the Mo atom and either internal or external electron carriers. Finally, the pterin could contribute to rate enhancement by participating in the transfer of the hydroxyl groups from or to substrates. In order to understand the role of the pterin, it is necessary to determine the oxidation state of the molybdopterin ring in the enzyme-bound state.

Oxidation State of the Pterin Ring

In addition to the fully oxidized and the fully reduced tetrahydro state, the pterin ring can exist in several isomeric dihydro states, as shown in Figure 4 (17). The fully oxidized pterin ring and the 7,8-dihydro form can be readily identified by their characteristic absorption bands, typified by the spectra shown in Figure 5 for the reduced forms of biopterin (18). As seen in Figure 6, the side chain of reduced pterins could exist in several alternative conformations. This stereochemical aspect of the structure of molybdopterin at the active sites of molybdoenzymes has yet to be elucidated.

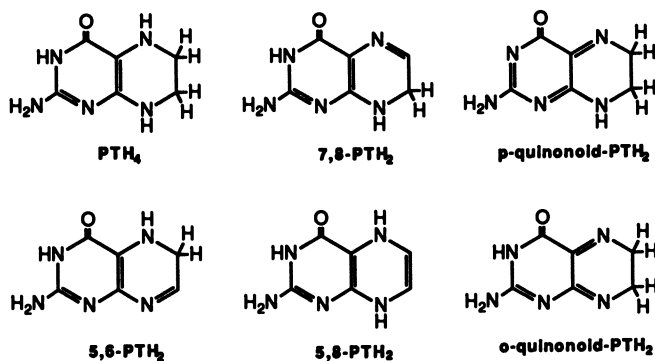


Figure 4. Electronic states of the pterin ring.

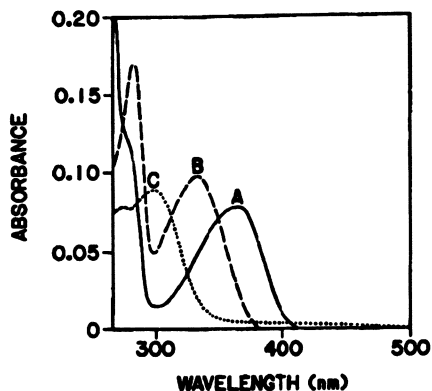


Figure 5. Absorption spectra of oxidized (A), 7,8-dihydro- (B) and tetrahydro (C) biopterin.

With the identification of a pterin as the organic component of the molybdenum cofactor, it was apparent that the inactivation of the cofactor in air could likely be initiated by the oxidation of a reduced pterin ring. Gardlik and Rajagopalan (19) have devised a procedure for probing the oxidation state of the pterin ring in native enzymes. For example, spectroscopic examination of anaerobically denatured milk xanthine oxidase revealed the absence of absorption bands attributable either to fully oxidized or

7,8-dihydro form of molybdopterin. When such a sample was treated with Hg^{2+} followed by the addition of dichlorophenolindophenol (DCIP), little or no reduction of the dye was observed (19). Since tetrahydropterins are known to be oxidized rapidly to p-quinonoid compounds by DCIP, these findings have been interpreted as evidence for the p-quinonoid state as the native form of molybdopterin in xanthine oxidase. Similar studies with sulfite oxidase (19) suggested that molybdopterin is present in the dihydro state in that enzyme as well but probably not in the quinonoid form. This inference was supported by the observation that in denatured sulfite oxidase the pterin was oxidized by two electron equivalents of DCIP to yield the fully oxidized pterin ring.

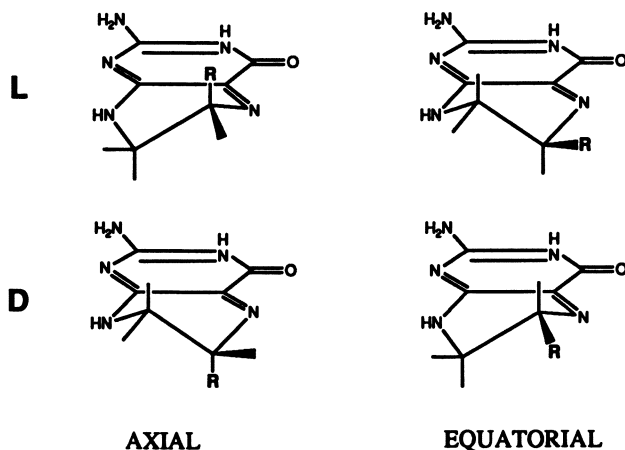


Figure 6. Conformations of the C-6 side chain (R) in quinonoid dihydro pterin.

Further evidence for the presence of the dihydro form of pterin in sulfite oxidase was derived from an investigation of the effect of ferricyanide on the enzyme (20). Reaction of 2 electron equivalents of ferricyanide per subunit of the native enzyme resulted in marked attenuation of the ability of the enzyme to transfer electrons to cytochrome *c* and ferricyanide but not to oxygen. Spectroscopic examination of the modified enzyme after denaturation revealed that molybdopterin had been converted to the fully oxidized form, verifying the presence of a dihydro pterin in the native enzyme. Gradual loss of Mo from ferricyanide-treated enzyme suggested that oxidation of the pterin ring destabilizes the ligand field of the metal. In contrast to the effect of ferricyanide, inactivation of sulfite oxidase by arsenite and periodate (21) was shown to involve reaction with sulfhydryl groups at the active site of the enzyme. In both cases loss of molybdenum occurred concomitant with inactivation, in contrast to the observations made with ferricyanide-treated enzyme.

Ligand Field of Molybdenum in Molybdoenzymes

The structure proposed in Figure 1 represents the molybdenum cofactor before the metal acquires additional ligands from apoproteins. Several questions arise with respect to the interactions between the cofactors and the proteins. What additional ligands are provided by the protein? Is the Mo-dithiolene bonding retained in all molybdoenzymes? Does the Mo atom undergo ligand exchange during the catalytic cycle? Does the Mo form bonds to the pterin ring?

As mentioned earlier, RR and MCD spectra of DMSO reductase have been interpreted to indicate a charge transfer interaction between dithiolene and Mo in that

enzyme. All of the visible absorption bands of the enzyme have been ascribed to the Mo-dithiolene interaction. Figure 7 shows a comparison of the absorption spectra of DMSO reductase and the Mo domain of sulfite oxidase. It is clear that some of the long wavelength bands of DMSO reductase are absent or greatly attenuated in sulfite oxidase. This suggests that the strength of the charge transfer interaction of the dithiolene with Mo may be considerably less in sulfite oxidase than that in DMSO reductase. Examination of the MCD spectra of several molybdoenzymes should provide further insight into the nature of the differences in their molybdenum ligation.

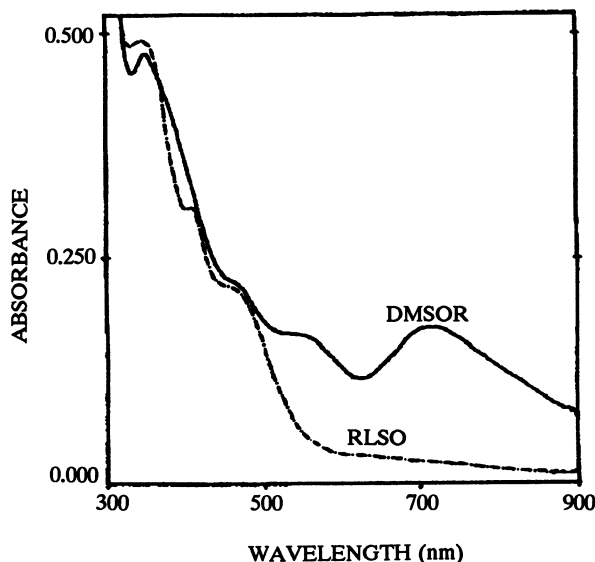


Figure 7. Absorption spectra of *R. sphaeroides* DMSO reductase (DMSOR) and the molybdenum domain of rat liver sulfite oxidase (RLSO). (Reproduced with permission from reference 22)

Xanthine oxidase (23), xanthine dehydrogenase (24) and aldehyde oxidase (25) have been shown to undergo substrate dependent inactivation by the -SH reagents *p*-chloromercuribenzoate, quinones and *F*-dinitrobenzene, respectively. The fact that inhibition by these reagents is not observed in the absence of substrates suggests that a thiol ligand of Mo becomes free during the catalytic cycle of each of these enzymes. Recent studies with aldehyde oxidase have indicated that the reactive thiol is not one of the dithiolene sulfurs, but is likely to be a cysteine residue. These findings constitute evidence for alterations in molybdenum ligation dependent on catalysis. Examination of the mechanism of the suicide inactivation of sulfite oxidase when oxidizing arsenite to arsenate has shown that the loss of activity results from removal of molybdenum from the enzyme. Presumably the excess arsenite present in the medium is able to bind to two Mo thiolate ligands that become accessible during catalysis. Identification of the labile thiolate ligands should provide crucial information on the dynamic nature of the Mo ligand field during catalysis.

Fischer and coworkers have recently examined the reaction of $\text{Mo(VI)O}_2\text{Cl}_2$ with tetrahydrobiopterin (26). The product, trichloro(1,5-quinoid-7,8-dihydro-6H-L-biopterin)oxo-Mo(IV), was examined by X-ray crystallography and was found to have the structure shown in Figure 8.

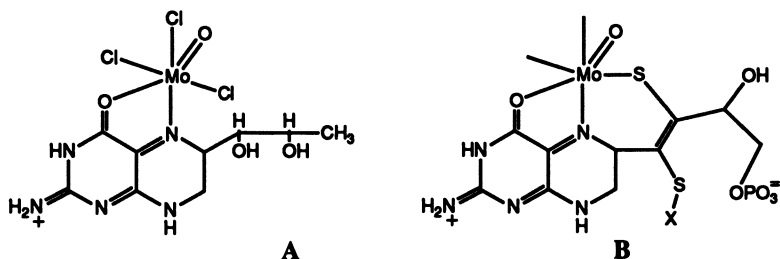


Figure 8. A. Structure of a model quinonoid-biopterin-Mo(IV) complex (see text). B. Proposed structure of the quinonoid form of molybdenum cofactor.

As mentioned earlier, the uniqueness of molybdopterin stems not so much from the fact that it is a pterin, as from the presence of the dithiolene moiety. Since this feature has remained immutable in all oxotransferases containing Mo or W and is not present in any other type of enzyme, the validity of using models lacking the dithiolene seems questionable. Further, the lack of information on the stereochemical aspects of the cofactor structure makes any model speculative at best. It is conceivable, however, that the aforementioned activity-dependent changes in the Mo ligand field could include bonding of the Mo to ligands provided by the pterin ring, possibly involving *cis-trans* isomerization of the dithiolene group. Perhaps this could explain the essentiality of the pterin ring as a component of the molybdenum cofactor.

Biosynthesis

The greater part of our information on the biosynthesis of the molybdenum cofactor has been obtained from a study of molybdopterin mutants of *E. coli*, as a group termed the chlorate-resistant mutants (*chl*), and from a molybdopterin mutant of *Neurospora crassa*, *nit-1*. The distribution of *chl* loci in the *E. coli* genome is shown in Figure 9. Mutants in these loci display pleiotropic lack of all molybdoenzyme activities. Two new mutants isolated in our laboratory, *chlM* and *chlN*, have been mapped to the *chlA* and *chlE* regions of the genome, respectively. These mutants and two other mutants studied earlier, *chlA1* and *chlE5*, were analyzed for molybdenum cofactor content by quantitating their ability to reconstitute nitrate reductase activity in a molybdopterin mutant of *Neurospora crassa*, *nit-1*, and by quantitating the presence of molybdopterin by conversion to the Form A derivative (27). The *chlA1*, *chlM* and *chlN* mutants were shown to be true molybdopterin mutants by the Form A assay. The *chlA* locus has been cloned and found to code for 5 peptides, *chlA1* representing the first reading frame (Dr. D. M. Boxer, University of Dundee, personal communication, 1992). The *chlE* segment encodes two proteins, ChlE5 and ChlN (28).

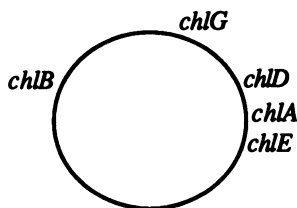


Figure 9. Genomic location of the *chl* loci in *Escherichia coli*.

Detailed studies on the *chlA1* showed that the mutant cells contained an activity which, when added to an extract of *N. crassa nit-1* cells caused the formation of molybdopterin from a precursor present in the low molecular weight fraction of the *nit-1* extract. The same precursor molecule, identified functionally in the *nit-1* low molecular weight fraction, was shown to accumulate also in the *chlM*, *chlN* and *chlE5* mutants of *E. coli* (29). It was further shown that extracts from those mutants which exhibited precursor activity were also the ones that produced an inactive fluorescent material, termed compound Z, upon iodine oxidation. Compound Z was isolated and chemically characterized in order to facilitate the characterization of the more labile precursor itself. These studies culminated in the structure shown below for compound Z (Figure 10). More recent studies on the structure of the precursor itself indicate that it contains a dihydro pterin ring but is similar to compound Z in all other respects. The active molecule has been termed precursor Z.

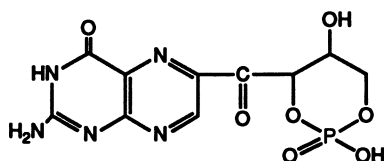


Figure 10. Structure of compound Z.

The activity in *chlA1*, required for the conversion of the precursor to molybdopterin, termed the converting factor (30), has been purified to homogeneity and has been shown to consist of two dissociable subunits, both of which are essential for activity. N-terminal amino acid sequencing has shown that the small subunit and the large subunit are the products of *chlA* genes 4 and 5, respectively.

Addition of purified converting factor to purified precursor leads to the formation of stoichiometric amounts of MPT, identified by conversion to Form A, Form B, and camMPT under appropriate derivatization conditions specific for each product. The smaller of the two subunits of the converting factor is essential for the sulfur addition reaction and appears to sequester an active sulfur sufficient for a single turnover activation reaction. *In vivo* this active sulfur must presumably be replenished by an activating system encoded by the *chlN* locus. Converting factor isolated from *chlN* mutants contains both subunit proteins and can bind precursor but cannot activate it to MPT unless the small subunit is itself activated by the product of a functional *chlN* gene. Electrospray mass spectrometry revealed that the mass of the small subunit of the converting factor purified from *chlA1* cells was 16 to 17 mass units greater than that of the small subunit from *chlN* cells. This difference suggests strongly that the active sulfur in functional converting factor displaces an oxygen atom and raises several interesting possibilities as to the potential residue and chemistry involved in the ligation of the reactive, transferable sulfur atom. The proposed pathway of sulfur transfer from a low molecular weight sulfur donor to its ultimate incorporation into molybdopterin is outlined in Figure 11.

The formation of the Mo cofactor from molybdopterin requires the ligation of the metal to the dithiolene sulfurs. Little is known about the proteins or the form of Mo required for these reactions, other than the implication of the *chlD* and *chlG* gene products in the uptake and further processing of molybdate (31). In prokaryotic organisms the appropriate dinucleotide forms of the cofactor also have to be synthesized. In *E. coli* it has been established that the *chlB* gene product is essential for the formation of MGD (32).

American Chemical
Society Library
1155 16th St. N. W.
Washington, D. C. 20036

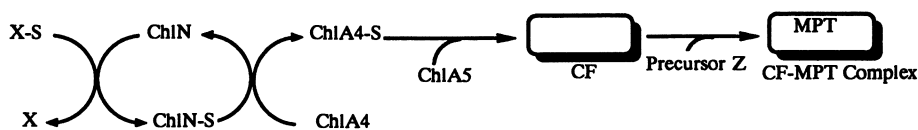


Figure 11. Pathway of S incorporation into MPT. ChlA4, ChlA5 and ChlN are products of *chlA4*, *chlA5* and *chlN* genes. CF is converting factor.

Molybdenum Cofactor Deficiency.

Molybdenum cofactor deficiency is generally a genetic disease of infancy characterized by severe neurological abnormalities, decreased brain size and, in most cases, dislocated ocular lens. Only two or three have survived beyond the first few weeks, with only one displaying normal mental acuity (33). Since individuals with xanthine dehydrogenase deficiency or combined xanthine dehydrogenase-aldehyde oxidase deficiency are asymptomatic, the pathological sequelae of cofactor deficiency are likely attributable to sulfite oxidase deficiency. Studies involving binary coculture of fibroblasts have revealed two clinical phenotypes, group A and group B. Patients in group A appear to have a block early in the biosynthesis of the cofactor; whereas group B patients excrete a molybdopterin precursor in the urine (34). The formation of compound Z upon iodine oxidation of group B urine showed that the patients have a block in the conversion of precursor Z to molybdopterin, analogous to *E. coli chlM* and *chlN*, and *N. crassa nit-1*. It is not yet established whether molybdopterin biosynthesis in humans is genetically as complex as it is in lower organisms, or whether a simpler pathway starting from a dietary precursor is operative. Isotopic tracer studies currently in progress are expected to provide the answer to this important question.

Literature Cited

- (1) Pateman, J. A.; Cove, D. J.; Rever, B. M.; Roberts, D. B. *Nature* **1964**, *201*, 58-60.
- (2) Nason, A.; Lee, K. Y.; Pan, S. S.; Erickson, R. H. *J. Less Common Metals* **1974**, *36*, 449-459.
- (3) Rajagopalan, K. V. In *Advances in Enzymology and Related Areas of Molecular Biology*; Meister, A., Ed.; John Wiley & Sons: New York, 1991; Vol. 64; pp 215-289.
- (4) Kramer, S. P.; Johnson, J. L.; Ribeiro, A. A.; Millington, D. S.; Rajagopalan, K. V. *J. Biol. Chem.* **1987**, *262*, 16357-16363.
- (5) Gardlik, S. J. Ph.D. Thesis, Duke University, 1988.
- (6) Hageman, R. V.; Rajagopalan, K. V. In *Nitrogen Fixation and CO₂ Metabolism*; Ludden, P. W.; Burris, J. E., Eds.; Elsevier Science Publishing Co.: New York, 1985; pp 133-141.
- (7) Kruger, B.; Meyer, O. *Biochim. Biophys. Acta* **1987**, *912*, 357-364.
- (8) Kruger, B.; Meyer, O. *Eur. J. Biochem.* **1986**, *157*, 121-128.
- (9) Johnson, J. L.; Bastian, N. R.; Rajagopalan, K. V. *Proc. Natl. Acad. Sci. USA* **1990**, *87*, 3190-3194.
- (10) Johnson, J. L.; Rajagopalan, K. V.; Meyer, O. *Arch. Biochem. Biophys.* **1990**, *283*, 542-545.
- (11) Borner, G.; Karrasch, M.; Thauer, R. K. *Febs. Lett.* **1991**, *290*, 31-34.
- (12) Mukund, S.; Adams, M. W. W. *J. Biol. Chem.* **1990**, *265*, 11508-11516.
- (13) Johnson, J. L.; Rajagopalan, K. V.; Mukund, S.; Adams, M. W. W. *J. Biol. Chem.* **1993**, *268*, 4848-4852.

- (14) Gruber, S.; Kilpatrick, L.; Bastian, N. R.; Rajagopalan, K. V.; Spiro, T. G. *J. Am. Chem. Soc.* **1990**, *112*, 8179-8180.
- (15) Finnegan, M. G.; Hilton, J.; Rajagopalan, K. V.; Johnson, M. K. *J. Inorg. Chem.* **1993**, *in press*.
- (16) Barber, M. J.; Coughlan, M. P.; Kanda, M.; Rajagopalan, K. V. *Arch. Biochem. Biophys.* **1980**, *201*, 468-475.
- (17) Pfeleiderer, W. In *Folates and Pterins*; Blakley R. L.; Benkovic, S. J., Eds.; John Wiley & Sons: New York, 1985; Vol. 2; pp 43-114.
- (18) Kaufman, S. *Proc. Natl. Acad. Sci. USA* **1963**, *50*, 1085-1093.
- (19) Gardlik, S.; Rajagopalan, K. V. *J. Biol. Chem.* **1990**, *265*, 13047-13054.
- (20) Gardlik, S.; Rajagopalan, K. V. *J. Biol. Chem.* **1991**, *266*, 4889-4895.
- (21) Gardlik, S.; Rajagopalan, K. V. *J. Biol. Chem.* **1991**, *266*, 16627-16632.
- (22) Bastian, N. R.; Kay, C. J.; Barber, M. J.; Rajagopalan, K. V. *J. Biol. Chem.* **1991**, *266*, 45-51.
- (23) Fridovich, I.; Handler, P. *J. Biol. Chem.* **1958**, *231*, 899-911.
- (24) Weaver, R. F.; Rajagopalan, K. V.; Handler, P.; Jeffs, P.; Byrne, W. L.; Rosenthal, D. *Proc. Natl. Acad. Sci. USA* **1970**, *67*, 1050-1054.
- (25) Rajagopalan, K. V.; Handler, P. *J. Biol. Chem.* **1964**, *239*, 2027-2035.
- (26) Fischer, B.; Strahle, J.; Viscontini, M. *Helv. Chim. Acta* **1991**, *74*, 1544-1554.
- (27) Johnson, M. E.; Rajagopalan, K. V. *J. Bacteriol.* **1987**, *169*, 117-125.
- (28) Nohno, T.; Kasai, Y.; Saito, T. *J. Bacteriol.* **1988**, *170*, 4097-4102.
- (29) Johnson, M. E.; Rajagopalan, K. V. *J. Bacteriol.* **1987**, *169*, 110-116.
- (30) Pitterle, D. M.; Rajagopalan, K. V. *J. Bacteriol.* **1989**, *171*, 3373-3378.
- (31) Stewart, V. *Microbiol. Rev.* **1988**, *52*, 190-232.
- (32) Johnson, J. L.; Indermaur, L. W.; Rajagopalan, K. V. *J. Biol. Chem.* **1991**, *266*, 12140-12145.
- (33) Johnson, J. L. In *The metabolic basis of inherited disease*; Scriver, C. R.; Beaudet, A. L.; Sly, W. S.; Valle, D., Eds.; McGraw-Hill: New York, 1989; pp 1463-1475.
- (34) Johnson, J. L.; Wuebbens, M. M.; Mandell, R.; Shih, V. E. *J. Clin. Invest.* **1989**, *83*, 897-903.

RECEIVED April 12, 1993

Chapter 4

The Bacterial Molybdenum Cofactor

O. Meyer, K. Frunzke, J. Tachil, and M. Volk

Lehrstuhl für Mikrobiologie, Universität Bayreuth, Universitätstrasse 30,
W-8580 Bayreuth, Germany

The molybdenum cofactor (Moco) is composed of a pterin moiety, molybdate and an O- or S-substituent attached to the metal. The bacterial Moco contains a molybdopterin dinucleotide which consists of molybdopterin (MPT) and a mononucleotide linked by a pyrophosphate bridge. Bacterial MPT dinucleotides identified so far are molybdopterin cytosine dinucleotide (MCD), molybdopterin adenine dinucleotide (MAD), molybdopterin guanine dinucleotide (MGD) and molybdopterin hypoxanthine dinucleotide (MHD). MPT has been resolved in bacterial xanthine dehydrogenases. Most molybdoenzymes studied exhibit a high specificity for the type of pterin utilized, even under conditions of coexpression of different molybdoenzymes.

We have obtained the *Hydrogenophaga pseudoflava* CO dehydrogenase pterin in amounts sufficient for structural analysis and describe the first ^1H - and ^{13}C -NMR spectra of a carboxamidomethylated MPT dinucleotide. The data fully agree with the chemical structure of a di(carboxamidomethyl)molybdopterin cytosine dinucleotide [di(cam)MCD].

Compound U, an excretion product of *H. pseudoflava*, was isolated and its chemical structure has been resolved as 2-amino-7-(1,2-dihydroxyethyl)-6-(methylthio)thieno[3,2-g]pteridine-4(3H)-one (urothione) employing uv-vis spectroscopy, electron impact mass spectroscopy, ^1H -NMR spectroscopy and HPLC. Evidence is presented, that urothione emerges from the degradation of the *H. pseudoflava* CO dehydrogenase Moco. The degradational pathway involves release of Moco from the enzyme, its dissociation into molybdate and MCD and conversion of MCD to urothione via MPT, phospho norurothione and norurothione.

The idea of the existence of an organic compound in the bacterial molybdenum cofactor different from molybdopterin emerged from analyses of CO dehydrogenases from different bacterial sources which revealed 8 mol of organic phosphate per mol of enzyme (1). That number was unexpectedly high since molybdopterin and flavin adenine dinucleotide in CO dehydrogenase would account for only 6 mol of organic phosphate. When CO dehydrogenases were precipitated with trichloroacetic acid or perchloro acid the additional organic phosphate appeared in the supernatant. On the basis of these and other results it was concluded that CO dehydrogenases contain an as yet unidentified, noncovalently bound, organic phosphorous compound in addition to molybdopterin and flavin adenine dinucleotide (1). In order to identify the unknown compound *Hydrogenophaga pseudoflava* (formerly *Pseudomonas carboxydoflava*) was cultivated with [³²P]phosphate and CO dehydrogenase was purified (2). One enzyme molecule contained an average of 8.32 molecules of organic phosphate. The entire phosphate content was confined to two molecules of FAD and two molecules of a pterin. These were not covalently bound. Molybdoenzyme cofactors could be extracted into N-methyl formamide and pterins were isolated by thin layer chromatography. The CO dehydrogenase pterin revealed the following characteristic features. (i) A relative molecular mass, M_r , of 730 which was much higher than that of molybdopterin (330). (ii) A content of 2 molecules of phosphate per molecule compared to only one phosphate in molybdopterin. (iii) The CO dehydrogenase pterin was three times less susceptible to air oxidation than molybdopterin. (iv) The pterin was cleaved by perchloric acid into two phosphorous-containing fragments with M_r of 330 and 420. The smaller one was believed to be very similar to molybdopterin, the larger one was not a pterin but was believed to contain an aromatic structure (2-4). The pterin contained a side chain at carbon atom 6 of the pterin ring as indicated by the formation of pterin-6-carboxylic acid upon alkaline permanganate oxidation. The affinity of the reduced pterin for thiol-Sepharose pointed to the presence of active thiol(s) in the molecule (5). On the basis of these results it was concluded that CO dehydrogenase contains a novel pterin which differs from molybdopterin in molecular mass, phosphate content and stability, implying a novel structure.

Since the large pterin was also identified in various molybdoenzymes from different bacterial sources, e.g. *Pseudomonas carboxydovorans* and *Pseudomonas carboxydohydrogena* CO dehydrogenases, *Clostridium barkeri* and *Veillonella atypica* (formerly *alcalescens*) xanthine dehydrogenases, *E. coli* nitrate reductase (2, 5), *Bacillus niacini* nicotinic acid dehydrogenase, *Pseudomonas stutzeri* nitrate reductase, and *Nitrobacter hamburgensis* nitrite oxidoreductase (6), it was tentatively named "bactopterin" (2).

In *H. pseudoflava* CO dehydrogenase the aromatic substituent could be identified as 5'-cytidine monophosphate by HPLC analysis and the structure of the CO dehydrogenase pterin was resolved as molybdopterin cytosine dinucleotide (MCD) (7). Molybdopterin guanine dinucleotide (MGD) has been

resolved in *Rhodobacter sphaeroides* dimethyl sulfoxide reductase (8). Since then a wide variety of bacterial molybdoenzymes has been examined for the type of pterin present in their molybdenum cofactor (Figure 1, Table I).

Chemical Structure of Molybdopterin Cytosine Dinucleotide (MCD)

The structure of the *Hydrogenophaga pseudoflava* CO dehydrogenase pterin has been investigated by alkylation and isolation of the carboxamidomethyl derivative (7). The alkylated pterin was identified as di(carboxamidomethyl)molybdopterin cytosine dinucleotide [di(cam)MCD] on the basis of its uv-vis absorption properties and by degradation with nucleotide pyrophosphatase yielding di(carboxamidomethyl)molybdopterin [di(cam)MPT] and cytidine monophosphate (CMP). However, a full structural characterization of the CO dehydrogenase pterin must involve $^1\text{H-NMR}$, $^{13}\text{C-NMR}$, COSY and mass spectroscopy. Amounts of di(cam)MCD sufficient for structural analysis were obtained as follows. CO dehydrogenase was isolated and purified from 500 g (wet weight) of CO-grown *H. pseudoflava* with a yield of 520 mg following published procedures (3, 9). The enzyme was unfolded with 2% (wt/vol) SDS under anoxic, reducing conditions. Carboxamidomethylation of pterins was performed as before (8). The pterin fraction was separated by ultrafiltration and further purified by anion exchange chromatography on QAE Sephadex A-25, isocratic C_{18} -reversed phase HPLC employing 50 mM ammonium acetate (pH 6.8) as the mobile phase, and gel filtration on Sephadex G-10 with water as the eluent. Di(cam)MCD was obtained with a yield of 2.2 mg and good purity as checked by HPLC (Figure 2).

Purified di(cam)MCD in its air oxidized state was yellow colored, showed a characteristic uv-vis absorption spectrum with maxima at 277 and 367 nm (Figure 2) and its spectrum was indistinguishable from that reported previously (7). The absorption maximum at 367 nm is in the range normally observed for oxidized 6-alkylpterins such as biopterin (10), di(cam)MPT (11) or form A and form B obtained from molybdopterin (12).

$^1\text{H-NMR}$ spectra (water decoupled mode) were recorded in water because of a much better solubility of di(cam)MCD compared to other solvents employed in NMR spectroscopy, e.g. dimethyl- d_6 -sulfoxide. Under these conditions signals from C-bound and N-bound protons were obtained (Figure 3).

Di(cam)MCD revealed signals of C-bound hydrogen at 8.5 ppm (singlet), 7.7 ppm (doublet), 5.75 ppm (two superimposed double doublets), 4.2 ppm (triplet), 4.1 ppm (multiplet), 4.05 ppm (multiplet), a multiplet centered at 3.95 ppm, 3.85 ppm (multiplet), around 3.58 ppm (double doublet), and 3.05 ppm (double doublet) which could be ascribed to C_7H (pterin moiety), C_6H (cytosine moiety), C_5H (cytosine moiety) and C_1H (ribose moiety), $\text{C}_3\text{'}(\text{OH})\text{H}$ (pterin side chain), $\text{C}_2\text{'}(\text{OH})\text{H}$ and $\text{C}_3\text{'}(\text{OH})\text{H}$ (ribose moiety), C_4H (ribose moiety), C_5H_2 (ribose moiety), C_4H_2 (pterin side chain), CH_2 (carboxamidomethyl group at $\text{C}_2\text{'}$ of the pterin side chain), and CH_2 (carboxamidomethyl group at

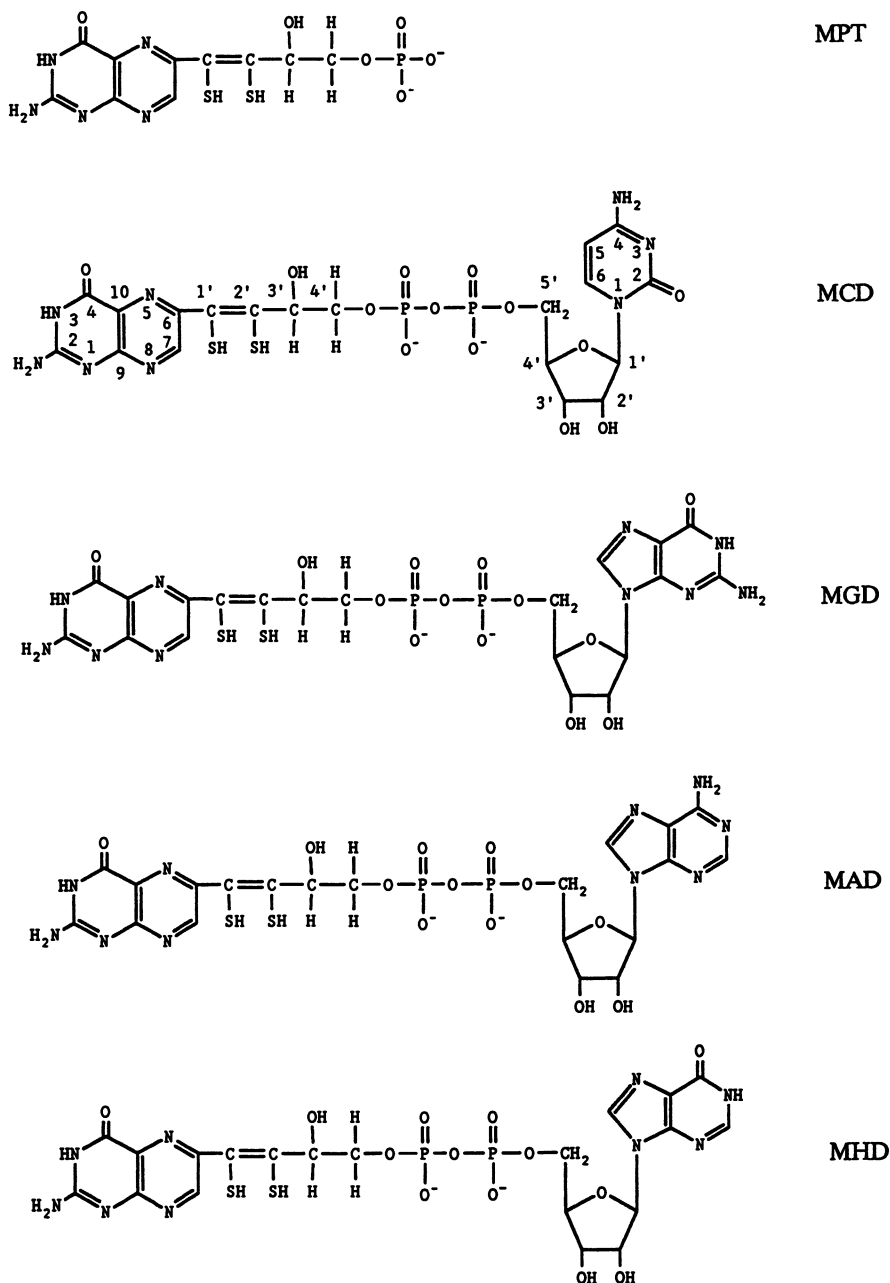


Figure 1. Chemical structures of bacterial pterins.

The structures show the pterins in their oxidized state. MPT, molybdopterin; pyrimidines: MCD, molybdopterin cytosine dinucleotide; purines: MGD, molybdopterin guanine dinucleotide; MAD, molybdopterin adenine dinucleotide; MHD, molybdopterin hypoxanthine dinucleotide. For references refer to Table I.

TABLE I. Occurrence of molybdopterin and molybdopterin dinucleotides in bacterial molybdoenzymes

Pterin ^a	Enzyme	Source and reference
MPT	Xanthine dehydrogenase	<i>Pseudomonas aeruginosa</i> (25) <i>Pseudomonas putida</i> (26)
MCD	CO dehydrogenase	<i>Hydrogenophaga pseudoflava</i> (7, 14) <i>Pseudomonas carboxydohydrogena</i> (14) <i>Pseudomonas carboxydovorans</i> (14) <i>Streptomyces thermoautotrophicus</i> (14, 16) <i>Pseudomonas putida</i> (26) <i>Rhodococcus</i> sp. (26)
	Quinoline oxidoreductase	
MGD	Dimethyl sulfoxide reductase	<i>Rhodobacter sphaeroides</i> (8)
	Formylmethanofuran dehydrogenase	<i>Methanosarcina barkeri</i> (28) <i>Methanobacterium thermoautotrophicum</i> (13) <i>Methanobacterium formicium</i> (29)
	Formate dehydrogenase	<i>Hydrogenophaga pseudoflava</i> (15)
	Nitrate reductase	<i>Pseudomonas stutzeri</i> (Frunzke et al. unpublished) <i>Escherichia coli</i> (17)
MAD, MHD	Formylmethanofuran dehydrogenase	<i>Methanobacterium thermoautotrophicum</i> (13)

^a MPT, molybdopterin; MCD, molybdopterin cytosine dinucleotide; MGD, molybdopterin guanine dinucleotide; MAD, molybdopterin adenine dinucleotide; MHD, molybdopterin hypoxanthine dinucleotide

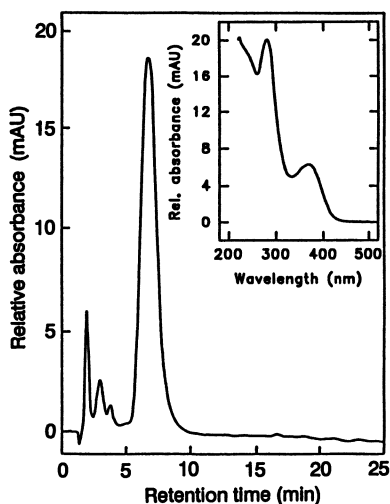


Figure 2. HPLC of the carboxamidomethylated pterin from *Hydrogenophaga pseudoflava* CO dehydrogenase.

Chromatography was isocratic on a C₁₈-reversed phase column in 50 mM ammonium acetate, pH 6.8. Absorbancies were recorded at 270 nm. The absorption spectrum of the compound eluting at 7 min is shown in the inset.

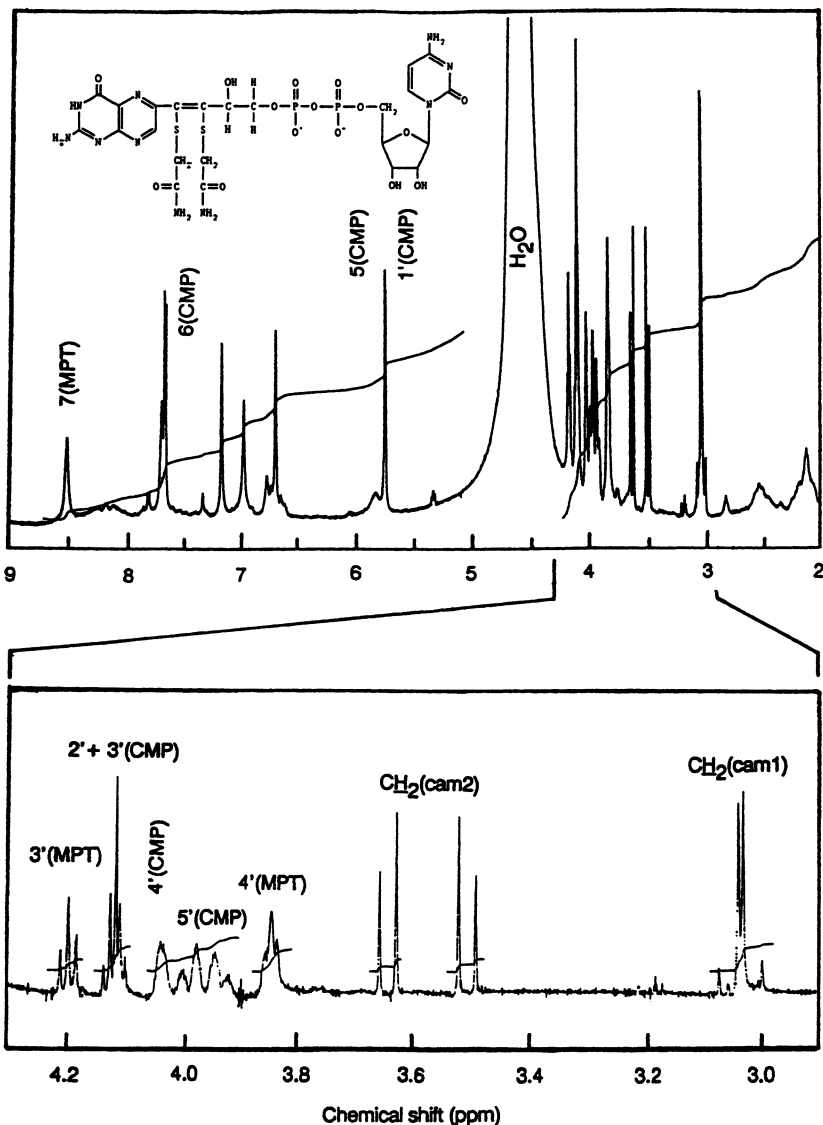


Figure 3. ¹H-NMR spectrum of the carboxamidomethylated pterin from CO dehydrogenase.

¹H-NMR spectra of a 6 mM sample of di(cam)MCD in a mixture of 90 % (vol/vol) H₂O and 10% D₂O (water decoupled) were recorded in a Bruker AM500 instrument at 25°C using pulse Fourier transform mode (256 scans). Chemical shifts are in ppm in relation to tetramethylsilane using water as internal standard.

C₁' of the pterin side chain), respectively. The signals at 7.2 ppm, 7.0 ppm and 6.7 ppm were ascribed to protons bound to nitrogen atoms since they exchanged in D₂O. Integration of the signals was in accord with the above assignments (Figure 3). The assignment of one of the double doublets at 5.75 ppm (C₅H, cytosine moiety) was further substantiated by cross peaks in COSY with the doublet at 7.7 ppm (C₆H, cytosine moiety). There were no signals detectable which could be ascribed to C-bound protons on C₁' and C₂' of the pterin side chain, indicating that there is a double bond between these C-atoms. The absence of any signals referring to a methyl group as well as the signals originating from the carboxamidomethyl groups show that MCD is not methylated at the sulfur atoms attached to the C₁' or C₂' atoms.

To test further the validity of the proposed structure, di(cam)MCD was subjected to ¹³C-NMR spectroscopy (Figure 4). The spectrum revealed signals that could be assigned to the methylene-C-atoms of the carboxamidomethyl groups (resonances at 36.5 and 38.9 ppm), to the C-atoms of the ribose moiety and to the C-atoms C₃' and C₄' of the pterin side chain. The resonances at 135.4 and 145.9 ppm are preliminarily assigned to the C₁' and the C₂' atoms of the molybdopterin side chain. This strongly suggests sp²-hybridization of these C-atoms.

Specificities of Molybdopterin Dinucleotides for their Target Proteins

As listed in the introduction, molybdopterin dinucleotides, the organic components of bacterial molybdenum cofactors, are specific for their target proteins with the exception of MGD, MAD, and MHD in *Methanobacterium thermoautotrophicum* formylmethanofuran dehydrogenase (13). All CO dehydrogenases studied so far harbored MCD (7, 14-16). Respiratory nitrate reductase in *E. coli* was reported to be a MGD-containing molybdoenzyme (17). For that reason we were interested in the specificity of molybdopterin dinucleotides for their target proteins. We found, that under denitrifying conditions and in the presence of CO *Hydrogenophaga pseudoflava* synthesizes respiratory nitrate reductase and CO dehydrogenase simultaneously (15). The contents of molybdenum, molybdopterin dinucleotides, and FAD of both enzymes are given in Table II. The data show that MGD is used in *H. pseudoflava* nitrate reductase exclusively, whereas MCD is specific for CO dehydrogenase of the bacterium (Hoffmüller, unpublished results). CO dehydrogenases from *Pseudomonas carboxydovorans*, *Pseudomonas carboxydohydrogena*, and *Streptomyces thermoautotrophicus* were demonstrated earlier to harbor MCD exclusively (see references in Table I). On the other hand there was low specificity for the utilization of dinucleotides in formylmethanofuran dehydrogenase from *M. thermoautotrophicum* (13). The enzyme contained MGD, MAD, and MHD at a molar ratio of 1 : 0.4 : 0.1. The reason for the significantly different specificities in the usage of dinucleotides in bacterial molybdenum cofactors is not yet known.

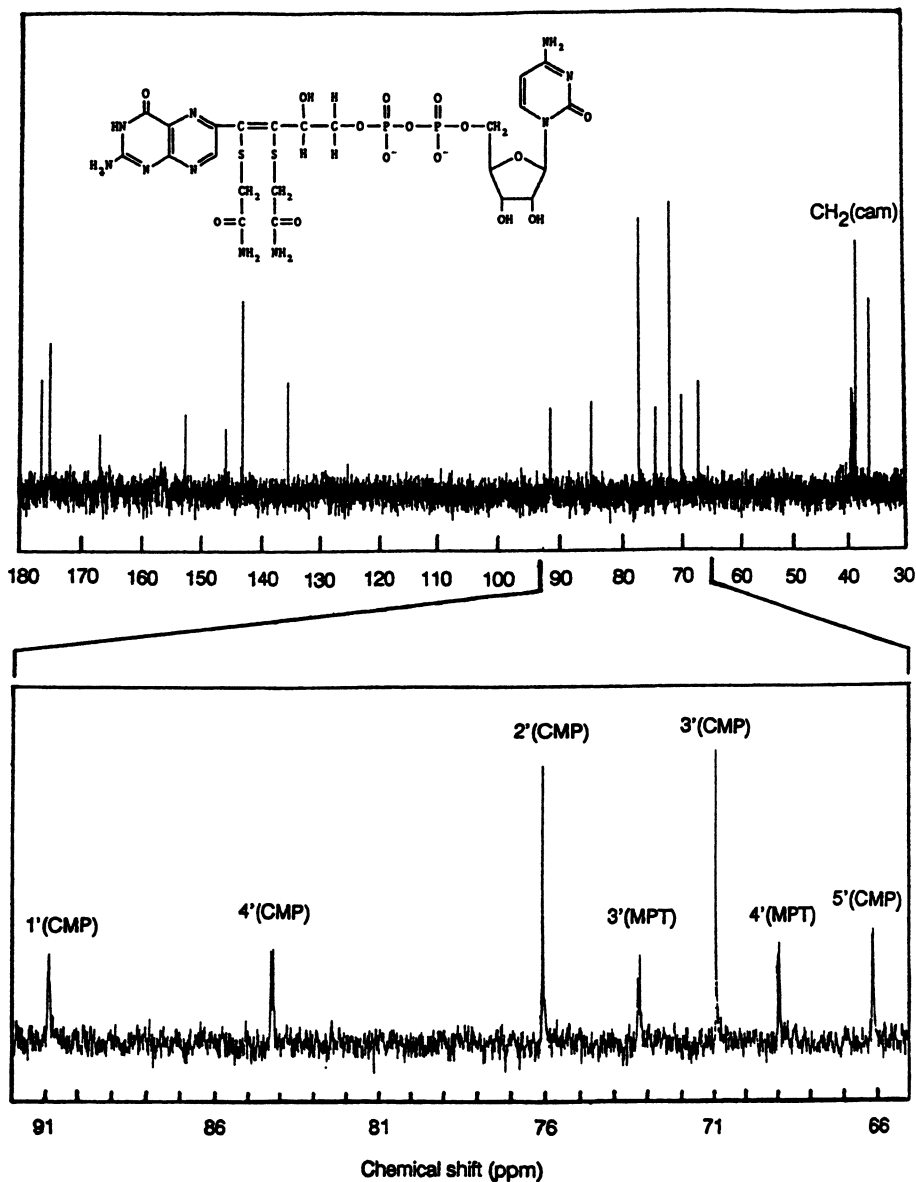


Figure 4. ^{13}C -NMR spectrum of the carboxamidomethylated pterin from CO dehydrogenase.

^{13}C -NMR spectroscopy (123,867 scans) was on the pterin sample specified in the legend to Figure 3.

Identification of Urothione as an Excretion Product of *Hydrogenophaga pseudoflava*

Urothione [2-amino-7-(1,2-dihydroxyethyl)-6-(methylthio)thieno[3,2-g]pteridine-4(3H)-one] is a stable nonfluorescing pterin containing the thiophene ring (compound I in Figure 5). It has been isolated from human urine (18-21) and is considered a degradation product of molybdopterin released from the molybdenum cofactor upon the turnover of hepatic xanthine dehydrogenase and sulfite oxidase (20, 21). Other sources of urothione have not been reported.

The starting observation of our work was, that fermentation media of CO-grown carboxidotrophic bacteria exhibited a bright blue fluorescence when exposed to uv-irradiation at 360 nm. Indeed, analyses for pterins revealed compounds which exhibited pterin-like uv-vis spectra (22). In 0.1 M NaOH one of these (compound U) showed absorption maxima at 272 and 398 nm. Compound U was isolated from 15 l of cell-free fermentation medium of *Hydrogenophaga pseudoflava*, rotoevaporated to dryness, extracted into methanol, rotoevaporated again, redissolved in distilled water and gel filtered on Sephadex G-10. The 1.4 mg of crude compound U obtained were purified by C₁₈-reversed phase HPLC employing 10 % (vol/vol) acetonitrile in water as mobile phase. The procedure yielded 1.1 mg of pure compound U.

Compound U was identified as urothione on the basis of the following considerations (23, 24). It has been reported that the uv-vis spectrum of urothione shows a characteristic dependence on the pH (19, 20). The same pH dependence occurred with compound U (Figure 6). We have, therefore, isolated urothione from human urine and found that it coeluted with compound U on HPLC. Cochromatography was also obtained after acetylation of both compounds with acetic anhydride, yielding the triacetyl derivatives (compound VI in Figure 5). Oxidation of compound U with alkaline potassium permanganate revealed a pterin which was identified as pterin-6-carboxylic-7-sulfonic acid on the basis of its fluorescence excitation and emission spectra and the same mobility on silica gel thin layer plates as pterin-6-carboxylic-7-sulfonic acid produced from urothione. The molecular mass of compound U as obtained from electron impact mass spectra of the acetylated derivative was 451, a value identical to that of triacetyl urothione (19). In addition, the fragmentation pattern was similar to that reported in the literature (19). Urothione contains three different types of carbon bound hydrogen atoms, a thiomethyl group, a CHOH group and a CH₂OH group (Figure 5). ¹H-NMR of compound U revealed signals at 6.97, 6.24, 5.28, 5.05, 3.57, and 2.55 ppm (Figure 7) which could be ascribed to C₇NH₂, C_{2a}OH, C_{2a}H, C_{2b}OH, C_{2b}H₂, and SCH₃, respectively. When water was partly decoupled all signals were reduced except those at 5.28, 3.57, and 2.55 ppm (Figure 7) indicating that the corresponding protons are water exchangeable and bound to heteroatoms. Integration of the multiplets at 5.28 and 3.57 ppm and the singlet at 2.55 ppm revealed a proton ratio of 1 : 2 : 3, referring to C_{2a}H, C_{2b}H₂ and SCH₃, respectively. In

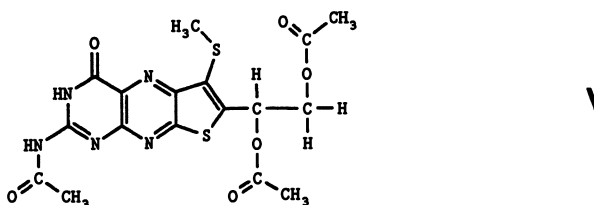
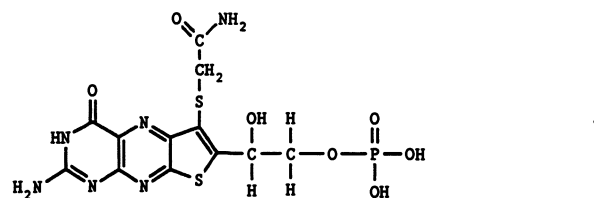
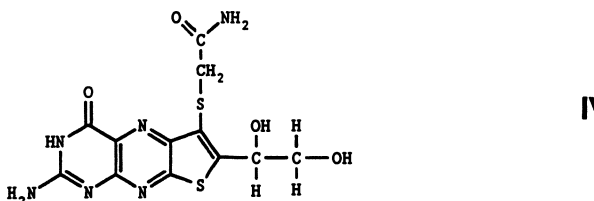
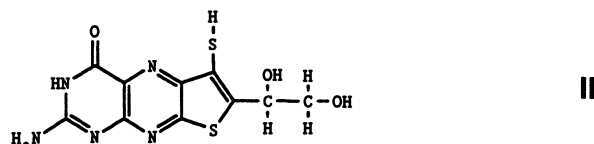
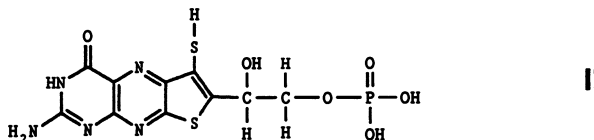
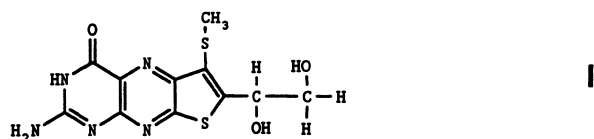


Figure 5. Chemical structures of *Hydrogenophaga pseudoflava* compound U (urothione) and derivatives thereof.

Urothione (I), phospho norurothione (II), norurothione (III), carboxamidomethyl norurothione (IV), phospho carboxamidomethyl norurothione (V) and triacetyl urothione (VI).

Table II. Quantitation of molybdenum, molybdopterin dinucleotides and FAD in *Hydrogenophaga pseudoflava* CO dehydrogenase and nitrate reductase

Method	CO dehydrogenase ^a				Nitrate reductase ^{a, b}		
	Mo	MCD	MGD	FAD	Mo	MCD	MGD
ICP-MS based on ⁹² Mo ^c	1.40				0.84		
Acid treatment of molybdoenzymes ^d		1.52	0	1.58		0	0.96
Carboxamidomethylation and extraction ^e		1.50	0	1.62		0	0.93

^a Bacteria were grown under denitrifying conditions in the presence of CO. Enzyme purification followed published procedures. Amounts of Mo and of dinucleotides are given as mol per mol of enzyme.

^b Hoffmüller *et al.* (unpublished results)

^c Induced coupled plasma mass spectroscopy

^d Enzyme samples were incubated in 3 % (vol/vol) aqueous sulfuric acid for 10 min at 95 °C.

^e For carboxamidomethylation of molybdopterin dinucleotides and extraction of (cam)derivatives refer to the text.

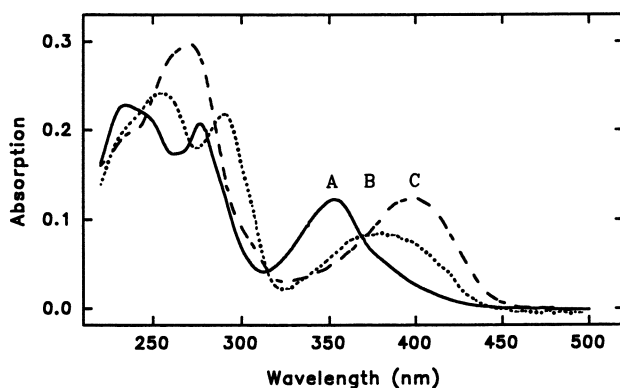


Figure 6. Absorption spectra of compound U under alkaline, neutral, and acidic conditions.

Absorption spectra of 3.7 μg compound U from *Hydrogenophaga pseudoflava* in 0.1 M HCl (A), 50 mM potassium phosphate buffer, pH 7.0 (B) or in 0.1 M NaOH (C) were recorded against solvents.

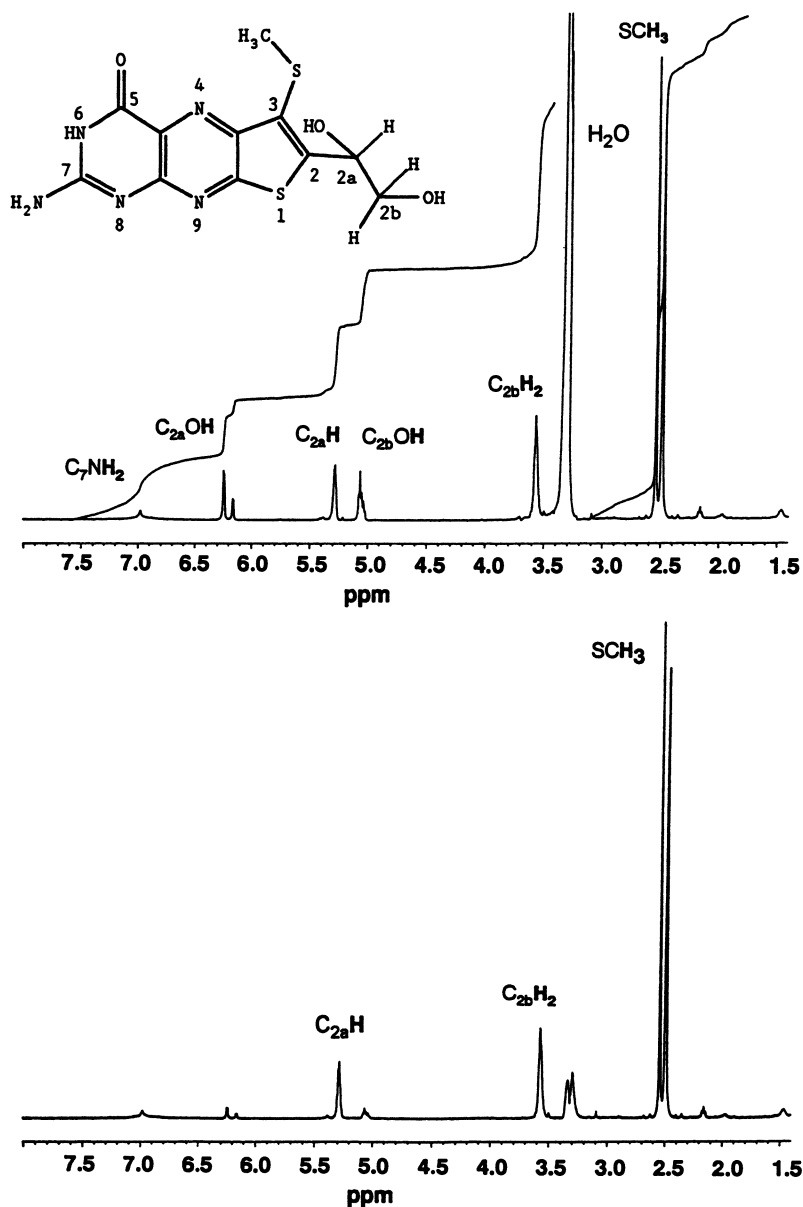


Figure 7. $^1\text{H-NMR}$ spectra of compound U.

$^1\text{H-NMR}$ spectra were recorded in $\text{dimethyl-}d_6\text{-sulfoxide}$ at 25°C in a 500 MHz NMR-spectrometer (model AM500, Bruker, Karlsruhe) using pulse Fourier transform mode (160 scans). Chemical shifts are in ppm in relation to tetramethylsilane using residual protons in $\text{dimethyl-}d_6\text{-sulfoxide}$ as internal standard. The water decoupled spectrum is shown below the $\text{dimethyl-}d_6\text{-sulfoxide}$ spectrum.

accordance with these interpretations were cross peaks in COSY of $C_{2a}H$ with $C_{2a}OH$ and $C_{2b}H_2$ and of $C_{2b}H_2$ with $C_{2b}OH$ and $C_{2a}H$.

Metabolic Relationship between the CO Dehydrogenase Molybdenum Cofactor and Urothione

Excretion of urothione by *Hydrogenophaga pseudoflava* showed a dependence on the growth phase (Figure 8). The onset of urothione production was in the mid-exponential growth phase. Urothione production reached its maximum during post-exponential growth (34 μg urothione per g of dry biomass). The coincidence of inactivation of CO dehydrogenase and excretion of urothione in the post-exponential growth phase points to a possible metabolic relationship between the CO dehydrogenase molybdenum cofactor and urothione. This was further substantiated by the finding that the excretion of urothione always coincided with conditions of CO dehydrogenase expression. Urothione excretion also occurred with other molybdoenzyme-containing bacteria (*Pseudomonas carboxydovorans*, *Streptomyces thermoautotrophicus*, *Escherichia coli*).

The degradation of the CO dehydrogenase molybdenum cofactor leads to urothione (Figure 9). The proposed pathway (Figure 10) involves the activities of nucleotide pyrophosphatase, phosphatase, and methyl transferase. The activities of nucleotide pyrophosphatase [6.7 nmol of di(cam)MCD cleaved ($\text{h} \times \text{mg protein}^{-1}$)] and alkaline phosphatase [250 nmol of p-nitrophenole formed from p-nitrophenylphosphate ($\text{h} \times \text{mg protein}^{-1}$)] have been identified in *H. pseudoflava*; so far we have not tested for methyl transferase activity. The procedure for the conversion of Moco to urothione detailed in Figure 10 was carried out under conditions of oxygen exclusion and in the presence of 0.7 mM dithionite and led to the formation of urothione, as was evident from cochromatographic and spectral identification of the product (Figure 9). That phospho norurothione (compound II in Figure 5) and norurothione (compound III in Figure 5) actually appeared as intermediates in the degradation of the molybdenum cofactor (Figure 10) is further substantiated by the finding that carboxamidomethyl norurothione (compound IV in Figure 5) was obtained from unfolded CO dehydrogenase treated with nucleotide pyrophosphatase, alkaline phosphatase and iodoacetamide. Phospho carboxamidomethyl norurothione (compound V in Figure 5) was obtained when alkaline phosphatase was omitted in the above procedure. It could be converted to carboxamidomethyl norurothione by alkaline phosphatase.

The results are in accord with the hypothesis that urothione excreted by *H. pseudoflava* originates from the CO dehydrogenase molybdenum cofactor.

Conclusions

The molybdenum cofactor (Moco) of the eu- and archaebacterial molybdoenzymes examined in that respect contains molybdopterin dinucleotides

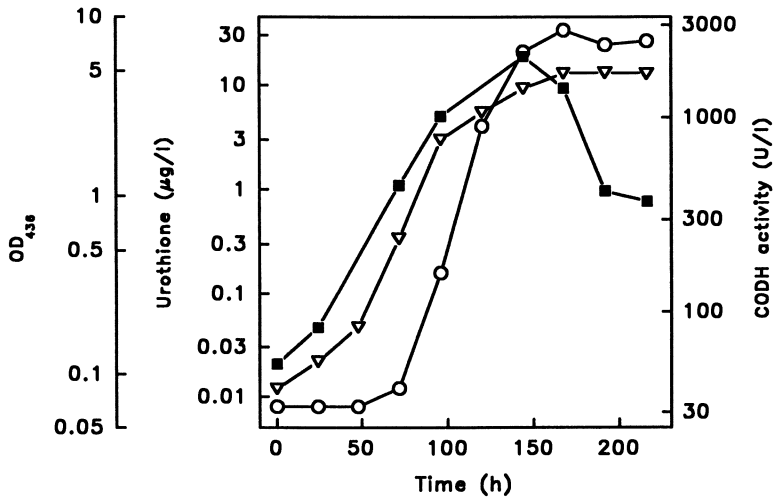


Figure 8. Excretion of urothione by growing cells of *Hydrogenophaga pseudoflava*.

H. pseudoflava was grown aerobically with CO as a substrate in 50-l culture volume. Growth was followed by OD₄₃₆ measurements (▽). CO dehydrogenase activities in cell extracts (■) were measured spectrophotometrically with idonitrotetrazolium chloride (INT) and 1-methoxyphenazinemethosulfate (MPMS) as electron acceptors (30). Urothione (○) was quantitated by HPLC in cell-free supernatants following published procedures (23).

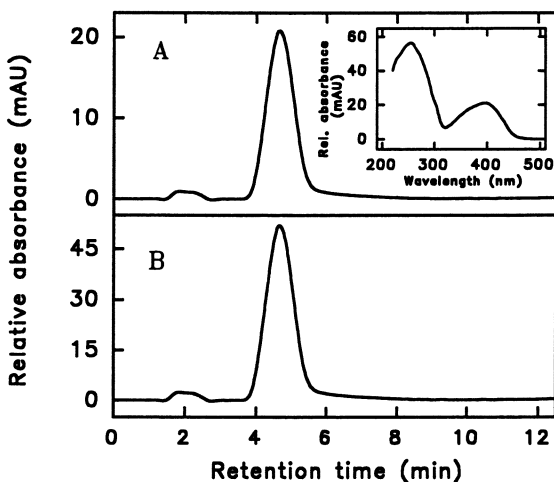


Figure 9. Identification of the *in vitro* conversion product of Moco.

Panel A: 2.1 μg of the final *in vitro* conversion product of the CO dehydrogenase Moco in 200 μl of 10 % (vol/vol) acetonitrile in 20 mM potassium phosphate buffer, pH 9.0, was subjected to C_{18} -reversed phase HPLC using the solvent as mobile phase. Panel B: A mixture of urothione (2.4 μg) and the above conversion product of Moco (2.1 μg) has been analyzed by HPLC as above. Relative absorbancies were recorded at 398 nm. The absorption spectrum of the compound eluting at 4.7 min is shown in the inset.

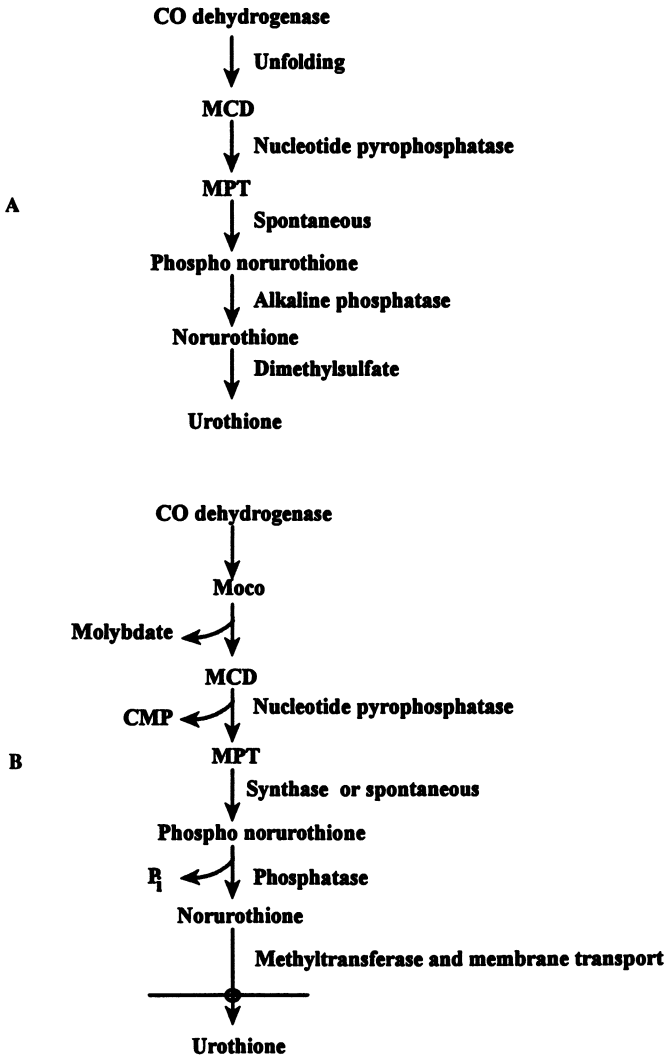


Figure 10. Formation of urothione from Moco *in vitro* (A) and proposed physiological pathway (B).

except with two eubacterial xanthine dehydrogenases (25, 26). It seems that molybdoenzymes from eukaryotic sources specifically contain molybdopterin (MPT) since MPT dinucleotides have not been resolved in any higher organism molybdoenzyme. MPT dinucleotides resolved so far are molybdopterin guanine dinucleotide (MGD), molybdopterin cytosine dinucleotide (MCD), molybdopterin adenine dinucleotide (MAD), and molybdopterin hypoxanthine dinucleotide (MHD). Among these, MCD is the only pyrimidine dinucleotide. Under appropriate conditions the molybdenum enzymes CO dehydrogenase and nitrate reductase are coexpressed in *Hydrogenophaga pseudoflava* and specifically contain MCD or MGD, respectively (15). On the other hand, usage of MPT dinucleotides in formylmethanofuran dehydrogenase of *Methanobacterium thermoautotrophicum* revealed a broad specificity, since the enzyme was found to contain MGD, MAD, and MHD simultaneously (13).

In this paper we have been able to prepare the *H. pseudoflava* CO dehydrogenase pterin in amounts sufficient for structural analysis and describe the first ^1H - and ^{13}C -NMR spectra of a carboxamidomethylated MPT dinucleotide. The data obtained fully support the chemical structure of a di(cam)molybdopterin cytosine dinucleotide [di(cam)MCD] as has been proposed before (2, 5, 7). It is, therefore, concluded that *H. pseudoflava* CO dehydrogenase contains MCD (Figure 1) in its Moco. The ^1H -NMR spectrum exhibited all signals predicted by the chemical structure of di(cam)MCD, and other signals were not apparent (Figure 3). The absence of protons at C_1 and C_2 of the pterin side chain is consistent with a C_1 - C_2 double bond. ^1H -NMR also proves the attachment of two distinct carboxamidomethyl groups to the pterin side chain and the absence of any methyl groups (Figure 3). The presence of a single proton at C_7 of the pterin ring refers to a fully oxidized state of the isolated compound. It does, however, not allow definite conclusions on the oxidation state of MCD in the native Moco.

Compound U is an excretion product of *H. pseudoflava*. It was isolated from fermentation media with good yield and purity and identified as urothione on the basis of its uv-vis spectral properties, electron impact mass spectroscopy, ^1H -NMR spectroscopy and cochromatography with authentic urothione on HPLC. Urothione was also traced in cultures of several other CO-oxidizing bacteria or of *Escherichia coli*. Human urine is another natural source of urothione.

The following findings suggest a metabolic relationship between urothione and the Moco from *H. pseudoflava* CO dehydrogenase. Urothione was only excreted under conditions where CO dehydrogenase was expressed (23). There was a coincidence of inactivation of CO dehydrogenase and the excretion of urothione. It was, therefore, tempting to assume that urothione is a degradation product of Moco. This assumption was further substantiated by the finding that the CO dehydrogenase Moco could be converted to urothione *in vitro*. The data currently available have been summarized in a hypothetical pathway (Figure 10). The *in vivo* conversion of Moco to urothione involves release of Moco from CO

dehydrogenase, its dissociation into molybdate and MCD, and conversion of MCD to urothione via MPT, phospho norurothione and norurothione (Figure 10).

Compound Z is a stable oxidized form of a MPT precursor in *E. coli chlM* and *chlN*, obtained by iodine oxidation (27). Recent results showed (M. Volk, unpublished) that besides urothione compound Z is another excretion product of *H. pseudoflava* growing with CO and significantly contributes to the blue fluorescence of bacterial cultures.

Acknowledgments

We are grateful to Dieter Willbold for significant help with NMR-spectroscopy and the interpretation of structural data. The research in our laboratory was financially supported by the Fonds der chemischen Industrie (Frankfurt) and stipends to M.V. and J.T. from the Deutsche Forschungsgemeinschaft (Bonn) and the State of Bavaria (Munich), respectively.

Literature cited

- (1) Meyer, O.; Rajagopalan, K.V. *J. Bacteriol.* **1984**, *157*, 643-648.
- (2) Krüger, B.; Meyer, O. *Eur. J. Biochem.* **1986**, *157*, 121-128.
- (3) Krüger, B. *Bactopterin, der universelle Kofaktor bakterieller Molybdoenzyme*; PhD Thesis; Universität Göttingen: Göttingen, Germany, 1986; pp 1-216.
- (4) Meyer, O.; Jacobitz, S.; Krüger, B. *FEMS Microbiol. Rev.* **1986**, *39*, 161-179.
- (5) Krüger, B.; Meyer, O. *Biochim. Biophys. Acta* **1987**, *912*, 357-364.
- (6) Krüger, B.; Meyer, O.; Nagel, M.; Andreesen, J.R.; Meincke, M.; Bock, E.; Blümle, S.; Zumft, W.G. *FEMS Microbiol. Lett.* **1987**, *48*, 225-227.
- (7) Johnson, J.L.; Rajagopalan, K.V.; Meyer, O. *Arch. Biochem. Biophys.* **1990**, *283*, 542-545.
- (8) Johnson, J.L.; Bastian, N.R.; Rajagopalan, K.V. *Proc. Natl. Acad. Sci. USA*, **1990**, *87*, 1390-1394.
- (9) Meyer, O. *J. Biol. Chem.* **1982**, *257*, 1333-1341.
- (10) Pfeleiderer, W. In *Folates and Pterins*; Blakeley, R.L.; Benkovic, S.J. Eds; John Wiley & sons: New York, USA, **1985**, Vol. 2; pp 43-114.
- (11) Kramer, S.P.; Johnson, J.L.; Ribeiro, A.A.; Millington; D.S.; Rajagopalan, K.V. *J. Biol. Chem.* **1987**, *262*, 16357-16363.
- (12) Johnson, J.L.; Hainline, B.E.; Rajagopalan, K.V.; Arison, B.H. *J. Biol. Chem.* **1984**, *259*, 5414-5422
- (13) Börner, G.; Karrasch, M.; Thauer, R.K. *FEBS Lett.* **1991**, *290*, 10158-10161.
- (14) Frunzke, K.; Meyer, O. *Bioforum*, **1991**, *14*, 83.
- (15) Hoffmüller, P.; Frunzke, K.; Meyer, O. *Bioforum*, **1991**, *14*, 47.

- (16) Willbold, D. *Isolierung und Charakterisierung von Kohlenmonoxid-Dehydrogenase aus dem thermophilen obligat chemolithoautotrophen Bakterium Streptomyces thermoautotrophicus*; Diploma thesis; Universität Bayreuth: Bayreuth, Germany, 1991.
- (17) Johnson, J.L.; Indermaur, L.W.; Rajagopalan, K.V. *J. Biol. Chem.*, **1991**, *266*, 12140-12145.
- (18) Koshara, W. *Hoppe Seiler Z. physiol. Chem.* **1940**, *263*, 78-79.
- (19) Goto, M.; Sakurai, A.; Ohta, K.; Yamakami, H. *J. Biochem.*, **1969**, *65*, 611-620.
- (20) Johnson, J.L.; Rajagopalan, K.V. *Proc. Natl. Acad. Sci. USA*, **1982**, *79*, 6856-6860.
- (21) Bamforth, J.F.; Johnson, J.L.; Davidson, G.F.; Wong, L.T.K.; Locktich, G.; Applegarth, D.A. *Clinic. Biochem.* **1990**, *23*, 537-542.
- (22) Volk, M. *Identifizierung und Charakterisierung von Exkretionsprodukten carboxidotropher Bakterien*; Diploma thesis; Universität Bayreuth: Bayreuth, Germany 1991.
- (23) Volk, M.; Frunzke, K.; Meyer, O. *Biol. Chem. Hoppe-Seyler* **1992**, *377*, 971-972.
- (24) Volk, M.; Frunzke, K.; Meyer, O. *Bio Engineering*, **1992**, *8* (supplement), 43.
- (25) Johnson, J.L.; Chaudhury, M.; Rajagopalan, K.V. *Biofactors*, **1991**, *3*, 103-107.
- (26) Hettrich, D.; Peschke, B.; Tshisuaka, B.; Lingens, F. *Biol. Chem. Hoppe-Seyler*, **1991**, *372*, 513-517.
- (27) Johnson, J.L.; Wuebbbers, M.M.; Rajagopalan, K.V. *J. Biol. Chem.* **1989**, *264*, 13440-13447
- (28) Karrasch, M.; Börner, G.; Thauer, R.K. *FEBS Lett.* **1990**, *274*, 48-52.
- (29) Johnson, J.L.; Bastian, N.R.; Schauer, N.L.; Ferry, J.G.; Rajagopalan, K.V. *FEMS Microbiol. Lett.* **1991**, *77*, 213-216.
- (30) Kraut, M.; Hugendieck, I.; Herwig, S.; Meyer, O. *Arch. Microbiol.* **1989**, *152*, 335-341.

RECEIVED April 30, 1993

Chapter 5

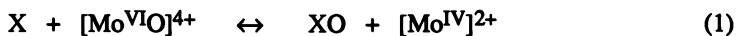
Models of Pterin-Containing Molybdenum Enzymes

Charles G. Young and Anthony G. Wedd

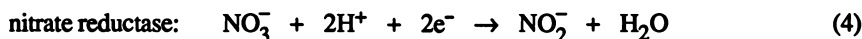
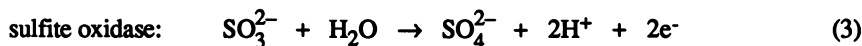
School of Chemistry, University of Melbourne, Parkville, Victoria 3052,
Australia

The pterin-containing molybdenum enzymes promote elegant and important biochemical transformations involving formal transfer of an oxygen atom. The understanding of these processes has been enhanced recently by a synergy between studies of the enzymes and synthetic models. This contribution surveys seminal discoveries from both areas. It focuses on recent models which span the biologically relevant oxidation states, accurately mimic enzyme EPR or EXAFS spectra and exhibit enzyme-like reactivity. New mechanistic insights derived from these models are presented and the reasons for Nature's exploitation of molybdenum are considered.

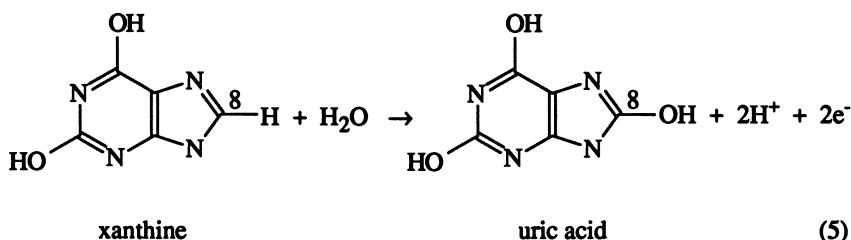
The pterin-containing molybdenum enzymes are typically complex systems featuring multiple redox centers (1-7). They are "molecular electrochemical cells": the two "electrode" sites promoting the individual half-reactions comprising the full catalytic process are connected by an internal electron transfer chain or "circuitry." The molybdenum centers are the primary catalytic sites. They promote two-electron redox reactions involving the net exchange of an oxygen atom between substrate and water. The redox processes at molybdenum and the substrate half-reactions may be represented by equations 1 and 2, respectively (where X = substrate or product).



Specific half-reactions for three of the more highly characterized enzymes are given in equations 3 to 5.



xanthine oxidase:



This Chapter outlines, in historical context, the vital synergy between enzyme and model studies and the role it has played in reaching the contemporary understanding of the molybdenum active sites of these enzymes.

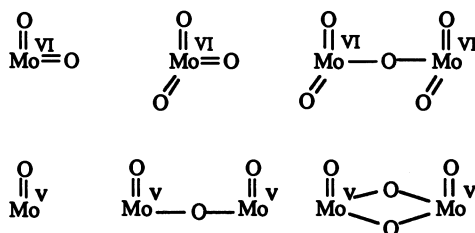
The Molybdenum Active Sites

Early Insights. Molybdenum was detected in xanthine oxidase in 1953 (8-10), nearly fifty years after the enzyme was formally named (11). It was suggested to be present in an assimilatory nitrate reductase at about the same time (12) and was detected in sulfite oxidase in 1971 (13). A full listing of the known and suspected molybdenum enzymes has been presented in this volume (6).

Xanthine oxidase was one of the first enzymes examined by electron paramagnetic resonance (EPR) spectroscopy (14) and the characteristic spectral pattern arising from hyperfine coupling to the naturally-occurring magnetic molybdenum nuclei, ^{95}Mo and ^{97}Mo ($I = 5/2$, 25%), became a signature for the presence of molybdenum in enzymes (15). The Mo^{V} level is but one of three high-valent states employed during enzyme turnover (1-7); fully oxidized and reduced forms of the enzymes contain Mo^{VI} and Mo^{IV} , respectively.

The first significant modeling experiment came in 1966 with the production of EPR signals characteristic of Mo^{V} upon reaction of $\text{Mo}^{\text{VI}}\text{O}_4^{2-}$ and glycolic acids $\text{HECH}_2\text{CO}_2\text{H}$ ($\text{E} = \text{O}, \text{S}$) (16). Average g and $a(^{95,97}\text{Mo})$ parameters for the sulfur system were, respectively, larger and smaller than those for the oxygen equivalent and strikingly similar to those of the so-called Very Rapid and Rapid signals of xanthine oxidase (16). The importance of ligand sulfur in the molybdenum enzymes was clearly indicated.

The high-valent coordination chemistry of the day was dominated by complexes of the mononuclear and binuclear centers shown below (17):



Work in subsequent years concentrated on binding sulfur co-ligands to such centers. Attempts to substitute thio ligands for oxo ligands were successful for both terminal and bridging sites of binuclear Mo^{V} complexes but unsuccessful in mononuclear systems (17). The study of binuclear species was justified at the time by the presence of two molybdenum atoms per molecule in the known enzymes.

Structural and Spectroscopic Probes. X-ray crystal structures to complement the recent progress in nitrogenase (18) do not exist for any of the pterin-containing enzymes. However, X-ray absorption (particularly fine structure analysis, i.e. EXAFS) and EPR studies of a variety of enzymes under a wide range of conditions have provided significant insights into the structures of the active sites. The X-ray absorption work showed that the two molybdenum atoms do not approach closely (4,5,19). Partial coordination spheres for the Mo^{VI} and Mo^{IV} centers of a number of systems were determined; those for sulfite oxidase (20,21) and xanthine oxidase/dehydrogenase (22-24) are given in Scheme I. The inactive desulfo forms of xanthine oxidase/dehydrogenase are formed upon hydrolysis or cyanolysis. Calibration with appropriate model complexes aided the assignment of these structures. The source of the thiolate ligands SR^- may be cysteinyl sidechains or molybdopterin (*vide infra*). Only one oxo ligand is detected in the Mo^{V} forms of the enzymes. An SH^- ligand formed by protonation of the original thio group appears to be present in the reduced forms of xanthine oxidase. In Scheme I, OR^- is the bound product anion derived from the substrate RH, e.g. xanthine as in equation 5.

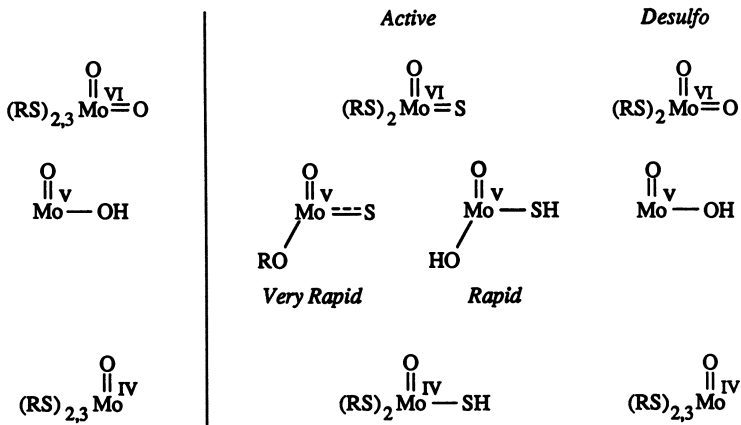
Complementary information for the Mo^{V} forms is available via hyperfine coupling observed in EPR-active enzyme samples (4,25-31) and model complexes of the ligands $\text{L-N}_2\text{S}_2$ and L-N_3 (Scheme II) (30-34). These sterically encumbering ligands, which limit dinucleation and enforce *cis* or *fac* stereochemistry on their co-ligands, permit the synthesis of $[\text{Mo}^{\text{V}}\text{O}_2]^+$, $[\text{Mo}^{\text{V}}\text{O}(\text{OH})]^{2+}$, $[\text{Mo}^{\text{V}}\text{OS}]^+$ and $[\text{Mo}^{\text{V}}\text{O}(\text{SH})]^{2+}$ complexes. The Mo^{V} structures displayed in Scheme I follow from detailed comparisons of the spectra of enzymes and these well defined models. The Very Rapid EPR signal ($t_{1/2} \approx 10$ ms) of xanthine oxidase appears under substrate limiting conditions and is accompanied by the Rapid signal ($t_{1/2} \approx 25$ ms) when excess xanthine is present.

The Molybdenum Cofactor. The pioneering work of Nason and coworkers (35) in 1970 provided the first evidence for a molybdenum cofactor (Mo-co) which is common to the pterin-containing molybdoenzymes (hence their name). A decade later, on the basis of degradation and spectroscopic studies, Mo-co was proposed (36,37) to comprise a 6-substituted pterin (molybdopterin) coordinated to molybdenum through a 1,2-dithiolene moiety on a four carbon C(6)-sidechain: known dithiolene-Mo chemistry strongly influenced the proposal of structure I for Mo-co. Dinucleotide derivatives of Mo-co have now been isolated from bacterial sources (38). The thiolate ligands discerned by EXAFS studies (Scheme I) may well be supplied by the Mo-co fragment. Timely reviews of the genetics and biochemistry of Mo-co have appeared (38,39). Synthetic approaches to Mo-co have now combined difficult pterin chemistry and established strategies for the generation of metal bound dithiolenes; the synthesis (40) of complexes such as $\text{Cp}_2\text{Mo}(\text{dithiolene})$, where the dithiolene contains pterin or quinoxaline substituents, augurs well for the eventual synthesis of models with biologically relevant co-ligands and supports the speculated binding of molybdenum to a pterin-dithiolene moiety. The modeling of Mo-co and progress towards its total synthesis are the subjects of other contributions to this volume (41).

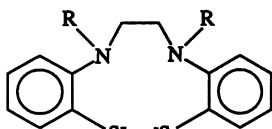
Further Insights from Model Chemistry. Further insights into enzyme behavior may be gleaned from the wealth of accumulated molybdenum chemistry (17,42,43). Firstly, molybdenum possesses great structural facility, especially in its $d^0 \text{Mo}^{\text{VI}}$ and $d^1 \text{Mo}^{\text{V}}$ complexes. A wide range of coordination numbers, geometries and structural and kinetic labilities characterize these complexes. Moreover, subtle structural changes may radically alter the redox potential of molybdenum complexes. Recently, Enemark *et al.* (44) demonstrated that altering the size of a single chelate

Sulfite oxidase

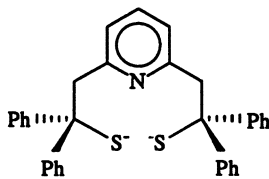
Xanthine oxidase/dehydrogenase



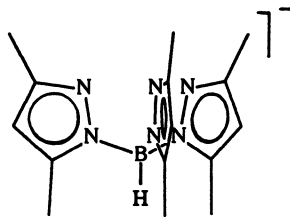
Scheme I



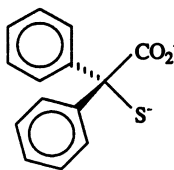
R = Me, L-N₂S₂
R = H, L-H₂



L-NS₂



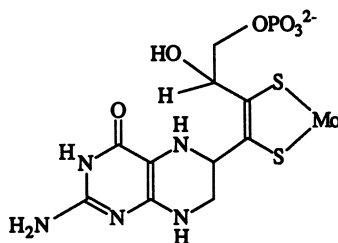
L-N₃



L-SO

Scheme II

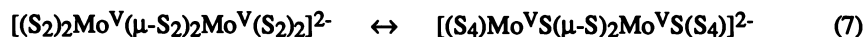
(I)



ring in Mo^V complexes produces striking redox changes. No doubt the nature of the donor atoms is an important determinant of the redox potential of the enzyme centers, but more subtle factors may also be of great significance.

Molybdenum-Sulfur Chemistry. An understanding of Mo-S chemistry is of great importance in the context of enzyme behavior, especially as Mo=S, Mo-SH, Mo-SR and/or Mo-dithiolene links appear to be important (Scheme I, and I). In particular, a [Mo^{VI}OS]²⁺ center has been established in the resting oxidized states of the hydroxylases (xanthine oxidase/dehydrogenase, aldehyde oxidase). The close energy matching of molybdenum 4*d* and sulfur 3*p* orbitals facilitates the redox interplay of these elements, especially when high valent molybdenum encounters the reducing thio (S²⁻) ligand. Bridging via sulfur is also a problem which besets the attempted modeling of mononuclear enzyme sites.

The redox non-innocence of sulfur is highlighted by induced internal electron transfer chemistry, where redox changes involving S_x²⁻ ligands are responsible for the seemingly paradoxical reduction of molybdenum by oxidizing agents (e.g., equation 6 (45)), and is reinforced by elegant studies of the facile and complex sulfur-based chemistry of Mo-S_x complexes (e.g., equation 7 (46)).



Not surprisingly then, [MoOS]²⁺ complexes are extremely rare and their synthesis has challenged researchers for over twenty years. Recently, the [MoOS]²⁺ complex (L-N₃)MoOS(S₂PPR₂) (Figure 1(a)) was synthesized and structurally characterized (47); although the [MoOS]²⁺ center is stabilized by an intramolecular sulfur-sulfur interaction, the Mo=S bond appears to be only slightly perturbed and the Mo-S(1) distance of 2.227 (2) Å falls within the range of Mo=S distances observed by EXAFS studies of the hydroxylases (2.15 - 2.25 Å (19,22-24)). The complex also provides a rare model for the cyanolysis of xanthine oxidase, being converted to (L-N₃)MoO₂(η¹-S₂PPR₂) upon reaction with CN⁻ in the presence of water and oxygen (c.f. desulfo enzyme centers in Scheme I).

Stabilization of enzymatic [MoOS]²⁺ centers through an active site interaction, possibly with cysteinyl sulfur or molybdopterin, provides an attractive reconciliation of the extreme reactivity of such groups and their presence in Nature. The (L-N₃)MoOS(S₂PPR₂) complex is the first model of such an interaction. Complexes like Cp₂Mo(S₃-Q) [Figure 1(b), S₃-Q = (2-quinoxaline)C(S)=C(S₂)C(O)Me], recently reported by Stiefel and coworkers (40), reflect one type of interaction possible between a [MoOS]²⁺ enzyme center and the dithiolene moiety of molybdopterin. Structural comparisons (Figure 1) support the formulation of (L-N₃)MoOS(S₂PPR₂) and Cp₂Mo(S₃-Q) as oxo-thio-Mo^{VI} and ene-1-perthiolate-2-thiolate-Mo^{IV} species, respectively, but theoretical studies of the bonding in these and related complexes are required to confirm these assignments. In enzymes, the severing of the stabilizing interaction upon reduction or initiation of catalysis would permit the generation of the [Mo^VOS]⁺ and [Mo^VO(SH)]²⁺ centers observed by EPR spectroscopy.

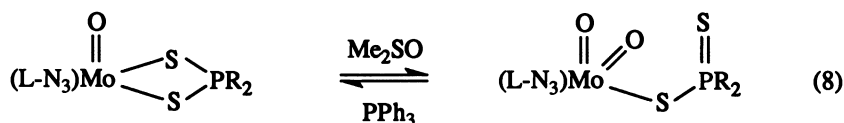
Chemical Models of the Substrate Reactions

Representations of the reactions promoted by the enzymes (equations 1 and 2) allow speculation in terms of oxygen atom transfer (5) and coupled electron-proton transfer (48) mechanisms.

Oxygen Atom Transfer Reactions. The interconversion of dioxo-Mo^{VI} and oxo-Mo^{IV} complexes may be effected by a variety of oxygen atom donors (+[O]) and acceptors (-[O]) (Scheme III); S- and N-oxides are typical oxidants and tertiary phosphines are typical reductants (5). A feature of many synthetic systems is the formation of binuclear [Mo^V₂O₃]⁴⁺ complexes via facile comproportionation of the

Mo^{IV} and Mo^{VI} species (Scheme III); this may be a reversible or irreversible process. In some cases, it has proven difficult to distinguish between the formation of mononuclear Mo^{IV} or binuclear Mo^V complexes, especially when the rapid formation of catalytically competent binuclear complexes occurs (7). Where the comproportionation reaction is reversible, inactive binuclear complexes will furnish Mo^{VI} and Mo^{IV} species which may be capable of catalyzing oxygen atom transfer reactions. This is the case in the classic dithiocarbamate system involving MoO₂(S₂CNR₂)₂, MoO(S₂CNR₂)₂ and Mo₂O₃(S₂CNR₂)₄, first reported by Barral *et al.* (49).

A number of ligand systems (Scheme II) have been designed with a view to preventing the biologically irrelevant comproportionation reaction (5,32,50-52) Complexes such as (L-N₃)MoO₂(η¹-S₂PR₂) and (L-N₃)MoO(η²-S₂PR₂) are capable of catalyzing oxygen atom transfer reactions without detectable dinucleation (50). Importantly, both the Mo^{VI} and Mo^{IV} complexes have been isolated and structurally characterized as mononuclear species; oxygen atom transfer is accompanied by a change in the denticity of the dithio ligand as indicated in equation 8. The reactions



are first order with respect to both complex and substrate, consistent with bimolecular reactions involving mononuclear species. Similar chemistry occurs with related L-N₃ complexes of molybdenum (34,51).

An important and more intensively studied system involves complexes of L-NS₂ (Scheme IV) (5,52). Complexes (L-NS₂)MoO₂ and (L-NS₂)MoO(DMF) (DMF = *N,N*-dimethylformamide) may be interconverted by a wide variety of reagents and both catalyze oxygen atom transfer reactions. While the Mo^{VI} complex has been structurally characterized it has not been possible to establish the mononuclearity of (L-NS₂)MoO(DMF). However, its reactions with oxidants XO, such as NO₃⁻ and *N*- and *S*-oxides, exhibit tight isosbestic points, consistent with the presence of two chromophores only. Substrate saturation kinetics, typical of enzyme systems, are observed for these substrates and kinetics studies have been interpreted in terms of a reversible substrate binding equilibrium (*K*_{eq}) followed by a rate-determining intramolecular oxygen atom transfer (*k*₁; Scheme IV). Interestingly, the reaction rates are independent of substrate. The above studies support the mononuclear nature of the enzyme centers and establish the thermodynamic competency of synthetic molybdenum complexes in oxygen atom transfer reactions (5).

Coupled Electron-Proton Transfer Reactions. An interpretation of enzyme behavior in terms of coupled electron-proton transfer reactions was provided by Stiefel in 1973 (48). π-Bonding in Mo=E (E = O, S) systems permits dramatic modulation of the *pK*_a of the E atom in Mo=E and Mo-EH units (and possibly other atoms in nearby ligands) when redox events occur at the molybdenum center. Thus, formal reduction of the metal center increases the basicity of the Mo=E ligands through the population of π* orbitals with significant ligand character. In xanthine oxidase, [MoOS]²⁺ and [MoO(SH)]⁺ forms only are observed in the Mo^{VI} and Mo^{IV} states, respectively (Scheme I). Both are observable at the Mo^V level and the unpaired electron in the Mo=S π* orbital in the Very Rapid center and in [(L-N₂S₂)Mo^VOS] has a spin density of 0.3 to 0.4 of an electron on the thio ligand. A number of facets of enzyme behavior are neatly accounted for by coupled electron-proton transfer reactions, notably the generation of Mo^V centers, observed proton coupling to these centers and the role of water in the regeneration of the active site.

Recent work involving the L-SO ligand (equation 9 (53)) and the electrochemical interconversion of amino-thiol and amido-thiol complexes (equation 10 (54)) nicely demonstrate the features of coupled electron-proton transfer reactions.

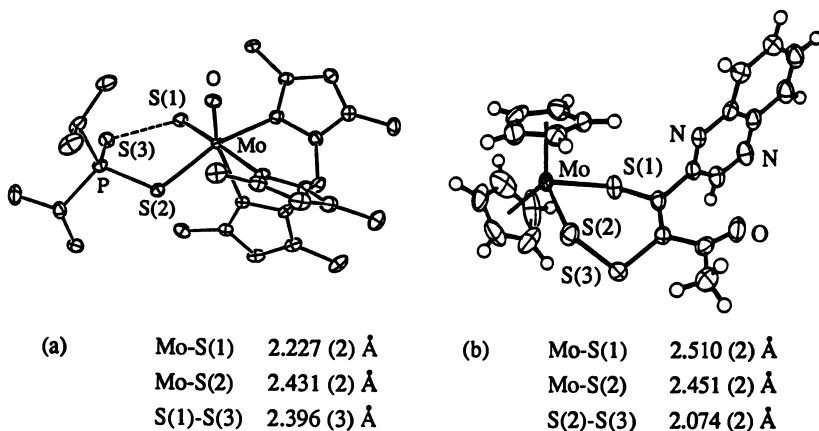
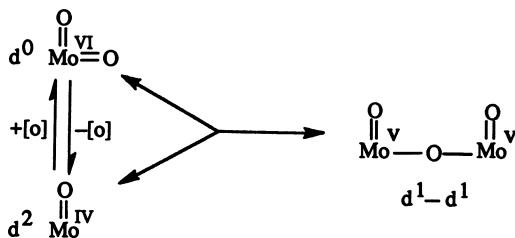
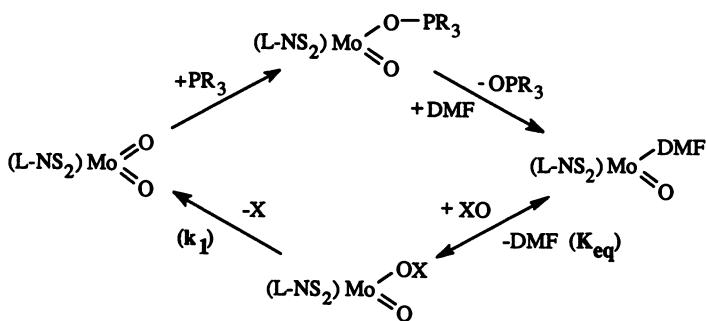


Figure 1. Molecular structures and parameters for (a) $(L-N_3)MoOS(S_2PPri_2)$ (adapted from ref. 47) and (b) $Cp_2Mo(S_3-Q)$ (adapted from ref. 40).



Scheme III



Scheme IV



A Model for Enzymes With $[\text{MoO}_2]^{2+}$ Oxidized Active Sites

In sulfite oxidase and related enzymes, transfer of the oxygen atom from molybdenum to substrate and its replacement from H_2O appear to both occur in the Mo^{VI} to Mo^{IV} transformation. Regeneration of the Mo^{VI} state is achieved by two one-electron oxidations, the first of which generates the transient Mo^{V} states observed by EPR spectroscopy (Scheme V) (5,55-57); these oxidation processes are mediated by the internal electron transfer chain. A number of model catalytic systems have been reported in which O_2 and/or H_2O are key participants but the role of water has not been clarified (49,58-62).

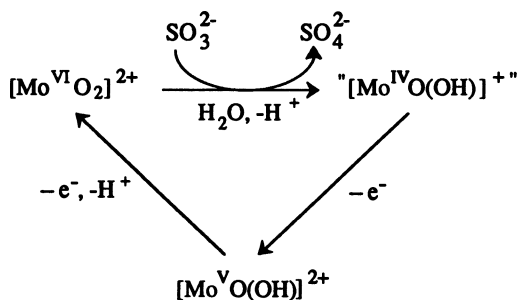
A new system (Scheme VI, 34) involving the L-N_3 ligand displays all the important centers and processes involved in catalysis by $[\text{MoO}_2]^{2+}$ -containing enzymes; it models the structure, spectroscopy and chemistry associated with the well-defined and arguably most important ligands on the molybdenum center (c.f. Scheme V). Reaction of $(\text{L-N}_3)\text{Mo}^{\text{VI}}\text{O}_2(\text{SPh})$ with PPh_3 produces coordinatively-unsaturated " $(\text{L-N}_3)\text{Mo}^{\text{VO}}(\text{SPh})$ " which can be trapped and structurally characterized in a number of ways, depending upon ligand availability (Scheme VI). In the presence of water and starting material, a one-electron process results in the formation of EPR-active $(\text{L-N}_3)\text{Mo}^{\text{VO}}(\text{OH})(\text{SPh})$. This in turn can be oxidized by O_2 to regenerate $(\text{L-N}_3)\text{Mo}^{\text{VI}}\text{O}_2(\text{SPh})$ and complete the cycle shown in Scheme VI (c.f. Scheme V). The two-electron Mo^{VI} to Mo^{IV} step is slower than the one-electron Mo^{IV} to Mo^{V} step, thus preventing direct access to the proposed $(\text{L-N}_3)\text{Mo}^{\text{IV}}\text{O}(\text{OH})_2(\text{SPh})$ intermediate. The system is also capable of catalyzing oxygen atom transfer from Me_2SO to PPh_3 (c.f. Scheme IV).

Oxygen isotope tracing shows that H_2O , not O_2 , is the source of the oxo ligand regenerated in the cycle. The system is thereby capable of catalyzing the net transfer of an oxygen atom from H_2O to PPh_3 with O_2 acting as electron acceptor (c.f. equation 2). Water prevents comproportionation to the inactive, coordinatively saturated $[\text{Mo}^{\text{V}}_2\text{O}_3]^{4+}$ species, permitting the one-electron oxidation chemistry characteristic of the enzymes to be observed. Note that the molybdenum oxidation state controls the level of protonation of the water-based ligand as previously outlined. The sulfite oxidase cycle (Scheme V) can be interpreted as oxygen atom transfer chemistry followed by coupled electron-proton transfer chemistry to regenerate the active site.

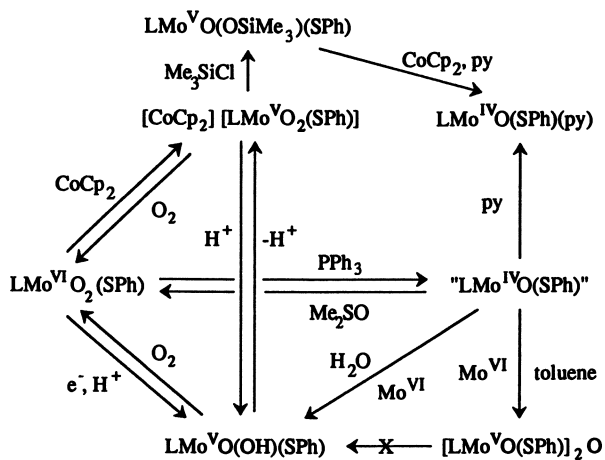
This system also provides access to the $[\text{Mo}^{\text{VO}}_2]^+$ center, isolated in substance for the first time as the cobaltocenium salt, $[\text{CoCp}_2][(\text{L-N}_3)\text{MoO}_2(\text{SPh})]$ (Scheme VI). Notably, it has not to date proven possible to observe any two-electron (i.e. oxygen atom transfer) chemistry with this species. This may be the reason that a $[\text{Mo}^{\text{VO}}_2]^+$ center has never been detected (via its characteristic EPR signal (32)) during turnover of any enzyme.

The Xanthine Oxidase Cycle

Xanthine oxidase and related hydroxylase enzymes exhibit broad substrate specificity and an apparently complex catalytic cycle (1). The important centers identified by EXAFS and EPR studies have been presented in Scheme I. Kinetics studies have also provided important results (28,56,57). In a particularly noteworthy study by Hille and Sprecher (56), single turn-over experiments under substrate-limiting conditions confirmed that the oxygen atom transferred to the substrate originates from the active site and not from solvent water. If oxygen atom transfer from a simple *cis*- $[\text{Mo}^{\text{VI}}\text{OS}]^{2+}$ center occurs, the transient existence of a deoxo- Mo^{IV} species is



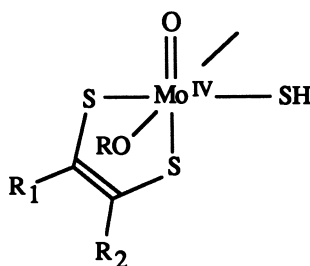
Scheme V

Scheme VI (L = L-N₃)

implied. However, a detailed comparison (31) of the enzyme EPR signals derived from *active* enzyme with the synthetic *cis* species $[(L-N_2S_2)Mo^{VOE}]^-$ and $(L-N_2S_2)Mo^{VO}(EH)$ ($E = O, S$) allows *three* ligands to be defined in each of the Mo^V enzyme centers: $[Mo^{VOS}(OR)]$ (Very Rapid) or $[Mo^{VO}(SH)(OH)]$ (Rapid 1 and 2) (Scheme I). The presence of bound product OR in the Mo^{IV} center has been implied from EXAFS and resonance Raman studies (24,63). The minimal catalytic cycle given in Scheme VII accounts for the observed behavior of the enzyme under *substrate-limiting* conditions.

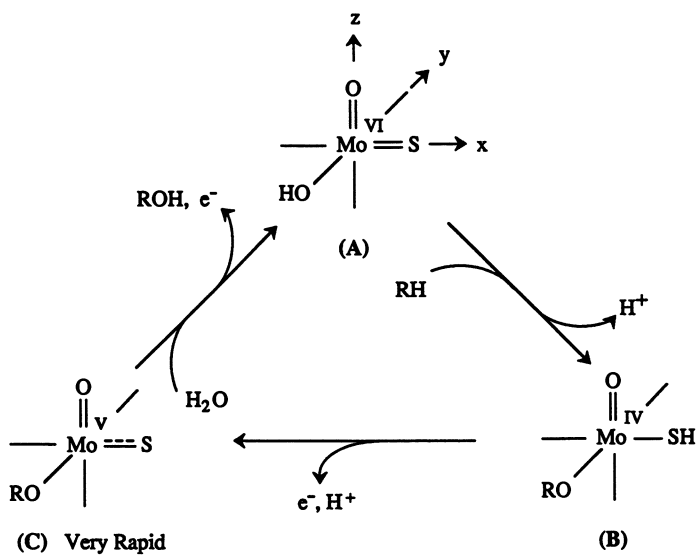
Formulation of the resting active site as a *fac*- $[Mo^{VIOS}(OH)]^+$ center (A) is not only consistent with available evidence but permits a $Mo=O$ group to be maintained at all stages of catalysis; possible stabilization of the thio ligand has been suggested (47) but as yet there is no direct evidence for this. The *cis*- $[Mo^{VI}O(OH)]^{3+}$ fragment is the equivalent of the *cis*- $[Mo^{VI}O_2]^{2+}$ unit in sulfite oxidase. Substrate activation takes place at A with the eventual formation of the Mo^{IV} center B, which contains bound oxidized substrate OR- and an SH- ligand. While details of the electronic rearrangements accompanying C(8)-H activation remain uncertain, it is likely that concerted changes in the acidity/basicity of the $Mo-OH$ and $Mo=S$ groups assist substrate activation and the formation of B. Oxidation may be initiated by interaction of the C-H bond with a $Mo=S$ π^* orbital of A, which induces formal transfer of hydride and formation of the $Mo-OR$ link in B. Conversely, interaction of C(8) with the hydroxy oxygen could lead to population of a $Mo=S$ π^* orbital, followed by deprotonation of the substrate by the basic thio ligand. The role of molybdopterin moieties or nearby amino acid sites in coupled electron-proton transfer reactions remains open to speculation. The Very Rapid center C is derived from the Mo^{IV} form B by a one-electron oxidation and the loss of a proton (57). The complications that obtain when substrate is in excess (observation of the Rapid signals) can be attributed to the effects of substrate binding prior to product release during the Mo^{IV} to Mo^{VI} one-electron transformations (31,57).

Definition of the three ligands allows speculation concerning the orientation of the dithiolene ligand apparently provided by molybdopterin (39). The stereochemistry of the structure given below for the Mo^{IV} center B permits interaction of the doubly occupied HOMO $Mo d_{xy}$ with the dithiolene π -framework, providing a ready pathway for electron transfer to the internal electron transfer chain via the pterin cofactor.



Why Molybdenum is Exploited by Nature

The pterin-containing molybdenum enzymes have exquisitely exploited the oxygen atom transfer and coupled electron-proton transfer capabilities of molybdenum and have tuned these for the performance of their vital functions. Oxo-, thio- and dithiolene-molybdenum centers appear to be uniquely tuned for the oxygen atom transfer and coupled electron-proton transfer chemistry displayed by these enzymes; they alone meet the kinetic and thermodynamic requirements for the substrate transformations observed. Moreover, the response of the acid-base properties of the $Mo=O(H)$ and $Mo=S(H)$ centers to changes in the oxidation state of the metal center appears to be crucial to substrate transformation and active site regeneration.



Scheme VII

Literature Cited

- (1) *Molybdenum and Molybdenum-containing Enzymes*; Coughlan, M. P., Ed.; Pergamon Press: Oxford, 1980.
- (2) Spence, J. T. *Coord. Chem. Rev.* **1983**, *48*, 59.
- (3) *Molybdenum Enzymes*; Spiro, T. G., Ed.; Wiley: New York, NY, 1985.
- (4) Bray, R. C. *Q. Rev. Biophys.* **1988**, *21*, 299.
- (5) Holm, R. H. *Coord. Chem. Rev.* **1990**, *110*, 183.
- (6) Stiefel, E.I. This Volume, Chapter 1.
- (7) Enemark, J. H.; Young, C. G. *Adv. Inorg. Chem.* submitted.
- (8) Green, D. E.; Beinert, H. *Biochem. Biophys. Acta* **1953**, *11*, 599.
- (9) Richert, D. A.; Westerfield, W. W. *J. Biol. Chem.* **1953**, *203*, 915.
- (10) De Renzo, E. C.; Kalieta, E.; Heytler, P.; Oleson, J. J.; Hutchings, B. L.; Williams, J. H. *J. Am. Chem. Soc.* **1953**, *75*, 753.
- (11) Burian, R. Z. *Physiol. Chem.* **1905**, *43*, 497.
- (12) Nicolas, D. S. D.; Nason, A. *J. Biol. Chem.* **1954**, *207*, 353.
- (13) Cohen, H. J.; Fridovich, I.; Rajagopalan, K. V. *J. Biol. Chem.* **1971**, *246*, 367.
- (14) Bray, R. C.; Malmstrom, B. G.; Vanngard, T. *Biochem. J.* **1959**, *73*, 193.
- (15) Bray, R. C.; Meriwether, L. S. *Nature* **1966**, *212*, 467.
- (16) Meriwether, L. S.; Marzluff, W. F.; Hodgson, W. G. *Nature* **1966**, *212*, 465.
- (17) Stiefel, E. I. *Prog. Inorg. Chem.* **1977**, *22*, 1.
- (18) (a) Rees, D. C.; Kim, J.; Georgiadis, M. M.; Komiya, H.; Chirino, A. J.; Woo, D.; Schlessman, J.; Chan, M. K.; Joshua-Tor, L.; Santillan, B.; Chakrabarti, P.; Chu, B. T. This Volume, Chapter 11. (b) Bolin, J.; Campobasso, N.; Muchmore, S. W.; Morgan, T. V.; Mortenson, L. E. This Volume, Chapter 12.
- (19) Cramer, S. P. *Adv. Inorg. Bioinorg. Mech.* **1983**, *2*, 259.
- (20) Cramer, S. P.; Gray, H. B.; Rajagopalan, K. V. *J. Am. Chem. Soc.* **1979**, *101*, 2772.
- (21) George, G. N.; Kipke, C. A.; Prince, R. C.; Sunde, R. A.; Enemark, J. H.; Cramer, S. P. *Biochem.* **1989**, *28*, 5075.
- (22) Tullius, T. D.; Kurtz, D. M., Jr.; Conradson, S. D.; Hodgson, K. O. *J. Am. Chem. Soc.* **1979**, *101*, 2776.
- (23) Hille, R.; George, G. N.; Eidness, M. K.; Cramer, S. P. *Inorg. Chem.* **1989**, *28*, 4018.
- (24) Turner, N. A.; Bray, R. C.; Diakin, G. P. *Biochem. J.* **1989**, *260*, 563.
- (25) Bray, R. C. *Polyhedron* **1986**, *5*, 591.
- (26) Bray, R. C.; Gutteridge, S. *Biochem.* **1982**, *21*, 5992.
- (27) Tanner, S. J.; Bray, R. C.; Bergmann, F. *Biochem. Soc. Trans.* **1978**, *6*, 1328.
- (28) George, G. N.; Bray, R. C. *Biochem. Soc. Trans.* **1987**, *13*, 570.
- (29) George, G. N.; Bray, R. C. *Biochem.* **1988**, *27*, 3603.
- (30) Wilson, G. J.; Greenwood, R. J.; Pilbrow, J. R.; Spence, J. T.; Wedd, A. G. *J. Am. Chem. Soc.* **1991**, *113*, 6803.
- (31) Greenwood, R. J.; Wilson, G. J.; Pilbrow, J. R.; Wedd, A. G. *J. Am. Chem. Soc.* in press.
- (32) Dowerah, D.; Spence, J. T.; Singh, R.; Wedd, A. G.; Wilson, G. L.; Farchione, F.; Enemark, J. H.; Kristofzski, J.; Bruck, M. *J. Am. Chem. Soc.* **1987**, *109*, 5655.
- (33) Wedd, A. G.; Spence, J. T. *Pure Appl. Chem.* **1990**, *62*, 1055.
- (34) Xiao, Z.; Young, C. G.; Enemark, J. H.; Wedd, A. G. *J. Am. Chem. Soc.* **1992**, *114*, 9194.
- (35) Ketchum, P. A.; Cambier, H. Y.; Frazier, W. A.; Madansky, C. H.; Nason A. *Proc. Nat. Acad. Sci. U.S.A.* **1970**, *66*, 1016.

- (36) Johnson, J. L.; Hainline, B. E.; Rajagopalan, K. V. *J. Biol. Chem.* **1980**, *255*, 1783.
- (37) Johnson, J. L.; Rajagopalan, K. V. *Proc. Nat. Acad. Sci. U.S.A.* **1982**, *79*, 6856.
- (38) (a) Rajagopalan, K. V. In *Advances in Enzymology and Related Areas of Molecular Biology*; Meister, A. Ed.; Wiley: New York, NY, 1991, Vol. 64; pp 215-290. (b) Rajagopalan, K. V. This Volume, Chapter 3. (c) Meyer, O. This Volume, Chapter 4.
- (39) Rajagopalan, K. V.; Johnson, J. L. *J. Biol. Chem.* **1992**, *267*, 10199.
- (40) Pilato, R. S.; Eriksen, K. A.; Greaney, M. A.; Stiefel, E. I.; Goswami, S.; Kilpatrick, L.; Spiro, T. G.; Taylor, E. C.; Rheingold, A. L. *J. Am. Chem. Soc.* **1991**, *113*, 9372.
- (41) (a) Pilato, R. S.; Gea, Y.; Erickson, K. E.; Greaney, M. A.; Taylor, E. C.; Goswami, S.; Kilpatrick, L.; Spiro, T. G.; Rheingold, A. L.; Stiefel, E. I. This Volume, Chapter 6. (b) Garner, C. D.; Armstrong, E. M.; Ashcroft, M. J.; Auterberry, M. S.; Birks, J. H.; Collison, D.; Goodwin, A. J.; Joule, J. A.; Larsen, L.; Rowe, D. J.; Russell, J. R. This Volume, Chapter 7.
- (42) Garner, C. D. In *Molybdenum Enzymes*; Spiro, T. G., Ed.; Wiley: New York, NY, 1985.
- (43) *Comprehensive Coordination Chemistry*; Wilkinson, G., Gillard, R. D., McCleverty, J. A. Eds.; Pergamon: Oxford, 1987, Vol. 3, Chapter 36, pp. 1229-1421.
- (44) Chang, C. S. J.; Collison, D.; Mabbs, F. E.; Enemark, J. H. *Inorg. Chem.* **1990**, *29*, 2261.
- (45) Coyle, C. L.; Harmer, M. A.; George, G. N.; Daage, M.; Stiefel, E. I. *Inorg. Chem.* **1990**, *29*, 14.
- (46) Coucouvanis, D.; Hadjikyriacou, A.; Toupadakis, A.; Koo, S.-M.; Ieperuma, O.; Draganjac, M.; Salifoglou, A. *Inorg. Chem.* **1991**, *30*, 754 and references therein.
- (47) Eagle, A. A.; Laughlin, L. J.; Young, C. G.; Tiekink, E. R. T. *J. Am. Chem. Soc.* **1992**, *114*, 9195.
- (48) Stiefel, E. I. *Proc. Nat. Acad. Sci. U.S.A.* **1973**, *70*, 988.
- (49) Barral, R.; Bocard, C.; Séree de Roch, I.; Sajas, L. *Tetrahedron Lett.* **1972**, *16*.
- (50) Roberts, S. A.; Young, C. G.; Cleland, W. E. Jr.; Ortega, R. B.; Enemark, J. H. *Inorg. Chem.* **1988**, *27*, 3044.
- (51) Roberts, S. A.; Young, C. G.; Kipke, C. A.; Cleland, W. E. Jr.; Yamanouchi, K.; Carducci, M. D.; Enemark, J. H. *Inorg. Chem.* **1990**, *29*, 3650.
- (52) Berg, J. M.; Holm R. H. *J. Am. Chem. Soc.* **1985**, *107*, 917 and 925.
- (53) Llopis, E.; Domenech, A.; Ramirez, J. A.; Cervilla, A.; Palanca, P.; Picher, T.; Sanz, V. *Inorg. Chim. Acta* **1991**, *189*, 29.
- (54) Rajan, O. A.; Spence, J. T.; Leman, C.; Minelli, M.; Sato, M.; Enemark, J. H.; Kroneck, P. M. H.; Sulger, K. *Inorg. Chem.* **1983**, *22*, 3065.
- (55) Rajagopalan, K. V. *Biochem. Elem.* **1984**, *3*, 149.
- (56) Hille, R.; Sprecher, H. *J. Biol. Chem.* **1987**, *262*, 10914.
- (57) McWirter, R. B.; Hille, R. *J. Biol. Chem.* **1991**, *266*, 23724.
- (58) Newton, W. E.; Corbin, J. L.; Bravard, D. C.; Searles, J. E.; McDonald, J. W. *Inorg. Chem.* **1974**, *13*, 100.
- (59) Chen, G. J.-J.; McDonald, J. W.; Newton, W. E. *Inorg. Chem.* **1976**, *15*, 2612.
- (60) Durant, R.; Garner, C. D.; Hyde, M. R.; Mabbs, F. E. *J. Chem. Soc., Dalton Trans.* **1977**, 955.
- (61) Speier, G. *Inorg. Chim. Acta* **1979**, *32*, 139.
- (62) Ueyama, N.; Yano, M.; Miyashita, H.; Nakamura, A.; Kamachi, M.; Nozakura, S. *J. Chem. Soc., Dalton Trans.* **1984**, 1447.
- (63) Oertling, W. A.; Hille, R. *J. Biol. Chem.* **1990**, *265*, 17446.

Chapter 6

Pterins, Quinoxalines, and Metallo-Ene-Dithiolates

Synthetic Approach to the Molybdenum Cofactor

Robert S. Pilato^{1,4}, K. Eriksen¹, M. A. Greaney¹, Y. Gea¹, E. C. Taylor²,
S. Goswami², L. Kilpatrick², T. G. Spiro², A. L. Rheingold³, and
Edward I. Stiefel¹

¹Exxon Research and Engineering Company, Clinton Township,
Route 22 East, Annandale, NJ 08801

²Department of Chemistry, Princeton University, Princeton, NJ 08540

³Department of Chemistry, University of Delaware, Newark, DE 19711

The syntheses of the molybdopterin decomposition products, such as Form A, provide starting points for the total synthesis of Moco. Specifically, C(6) alkyne-substituted pterins similar to Form A react with metal polysulfides to yield the molybdenum-ene-dithiolate moiety of Moco. Syntheses are reported for the pterin-ene-dithiolate and quinoxaline-ene-dithiolate complexes $(C_5H_5)_2Mo-\{S_2C_2[C(O)R]R'\}$ where $R = CH_3, CH_2OSiPh_2^tBu$, and $R' = N$ -pivaloyl-6-pterin, 2-quinoxaline. Intermediates in the preparation are the unprecedented ene-1-thiolate-2-perthiolate (trithiolene) complexes. Reactions of the molybdenum ene-dithiolate complexes include the oxidation of Mo(IV) to Mo(V), reduction of the side-chain carbonyl, and transmetallation. The complexes $(C_5H_5)_2Mo-\{S_2C_2[C(O)CH_3]R'\}$ have been $\geq 81\%$ ³⁴S enriched. Resonance Raman studies identify a $\nu(Mo-S)$ stretch at 350 cm^{-1} , similar to a band in DMSO reductase. Fluorescence of the oxidized pterin is quenched in the metal ene-dithiolate and ene-1-thiolate-2-perthiolate complexes.

The proposed structure for Moco, the cofactor found in all the molybdoenzymes except nitrogenase, is shown in figure 1. The first coordination sphere of molybdenum has been defined by EXAFS (Extended X-ray Absorption Fine Structure) (1-3) and all of the enzymes appear to possess thiolate ligation of molybdenum and (with the possible exception of dissimilatory nitrate reductase and formate dehydrogenase) either dioxo or oxo-sulfido ligation of the Mo(VI) state. The molybdopterin derivatives Form A, camMPT, Form B and urothione, shown in figure 2 have been isolated and when combined with EXAFS results have led to the proposed Moco structure (4-7). The isolated C(6)-substituted pterins possess unsaturated carbon atoms α and β to the pterin ring. Sulfur functionalities are associated with these unsaturated carbons in camMPT, Form B and urothione. The formation of these compounds is consistent with the decomposition of the proposed

⁴Current address: Department of Chemistry and Biochemistry, University of Maryland, College Park, MD 20742

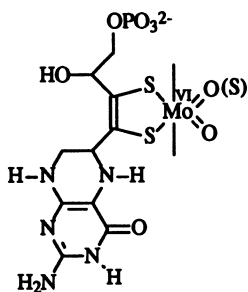


Figure 1. The proposed structure for Moco with Mo(VI).

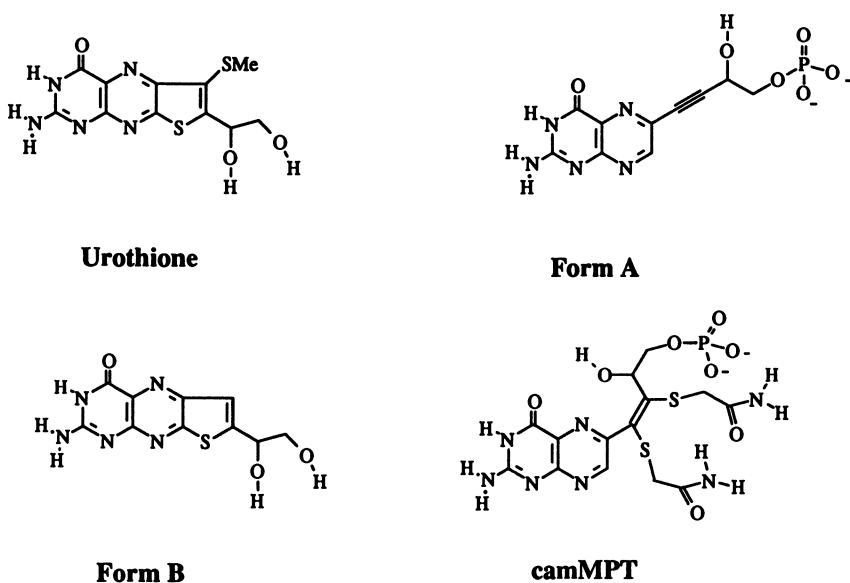


Figure 2. The oxidative decomposition products of Moco and the Moco metabolite urothione.

1,2-ene-dithiolate Moco structure (see Rajagopalan, K. V., Chapter 3 and Meyer, O., Chapter 4, this volume). Moreover, the oxidative decomposition of quinoxaline-substituted 1,2-ene-dithiolate molybdenum complexes has yielded thiophenes similar to Form B and urothione (8).

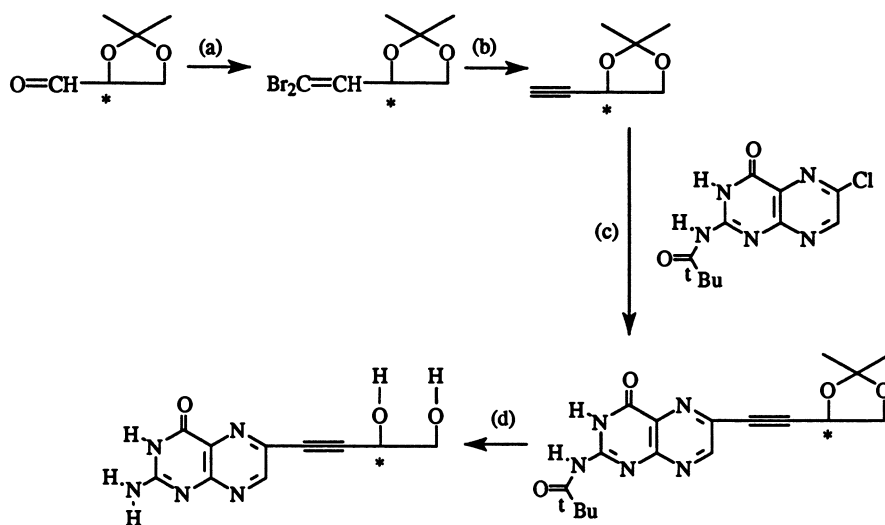
The structures of the molybdopterin derivatives; Form A, dephospho Form A, Form B and urothione, have been confirmed by direct synthesis. The absolute configuration of Form A was determined by comparing the circular dichroism spectra of synthetic Form A (the S isomer) with enzyme isolated Form A (9-10). The synthesis of the S isomer of Form A is shown in scheme 1.

Synthetic Strategy for Moco

Our current research program is directed at the total synthesis of Moco and includes both synthetic organic and inorganic components (11). We have concentrated to date on the synthesis of the pterin substituted 1,2-ene-dithiolate portion of Moco, termed molybdopterin. A limited number of 1,2-ene-dithiolates can be isolated as the disodium salts and many of these contain electron-withdrawing groups (12-17). However, many 1,2-ene-dithiolates can be prepared as metal complexes where the 1,2-ene-dithiolate is stabilized as a chelating ligand (as is suggested for Moco) (18-28). Synthetic routes to metallo-1,2-ene-dithiolate complexes include the reactions of metal complexes (containing labile ligands) with dithines (26), dithiolium salts (19, 29) or α -hydroxy ketones in the presence of P_4S_{10} (17), as shown in equations 1, 2, and 3, respectively. Another interesting synthetically useful method for the preparation of dithiolenes is the reaction of a metal polysulfido complex with an alkyne as shown in equation 4 (8, 11, 18, 21, 22, 24). The previously reported synthesis of C(6)-alkyne-substituted pterin derivatives (such as Form A) (9, 10) should, in conjunction with the reaction shown in equation 4, allow the preparation of molybdenum 1,2-ene-dithiolate (dithiolene) complexes that approach the structure of Moco.

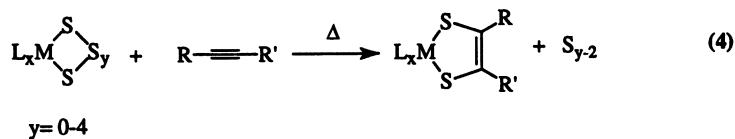
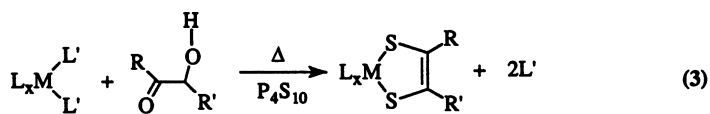
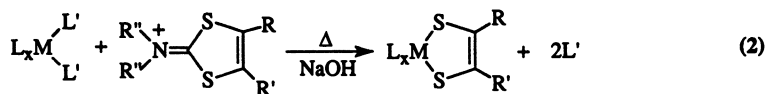
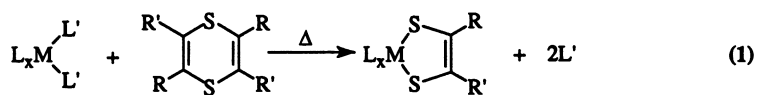
A proposal for the total synthesis of Moco is shown scheme 2. N-Pivaloyl pterins are used to increase the solubility of the pterin ring in common organic solvents. The pivaloyl group can be removed by saponification of the amide without decomposing the pterin. The alkyne functionality is appended to the pterin in a Pd catalyzed coupling reaction (the reaction of C(6)-chloro-pivaloyl-pterin with a terminal alkyne). The subsequent reaction of the alkyne with a metal polysulfido complex should yield a metallo-1,2-ene-dithiolate. The dithiolene need not be a molybdenum complex since dithiolene metal exchange reactions are known and in theory can be used to introduce the $[MoO_2]^{2+}$ or $[Mo(O)(S)]^{2+}$ fragment once the side-chain is complete and the pivaloyl protecting group removed. Our goal is to prepare biologically active materials. At any point in the synthesis the biological activity can be tested with the Nit-1 assay, the standard test for Moco activity (30, 31).

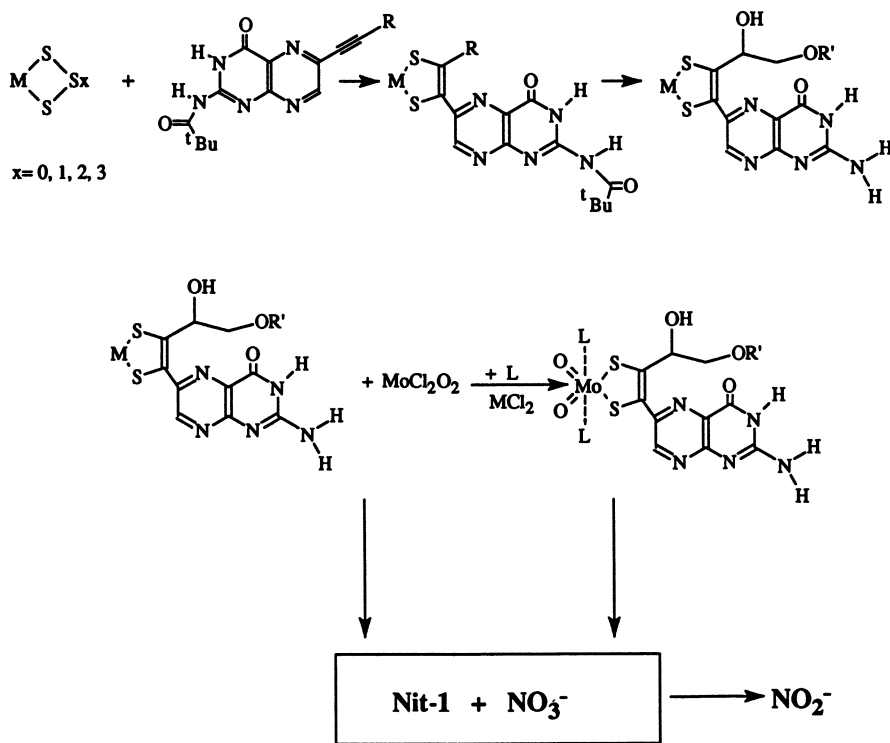
In selecting a metal polysulfido complex for the synthesis of molybdopterin (scheme 2) several factors must be considered. First, a robust metal framework is required that will allow subsequent reaction of the pterin and the appended side chain of the dithiolene complex. Second, it would be useful for the metal dichloride derivative of the framework to be relatively insoluble in common solvents to drive the metal chloride-metal-1,2-ene-dithiolate metathesis (used to introduce the $[MoO_2]^{2+}$ or $[Mo(O)(S)]^{2+}$ functionalities) (16). Third, to simplify subsequent reactions and to better approximate the active site, the polysulfido complex should yield a mono-1,2-ene-dithiolate complex upon reaction with the alkyne rather than the more common tris-ene-dithiolate complex. Finally, it would be advantageous to find a metal framework



- (a) CBr_4 , PPh_3 (2 equiv), CH_2Cl_2 , 0°C to RT.
 (b) $n\text{-BuLi}$ (2 equiv), THF, -78°C to RT.
 (c) $\text{Pd}(\text{o-Ac})_2$, $(\text{o-tolyl})_3\text{P}$, CuI , Et_3N , CH_3CN , 100°C .
 (d) 0.5 N HCl , dioxane, reflux.

Scheme 1





Scheme 2

that meets the above criteria and contains molybdenum such that intermediates in the total syntheses will be potential reactivity and spectroscopic models for Moco.

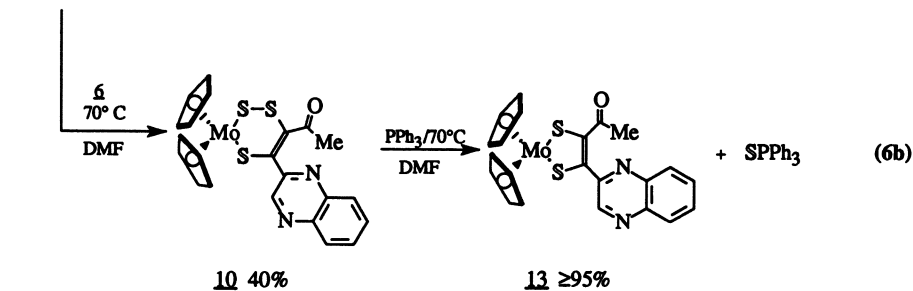
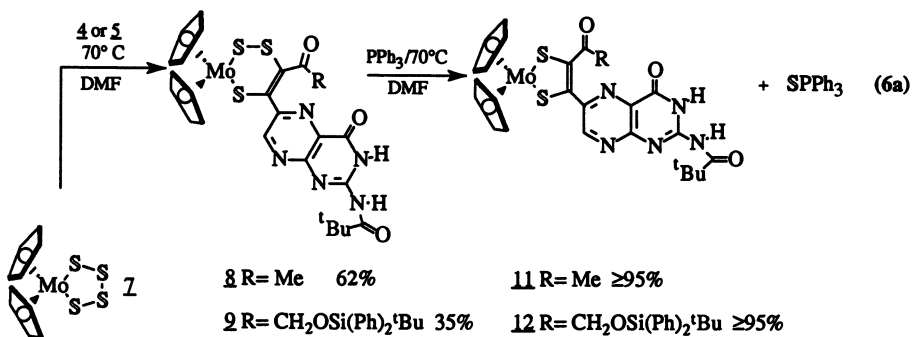
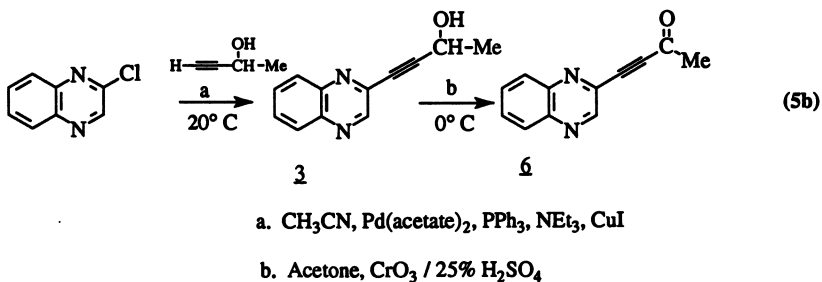
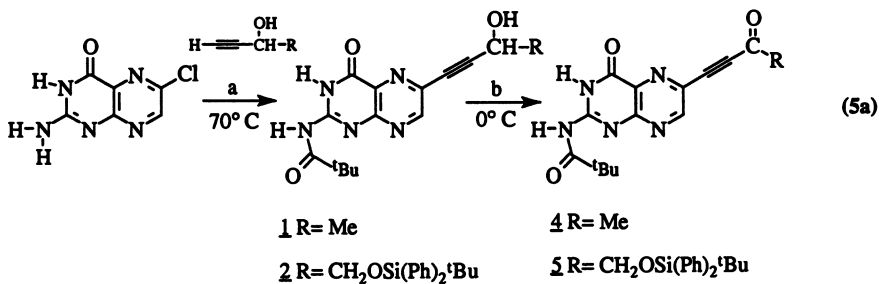
We have investigated a relatively large number of metal polysulfido complexes and have prepared several metallo-1,2-ene-dithiolate complexes with either N-pivaloyl-pterins or quinoxalines (quinoxalines were chosen to facilitate product crystallization while retaining the pyrazine redox site of the pterin). Of these, the bis-cyclopentadienyl molybdenum metal framework meets most if not all of the synthetic criteria. Here we describe our progress in the total synthesis of Moco as well as the chemistry of molybdenum-containing intermediates which may be pertinent to the catalysis of the molybdoenzymes and/or the synthesis of Moco.

Pterin-ene-dithiolate and Quinoxaline-ene-dithiolate Synthesis

While a broad range of N-pivaloylated-C(6)-alkyne substituted pterins (PPT-CC-CH(OH)R) and C(2)-alkyne substituted quinoxalines (Quin-CC-CH(OH)R) can be prepared, our discussion here is limited to the derivatives where R = Me and CH₂(OSiPh₂^tBu). These R groups were selected since they possess four-carbon side chains and should allow ultimate conversion to the proposed molybdopterin side chain. Compounds **1-3** were prepared by the palladium catalyzed coupling of the corresponding terminal alkynes with either C(6) chloro-N-pivaloyl-pterin or C(2) chloro-quinoxaline and were isolated in fair yield, as shown in equations 5a and 5b. While compounds **1-3** contain a hydroxyl group γ to the pterin they were not sufficiently activated to allow coupling with any transition metal polysulfido complex investigated. To activate the alkynes the hydroxyl groups of compounds **1-3** were oxidized in the corresponding ketones, compounds **4-6**. Of the oxidants investigated CrO₃ in 25% H₂SO₄ (Jones' reagent) at 0°C gave the best yields as is shown in equation 5a and 5b.

The reaction of compounds **4-6** with the molybdenum polysulfido complex (C₅H₅)₂MoS₄, **7** (**32**) affords a family of complexes that contains a new ligand type, an ene-1-per-thiolate-2-thiolate (trithiolene) **8-10** as shown in equation 6a and 6b (**11**). The product was confirmed by a combination of spectroscopic analysis including a single crystal X-ray study of **10** the results of which are shown in figure 3. Crystallographic data for complex **10** and spectroscopic data for complexes **8-10** implicate a single trithiolene isomer. The S₂ linkage in the trithiolene is bound to the alkene carbon flanked by the carbonyl functionality. The four-atoms, S(1), S(3), C(19) and C(20), form a plane within the estimated standard deviations for the atomic positions. The Mo-S(1) bond length 2.510(2) Å is rather long. The Mo-S(2) bond length at 2.451(2) Å is similar to the Mo-S distances found in molybdenum 1,2-ene-dithiolene and di- or polysulfide complexes. The S(2)-S(3) bond length at 2.074(2) Å is best described as a S-S single bond. The Mo and S(3) are not within bonding distance [(Mo-S(3) 3.704(2) Å)]. The plane of the quinoxaline ring forms a 94.0° angle with the S(1), C(19), C(20), S(3) plane in complex **10**.

Complexes **8-10** are readily converted to the desired 1,2-ene-dithiolate complexes (dithiolenes) in $\geq 95\%$ yield by the addition of triphenylphosphine which acts as a sulfur atom acceptor as shown in equations 6a and 6b. The identity of the 1,2-ene-dithiolene complexes **11-13** was confirmed by a combination of spectroscopy, including ¹H NMR, ¹³C NMR, mass spectrometry, and the single crystal X-ray crystallographic study of complex **13**, the results of which are shown in figure 4. The crystallographic characterization of the 1,2-ene-dithiolene complex, **13**, shows the five-membered metalocycle formed by Mo, S(1), S(2), C(13) and C(14) to be essentially planar with a deviation from planarity of only 0.01 Å. The bond lengths and angles in complex **13** are similar to those of other crystallographically characterized 1,2-ene-



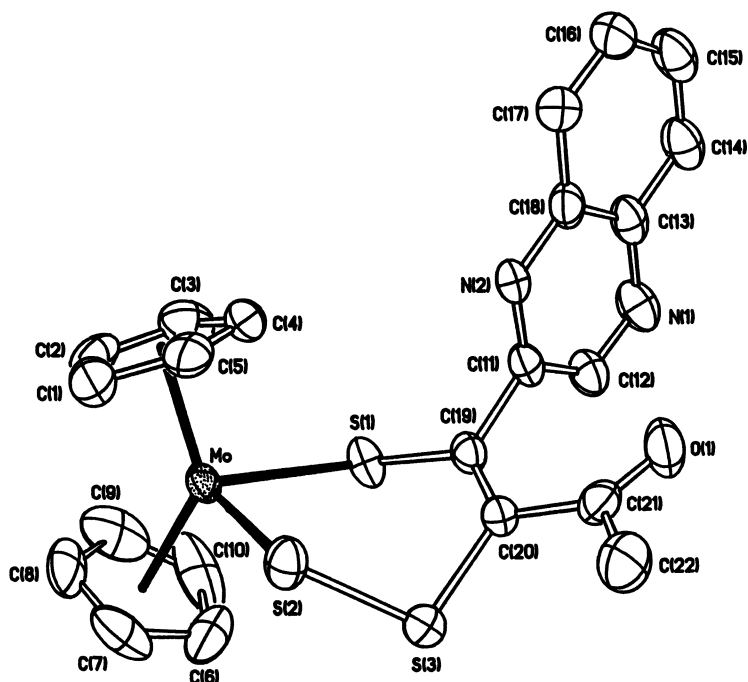


Figure 3. An ORTEP drawing of complex **10** with the thermal ellipsoids drawn at 35% probability.

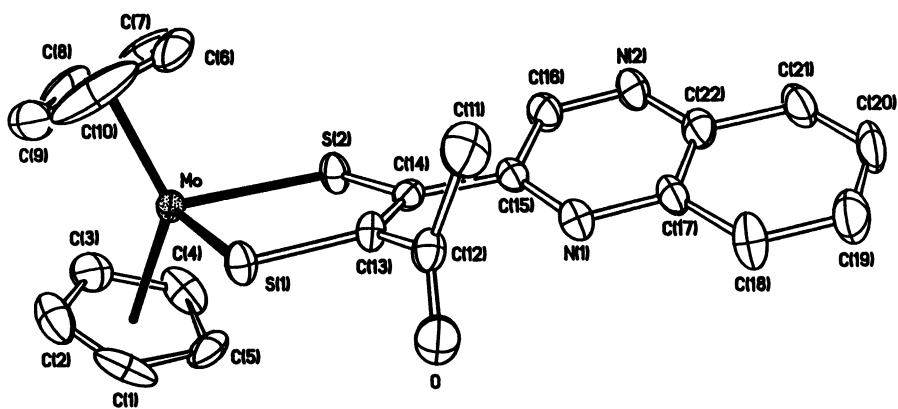


Figure 4. An ORTEP drawing of complex **13** with the thermal ellipsoids drawn at 35% probability.

dithiolate complexes of molybdenum. The plane of the quinoxaline ring forms a 19.5° angle with the S(1), C(13), C(14), S(2) plane of complex **13**.

Spectroscopic, Electrochemical and Theoretical Studies

Complexes **11** and **13** have been $\geq 81\%$ enriched in ^{34}S and have been subject to study by resonance Raman spectroscopy. The $\nu(\text{Mo-S})$ modes can be identified by comparing the resonance Raman spectra of natural abundance and ^{34}S enriched samples. In complex **11** the major sulfur-sensitive band appears at 351 cm^{-1} and shifts to 340 cm^{-1} upon ^{34}S enrichment (the isotopic $^{34}\text{S}/^{32}\text{S}$ shift for a band at 351 cm^{-1} is predicted by reduced mass equations to be $\approx 10\text{ cm}^{-1}$). This datum compares favorably with a recent resonance Raman study of DMSO reductase from *Rhodobacter sphaeroides*, which shows a major sulfur-sensitive band at 350 cm^{-1} for the oxidized form of the enzyme (**23**).

Many oxidized pterins (including the C(6)-alkyne-substituted-N-pivaloyl pterins **12**, **4**, and **5**) exhibit fluorescence associated with excitation of electronic transitions in the UV and visible regions (**33**). An interesting feature of both the pterin containing trithiolene, **8**, and dithiolene, **11**, complexes is the quenching of the pterin fluorescence as compared to compound **4**.

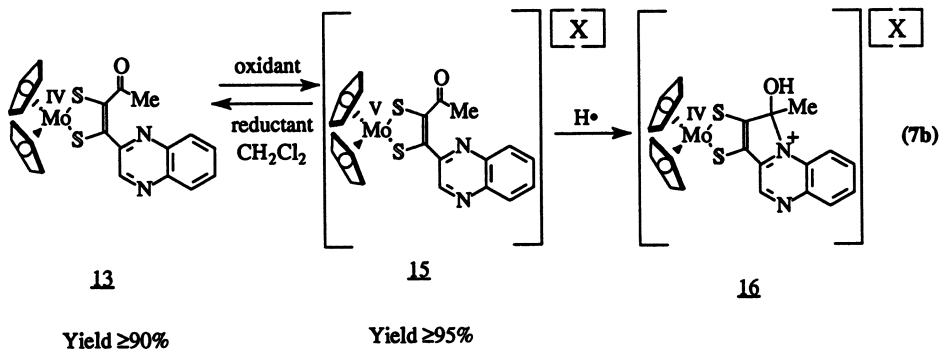
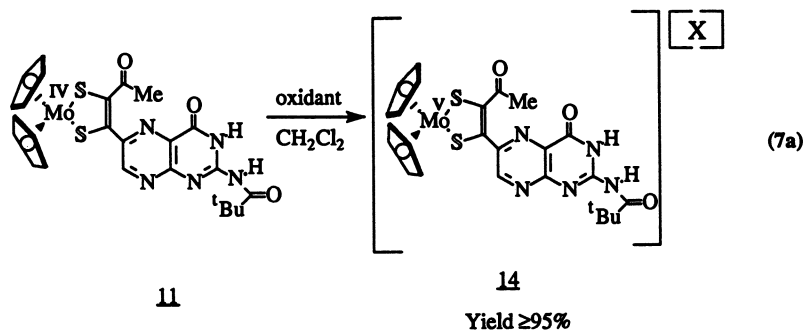
Complexes **11** and **13** have been investigated electrochemically and both show reversible one-electron oxidation waves centered at 317 and 403 mV, respectively (**34**). The potentials are insensitive to solvent although the redox potential for complex **13** is extremely sensitive to the presence of acid in the solution. When a solution of complex **13** is titrated with EtSO_3H a new reversible wave centered at 645 mV appears and the titration is complete upon the addition of 1.5 equivalents of the acid.

A ZINDO (**35**) calculation of complex **13** suggests that the HOMO, the source of the electron removed upon oxidation, is comprised mainly of 1,2-ene-dithiolate carbon and sulfur molecular orbitals (C-C π bonding and C-S π antibonding) with only a small contribution from the metal center. The lowest energy electronic transition should be from the HOMO to an unfilled essentially π^* orbital of the quinoxaline ligand. In addition to the UV-visible bands associated with the $\pi \rightarrow \pi^*$ and $n \rightarrow \pi^*$ electronic transitions of the pterin and quinoxaline, complexes **11** and **13** each show a band that we have assigned to the HOMO to LUMO transition centered at 510 ($\epsilon \approx 3,000\text{ M}^{-1}\text{cm}^{-1}$) and 496 nm ($\epsilon \approx 3,500\text{ M}^{-1}\text{cm}^{-1}$), respectively.

Redox and Acid Base Reactivity of the Molybdenum Ene-dithiolate Complexes

Complexes **11** and **13** can be chemically oxidized using $[(\text{C}_5\text{H}_5)_2\text{Fe}][\text{PF}_6]$, I_2 or $[\text{Ph}_3\text{C}][\text{BF}_4]$ to yield **14** and **15** as shown in equations 7a and 7b. The room temperature electron paramagnetic resonance (EPR) spectra of complexes **14** and **15** are characterized by g-values of 2.009 and 2.011 with A values of 10.7 G and 10.8 G for the six-line $^{95,97}\text{Mo}$ pattern, respectively. The $^{95,97}\text{Mo}$ splitting is quite small compared to that of $[(\text{C}_5\text{H}_5)_2\text{MoCl}_2]^+$ which has a more typical A-value of 36 G. The small $^{95,97}\text{Mo}$ hyperfine suggests that the partially filled HOMO in **14** and **15** is significantly ligand based rather than metal centered as is also suggested for the HOMO of **13** from the ZINDO calculations.

Complex, **14** and **15**, can be isolated and quantification of the EPR signal suggests that $\geq 95\%$ of samples contain a single unpaired electron. However, attempts to obtain X-ray quality crystals of **15** (I_2 as the oxidant) led to the isolation of the new Mo(IV) complex **16**, which is shown in figure 5. As shown in the X-ray study this complex has a new ring formed by the reaction of the side chain carbonyl with the



oxidant: $[(\text{C}_5\text{H}_5)_2\text{Fe}][\text{PF}_6]$, $[\text{Ph}_3\text{C}][\text{BF}_4]$, I_2

reductant: $(\text{C}_5\text{H}_5)_2\text{Co}$

X: PF_6^- , BF_4^- , I^- , or I_3^-

nitrogen atom of the quinoxaline. The metal center in complex **16** is little perturbed from that of complex **13** even though the 1,2-ene-dithiolate ligand is perturbed as evident from the shortening of the S(1)-C(11) bond to 1.706 Å compared to the more typical S(2)-C(12) bond distance of 1.764(2) Å. The reduction of the C(13)-O(1) bond order is evident from the lengthening of this bond from 1.206(10) Å in **13** to 1.384(29) Å in complex **16** as well as by pseudo-tetrahedral geometry about C(13) in **16**. The C(13)-N(1) bond distance of 1.520(22) Å in complex **16** is a long single bond but all of the C-C and C-N bonds of the quinoxaline ring are similar to those observed for complex **13**. The crystal data in combination with the disappearance of the C=O stretch in the IR, led to the conclusion that the ketone functionality was indeed absent.

We can easily distinguish complexes **15** and **16** by IR spectroscopy (complex **15** has a ketone stretch at 1668 cm⁻¹) as well as the EPR signal associated with **15** and the NMR signals associated with **16**. The mechanism for the conversion of the Mo(V) species, **15**, to the protonated Mo(IV) species, **16**, is currently under investigation.

Interestingly, an alternate route to complex **16** is the addition of acid to complex **13**, as shown in equation 8. This reaction is easily monitored by the large red shift of the bands in the UV-visible spectra of **13** upon the addition of acids and the formation of **16**. Particularly worth noting is the large shift in the HOMO to LUMO transition of **13** upon protonation, from 496 nm ($\epsilon \approx 3,500 \text{ M}^{-1}\text{cm}^{-1}$) to 746 nm ($\epsilon \approx 6,900 \text{ M}^{-1}\text{cm}^{-1}$). This protonation is reversible and the addition of NEt₃ to **16** leads to the quantitative reformation of complex **13**. Clearly, the acid-base and redox properties of these complexes are strongly coupled, a feature that may be critical to the activity of similar sites in the molybdenum cofactor enzymes.

Reduction of the Side-chain. To further our synthetic efforts, we investigated the reduction of the side-chain ketone functionality in complexes **11-13** to the corresponding alcohols. For this reaction we found NaBH₄ to be the best reducing agent, and while we are still optimizing this reaction, the ketone can be reduced in $\approx 40\%$ yield as shown for complex **13** in equation 9.

Transmetalation of the Molybdenum Ene-dithiolate Ligand. We have clearly demonstrated that it is possible to prepare 1,2-ene-dithiolates containing pterins from the reaction of metal polysulfido complexes and pterin substituted alkynes. However, to show that the total synthesis of Moco is possible, we must now demonstrate that the 1,2-ene-dithiolate ligand can be transferred to a [MoO₂]²⁺-fragment. While complexes **11** and **13** react with MoO₂Cl₂ to eliminate (C₅H₅)₂MoCl₂, we have not yet obtained tractable pterin containing products. To demonstrate the principle of dithiolene metathesis, we have reacted complex **11** with [(C₅Me₅)RhCl₂]₂ and obtained the rhodium dithiolene complex, **17**, in 89% yield as shown in equation 10.

Summary

Our results confirm that the reaction of metal polysulfido complexes and alkynes can be used as a component of the total synthesis of Moco. The intermediate pterin-dithiolene complexes are close structural analogues to the pterin-1,2-ene-dithiolate portion of Moco and allow spectroscopic and reactivity studies of this feature of Moco. Moreover, the acid-base and redox reactivity of the complexes demonstrate the strong electronic interaction of the metal and ligand in these systems. It is not surprising that none of the compounds prepared to date reconstitute the apo-proteins of Nit-1 in light of the lack of the terminal phosphate and the presence of the pivaloyl protecting group. However, as continuing synthetic efforts approach the proposed structure of Moco, the

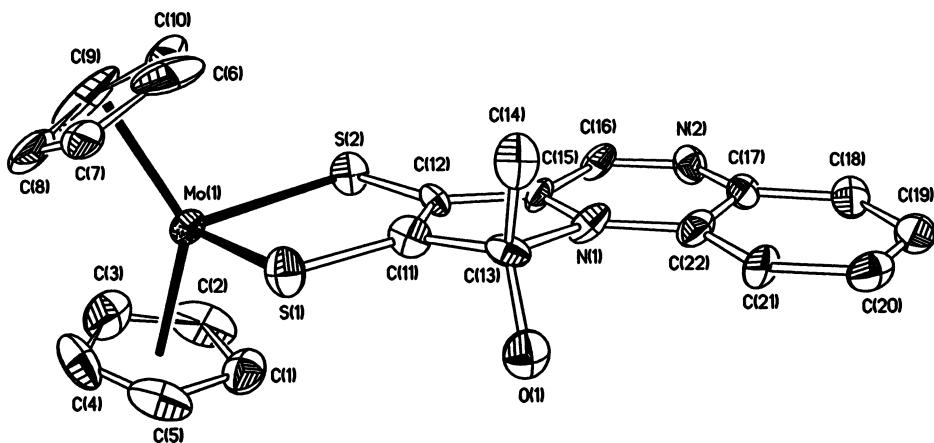
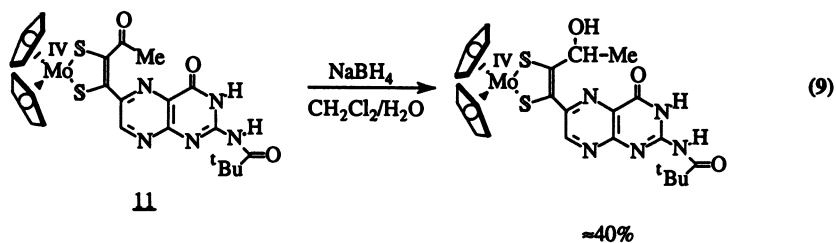
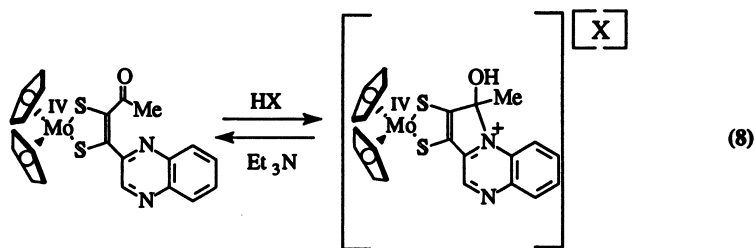
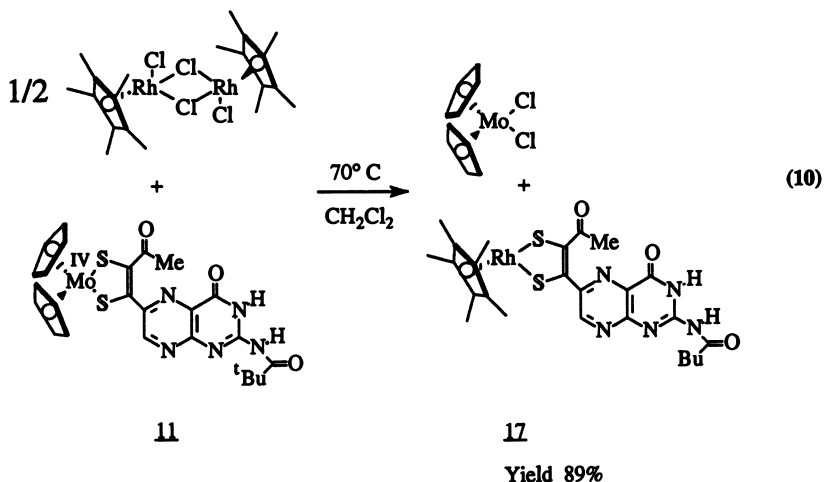


Figure 5. An ORTEP drawing of complex **16** with the thermal ellipsoids drawn at 35% probability.





Nit-1 assay remains the final test for the structural integrity of both synthetic and natural cofactor.

Literature Cited

1. Cramer, S. P.; Wahl, R.; Rajagopalan, K. V. *J. Am. Chem. Soc.* **1981**, *103*, 7721-7.
2. Cramer, S. P.; Solomonson, L. P.; Adams, M. W. W.; Mortenson, L. E. *J. Am. Chem. Soc.* **1984**, *106*, 1467.
3. George, G. N.; Turner, N. A.; Bray, R. C.; Morpeth, F. F.; Boxer, D. H.; Cramer, S. P. *Biochem. J.* **1989**, *259*, 693.
4. Johnson, J. L.; Rajagopalan, K. V. *Proc. Natl. Acad. Sci. U. S. A.* **1982**, *79*, 6856.
5. Kramer, S. P.; Johnson, J. L.; Ribeiro, A. A.; Millington, D. S.; Rajagopalan, K. V. *J. Biol. Chem.* **1987**, *262*, 16357.
6. Johnson, J. L.; Hainline, B. E.; Rajagopalan, K. V.; Arison, B. H. *J. Biol. Chem.* **1984**, *259*, 5414.
7. Johnson, J. L.; Wuebbens, M. M.; Rajagopalan, K. V. *J. Biol. Chem.* **1989**, *264*, 13440.
8. Soricelli, C. L.; Szalai, V. A.; Burgmayer, S. J. N. *J. Am. Chem. Soc.* **1991**, *113*, 9877.
9. Taylor, E. C.; Ray, P. S.; Darwish, I. S. *J. Am. Chem. Soc.* **1989**, *111*, 7664.
10. Taylor, E. C.; Ray, P. S. *J. Org. Chem.* **1987**, *52*, 3997.
11. Pilato, R. S.; Eriksen, K. A.; Greaney, M. A.; Stiefel, E. I.; Goswami, S.; Kilpatrick, L.; Spiro, T. G.; Taylor, E. C.; Rheingold, A. L. *J. Am. Chem. Soc.* **1991**, *113*, 9372.
12. Schroth, W.; Peschel, J. *Chimia* **1964**, *18*, 171.
13. Schroth, W. *Tetrahedron Lett.* **1965**, 195.
14. Bähr, G.; Schleitzer, G. *Chem. Ber.* **1955**, *88*, 1771.
15. Locke, J.; McLeverty, J. A. *Inorg. Chem.* **1966**, *5*, 1157.
16. Krespan, C. G.; McKusick, B. C. *J. Am. Chem. Soc.* **1961**, *83*, 3438.
17. Schrauzer, G. N.; Mayweg, V. P.; Heinrich, W. *Inorg. Chem.* **1965**, *4*, 1615.

18. Bolinger, C. M.; Rauchfuss, T. B. *Inorg. Chem.* **1982**, *21*, 3947.
19. Boyde, S.; Garner, C. D.; Joule, J. A.; Rowe, D. J. *J. Chem. Soc. Chem. Commun.* **1987**, 800.
20. Brown, G. F.; Stiefel, E. I. *Chem. Comm.* **1970**, 728.
21. Coucouvanis, D.; Toupadakis, A.; Lane, J. D.; Koo, S. M.; Kim, C. G.; Hadjikyriacou, A. *J. Am. Chem. Soc.* **1991**, *113*, 5271.
22. Coucouvanis, D.; Toupadakis, A.; Koo, S.-M.; Hadjikyriacou, A. *Polyhedron* **1989**, *8*, 1705.
23. Gruber, S.; Kilpatrick, L.; Bastian, N. R.; Rajagopalan, K. V.; Spiro, T. G. *J. Am. Chem. Soc.* **1990**, *112*, 8179.
24. Halbert, T. R.; Pan, W.-H.; Stiefel, E. I. *J. Am. Chem. Soc.* **1983**, *105*, 5476.
25. Johnson, J. L.; Rajagopalan, K. V.; Meyer, O. *Arch. Biochem. Biophys.* **1990**, *283*, 542.
26. Kajitani, M.; Ochiai, R.; Kikuchi, R. O., M.; Akiyama, T.; Sugimori, A. *Polyhedron* **1990**, *9*, 1123.
27. Rajan, O. A.; McKenna, M.; Noordik, J.; Haltiwanger, R. C.; Rakowski DuBois, M. *Organometallics* **1984**, *3*, 831.
28. Weberg, R. T.; Haltiwanger, R. C.; Rakowski DuBois, M. *New. J. Chem.* **1988**, *12*, 361.
29. Rowe, D. J.; Garner, C. D.; Joule, J. A. *J. Chem. Soc. Perkin Trans. 1* **1985**, 1907.
30. Nason, A.; Lee, K. Y.; Pan, S. S.; Ketchum, P. A.; Lamberti, A.; DeVries, J. *Proc. Nat. Acad. Sci. U. S.* **1971**, *68*, 3242.
31. Ketchum, P. A.; Downey, R. J. *Biochim. Biophys. Acta* **1975**, 385.
32. Köpf, H. *Angew. Chem. Int. Ed. Engl.* **1969**, *81*, 375.
33. Hurst, D. T. *Chemistry and Biochemistry of Pyrimidines, Purines, Pteridines*; John Wiley and Sons: New York, 1980.
34. All electrochemical experiments were conducted on a BAS100 in the CV mode with [Bu₄N][PF₆] as the supporting electrolyte, a glassy carbon working electrode, and SCE as the reference. The values reported in text are those in CH₂Cl₂.
35. The ZINDO calculations were conducted on a Cache system with the crystallographic input for **13** providing the atomic positions for all the non-hydrogen atoms. The calculations were run with standard INDO/1 input for molybdenum, see Zerner, M.C. *Reviews in Computational Chemistry II*; Lipkowitz, B.; Boyd B., Eds.; VCH Publishers Inc., New York, 1991, p 313.

RECEIVED April 20, 1993

Chapter 7

Strategies for the Synthesis of the Cofactor of the Oxomolybdoenzymes

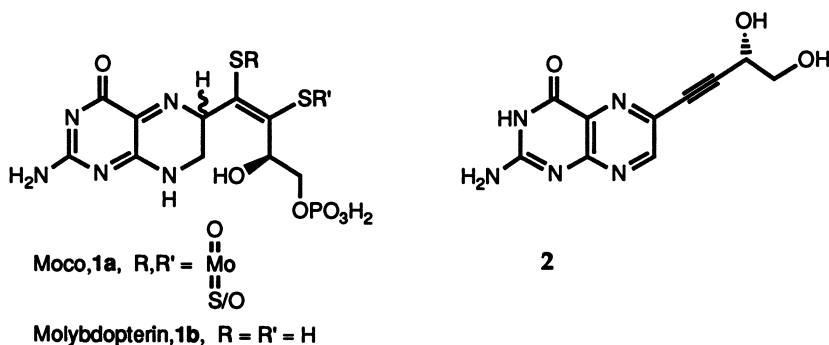
C. D. Garner, E. M. Armstrong, M. J. Ashcroft, M. S. Austerberry, J. H. Birks, D. Collison, A. J. Goodwin, L. Larsen, D. J. Rowe, and J. R. Russell

Department of Chemistry, University of Manchester,
Manchester M13 9PL, England

Strategies for the total synthesis of the cofactor of the oxomolybdoenzymes (Moco) have been developed. Initially, the approaches involve quinoxaline and other aromatic groups in the place of the pteridine; these have led to general routes for the synthesis of complexes of unsymmetrical dithiolenes. The extension of these studies to include pteridines is also described. Electrochemical experiments on $[\text{CpCo}\{\text{S}_2\text{C}_2\text{H}(\text{quinoxalin-2-yl})\}]$, which contains a pyrazine ring with a dithiolene substituent as proposed for Moco, demonstrate how reduction of a metal center may be coupled to the protonation of the pyrazine group. Such cooperativity could confer operational advantages in respect of the two-electron changes catalyzed by Moco.

The concept that a small molybdenum-containing unit might act as a cofactor for some or all of the molybdoenzymes was first suggested by Pateman *et al.* (1) in 1964. As a result of work on a series of mutant cells lacking both nitrate reductase and xanthine oxidase activity, it was proposed that the two enzymes share a common cofactor. Support for this idea came from work by Nason *et al.* (2) who showed that a molybdenum-deficient nitrate reductase from a mutant strain of *Neurospora crassa*, Nit-1, could be reactivated by an acid-denatured extract from any molybdoenzyme. Subsequent studies, principally by Brill *et al.*, achieved the isolation (3) of a cofactor from Component I of nitrogenase, containing iron,

molybdenum, and acid-labile sulfide. This cofactor, *FeMoco*, is capable of reconstituting molybdenum-deficient nitrogenase Component I from the *Azotobacter vinelandii* mutant strain, UW45, but does not reconstitute the nitrate reductase mutant, Nit-1. On the other hand, a cofactor from xanthine oxidase was shown to reactivate the Nit-1 strain, but not the nitrogenase mutant, UW45. Subsequently, activity has been returned to Nit-1 nitrate reductase using cofactor produced from the oxomolybdoenzymes, xanthine oxidase, aldehyde oxidase, sulfite oxidase, and nitrate reductase derived from organisms ranging from *Escherichia coli* to the rat (4). This cofactor is termed *Moco* (see 1a).



Spectroscopic and biochemical studies have established that Moco is the catalytic center of all molybdoenzymes, except nitrogenase. There is now a considerable body of evidence (5-8) which shows that the molybdenum in Moco has sulfur ligands (6,7) and is probably linked *via* an ene-1,2-dithiolate unit (8) on the side-chain of an organic component known as **molybdopterin**. Because Moco and molybdopterin are extremely unstable, neither has been isolated and most of the structural evidence has come from identifications of fully aromatic pteridines, believed to be oxidative degradation products. There is evidence (9) that in Moco itself the pyrazine ring is in a reduced state; early views favored a tetrahydro-level but the most recently reported work (10) suggests that molybdopterin is a dihydropterin, as the quinonoid tautomeric form, 1b, implying partial structure, 1a, for Moco. Other natural, reduced pterins have been identified, for example sepiapterin and congeners, 7,8-dihydropterins, are present in the yellow eye pigment of *Drosophila melanogaster* (11) and of possible relevance to the cofactor function of Moco, 5,6,7,8-tetrahydrobiopterin is the cofactor for monoamine-synthesising monoxygenases (12).

No comment has yet been made on the stereochemistry at the pteridine 6-position in Moco, though a CD study establishing the

absolute configuration at C-6 of 5,6,7,8-tetrahydrobiopterin has been reported (9). The absolute configuration of the side-chain hydroxyl-bearing carbon has been deduced to be that shown in **1**, on the basis of a CD comparison between samples of alkyne, **2**, produced in homochiral form by total synthesis (13), and by degradation of the enzyme, respectively. The structure of molybdopterin is thus seen to comprise a (partially) reduced pterin, carrying at C-6 a highly functionalised C₄-side-chain on which are situated the two sulfur atoms which coordinate the metal.

Recently, the previously homogeneous picture of molybdenum enzymes' cofactor constitution has had to be modified: thus there could be a family of Mocos, having in common the 'western' portion of the molecule, *i.e.* molybdopterin, but linked *via* the phosphate to a particular nucleotide (14).

Nature of the Molybdenum Center in the Oxomolybdoenzymes

X-ray Absorption Spectroscopy (XAS). XAS, particularly the Extended X-ray Absorption Fine Structure (EXAFS) associated with the molybdenum *K*-edge, has played a vital role in defining the nature of the molybdenum centers of the oxomolybdoenzymes (6). Also, these studies have addressed the manner in which these centers respond to changes in the oxidation level of the protein and/or the presence of substrates, substrate analogues, and inhibitors of enzymic activity.

Sulfite Oxidase. The molybdenum *K*-edge EXAFS investigations (15) of sulfite oxidase represent a prototype for such studies of oxomolybdoenzymes. Molybdenum(VI) is coordinated by two oxo-groups at *ca.* 1.70Å, one oxygen (or nitrogen) - and three sulfur-donor ligands at *ca.* 2.06 and 2.42Å, respectively. Molybdenum(V) and (IV) each possess a single oxo-ligand at *ca.* 1.69Å, one oxygen (or nitrogen) - and three sulfur-donor ligands at *ca.* 2.00 and 2.37Å, respectively. Both of the reduced centers have an additional coordination site available and are capable of binding chloride at pH6 in 0.3M KCl.

The minimal chemical interpretation of this information is to consider that a *cis*-dioxomolybdenum(VI) center exists, ligated by the dithiolene group of the molybdopterin (as in **1a**) plus a cysteine from the protein, and possibly an oxygen from the phosphate of the molybdopterin completing the coordination sphere. Reduction of molybdenum(VI) does not affect the sulfur ligation but one oxo-group is lost, presumably due to protonation and the formation of a water molecule or hydroxide ligand. The chloride ion would be expected to bind initially *trans* to the oxo-group but rearrangement to a *cis* site is clearly possible. This pattern of substitution has been well

developed for an oxomolybdenum(V) center interacting with anions (16) and for nitrate the site *cis* to the oxo-group has been shown (17) to fulfill the requirements for a facile redox reaction, transferring an oxygen atom from nitrate to molybdenum. The geometric and electronic conditions for oxygen atom transfer from a *cis*-dioxomolybdenum(VI) center to a suitable substrate are essentially the reverse of these and oxygen atom transfer reactions, wholly compatible with the function of molybdenum centres of the oxomolybdoenzymes, are now well established for several $\text{MoO}_2^{2+}/\text{MoO}^{2+}$ couples (18).

Therefore, it would appear that one functionality of the molybdenum center of Moco is the *direct* transfer of oxygen atoms to, or from, the substrate. However, several sophistications of the possible redox chemistry of Moco, beyond oxygen atom transfer need to be addressed.

Xanthine oxidase. This enzyme exists in two forms, active and desulfo. Molybdenum *K*-edge EXAFS studies (19) have shown that the environment of molybdenum(VI) and (IV) in desulfo xanthine oxidase closely resemble that of the corresponding oxidation state for sulfite oxidase. The principal difference between the molybdenum(VI) center of the oxidized active form, compared with the oxidised desulfo form, is the presence of one sulfide-group (at *ca.* 2.18Å) plus one oxo-group (1a), rather than two oxo-groups.

The molybdenum center of xanthine oxidase is very reactive and both molybdenum *K*-edge and EPR data (7) indicate that this is primarily due to the Mo=S bond. This terminal sulfide group is not retained upon reduction, presumably due to coupled electron addition to the metal center and protonation of the ligand. However, since the oxo-group does remain in reduced xanthine oxidase, an alternative interpretation of the role of the molybdenum center in the oxidation of xanthine is the binding of H^- from C-8-H by the Mo=S group, concomitant with attack by OH^- at C-8 (20).

Investigations (21,22) of the redox properties of xanthine oxidase, at room temperature and as a function of pH, demonstrate a minimal effect of desulfurization on the redox potential of the $\text{Mo}^{\text{VI}}/\text{Mo}^{\text{V}}$ couple. Barber and Siegel (21) have concluded that "the conversion of a terminal sulfur to a terminal oxygen ligand has little effect on the intrinsic electron affinities of the various molybdenum oxidation states". This conclusion is in stark contrast to the redox-potential changes of *ca.* 350-550 mV, on replacement of S by O (= Y) in the series of complexes *cis*- $[\text{MoY}_2(\text{C}_5\text{H}_{10}\text{NO})_2]$ (23). Thus, the inherent differences of the MoOS^{2+} and MoO_2^{2+} centers must be modified by other effects in the enzymes. One possibility is that

reduction of Moco could involve a cooperativity between the molybdenum and the pyrazine ring of the pterin.

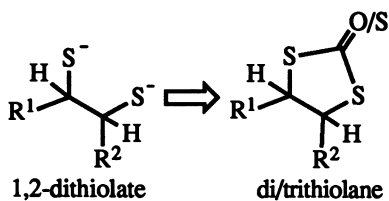
Other Physical Methodologies. EXAFS has provided the only structural information to date concerning the nature of the molybdenum centers in the various oxomolybdoenzymes (6,15,19). The results of protein crystallographic studies are eagerly awaited to establish the structural relationships between the various components of molybdopterin and molybdenum and to view the location of the catalytic center within the overall molecular architecture of the protein. However, the definition of the structure-function relationships, *not least the definition of the electronic structure of the states of Moco involved in the catalytic cycle*, will need the information provided by complementary physical techniques. Resonance Raman spectroscopic studies of oxidized and reduced Moco in DMSO reductase has provided direct support for the postulated dithiolene ligation of the molybdenum (8). EPR spectroscopy has been of immense value in characterizing the molybdenum(V) centers of the oxomolybdoenzymes (7). Furthermore, these paramagnetic states can be probed by MCD spectroscopy (Thomson, A. J. *et al. FEBS Lett.*, in press) and the data presented in Figure 1 clearly demonstrate the potential of this technique for "fingerprinting" molybdenum(V) centers and providing new information concerning their electronic structure.

The interpretation of the data obtained from these and other physical techniques will be greatly aided by the availability of the corresponding information on fully characterized chemical analogues of the natural systems. Given the amalgam of chemical functionalities within Moco, such an approach to the delineation of the structure-function relationships requires the availability of chemical analogues which contain most, if not all, of the constituent groups. Indeed, the total synthesis of Moco would appear necessary to remove uncertainties concerning its structure and the chemical bases of its biological activity.

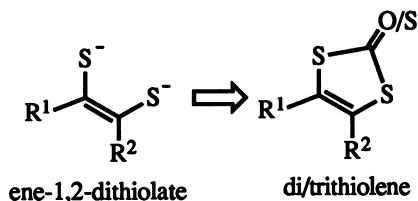
Towards the Synthesis of Molybdopterin

Strategy. In devising a route for the synthesis of Moco we have subdivided the task into distinct and separate objectives. We consider that at a late stage in the synthesis it will be necessary to provide the organic ligand to coordinate molybdenum. When we began our work, the structural postulate for Moco had the metal coordinated by two sulfur atoms forming a *saturated* five-membered ring: thus Goal 1 was a route to a suitably substituted 1,2-dithiolate. Later, it was suggested that the sulfur atoms in Moco may form part of a

dithiolene unit, (β) *i.e.* the metal is coordinated by two sulfurs in an *unsaturated* five-membered ring. Goal 2 was to develop a route to suitably substituted ene-1,2-dithiolates. For these goals (24,25) we envisaged carrying the sulfurs through as cyclic di/trithiolane and di/trithiolene groups, respectively, anticipating that these would be much more stable and that some means for the release of the ligand could be found. Also, it was necessary to devise a synthesis which would allow R^1 and R^2 to be, eventually, a pterin and the phosphorylated dihydroxyethyl side-chain, respectively.

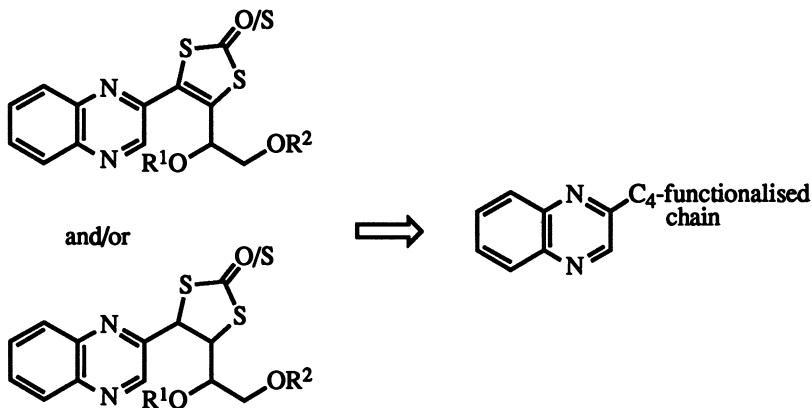


Goal 1



Goal 2

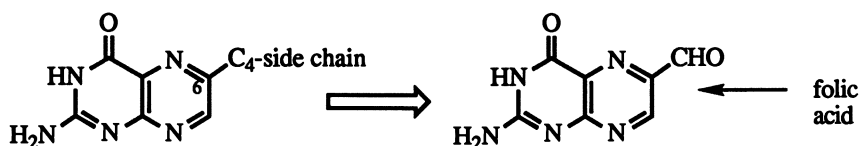
Ene-1,2-dithiolates can be used to prepare metal complexes (26). More importantly, trithiolenes can be made to react directly with $[\text{CpCo}(\eta^4\text{-C}_8\text{H}_{12})]$ to produce dithiolene complexes such as $[\text{CpCo}\{\text{S}_2\text{C}_2\text{H}(\text{quinoxalin-2-yl})\}]$ (*vide infra* (Armstrong, E. A.; Austerberry, M. S.; Garner, C. D.; Joule, J. A. *Heterocycles*, 1993, in press)).



Given the legendary insolubility of pteridines, and that, in terms of enzyme mechanism, co-operativity between metal center and heterocycle probably involves only the pyrazine ring of the pteridine,

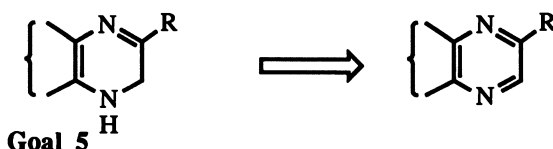
Goal 3 was the evolution (27) of a viable route to models with appropriately functionalised C₄-side-chains attached to the heterocyclic ring of *quinoxaline*.

Goal 4 was the development of regioselective syntheses of pteridines carrying functionalized C₄-side chains at C-6; Wittig chemistry seemed to be the method of choice; though, since this was to be the first occasion on which such chemistry would be used with pteridines, whether the unfavorable solubility properties would allow its successful employment was a concern, which turned out to be unfounded. The obvious starting material was 6-formylpterin, a known degradation product of the readily available folic acid.



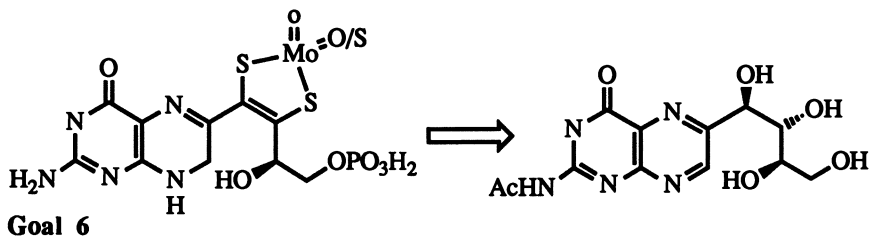
Goal 4

Goal 5, thus far only partially completed, (28) is the establishment of a method for the partial reduction of the pyrazine ring in anticipated synthetic intermediates, to the *dihydro*-oxidation level, now believed (10) to pertain in Moco itself.



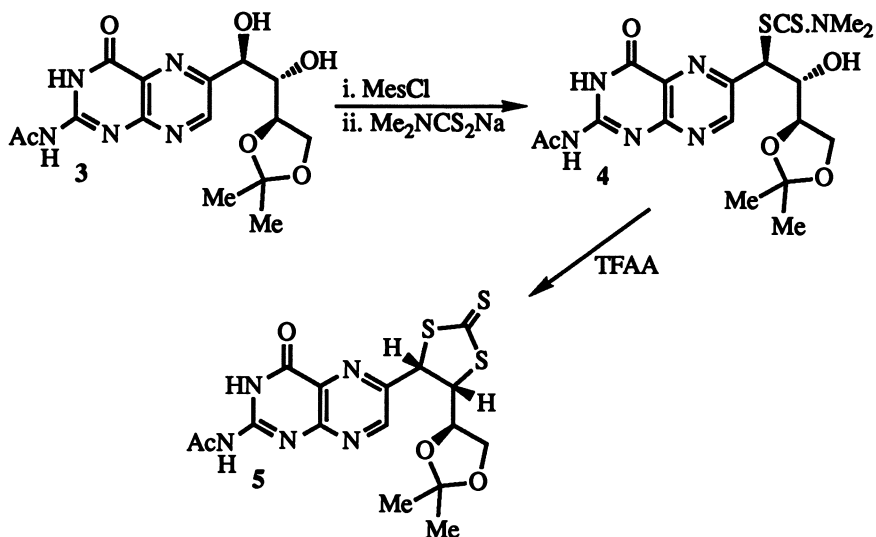
Goal 5

Current work, **Goal 6** (28,29) draws on previous results. This utilises a pteridine-C₄-tetrol obtained *via* a condensation using readily available sucrose and 6-hydroxy-2,4,5-triaminopyrimidine, and is targeted at Moco itself.



Goal 6

In our recent work, the acetal-diol-acetamide **3** has been converted into dimethyldithiocarbamate **4** and this cyclised to trithiolane **5**. It remains to dehydrogenate this to the trithiolene, remove protecting groups and bring the trithiolene to an MoO_2^{2+} (or MoOS^{2+}) center in order to synthesise a close analogue of the structure proposed for Moco (**1a**).



Coupled Proton Electron Transfer Relevant to Moco

Quinoxaline-2,3-dithiolates. We have investigated complexes of quinoxaline-2,3-dithiolate (qdt), especially since some complexes of this ligand undergo reversible protonation of the ligand nitrogen atoms, in addition to the one-electron transfer reactions typical of metal dithiolenes (30-32). This ligand protonation induces changes in the electronic spectra of the complexes, implying that the relative energies of the frontier molecular orbitals alter. The redox properties of the complex should also vary with protonation and thus it should be possible to fine-tune their electrochromic properties by control of the acidity of the medium.

The cyclic voltammetry of $[\text{Mo}(\text{qdt})_3]^{2-}$ (Figure 2) in DMF has been measured, during titration with trifluoroacetic acid (TFA) (32) In aprotic solution two reversible, Nernstian, waves were detected, at $E_2^1 = 0.265$ and -1.28 V (versus SCE), corresponding to the one-electron oxidation and reduction of the complex, respectively. On addition of TFA, the oxidation process shifted to higher potential and became

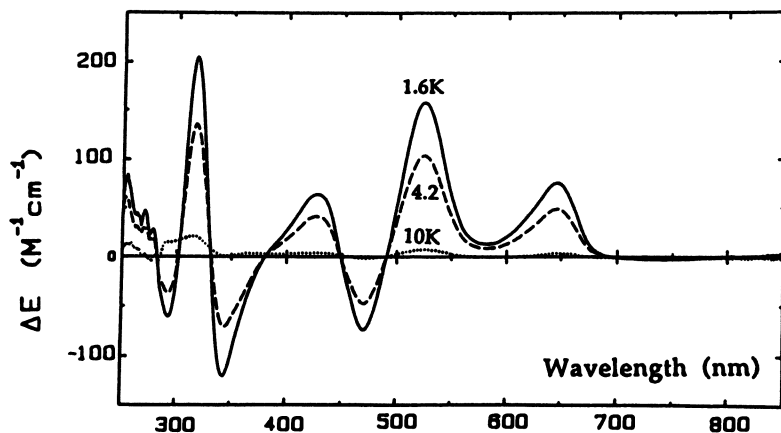


Figure 1. MCD spectra of $[\text{PPh}_4][\text{MoO}(\text{SCH}_2\text{CH}_2\text{S})_2]$ (0.964mM in DMF: CH_2Cl_2 3:20) (Garner, C. D.; Thomson, A. J. *et al.* unpublished data).

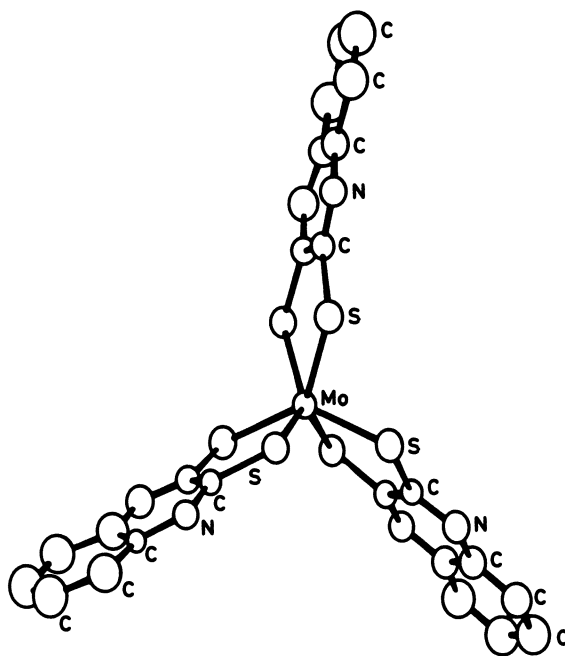


Figure 2. The structure of $[\text{Mo}(\text{qdt})_3]^{2-}$. (Adapted from ref. 31.)

non-Nernstian, with $E_{\frac{1}{2}}$ dependent upon [TFA], while the one-electron reduction of the complex was replaced by a *three*-electron, quasi-reversible wave at $E_{\frac{1}{2}} = ca. -0.35V$ (Figure 3). It is proposed that the latter process corresponds to the addition of one electron and one proton to each ligand, to form a complex containing three independent, coordinated quinoxalinium radicals. Therefore, $[Mo(qdt)_3]^{2-}$ contains two distinct redox-active sites. These are the metal atom and the quinoxaline group of the qdt ligands, with the relative potentials of these sites being controlled by the acidity of the medium. The ligand reduction is a property of the complex: cyclic voltammograms of the free ligand in DMF solution in the presence of TFA do *not* manifest such behaviour. This type of reactivity appears to be a general feature of qdt complexes which are stable with respect to protonation.

[CpCo(S₂C₂H(quinoxalin-2-yl))]. Cyclopentadienylcobaltdithiolene complexes have been prepared previously, [CpCo(S₂C₂(CF₃)₂) (33) and [CpCo(S₂C₂(CN)₂)] (34) have been characterised by X-ray crystallography, and several of these compounds have been shown to undergo a reversible, one-electron reduction (35). Trithiolenes can be reacted with [CpCo(η^4 -C₈H₁₂)] and [CpCo(S₂C₂H(quinoxalin-2-yl))] (Figure 4) has been prepared using the procedure developed by Siedle (36). In this molecule, single crystal X-diffraction reveals that the cobalt-dithiolene metallocycle is essentially planar, as is the quinoxalin-2-yl group and these two planes are mutually disposed at an angle of 10.6°. The NMR chemical shift of the hydrogen of the dithiolene group is at 9.74 p.p.m., consistent with the presence of an aromatic ring current within the CoSCCS ring. This, plus the relative lengths of C-C and C-N bonds, favors the description of the electronic structure shown for A in Scheme 1.

As for other compounds of this type, [CpCo(S₂C₂H(quinoxalin-2-yl))] undergoes a reversible, one-electron reduction. However, the redox behavior becomes dramatically different in the presence of protons (Figure 5). The addition of one equivalent of TFA produces four closely spaced reduction peaks; the cathodic peak positions at 100 mVs⁻¹ are : -330 (A), -560 (B), -660 (Q) and -830(C) mV (versus SCE). Q corresponds to reduction of the parent compound. The two processes at less negative potential are assigned to the two singly protonated forms of the parent molecule (A and B) and the particular processes have been suggested by analogy with the behaviour of the pyridin-2'-yl and -3'-yl derivatives. The reduction at -830mV is suggested to involve further electron and proton addition to produce C, which can be considered to involve (at least) two resonance forms. These

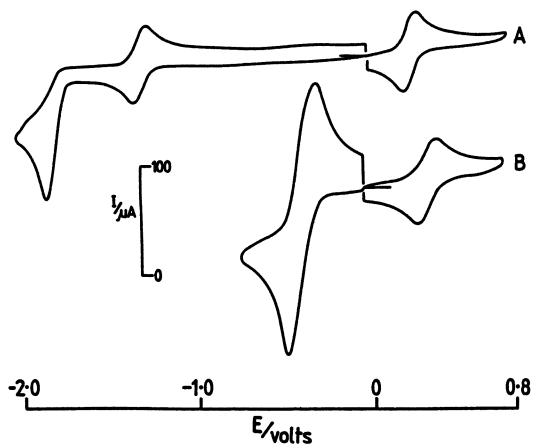


Figure 3. Cyclic voltammograms recorded for $[\text{PPh}_4]_2[\text{Mo}(\text{qdt})_3]$ (2mM) in DMF during titration with TFA at: $[\text{TFA}] = 0$, A; $[\text{TFA}] = 20\text{mM}$, B. (Adapted from ref. 32.)

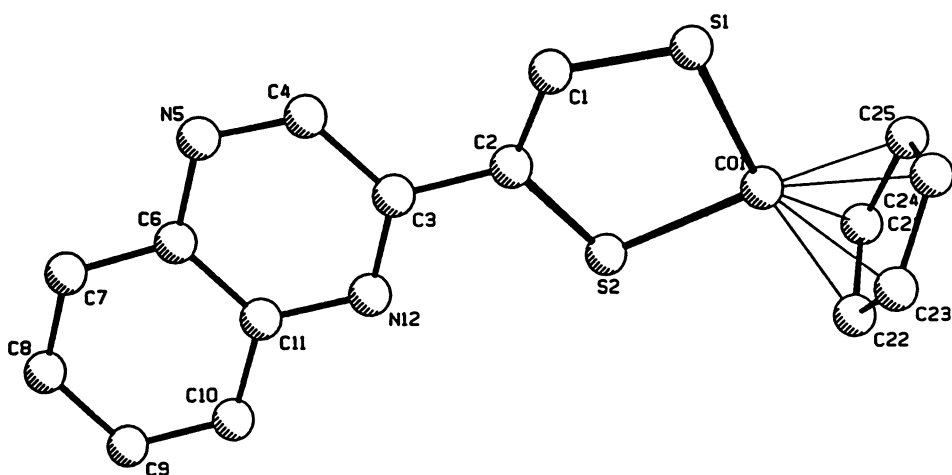
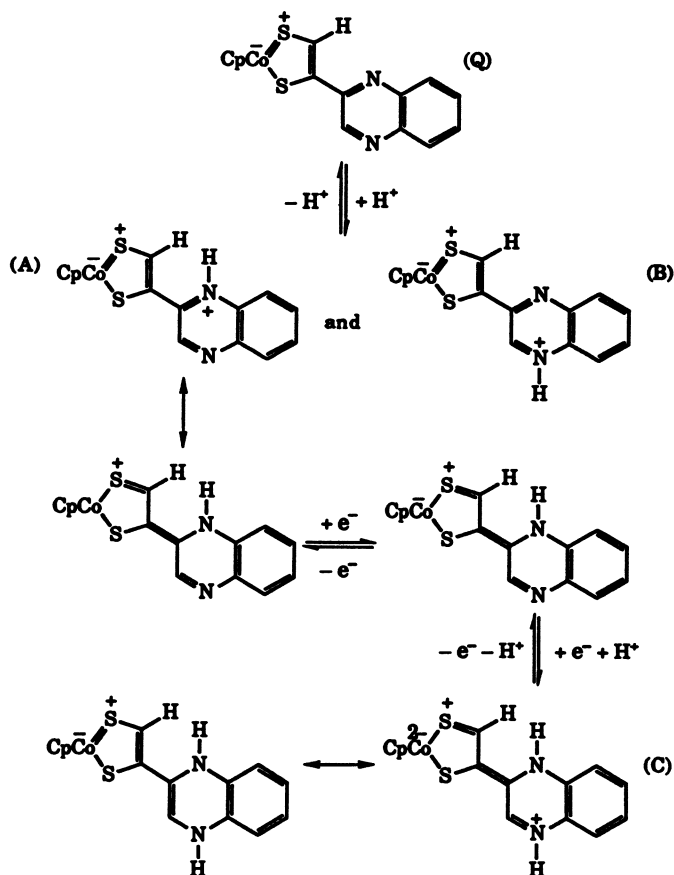


Figure 4. Structure of $[\text{CpCo}(\text{S}_2\text{C}_2\text{H}(\text{quinoxalin-2-yl}))]$.



Scheme 1. The suggested sequence of protonation and reduction events for $[CpCo(S_2C_2H(quinoxalin-2-yl))]$ in the electrochemical cell.

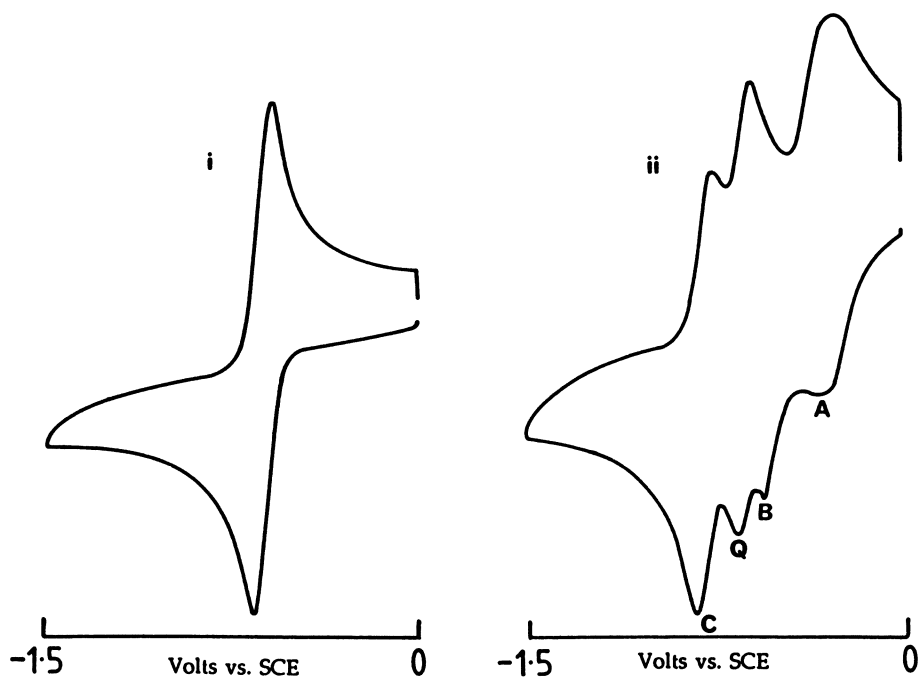


Figure 5. The cyclic voltammogram of $[\text{CpCo}(\text{S}_2\text{C}_2\text{H}(\text{quinoxalin-2-yl}))]$ in MeCN containing $[\text{NBu}_4][\text{BF}_4]$ (0.2M) in the presence of: (i) 0 and (ii) 1 equivalent of TFA.

differ in the extent of the reduction of the metal *versus* the pyrazine ring; at one extreme the overall $2e^-/2H^+$ addition to $[CpCo(S_2C_2H(\text{quinoxalin-2-yl}))]$ can be represented as the reduction of the fully oxidized pyrazine ring to its dihydro-form, leaving the metal center unchanged.

Conclusions

The combination of spectroscopic studies of the molybdenum centers of the oxomolybdoenzymes, coupled with the information derived from molecules which serve as analogues of the molybdenum or ligand functionalities, support the structure proposed for Moco (1a). An intriguing aspect of the properties of this cofactor is the extent to which the molybdenum and the pterin jointly participate in the redox changes of this center. Not only may the extent and nature of this cooperation vary from enzyme to enzyme but also it may be meaningless to attempt to separate the metal and ligand redox contributions (see the bottom line of Scheme 1). Also, such behavior provides an attractive mechanism for modulating the redox potential of Moco by a protein *via* a control of the state and extent of protonation of the pyrazine ring *and* the stabilisation of particular tautomers (10) of the partially reduced forms of the pteridine.

Acknowledgements

We are grateful for the financial support provided by the Science and Engineering Research Council and The Royal Society. Thanks are due to Professor A. J. Thomson and Ms. J. A. Farrar for recording the MCD spectrum shown herein and to Dr. S. Boyde for electrochemical studies.

Literature Cited

- (1) Pateman, J. A.; Cove, D. J.; Rever, B. M.; Roberts, D. B. *Nature*, **1964**, *201*, 58-60.
- (2) Ketchum, P. A.; Cambrier, H. Y.; Frazier, W. A.; Madansky, C. H.; Nason, A. *Proc. Natl. Acad. Sci. USA*, **1970**, *66*, 1016-1023; Nason, A.; Lee, K.Y.; Pan, S. S.; Ketchum, P. A.; Lamberti, A.; Devries, J. *ibid*; **1971**, *68*, 3242-3246.
- (3) Shah, V. K.; Brill, W. J. *Proc. Natl. Acad. Sci. USA*, **1977**, *74*, 3249-3253; Pienkos, P. T.; Shah, V. K.; Brill, W. J. *ibid*, 5468-5471.
- (4) Johnson, J. L., in *Molybdenum and Molybdenyum Containing Enzymes*, Coughlan, M. P., Ed.; Pergamon Press, Oxford, **1980**, pp. 345-383.

- (5) Johnson, J. L.; Hainline, B. E.; Rajagopalan, K. V.; Arison, B. H. *J. Biol. Chem.*, **1984**, *259*, 5414-5422; Cramer, S. P.; Solomonson, L. P.; Adams, M. W. W.; Mortensen, L. E. *J. Am. Chem. Soc.*, **1984**, *106*, 1467-1471; Solomonson, L. P.; Barber, M. J.; Howard, W. D.; Johnson, J. L.; Rajagopalan, K. V. *J. Biol. Chem.*, **1984**, *259*, 849-853; Kramer, S.; Johnson, J. L.; Ribeiro, A. A.; Millington, D. S.; Rajagopalan, K. V. *J. Biol. Chem.*, **1987**, *34*, 16357-16363; Johnson, J. L.; Wuebbens, M. M.; Rajagopalan, K. V. *J. Biol. Chem.*, **1989**, *264*, 13440-13447.
- (6) Cramer, S. P. *Advances in Inorganic and Bioinorganic Mechanisms*, Vol 2; Sykes, A. G., Ed.; Academic Press, London **1983**, pp 259-316; Hedman, B.; Hodgson, K. O.; Garner, C. D. in *Synchrotron Radiation and Biophysics*; Hasnain, S. S., Ed.; Ellis Horwood, Chichester, **1990**, 43-62.
- (7) Bray, R. C. *Quart. Rev. Biophys.* **1988**, *21*, 299-329.
- (8) Gruber, S.; Kilpatrick, L. T.; Bastian, N. R.; Rajagopalan, K. V.; Spiro, T. G. *J. Am. Chem. Soc.*, **1990**, *112*, 8179-8180.
- (9) Rajagopalan, K. V.; Kramer, S.; Gardlik, S. *Polyhedron*, **1986**, *5*, 573-576.
- (10) Gardlik, S.; Rajagopalan, K. V. *J. Biol. Chem.*, **1990**, *265*, 13047-13054.
- (11) Baur, R.; Sugimoto, T.; Pfeleiderer, W. *Chem. Lett.*, **1984**, 1025-1028; *idem*, *Helv. Chim. Acta*, **1988**, *71*, 531-534.
- (12) Matura, S.; Sugimoto, T.; Murata, S.; Sugawara, Y.; Iwasaki, H. *J. Biochem.*, **1985**, *98*, 1341-1348; Dix, J. A.; Benkovic, S. J. *Acc. Chem. Res.* **1988**, *21*, 101-107.
- (13) Taylor, E. C.; Goswami, S. *Tetrahedron Lett.* **1991**, *32*, 7357-7360.
- (14) Kruger, B.; Meyer, O. *Eur. J. Biochem.*, **1986**, *157*, 121-128; Johnson, J. L.; Rajagopalan, K. V.; Meyer, O. *Arch. Biochem. Biophys.*, **1990**, *283*, 542-545; Johnson, J. L.; Bastian, N. R.; Rajagopalan, K. V. *Proc. Natl. Acad. Sci.*, **1990**, *87*, 3190-3194.
- (15) George, G. N.; Kipke, C. A.; Prince, R. C.; Sunde, R. A.; Enemark, J. H.; Cramer, S. P. *Biochemistry*, **1989**, *28*, 5075-5080.
- (16) Garner, C. D.; Hyde, M. R.; Mabbs, F. E.; Routledge, V. I. *J. Chem. Soc., Malton Trans.* **1975**, 1175-1180; *idem*, *ibid*, 1180-1185.
- (17) Garner, C. D.; Hyde, M. R.; Mabbs, F. E.; Routledge, V. I. *Nature*, **1974**, *252*, 579-580.
- (18) Holm, R. H.; Berg, J. M. *Acc. Chem. Res.* **1986**, *19*, 363-370.
- (19) Cramer, S. P.; Hille, R. *J. Am. Chem. Soc.* **1985**, *107*, 8164-8169; Turner, N. A.; Bray, R. C.; Diakun, G. P. *Biochem. J.* **1989**, *260*, 563-571.
- (20) Wootton, J. C.; Nicholson, R. E.; Cock, J. M.; Walters, D. E.; Burke, J. F.; Doyle, W. A.; Bray, R. C. *Biochim. Biophys. Acta*, **1991**, *1057*, 157-185.

- (21) Barber, M. J.; Siegel, L. M. *Biochemistry*, **1982**, *21*, 1638-1647.
- (22) Porras, A. G.; Palmer, G. J. *Biol. Chem.*, **1982**, *257*, 11617-11626.
- (23) Bristow, S.; Garner, C. D.; Pickett, C. J. *J. Chem. Soc., Dalton Trans.*, **1984**, 1617-1619.
- (24) Rowe, D. J.; Garner, C. D.; Joule, J. A. *J. Chem. Soc., Perkin Trans.1*, **1989**, 1907-1910.
- (25) Larsen, L.; Garner, C. D.; Joule, J. A. *J. Chem. Soc., Perkin Trans.1*, **1989**, 2311-2316.
- (26) Boyde, S.; Garner, C. D.; Joule, J. A.; Rowe, D. J., *J. Chem. Soc., Perkin Trans.1*, **1987**, 800-801.
- (27) Larsen, L.; Rowe, D. J.; Garner, C. D.; Joule, J. A. *J. Chem. Soc., Perkin Trans.1*, **1989**, 2317-2327.
- (28) Russell, J. R.; Garner, C. D.; Joule, J. A. *J. Chem. Soc., Perkin Trans.1*, **1992**, 1245-1249; Russell, J. R.; Garner, C. D.; Joule, J. A. *Acta Crystallogr.*, **1992**, *C48*, 2075-2078.
- (29) Russell, J. R.; Garner, C. D.; Joule, J. A. *Tetrahedron Lett.*, **1992**, *33*, 3371-3374; Russell, J. R.; Garner, C. D.; Joule, J. A. *Synlett*, **1992**, 711-712.
- (30) Pignedoli, A.; Peyronel, G.; Malavasi, W. J. *Inorg Nucl. Chem.* **1976**, *38*, 1963-1966; Theriot, L. J.; Ganguli, K. K.; Kavarnos, S.; Bernal, I. J. *Inorg. Nucl. Chem.* **1969**, *31*, 3133-3140.
- (31) Boyde, S.; Garner, C. D.; Enemark, J. H.; Ortega, R. B. *J. Chem. Soc., Dalton Trans.* **1987**, 297-302; Boyde, S.; Garner, C. D.; Enemark, J. H.; Bruck, M. A.; Kristofski, J. G. *ibid.* **1987**, 2267-2271.
- (32) Boyde, S.; Garner, C. D. *J. Chem. Soc., Dalton Trans.* **1991**, 713-716.
- (33) Baird, H. W.; White, B. M. *J. Am. Chem. Soc.* **1966**, *88*, 4744-4745.
- (34) Churchill, M. R.; Kennessey, J. P. *Inorg. Chem.* **1968**, *7*, 1123-1129.
- (35) Kajitani, M.; Akiyama, T.; Sugimori, A.; Hirakata, K.; Hushino, Y.; Satsu, Y.; Satô, G. P.; Shimizu, K.; Kaise, M.; Nishihara, J. *Electroanal. Chem. Interfacial Electrochem.* **1988**, 421-428.
- (36) Siedle, A. J. *Organomet. Chem.* **1976**, *120*, 369-374.

RECEIVED March 8, 1993

Chapter 8

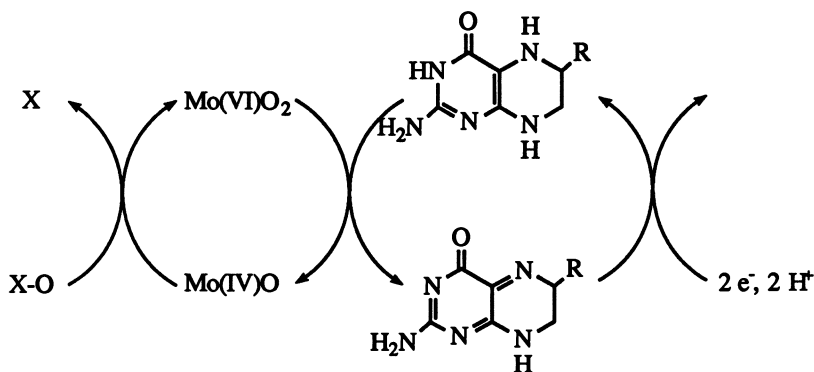
Molybdenum Complexes of Reduced Pterins

Sharon J. Nieter Burgmayer, Kristin Everett, and Laura Bostick

Department of Chemistry, Bryn Mawr College, Bryn Mawr, PA 19010

The reactions of molybdenum(VI) complexes and tetrahydropterins is described. The products of these reactions are formulated as Mo(VI)-tetrahydropterin complexes, *not* the expected Mo(IV)-dihydropterin products. This formulation is supported by an X-ray crystal structure and ligand substitution experiments. Tetrahydropterin coordinates as an anionic ligand to Mo(VI) through deprotonated pyrazine N5 and carbonyl O4. These complexes are intensely colored, a physical property consistent with considerable electronic delocalization over the pterin and Mo-oxo core. The tetrahydropterin in these Mo(VI) complexes is oxidized by oxygen to 7,8-dihydropterin.

The function of the pterin component, *molybdopterin*, of the molybdenum cofactor from the oxo-molybdoenzymes is unknown (1). A look at the roles of reduced pterins in other enzymes, c.f., phenylalanine hydroxylase, suggests a purpose for molybdopterin. Other pterin-dependent enzymes use the redox capability of pterin for substrate transformation (2). Hence, it is reasonable to anticipate a redox role for molybdopterin. A simple example of how pterin could be involved in catalytic substrate reduction is below. The reducible substrate XO oxidizes Mo(IV) to Mo(VI) and tetrahydropterin (H₄pterin) is used to regenerate Mo(IV).



The possibility that the above reaction could operate in Mo-co motivated our inquiry into the reactions of oxidized Mo(VI) complexes with reduced, tetrahydropterins. To date there is no detailed understanding of how transition metals react with semi- and fully reduced pterins.

Redox Reactions of Tetrahydropterins

Tetrahydropterin is related to its oxidized parent compound, pterin, by a four electron/four proton oxidation (3). This four electron oxidation can occur in two discrete steps via the semi-reduced dihydropterin, which can exist in several isomeric forms. Figure 1 illustrates this process for the parent pterin 6,7-dimethylpterin (DMP) and indicates the abbreviations used for the corresponding redox partners.

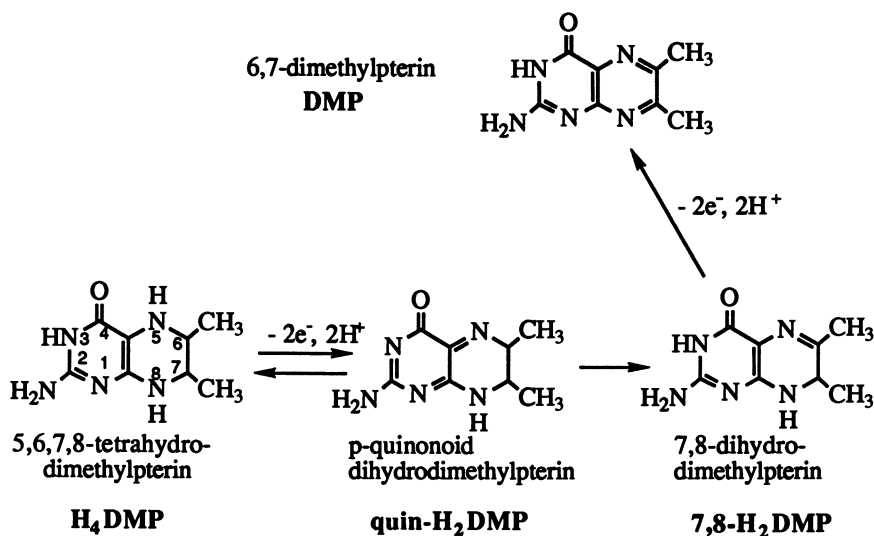


Figure 1. Oxidation Products of 5,6,7,8-Tetrahydro-6,7-Dimethylpterin.

Electrochemical and enzymatic studies have shown that initial oxidation of H₄DMP produces a semi-reduced quinonoid dihydropterin (4-5). Figure 1 shows one of several possible tautomeric structures for quin-H₂DMP. Quinonoid dihydropterin is the kinetic product but it is thermally unstable and rearranges to the 7,8-dihydro isomer. A second, considerably slower oxidation of 7,8-H₂DMP yields fully oxidized DMP. Of the four species, only H₄DMP, 7,8-H₂DMP and DMP can be chemically synthesized and isolated (6). Quin-H₂DMP has been observed spectroscopically using ¹H and ¹³C NMR and ultraviolet spectroscopy (7).

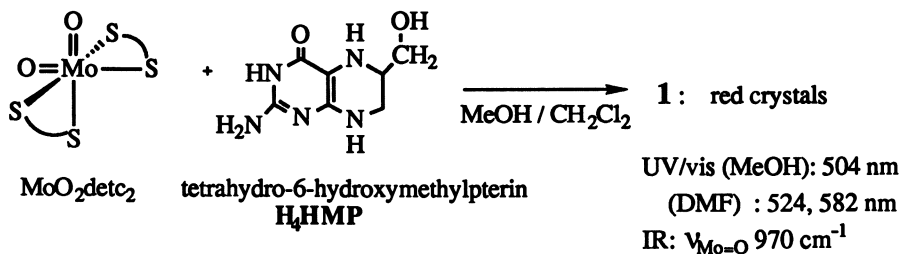
Tetrahydropterin Reactions of Molybdenum Dioxo Bis(dithiocarbamate) Complexes

Molybdenum dithiocarbamate complexes have been intensely studied because they demonstrate reactivity that models aspects of Mo-co as well as the cofactor of nitrogenase, FeMo-co (8-10). In particular, reversible oxo-transfer reactions are features of the Mo-dtc system that mimic the Mo-co enzyme counterparts (11). These reactions are typified by reduction of cis-dioxo-Mo(VI) complexes to mono-

oxo Mo(IV) products. MoO₂detc₂ reduction is facilitated by the four sulfur atoms in the inner coordination sphere as compared to reductions of complexes having oxygen or nitrogen donor atoms from ancillary ligands. For this reason we chose MoO₂detc₂ for initial experiments with tetrahydropterins.

Reaction of MoO₂detc₂ and H₄DMP. Addition of H₄DMP to MoO₂detc₂ caused an immediate solution color change to magenta, observed spectroscopically at 504 nm. Since the known reduction products of MoO₂detc₂, i.e., Mo(IV)Odetc₂ and dimeric Mo(V)₂O₃detc₄, both absorb near 500 nm, it appeared that a redox reaction had occurred. Repeating this reaction as a titration showed that the stoichiometry for formation of the 500 nm species was 1:1 in Mo:H₄DMP. This titration suggested that reasonable reaction products were Mo(IV)Odetc₂ and a dihydropterin. ¹H NMR was used to verify the fate of the H₄DMP. To our surprise, the NMR spectrum of the reaction mixture (Figure 2) did not show the appearance of 7,8-H₂DMP but instead two double quartet signals at 5.7 and 4.3 ppm. H₄DMP protons H6 and H7 give double quartet signals but the large downfield chemical shifts observed from the reaction product were characteristic of quinonoid dihydropterin. Unlike previous reports wherein quin-H₂DMP demonstrated only fleeting stability at room temperature, the new species generated in our reaction was stable for days. The likely explanation for this unusual stability was that the quin-H₂DMP was coordinated to Mo(IV). The most probable metal binding sites would be the carbonyl O4 and the pyrazine ring nitrogen N5. Coordination at this site would also explain the larger downfield shift (>2.00 ppm) of H6 relative to H7. When this new species was generated in the presence of d⁶-DMSO, the double quartet signals disappeared as resonances due to 7,8-dihydropterin grew in. This observation was interpreted as the dissociation of the coordinated quin-H₂DMP due to DMSO oxidation of Mo(IV) to Mo(VI) followed by its rearrangement to the more stable dihydropterin isomer (12). Unfortunately, when the reaction scale was increased to allow the isolation and detailed characterization of this intriguing product, the resultant dark purple solids were insoluble and defied purification.

A different tetrahydropterin, 6-hydroxymethylpterin, gave better results in synthetic preparations. Red crystals isolated in 60% yield were obtained from the reaction below. The reaction progress was marked by the increase in absorbance at 504 nm as observed in the reaction between H₄DMP and MoO₂detc₂. The ¹H NMR spectrum of the product indicated that the isolated product contained a coordinated reduced pterin, clearly shown by the downfield signature resonances for H6 and H7. Integration of the spectrum revealed a 1:1 ratio of HMP to detc ligand.



This result was verified by microanalysis on crystalline material and this data yielded an empirical formula of MoO(detc)(H₂HMP)Cl₂ for **1**. Chloride in the product is introduced into the reaction system via the H₄HMP reagent, isolated as a hydrochloride salt (13). The $\nu_{\text{Mo-O}}$ at 970 cm^{-1} in the infrared spectrum was appropriate for a Mo(IV)-mono-oxo complex. Conductivity measurements made on

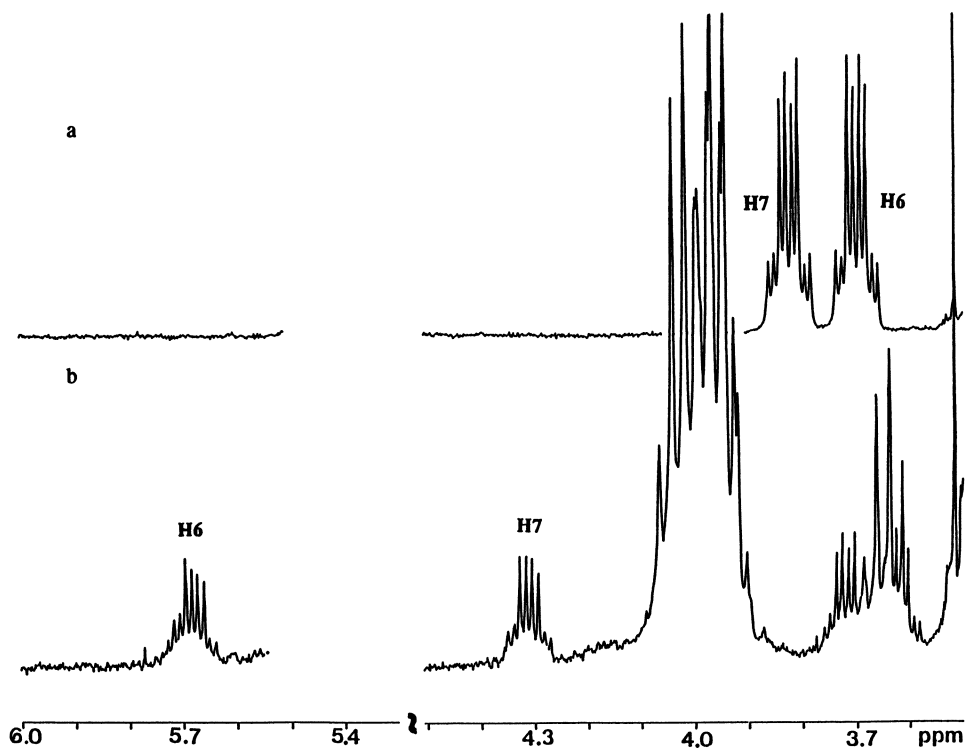
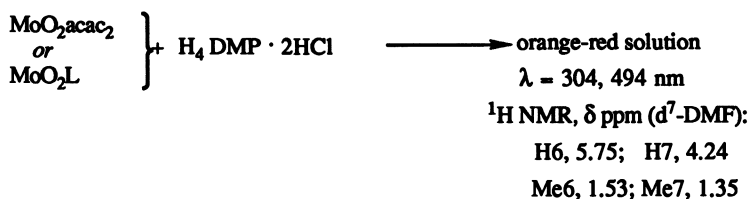


Figure 2. a) ^1H NMR spectra of H_4DMP in $\text{d}_4\text{-MeOH}$. b) ^1H NMR spectra of the reaction mixture of H_4DMP and $\text{MoO}_2\text{detc}_2$ in $\text{d}_4\text{-MeOH}/\text{CDCl}_3$

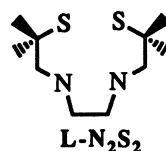
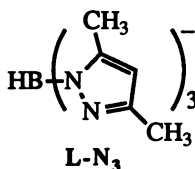
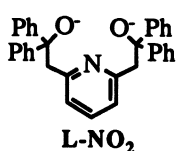
methanolic and dimethylformamide solutions of **1** first indicated that it demonstrated different behavior in these two solvents. **1** behaved as a 1:1 salt in methanol whereas in dimethylformamide, **1** appeared to be a non-electrolyte. Different electronic spectral features of **1** dissolved in MeOH compared to DMF solutions also offered evidence of solvent dependent behavior.

Tetrahydropterin Reactions of Other Mo(VI) Complexes

The ability of tetrahydropterins to react with molybdenum dioxo complexes having different inner coordination spheres was investigated. A variety of ancillary ligands



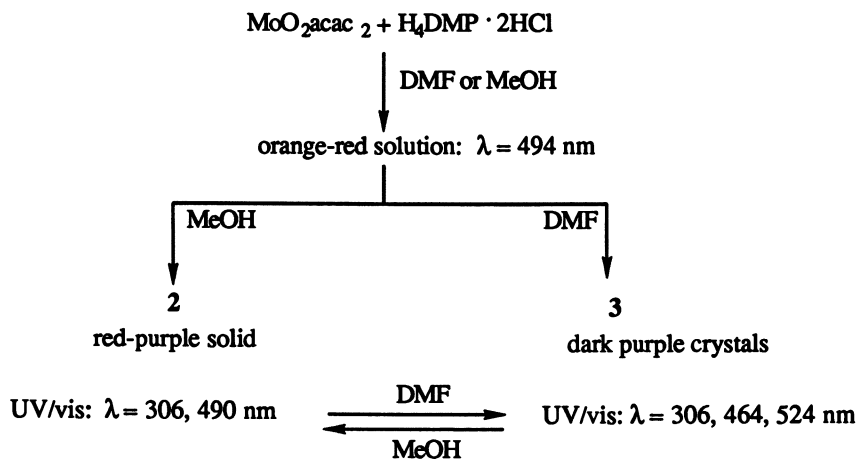
L =



donating sulfur, oxygen or nitrogen donor atoms were used to prepare Mo-dioxo complexes and these were allowed to react with H₄DMP. Using UV/visible and ¹H NMR spectroscopy to monitor the reaction, the same spectral changes were observed in each case. The reaction solution, initially yellow or yellow-orange, became an orange-red color due to the growth of an absorbance at 490 nm. When reactions were performed in DMF, one set of resonances corresponding to the now familiar H6 and H7 signals of the coordinated pterin appeared in the ¹H NMR spectra. When reactions were performed in methanol, multiple sets of H6, H7 signals developed. Because all of these reactions produced the same species, it became clear that the ancillary ligand L was dissociating, a result likely due to the HCl present in the H₄DMP. This hypothesis was confirmed by identifying the free, uncoordinated ligand in the NMR spectra. The rates of reaction, monitored spectroscopically, varied substantially with the nature of the ancillary ligand and suggested that ancillary ligand dissociation preceded formation of the product absorbing at 490nm. For example, the reaction using MoO₂acac₂ was complete after four hours whereas the reaction using MoO₂(L-NO₂) and MoO₂ssp required 17 hours and four days, respectively. The identity of this product was revealed from further studies using MoO₂acac₂, the fastest reacting Mo(VI) complex.

The identity of the Mo-Pterin Product from MoO₂L Reactions. Reactions of MoO₂acac₂ and either H₄DMP or H₄HMP were carried out in both methanol and dimethylformamide solvents. Precipitated products from these reactions gave IR spectra where the primary features are $\nu_{\text{Mo=O}}$ 960 and $\nu_{\text{C=O, C=N}}$ 1660, 1590 cm⁻¹. In contrast, UV/vis spectroscopy indicated the isolated compounds were not identical but interconverted as depicted in the scheme below. The UV

absorbance at 306 nm in complexes 2 and 3 could be assigned to quin-H₂DMP in accordance with previous assignments.



The microanalysis of 3 indicated the empirical formula $\text{MoOCl}(\text{H}_2\text{DMP})(\text{DMF})_2$ but a subsequent x-ray crystal structure determination of 3 showed its true dimeric nature (14). Figure 3 provides two views of the dimer; one illustrating the atomic labeling scheme and the second side view illustrating the half-chair conformation of a reduced pterin. A crystallographic C2 axis bisects the Mo-Mo vector. Figure 4 is a schematic of the structure showing the bond distances and angles in one dimer. This structure is one of the first to demonstrate the ability of a reduced pterin to coordinate to a metal and it is important in that regard (15). An analysis of the structural parameters leads to the conclusion that *this molecule is a Mo(VI) dimer, not Mo(IV), and the reduced pterin is in the tetrahydro-, not quinonoid dihydro-, reduced state*. The key data supporting this formulation are the following. The Mo_2O_4 core is common in Mo(V) dimers and is observed less frequently in Mo(VI) complexes. The long Mo-Mo separation, an indication of no Mo-Mo bond, is appropriate only for the d^0 Mo(VI) oxidation state. Having determined this, the $\text{Mo}_2\text{O}_4^{4+}$ core requires four anionic ligands to generate this neutral complex. This requires that the pterin serves as a deprotonated, anionic ligand at each Mo atom in addition to the chloride and oxide ligands. Unlike other anionic pterin ligands where the site of deprotonation is the amide proton on N3, the short C=O distance in this dimer and long Mo-O bond indicates this proton is intact. This amide proton can, in fact be observed in the ¹H NMR spectrum at 9.4 ppm. A short Mo-N5 distance, 2.03 Å, and the approximately 120° angles about N5 suggest that N5 is a deprotonated, imide nitrogen donating to Mo. The surprising result of this structure analysis is that the appropriate molecular formula of 3 is $\text{Mo}_2\text{O}_4\text{Cl}_2(\text{H}_4\text{DMP})_2 \cdot 4\text{DMF}$. The C-C and C-N distances within the pterin ligand are of little aid in verifying the reduction level of the pterin since these values indicate considerable delocalization, rather than the easily identifiable localized bond distribution of tetrahydro- and dihydropterin structures. Additional evidence corroborating a tetrahydropterin assignment in $\text{Mo}_2\text{O}_4\text{Cl}_2(\text{H}_4\text{DMP})_2$ comes from further reactivity studies.

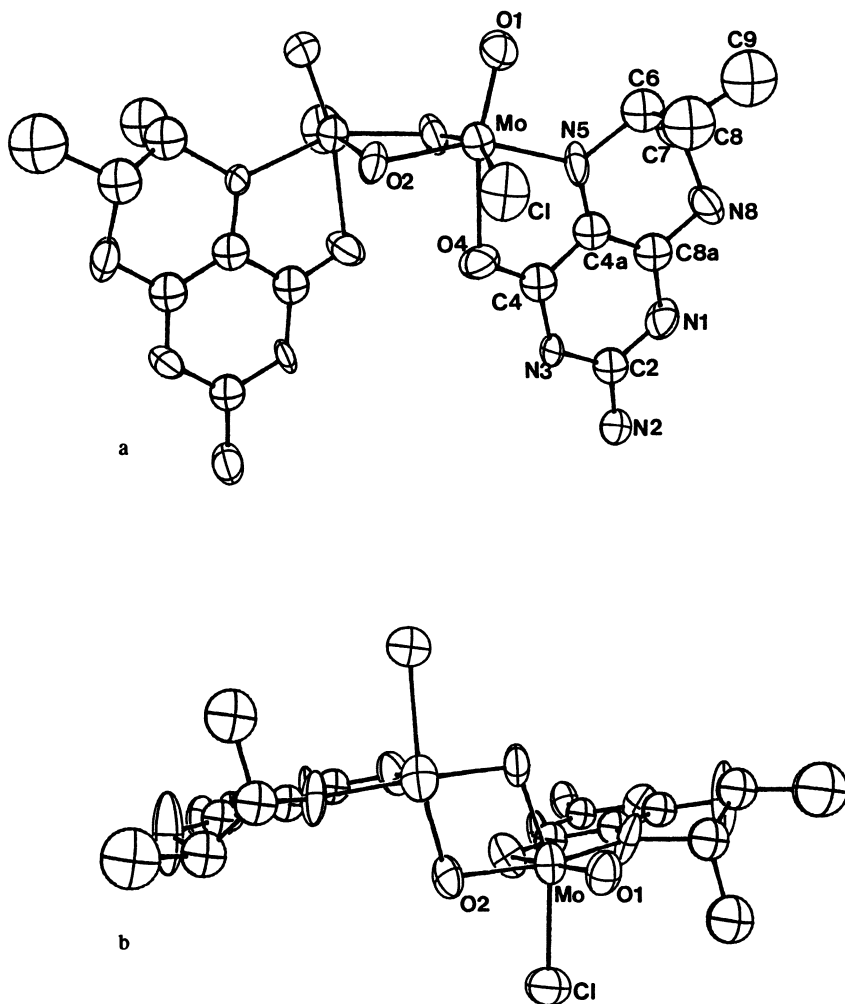


Figure 3. (a) Ortep drawing of one unique dimer showing the atomic labelling scheme. (b) A rotated view of the dimer in (a).

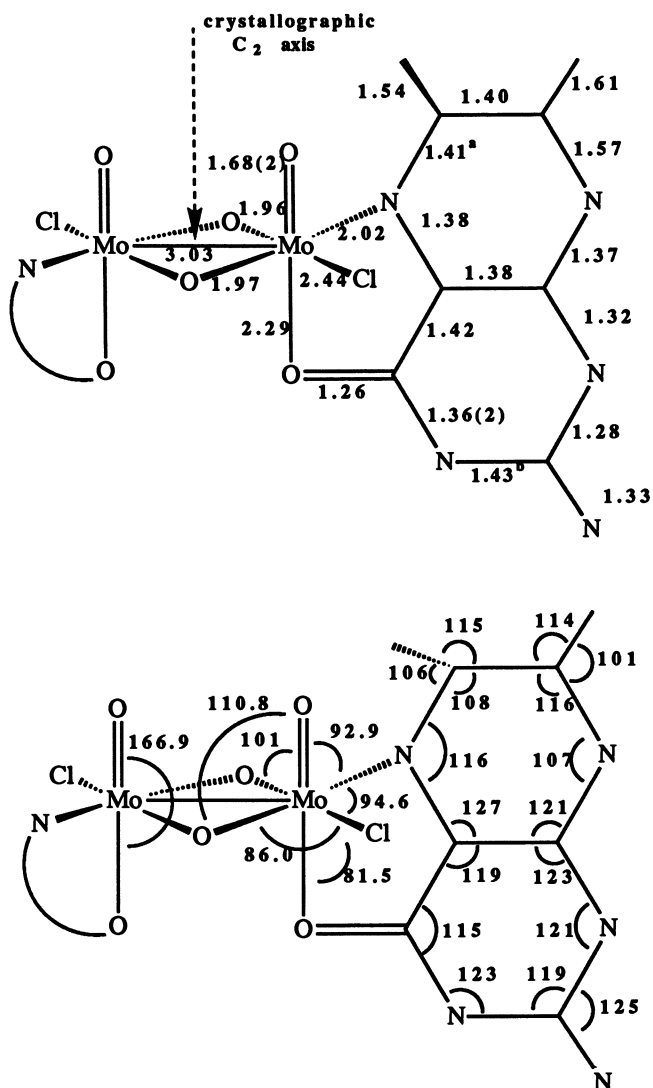


Figure 4. Average bond distances and angles in 3. The bond distances vary ± 0.02 Å in the two independent dimers and the angles vary ± 2 deg with the following exceptions: a) this distance is 1.55 Å in the other dimer, and b) this distance is 1.32 Å in the other dimer. The esd's in the bond distances is .03 and 2 deg in the angles.

Proof for Tetrahydropterin Complexes of Molybdenum(VI)

Ligand substitution experiments confirmed the tetrahydropterin formulation of **3**. Hydroxyquinoline (HQ) was chosen to displace the reduced pterin ligand because it has a similar binding site and because its ionizable proton could aid dissociation of reduced DMP. The identity of the dissociated reduced pterin was revealed using ^1H NMR since this technique can easily distinguish H_4DMP and 7,8- H_2DMP . 7,8- H_2DMP is the expected pterin product from the rearrangement of dissociated quin- H_2DMP ligand, whereas H_4DMP is expected if the coordinated pterin is an anionic H_4DMP ligand. Figure 5 shows the ^1H NMR spectrum resulting from addition of HQ to **3** after 4 hours. The results of this experiment are understood by recognizing that either chloride or the reduced DMP can be substituted by HQ. The NMR spectrum clearly shows free H_4DMP (signals marked 'b') but also that a new DMP species is formed (signals marked 'c'). Over the first 24 hours, H_4DMP and the new species increases in concentration at approximately equal rates. There is *no* evidence of 7,8- H_2DMP . The results indicate the coordinated ligand is H_4DMP . Furthermore, the slow substitution of H_4DMP by HQ suggest that this pterin is a reasonably good chelate. The above HQ substitution experiment repeated using compound **1** of empirical formula $\text{MoO}(\text{detc})(\text{H}_x\text{HMP})\text{Cl}_2$ gave the same results: resonances from free H_4HMP as well as from a different H_4DMP complex were observed in the ^1H NMR. Dithiocarbamate and H_4HMP are both substituted by HQ in the ratio of 1 to 5, respectively.

A second set of experiments provided corroborating evidence for the Mo(VI) / H_4pterin formulation in compounds **1** and **3**. DCl added to these compounds liberated free H_4pterin , the *only* pterin identified by NMR.

Spectral Properties of the New Mo(VI)- H_4pterin Complexes

Certainly the brilliant purple color of these new compounds influenced their early, incorrect assignment as $\text{O}=\text{Mo}(\text{IV})(\text{quin}-\text{H}_2\text{pterin})$ complexes. Having proved their identity by the above decomposition reactions, the extraordinary spectroscopic properties demanded an explanation.

Table I lists the electronic and infrared absorptions. The solvent-dependent

Table I. Spectral Properties and Empirical Formulae of Complexes 1-3

compound	UV/vis λ, nm ($\epsilon, \text{M}^{-1}\text{cm}^{-1}$)	infrared $\nu_{\text{Mo}=\text{O}}, \text{cm}^{-1}$	empirical formula
1	304; 490 (16,000) ^a	960	$\text{MoO}_2\text{Cl}_2(\text{H}_4\text{DMP})\cdot 2\text{MeOH}$
2	304; 464 (9310) ^b 524 (9500)	962	$\text{MoO}_2\text{Cl}(\text{H}_4\text{DMP})\cdot 2\text{DMF}$
3	304; 504 (13,900) ^a 304; 522 (10,900) ^b 580(9200)	970	$\text{MoO}(\text{detc})(\text{H}_4\text{HMP})\text{Cl}_2$

^a In MeOH. ^b In DMF.

spectral behavior of the Mo- H_4DMP compounds has been traced to an acid/base sensitivity. Figure 6 shows the effect of HCl followed by $\text{N}(\text{CH}_2\text{CH}_3)_3$ additions to **1**. The site of protonation is likely the pterin ligand, but this speculation can not be proved due to the disappearance of all ionizable protons from the ^1H NMR spectrum, probably due to rapid exchange reactions under the acidic/basic conditions. These

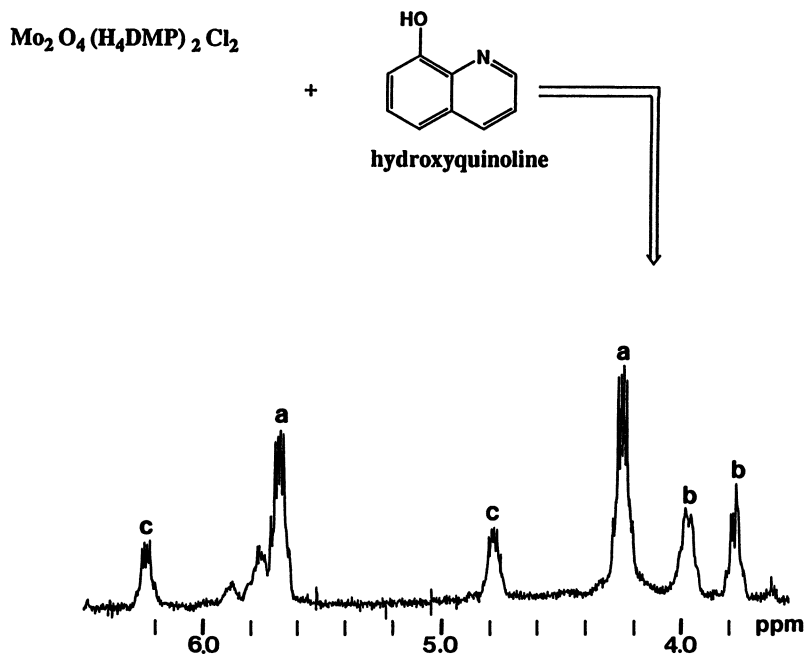


Figure 5. ^1H NMR spectra before and after addition of HQ to 3. Signals marked 'a' are due to $\text{Mo}_2\text{O}_4(\text{H}_4\text{DMP})_2\text{Cl}_2 \cdot \text{H}_4\text{DMP}$. Signals marked 'b' are due to uncoordinated H_4DMP . Signals marked 'c' are due to new DMP species.

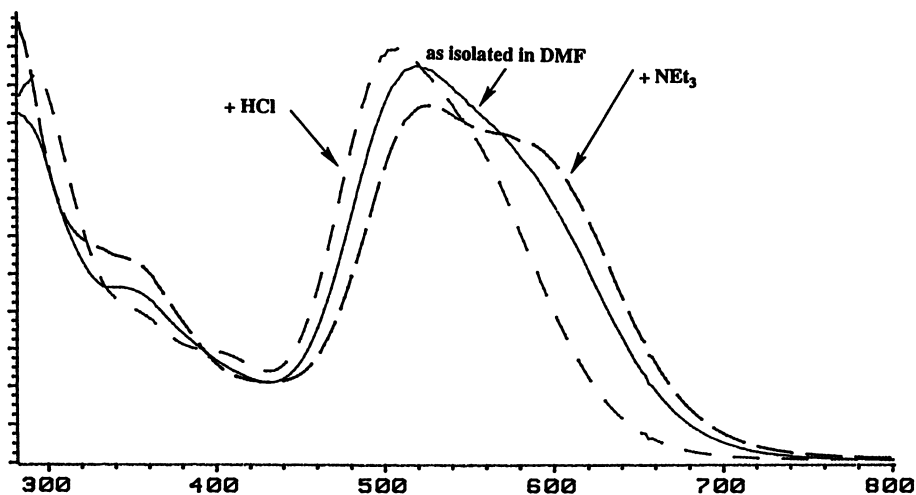
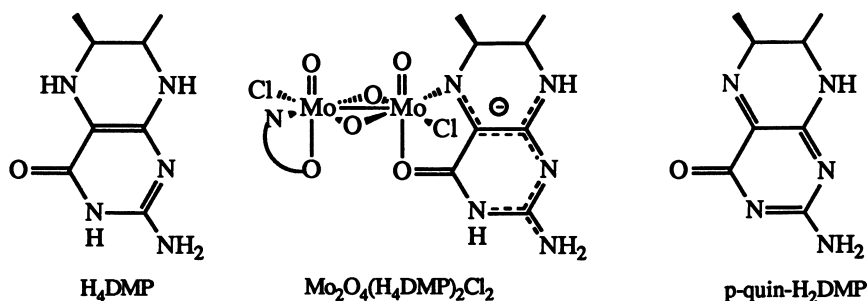


Figure 6. Visible spectra of 3 showing the effect of HCl and Triethylamine addition.

compounds are all non-fluorescent, as expected for tetrahydropterin compounds. Mo(VI)-oxo compounds, monomeric and dimeric, are typically yellow or yellow-orange in color. The purple colors observed in these Mo(VI)-H₄pterin compounds and the large extinction coefficients for the associated visible absorptions are peculiar. A similar observation has been made for another group of Mo(VI)-mono-oxo compounds, MoO(catecholate)L₂ [L= detc, hydroxylamide] and MoO(catecholate)(ssp) (16-18). These seven- and six-coordinate complexes have purple to blue colors and absorptivities near 5000 M⁻¹cm⁻¹. The explanation offered for the unusual energies and absorptivities of these complexes was that the virtual orbitals of Mo and catecholate were close in energy. Applying this idea to the Mo(VI)-H₄pterin complexes, it might be concluded that even greater delocalization results from energetically close orbitals. The crystal structure indicates a highly delocalized π-system. Inspection of the pterin C-C and C-N distances point to an electronic distribution between the limiting structures of H₄pterin and p-quin-



H₂pterin. From this perspective, perhaps the attempt to formulate these complexes as "Mo(VI)-H₄pterin" species is invalid. Although the electronic spectral properties of complexes 1 and 3 are similar to those of MoO(catecholate)L₂ complexes, the energies of the $\nu_{\text{Mo=O}}$ are significantly different. MoO(catecholate)L₂ have $\nu_{\text{Mo=O}}$ in the range 900-930 cm⁻¹; the values of the pterin complexes 1 and 3 are in the range 960-970 cm⁻¹. This latter range is anomalously high for Mo(VI) oxo complexes. Only one other example exists having the Mo(VI)₂O₄ core (19). Trans-Mo₂O₄(Et₂NO)₂(C₂O₄)₂ has structural parameters nearly identical with 3 and displays a $\nu_{\text{Mo=O}}$ at 942 cm⁻¹ and a bridging mode, $\nu_{\text{Mo-O-Mo}}$, near 770 cm⁻¹. Indeed sharp, moderately strong bands are observed near 770 cm⁻¹ for both 1 and 3. However, this assignment remains uncertain since H₄pterins have similar bands in this region.

Electrochemistry of Mo₂O₄(H₄DMP)₂Cl₂

Cyclic voltammograms of Mo₂O₄(H₄DMP)₂Cl₂ are shown in Figure 7. Three irreversible reductions and two irreversible oxidations are observed at scan rates of 50 mV/s. Increasing the cycling rate to 300 mV/s causes the appearance of a return wave to the first reduction. Addition of HClO₄ causes the appearance of a reversible wave at -0.33 V, assigned to the H₄DMP/quin-H₂DMP couple from dissociated H₄DMP. No significant current is observed for return waves of either oxidation at a scan rate of 300 mV/s. The limited solubility of this compound in MeOH prevents a comparison.

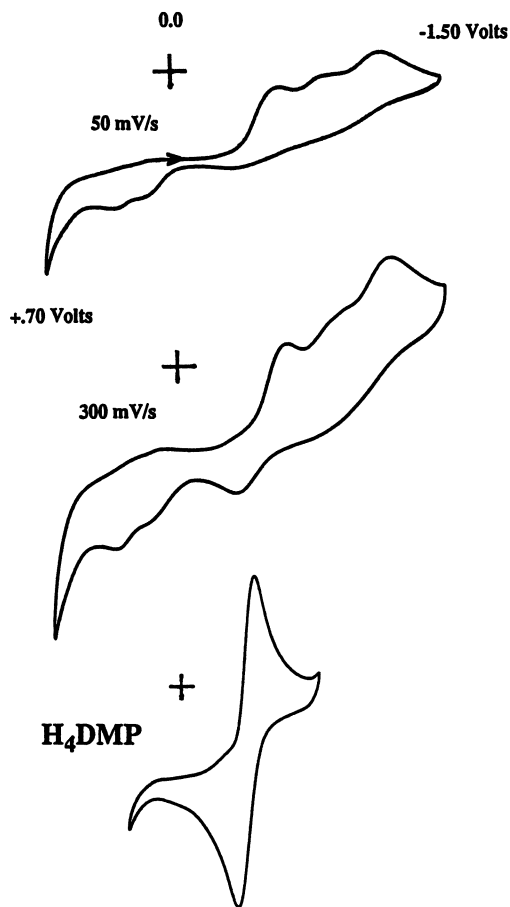


Figure 7. Cyclic Voltammograms of $\text{Mo}_2\text{O}_4(\text{H}_4\text{DMP})_2\text{Cl}_2$ in TEAP/DMF using a Pt disk working electrode. Potentials are referenced to a Ag/AgCl reference electrode. The $\text{Fe}^{3+}/\text{Fe}^{2+}$ couple of ferrocene occurs at +.500 V.

Oxidation Reactions of Mo(VI)-H₄pterin Complexes

Complexes **1** and **3** are unstable to the atmosphere, reactivity that initially was interpreted as evidence for the Mo(IV)(=O) core. Figure 8 shows the decay of MoO(H₄hmp)(detc)Cl₂ over 2 hours. The absorptions at 504 and at 304 nm decrease in parallel and simultaneously with the increase at 328 nm. The oxidation product absorbing at 328 nm is uncoordinated 7,8-H₂pterin, verified by a control experiment. The observed isosbestic points prove there are no intermediates in the oxidation of [Mo(VI)-H₄pterin] compounds to Mo(VI) and free 7,8-H₂pterin. Both MoO(H₄hmp)(detc)Cl₂ and Mo₂O₄(H₄DMP)₂Cl₂ are more reactive to oxygen in methanolic solution than in dimethylformamide solutions. Figure 9 illustrates how the oxidation of Mo₂O₄(H₄DMP)₂Cl₂ proceeds through its "acid" form ($\lambda = 504$ nm) to ultimately yield 7,8-H₂DMP, a decomposition requiring 4 hours. In contrast, Mo₂O₄(H₄DMP)₂Cl₂ in DMF solution exhibits no decay over 24 hours and only a 25% decay after 7 days.

Reactivity with DMSO. MoO(H₄hmp)(detc)Cl₂, but not Mo₂O₄(H₄DMP)₂Cl₂, reacts with DMSO. The reaction of **1** in DMSO is still under study but initial results suggest interesting chemistry exists. Using ¹H NMR to follow the reaction over several days, the products detected are water, HMP, free detc and an oxidized HMP product, possibly 6-formyl-pterin. In contrast, solutions of dimer **3** in DMSO show less than 10% decomposition after 4 days.

Does Mo(VI)-Tetrahydropterin Redox Occur?

The isolated products from reactions of Mo(VI)-dioxo complexes and tetrahydropterins give Mo(VI)-H₄pterin complexes, that is, only non-redox products, when reactions are done in methanolic solutions. If the reactions are performed under basic conditions, a condition accomplished by adding triethylamine to neutralize the two equivalents of HCl present in the tetrahydropterin reagents, significantly different reaction behavior is observed. Using MoO₂detc₂, a small amount of the *reduced* complex, Mo(IV)Odetc₂ is observed in addition to an insoluble blue pterin-containing product. When MoO₂ssp is the metal reagent, the reduced product Mo₂O₃ssp₂ is obtained in nearly 50% yield (20). It appears that in the absence of a protic environment promoting detc or ssp dissociation and subsequent H₄pterin coordination, H₄pterin is able to reduce Mo(VI) to Mo(IV).

Concluding Remarks

Our study began with the anticipation that redox chemistry was likely between a reduced tetrahydropterin and an oxidized Mo(VI)-dioxo complex. Early solution spectroscopic evidence suggested that the reaction products were Mo(IV)-quinonoid-dihydropterin complexes, thereby encouraging this expectation. However, structural data and ligand substitution experiments convinced us that these products were Mo(VI)-tetrahydropterin complexes and *not* the results of a redox reaction. The surprising chelation by H₄pterins at Mo(VI) observed in this work leads us to conclude that alternative coordination modes, such as the tridentate example illustrated below, may play a role during enzyme turnover or may be formed during isolation procedures.

Tetrahydropterins have not been previously considered viable metal chelates because of their instability to oxidation, the unfavorable geometry at the protonated pyrazine N5 and their basic pK_a's. Our studies of the reaction products of Mo(VI)-oxo reagents and tetrahydropterins are the first to lead to complexes having the

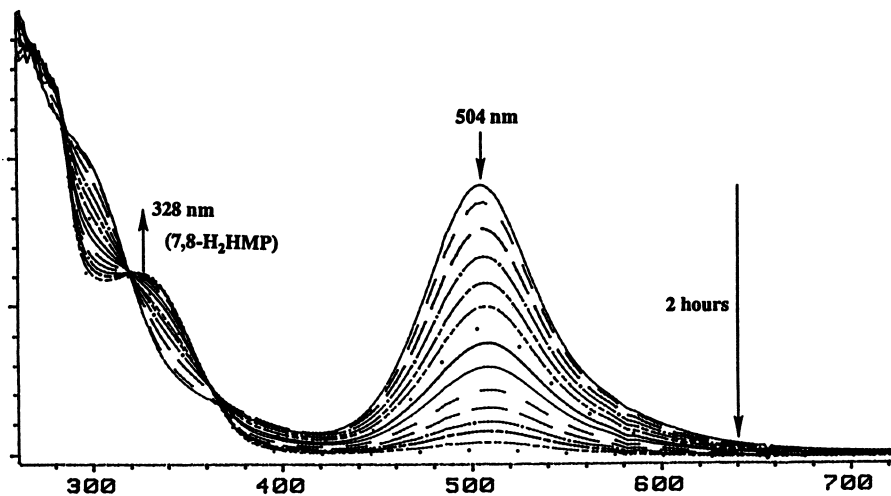


Figure 8. Oxidation of $\text{MoO}(\text{detc})(\text{H}_4\text{HMP})\text{Cl}_2$ by Oxygen.

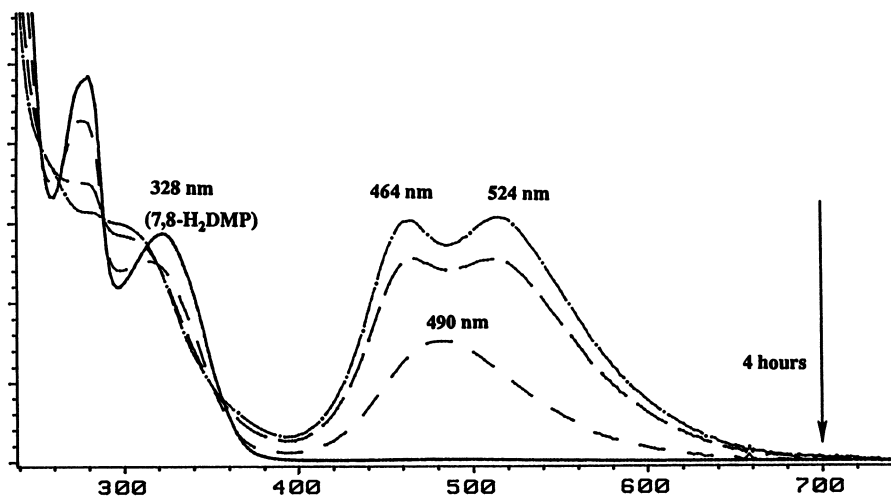
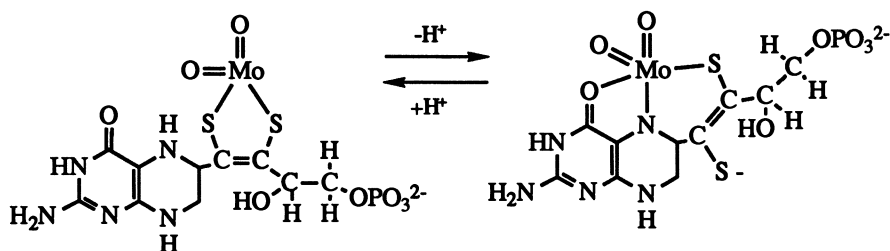


Figure 9. Oxidation of $\text{Mo}_2\text{O}_4(\text{H}_4\text{DMP})_2\text{Cl}_2$



Mo(VI)-H₄pterin formulation. In other projects within our research effort, we have observed that Cu(II) also coordinates H₄pterin, but much more weakly so that the Cu(II)H₄pterin complex decomposes over several hours to Cu(I) and 7,8-H₂pterin (21).

The chemistry of reduced pterins with transition metals may be similar to that of another redox active organic ligand, catechol. Metal complexes are known for all three oxidation states of the catechol–semi-quinone–quinone series. The study of a large number and variety of metal complexes having these ligands has led to a molecular orbital interpretation of the following trend. High oxidation state, "hard" metals of the second and third periods prefer reduced catechol ligands while low oxidation state, "soft" first row metals prefer oxidized, quinone, ligands (22-24). It will be interesting to see if the emerging chemistry of metal-pterin complexes will parallel this catechol coordination chemistry.

Literature Cited

1. Rajagopalan, K. V. *Adv. in Enzymology and Related Areas of Molecular Biology*, Meister, A., Ed.; Wiley: New York, 1991, Vol.64, pp 215-290.
2. Dix, T. A.; Benkovic, S. J. *Acc. Chem. Res.* **1988**, *21*, 101-107.
3. Dryhurst, G.; Raghavan, R.; Ege-Serpken, D.; Karber, L. *Electrochemical and Spectrochemical Studies of Biological Redox Components*, Kadish, K., Ed.; A.C.S. Symposium Series #201; American Chemical Society: Washington, D. C., 1982, Vol. 201; pp 458-487.
4. Pfeleiderer, W.; Gottlieb, R. *Biochemical and Clinical Aspects of Pteridines*, Wachter, H.; Curtius, H.; Pfeleiderer, W., Eds.; DeGruyter: Berlin, 1985, Vol.4; pp 3-71.
5. Archer, M. C.; Scrimgeour, K. G. *Can. J. Biochem.*, **1970**, *48*, 278.
6. Viscontini, M. *Methods in Enzymology*, 1971, Vol. XVIII B, pp 678-705.
7. Lazarus, R. A.; DeBrosse, C. W.; Benkovic, S. J. *J. Amer. Chem. Soc.* **1982**, *104*, 6871.
8. Newton, W. E.; Watt, G. D.; McDonald, J. W. *Chem. Uses Molybdenum, Proc. Int. Conf.* 1979, *3*, 259.
9. Mitchell, P.; Scarle, R. *J. Chem. Soc., Dalton Trans.* **1975**, 2552.
10. McDonald, J. W.; Corbin, J. L.; Newton, W. E. *Inorg. Chem.* **1976**, *15*, 2056.
11. Holm, R. *Chem. Rev.* **1987**, *87*, 1401.
12. Burgmayer, S. J. N.; Baruch, A.; Kerr, K.; Yoon, K. *J. Amer. Chem. Soc.* **1989**, *111*, 4982.
13. Baugh, C. M.; Shaw, E. *J. Org. Chem.* **1964**, *29*, 3610.

14. X-ray parameters: space group Pbcn (orthorhombic), $a=19.945(3)$, $b=20.855(4)$, $c=20.584(4)$, $Z=8$, #data, $I>\# \sigma=2217$, #variables=320, $R=7.7\%$, $R_w=10.8\%$. The ratio of data/variables is limited due to crystal decomposition in the X-ray beam. There are two unique dimer halves in the asymmetric unit, each half dimer related to the rest of the molecule by a crystallographic C2 axis bisecting the Mo-Mo vector parallel to the Mo=O bonds.
15. A monomeric, octahedral Mo complex of reduced biopterin is reported by Fischer, B; Strahle, J.; and Viscontini, M. in *Helv. Chim. Acta*, **1991**, *74*, 1544. Although these authors claim that this complex is a Mo(IV)-quinonoid-dihydrobiopterin complex, we feel the formulation is incorrect and should be Mo(VI)-tetrahydrobiopterin. The reported structural data are identical to the Mo(VI) dimer reported in this manuscript and the complex is reported to decompose in methanol to free tetrahydrobiopterin and a Mo(VI) complex.
16. Bradbury, J.; Schultz, F. *Inorg. Chem.* **1986**, *25*, 4461.
17. Mondal, J.; Schultz, F.; Brennan, T.; Scheidt, W. *Inorg. Chem.* **1988**, *27*, 3950.
18. Geller, S.; Newton, B.; Majid, L.; Bradbury, J.; Schultz, F. *Inorg. Chem.* **1988**, *27*, 359.
19. Wieghardt, K.; Hahn, M.; Swiridoff, W.; Weiss, J. *Inorg. Chem.* **1984**, *23*, 94.
20. The Mo(IV) product, Mo=O(ssp) is not stable; only the Mo(V) dimer can be isolated from reductions of MoO₂ssp (in the absence of excess amounts of a third ligand). Craig, J.; Harlan, E.; Snyder, B.; Whitener, M; Holm, R. *Inorg. Chem.* **1989**, *28*, 2082.
21. Burgmayer, S. J. N.; Bharwani, L.; Mosny, K.; McCracken, J.; manuscript in preparation.
22. Pierpont, C.; Larsen, S.; Boone, S. *Pure Appl. Chem.* **1988**, *60*, 1331.
23. Buchanan, R.; Wilson-Blumenberg, C.; Trapp, C.; Larsen, S.; Larsen, S.; Greene, D.; Pierpont, C. G. *Inorg. Chem.* **1986**, *25*, 3070.
24. Buchanan, R.; Pierpont, C. G. *J. Amer. Chem. Soc.* **1980**, *102*, 4951.

RECEIVED April 30, 1993

Chapter 9

Chemical and Physical Coupling of Oxomolybdenum Centers and Iron Porphyrins

Models for the Molybdenum–Iron Interaction in Sulfite Oxidase

Michael J. LaBarre, Arnold Raitsimring, and John H. Enemark¹

Department of Chemistry, University of Arizona, Tucson, AZ 85721

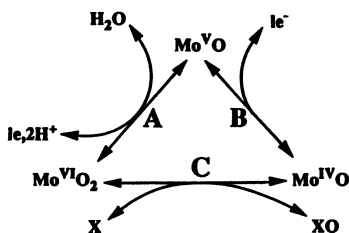
The hydrotris(3,5-dimethyl-1-pyrazolyl)borate ligand (L) stabilizes a wide range of six-coordinate mononuclear complexes possessing *fac* stereochemistry and containing the $[\text{LMo}^{\text{IV}}\text{O}]^+$, $[\text{LMo}^{\text{V}}\text{O}]^{2+}$, and $[\text{LMo}^{\text{VI}}\text{O}_2]^+$ fragments. Covalent coupling of a $[\text{LMo}^{\text{V}}\text{O}]^{2+}$ fragment to a tetraarylporphyrin Fe(III)Cl unit gives binuclear complexes with controlled Mo...Fe distances. EPR spectroscopy at 4 K shows static dipolar coupling between Mo(V) and high spin Fe(III) that is distance dependent. At 77 K the dipolar coupling is modulated by rapid relaxation of the Fe(III) center. The iron-free complexes and the Mo(V)/Zn(II) analogues show unperturbed EPR spectra similar to the known $\text{LMo}^{\text{V}}\text{O}(\text{catecholate})$ complexes.

Sulfite oxidase is a pterin-containing molybdoenzyme (1) that catalyzes the oxidation of sulfite to sulfate and that is absolutely essential for human life. Each of the two identical subunits contains one oxo-molybdenum center and one b_5 -type heme center. During turnover electrons appear to flow from sulfite to the molybdenum center to the heme group and then to exogenous cytochrome c.

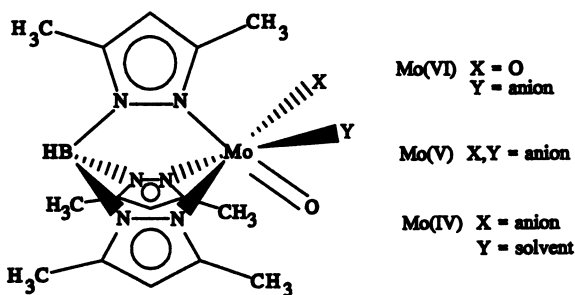
Scheme I shows a simplified sequence of reactions that has been used to describe the chemical transformations occurring at the molybdenum center of sulfite oxidase and related enzymes. Step C, a formal oxygen atom transfer reaction, has been modeled by several chemical systems and extensively reviewed (2). New analogues for reaction C have recently been reported (3).

We have previously prepared a wide range of mononuclear oxomolybdenum complexes of the general form $\text{LMo}^{\text{VI}}\text{O}_2\text{X}$, $\text{LMo}^{\text{V}}\text{O}(\text{X},\text{Y})$, and $\text{LMo}^{\text{IV}}\text{OX}(\text{Solvent})$ (where L is hydrotris(3,5-dimethylpyrazolyl)borate) as shown in Figure 1 (4-6). To our knowledge this is the only family of oxo-molybdenum complexes for which x-ray structures and spectroscopic data are available for all three oxidation states of

¹Corresponding author



Scheme I. Reaction Cycle for Oxomolybdenum Centers.

Figure 1. Structures of the $\text{LMo}^{\text{VI}}\text{O}_2\text{X}$, $\text{LMo}^{\text{V}}\text{O}(\text{X},\text{Y})$ and $\text{LMo}^{\text{IV}}\text{OX}(\text{solvent})$ species

Scheme I, Mo(IV,V,VI). The redox potentials and spectroscopic properties of these species are strongly dependent upon the nature of the X and Y groups. Reaction conditions for the chemical transformations of steps A, B and C of Scheme I have also been developed (7,8).

Intramolecular electron transfer between the molybdenum and heme centers of sulfite oxidase has been investigated by laser flash photolysis techniques (9) and shown to be strongly inhibited by anions in the media (10). No crystal structures are available for any pterin-containing molybdoenzyme, and the iron-molybdenum distance in sulfite oxidase is unknown. Thus, there is presently no structural basis for interpreting the observed intramolecular electron transfer reactions between the molybdenum and iron centers.

As part of our ongoing studies of the chemistry and biochemistry of molybdenum in enzymes we have begun to investigate model systems that can be used to quantitate the interactions between an oxo-molybdenum center and an iron porphyrin center. Herein we describe the synthesis and properties of novel Fe(III) porphyrins possessing pendant oxo-Mo(V) centers.

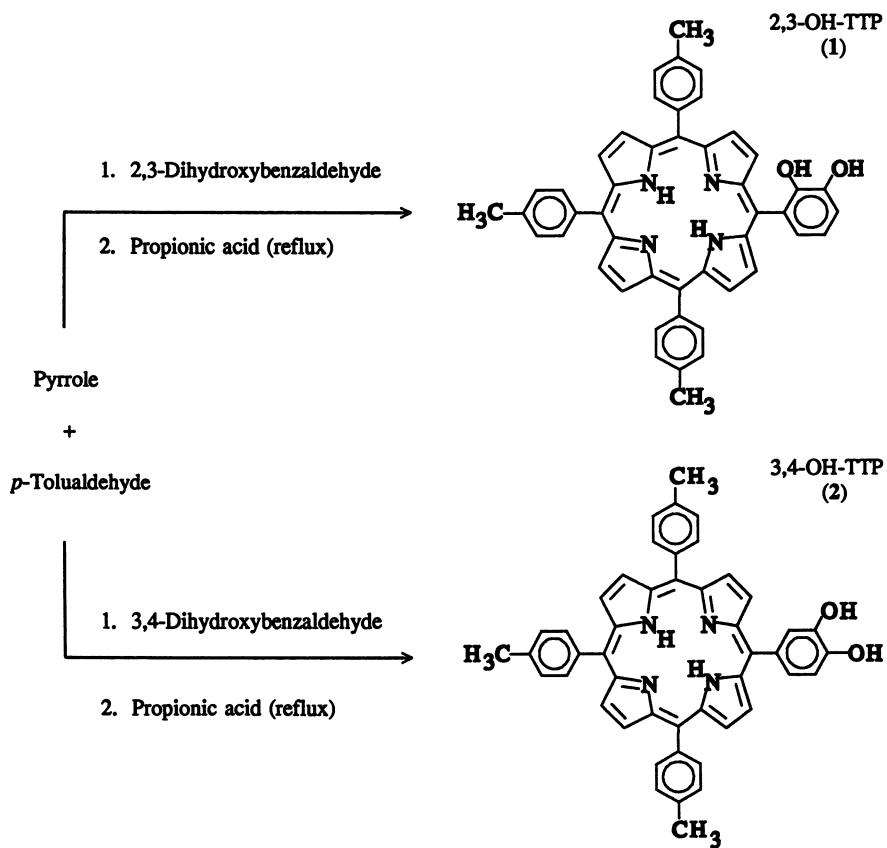
Experimental Results

The catecholate-substituted porphyrins 2,3-OH-TTP (1) (11) and 3,4-OH-TTP (2) were obtained in low yield (1-3%) via modifications of the mixed aldehyde synthetic procedure for substituted tetraaryl porphyrins (Scheme II) (12,13). The oxo-Mo(V) group was attached to the catecholate functions of 1 and 2 by reacting each with LMoO(eth-gly) (L = hydrotris(3,5-dimethyl-1-pyrazolyl)borate; eth-gly = ethylene glycolate) in refluxing toluene to give 2,3-Mo-TTP (3) and 3,4-Mo-TTP (4), respectively, in high yield (90%) (Scheme III). Zinc and iron can be inserted into the porphyrin ring. Metallation of 3 and 4 with FeCl₂ in DMF (14-16) yielded FeCl(2,3-Mo-TTP) (5) and FeCl(3,4-Mo-TTP) (6) in good yield (17).

All attempts to crystallize 3-6 to date have been unsuccessful. However, molecular modeling calculations show that the steric constraints of the porphyrin moiety and the facially coordinating pyrazolylborate ligand severely restrict the conformations available to 5 and 6 (Figure 2). For square planar geometry at the porphyrin center the calculated metal-metal distances for 5 and 6 are 7.3 and 9.4 Å, respectively.

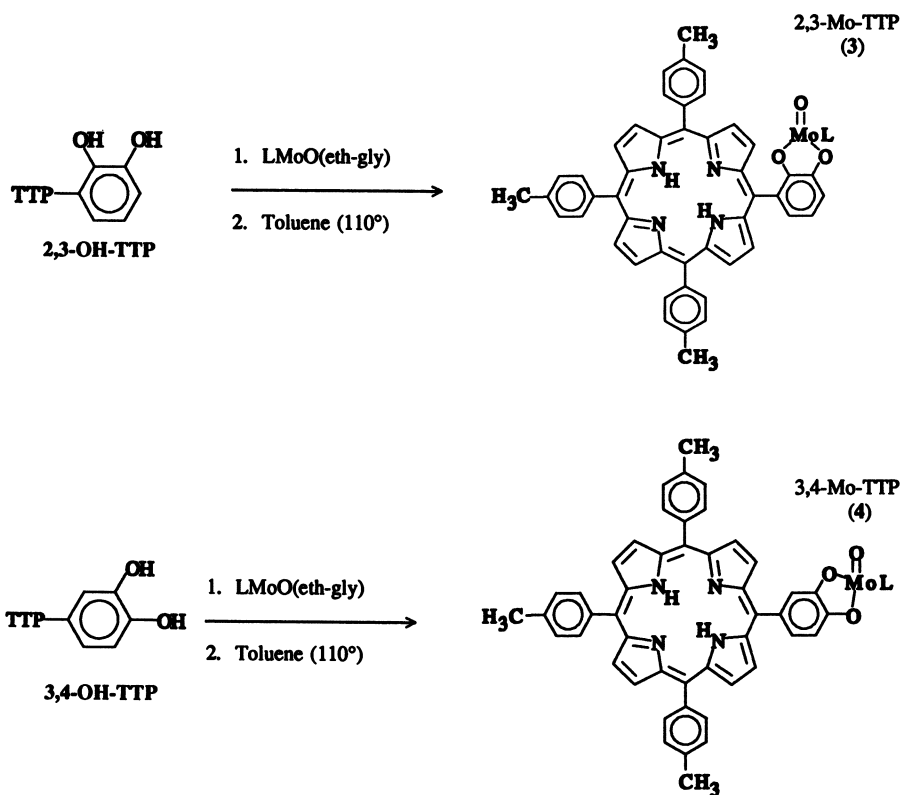
At room temperature 3-6 exhibit isotropic EPR spectra that are nearly identical in g-value, line width and $A(^{95,97}\text{Mo})$ to LMoO(cat). At 77 K, 3 and 4 show pseudo-axial EPR spectra that are virtually indistinguishable from the spectrum of LMo(cat) at 77 K (4). However, the EPR spectra of the molybdenum centers of 5 and 6 at 77 K are dramatically different from 3 and 4. Figure 3 compares the Mo(V) EPR signal of 4 and 6 at 77 K. The peak heights of 6 are reduced relative to 4, and much of the signal of 6 is broadened into the wings due to coupling of Mo(V) to the high-spin Fe(III) center of the porphyrin (Fe...Mo distance ~9.4Å). Figure 4 shows that the reduction in peak heights of the Mo EPR signal of 5 relative to 3 is much more dramatic because of the shorter distance (7.3Å) between the Fe and Mo centers. This is reasonable since dipolar coupling is proportional to $1/r^3$ (18).

Addition of excess N-methylimidazole to 6 produces a dramatic change in the EPR spectrum. The Fe(III) center becomes low-spin with g-values similar to those



Yield = 1-2%

Scheme II. Synthesis of Bis-Hydroxy-Substituted Porphyrins.



Scheme III. Synthesis of 2,3-Mo-TTP (3) and 3,4-Mo-TTP (4).

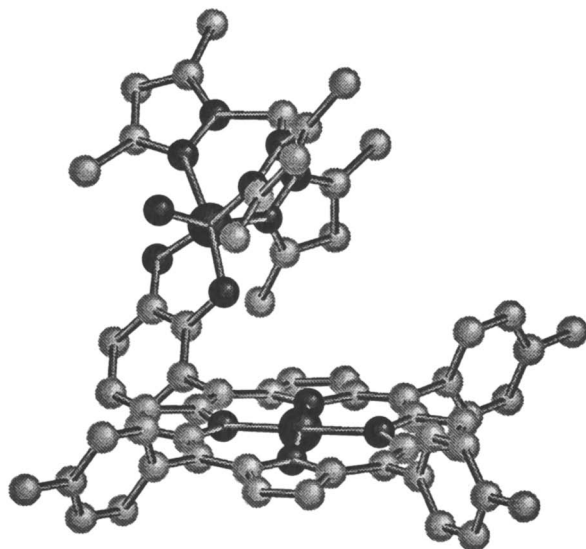


Figure 2a. Calculated conformation for the [Fe(2,3-Mo-TPP)]⁺ fragment related to 5. The Fe...Mo distance is 7.3Å.

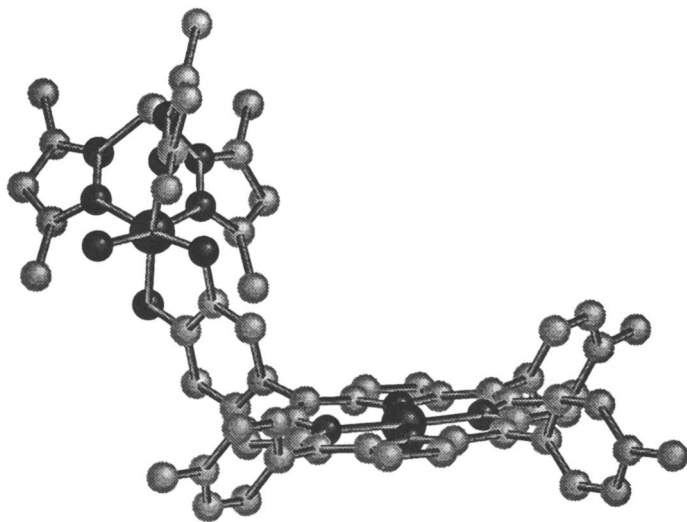


Figure 2b. Calculated conformation for the [Fe(3,4-Mo-TPP)]⁺ fragment related to 6. The Fe...Mo distance is 9.4Å.

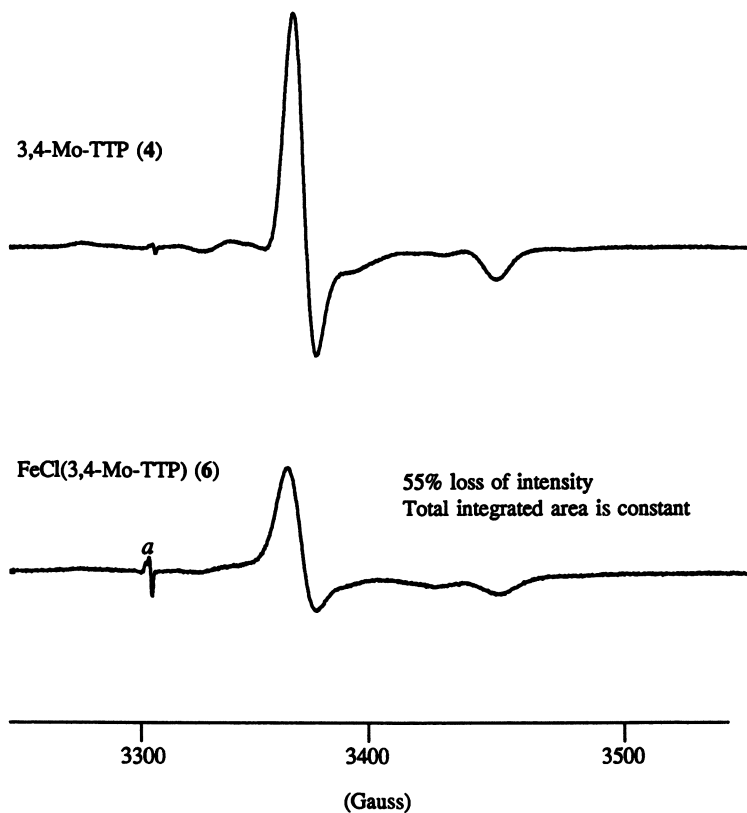


Figure 3. EPR spectra of the Mo(V) complexes **4** and **6** normalized to 1.0 mM solutions in dichloromethane:toluene (1:1) glasses recorded on a Bruker ESR 300. The signal arising at *a* is due to the quartz Dewar used to maintain 77 K.

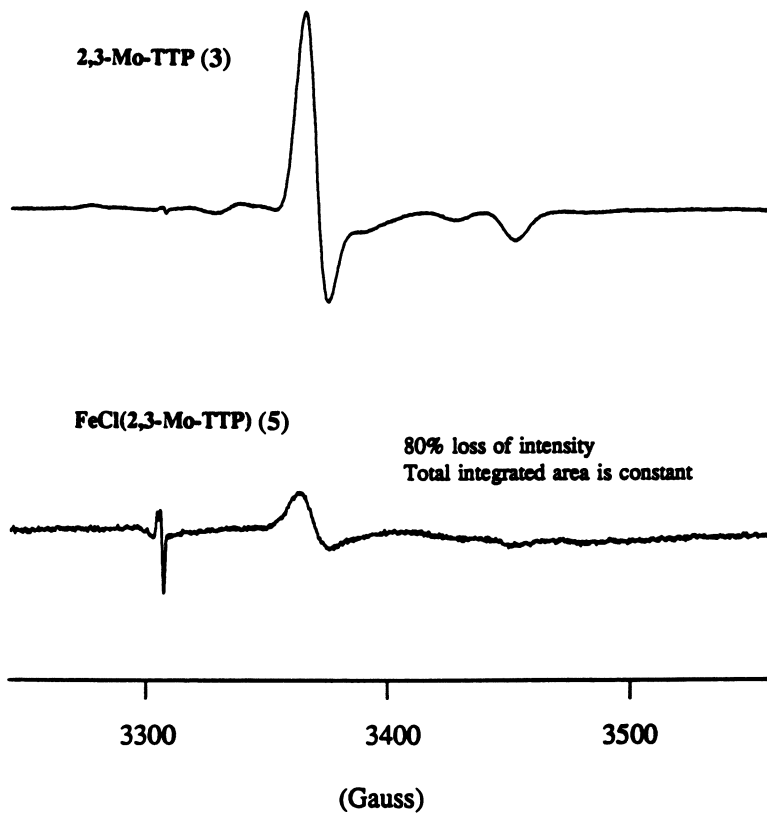


Figure 4. EPR spectra of the Mo(V) centers of **3** and **5**; spectra are normalized to a Mo concentration of 0.5 mM in dichloromethane:toluene (1:1) glasses and recorded as in Figure 3.

reported previously for $[(\text{TPP})\text{Fe}(\text{imid})_2]^+$ complexes (19). The EPR spectrum of the Mo(V) center is also different in the presence of excess N-methylimidazole. The main features consist of shifting of the original g_{\perp} peak to higher field and splitting of the g_{\perp} feature. (Figure 5).

The simulation of these coupled spectra is not simple. The coupling is anisotropic and both dipolar and exchange terms appear to be important, with dipolar coupling being the dominant feature. A more detailed analysis of the coupling between the Fe(III) and Mo(V) centers is in progress.

The half wave reduction potentials for the series of bis-hydroxy substituted porphyrins and their $[\text{FeCl}]^{2+}$ insertion products are listed in Table I and several

Table I. Half-Wave Reduction Potentials^a

Complex	Redox Process			
	$\text{Fe}^{\text{III}}/\text{Fe}^{\text{II}}$	$\text{Mo}^{\text{V}}/\text{Mo}^{\text{IV}}$	$\text{Fe}^{\text{II}}/\text{Fe}^{\text{I}}$	$\text{TTP}^0/\text{TTP}^{-1}$
TTP				-1.14 (140)
3,4-OH-TTP (2)				-1.18 (140)
3,4-Mo-TTP (4)		-0.68 (150)		-1.20 (140)
2,3-OH-TTP (1)				-1.22 (150)
2,3-Mo-TTP (3)		-0.74 (150)		-1.28 (140)
FeCl(TTP)	-0.23 (150)		-1.00 (150)	
FeCl(3,4-Mo-TTP) (6)	-0.25 (160)	-0.71 (150)	-1.06 (150)	
FeCl(2,3-Mo-TTP) (5)	-0.28 (160)	-0.74 (150)	-1.13 (150)	
LMO(catecholate)		-0.71 (170)		

^aCyclic voltammetry was performed on 1.0 mM CH_2Cl_2 solutions with 100 mM tetrabutylammonium tetrafluoroborate as supporting electrolyte. Half-wave reduction potentials are listed in volts with ΔE_p in parentheses. Voltammograms were recorded at 100 mV/sec and potentials are referenced to SCE.

representative voltammograms are seen in Figure 6. The data show a distinctive decrease in reduction potentials as the porphyrin substitution pattern shifts from unsubstituted to 3,4- to 2,3-substituted complexes. This trend is independent of the redox process examined and the nature of the substituent. The first porphyrin ring reduction in 3 is 80 mV lower than in 4, and 140 mV more negative than in TTP. This pattern corresponds with the decreasing distance from the Mo atom of the LMO(catecholate) substituent to the center of the porphyrin. The $\text{Mo}^{\text{V}}/\text{Mo}^{\text{IV}}$ redox

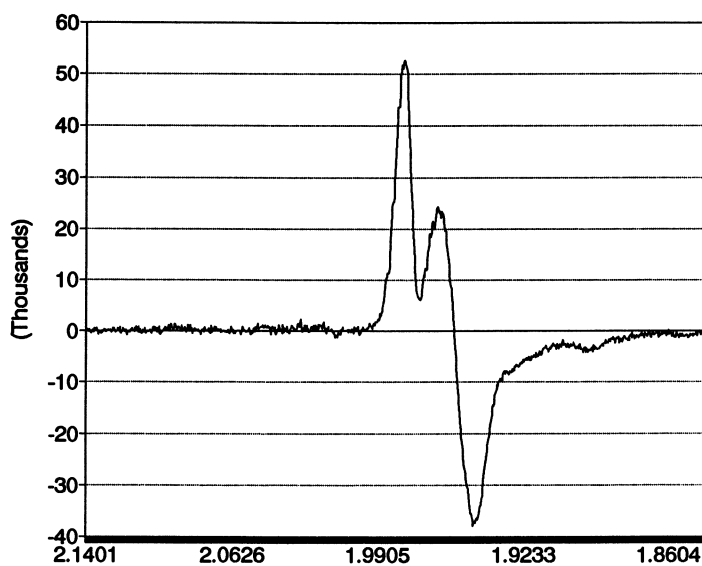


Figure 5. EPR spectrum of the Mo(V) center of **6** at 77 K in the presence of excess *N*-methylimidazole.

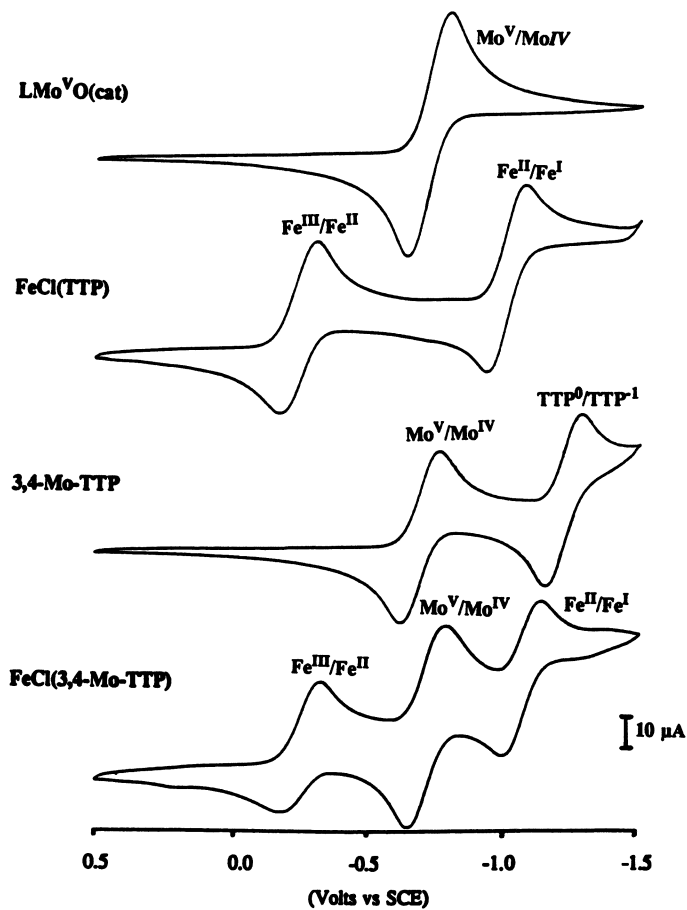


Figure 6. Cyclic voltammograms of 1 mM solutions in CH_2Cl_2 with 100 mM $[\text{Bu}_4\text{N}][\text{BF}_4]$ as supporting electrolyte, a Pt disk working electrode, Pt wire counter electrode, and SCE as reference electrode.

process is less affected by $[\text{FeCl}]^{2+}$ insertion than is the Fe center upon $[\text{LMoO}]^{2+}$ attachment to the porphyrin periphery.

The electronic spectra of **5** and **6** are very similar to the parent (TTP)FeCl complex, consistent with little electron delocalization between the Mo and Fe systems. The electronic spectra are also consistent with the electrochemical results which show that distinct one electron redox processes are maintained for the Mo and Fe portions of **5** and **6**.

Summary

Complexes **5** and **6** are initial models for investigating the long range coupling between the Mo and Fe centers of sulfite oxidase. The present choice of porphyrin substituents and ligands to the molybdenum atom gives complexes which are most stable in the Mo(V)/Fe(III) state, and therefore are well suited for EPR coupling studies. Variation of the Mo...Fe distance in related complexes will provide benchmarks for interpreting the EPR spectra of the Mo(V)/Fe(III) states of sulfite oxidase itself.

Acknowledgments

We thank Mr. Ish Dhawan for assistance with the molecular modeling calculations and Professor F.A. Walker for helpful discussions. Support of this research by the National Institute of Health, Grant GM 37773, is gratefully acknowledged.

Literature Cited

- (1) Rajagopalan, K.V. *Adv. Enzymol. Relat. Areas Mol. Biol.* **1991**, *64*, 215-290.
- (2) Holm, R.H. *Coord. Chem. Rev.* **1990**, *100*, 183.
- (3) Gheller, S.F.; Muetterties, M.C.; Schultz, B.E.; Scott, M.J.; Holm R.H.; *J. Am. Chem. Soc.* **1992**, *114*, 6934.
- (4) Cleland, W.E., Jr.; Barnhart, K.M.; Yamanouchi, K.; Collison, D.; Mabbs, F.E.; Ortega, R.B.; Enemark, J.H. *Inorg. Chem.*, **1987**, *26*, 1017.
- (5) Roberts, S.A.; Young, C.G.; Cleland, W.E., Jr.; Ortega R.B.; Enemark, J.H. *Inorg. Chem.*, **1988**, *27*, 3044.
- (6) Roberts, S.A.; Young, C.G.; Kipke, C.A.; Cleland W.E., Jr.; Yamanouchi, K.; Carducci, M.D.; Enemark, J.H. *Inorg. Chem.*, **1990**, *29*, 3650-3656.
- (7) Xiao, Z.; Young, C.G.; Enemark, J.H.; Wedd, A.G. *J. Am. Chem. Soc.*, **1992**, *114*, 9194-9195.
- (8) Young, C.G.; Wedd, A.G. *This ACS Symposium Series*, Ch. 5, **1992**.
- (9) Kipke, C.A.; Cusanovich, M.A.; Tollin, G.; Sunde, R.A.; Enemark, J.H. *Biochemistry*, **1988**, *27*, 2918
- (10) Sullivan, E.P., Jr.; Hazzard, J.T.; Tollin, G.; Enemark, J.H. *J. Am. Chem. Soc.* **1992**, *114*, 9662-9663.
- (11) Gust, D.; Moore, T.A.; Bensasson, R.V.; Mathes, P.; Land, E.J.; Chachaty, C.; Moore, A.L.; Liddle, P.A. *J. Am. Chem. Soc.* **1985**, *107*, 3631.

- (12) Little, R.G.; Anton, J.A.; Loach, P.A.; Ibers, J.A. *J. Heterocyclic Chem.* **1975**, *12*, 343.
- (13) Little, R.G. *J. Heterocyclic Chem.* **1981**, *18*, 129.
- (14) Adler, A.D.; Longo, F.R.; Kampas, F.; Kim, J. *J. Inorg. Nucl. Chem.* **1970**, *32*, 2443.
- (15) Walker, F.A.; Balke, V.E.; McDermott, G.A. *J. Am. Chem. Soc.* **1982**, *104*, 1569.
- (16) Sadasivan, N.; Eberspaecher, H.I.; Fuchsman, W.H.; Caughey, W.S. *Biochem.* **1969**, *8*, 53.
- (17) LaBarre, M.J. *Ph.D. Dissertation*, University of Arizona, 1992.
- (18) Wertz, J.E.; Bolton, J.R. In *Electron Spin Resonance*, Chapman and Hall, New York City, NY, 1986.
- (19) Walker, F.A.; Reis, D.; Balke, V.L.; *J. Am. Chem. Soc.* **1984**, *106*, 6888.

RECEIVED March 8, 1993

Chapter 10

Nitrogenase Structure, Function, and Genetics

Barbara K. Burgess

Department of Molecular Biology and Biochemistry, University
of California, Irvine, CA 92717

This paper is an overview of what is currently known about the structure and biosynthesis of the two component proteins of Mo nitrogenase. It focuses initially on the Fe protein polypeptide, the assembly of the holoprotein, its three dimensional structure, the properties of its [4Fe-4S] cluster and the effects of MgATP/MgADP binding. This is followed by a consideration of the MoFe protein polypeptides, the properties of the "P" clusters, the assembly of the FeMo-co deficient MoFe protein, the physical properties and biosynthesis of FeMo-cofactor and the organization of the holoprotein. The flow of electrons from reductant, to the Fe protein, to the MoFe protein, to substrate, is then considered with emphasis on the role of ATP and the reduction of the physiological substrates N₂ and H⁺. Nitrogen fixation (*nif*) genes are mentioned throughout this discussion and their organization is summarized. The vanadium and "Fe-only" nitrogenase systems are also briefly discussed.

Molybdenum nitrogenase is composed of two separately purified proteins called the iron protein (Fe protein) and the molybdenum-iron protein (MoFe protein). As shown in Figure 1 the Fe protein is a dimer of two identical subunits, with a single [4Fe-4S]^{2+/1+} cluster, and two binding sites for MgATP.

The MoFe protein is an $\alpha_2\beta_2$ tetramer. It contains two different types of metal clusters designated the "P-clusters" and the iron-molybdenum cofactor (FeMoco) centers, with FeMoco believed to be the site of substrate binding and reduction. In addition to these two component proteins the assembly of a functional Mo nitrogenase system within a bacterial cell requires the participation of a large number of other proteins encoded by nitrogen fixation (*nif*) specific genes. *Azotobacter vinelandii* and some other organisms have two other nitrogenase systems that are expressed under different growth condition. One, the *vnf* system, functions using vanadium instead of Mo, whereas the other, the *anf* system, is

expressed in the absence of both Mo and V. N₂ fixation, and all other reductions catalyzed by all three nitrogenase systems, require both component proteins, a source of low potential electrons, MgATP, protons and an anaerobic environment. The general direction of electron flow is from an electron donor to the Fe protein to the MoFe protein to substrate, with the electron transfer between the Fe and MoFe proteins coupled to MgATP hydrolysis.

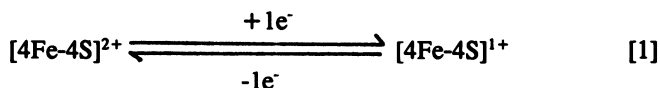
This overview covers what has been learned recently about the structure, substrate reactions and assembly of the Fe protein, the MoFe protein and their vnf and anf analogues.

Fe Protein

The Fe protein is a dimer of two identical subunits encoded by the nifH gene. At the protein level over 20 sequences have now been compared (1). These data show that there is a remarkable degree of conservation of the amino acid sequence (range 45 to 90%) not only when archaeobacterial, eubacterial and cyanobacterial sequences are compared to each other, but also when Mo system versus non-Mo system sequences are compared within the same organism (2). The consensus sequence is illustrated in Figure 2 and specific regions of interest are discussed below.

Redox Properties. Biochemical, genetic and spectroscopic data have established that the Fe protein has a single [4Fe-4S] cluster (3) bridged symmetrically between the two subunits using conserved cysteines 97 and 132 of the Azotobacter vinelandii sequence (4,5). D₂O exchange experiments have shown that this [4Fe-4S] cluster is more exposed to solvent than similar clusters found in other proteins (6). The Fe protein's [4Fe-4S] cluster is also more O₂ sensitive leading to the recent suggestion that under some physiological circumstances the cluster might serve as an O₂ reductase (7). The three dimensional structure of the A. vinelandii Fe protein has recently been determined to 2.9 Å resolution (8,9). The above data are all consistent with that structure which shows that the [4Fe-4S] cluster is close to the surface of the protein and that it forms the major connection between the two subunits.

As shown in equation [1] the [4Fe-4S]²⁺ cluster can be reversibly reduced by one electron with a reduction potential of ~ -320 mV versus SHE (10).



The reduced cluster exhibits low temperature EPR spectra that have been interpreted in terms of a mixture of interconvertible S=1/2 and S=3/2 spin states, which together integrate to one spin per [4Fe-4S]¹⁺ (11-14). The two spin states can be interconverted by changes in solvent or temperature, leading to the suggestion, based on NMR studies, that the S=3/2 state might only arise during freezing of the samples for spectroscopy (15). Mixed S=1/2 and S=3/2 spin states of [4Fe-4S]¹⁺ clusters have also been reported for a number of other proteins and this topic has been recently reviewed (16).

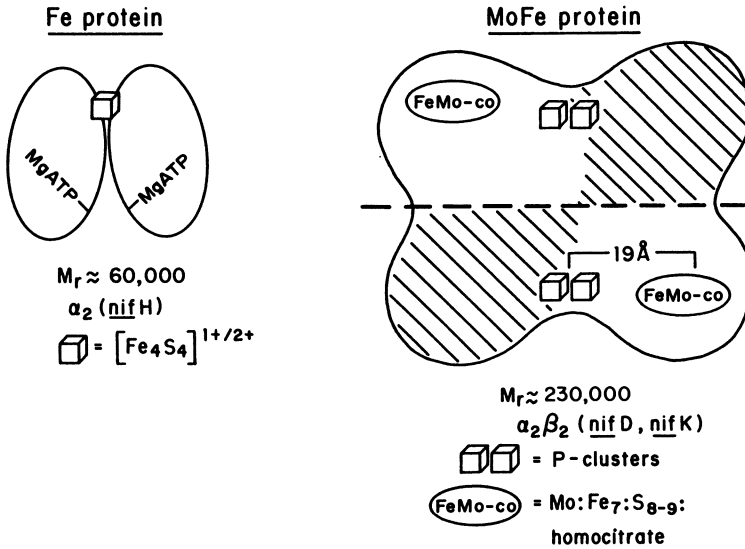


Figure 1. The two component protein of Mo nitrogenase.

m-m--lrqiafYGGKGIgKSTtsqntlaalae-mgqkilivGCDPKaDsTrliihskaqd
 tvldaae-gsvdedledvkeGyggikCvEsGGPePGvGC^{*}AGRGvItsinfleengay-
 dlddvsyDvLGDVV^{*}CGGFAmPirenkAqeiYiVmsgemMAMYAANNIskGilk
 yansggvrLGGlicNsRtdreleleala-klgtqlihfvPrdnivqhaElrrmTviey-
 pdsqadeyr-LArkhhn.gkgviPtPitmdelee.lmefgim..ede.

Figure 2. NifH consensus sequence. Capital letters indicate residues that are invariant. (*) above the C's indicates cluster ligands.

In vitro, the reduction of $[4\text{Fe-4S}]^{2+}$ is accomplished using dithionite, where SO_3^{2-} is the actual one electron donor, and the reoxidation is carried out using dyes (17). The Fe protein is also known to "self-oxidize" without loss of activity when stored anaerobically in the presence of dithionite (18). It is therefore not clear if the Fe protein samples used for the recent crystallographic studies (8,9) were in the oxidized or reduced states.

The physiological electron donor to the Fe protein differs depending upon the organism. For example, in the obligate anaerobe *Clostridium pasteurianum* (Cp) the electron donor appears to be a $2[4\text{Fe-4S}]$ -containing ferredoxin (19). In contrast, in the facultative anaerobe *Klebsiella pneumoniae* (Kp), the *nif* specific electron transfer sequence does not involve ferredoxin. In that case, the *nifJ* gene product catalyzes the two electron oxidation of pyruvate to acetyl-SCoA + CO_2 with the two electrons being used to reduce two molecules of the *nifF* gene product, a flavodoxin (20,21). The flavodoxin then fluctuates between the semi-quinone and hydroquinone states in transferring one electron to the oxidized Fe protein (21,22). A flavodoxin encoded by the *nifF* gene is also the likely physiological electron donor in *A. vinelandii* (Av) (23,24). The region of the *A. vinelandii* Fe protein involved in flavodoxin binding, however, has not as yet been established.

Binding of MgATP and MgADP to Isolated Fe Protein. The oxidized and reduced states of Fe proteins from all sources tested, bind 2MgATP or 2MgADP molecules with reported dissociation constants for MgATP ranging from <5 to $560 \mu\text{M}$ (3,10). Sequence comparisons (25), site-directed mutagenesis (26) and X-ray crystallography (8,9) are all consistent with a model whereby the terminal phosphate of MgATP interacts with the sequence GYGXXGKS located between residues 9-16 of *A. vinelandii* (Figure 2). This sequence is known as a Walker's motif and is found in a large number of mononucleotide binding proteins (27). In the structure of some of those proteins the bound Mg^{2+} has been shown to interact with an aspartate residue analogous to Asp-125 of the Fe protein sequence (9).

One of the most intriguing aspects of the Fe protein is that somehow the binding of mononucleotides influences the environment of the $[4\text{Fe-4S}]$ cluster (3,10) even though the binding site of the terminal phosphate is located $\sim 20\text{\AA}$ away from the cluster (9). Changes in the $[4\text{Fe-4S}]$ that occur upon MgATP binding include: 1) the E^0 is lowered by ca. 100 mV (14,28); 2) the $S=1/2$ EPR signal changes from rhombic to more axial (29-31); 3) the O_2 sensitivity increases; 4) large changes occur in the circular dichroism spectrum of the oxidized protein (32); and 5) the cluster's Fe atoms, which are inert to chelators in the absence of MgATP, become accessible to chelators in its presence (33,34). It is interesting to note that the effects of MgATP and MgADP are not identical. MgADP causes similar changes in the E^0 and the CD spectrum (14,28,32) but is an inhibitor of the chelation reaction (33,34). The kinetics of the chelation reaction are complex involving two sequential steps with the formation of a discrete $[2\text{Fe-2S}]^{2+}$ intermediate (35). This $[2\text{Fe-2S}]^{2+}$ intermediate also appears to form upon addition of MgATP to oxidized Fe protein in the absence of chelators, leading to the suggestion that it might be responsible for the observed changes in CD (36).

The recent X-ray structural analysis of the *A. vinelandii* Fe protein was carried out on a preparation that appeared to have copurified with a small amount

of a bound nucleotide. This was modeled as ADP bound to one of the two subunits and led to the assignment of residues involved in ribose and adenine binding (9). Interestingly, like the cluster itself, which bridges the two subunits, the adenine and ribose portions of ADP in the model protrude into a cleft at the subunit interface and interact with residues on the adjacent subunit. For example, in the model the adenine ring of an ADP whose phosphates bind to one subunit, crosses the interface to interact with Y159, A160 and N163 of the other subunit (9).

The structural data discussed above, which show that the cluster and nucleotide are to distant too interact directly, confirm the prior data that also suggested a lack of direct contact (6). These and other biochemical experiments (33,34) have led to a working hypothesis that nucleotide binding induces a conformational change in the Fe protein that affects the [4Fe-4S] cluster. This hypothesis represents the limiting situation for a recently proposed allosteric model for how the cluster and nucleotide might communicate over long distances via residues located at the subunit interface (9). That model suggests that significant quantities of different conformational states of the Fe protein normally exist, and that it is the equilibrium between the states that is sensitive to oxidation and nucleotide binding (9,35). Site-directed mutagenesis experiments have begun to examine the role of specific residues in the conformational change. Residues modified to date include "Walker" motif residue K15 (26) and residue A157, which is near the proposed adenine binding site (37). Mutations at both of these sites prevent the MgATP induced conformational change.

Binding of the Fe Protein to the MoFe Protein. Kinetic studies of nitrogenase, involving the measurement of substrate reduction activity, have shown that there are two Fe protein binding sites per MoFe protein and that the two proteins associate only transiently (17). Chemical cross-linking studies have identified Fe protein residue Q112 as a residue that can form a specific cross-linked product with K399 of the β subunit of the MoFe protein (38,39). Q112 is on the same "top" surface of the Fe protein as the [4Fe-4S] cluster (8,9). Also located on that surface is the conserved R100, a residue that has been proposed to be involved in Fe protein/MoFe protein interaction (40,41). Analysis of site-directed mutations of that residue have led to the suggestion that it may be involved in a salt bridge with the MoFe protein (41). The chemical cross-linking reaction was insensitive to the presence or absence of nucleotides and thus, Fe protein/MoFe protein complexes appear to form in the absence of MgATP or MgADP (38). Recently, however, two reports have provided evidence that the MoFe protein may have a strong preference for the MgATP-bound conformation of the Fe protein (26,37). Thus, site-directed mutations that allow MgATP binding but prevent the MgATP induced conformational change, result in Fe proteins that do not compete successfully with wild-type Fe protein in an activity assay (26,37).

The MoFe Protein

The MoFe protein is a ca. 220,000 Mr tetramer of two α and two β subunits encoded by the *nifD* and *nifK* genes, respectively. Unlike the *nifDK* genes, which

are contiguous on the chromosome, both the *vnf* and *anf* systems, have another gene designated G, inserted between D and K. The *vnfG* and *anfG* genes each appear to encode a ca. 13,000 Mr protein, which may be a third type of subunit (designated δ) associated with the vanadium and alternative versions of the MoFe protein (42). Thus, these have been reported to be hexamers with $\alpha_2\beta_2\delta_2$ subunit patterns. It is not clear, however, if the δ subunits are required for activity. Two types of metal centers are believed to be contained within the $\alpha_2\beta_2$ units of the MoFe protein, designated the P-clusters and the FeMoco centers, respectively. A similar organization is likely for the *vnf* and *anf* systems (2,42). The MoFe protein has long been believed to be a dimer of two identical halves that do not communicate with each other, with each half containing a single FeMoco cluster (43). This view was recently confirmed by X-ray crystallographic analysis of the *C. pasteurianum* MoFe protein, that showed that the two FeMoco sites are 70Å apart (44). The same structural analysis showed that the P-clusters are 19Å from the FeMoco centers.

The P-clusters. The Fe atoms. The P-cluster concept was originally introduced by Zimmerman *et al.* in 1978 based on Mössbauer analysis of the MoFe protein of *A. vinelandii* nitrogenase (45). These and subsequent Mössbauer studies (46-49), combined with analytical data and quantitative cluster extrusion experiments (46,50), led to a dominant P-cluster hypothesis that was almost universally accepted by 1987 (for reviews see 51-53). At that time, the P-clusters were believed to be discrete, albeit spectroscopically unusual, [4Fe-4S]-type clusters and each $\alpha_2\beta_2$ tetramer was thought to contain four P-clusters. In the dithionite reduced state the P-clusters are diamagnetic and were designated P^N , with each P^N proposed to contain four ferrous Fe atoms. The individual Fe atoms within each P^N cluster were further differentiated into three subtypes, designated Fe^{2+} , D and S. The dithionite reduced MoFe holoprotein thus appeared to contain four P^N clusters occurring in two slightly different pairs: $2[D_3Fe^{2+}] + 2[D_2SFe^{2+}]$.

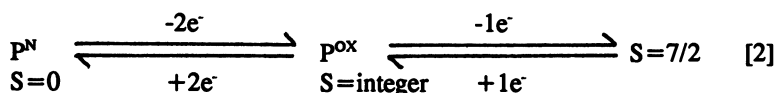
A major argument in favor of this P-cluster model came from studies of the dye oxidation of P^N to yield a state P^{OX} . This oxidation occurred with an $E^0 \approx -420$ mV vs. SHE. Mössbauer analysis of P^{OX} was initially interpreted in terms of P^{OX} being a system with an odd number of electrons (45). This required that an odd number of electrons had to be removed in order to undergo the transition from the $S=0$ P^N state, to the P^{OX} state. When this information was combined with electron counting and metal analysis data, it followed that P^{OX} must be a $1e^-$ oxidation product of P^N . Since P^N was viewed at the time as a $[4Fe-4S]^0$ cluster, its one electron oxidation should have yielded a $[4Fe-4S]^{1+}$ cluster. $[4Fe-4S]^{1+}$ clusters are common in proteins and are generally EPR active exhibiting $S=1/2$ and/or $S=3/2$ signals (16). One puzzling feature of the P-clusters was that although transient $S=1/2$ type EPR signals were sometimes observed during oxidative titration of the MoFe protein, P^{OX} was a stable, paramagnetic, but EPR silent cluster. Low temperature magnetic circular dichroism (MCD) studies further suggested that P^{OX} was probably a $S=5/2$ or $S=7/2$ system (54,55).

The dominant P-cluster hypothesis discussed above was first challenged in 1987 by Hagen *et al.* based on EPR studies of the MoFe protein (56). They observed a stable $S=7/2$ EPR signal for the MoFe protein P-clusters following

oxidation with solid thionine. Because this oxidized state was EPR active it had to be distinct from P^{OX} . To explain their data, they proposed that there might be only two P-clusters per MoFe protein, each containing 8Fe atoms. In this model the $S=7/2$ state was proposed to arise from the three electron oxidation of an 8Fe containing $S=0$ P^N . This model was initially rejected by Lindahl *et al.* in 1988 based on a combined EPR and Mössbauer study (57).

A major breakthrough in the understanding of P-clusters came in 1990 when Bolin and co-workers published the analysis of anomalous scattering data for crystals of the *C. pasteurianum* MoFe protein. These data showed that there were only four metal clusters of approximately equal density per MoFe protein $\alpha_2\beta_2$ tetramer. Because two of the four were FeMoco centers, it followed that there could only be two P-clusters per $\alpha_2\beta_2$ tetramer, each containing 8Fe atoms (44). To be consistent with other data, it also followed that if the P-clusters were composed of $[4Fe-4S]^0$ units, then each P-cluster would contain two $[4Fe-4S]^0$ clusters, somehow bridged so that they were no more than 4.5 Å center-to-center (44).

In light of this information and with new data for a number of model compounds, the Mössbauer data were reanalyzed to show that P^{OX} was actually an integer spin system (58) and not a Kramers system as previously reported (45). This brought the Mössbauer analysis in line with the Hagen proposal (56) and the structural data (44). Thus, the eight-iron P-clusters are now believed to undergo the oxidation shown in equation [2].



The transient $S=1/2$ EPR signals observed during MoFe protein oxidation could then arise from $1e^-$ oxidation of the 8Fe P^N clusters. Although P^{OX} is now believed to be an integer-spin system its precise spin state is still unknown and the MCD data, which led to the interpretation of P^{OX} as an $S=7/2$ or $S=5/2$ state, have yet to be reanalyzed.

P-cluster ligands. The data discussed above are now consistent with the view that P^N is best represented as two bridged $[4Fe-4S]^0$ clusters. Such highly reduced $[4Fe-4S]^0$ cluster units have never been observed in proteins and can only be produced in synthetic systems at extremely low potentials. Stable protein-bound all ferrous $[3Fe-4S]^2$ clusters have been produced electrochemically at low potential (59). It is likely that these clusters are stabilized by protonation (59) and this has been suggested as a possibility for the P-clusters as well (60). Another possibility that has been repeatedly suggested is that the P-clusters might have non-cysteine ligation and/or a ligation pattern other than one cysteine per Fe atom (52,60).

Support for the last idea has come from detailed comparisons of the primary sequences for MoFe proteins from different organisms and from site-directed mutagenesis studies (61-64). Figure 3 shows the consensus view that has emerged, with each P-cluster likely to have a total of only six cysteine ligands. These are three conserved Cys residues 62,88,154 in the α subunit, which are located within

62		88	154		
R G C A Y		H G P V G C	C P I G L I G D D	Av	
R G C A Y		H G P V G C	C P V G L I G D D	Bj	
R G C A Y		H G P V G C	C P I G S I G D D	An	α
R G C A Y		H G P I G C	C P V G L I G D D	Cp	
K A C Q P		H G S Q G C	C M A E V I G D D	Av	
K A C Q P		H G S Q G C	C M A E V I G D D	Bj	
K G C Q P		Q G S Q G C	C M A E V I G D D	An	β
K T C Q P		H G S Q G C	C L S E T L G D D	Cp	
70		95	153		

Figure 3. Comparison of sequences surrounding P-cluster ligands.

regions that have amino acid sequence identity when compared to the corresponding regions surrounding the other three putative ligands, Cys residues 70,95,153 in the β subunit. Thus, as predicted (62), the P-clusters appeared to bridge between the two subunits. No direct evidence for P-cluster ligands other than these six cysteines has been obtained for the wild-type MoFe protein. It should be noted, however, that two of the putative Cys ligands, $\alpha 88$ and $\beta 153$ can tolerate some substitutions to other residues with partial retention of activity.

P-cluster Structure. Recently Kim and Rees have presented a P-cluster model that is consistent with the above data based on crystallographic analysis of the *A. vinelandii* MoFe protein (65). The model shows two [4Fe-4S] clusters bridged by two cysteine thiols ($\alpha 88$, $\beta 95$) with the other four cysteines singly coordinating the remaining Fe sites. It is not known if the presence of six, rather than eight, thiol ligands for the two bridged [4Fe-4S] clusters, removes enough negative charge to stabilize an all ferrous state, or if the stabilization requires protonation or other, as yet unrecognized, protein interactions.

FeMo cofactor. FeMoco can be studied when it is within the MoFe protein or after extraction into N-methyl formamide (66). Since this subject has recently been reviewed in detail (53,67,68) this section will only briefly summarize and update that information.

Metal composition and organization. The following is a brief summary of conclusions about cluster organization drawn from spectroscopic experiments that are reviewed elsewhere (53,67,68). Analytical and spectroscopic data have long been consistent with the stoichiometry $\text{Mo:Fe}_{6-8}:\text{S}^{2-}_{8-9}$, with most data favoring the lower Fe numbers. The metal atoms are arranged in a spin-coupled cluster. In the presence of dithionite this cluster gives rise to the $S=3/2$ EPR signal that is exhibited by both the protein and the isolated FeMoco. The three unpaired electrons appear to be delocalized among the Fe atoms with the Mo atom playing a minor role in this $S=3/2$ system. In this dithionite reduced state, the Mo atom is most likely in the +4 formal oxidation state. X-ray absorption spectroscopy shows that the Mo atom is surrounded by a mixed S, O(N) ligation sphere having, most likely, a distorted octahedral geometry. The O(N) ligands must be anionic with Mo-O(N) distances of 2.1Å. The Fe atoms exist in at least two different sets, those which "see" the Mo (~ 3) and those which do not. The Fe atoms are most likely connected to the Mo atoms and to each other via sulfide bridges using a total of 8-9 sulfides. The relevant distances are Mo-S 2.3Å, Fe-S 2.2-2.5Å and Mo-Fe 2.7Å. Some Fe atoms also appear to "see" other Fe atoms at 3.68Å. Isolated FeMoco has an overall negative charge which probably arises due to some exogenous thiosulfate ligands on iron. FeMoco is highly asymmetric when bound to the protein with at least five different Fe environments. When it is released, it becomes more symmetric without major change in the magnetic properties of the $S=3/2$ state.

Ligands for protein-bound FeMoco. In addition to its metal atoms, FeMoco is now known to have the endogenous organic component (R)-homocitric

acid in a ratio of one homocitrate per Mo (69). By analogy to aconitase, where the substrate citrate binds to a single Fe atom of a [4Fe-S] cluster, the homocitrate has been suggested to be a terminal ligand to either Mo or Fe (67). The former is most likely based on Mo and Fe EXAFS experiments which show anionic O(N) ligands on Mo (70) and, in one report, no O(N) atoms on Fe (71). The same analogy with aconitase would suggest that the homocitrate might bind through the carboxylate oxygen attached to the chiral carbon atom and through the hydroxyl group. Indirect evidence from biochemical (69) and genetic (72) experiments indicates that the FeMoco retains its homocitrate when it is extracted from the protein.

In 1978, Rawlings *et al.* reported that the addition of thiophenol to isolated FeMoco in NMF caused its EPR signal to sharpen, making it look more like the signal exhibited by the FeMoco center of the MoFe protein (73). Since then, the reactivity of FeMoco with thiolate ligands has been studied in detail. The results show that there is a single thiol binding site on isolated FeMoco and that it is on Fe and not on Mo (67). These data, combined with sequence comparisons, suggest strongly that there is a single Cys ligand to FeMoco in the MoFe protein. This was predicted to be α Cys²⁷⁵ based on sequence comparisons (61), and this prediction has been confirmed by site-directed mutagenesis (64,74,75).

Recently, evidence for N ligation to FeMoco in the MoFe protein has been obtained by comparing electron spin echo data for the MoFe protein to that for isolated FeMoco (76). The electron spin echo modulation spectrum of the protein, but not of the isolated FeMoco, was shown to contain lines characteristic for N coordination to a paramagnetic metal center. The site-directed mutation of α subunit His 195 to an Asn residue resulted in the disappearance of this spectrum, and caused changes in the S=3/2 EPR signal and the loss of N₂ fixation activity (77). Taken together, these data provided strong evidence that His 195 was a ligand to FeMoco (77). However, an alternative interpretation was also offered, namely that mutation of His 195 somehow affected the protein structure causing alteration of N coordination at a distant site.

Structure of Protein Bound FeMoco. In a recent historic paper Kim and Rees presented a model for the FeMoco center of the MoFe protein that is consistent with the above data (65). This model was based on crystallographic analysis of the *A. vinelandii* MoFe protein. That model gives a stoichiometry of Mo:Fe₇:S₈: homocitrate, and shows the FeMoco to be composed of a [4Fe-3S] cluster and a [Mo-3Fe-3S] cluster bridged by three non-protein ligands, at least two of which are S²⁻ atoms. The homocitrate is a terminal ligand to Mo, binding through one carboxylate oxygen and the hydroxyl group in a manner similar to the way citrate appears to bind to aconitase. The Mo also has a single N ligand from Histidine. However, that His is not α His195 but rather α His442. The only other protein ligand appears to be α C275 which is a terminal ligand to a single Fe atom. To date, no structure of the isolated FeMo cofactor is available.

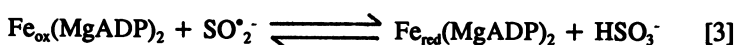
vnf and anf Metal Clusters. The limited information that is available from sequence comparisons and MCD data on the VFe protein would support the suggestion that it contains P-clusters that are similar, if not identical, to those of

the MoFe protein. The FeVaco site of that protein and isolated FeVaco have been studied by EPR, and Fe and Mo EXAFS and the data are consistent with the VFe protein having a Fe-V-S cluster analogous to the FeMoco site of the MoFe protein (2,42). The alternative (i.e., *anf*) version of the MoFe protein has been purified from two organisms and preliminary characterization indicates that it is likely to be an "Fe-only" nitrogenase with a cofactor site that gives rise to an S=3/2 EPR signal (78). Homocitrate is needed for all three cofactors (79).

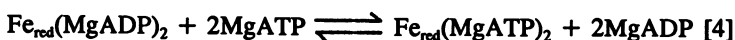
Nitrogenase Turnover

As indicated in the introduction, the general direction of electron flow is from reductant to the Fe protein to the MoFe protein to substrate. What is known about the details of this electron transfer sequence is reviewed elsewhere (3,17) and will be only briefly treated here. There are no known species differences or known differences between the Mo, V and alternative systems with respect to the overall steps, although the individual rate constants do vary.

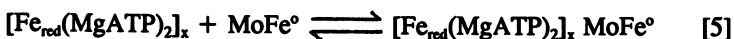
Almost everything that is known about nitrogenase turnover comes from steady state and pre-steady state kinetic experiments that were carried out using SO_2^- as the reductant for the Fe protein. As discussed in section 2.2 above, the oxidized Fe protein can exist in at least three forms; 1) uncomplexed; 2) complexed with 2MgATP; and 3) complexed with 2MgADP. Although any of these forms can be reduced by SO_2^- the bulk of kinetic data support the suggestion that the first step is the reduction of the $\text{Fe}_{\text{ox}}(\text{MgADP})_2$ complex as shown in equation [3].



As shown in equation [4], for electron flow to continue the MgADP must then exchange with MgATP.

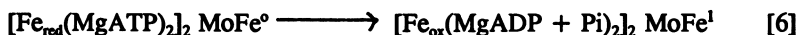


The next step in nitrogenase turnover involves complex formation between the Fe protein and the MoFe protein, which is initially in its dithionite-reduced state, designated MoFe° . Cross-linking studies indicate that Fe and MoFe protein complexes can form in the absence of nucleotides (38) and kinetic studies demonstrate that complexes between oxidized $\text{Fe}(\text{MgATP})_2$ and the MoFe protein can also form (80). However, during turnover, complex formation is probably best described by equation [5].



Recent mutagenesis data support this suggestion by showing that the MoFe protein appears to have a strong preference for the MgATP conformation of the Fe protein (26,37). The value of X has been extensively investigated (3,10,17) to show: 1) that there are two binding sites for the Fe protein on the MoFe protein; 2) that active 2Fe/MoFe protein complexes exist; and 3) that active 1Fe/MoFe complexes can also exist when Fe protein is limiting. Thus the maximum value for X is 2.

The overall next step in nitrogenase turnover involves MgATP hydrolysis and electron transfer as shown in equation [6]

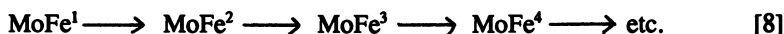


MoFe^1 represents a species where each half of the MoFe protein has been reduced by one electron. The minimum stoichiometry is two MgATPs hydrolyzed per electron transferred. Until 1987, all available data suggested that electron transfer from the Fe protein to the MoFe protein occurred with concomitant MgATP hydrolysis (3,10,17). However, more recent data suggest that MgATP hydrolysis may precede electron transfer (81,82). This MgATP hydrolysis represents the major energy expenditure for N_2 reduction and its function at the molecular level is not understood.

The final step in the catalytic cycle is the dissociation of the complex (equation [7]).



This dissociation step is believed to be the rate-limiting step in a single catalytic cycle for nitrogenase turnover (17). At the end of the step illustrated in equation [7] the reduced MoFe^1 is free in solution and may complex with the Fe protein again to be reduced by additional electrons as shown in [8]



Where Do the Electrons Go In the MoFe Protein? During nitrogenase turnover the $S=3/2$ FeMoco center of the MoFe protein is reduced to an EPR-silent, but paramagnetic state (83-85). The one-electron reduction of isolated FeMoco to an EPR silent state has also been accomplished electrochemically, but this state does not reduce substrates (86). For the protein, the disappearance of the EPR signal occurs following the addition of one electron per FeMoco center, indicating that FeMoco is the final location for the first electron that enters from the Fe protein (46). Although it seems likely that the electrons are transferred from the Fe protein to the P-clusters and then to FeMoco, there is currently no compelling experimental evidence to suggest that is the case.

As indicated below, all products that leave nitrogenase have been reduced by multiples of two electrons. Thus, the MoFe protein must be able to accumulate several electrons before products are released. At present it is not clear if those electrons are stored in the P-clusters, in the FeMoco or if, when they enter the protein one at a time, they are immediately used to produce enzyme-bound reduced substrate intermediates. It is interesting to note, however, that the recently determined structures of both the P-clusters and the FeMoco suggest that either might be capable of two electron transfers (65).

General Features of Substrate Reduction by Wild-Type MoFe Protein. The substrate reactions of nitrogenase were recently reviewed in detail (3,87). This

section will briefly summarize some of that general information with emphasis on recent studies showing how substrate reactivity can be modified by alteration of the FeMoco site of the MoFe protein:

Substrate Binding. As indicated below, mounting circumstantial evidence is consistent with FeMoco being the substrate reducing site of nitrogenase. As shown in Figure 4, nitrogenase is a promiscuous enzyme capable of reducing a wide variety of substrates. These range in size from 2H^+ to substrates as large as 1-butyne and the the isonitrile $\text{CH}_2=\text{CHNC}$. Despite its size, this isonitrile is a fairly good substrate with a K_m of ~ 0.8 mM, indicating that it binds more tightly than N_2O or N_3^- (87). Kinetic evidence suggests that some substrates (e.g. CH_3NC) can bind in more than one orientation to the same site, and that two molecules of different substrates and/or inhibitors can be bound simultaneously (87). These data indicate that the substrate binding site must be both large enough and flexible enough to accommodate the variety of structures shown in Figure 4. It must also be able to accept both neutral and anionic substrates.

Most proposals for substrate reduction have involved end-on binding to a single metal-atom, side-on binding to a single metal-atom, or having the substrate bridged between two metal atoms. Although most early proposals involved direct binding to Mo, the observation that V based nitrogenase, and probably "Fe only" nitrogenase can also fix N_2 suggests that substrate binding may occur through Fe (2). The recently published model for the structure of FeMoco included speculation that substrates might be bound between two Fe atoms, or be held in a cavity in the inside of FeMoco that might allow six Fe atoms to interact with substrates (65).

Unfortunately, at present, there is very little direct evidence for substrate binding to protein-bound FeMoco. EPR studies have provided some indirect evidence for C_2H_2 and CO binding to the $S=3/2$ center of the MoFe protein (85,88). However, MoK absorption edge and EXAFS spectra for the dithionite-reduced MoFe protein are identical before and after the addition of C_2H_2 , CO, N_2 , NaN_3 , NaCN or CH_3NC (89). Thus, if these species do bind to the $S=3/2$ center of the MoFe protein, they do not appear to bind to Mo.

One possible reason for the lack of direct spectroscopic evidence for substrate binding is that some substrates may only bind to protein-bound FeMoco after it has been reduced by one or more electrons. For example, pre-steady state data provide strong evidence that N_2 only binds to a highly reduced state of the MoFe protein (17). Another possibility is that the FeMoco site might be somehow oriented within the protein such that the substrate binding site is only accessible under turnover conditions. If this is the case, then some substrates might be expected to bind to the isolated FeMoco in NMF. In fact, EPR (53) and NMR (89) data do indicate that cyanide and CH_3NC can bind to isolated FeMoco in NMF but that they are unlikely to bind to Mo. Because isolated FeMoco does not reduce these substrates it is not clear whether (or if) this binding is related to the productive binding that occurs at the enzyme active site.

General characteristics of substrate reduction. (Unless otherwise indicated this information is taken from reference 87). Most reducible substrates

contain NN, NO, NC or CC triple or potential triple bonds. Exceptions are allene, cyclopropene, diazirine, nitrite (90) and ethylene (91) which contain double bonds, and hydrazine which contains a single NN bond. The CO triple bond is not reduced by nitrogenase. Nitrogenase can cleave NN, NO (in N_2O and NO_2^- but not in NO) or NC bonds, but not CC bonds.

Substrate reduction requires the transfer of electrons from FeMoco to bound substrate. Regardless of which substrate is being reduced, all products are reduced by multiples of two electrons and products reduced by 2,4,6,8,10,12 and 14 electrons have been reported. Similarly, all direct evidence for the formation of enzyme bound intermediates during substrate reduction suggests that those intermediates are also reduced by multiples of two electrons. Thus, it is possible that electrons are transferred from FeMoco to substrate either one at a time or two at a time.

With the exceptions of NO_2^- and N_3^- , all substrate reductions incorporate an equal number of protons and electrons. In the case of acetylene reduction, the protonation reaction has been studied by monitoring substrate reduction in D_2O . For example, C_2H_2 reduction in D_2O gives only *cis* $C_2H_2D_2$ as a product. The geometric specificity of this reaction and the retention of the acetylene protons has been used to support a concerted $2H^+/2e^-$ transfer mechanism. Currently no direct information is available concerning how protons are transferred to the FeMoco site of the protein or where they reside on FeMoco prior to their transfer to substrate. Thus, in addition to the possibility of hydrides (17), the sulfur atoms on FeMoco could be protonated directly, or the protonation could involve homocitrate, the protein ligands to FeMoco, or nearby amino acid residues. In addition, there is evidence for protonation of isolated FeMoco in NMF (92).

Changes in Substrate Reactivity. Caused by Changes in Electron Flux. One complication of studying nitrogenase is that protons are always available and they can be reduced by the enzyme to form H_2 -gas. Thus, even in the absence of added reducible substrates, once dithionite, MgATP and the Fe protein are added, the MoFe protein turns over with electrons entering from dithionite and leaving as H_2 gas. When other substrates like N_2 are added, the rate of electron flow through the enzyme does not change but now the enzyme chooses whether to use the electrons to produce H_2 or to reduce N_2 to ammonia. The choice the enzyme makes varies depending upon: 1) the substrate being reduced and its concentration; and 2) the rate at which the electrons are transferred to the substrate reduction site. For example, for N_2 , high rates of electron flux favor N_2 reduction over H_2 evolution. However, even in the presence of very high $[N_2]$ and at high flux, ca. 25% of the electrons are still used to evolve H_2 (17,87). In contrast, for HCN reduction high rates of flux favor H_2 evolution over HCN reduction, but at high enough $[HCN]$ H_2 evolution can be almost eliminated (87). Some nitrogenase substrates (e.g., HCN, CH_3NC) are reduced primarily by six electrons but with some lesser reduced, $2e^-$ and $4e^-$ products being released along the way. In that case, the rate at which electrons are delivered to the MoFe protein changes the ratios of the 2:4:6 e^- products, presumably by changing the lifetimes of the enzyme-bound intermediates that give rise to those products.

The above discussion indicates that any process that increases the time it

takes for the next electron to reach the substrate reduction site is expected to change: 1) the ratio of H_2 evolved to substrate reduced; and 2) the ratios of 2:4:6 e^- substrate reduction products. For wild-type Mo nitrogenase, factors that change the time it takes for the next electron to reach the substrate reduction site include changes in the Fe/MoFe protein ratio and/or the MgATP/MgADP ratio as well as changes in physical parameters like the pH, [salt] or temperature (87). Heterologous crosses between Fe proteins from one organism and MoFe proteins from another can also have altered substrate reactivity. In site-directed mutagenesis studies then, any mutation in the Fe protein or MoFe protein that changes the interaction between the two proteins (93), or otherwise interferes with the pathway of electron transfer to the FeMoco site, might change substrate reactivity even though the mutated residues are not directly involved in substrate binding and reduction.

Changes in Reactivity for Mo Versus V and "Fe Only" Nitrogenases.

As shown in Table I there are significant differences in substrate reactivity when the MoFe protein, the VFe protein and the proposed "Fe only" protein are compared (2,42,53). The non-Mo nitrogenases both appear to turnover more slowly than the Mo system with specific activity for VFe protein being 70-80% and for "Fe only" being only ca. 10% of the MoFe protein. It should be noted, however, that the assay conditions used were originally optimized for the Mo system and further purification, characterization and optimization of the VFe and especially "Fe only" systems may eventually lead to higher values for specific activity.

Another major difference in substrate reactivity concerns the efficiency of the three systems with respect to N_2 -reduction. Under optimal conditions ca. 75% of the electrons and MgATP that are used by the MoFe protein are directed into N_2 reduction with the remainder being "lost" as H_2 evolution. As shown in Table I for the VFe protein only 36% of the electrons are used to reduce N_2 . The "Fe only" system is even less efficient with only 24% of the electrons being used to reduce N_2 , the remainder going to H_2 evolution. The MoFe protein is also much more efficient at C_2H_2 reduction to C_2H_4 (Table I).

Some of these differences in reactivity may reflect differences in the affinity of the various active sites for the same substrate. For example the reported K_m C_2H_2 for the VFe protein is much larger than the K_m C_2H_2 for the MoFe protein.

All three nitrogenase systems reduce C_2H_2 to C_2H_4 , however, only the V and "Fe only" nitrogenases normally reduce C_2H_2 to C_2H_6 . Thus, for the VFe protein C_2H_6 production can use up to 7.4% of the total electron flow (94), while for the wild-type MoFe protein C_2H_6 has never been observed as a C_2H_2 reduction product. The VFe protein also produces a different product during N_2 reduction. Thus, while the reduction of N_2 by the MoFe protein yields only the six electron product ammonia, the reduction of N_2 by the VFe protein yields very small amounts (ca. 0.5% of electron flow) of free N_2H_4 , in addition to ammonia (95).

At present it is not known if the differences in the reactions described above are due to simple substitution of one metal for another in FeMoco or if they reflect a different fit of the cofactor in the protein or a different protein environment. For example, the *vnfD* and *anfD* gene products each share only 33% identity with the

1.	H ⁺	9.	C ₂ H ₂	16.	$\begin{array}{c} \text{CH}_2 \\ \diagup \quad \diagdown \\ \text{N}=\text{N} \end{array}$
2.	N ₂	10.	C ₂ H ₄		
3.	N ₂ H ₄	11.	CH ₃ C≡CH	17.	HCN/CN ⁻
4.	N ₃ ⁻	12.	C ₂ H ₅ C≡CH	18.	CH ₃ CN
5.	N ₂ O	13.	H ₂ C=C=CH ₂	19.	C ₂ H ₃ CN
6.	NO ₂ ⁻	14.	$\begin{array}{c} \text{CH}_2 \\ \diagup \quad \diagdown \\ \text{HC}=\text{CH} \end{array}$	20.	C ₃ H ₇ CN
7.	H ₂	15.	N≡CNH ₂	21.	CH ₃ NC
8.	CO			22.	C ₂ H ₅ NC
				23.	H ₂ C=CHNC

Figure 4. Nitrogenase substrates and inhibitors.

TABLE I. The V and "Fe-only" nitrogenases show different substrate reactions when compared to the MoFe protein (2)

	MoFe	VFe	"Fe-only"
Sp. Activity (nmoles H ₂ /min/mg)	2100	1348	253
%e ⁻ to N ₂	70%	36%	21%
%e ⁻ to C ₂ H ₂	85-95%	45%	11%
C ₂ H ₂ Products	C ₂ H ₄	C ₂ H ₄ /C ₂ H ₆	C ₂ H ₄ /C ₂ H ₆
N ₂ Products	NH ₃	NH ₃ /N ₂ H ₄	NH ₃ /?

Nif D protein and similar values are obtained for comparisons of the K gene products (42). Thus, the polypeptides are substantially different. In order to get information on that point Smith *et al.* removed the FeVaco from the VFe protein and inserted it into the MoFe polypeptides (96). Unfortunately, the product did not behave like either of the parent species, and was no longer capable of fixing N_2 although it was still capable of C_2H_2 reduction to both C_2H_4 and C_2H_6 .

Changes caused by changes in the MoFe protein. Two site-directed mutant variants of the MoFe protein have also been shown to have altered substrate reactivity. The two α subunit residues, Q191 and H195 were originally chosen for mutagenesis as putative FeMoco ligands (77,97). Recent crystallographic analysis now shows that both residues are close to the FeMoco site but that neither is directly coordinated to FeMoco (65). Neither of the two mutants, Q191K or H195N was capable of N_2 reduction and both had altered FeMoco EPR signals. Interestingly both reduced C_2H_2 to C_2H_6 , a reaction that is not normally carried out by the MoFe protein but is carried out by the VFe and "Fe only" proteins. Thus, it is possible to obtain non-Mo type reactivity with the MoFe protein, by altering specific amino acid residues near the FeMoco site.

Changes caused by alteration in homocitrate. Using an *in vitro* system for the synthesis of FeMoco, a number of analogues have been produced using organic acids other than R-homocitrate (98,99,100). To be competent for Mo incorporation in the MoFe polypeptides and to give some substrate reduction activity these appear to need: 1) stereochemistry at the chiral C-2 carbon like that of the R isomer of homocitrate; 2) a hydroxyl group on the chiral carbon atom; 3) a carboxyl group on the chiral carbon atom; 4) a carboxyl group α to the chiral center; and 5) a four to six carbon chain with two terminal carboxylates (99). This information is consistent with the FeMoco model based on crystallographic analysis, which shows that the Mo atom receives two ligands from homocitrate, one the hydroxyl group and one a carboxyl group from the chiral C atom (65). Comparisons of substrate reduction activities for sixteen analogues, substituted at C_1 , C_2 , C_3 and C_4 indicate that the requirements for H_2 evolution by FeMoco are not very stringent. C_2H_2 reduction is more sensitive, with some organic substitutions (e.g. isocitrate and homoisocitrate) giving H_2 reduction activity almost as high as for homocitrate but showing only 10-20% of the C_2H_2 reduction activity. By far the most stringent requirements are for N_2 reduction. Significant levels of NH_3 were only observed for homocitrate, erythro-fluorohomocitrate and R-citroylformate that has a (-CO-) substituted for a (- CH_2 -) at the C_4 position.

Substitution of homocitrate by other organic acids has also produced MoFe proteins with altered reactivity toward CO. When CO is added to wild-type MoFe protein it serves as a non-competitive inhibitor of substrate reduction but does not inhibit H_2 evolution (17). Some homocitrate analogues with substitutions at the C_1 carbon, and citrate, which is missing C_4 , have MoFe proteins where CO is now an inhibitor of H_2 evolution (100). Again, however, similar changes in substrate reactivity can occur for homocitrate containing MoFe protein. Thus, the site-directed Q191N mutant described in section 4.3b above also exhibits CO inhibition of H_2 evolution (97).

At present it is not known if homocitrate participates directly in substrate reduction, for example by serving as a proton donor or if, it is simply important as a ligand for Mo. In that capacity it may be needed to guarantee the required geometry at the Mo site, the proper fit of the cluster in the protein, or the proper juxtaposition of other catalytic groups. Taken together, the above information suggests that the FeMoco site of the MoFe protein is extremely fine tuned to serve as an N₂ reductase. Changes in metal composition, protein environment or homocitrate often result in proteins that can still evolve H₂ but usually they are no longer effective nitrogenases. This, unfortunately, increases the difficulty of trying to produce effective synthetic systems for N₂ reduction based on FeMoco or its analogues.

Nitrogenase Assembly

Several recent reviews have focused on what is known about FeMoco biosynthesis and the assembly of the Fe protein and MoFe proteins (53,67,68,101,102). Therefore that subject will be only briefly treated here.

Fe Protein Assembly. When the *K. pneumoniae* Fe protein polypeptides were expressed in a foreign background in *E. coli*, no active Fe protein was assembled (103). When the same polypeptides were expressed along with the *nifM* gene products active Fe protein was obtained (103). These data, combined with studies showing that mutation of the *nifM* gene in *K. pneumoniae* or *A. vinelandii* results in the synthesis of inactive Fe protein (104,105), lead to the conclusion that the *nifM* gene product is required for the synthesis of active Fe protein. To date, there are no reports of purification of either the *nifM* product or of the inactive Fe protein from *NifM* mutants. It is therefore not clear what the *nifM* product does. It does not appear to be required for dimer formation (106) and it may (103) or may not (5) be involved in [Fe-S] cluster assembly.

Some of the above data indicate that *nifH* and *nifM* are sufficient to form a fully functional Fe protein. In contrast to this conclusion, it has been demonstrated that deletion of either the *nifU* or the *nifS* genes in *A. vinelandii* leads to the production of Fe proteins with only very low levels of activity, while deletion of both genes yields essentially no active Fe protein (102). Thus, at least in this organism, these gene products must be involved either in the assembly of active Fe protein or in the stability of that protein. Again the inactive Fe proteins from $\Delta nifS$ and $\Delta nifU$ strains have not been purified so the cause for their lack of activity is not known. In *A. vinelandii*, the processing of the *vnfH* and *anfH* gene products also appears to require the *nifM*, S and U gene products (79).

FeMoco Biosynthesis. *nifV*. The *nifV* gene product is required for all three nitrogenase systems (79) and it is believed to encode the enzyme homocitrate synthase (69). The specific function of homocitrate in FeMoco biosynthesis is currently unknown. The fact that it is excreted into the medium of N₂-fixing *K. pneumoniae* cultures suggests that it might have a role in molybdenum chelation, uptake and/or initial processing (109). Thus, for the Mo system it may serve as a ligand for Mo throughout the biosynthesis of FeMoco.

nifQ. Mo is usually supplied to N₂-fixing bacterial cultures in the form of MoO₄²⁻. Thus, at some point during FeMoco biosynthesis the Mo atom in MoO₄²⁻ must be reduced and its ligation sphere changed from all O to mixed S and O(N). One nif specific protein that is probably involved in Mo processing is the nifQ gene product. The Nif Q protein has never been identified, but the nifQ sequence has been determined and it does contain a putative cluster binding site with the sequence Cys-X₄-Cys-X₂-Cys-X₅-Cys (102).

Mutants of *K. pneumoniae* with defects in the nifQ gene can only fix N₂ when extremely high (>10 μM vs. 10 nM for wild-type cells) MoO₄²⁻ concentrations are available. The Nif Q gene product, however, is not believed to be involved in MoO₄²⁻ transport but rather, in Mo accumulation or processing (107). When Nif Q mutants were supplied with a reduced form of sulfur, by substituting SO₄²⁻ with cysteine in the growth media, they fixed N₂ at low [MoO₄²⁻] and accumulated higher levels of Mo (108). Thus the nifQ gene product may be involved in the synthesis of a Mo-S unit for eventual incorporation into FeMoco. It is not known if there are vnf and/or anf analogues of nifQ.

nifB. Organisms with defects in the nifB gene accumulate inactive FeMoco-deficient forms of the MoFe protein but do not accumulate FeMoco. Their inactive MoFe proteins can be activated in vitro by the addition of isolated FeMoco in NMF (66). The nifB product is required for the synthesis of FeMoco, FeVaco and the "Fe-only" cofactor and therefore it is believed to be involved in assembly of the [FeS] portion of the cofactor, and not the Mo portion. Although the nifB gene product has not been purified its sequence indicates that it has a cysteine rich, highly conserved region that may serve as a cluster binding site (102).

nifN and nifE. It is currently well established that FeMoco is accumulated in vivo in the absence of the MoFe protein polypeptides, which leads to the conclusion that it must be assembled elsewhere in the cell and later incorporated into the MoFe protein polypeptides (110-112). Since isolated FeMoco is water sensitive (66) it follows that the cell must have some protein which serves as a site for FeMoco assembly. The nifE and nifN gene products have been proposed to fulfill this function (113,102). This proposal was based on sequence comparisons showing that the nifE gene shared sequence identity with the nifD gene while the nifN gene shared sequence identity with the nifK gene. This led to the proposal that nifEN might form an α₂β₂-protein analogous to the α₂β₂ nifDK-encoded MoFe protein with the putative nifEN protein possibly containing both P-clusters and a FeMoco assembly site, analogous to the FeMoco binding site of the MoFe protein (102,113).

A nifEN complex has been purified from *K. pneumoniae* and shown to be an O₂ sensitive, Fe containing α₂β₂ tetramer (114). That protein was purified from a Nif B⁻ mutant and therefore was not expected to contain FeMo cofactor. For the same reason it is not known if the α₂β₂ tetramer is normally associated with the nifB gene product. It is interesting to note however, that in one organism, *C. pasteurianum*, nifN and B are synthesized as a single protein suggesting that the nifNE complex may also associate with the nifB product in other organisms (102).

Strains with mutations in *nifE* and *nifN* genes synthesize inactive FeMoco deficient MoFe proteins analogous to the protein synthesized by Nif⁻ strains (66,115). These proteins can be activated *in vitro* by addition of isolated FeMoco. It should be noted that there are *vnfEN* and *anfEN* genes, indicating that the *nifEN* protein complex contains at a minimum, the Mo portion of FeMoco (2,42).

nifH. Surprisingly, the *nifH* gene, which encodes the Fe protein of nitrogenase, is also required for an early step in FeMoco biosynthesis (111,112,116). A *nifH* deletion strain of *A. vinelandii* accumulates an inactive FeMo cofactor-deficient MoFe protein that can be activated *in vitro* by addition of isolated FeMoco (112,116). Recently, a number of Fe protein mutants have been examined that do not function in nitrogenase turnover but do function in FeMoco biosynthesis. The mutant Fe proteins purified to date all contain normal [4Fe-4S]^{2+/1+} clusters (26,37). In addition, site-directed mutation of that cluster's ligands results in an Fe protein that can no longer participate in FeMo cofactor biosynthesis (5). Thus, a normal [4Fe-4S]^{2+/1+} cluster is likely to be required for this Fe protein function. Mutants purified to date also bind MgATP so this activity might be required. However, the same analysis shows that to participate in FeMoco biosynthesis the Fe protein does not have to be able to undergo the MgATP induced conformational change, does not have to hydrolyze ATP in the usual way, and does not have to transfer electrons to the MoFe protein (26,37).

As indicated above the *nifM*, U and S genes are required for the synthesis of fully active Fe protein. It is interesting to note that mutation of any of these three genes gives some MoFe protein activity indicating that some FeMoco can be synthesized by these strains. It is also important to note however, that these mutants give much lower than wild-type levels of MoFe protein activity. Whether this decrease in activity is due to a difference in FeMoco biosynthesis is currently unknown.

The function of the Fe protein in FeMoco biosynthesis is also currently unknown. The sequence similarity between the $\alpha_2\beta_2$ *nifDK* encoded MoFe protein and the $\alpha_2\beta_2$ *nifEN* encoded protein, make it tempting to speculate that during FeMoco biosynthesis the Fe protein binds to the *nifEN* product (116,117).

MgATP. In addition to the *nifQ*, B, N, E, V and H gene products, MgATP is required for FeMoco biosynthesis (118). The function of the MgATP is not known. However, the Fe protein normally binds MgATP and these two requirements may be related (117). The *nifEN*, $\alpha_2\beta_2$ protein may also bind MgATP (53,114).

Assembly of a FeMoco-deficient MoFe protein. In the absence of FeMoco *in vivo*, FeMoco-deficient MoFe proteins are assembled (111,115,119) that do contain P-clusters (120). It is likely that several *nif* specific proteins are somehow involved in this process. For example, mutations in *nifW* or *nifZ* give MoFe proteins with lower activity indicating that these are somehow involved in the assembly or stability of active MoFe protein in both *A. vinelandii* and *K. pneumoniae* (102). However, the MoFe proteins from Nif⁻ W⁻ and Nif⁻ Z⁻ cells have not yet been purified so their specific defects have not been identified. The

nifY and *nifT* gene products are not required for diazotrophic growth but they have been suggested to be somehow involved in maturation of a FeMoco-deficient MoFe protein (121). FeMoco-deficient MoFe proteins isolated from *NifB*⁻ strains also seem to be associated with a 20 KD protein of unknown origin (111,119).

Interestingly, the Fe protein also seems to be involved in modification of the non-FeMoco part of the MoFe protein. Thus, a Δ *nifH* strain of *A. vinelandii* does not synthesize FeMoco because of the Fe protein requirement for FeMoco biosynthesis discussed above. It does synthesize a stable, Fe containing but inactive, FeMoco-deficient MoFe protein. This MoFe protein can be fully activated by addition of FeMoco *in vitro* but only if the Fe protein and MgATP are added as well (117). Thus, the Fe protein together with MgATP modifies the FeMoco-deficient MoFe protein in such a way that it can accept FeMoco. To be functional in this insertion reaction the Fe protein probably must have a [4Fe-4S] cluster but it does not have to undergo the MgATP induced conformational change, normal MgATP hydrolysis or normal e⁻ transfer to the MoFe protein (37). Although it seems likely that MgATP and the Fe protein work together in this reaction, that is not necessarily the case (115) because the MoFe protein has also been shown to be a nucleotide binding protein (3). As indicated above, *nifM*⁻, *nifU*⁻ and *nifS*⁻ strains that contain inactive Fe proteins also have lowered levels of MoFe protein activity and these genes might therefore be indirectly involved in MoFe protein processing (102,121). Perhaps one or more of these genes serve to modify the Fe protein from a species that interacts optimally with Nif EN to one that acts optimally with Nif DK or, from one that functions in FeMoco insertion to one that functions in electron donation to the MoFe protein.

Some mutants (e.g. *Nif B*⁻, *Nif N*⁻ or *Nif E*⁻) do not synthesize FeMoco but do contain the Fe protein and MgATP. In these strains the modification appears to have already taken place. Thus, not only are the *nifB*⁻, *N*⁻ or *E*⁻ FeMoco-deficient proteins physically quite different from the Δ *nifH* protein (115) but *in vitro* activation of these proteins with FeMoco no longer requires the Fe protein and MgATP (119). In wild-type cells *in vivo*, it is possible that the modification of the FeMoco-deficient MoFe protein by the Fe protein and MgATP immediately precedes FeMoco insertion.

Concluding Remarks

In the past three decades, research has focused on solving the structures of the Fe and MoFe proteins, on defining the overall steps in nitrogenase turnover, on cataloging the substrate reactions of the enzyme, and on isolating and characterizing the *nif*, *vnf* and *anf* genes. Now that the structural problems are being rapidly solved (8,9,49,65) efforts in the near future are likely to focus on trying to determine the molecular level details of nitrogenase turnover, substrate binding and reduction, and on the purification and functional characterization of the numerous proteins involved in nitrogenase assembly.

Acknowledgments

We are grateful to Drs. Rees, Orme-Johnson and Münck for providing research results prior to publication and to NIH Grant No. GM43144 for funding our recent research on nitrogenase.

Literature Cited

1. Normand, P.; Bousquet, J. *J. Mol. Evol.* **1989**, *29*, 436-447.
2. Eady, R.R. *Adv. in Inorg. Chem.* **1991**, *36*, 77-102.
3. Yates, M.G. in *Biological Nitrogen Fixation*; Stacey, G.; Burris, R.H.; Evans, H.J. Chapman and Hall: New York, **1992**; pp 685-735.
4. Hausinger, R.P.; Howard, J.B. *J. Biol. Chem.* **1983**, *258*, 13486-13492.
5. Howard, J.B.; Davis, R.; Moldenhauer, B.; Cash, V.L.; Dean, D. *J. Biol. Chem.* **1989**, *264*, 11270-11274.
6. Morgan, T.V.; McCracken, J.; Orme-Johnson, W.H.; Mims, W.B.; Mortenson, L.E.; Peisach, J. *Biochemistry*, **1990**, *29*, 3077-3082.
7. Thorneley, R.N.F.; Ashby, G.A. *Biochem. J.*, **1989**, *261*, 181-187.
8. Georgiadis, M.M.; Chakrabarti, P.; Rees, D.C. In *Nitrogen Fixation: Achievements and Objectives*. Gresshoff, P.M.; Roth, L.E.; Stacey, G.; Newton, W.E. Chapman and Hall: New York, **1990**; pp. 111-116.
9. Georgiadis, M.M.; Chakrabarti, P.; Woo, D.; Kornuc, J.J.; Rees, D.C. "Crystallographic Structure of the Nitrogenase Iron Protein from *Azotobacter vinelandii*" Submitted to Science 6/18/92.
10. Burgess, B.K. In *Advances in Nitrogen Fixation Research*. Veeger, C.; Newton, W.E. Martinus-Nijhoff: The Hague, **1983**, pp. 103-114.
11. Lindahl, P.A.; Day, E.P.; Kent, T.A.; Orme-Johnson, W.H.; Münck, E. *J. Biol. Chem.* **1985**, *260*, 11160-11173.
12. Watt, G.D.; MacDonald, J.W. *Biochemistry* **1985**, *24*, 7226-7231.
13. Hagen, W.R.; Eady, R.R.; Dunham, W.R.; Haaker, H. *FEBS Lett.* **1985**, *189*, 250-254.
14. Morgan, T.V.; Prince, R.C.; Mortenson, L.E. *FEBS Lett.* **1986**, *206*, 4015-4018.
15. Meyer, J.; Gaillard, J.; Moulis, J.M. *Biochemistry* **1988**, *27*, 6150-6156.
16. Stiefel, E.I.; George, G.N. In *Bioinorganic Chemistry: Structure and Mechanisms*. Bertini, I; Gray, H.B.; Lippard, S.J.; Valentine, J.S. University Science Books: New York, **1993**, in press.
17. Thorneley, R.N.F.; Lowe, D.J. In *Molybdenum Enzymes*; Spiro, T.G. Wiley: New York, **1985**, pp. 222-284.
18. Dao, C. Ph.D. Thesis, **1990**. "Self-oxidation of Dithionite-Av2 solutions". Dept. of Chemistry, University of Southern California.
19. Mortenson, L.E. *Biochim. Biophys. Acta.* **1964**, *81*, 473-478.
20. Nieva-Gomez, D.; Roberts, G.P.; Klevickis, S.; Brill, W.J. *Proc. Natl. Acad. Sci. USA.* **1980**, *77*, 2555-2558.
21. Shah, V.K.; Stacey, G.; Brill, W.J. *J. Biol. Chem.* **1983**, *258*, 12064-12068.
22. Thorneley, R.N.F.; Deistung, J. *Biochem. J.* **1988**, *253*, 587-595.
23. Bennett, L.T.; Jacobson, M.R.; Dean, D.R. *J. Biol. Chem.* **1988**, *263*, 1364-1369.
24. Martin, A.E.; Burgess, B.K.; Iismaa, S.E.; Smartt, C.T.; Jacobson, M.R.; Dean, D.J. *J. Bacteriol.* **1984**, *171*, 3162-3167.
25. Robson, R.L. *FEBS Lett.* **1984**, *173*, 394-398.
26. Seefeldt, L.C.; Morgan, T.V.; Dean, D.R.; Mortenson, L.E. *J. Biol. Chem.* **1992**, *267*, 6680-6688.

27. Walker, J.E.; Saraste, M.; Runswick, M.J.; Gay, N.J. *EMBO J.* **1982**, *8*, 945-951.
28. Zumft, W.G.; Mortenson, L.E.; Palmer, G. *Eur. J. Biochem.* **1974**, *46*, 525-535.
29. Zumft, W.G.; Cretney, W.C.; Huang, W.C.; Mortenson, L.E.; Palmer, G. *Biochem. Biophys. Res. Commun.* **1972**, *48*, 1525-1532.
30. Orme-Johnson, W.H.; Hamilton, W.D.; Jones, T.L.; Tso, M.-Y.W.; Burris, R.H.; Shah, V.K.; Brill, W.J. *Proc. Natl. Acad. Sci. USA* **1972**, *69*, 3142-3145.
31. Smith, D.E.; Lowe, D.J.; Bray, R.C. *Biochem. J.* **1973**, *135*, 331-341.
32. Stephens, P.J.; McKenna, C.E.; Smith, B.E.; Nguyen, H.T.; McKenna, M.-C.; Thomson, A.J.; Devlin, F.; Jones, J. *Proc. Natl. Acad. Sci. USA* **1979**, *76*, 2585-2589.
33. Walker, G.A.; Mortenson, L.E. *Biochem. Biophys. Res. Commun.*, **1973**, *53*, 904-909.
34. Walker, G.A.; Mortenson, L.E. *Biochemistry*, **1974**, *13*, 2382-2388.
35. Deits, T.L.; Howard, J.B. *J. Biol. Chem.* **1989**, *264*, 6619-6628.
36. Fu, W.; Morgan, T.V.; Mortenson, L.E.; Johnson, M.K. *FEBS Lett.* **1991**, *284*, 165-168.
37. Gavini, N.; Burgess, B.K. *J. Biol. Chem.* **1992**, 21179-21186.
38. Willings, A.H.; Georgiadis, M.M.; Rees, D.C.; Howard, J.B. *J. Biol. Chem.* **1989**, *264*, 8499-8503.
39. Willings, A.; Howard, J.B. *J. Biol. Chem.* **1990**, *265*, 6596-6599.
40. Pope, M.R.; Murrell, S.A.; Ludden, P.W. *Proc. Natl. Acad. Sci. USA*, **1985**, *82*, 3173-3177.
41. Wolle, D.; Kim, C.H.; Dean, D.; Howard, J.B. *J. Biol. Chem.* **1991**, *267*, 3667-3673.
42. Bishop, P.E.; Premakumar, R. in *Biological Nitrogen Fixation*; Stacey, G.; Burris, R.H.; Evans, H.J. Chapman and Hall: New York, **1992**; pp. 736-762.
43. Hageman, R.V.; Burris, R.H. *Biochemistry* **1978**, *17*, 4117-4124; *Proc. Natl. Acad. Sci. USA* **1978**, *75*, 2699-2702.
44. Bolin, J.T.; Ronco, A.E.; Mortenson, L.E.; Morgan, T.V.; Williamson, M.; Xuong, N.-h. In *Nitrogen Fixation: Achievements and Objectives*. Gresshoff, P.M.; Roth, L.E.; Stacey, G.; Newton, W.E. Eds. Chapman and Hall: New York, **1990**; pp. 117-124.
45. Zimmermann, R.; Münck, E.; Brill, W.J.; Shah, V.K.; Henzl, M.T.; Rawlings, J.; Orme-Johnson, W.H. *Biochim. Biophys. Acta.* **1978**, *537*, 185-207.
46. Orme-Johnson, W.H.; Münck, E. In *Molybdenum and Molybdenum Containing Enzymes*; Coughlin, M.P. Ed. Pergamon Press, Oxford **1980**; pp. 427-438.
47. Smith, B.E. In *Nitrogen Fixation: The Chemical-Biochemical-Genetic Interface*. Müller, A.; Newton, W.E. Eds. Plenum Press, New York **1983**, pp. 23-62.
48. Zimmermann, R.; Trautwein, A.X. In *Nitrogen Fixation: The Chemical-Biochemical-Genetic Interface*. Müller, A.; Newton, W.E. Ed. Plenum Press, New York **1983**, pp. 63-81.

49. Huynh, B.H.; Henzl, M.T.; Christner, J.A.; Zimmermann, R.; Orme-Johnson, W.H.; Münck, E. *Biochim. Biophys. Acta.* **1980**, *623*, 124-138;
- McLean, P.A.; Papaefthymiou, G.; Orme-Johnson, W.H.; Münck, E. *J. Biol. Chem.* **1987**, *262*, 12900-12903.
50. Kurtz, D.M.; McMillan, R.S.; Burgess, B.K., Mortenson, L.E.; Holm, R.H. *Proc. Natl. Acad. Sci. USA.* **1979**, *76*, 4986-4989.
51. Orme-Johnson, W.H. *Ann. Rev. Biophys. Biophys. Chem.* **1985**, *14*, 419-459.
52. Stephens, P.J. In *Molybdenum Enzymes*; Spiro, T.G. Wiley: New York, **1985**, pp. 117-160.
53. Smith, B.E.; Eady, R.R. *Eur. J. Biochem.* **1992**, *205*, 1-15.
54. Johnson, M.K.; Thomson, A.J.; Robinson, A.E.; Smith, B.E. *Biochim. Biophys. Acta.* **1981**, *671*, 61-70.
55. Morningstar, J.E.; Johnson, M.K.; Case, E.E.; Hales, B.J. *Biochemistry* **1987**, *26*, 1795-1800.
56. Hagen, W.R.; Wassink, H.; Eady, R.R.; Smith, B.E.; Haaker, H. *Eur. J. Biochem.* **1987**, *169*, 457-465.
57. Lindahl, P.A.; Papaefthymiou, V.; Orme-Johnson, W.H.; Münck, E. *J. Biol. Chem.* **1988**, *263*, 19412-19418.
58. Surerus, K.K.; Hendrich, M.P.; Christie, P.D.; Rottgardt, P.; Orme-Johnson, W.E.; Münck, E. *J. Am. Chem. Soc.* **1992**, in press.
59. Armstrong, F.A.; Butt, J.N.; George, S.J.; Hatchlian, E.C.; Thomson, A.J. *FEBS Lett.* **1989**, *259*, 15-18.
60. Holm, R.H.; Ciurli, S.; Weigel, J.A. In *Progress in Inorganic Chemistry: Bioinorganic Chemistry*. Lippard, S.J. editor John Wiley & Sons: New York **1990**, *38*, 1-74.
61. Brigle, K.E.; Newton, W.E.; Dean, D.R. *Gene*, **1985**, *37*, 37-44.
62. Dean, D.R.; Setterquist, R.A.; Brigle, K.E.; Scott, D.J.; Laird, N.F.; Newton, W.E. *Molecular Micro.* **1990**, *4*(9), 1505-1512.
63. May, H.D.; Dean, D.R.; Newton, W.E. *Biochem. J.* **1991**, *277*, 457-464.
64. Kent, H.M.; Ioannidis, I.; Gormal, C.; Smith, B.E.; Buck, M. *Biochem. J.* **1989**, *264*, 257-264.
65. Kim, J.; Rees, D.C. *Science*, **1992**, in submission.
66. Shah, V.K.; Brill, W.J. *Proc. Natl. Acad. Sci. USA*, **1977**, *74*, 3249-3253.
67. Burgess, B.K. *Chem. Rev.* **1990**, *90*, 1377-1406.
68. Newton, W.E. In *Biological Nitrogen Fixation*, Stacey, G.; Burris, R.H.; Evans, H.J. Eds. Chapman and Hall: New York, **1992**; pp. 877-930.
69. Hoover, T.R.; Imperial, J.; Ludden, P.W.; Shah, V.K. *Biochemistry*, **1989**, *28*, 2768-2771.
70. Conradson, S.D.; Burgess, B.K.; Newton, W.E.; Mortenson, L.E.; Hodgson, K.O. *J. Am. Chem. Soc.* **1987**, *109*, 7507-7515.
71. Arber, J.M.; Flood, A.C.; Garner, C.D.; Gormal, C.A.; Hasnain, S.S.; Smith, B.E. *Biochem. J.* **1988**, *252*, 421-425.
72. Hawkes, T.R.; McLean, P.A.; Smith, B.E. *Biochem. J.* **1984**, *217*, 317-321.
73. Rawlings, J.; Shah, V.K.; Chisnell, J.R.; Brill, W.J.; Zimmermann, R.; Münck, E.; Orme-Johnson, W.H. *J. Biol. Chem.* **1978**, *253*, 1001-1004.

74. Dean, D.R.; Brigle, K.E.; May, H.D.; Newton, W.E. In *Nitrogen Fixation: Hundred Years After*; Bothe, H.; de Bruijn, R.J.; Newton, W.E.: Eds. Fisher: Stuttgart, 1988, pp. 107-113.
75. Brigle, K.E.; Setterquist, R.A.; Dean, D.R.; Cantwell, J.S.; Weiss, M.C.; Newton, W.E. *Proc. Natl. Acad. Sci. USA* 1987, 84, 7066-7069.
76. Thomann, H.; Morgan, T.V.; Jun, H.; Brugmayer, S.J.N.; Bare, R.E.; Stiefel, E.I. *J. Am. Chem. Soc.* 1987, 109, 7913-7914.
77. Thomann, H.; Bernardo, M.; Newton, W.E.; Dean, D.R. *Proc. Natl. Acad. Sci. USA* 1991, 88, 6620-6623.
78. Müller, A.; Schneider, K.; Knittel, K.; Hagen, W.R. *FEBS Lett.* 1992, 303, 36-40.
79. Kennedy, C.; Dean, D. *Mol. Gen. Genet.* 1992, 231, 494-498.
80. Cordewener, J.; Krüse-Wolters, M.; Wassink, H.; Haaker, H.; Veeger, C. *Eur. J. Biochem.* 1988, 172, 739-745.
81. Cordewener, J.; Asbroek, A.T.; Wassink, H.; Eady, R.R.; Haaker, H.; Veeger, C. *Eur. J. Biochem.* 1987, 162, 265-270.
82. Thorneley, R.N.F.; Ashby, G.A.; Howarth, J.V.; Millar, N.C.; Gutfreud, H. *Biochem. J.* 1989, 264, 657-661.
83. Orme-Johnson, W.H.; Hamilton, W.D.; Ljones, T.; Tso, M.-Y.W.; Burris, R.H.; Shah, V.K.; Brill, W.J. *Proc. Natl. Acad. Sci. USA* 1972, 69, 3142-3145.
84. Mortenson, L.E.; Zumft, W.G.; Palmer, G. *Biochim. Biophys. Acta.* 1973, 292, 422-435.
85. Smith, B.E.; Lowe, D.J.; Bray, R.C. *Biochem. J.* 1973, 135, 331-341.
86. Schultz, F.A.; Gheller, S.F.; Newton, W.E. *Biochem. Biophys. Res. Comm.* 1988, 152, 629-635.
87. Burgess, B.K. In *Molybdenum Enzymes*, Spiro, T.G. Ed. Wiley: New York, 1985, pp. 161-220.
88. Hawkes, T.R.; Lowe, D.J.; Smith, B.E. *Biochem. J.* 1983, 211, 495-497.
89. Conradson, S.D.; Burgess, B.K.; Vaughn, S.A.; Roe, A.L.; Hedman, B.; Hodgson, K.O.; Holm, R.H. *J. Biol. Chem.* 1989, 264, 15967-15974.
90. Vaughn, S.A.; Burgess, B.K. *Biochemistry* 1989, 28, 419-424.
91. Ashby, G.A.; Dilworth, M.J.; Thorneley, R.N.F. *Biochem. J.* 1987, 247, 547-554.
92. Newton, W.E.; Gheller, S.F.; Feldman, B.J.; Dunham, W.R.; Schultz, F.A. *J. Biol. Chem.* 1989, 264, 1924-1927.
93. Jacobson, M.R.; Cantwell, J.S.; Dean, D.R. *J. Biol. Chem.* 1990, 265, 19429-19433.
94. Dilworth, M.J.; Eady, R.R.; Eldridge, M. *Biochem. J.* 1988, 249, 745-751.
95. Dilworth, M.J.; Eady, R.R. *Biochem. J.* 1991, 277, 465-468.
96. Smith, B.E.; Eady, R.R.; Lowe, D.J.; Gormal, C. *Biochem. J.* 1988, 250, 299-302.
97. Scott, D.J.; May, H.D.; Newton, W.E.; Brigle, K.E.; Dean, D.R. *Nature* 1990, 188-190.
98. Imperial, J.; Hoover, T.R.; Madden, M.S.; Ludden, P.W.; Shah, V.K. *Biochemistry* 1989, 28, 7796-7799.

99. Madden, M.S.; Kindon, N.D.; Ludden, P.W.; Shah, V.K. *Proc. Natl. Acad. Sci. USA* 1990, 87, 6517-6521.
100. Madden, M.; Krezel, A.M.; Allen, R.M.; Ludden, P.W.; Shah, V.K. *Proc. Natl. Acad. Sci. USA* 1992, 89, 6587-6591.
101. Hoover, T.R.; Imperial, J.; Ludden, P.W.; Shah, V.K. *Biofactors* 1988, 1, 199-205.
102. Dean, D.R.; Jacobson, M.R. In *Biological Nitrogen Fixation*; Stacey, G.; Burris, R.H.; Evans, H.J. Chapman and Hall: New York 1992, pp. 763-834.
103. Howard, K.S.; McLean, P.A.; Hansen, F.B.; Lemley, P.V.; Koblan, K.S.; Orme-Johnson, W.H. *J. Biol. Chem.* 1986, 261, 772-778.
104. Roberts, G.P.; MacNeil, T., MacNeil, D.; Brill, W.J. *J. Bacteriol.* 1978, 136, 267-279.
105. Jacobson, M.R.; Cash, V.L.; Weiss, M.C., Laird, N.F.; Newton, W.E.; Dean, D.R. *Mole. Gen. Genet.* 1989, 219, 49-57.
106. Berman, J.; Gershani, J.M.; Zamir, A. *J. Biol. Chem.*, 1985, 260, 5240-5243.
107. Imperial, J.; Ugalde, R.A.; Shah, V.K.; Brill, W.J. *J. Bacteriol.* 1984, 158, 187-194.
108. Ugalde, R.A.; Imperial, J.; Shah, V.K.; Brill, W.J. *J. Bacteriol.* 1984, 164, 1081-1087.
109. Hoover, T.R.; Robertson, A.D.; Cerny, R.L.; Hayes, R.N.; Imperial, J.; Shah, V.K.; Ludden, P.W. *Nature* 1987, 329, 855-857.
110. Ugalde, R.A.; Imperial, J.; Shah, V.K.; Brill, W.J. *J. Bacteriol.* 1984, 159, 888-893.
111. Filler, W.A.; Kemp, R.M.; Ng, J.C.; Hawkes, T.R.; Dixon, R.A.; Smith, B.E. *Eur. J. Biochem.* 1986, 160, 371-377.
112. Robinson, A.C.; Burgess, B.K.; Dean, D.R. *J. Bacteriol.* 1986, 166, 180-186.
113. Dean, D.R.; Brigle, K.E. *Proc. Natl. Acad. Sci. USA* 1985, 82, 5720-5723.
114. Paustian, T.D.; Shah, V.K.; Roberts, G.P. *Proc. Natl. Acad. Sci. USA* 1989, 86, 6082-6086.
115. Tal, S.; Chun, T.W.; Gavini, N., Burgess, B.K. *J. Biol. Chem.* 1991, 266, 10654-10657.
116. Robinson, A.C.; Dean, D.R.; Burgess, B.K. *J. Biol. Chem.* 1987, 262, 14327-14332.
117. Robinson, A.C.; Chun, T.W.; Li, J.-G.; Burgess, B.K. *J. Biol. Chem.* 1989, 264, 10088-10095.
118. Shah, V.K.; Imperial, J.; Ugalde, R.A.; Ludden, P.W.; Brill, W.J. *Proc. Natl. Acad. Sci. USA* 1986, 83, 1636-1640.
119. Paustian, T.D.; Shah, V.K.; Roberts, G.P. *Biochemistry* 1990, 29, 3515-3522.
120. Robinson, A.E.; Richard, A.J.M.; Thomson, A.J.; Hawkes, T.R.; Smith, B.E. *Biochem. J.* 1984, 219, 495-503.
121. Harris, G.S.; White, T.C.; Flory, J.E.; Orme-Johnson, W.H. 1990, 265, 15909-15919.

Chapter 11

Crystal Structures of the Iron Protein and Molybdenum–Iron Protein of Nitrogenase

D. C. Rees¹, J. Kim¹, M. M. Georgiadis^{1,3}, H. Komiya¹, A. J. Chirino¹,
D. Woo¹, J. Schlessman¹, M. K. Chan¹, L. Joshua-Tor¹, G. Santillan²,
P. Chakrabarti^{1,4}, and B. T. Hsu¹

¹Division of Chemistry and Chemical Engineering, 147–75CH,
California Institute of Technology, Pasadena, CA 91125

²Department of Chemistry, California State University
Los Angeles, CA 91030

Three-dimensional structures of the nitrogenase iron protein and molybdenum-iron protein from *Azotobacter vinelandii* have been determined by x-ray crystallography. The iron protein contains a single 4Fe:4S cluster symmetrically liganded by two identical subunits. The molybdenum-iron protein is an $\alpha_2\beta_2$ tetramer, where the homologous α and β subunits surround two different types of metal centers: the FeMo-cofactor and the P-cluster pair. Both centers are constructed from two bridged clusters; the FeMo-cofactor has 4Fe:3S and 1Mo:3Fe:3S cluster bridged by three non-protein ligands, while the P-cluster pair contains two 4Fe:4S clusters bridged by two cysteine ligands located at the $\alpha\beta$ subunit interface. Docking studies between the iron protein and molybdenum iron protein suggest a possible interaction mode between these two proteins.

The conversion of atmospheric dinitrogen to ammonia during the biological process of nitrogen fixation is catalyzed by the nitrogenase enzyme system (*1-7*). Nitrogenase consists of two component proteins, the iron (Fe-) protein and molybdenum iron (MoFe-) protein, that together mediate the ATP dependent reduction of substrates such as N_2 and H^+ to products. Three basic types of electron transfer reactions occur in this system: the reduction of Fe-protein by low molecular weight proteins such as ferredoxin or flavodoxin; the transfer of electrons from Fe-protein to MoFe-protein coupled to the hydrolysis of MgATP; and the final transfer of electrons to the substrate. The overall reaction stoichiometry for the reduction of N_2 has been established (*8*):



³Current address: Department of Biochemistry and Molecular Biophysics, Columbia University, New York, NY 10032

⁴Current address: Physical Chemistry Division, National Chemical Laboratory, Pune 411008, India

Since only single electrons are transferred from Fe-protein to MoFe-protein, at least eight cycles of this electron transfer step must occur for the complete conversion of dinitrogen to ammonia. Studies of the kinetics of dinitrogen reduction show that this reaction is relatively slow, with a turnover time of $\sim 5 \text{ sec}^{-1}$, and the rate determining step being dissociation of the Fe-protein:MoFe-protein complex following each electron transfer (9-11). Important mechanistic questions to be addressed include the role of MgATP in this process, and the molecular details of dinitrogen reduction by nitrogenase.

The MoFe-protein is an $\alpha_2\beta_2$ tetramer with total molecular weight $\sim 240 \text{ kD}$, and the Fe-protein is a γ_2 dimer of total molecular weight $\sim 60 \text{ kD}$. Three distinct types of redox centers are associated with these proteins: the MoFe-protein contains two types of centers: the FeMo-cofactor and the P-cluster pair, while the Fe-protein dimer contains one 4Fe:4S cluster. The metal centers of the MoFe-protein have attracted considerable attention since they almost certainly provide the active site of substrate reduction. The FeMo-cofactor, first identified by Shah and Brill (12) has the approximate composition 1 Mo: 6-8 Fe: 8-9 S:1 homocitrate (5), and is likely to represent the actual site for dinitrogen binding and reduction (13). The P-cluster pair is believed to contain two 4Fe:4S clusters in close proximity (14-19), which could function in the transfer of electrons from Fe-protein to the FeMo-cofactor and/or substrates. The overall metal composition of the MoFe-protein, approximately 2 Mo: 30 Fe: 30 S, is consistent with the presence of two copies each of the FeMo-cofactor and P-cluster pairs per MoFe-protein tetramer. Despite extensive study, the detailed structures of the FeMo-cofactor and P-cluster pair have been elusive.

Availability of an enzyme structure is indispensable for the formulation of a mechanistic description. For proteins the size of nitrogenase, x-ray crystallographic methods provide the only feasible approach for determining the three-dimensional structures. We have pursued the crystallographic analysis of the Fe-protein and MoFe-protein structures to determine the polypeptide and cofactor structures, and to provide a structural basis to address questions concerning the substrate reduction mechanism and assembly of nitrogenase.

Structure Determinations of Nitrogenase Fe-protein and MoFe-protein

Since descriptions of the structure determinations for Fe-protein and MoFe-protein have been published (20, 21), only general features of that process will be presented here. Both the Fe-protein and MoFe-protein were isolated from *Azotobacter vinelandii* and *Clostridium pasteurianum* and crystallized in forms suitable for diffraction analysis. The proteins are designated Av1 and Av2 for the MoFe-protein and Fe-protein from *A. vinelandii*, respectively, and Cp1 and Cp2 for the MoFe-protein and Fe-protein from *C. pasteurianum*, respectively. Three crystal forms each of Fe-protein and MoFe-protein were employed in their respective structure determinations: for Fe-protein, Av2 was crystallized in space group $P2_12_12_1$ ($a=94.6\text{\AA}$, $b=179.9\text{\AA}$, $c=74.1\text{\AA}$) and $P2_1$ ($a=56.8\text{\AA}$, $b=92.9\text{\AA}$, $c=63.6\text{\AA}$, $\beta=100.0^\circ$), while Cp2 was crystallized in space group $P2_1$ ($a=67.6\text{\AA}$, $b=75.7\text{\AA}$, $c=53.6\text{\AA}$, $\beta=114.2^\circ$); and for MoFe-protein, Av1 was crystallized in space group $P2_1$ ($a=108.4\text{\AA}$, $b=130.5\text{\AA}$, $c=81.5\text{\AA}$, $\beta=110.8^\circ$), while Cp1 was crystallized in two $P2_1$ forms (cell constants $a=70.0\text{\AA}$, $b=151.3\text{\AA}$, $c=121.9\text{\AA}$, $\beta=110.4^\circ$, and $a=87.9\text{\AA}$, $b=171.4\text{\AA}$, $c=73.6\text{\AA}$, and $\beta=91.5^\circ$). Every crystal form had one complete molecule in the asymmetric unit, with the exception of the Av2 $P2_12_12_1$ form that had two Fe-protein dimers/asymmetric unit. The presence of this non-crystallographic symmetry (NCS) was invaluable in the structural analysis (22, 23).

The structure determination of the two nitrogenase proteins was complicated by the extreme oxygen sensitivity of the proteins, especially the Fe-protein. Since most heavy metal reagents traditionally used to prepare isomorphous derivatives for phase determination are oxidants (relative to these proteins), crystal soaking with these

compounds often resulted in crystal bleaching and/or loss of diffraction. After an exhaustive search, the anti-arthritis drug myochrisine (gold sodium thiomalate) was found to produce a satisfactory heavy atom derivative for the Fe-protein; the MoFe-protein crystals were somewhat harder and derivatives could be prepared by soaking crystals in ethylmercurithiosalicylate, K_2PtCl_4 and di- μ -iodobis(ethylenediamine)-diplatinum (II) nitrate. The locations of the heavy atom sites were determined from analysis of isomorphous difference Patterson maps. From these sites, phases were calculated by the method of isomorphous replacement. Although electron density maps calculated from these phases were encouraging, they were not of sufficient quality to permit model building. The electron density maps were improved by averaging with the NCS, both within single crystal forms, as well as between them. Even though the Av1 and Cp1 sequences are only 36% identical, and the Av2 and Cp2 sequences are 69% identical, averaging between Av and Cp crystal forms significantly improved the initial electron density maps for both the MoFe-protein and Fe-protein. The final structural models for Fe-protein and MoFe-protein are the product of an iterative process of map calculation, NCS averaging, model building (with the program TOM (24)), refinement and phase combination. Models have been presently constructed for Av1 and Av2, with the Cp1 and Cp2 refinements currently underway. The program TNT (25) was used for the Av2 refinement, while both TNT and X-PLOR (26) were used for the Av1 refinements. At present, the Av2 model contains all but the last 3-5 residues of the 289 present per subunit (although not every side chain has adequate density to justify complete building) and has been refined to an R of 0.183 at 2.9Å resolution, with rms deviations from ideal bond lengths and angles of 0.017 and 2.23°. The Av1 model is complete except for 23 residues in each α subunit, and has been refined to an R of ~0.196 at 2.7Å resolution, with rms deviations from ideal bond lengths and angles of 0.018Å and 3.54°, respectively

Structures of the Metal Centers in the Nitrogenase Proteins (20, 21)

Fe-protein. As predicted from chemical modification, genetic and spectroscopic studies (27-29), the 4Fe:4S cluster of Fe-protein is symmetrically coordinated by two cysteines, 97 and 132, from each subunit. Coordination of metal centers by residues from identical (or homologous) subunits has been observed in the photosynthetic reaction center (30, 31), nitrite reductase (32) and the MoFe-protein (21), and may be a common feature of multisubunit metalloproteins. The 4Fe:4S cluster has significant solvent exposure, which had been recognized in spectroscopic studies (33-37). This solvent exposure may contribute to the considerable sensitivity of Fe-protein to inactivation by oxygen. The protein environment surrounding the cluster appears to be rather loose; other than the ligating cysteines, the only side chains that contact the cluster are Ala 98 from each subunit. Both cluster ligands are located near the N-terminal end of α -helices that are directed towards the cluster, permitting favorable electrostatic interactions between the terminal amide groups of the helix and the anionic cluster.

MoFe-protein. At the current resolution of the MoFe-protein structure analysis (2.7Å), it is not possible to unambiguously establish the detailed geometry and chemical identities of all the constituents of novel metal centers such as the FeMo-cofactor and P-cluster pair. Consequently, models for these centers were built into electron density maps using fragments of well-characterized clusters as the basic building blocks (38, 39). This is rather like the use of amino acid fragments to fit electron density maps for proteins of unknown sequence. It should be emphasized that at this stage, the proposed cluster models are consistent with the general shape and features of the electron density map, but the unambiguous identification of

individual atoms, including the possible presence of hydrides or light atoms adjacent to more electron dense ones, and a more detailed description of the geometry and oxidation states will require higher resolution diffraction data. This analysis is currently underway in our lab at 2.2Å resolution for the *A. vinelandii* MoFe-protein.

FeMo-cofactor. The FeMo-cofactor has been modeled by two clusters of composition 4Fe:3S and 1Mo:3Fe:3S, that are bridged by three non-protein ligands (Figure 1). The Fe-Fe separation distance between bridged iron sites is ~2.7Å, whereas the separation distance is ~3.8Å between nonbridged iron sites on different cluster fragments (such as Fe2 to Fe5). Based on the electron density values at the bridging ligands, two are assigned as sulfur, while the third ligand (designated Y in Figure 1) has lower electron density (Figure 2), and has been modeled by a nitrogen containing group. This site could also be occupied by an oxygen containing group, a dithionite derived species, or a less well ordered sulfur, for example. There is also no evidence in the electron density maps for a hexacoordinate sulfur atom at the center of the cluster (Figure 2). Homocitrate, which is an essential component of FeMo-cofactor (41, 42), coordinates the Mo through both hydroxyl and carboxyl oxygens. As discussed in (21), these structural features of the FeMo-cofactor model are generally consistent with the results of analytical and spectroscopic (EXAFS (43-45), ENDOR (46) and Mössbauer (15, 47)) studies of the cofactor.

Neglecting the protein environment and the precise atomic identities, the cofactor has approximate D_3 symmetry, with the Fe1 and Mo sites located on the threefold axis, and separated by ~7.5Å. The approximate three-fold symmetric nature of the FeMo-cofactor can be illustrated by a rotation function analysis of unbiased electron density maps (Figure 3). For this calculation, an Fo-Fc electron density map, using Fe's calculated from a MoFe-protein model refined at 2.7Å resolution without the metal centers, was skewed into a cylinder of height 12Å and radius 6Å. The origin of the cylinder was positioned at the center of the FeMo-cofactor, with the cylinder axis oriented along the direction linking the centers of the two component clusters. The cylinder was then placed in an empty cube with 30Å sides. Structure factors calculated between 5-3Å resolution from inversion of this map were used for a rotation function analysis (43), using an integration radius of 12Å. The rotational symmetry about the axis linking the centers of the component clusters shows a maximum at ~120°, corresponding to an approximate three-fold symmetry of FeMo-cofactor along this axis.

The protein environment around the FeMo-cofactor is primarily provided by the α subunit. Cys α 275 coordinates Fe1, while the Mo is liganded by the side chain of His α 442. Two other side chains, His α 195 and Gln α 191, are within 5Å of Fe2 and Fe6, respectively, but are not directly liganded to any metal. The side chain of Gln α 191 does interact with one of the carboxyl groups of homocitrate. Cys α 275, His α 442, His α 195 and Gln α 191 are conserved in all known MoFe-protein sequences; additionally, mutagenesis studies have implicated Cys α 275 (49-51) and His α 195 (52, 53) as involved in binding of FeMo-cofactor to the MoFe-protein. The position of Gln α 191 seen in this structure supports the proposal that Gln α 191 interacts with homocitrate (54). Based on sequencing of Nif⁻ mutants altered in the α subunit, Zamir had proposed that His α 442 might coordinate the FeMo-cofactor (55).

An unusual feature of this model for the FeMo-cofactor is the approximate trigonal planar geometry of the sulfurs surrounding the six Fe sites that bind the bridging ligands (although strictly speaking, the sulfurs are not co-planar with an iron; trigonal pyramidal might be a more accurate description of the coordination geometry). Neither protein groups nor solvent molecules that might possibly serve as fourth ligands have been observed within coordinating distance of any of these sites, although it is possible that a less electron dense group (such as O or N) could be present in the cluster interior. It is also possible that Fe-Fe bonding interactions occur between bridged Fe sites that effectively provide a four coordinate iron environment.

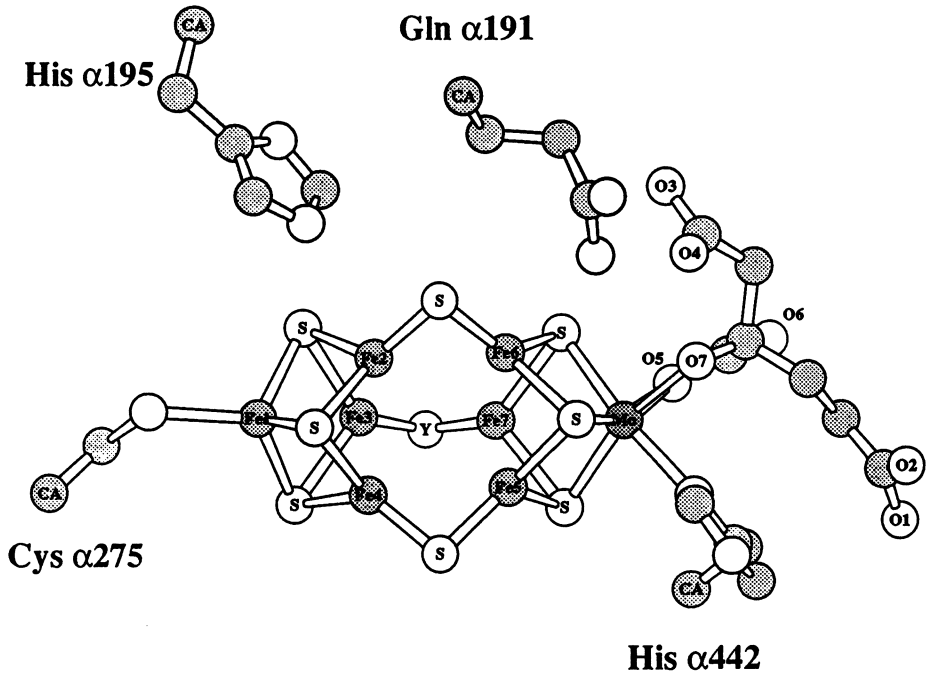


Figure 1. Structure of the FeMo-cofactor and surrounding protein, prepared with the program MOLSCRIPT (40).

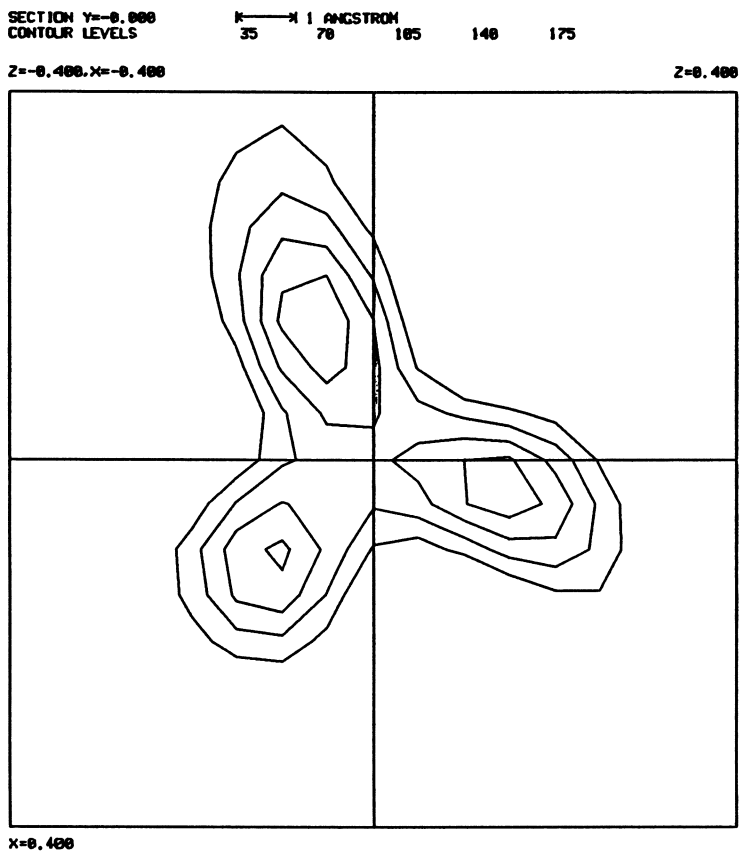


Figure 2. Electron density section through the bridging ligands of the FeMo-cofactor, illustrating the absence of significant electron density at the cofactor center.

No matter what the detailed geometry turns out to be, the coordination environments of the bridged Fe sites (a) are non-tetrahedral and (b) lack protein ligands.

P-cluster Pair. The P-cluster pair model (Figure 4) contains two 4Fe:4S clusters that are bridged by two cysteine thiol ligands (from residues $\alpha 88$ and $\beta 95$), with the four remaining Fe liganded by singly coordinating cysteine thiols (from residues $\alpha 62$, $\alpha 154$, $\beta 70$, and $\beta 153$). The nonbridging cysteines coordinated to a specific 4Fe:4S cluster are from the same subunit. The ligands and location of the P-cluster pair at the interface between the α and β subunits had been proposed from mutagenesis experiments (49-51, 56), and is reminiscent of the location of the 4Fe:4S cluster between the two Fe-protein subunits. In addition to the cysteine ligands, Ser $\beta 188$ is close to Fe6 and may be able to coordinate this site along with Cys $\beta 153$. The coordination environments of both Fe6 and Fe2 are distorted from ideal tetrahedral geometry, due to interactions with Ser $\beta 188$ and the mainchain of Gly $\alpha 185$, respectively. Individual replacement of any of the six cysteines by alanine eliminates diazotropic growth of the mutant strains; substitution of Gly $\alpha 185$ by Asp has also been identified in a Nif⁻ mutant (55). To a first approximation, the P-cluster pair model has D₂ symmetry, with one of the twofolds passing through the centers of the individual clusters, as can be illustrated by a rotation function analysis of unbiased electron density maps (Figure 3). Comparison of the rotation function analyses for the FeMo-cofactor and the P-cluster pair in Fig. 3 illustrates that the rotational symmetry along the axis joining the centers of the component clusters differs for these two centers; in the FeMo-cofactor, this axis approximates a three-fold rotation axis, while in the P-cluster pair, this axis approximates a two-fold rotation axis.

Structural Descriptions of Nitrogenase Proteins

Fe-protein. The quarternary structure arrangement of Fe-protein (20) consists of two subunits, each folded as a single α/β type domain and connected at one surface by the 4Fe:4S cluster (Figure 5). At the core of each subunit is an eight-stranded β sheet (with seven of the eight β strands oriented in parallel fashion) flanked by nine α helices. Each subunit contains a characteristic structural motif near the amino terminus (residues 9-16) that is found in a major class of mononucleotide binding proteins. The two nucleotide binding sites in Fe-protein are located in the cleft formed between the two subunits. Molybdate ions from the crystallization solution are bound at positions $\sim 20\text{\AA}$ from the 4Fe:4S cluster that correspond to the location of the nucleotide phosphate groups in other nucleotide binding proteins. Furthermore, the crystal structure analysis identified a nucleotide, modeled as ADP, that was bound to only one of the two nucleotide binding sites present in the dimer. The occupancy of this ADP has been estimated as ~ 0.4 . Since the two potential nucleotide binding sites are not related by crystallographic symmetry, both sites need not be equally occupied. The nucleotide interacts with residues from both subunits: the terminal phosphate groups interact with residues 9-16, while the adenine ring contacts Tyr 159, Ala 160, Asn 163 and the main-chain atoms of 128-130 of the neighboring subunit. The ribose spans the subunit cleft and interacts with residues Lys 41 and Asp 129 from the different subunits. This nucleotide co-purified with Av2 and must represent a tightly bound species of the type identified by Lindahl, *et al* (57). The functional significance of the tightly bound nucleotide, if any, is unclear.

Since the phosphate groups of the nucleotide and the cluster are too distant ($\sim 20\text{\AA}$) to permit direct chemical coupling of electron transfer and ATP hydrolysis, the location of both sites at the subunit interface suggests that the interface provides the coupling mechanism. The simplest picture envisions two (or more) conformational states of Fe-protein that differ in the details of the intersubunit interactions, with the

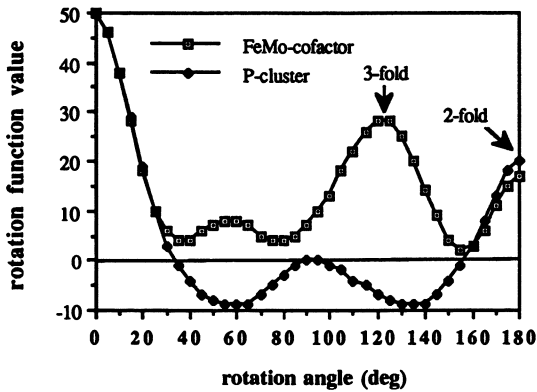


Figure 3. Rotation function analysis of the rotational symmetry along the axis connecting the centers of the component clusters for the FeMo-cofactor and P-cluster pair. Details of the calculation are described in the text.

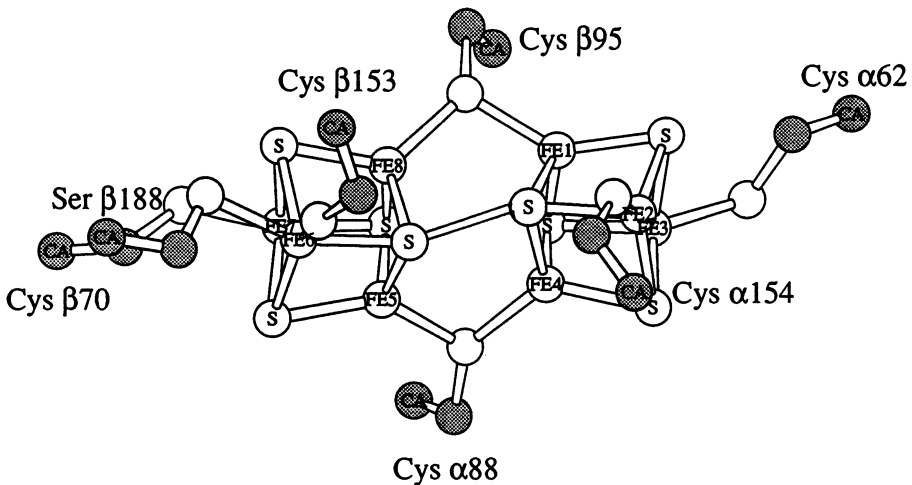


Figure 4. Structure of the P-cluster pair and surrounding protein, prepared with the program MOLSCRIPT (40).

equilibrium between the two states sensitive to oxidation state of the cluster and nucleotide binding. This allosteric model for Fe-protein function naturally directs attention to interactions that might stabilize alternate quaternary structure arrangements of the subunits, such as salt-bridges. An intriguing set of inter-subunit salt bridges in Fe-protein that may function in this capacity are a cyclic arrangement of Asp 129 and Lys 41 in alternating fashion from both subunits, organized about the dimer twofold axis. Since both Lys 41 and Asp 129 interact with the bound nucleotide, this observation indicates that the Asp 129 - Lys 41 interactions, and their respective interactions with nucleotide could be mutually exclusive, thereby providing a mechanism for coupling protein conformational state with nucleotide binding.

MoFe-protein. The α and β subunits of the MoFe-protein exhibit similar polypeptide folds consisting of three domains of the α/β type, with some extra helices ((21), Figure 6). Regions of similarities between α and β subunits were originally recognized in sequence analyses (58). In each subunit, there is a wide, shallow cleft between the three domains; in the α subunit, the FeMo-cofactor occupies the bottom of this cleft. The location for the FeMo-cofactor at the boundary between three domains is reminiscent of the site for the iron-sulfur cluster in aconitase (59). Although there are no permanent channels leading from the surface to the FeMo-cofactor, it is possible that transient openings could be created between the α subunit domains that allow cluster insertion, substrate access and product egress. Extensive contacts occur between the α and β subunits in an $\alpha\beta$ dimer; this is especially evident in the bridging of the two subunits through the P-cluster pair. The α and β subunits within an $\alpha\beta$ dimer are approximately related by a twofold axis that passes through the P-cluster pair. The quaternary structure of the MoFe-protein may be considered to consist of a pair of $\alpha\beta$ dimers, where each $\alpha\beta$ dimer is related to the other by the intratetramer twofold axis used for NCS averaging. Although the α and β subunits in an $\alpha\beta$ dimer are also approximately related by a twofold rotation, the MoFe-protein does not exhibit 222 symmetry. The $\alpha\beta$ twofold and the tetramer twofold axes form an angle of $\sim 97^\circ$, and at the positions of closest approach are separated by $\sim 12\text{\AA}$. Packing between helices from the β subunit dominate the interactions at the tetramer interface, with some contributions from helices in the α subunit. Interestingly, the center of the six α -helical barrel that surrounds the tetramer twofold axis is not filled with sidechains; rather, an open channel of $\sim 8\text{-}10\text{\AA}$ diameter and length $\sim 35\text{\AA}$ exists that may serve as a model for helical pores in membrane spanning proteins, and which could conceivably serve as a conduit for substrates and products to access the active sites.

The observation that interactions between β subunits contribute predominantly to the formation of the tetramer is consistent with the observation that proteins corresponding to the MoFe-protein in alternate nitrogenase systems may be isolated in a trimeric $\alpha\beta_2$ form (60). The MoFe-protein structure is compatible with the loss of individual α subunits from the tetramer, creating either $\alpha\beta_2$ or β_2 species. Forms of the MoFe-protein containing either $\alpha\beta_2$ or α_2 oligomers could not be generated using only those interactions observed in the tetrameric structure.

Interactions between MoFe-protein and Fe-protein

With the availability of the crystal structures for both proteins isolated from *A. vinelandii*, some general features of the complex between the two proteins may now be addressed. Two residues of Fe-protein that have been identified as interacting with the MoFe-protein, Arg 100 and Glu 112, are located on the same side of the protein as the 4Fe:4S cluster. Hence, this surface almost certainly includes at least part of the interaction region between the two proteins. Relevant features of the interaction

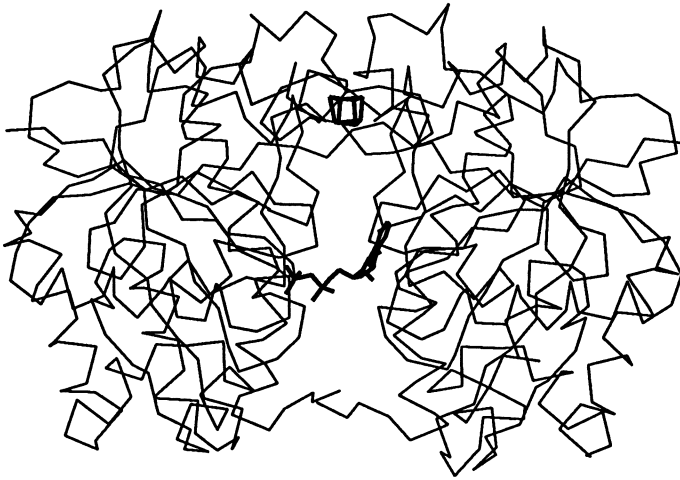


Figure 5. Alpha carbon chain trace of the Fe-protein polypeptide fold, with the 4Fe:4S cluster and ADP indicated by dark lines.

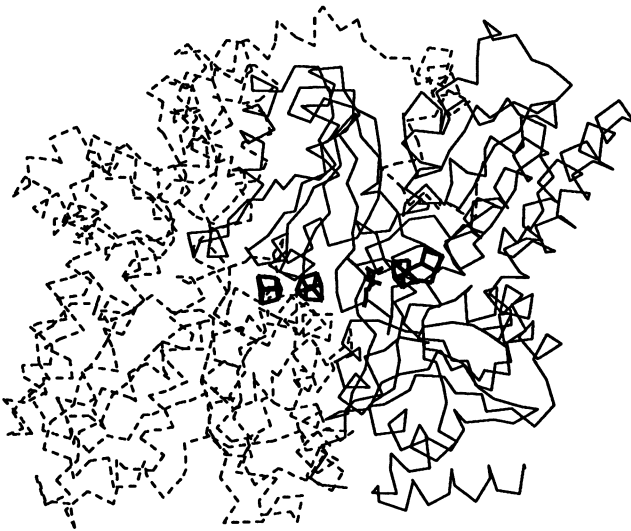


Figure 6. Alpha carbon chain trace of an $\alpha\beta$ subunit pair of MoFe-protein, with the α and β subunits represented by solid and dashed lines, respectively. The P-cluster pair (left) and FeMo-cofactor (right) are indicated by dark lines.

between Fe-protein and MoFe-protein that have been established biochemically include the ability of Glu 112 to crosslink with Lys β 400 (61), and the likely occurrence of salt bridges in the interface region, as established by salt effects on nitrogenase activity (62) and the effects of replacing Arg 100 with other residues (63). As the Fe-protein dimer has a twofold symmetry axis, a plausible model (21) for docking the two proteins involves superposition of the Fe-protein twofold axis with the twofold axis passing through the P-cluster pair that relate the α and β subunits of the MoFe-protein (Figure 7). The surfaces of the two proteins are complementary in this region; the MoFe-protein surface near the P-cluster pair has a convex shape, while the Fe-protein surface is concave about the 4Fe:4S cluster. To either side of the P-cluster pair there are two wide and shallow clefts related by the pseudo-twofold axis, that could accommodate the two Fe-protein subunits. With this orientation, the side chains of Glu 112 and Lys β 400 can be positioned sufficiently close to permit crosslinking. Four short helices (α 155- α 159; α 120- α 125; β 153- β 158 and β 120- β 125) which are related by pseudo twofold axis, are oriented in parallel from the P-cluster pair toward surface forming a four-helical bundle, and the 4Fe:4S cluster of Fe-protein could bind to the top surface of these helices. Kinetic studies of site-directed mutants at Phe β 125 indicate that these alterations interfere with the Fe-protein - MoFe-protein interaction (64). Additionally, substitutions of Glu α 120 and Gly α 160 in or near these helices have been identified in Nif⁻ mutants, possibly due to disruption of the Fe-protein - MoFe-protein interaction (55). The edge-edge distance from the P-cluster pair to the end of these helices is about 12Å, thus the edge-edge distance from the P-cluster pair to the 4Fe:4S cluster of Fe-protein may be about 15Å. Charged and polar residues on the MoFe-protein surface in this region may be important for the formation of salt bridges/hydrogen bonds with Fe-protein. Asp α 162 and Asp β 161, which are related by the pseudo twofold axis, are completely exposed to the solvent and are located about 15Å from the P-cluster pair. Other solvent exposed side chains near the Fe-protein binding site include His β 185, Asp α 128, Asp α 161 and Glu β 156.

Kinetic studies indicate that nucleotide hydrolysis precedes electron transfer in the Fe-protein - MoFe-protein complex (9, 10, 65). Although the detailed structural consequences of nucleotide binding on the Fe-protein structure have not been established, it is likely that MgATP hydrolysis is accompanied by a change in Fe-protein structure, such as an alteration in the relative orientations of the two subunits. Presumably, this transition leads to the formation of an activated species that is competent for electron transfer from the Fe-protein to MoFe-protein (in particular, to the P-cluster pair in this model). A speculative model for the coupling of ATP hydrolysis to electron transfer involves the participation of residues ~62-70 of Fe-protein in the binding interaction with MoFe-protein (20). These residues, which exhibit a relatively large degree of sequence variability between different Fe-proteins, protrude from the same side of the Fe-protein surface as the cluster, Arg 100 and Glu 112. Residues 62-70 are part of a Fe-protein subdomain that encompasses residues 39-80. Changes upon binding to MoFe-protein in the position of this subdomain, relative to the remainder of Fe-protein, could be transmitted to Asp 39 or Asp 43 which are located within this region. Upon binding of Fe-protein to MoFe-protein, these residues, which are near the terminal phosphate groups of the nucleotide, could be repositioned to function as a general base catalyst in ATP hydrolysis. The coupling between nucleotide hydrolysis and conformational changes associated with intermolecular interactions is widespread in biochemistry, and has been described for such diverse systems as the H-ras p21 oncogene protein (66, 67) and the rec A protein (68) that participates in DNA recombination.

As the nucleotide binding site in this model for the complex (Figure 7) is on the opposite surface of the Fe-protein to the interaction region with the MoFe-protein, it



Figure 7. Model for a complex formed between Fe-protein (top) and an $\alpha\beta$ subunit pair of the MoFe-protein. The α and β subunits are represented by solid and dashed lines, respectively, with the various clusters and ADP indicated by dark lines.

should be possible for MgATP to exchange with MgADP without dissociation of the two proteins, as has been proposed from kinetic analyses of the nitrogenase reaction (65). Kinetic studies also indicate that reduction of oxidized Fe-protein requires dissociation of complex. Since the 4Fe:4S cluster of Fe-protein would be buried in the interface region, reduction of oxidized Fe-protein would seem to require dissociation of the two proteins. Experimental studies have also indicated that oxidized MoFe-protein can bind MgADP (69), although it is not clear from the present studies where this site would be located, and what the relationship of this site might be to the MoFe-protein metal centers and the proposed Fe-protein binding site.

Similarities between MoFe-protein and the Photosynthetic Reaction Center

Although the electron transfer processes catalyzed by nitrogenase and the photosynthetic reaction center (RC; reviewed in (70)) are quite different, there are striking similarities in the structural organization of the two systems: (1) Both the MoFe-protein and the RC are composed of two homologous subunits approximately related by a twofold rotation: the α and β subunits of the MoFe-protein, and the L and M subunits of the reaction center. The initial electron carriers for both systems, the P cluster pair and the special pair, are buried in the interface between the two subunits. The location of these redox centers at the subunit interface may provide a convenient assembly mechanism for the incorporation of powerful reductants in the protein interior, isolated from contact with solvent. (2) Despite the general twofold symmetry in the protein organization, electron transfer from the initial donor proceeds in only one direction. In the reaction center case, only one of the two electron transfer branches present is actually utilized. In the MoFe-protein, however, the FeMo-cofactor is present in only one of the two homologous subunits, so that electron transfer necessarily proceeds in this direction. Whether the original MoFe protein was a homodimer or tetramer containing equivalent branches is an interesting question in molecular evolution. (3) The binding sites for the terminal electron acceptors are buried in both the MoFe-protein and RC, so that the protein structures must accommodate both entry and exit of the relevant groups. (4) In the RC, it has been established that separate pathways exist for electron transfer and proton transfer within the protein, and it seems quite likely that the MoFe-protein behaves similarly. (5) A significant fraction of the energy input into these systems (light for the RC and MgATP for nitrogenase) is lost during the overall reaction. This apparently is a consequence of ensuring that the electron transfer reactions are essentially irreversible, so that short-circuits or futile cycles are minimized.

Concluding Remarks

The structures of the nitrogenase Fe-protein and MoFe-protein provide a framework for addressing detailed questions concerning the mechanism and assembly of this complex system. While nitrogenase may catalyze a (bio)chemically unique reaction, general features of the nitrogenase proteins are common to numerous other systems, including G-proteins, membrane translocators and complex electron transfer systems. Although considerable attention has been justifiable focused on the FeMo-cofactor as a novel type of cluster carrying out unusual chemistry, from the viewpoint of protein structure, the Fe-protein appears extraordinarily interesting. The sensitivity of Fe-protein conformation to oxidation and nucleotide binding states suggests that the affinity of Fe-protein for electron donors (such as ferredoxin) and acceptors (MoFe-protein) can be sequentially altered during the catalytic cycle. In essence, these conformational changes could permit Fe-protein to function as a molecular clock that

can both set the temporal sequence and provide the driving force for multiple electron transfer events during substrate reduction by nitrogenase. These properties of Fe-protein, together with the metal centers and polypeptide chain of the MoFe-protein, create the molecular machinery responsible for biological nitrogen fixation.

Acknowledgements. Stimulating discussions with J.B. Howard, J.E. Bercaw and H.B. Gray are greatly appreciated. This work was supported by NSF DMB91-18689 and NIH GM45162. The rotation camera facility at the Stanford Synchrotron Radiation Laboratory is supported by the DOE Office of Basic Energy Sciences and the NIH Biomedical Resource Technology Program, Division of Research Resources. X-PLOR calculations were performed on the CRAY-YMP at the San Diego Supercomputer Center, supported by NSF.

Note Added in Proof. Since this manuscript was prepared, our paper describing the three-dimensional structure of the MoFe-protein has appeared (J. Kim and D.C. Rees, *Nature* **360**, 553-560 (1992)). High resolution (2.2Å) refinement of the Av1 structure using diffraction data collected at SSRL have verified the models for the FeMo-cofactor and P-cluster pair described in this manuscript, with the additional identification of a disulfide bridge between two of the cluster sulfurs in the P-cluster pair (M.K. Chan, J. Kim, D.C. Rees, submitted (1993)).

Literature Cited

- (1) Burgess, B. K. in Veeger, C.; Newton, W. E.; Martinus Nijhoff, Boston, 1984; pp 103-114.
- (2) Orme-Johnson, W. H. *Ann. Rev. Biophys. Biophys. Chem.* **1985**, *14*, 419-459.
- (3) Holm, R. H.; Simhon, E. D. in Spiro, T. G.; Wiley-Interscience, New York, 1985; pp Chapter 1.
- (4) Stiefel, E. I.; Thomann, H.; Jin, H.; Bare, R. E.; Morgan, T. V.; Burgmayer, S. J. N.; Coyle, C. L. in Que, L.; American Chemical Society, Washington, D.C., 1988; pp 372-389.
- (5) Burgess, B. K. *Chem. Rev.* **1990**, *90*, 1377-1406.
- (6) Burris, R. H. *J. Biol. Chem.* **1991**, *266*, 9339-9342.
- (7) Smith, B. E.; Eady, R. R. *Eur. J. Biochem.* **1992**, *205*, 1-15.
- (8) Simpson, F. B.; Burris, R. H. *Science* **1984**, *224*, 1095-1097.
- (9) Lowe, D. J.; Thorneley, R. N. F. *Biochem. J.* **1983**, *215*, 393-405.
- (10) Lowe, D. J.; Thorneley, R. N. F. *Biochem. J.* **1984**, *224*, 895-901.
- (11) Hageman, R. V.; Burris, R. H. *Biochem.* **1978**, *17*, 4117-4124.
- (12) Shah, V. K.; Brill, W. *Proc. Natl. Acad. Sci. USA* **1977**, *74*, 3249-3253.
- (13) Hawkes, T. R.; McLean, P. A.; Smith, B. E. *Biochem. J.* **1984**, *217*, 317-321.
- (14) Kurtz, D. M.; McMillan, R. S.; Burgess, B. K.; Mortenson, L. E.; Holm, R. H. *Proc. Natl. Acad. Sci. USA* **1979**, *76*, 4986-4989.
- (15) Zimmermann, R.; Münck, E.; Brill, W. J.; Shah, V. K.; Henzl, M. T.; Rawlings, J.; Orme-Johnson, W. H. *Biochem. Biophys. Acta* **1978**, *537*, 185-207.
- (16) Lindahl, P. A.; Papaefthymiou, V.; Orme-Johnson, W. H.; Münck, E. *J. Biol. Chem.* **1988**, *263*, 19412-19418.
- (17) Sureus, K. K.; Hendrich, M. P.; Christie, P. D.; Rottgardt, D.; Orme-Johnson, W. H.; Münck, E. *J. Amer. Chem. Soc.* **1992**, in press.
- (18) Hagen, W. R.; Wassink, H.; Eady, R. R.; Smith, B. E.; Haaker, H. *Eur. J. Biochem.* **1987**, *169*, 457-465.

- (19) Bolin, J. T.; Ronco, A. E.; Mortenson, L. E.; Morgan, T. V.; Williamson, M.; Xuong, N.-H. in Gresshoff, P. M.; Roth, L. E.; Stacey, G.; Newton, W. E.; Chapman and Hall, New York, 1990; pp 117-124.
- (20) Georgiadis, M. M.; Komiya, H.; Chakrabarti, P.; Woo, D.; Kornuc, J. J.; Rees, D. C. *Science* **1992**, *257*, 1653-1659.
- (21) Kim, J.; Rees, D. C. *Science* **1992**, *257*, 1677-1682.
- (22) Rossmann, M. G. *Molecular Replacement Method*; Gordon and Breach: New York, 1972; pp
- (23) Bricogne, G. *Acta Cryst.* **1976**, *A32*, 832-847.
- (24) Jones, T. A. *Meth. Enzym.* **1985**, *115*, 151-171.
- (25) Tronrud, D. E.; Ten Eyck, L. F.; Matthews, B. W. *Acta Cryst.* **1987**, *A43*, 489-501.
- (26) Brünger, A. T. *J. Mol. Biol.* **1988**, *203*, 803-816.
- (27) Hausinger, R. P.; Howard, J. B. *J. Biol. Chem.* **1983**, *258*, 13486-13492.
- (28) Meyer, J.; Gaillard, J.; Moulis, J.-M. *Biochem.* **1988**, *27*, 6150-6156.
- (29) Howard, J. B.; Davis, R.; Moldenhauer, B.; Cash, V. L.; Dean, D. *J. Biol. Chem.* **1989**, *264*, 11270-11274.
- (30) Deisenhofer, J.; Epp, O.; Miki, K.; Huber, R.; Michel, H. *Nature* **1985**, *318*, 618-624.
- (31) Allen, J. P.; Feher, G.; Yeates, T. O.; Komiya, H.; Rees, D. C. *Proc. Natl. Acad. Sci. USA* **1987**, *84*, 5730-5734.
- (32) Godden, J. W.; Turley, S.; Teller, D. C.; Adman, E. T.; Liu, M. Y.; Payne, W. J.; LeGall, J. *Science* **1991**, *253*, 438-442.
- (33) Lindahl, P. A.; Day, E. P.; Kent, T. A.; Orme-Johnson, W. H.; Münck, E. *J. Biol. Chem.* **1985**, *260*, 11160-11173.
- (34) Hagen, W. R.; Eady, R. R.; Dunham, W. R.; Haaker, H. *FEBS Lett.* **1985**, *189*, 250-254.
- (35) Watt, G. D.; McDonald, D. W. *Biochem.* **1985**, *24*, 7226-7231.
- (36) Morgan, T. V.; Prince, R. C.; Mortenson, L. E. *FEBS Lett.* **1986**, *206*, 4-8.
- (37) Morgan, T. V.; McCracken, J.; Orme-Johnson, W. H.; Mims, W. B.; Mortenson, L.; Peisach, J. *Biochem.* **1990**, *29*, 3077-3082.
- (38) Herkovitz, T.; Averill, B. A.; Holm, R. H.; Ibers, J. A.; Phillips, W. D.; Weiher, J. F. *Proc. Natl. Acad. Sci. USA* **1972**, *69*, 2437-2441.
- (39) Coucouvanis, D. *Acc. Chem. Res.* **1991**, *24*, 1-8.
- (40) Kraulis, P. J. *J. Appl. Cryst.* **1991**, *24*, 946-950.
- (41) Hoover, T. R.; Robertson, A. D.; Cerny, R. L.; Hayes, R. N.; Imperial, J.; Shah, V. K.; Ludden, P. W. *Nature* **1987**, *329*, 855-857.
- (42) Madden, M. S.; Kindon, N. D.; Ludden, P. W.; Shah, V. K. *Proc. Natl. Acad. Sci. USA* **1990**, *87*, 6517-6521.
- (43) Eidsness, M. K.; Flank, A. M.; Smith, B. E.; Flood, A. C.; Garner, C. D.; Cramer, S. P. *J. Am. Chem. Soc.* **1986**, *108*, 2746-2747.
- (44) Conradson, S. D.; Burgess, B. K.; Newton, W. E.; Mortenson, L. E.; Hodgson, K. O. *J. Amer. Chem. Soc.* **1987**, *109*, 7507-7515.
- (45) Arber, J. M.; Flood, A. C.; Garner, C. D.; Gormal, C. A.; Hasnain, S.; Smith, B. E. *Biochem. J.* **1988**, *252*, 421-425.
- (46) True, A. E.; Nelson, M. J.; Venters, R. A.; Orme-Johnson, W. H.; Hoffman, B. M. *J. Amer. Chem. Soc.* **1988**, *110*, 1935-1943.
- (47) Rawlings, J.; Shah, V. K.; Chisnell, R. J.; Brill, W. J.; Zimmermann, R.; Münck, E.; Orme-Johnson, W. H. *J. Biol. Chem.* **1978**, *253*, 1001-1004.
- (48) Crowther, R. A. in Rossmann, M. G.; Gordon and Breach, New York, 1972; pp 173-178.
- (49) Kent, H. K.; Ioannidis, I.; Gormal, C.; Smith, B. E.; Buck, M. *Biochem. J.* **1989**, *264*, 257-264.

- (50) Kent, H. M.; Baines, M.; Gormal, C.; Smith, B. E.; Buck, M. *Mol. Microbiol.* **1990**, *4*, 1497-1504.
- (51) Dean, D. R.; Setterquist, R. A.; Brigle, K. E.; Scott, D. J.; Laird, N. F.; Newton, W. E. *Mol. Microbiol.* **1990**, *4*, 1505-1512.
- (52) Scott, D. J.; May, H. D.; Newton, W. E.; Brigle, K. E.; Dean, D. R. *Nature* **1990**, *343*, 188-190.
- (53) Thomann, H.; Bernardo, M.; Newton, W. E.; Dean, D. R. *Proc. Natl. Acad. Sci. USA* **1991**, *88*, 6620-6623.
- (54) Scott, D. J.; Dean, D. R.; Newton, W. E. in Gresshoff, P. M.; Roth, L. E.; Stacey, G.; Newton, W. E.; Chapman and Hall, New York, 1990; pp 169.
- (55) Govenzensky, D.; Zamir, A. *J. Bact.* **1989**, *171*, 5729-5735.
- (56) May, H. D.; Dean, D. R.; Newton, W. E. *Biochem. J.* **1991**, *277*, 457-464.
- (57) Lindahl, P. A.; Gorelick, N. J.; Münck, E.; Orme-Johnson, W. H. *J. Biol. Chem.* **1987**, *262*, 14945-14953.
- (58) Lammers, P. J.; Haselkorn, R. *Proc. Natl. Acad. Sci. USA* **1983**, *80*, 4723-4727.
- (59) Robbins, A. H.; Stout, C. D. *Proteins: Struct. Func. Gen.* **1989**, *5*, 289-312.
- (60) Eady, R. R. *Adv. Inorg. Chem.* **1991**, *36*, 77-102.
- (61) Willing, A.; Howard, J. B. *J. Biol. Chem.* **1990**, *265*, 6596-6599.
- (62) Deits, T. L.; Howard, J. B. *J. Biol. Chem.* **1990**, *265*, 3859-3867.
- (63) Wolle, D.; Kim, C.-H.; Dean, D.; Howard, J. B. *J. Biol. Chem.* **1992**, *267*, 3667-3673.
- (64) Thorneley, R. N. F.; Ashby, G. A.; Fisher, K.; Lowe, D. J. in Stiefel, E.; Coucouvanis, D. Newton, W. E.; American Chemical Society, Washington, D.C., 1993; in press.
- (65) Thorneley, R. N. F. in Gresshoff, P. M.; Roth, L. E.; Stacey, G.; Newton, W. E.; Chapman and Hall, New York, 1990; pp 103-109.
- (66) Brünger, A. T.; Milburn, M. V.; Tong, L.; DeVos, A. M.; Jancarik, J.; Yamaizumi, A.; Nishimura, S.; Ohtsuka, E.; Kim, S. H. *Proc. Natl. Acad. Sci. USA* **1990**, *87*, 4849-4853.
- (67) Pai, E. F.; Krengel, U.; Petsko, G. A.; Goody, R. S.; W., K.; Wittinghofer, A. *EMBO J.* **1990**, *9*, 2351-2359.
- (68) Story, R. M.; Steitz, R. A. *Nature* **1992**, *355*, 374-376.
- (69) Miller, R. W.; Eady, R. R. *Biochem. J.* **1989**, *263*, 725-729.
- (70) Feher, G.; Allen, J. P.; Okamura, M. Y.; Rees, D. C. *Nature* **1989**, *339*, 111-116.

RECEIVED March 8, 1993

Chapter 12

Structure and Environment of Metal Clusters in the Nitrogenase Molybdenum–Iron Protein from *Clostridium pasteurianum*

Jeffrey T. Bolin¹, Nino Campobasso¹, Steven W. Muchmore¹,
T. Vance Morgan², and Leonard E. Mortenson²

¹Department of Biological Sciences, Purdue University,
West Lafayette, IN 47907

²Center for Metalloenzyme Studies, Department of Biochemistry,
University of Georgia, Athens, GA 30602

The MoFe protein of Mo-dependent nitrogenases binds large and unusual metal-sulfur clusters of two types. These clusters are believed to be involved in the catalytic reduction of dinitrogen to ammonia by the enzyme. An analysis of the crystal structure of the MoFe protein from *Clostridium pasteurianum* at 2.2Å resolution is underway. On the basis of this analysis, atomic models for the structure of the FeMo cofactor and the Fe₈S₈ cluster, the interactions of these clusters with the protein, and general features of the protein structure are described. Two possible through-bond paths for electron transfer the two clusters are identified.

Nitrogenase catalyzes the reduction of dinitrogen to ammonia. The Mo-dependent form of the enzyme is a complex of two easily separated components known as the MoFe protein (component 1) and the Fe protein (component 2). MoFe protein is an $\alpha_2\beta_2$ tetramer, $M_r = 220\text{--}230,000$, which binds two Mo atoms and 30 Fe atoms in the form of four large metal-sulfur clusters of two types; two clusters of each type are present per tetramer. Fe protein is a homodimer, $M_r = 60\text{--}70,000$, which binds a single Fe₄S₄ cluster symmetrically between the subunits. The crystal structure of the Fe-protein has been described by Georgiadis *et al.* (1).

One of the metallic components of MoFe protein, the FeMo-cofactor (FeMoco), has been associated with substrate binding and reduction (2). Each FeMoco consists of one Mo, seven Fe, at least eight inorganic S atoms, plus one molecule of homocitrate. The two FeMoco units bound by the protein account for all of the Mo and 47% of the Fe content. Until recently, most models for the structure of MoFe protein assigned the remaining 16 Fe atoms to four atypical Fe₄S₄ clusters commonly referred to as "P-clusters." In 1987, Hagen *et al.* (3) challenged the conventional model for the structure and redox chemistry of P-clusters and described possible alternatives, including the possibility of 8-Fe rather than 4-Fe clusters. Subsequently we reported X-ray anomalous diffraction experiments which conclusively demonstrated that MoFe protein binds four metal-sulfur clusters of roughly equivalent metal content, and that the non-cofactor Fe atoms are associated with two large FeS clusters of a previously undescribed type (4). We now know these clusters

are identical, contain eight Fe atoms, and are constructed of two multiply-bridged 4-Fe subclusters structurally similar to typical Fe_4S_4 clusters (see below).

Within the past year, the crystal structures of Av1 and Cp1, the MoFe proteins from *Azotobacter vinelandii* and *Clostridium pasteurianum*, respectively, have been determined to high resolution. Kim and Rees (5) published atomic models for both FeMoco and the 8-Fe cluster based on a 2.7Å resolution structure of Av1; we will treat these initial "KR" models as reference structures for both clusters. We independently determined the structure of Cp1 at 2.7Å resolution and subsequently extended this analysis to 2.2Å resolution. Here we describe structural features of Cp1 based on this 2.2Å resolution analysis with an emphasis on the structures of the clusters and their protein environments. We will compare these results with the KR models as well as with the results of our 2.7Å resolution analysis, both of which were presented orally at the symposium upon which this volume is based. Kim and Rees (6) revised their model for the 8-Fe cluster subsequent to the symposium and this revised model also will be considered.

Procedures and Status of the Cp1 Model

Monoclinic crystals of Cp1 containing one $\alpha_2\beta_2$ tetramer per asymmetric unit were prepared in a glove box under N_2 atmosphere (less than 1 ppm O_2) as previously described (4). Diffraction data were recorded on a variety of instruments including multiwire area detector systems relying on conventional X-ray generators as well as instruments at the Stanford Synchrotron Radiation Laboratory and the Photon Factory synchrotron in Tsukuba, Japan.

Initial phases were obtained to 3.0Å resolution by a combination of multiwavelength anomalous diffraction and multiple isomorphous replacement methods. Scattering factors used for metal-sulfur clusters in the anomalous diffraction phase calculations were constructed from rotationally averaged tetrahedra rather than atomic models. Three heavy atom derivatives (two Pt and one Ir) with common sites contributed to the isomorphous replacement phases. Solvent flattening and two-fold molecular averaging were used to improve and extend the phase set in two rounds of phase extension, which stopped at 2.7Å and 2.2Å resolution, respectively. Co-K α and Cu-K α Bijvoet difference maps were used throughout the study in the interpretation of the structures of the metal-sulfur clusters. For example, Co-K α Bijvoet difference maps define the positions of the Mo atoms as the highest density features in the map. This is the expected result inasmuch as the anomalous scattering factors, f'' , for Mo, Fe, and S are 3.5, 0.5, and 0.7 electrons, respectively, for Co-K α radiation ($\lambda=1.79$ Å). Similarly, the positions of the Fe atoms in Cu-K α Bijvoet difference maps correspond to the highest density features: for Cu-K α radiation ($\lambda=1.542$ Å), f'' values for Mo, Fe, and S are 2.7, 3.2, and 0.6 electrons, respectively. In fact, the Fe and Mo atoms are represented by virtually resolved maxima in a 2.5 Å resolution Cu-K α Bijvoet difference map calculated using phases provided by the second round of phase extension. We also note that all Co-K α Bijvoet anomalous difference maps calculated subsequent to the first round of phase extension show high density peaks for all but one of the 48 protein S atoms in the $\alpha\beta$ dimer. These maps thus served as an invaluable aid during the reconciliation of amino acid sequence data and electron density.

Although atomic parameter refinement is underway, the results presented in this report are derived solely from the interpretation of electron density maps calculated with experimental phases; thus these maps possess no bias from particular atomic models (cf. 7). The current model is based on the interpretation of two-fold averaged standard electron density maps at 2.2Å resolution as well as averaged Cu-K α and Co-K α Bijvoet anomalous difference maps at 2.5 and 3.0Å resolution, respectively. The native data set includes more than 720,000 observations for 110,000 of 120,000 possible reflections to 2.2Å resolution; $R_{\text{merge}} = 6.3\%$. For reflections with

spacings between 2.3 and 2.2 Å, the data are 70% complete and $R_{\text{merge}} = 12\%$. The model includes 508 of the 534 residues in the Cp1 α -chain and all 458 residues in the β -chain; the sidechains of a small fraction of the residues have been truncated because of weak density. The crystallographic R-factor for this unrefined model, based on all measured reflections to 2.2 Å resolution, is 33%. A detailed description of all procedures used for data collection, phase determination, model construction, and refinement will be published elsewhere.

The Tertiary Structure of the α and β Subunits

As shown in Figure 1, the tertiary structures of the α and β subunits of Cp1 are quite similar. Moreover, both subunits have three similar domains, all of which belong to the doubly-wound, parallel β class (β). The six domains share a common core, which includes a parallel β sheet of four strands with three dimensional order B,A,C,D, where the order in the amino acid sequence is A,B,C,D. The core structure also includes helices between β A and β B and after β D on one side of the sheet, and a helix between β C and β D on the other side. Among the variations in structure is the presence of an additional helix preceding β A in the N-terminal domain of both subunits; in both cases, a cysteinyl residue (α Cys52, β Cys23) near the N-terminus of the helix provides a ligand to the 8-Fe cluster. All of the above features are consistent with the structure of Av1 as reported by Kim and Rees (5,6).

The Quaternary Structure of MoFe Protein.

In general, past studies of the external shape and gross structure of MoFe protein by low resolution techniques such as electron microscopy (9) and low-angle neutron scattering (10) underestimated the size of MoFe protein, yielding a typical maximum dimension of approximately 90 Å. The true dimensions of MoFe protein are roughly 125 Å by 70 Å in a projection perpendicular to the molecular twofold axis and 75 Å along the axis.

Similarly, predictions about the quaternary structure based on low resolution methods were in error. Although the α and β subunits have the same general shape, they do not assemble into a particle with 222 (D_2) point group symmetry, as suggested by low resolution X-ray diffraction studies (11,12) and supported by sequence comparisons between α and β subunits (13,14). Rather, a single molecular twofold axis relates two $\alpha\beta$ dimers, whereas two non-intersecting local twofold axes approximately relate the α and β subunits within each dimer (see below).

The quaternary interactions of MoFe protein can be understood by analogy to a model constructed from two pairs of boots or shoes. For each subunit, the N-terminal domain is represented by the toe of the boot up to the arch, the middle domain by the heel, and the C-terminal domain by the ankle piece. To construct the packing model, two equivalent β boots (say, the left boots from the two pairs) are placed sole down on the floor such that they are related by a vertical two-fold symmetry axis and interact extensively from arch to heel along their inside (medial) surfaces. The toes, or N-terminal domains, are thus well separated and effectively free from β - β interactions. Each α boot is then turned sole upward and placed across the toe of one β boot such that the heel-to-toe axes of α and β are perpendicular and each α subunit interacts extensively with one β subunit through the top surfaces of their toe portions; it is this interaction that defines the local axis of pseudo symmetry between α and β subunits belonging to the same $\alpha\beta$ dimer. Each α subunit interacts with the other β subunit through heel and ankle contacts. Thus the α subunits interact with both β subunits, but are well separated from each other (by roughly 35 Å at closest approach).

Structure and Binding of the FeMo-cofactor

Figure 2 provides schematic drawing of our current model for FeMoco, whereas Figure 3 shows the model along with the corresponding electron density from a 2.2Å resolution map. The metal-sulfur framework of the cofactor consists of bridged MoFe₃S₃ and Fe₄S₃ fragments geometrically analogous to pieces derived from MoFe₃S₄ and Fe₄S₄ cubane-like clusters. Three bridging atoms connect the two fragments by linking pairs of Fe atoms from different fragments such that the six central Fe atoms form a trigonal prism; within the prism, the average distances between bridged Fe atoms and between non-bridged Fe atoms from different fragments are 2.8Å and 3.9Å, respectively. Homocitrate ((*R*)-2-hydroxy-1,2,4-butanetricarboxylic acid) is coordinated to the Mo atom through its 2-hydroxy and 2-carboxyl groups, and the only two protein ligands are provided by the conserved residues αHis481 and αCys261. The former binds to Mo through its Nδ1 atom, whereas the latter binds through its Sγ atom to the tetrahedral Fe atom (Fe1) at the opposite end of the cluster.

The major features of our model are thus wholly analogous to the that proposed by Kim and Rees on the basis of their 2.7Å resolution study of Av1 (5). The models differ in the identity of the bridging atoms. Whereas Kim and Rees, on the basis of relative electron density values, model the three bridging groups as two S atoms and one atom of lower atomic number (or a disordered S), our data indicate that all three are S atoms. In our case, the interpolated electron density values at all three positions are within 0.5 σ (standard deviation) of the mean for all protein and cluster S atoms in the αβ dimer and are 2 σ larger than the mean density of all carbonyl O atoms. Moreover, the position of each bridging atom is associated with significant density in the Cu-Kα and Co-Kα Bijvoet anomalous difference maps.

Our current model and the KR model are consistent with respect to the unusual character of the six central Fe atoms in that each is modeled as three-coordinate Fe displaced out of the plane of its three S ligands toward the center of the cluster. The first maps we obtained at 2.7Å resolution had significant electron density at the center of the cluster, thus suggesting but not confirming the presence of a hexavalent central atom, presumably S, which could provide a fourth ligand for each of the six central Fe atoms. However, the 2.2Å resolution maps have low electron density at the center and do not indicate the presence of a central atom; calculations based on models with and without a central S atom indicate that significant density would be observed if such an atom were present. Our maps also provide no indication of an external fourth ligand for any of the six Fe atoms, although it should be noted that we would not observe external or internal hydride ligands if they are present.

The FeMo cofactor binds at a point where all three domains of the α subunit converge, and residues from each domain make contact with the cluster. Although we will not document all of the contacts here, we will note a few interesting features of the cofactor binding site not described by Kim and Rees (5). For example, we observe that each of the bridging S atoms is potentially involved in hydrogen bonded interactions with the protein: the S atom between Fe2 and Fe6 is 3.3Å from Nε2 of conserved αHis185; the S atom between Fe4 and Fe5 is in a pocket formed by the backbone atoms of residues α342 through α346 and could accept hydrogen bonds from two or more of the amide protons in this loop; and the S between Fe3 and Fe7 (position Y in the KR model) is 2.8Å from atom Nη2 of conserved αArg86. The interactions of αArg86 also include a potential hydrogen bond between Nε and a cluster S atom directly bound to the Mo. Because αArg86 is separated by only two turns of helix from one of the ligands to the 8-Fe cluster, αCys78, this helix must be considered a possible path for electron transfer between the two metal centers.

Another remarkable feature of the cofactor site not noted by Kim and Rees is the fact that the homocitrate end of the cofactor is highly hydrated and in close proximity

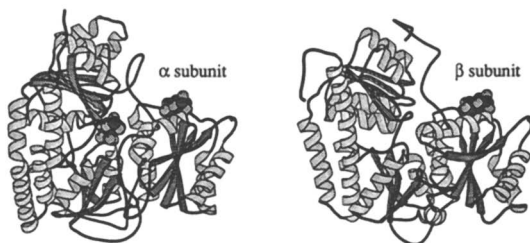


Figure 1. Ribbon drawings of the α and β subunits of MoFe protein. The two subunits have been placed in the same orientation and the similarity of the secondary and tertiary structures is evident. Helical structure is lightly shaded whereas the β structure and connecting segments are darkly shaded. The metal and sulfur atoms of the FeMo cofactor and Fe_8S_8 cluster are shown as shaded spheres; the former is near the center of the α subunit whereas the latter is directly beneath the subunit label in both subunits. The drawings were prepared with the program MOLSCRIPT (Per Kraulis, Uppsala University).

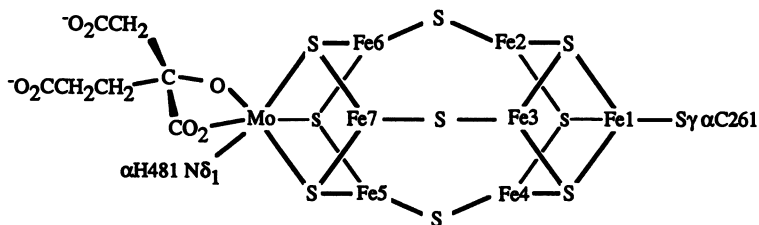


Figure 2. A schematic drawing of the structure of the MoFe cofactor and its protein ligands.

to residues from the β subunit. We observe resolved electron density features indicating the presence of at least 12 water molecules that appear to form part of a hydrogen bonded network that includes all carboxylate groups of homocitrate as well as sidechain and backbone atoms from both subunits. Among the protein groups involved are the sidechains of conserved residues β Tyr51 and β Arg58. Clearly, these water molecules provide a likely source of protons needed for substrate reduction, and they may also provide alternative electron transfer paths. Among the possible paths is one which passes along a β -subunit helix that includes the 8-Fe cluster ligand β Cys48 as well as β Arg58; this helix is structurally homologous to the α -subunit helix that includes α Arg86 and α Cys78, as described above.

Structure and Environment of the 8-Fe Cluster.

Two 4-Fe subclusters similar in structure to standard Fe_4S_4 clusters are joined to form the 8-Fe cluster, which is bound at the pseudo-symmetric (toe-to-toe) interface between the N-terminal folding domains of α and β subunits belonging to the same dimer. Three conserved cysteine residues from each domain (α Cys52, α Cys78, α Cys144; β Cys23, β Cys48, β Cys106) serve as the only protein ligands to the cluster's metal atoms. The connections between the subclusters include two Fe-S-Fe bridges involving protein thiolate groups, the S γ atoms of α Cys78 and β Cys48. Thus each subcluster is bound by three cysteines from the same subunit and one bridging cysteine residue from the other. Moreover, each of the 8 Fe atoms has a single cysteinyl S as a ligand, but only six cysteine residues are required. A schematic drawing of this structure is presented in Figure 4.

Our maps at both 2.7 and 2.2Å resolution clearly indicate the presence of a third link between subclusters, a feature not present in the original KR model. Thus when known $\text{Fe}_4\text{S}_4(\text{SR})_4$ structures are fit independently to the density for the two halves of the 8-Fe cluster, we observe a 1Å separation between two S atoms from different subclusters. We obtain a similar separation regardless of whether we fit model structures to standard electron density maps, or to a 2.5Å resolution Cu-K α Bijvoet difference map, which shows resolved maxima for each Fe atom. In general, the positions of the core atoms and terminal S atoms agree well with the electron density, as illustrated by Figure 5, which shows the result of a fit with a 1Å S-to-S separation and the corresponding features from a 2.2Å resolution standard electron density map.

Clearly, a model which includes a 1Å S-to-S separation is chemically unreasonable. At present, our model and the revised model of Kim and Rees (6) both include a disulfide bond roughly 2Å in length between subclusters at this position, a possibility suggested by Dr. E. I. Stiefel during the symposium. However, to obtain a good fit to the standard electron density and maintain terminal Fe-S bonds of appropriate length, this model must include significant distortions from tetrahedral bonding geometry for the two S atoms involved in the disulfide bond as well as for the Fe atoms bonded to α Cys144 and β Cys106 (Fe2 and Fe6, respectively). Some of these distortions would be relieved if the two subclusters were linked by a single shared S atom rather than by a disulfide bond, and such a model remains compatible with the high resolution electron density maps. This model, whose features include an Fe_3S_7 core, two bridging cysteinyl ligands, and a hexavalent S atom bonded to three Fe atoms from each subcluster, is the model we presented at the symposium upon which this volume is based.

In addition to the covalent cluster ligands, we have identified three β chain residues whose sidechain atoms should donate hydrogen bonds to S atoms of the cluster. These interactions involve the O γ atoms of conserved serine residues β Ser45 and β Ser141, and the Ne2 atom of β His52, a non-conserved residue. The sidechain of β Ser141 lies near the center of one face of the β subcluster (the Fe6,Fe7 face) and its electron density suggests that it may interact, through different

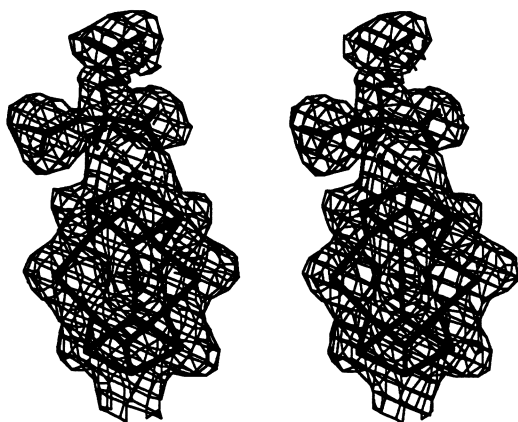


Figure 3. A model for the FeMo cofactor and the corresponding electron density. The metal and sulfur core as well as the homocitrate moiety are illustrated with thick solid lines whereas the bonds between the two groups are indicated by thick dashed lines. This stereo pair is oriented so that the Fe4-S-Fe5 bridge is toward the viewer and the Fe3-S-Fe7 bridge is toward the right. The electron density is from a 2.3Å resolution map calculated with experimental phases and was contoured at a value corresponding to 1.2 times the root mean square value of density values in the asymmetric unit. Density features associated with nearby protein atoms, including the Mo ligand α H481, have been edited for the sake of clarity. The figure was prepared using the program MACINPLOT II (see Smith, T. J. *J. Appl. Crystallogr.* 1990, 23, 141-142).

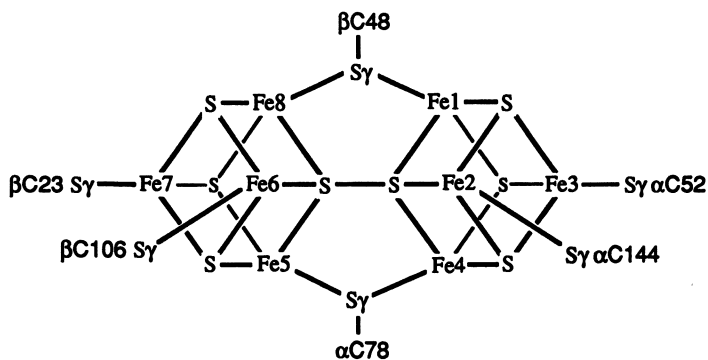


Figure 4. A schematic drawing of the structure of the Fe_8S_8 cluster and its protein ligands.

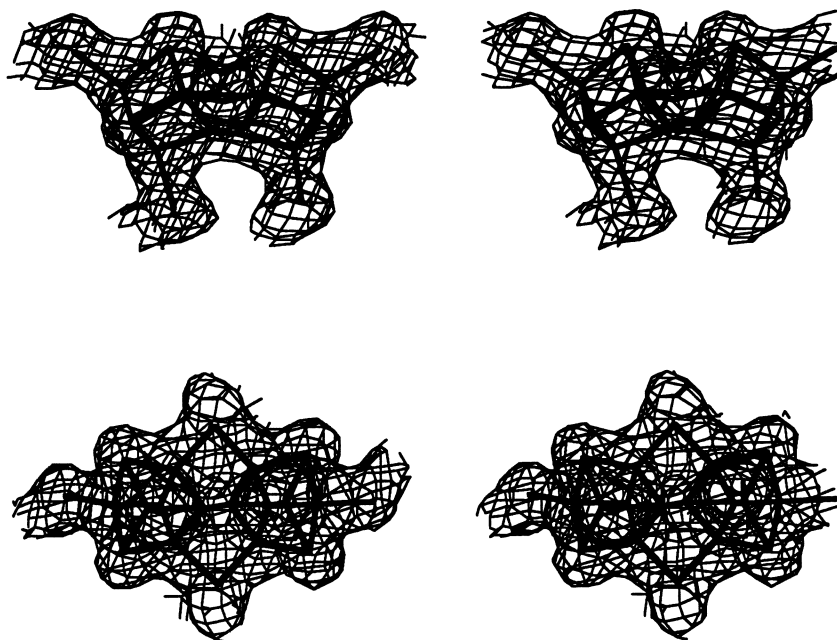


Figure 5. A model for the Fe₈S₈ cluster and the corresponding electron density. The figure illustrates a "best fit" structure for the Fe₈S₈ cluster in two perpendicular stereo pairs. This structure contains an unreasonable 1Å separation between two cluster S atoms, rather than a 2Å disulfide bond (see text). Bonds between the cluster and cysteinyl S_γ atoms as well as bonds between cluster atoms are illustrated as thick solid lines. The source map, contouring, and figure preparation are as described Figure 3.

conformers, with both of the core S atoms on this face. The density for the sidechain of β Ser141 is clearly resolved from the Fe atoms of this face, and we think it unlikely that its O γ atom coordinates with Fe6, as suggested by Kim and Rees (5,6), unless it is through a long distance contact roughly 3.0Å in length; in our current model the O γ -to-Fe6 distance is 3.2Å.

Adjacent to the 8-Fe cluster we also observe several resolved electron density features that are likely to represent bound water molecules. One of the possible water positions is 3.1Å from S γ of α Cys144 and 3.3Å from S γ of β Cys48, two of the cluster's cysteinyl ligands. In addition to serving as a hydrogen bond donor to these atoms, a water at this site could accept hydrogen bonds from O γ 1 of β Thr105, a conserved residue, as well as from the backbone amide group of β Ser45. Moreover, this site is within 3.8Å of one of the sulfur atoms involved in the possible disulfide bond between subclusters. A second potential water position has been identified 4Å away from the cluster S atom bound by Fe1, Fe3, and Fe4. This site is particularly interesting because it seems to be connected by a network of additional bound waters and protein groups to the homocitrate group of the FeMo cofactor (see above).

Summary

We have presented models for the metal-sulfur clusters bound by Cp1 as well as descriptions of their binding sites. Our models for the clusters are comparable to the initial models of Kim and Rees (5) with three notable exceptions: (1) we have identified all three bridging atoms in the FeMo-cofactor as S atoms; (2) we observe three covalent links between the two Fe $_4$ S $_4$ subclusters of the Fe $_8$ S $_8$, including one not mediated by protein atoms and currently modeled as a disulfide bond (see also (6)); (3) the position of the sidechain of β Ser141 in our model suggests that it interacts with the 8-Fe cluster through a hydrogen bond involving a cluster S atom rather than through a direct bond to an Fe atom. These differences should be interpreted with caution until crystallographic refinement of the Cp1 structure has been completed.

Acknowledgments

J.T.B. gratefully acknowledges support from the USDA (NRI-CRGO), the Lucille P. Markey Foundation, and Exxon Corporation as well as helpful conversations with Profs. D. Coucouvanis, A. Davison, and R. Holm on the structures of metal-sulfur clusters. N.C. and S.W.M. were supported in part by a Biophysical Studies training grant funded by NIH.

Literature Cited

1. Georgiadis, M. M.; Komiya, H.; Chakrabarti, P. K.; Woo, P., Kornuc, J. J.; Rees, D. C. *Science* **1992**, *257*, 1653-1659.
2. Burgess, B. K. *Chem. Rev.* **1990**, *90*, 1377-1406.
3. Hagen, W. R.; Wassink, H.; Eady, R. R.; Smith, B. E.; Haaker, H. *Eur. J. Biochem.* **1987**, *169*, 457-465.
4. Bolin, J. T.; Ronco, A. E.; Mortenson, L. E.; Morgan, T. V.; Williamson, W. E.; Xuong, N.-h. In *Nitrogen Fixation: Achievements and Objectives*; Greshoff, P. M.; Roth, L. E.; Stacey, G.; Newton, W. E., Eds.; Chapman and Hall: New York, NY, 1990; pp. 117-122.
5. Kim, J.; Rees, D. C. *Science* **1992**, *257*, 1677-1682.
6. Kim, J.; Rees, D. C. *Nature(London)* **1992**, *360*, 553-560.
7. Donahue, J. *Science* **1969**, *169*, 1091-1096.
8. Richardson, J. S. *Adv. Prot. Chem.* **1981**, *34*, 167-339.

9. Voorduow, G.; Haaker, H.; van Bruggen, J. F. L.; van Bruggen, E. F. J.; Eady, R. R. *Eur. J. Biochem.* **1983**, *136*, 397-401.
10. Meyer, J.; Zaccari, G. *Biochem. Biophys. Res. Commun.* **1981**, *98*, 43-50.
11. Yamane, T.; Weininger, M. S.; Mortenson, L. E.; Rossmann, M. G. *J. Biol. Chem.* **1982**, *257*, 1221-1223.
12. Sosfenov, N. I.; Andrianov, V. I.; Vagin, A. A.; Strokopytov, B. V.; Vainshtein, B. K.; Shilov, A. E.; Gvozdev, R. I.; Likhtenstein, G. I.; Mitsova, I. Z.; Blazhchuk, I. S. *Sov. Phys. Dokl.* **1986**, *31*, 933-935.
13. Lammers, P. J.; Haselkorn, R. *Proc Natl. Acad. Sci. U.S.A.* **1983**, *80*, 4723-4727.
14. Thony, B.; Kaluza, K.; Hennecke, H. *Mol. Gen. Genet.* **1985**, *198*, 441-448.

RECEIVED April 12, 1993

Chapter 13

Biosynthesis of the Iron–Molybdenum Cofactor of Nitrogenase

Paul W. Ludden¹, Vinod K. Shah¹, Gary P. Roberts², Mary Homer²,
Ronda Allen¹, Tim Paustian², Jon Roll², Ranjini Chatterjee¹,
Mark Madden¹, and Jeff Allen¹

Departments of ¹Biochemistry and ²Bacteriology, University of Wisconsin,
Madison, WI 53706

The in vitro biosynthesis of the iron-molybdenum cofactor (FeMo-co) of nitrogenase requires the NifB, NifNE and NifH (dinitrogenase reductase) proteins, molybdate, homocitrate and MgATP. The various components required for FeMo-co synthesis are described in this chapter. Many homologs of homocitrate have been employed in the biosynthesis of FeMo-co and the structural requirements for effective incorporation have been established. The catalytic properties of dinitrogenases containing FeMo-cos synthesized with homocitrate analogs are presented. The specificity of the FeMo-co synthetic system for nucleotides and divalent metals has been tested and compared to the requirements for metal-nucleotide by dinitrogenase reductase in its catalytic role. Tritium-labelled homocitrate has been used to follow the incorporation of the organic acid into FeMo-co and its precursors.

The iron-molybdenum cofactor (FeMo-co) is at the active site of nitrogenase and an elucidation of its biosynthesis is essential to an understanding of both the biology and chemistry of nitrogen fixation. Nitrogen fixation was shown to be dependent on molybdenum (1) and, until the work by Bishop and coworkers and the Sussex group (2-7), this element was thought to be specifically required for all biological systems of N₂ reduction to ammonia. The discovery of the molybdenum cofactor (Mo-co) associated with nitrate reductase and its ability to reconstitute active enzyme in extracts from mutant *Neurospora sperassa* cell lines (8) led to speculation that a similar cofactor might exist in the dinitrogenase protein (the dinitrogenase protein is also referred to as the MoFe protein or component I elsewhere in this volume and abbreviated as Kp1, for example, for the dinitrogenase protein from *Klebsiella pneumoniae*). After preliminary work by Pienkos et al. (9), such a cofactor was isolated and reported by Shah and Brill in 1977 (10), but the primary similarity between the iron-molybdenum cofactor of nitrogenase and the pterin-containing cofactor of nitrate reductase and other molybdenum enzymes is the presence of molybdenum (11). The iron-molybdenum cofactor of nitrogenase (FeMo-co) apparently is unique to molybdenum nitrogenases; its analogs in non-molybdenum nitrogenases probably are structurally similar entities with another metal in place of molybdenum (3, 5).

FeMo-co consists of iron, sulfur, molybdenum and the organic acid homocitrate

in a ratio of Fe₇S₈MoHomocitrate (10, 12-15). The arrangement of the components of FeMo-co was a major scientific puzzle from the time of FeMo-cofactors' discovery until the elucidation of its basic structure by the Rees and Bolin groups as presented elsewhere in this volume. Although the models presented by the two groups differ in some substantial ways, the basic arrangement of metals is agreed upon.

Our approach for determining the biosynthetic pathway of FeMo-co was built on genetic studies by Brill and coworkers who defined the involvement of several *nif* gene products in the in vivo biosynthesis of FeMo-co (16, 17); Filler and Smith (18) later added *nifH* to this list of biosynthetic genes. The biochemical analysis of FeMo-co synthesis was facilitated by the development of a system for the in vitro biosynthesis of FeMo-co (19). This in vitro FeMo-co biosynthesis system provided a means to assay individual components of the system when other components were present in excess. The assay provides a means to follow the purification of the proteins and other factors involved in the biosynthesis. FeMo-co synthesis is defined as the *nif*-specific processing of molybdenum, iron and sulfur along with the synthesis and utilization of homocitrate or its analogs. The synthesis ends when a molecule capable of activating apo-dinitrogenase is obtained. The insertion of FeMo-co into apo-dinitrogenase is thus considered to be a separate process. Activation of apo-dinitrogenase is defined as insertion of FeMo-co (or an analog) so that the enzyme is capable of reduction of any of the known nitrogenase substrates including protons, acetylene and dinitrogen.

The in vitro biosynthetic system recognizes as "FeMo-co" any chemical entity that will activate apo-dinitrogenase, and thus is a functional definition rather than a chemical one. While it was always assumed that FeMo-co produced by the wild-type organism had a single, precise chemical composition, it is now clear that functional variants of FeMo-co with altered chemical compositions and properties can be prepared in vitro and in vivo.

The *nif* Gene Products Required for FeMo-co Synthesis. In their investigation of the *nif* genes of *pneumoniae*, Roberts et al. identified the *nifB*, *N*, and *E* genes as necessary for synthesis of FeMo-co (17, 20). Extracts of *nifB*, *nifN* or *nifE* strains lacked active dinitrogenase (called component I in the original manuscript) but the inactive proteins accumulated in the cell. These inactive dinitrogenases could be activated by addition of purified FeMo-co to the extract. Under molybdenum-limiting conditions, *nifQ* mutants were also phenotypically Nif⁻, and extracts of these strains could also be activated by addition of FeMo-co (21). The *nifQ* strains were not defective in MoO₄²⁻ uptake or in the accumulation of the *nifH* or *nifDK* gene products which encode dinitrogenase reductase and dinitrogenase proteins, respectively.

Strains with point mutations in *nifV* displayed slow growth on N₂, but exhibited significant acetylene reduction. McLean and Smith then demonstrated that the dinitrogenase protein of *nifV* strains differed in its substrate specificity and inhibitor susceptibility. In a set of experiments in which FeMo-co was isolated from wild-type or *nifV* strains and used to activate apo-dinitrogenase, Hawkes et al. demonstrated that the aberrant properties of the *nifV* dinitrogenase were due to the FeMo-co of that protein, thus implicating the *nifV* gene in FeMo-co synthesis, processing or insertion (22). The role of the *nifV* gene product in producing the homocitrate component of FeMo-co is discussed below.

The *nifH* gene had long been known to encode the structural gene for dinitrogenase reductase (also known as NifH, the Fe protein or component II and abbreviated as, for example, Kp2), so it was surprising when Filler et al. presented evidence that a form of NifH was required for FeMo-co synthesis in vivo (18). Biochemical evidence for the role of NifH in FeMo-co synthesis was provided by Robinson et al. using the in vitro FeMo-co biosynthesis assay (23). The proposal that the role of NifH in FeMo-co synthesis differs mechanistically from its role in MgATP-dependent electron transfer to dinitrogenase is supported by the observations that

ADP-ribosylated NifH in *R. rubrum* (which is unable to transfer electrons to dinitrogenase) will support in vitro FeMo-co synthesis (24) and that the dinitrogenase reductase from a *nifM* mutant is able to promote FeMo-co synthesis in vivo (17).

While definitive biochemical and genetic evidence has been presented for the roles of *nifB*, *N*, *E*, *V* and *H* gene products as well as a role for the *nifQ* product under some conditions of growth, no role in the synthesis has been suggested for the *nifKD* gene products that constitute the dinitrogenase protein. In fact, FeMo-co synthesis occurs readily in vivo and in vitro in the absence of NifK and NifD (25). In vivo, ⁹⁹Mo labelling studies by Ugalde et al. showed that ⁹⁹Mo accumulated on protein in a form that could activate apo-dinitrogenase, thus fitting the functional definition of FeMo-co. The identity of this FeMo-co carrier is not known, but it does not appear to be NifNE or NifB. These results suggest that FeMo-co is built on some other protein and then transferred to the apo-dinitrogenase protein (lacking FeMo-co), although the model in which FeMo-co accumulates on another protein only in the absence of apo-dinitrogenase cannot be ruled out.

The In Vitro FeMo-co Synthesis Assay. In order to further define the roles of the various gene products in FeMo-co synthesis, it was necessary to develop a system for in vitro FeMo-co synthesis. It has been assumed in these studies that all intermediates of FeMo-co synthesis will be protein-bound, or at least not free intermediates, and this makes the isolation of intermediates all the more difficult. Once a crude extract system was available, it would be possible to purify the various gene products from the extract(s). The initial success towards an in vitro system came when extracts of two organisms were mixed: an extract of *K. pneumoniae* strain UN1100 (a NifE⁻ strain) and an extract of *Azotobacter vinelandii* strain UW45 (a NifB⁻ strain) (26); this strain had long been used as a source of apo(lacking FeMo-co)-dinitrogenase protein (19). *K. pneumoniae* appears to be a good source of NifB, while *A. vinelandii* is a better source of the NifNE protein. Both extracts provide apo-dinitrogenase that can bind FeMo-co and reconstitute active dinitrogenase that is then measured by reduction of acetylene or other nitrogenase substrate. In subsequent studies, it has been possible to achieve FeMo-co synthesis with extracts of a single organism. In order to establish the validity of the in vitro FeMo-co synthesis assay, it was demonstrated that the production of FeMo-co was linear over the time course of the assay and that the assay could be saturated with either NifNE or NifB. The molybdenum-dependence of the assay was established using extracts of each type of cell grown in the absence of added molybdate and the presence of excess sodium tungstate. Under these conditions, the activity of the FeMo-co synthesis assay in the absence of added MoO₄²⁻ was only 3% that of the complete assay mixture. The ATP-dependence of FeMo-co synthesis was demonstrated, but the stoichiometry of the ATP per FeMo-co is not known, nor is it known if ATP is hydrolyzed during synthesis of FeMo-co.

As a final proof of the validity of the in vitro FeMo-co synthesis assay, the characteristic EPR signal of the dinitrogenase protein at $g = 3.65$ was observed with dinitrogenase activated with FeMo-co synthesized in vitro (Figure 1).

It is interesting that 1-5% of the acetylene reduction activity of the complete assay system is observed in assay mixtures lacking one or more essential component. It is not known if this results from non-enzymatic assembly of FeMo-co or from the assembly of a non-FeMo-co entity capable of low levels of acetylene reduction.

Purification and Characterization of the NifNE Gene Products. The NifNE proteins were purified to homogeneity with a 20% yield by Paustian et al. using a combination of ion exchange, affinity and reverse-phase chromatography (27). The purification was monitored by increasing specific activity of the proteins in the FeMo-co synthesis assay. A unit of NifNE activity is defined as one nmole of acetylene reduced per minute of incubation of the FeMo-co synthesis assay. It had been

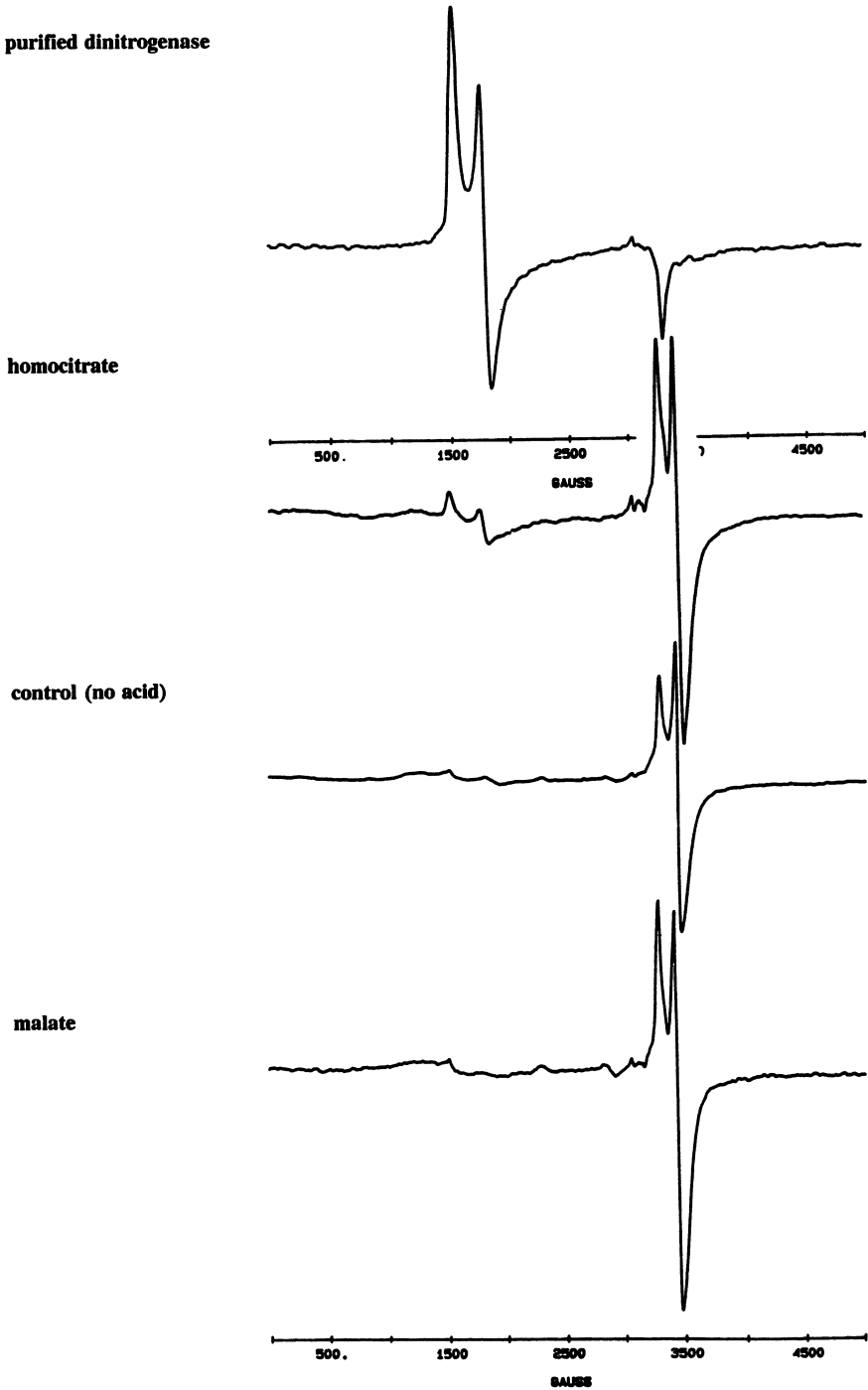


Figure 1. EPR spectra of dinitrogenases containing in vitro synthesized FeMo-cofactors.

suggested by Roberts et al. (17, 28) that the products of the *nifNE* genes might form a dimer or tetramer because neither protein was stable *in vivo* in the absence of the other. Dean and Brigle noted the sequence similarity of the *nifD* and *nifE* genes and suggested that *nifNE* might encode products that formed a tetramer and serve as a "surrogate" MoFe protein (29). Most notably, an analogous cysteine is found at position 275 of NifD and 231 of NifE. This cysteine is thought to be involved in FeMo-co binding in NifD (30, 31 and Paustian, Roberts & Howard, unpublished) and suggests that NifNE may serve that purpose in the final stages of the cofactor synthesis. Analysis of purified NifNE by SDS PAGE and by native gel filtration confirmed that the protein consisted of two subunits and that the native molecular weight is consistent with an $\alpha_2\beta_2$ tetramer of the *nifN* and *nifE* products (27).

Metal analysis revealed 4.6 iron atoms per tetramer of NifNE. Zinc and copper atoms were also found in the purified protein solution at nearly stoichiometric levels, but the significance of these metals to the role of NifNE is not known at this time. The protein exhibited a UV-vis spectrum characteristic of Fe-S proteins and could be reversibly oxidized and reduced. Further spectroscopic analysis of the protein should reveal the type of metal center in the protein. No molybdenum was found in the NifNE protein purified from *A. vinelandii* strain UW45 even though the protein was purified from cells grown in the presence of Mo, demonstrating that NifNE is not the obligate molybdenum source in the *in vitro* synthesis assay. The activity of NifNE protein is oxygen labile with a half-life in air of less than 3 minutes.

Because iron and sulfur are present in the protein that functions *in vitro*, it is tempting to conclude that NifNE might serve as the donor of some or all of the Fe and S of FeMo-co, although direct biochemical evidence to support this hypothesis is lacking. NifNE has only been purified from a NifB⁻ strain and it is likely that the form of NifNE that accumulates in this strain differs from the predominant form of the enzyme in the *nif*-derepressed wild-type. It has not been possible to detect NifNE activity in extracts of *A. vinelandii* wild-type (Paustian, Shah and Roberts, unpublished), suggesting that NifNE might only accumulate in a "charged" form in strains blocked elsewhere in FeMo-co synthesis. Calculations of the amount of FeMo-co that can be synthesized with a known amount of purified NifNE show that NifNE can turn over no more than twice in the *in vitro* FeMo-co synthesis assay. The conclusion from this set of experiments has been that NifNE contributes a portion of FeMo-co and then cannot be regenerated *in vitro*. Another conceivable role for NifNE is to provide reductant during the synthesis of FeMo-co. The source of molybdenum *in vivo* and *in vitro* is usually MoO_4^{2-} , whereas the molybdenum atom of FeMo-co is thought to be in a much more reduced state (32).

The ability of NifNE to bind the affinity resin Reactive Red 120 suggests the presence of a nucleotide-binding site on the protein. ATP-binding sites on the dinitrogenase protein have been characterized and the NifNE protein has significant presence of MoO_4^{2-} or homocitrate (Paustian, unpublished). Nucleotide is required for FeMo-co synthesis and perhaps NifNE serves as a nucleotide-binding protein in sequence similarity to that protein. The NifNE protein does not hydrolyze ATP in the the process.

Purification and Characterization of NifB. The NifB protein has been extremely resistant to purification. It is an oxygen-labile, membrane protein and is not easily solubilized (24). It has not been observed on two-dimensional gels and behaves anomalously on many protein purification matrices. The protein can be solubilized by N-lauroylsarcosine and sulfobetaine detergents (SB-12, SB-14) and then purified by ion exchange chromatography although NifB behaves anomalously here as well, eluting in 2-3 column volumes (Shah and J. Allen, unpublished results). Further purification is achieved on gel filtration and reverse phase columns. Iron is observed in

metal analysis of the most purified NifB fraction and the fraction has the brown color characteristic of Fe-S proteins (Shah, unpublished results). The protein has a requirement for or is greatly stimulated by lipid, but this requirement appears not to be specific to a unique lipid, as commercial lecithin preparations will stimulate the *in vitro* FeMo-co synthesis 8-10 fold when purified NifB is used in the assay.

The Discovery of Homocitrate as a Component of FeMo-co. By far the most significant result to come from our investigation of the biosynthesis of FeMo-co has been the unanticipated finding that FeMo-co contains the unusual organic acid, homocitrate (14, 33). While attempting to purify the NifNE protein, Hoover found that all FeMo-co synthesis activity was lost on a gel filtration column. The activity could be regained when all fractions from the column were recombined. The unknown factor was determined to be low-molecular weight and stable to heat, oxygen and a range of pH. The factor was produced only under *nif*-derepressing conditions by cells possessing a functional *nifV* gene, thus the original name V-factor (34). V-factor was produced by all nitrogen-fixing cells tested and a test of the cell medium revealed that the predominant amount of V-factor was present in the extracellular medium rather than inside the cell. This suggested to us initially that V-factor might function as a molybdenum siderophore that accumulated molybdenum for the synthesis of FeMo-co. This result seemed at odds with the results of McLean, Hawkes and Smith (35, 36).

Large amounts of V-factor were purified and the compound was identified as *R*-homocitrate ([*R*]2-hydroxy-1,2,4-butanetricarboxylic acid) by NMR and high resolution mass spectroscopy (Figure 1) (14). The *R* configuration of the natural product was established by polarimetry and comparison of the values obtained with literature values for the synthetic *S* isomer of the compound.

Tritiated homocitrate was prepared and the incorporation of the labelled compound into FeMo-co was observed *in vitro*. The labelled compound was incorporated into the dinitrogenase in the complete reaction mixture, while the control reaction mixture lacking NifB showed no label incorporation. Unlabelled, purified dinitrogenase protein was then added to the labelled dinitrogenase mixture, the dinitrogenase was repurified, and FeMo-co was extracted from the repurified protein. The fraction was then chromatographed on a Sephadex G-100 column and the ability to activate apo-dinitrogenase co-chromatographed with the ³H label, confirming that homocitrate or a portion of the molecule had been incorporated into FeMo-co (33).

From the known specific radioactivity of the homocitrate in the reaction mixture, a ratio of one homocitrate per molybdenum atom was calculated. A large amount of crystallized dinitrogenase protein was then extracted and the organic acid was purified from the extract. The identity of the organic acid as homocitrate was established by NMR (33). Since a high yield of the ³H label that was incorporated into dinitrogenase in the previous experiment could be recovered in the FeMo-co fraction, the homocitrate that was isolated from crystallized dinitrogenase protein must have been present in FeMo-co in the enzyme. The composition of FeMo-co is thus MoFe₇S₈Homocitrate. Attempts to remove homocitrate, while retaining the activity of the cofactor, have been unsuccessful (Shah, Madden, Imperial, unpublished results). It was thought that the molybdenum-containing moiety obtained by extracting FeMo-co solution with methylethylketone (MEK) might be the metal component of the cofactor without homocitrate, but attempts to add the MEK extract to homocitrate failed to reconstitute FeMo-co. Our current concept of FeMo-co is that the presence of homocitrate or a suitable analog is essential for FeMo-co activity. Attempts to substitute organic acids for homocitrate after isolation of FeMo-co have failed in our hands.

Substitution of Other Organic Acids in the *In Vitro* FeMo-co Synthesis Assay. The observation that homocitrate is required for FeMo-co synthesis and is a component of the finished product led to a structure/function investigation of the organic acids

that might serve as analogs of homocitrate. First and foremost, an effort was made to determine if the substitution of another organic acid might provide an explanation for the properties of the dinitrogenase isolated from *NifV*⁻ strains of *K. pneumoniae*. Studies by the Sussex group had established that the *nifV* gene was required for production of fully functional dinitrogenase and identified FeMo-co as the defective component of nitrogenase isolated from a *nifV* strain (22, 37). The *NifV*⁻ nitrogenase showed nearly wild-type levels of proton reduction and acetylene reduction but very poor rates of N₂ reduction. Furthermore, the proton reduction by the *NifV*⁻ dinitrogenase protein was inhibited by CO, in contrast to the wild-type enzyme. Use of citrate in the in vitro FeMo-co synthesis assay resulted in production of a dinitrogenase that mimicked the dinitrogenase isolated from *nifV* strains (38). The *nifV* gene is thought to encode homocitrate synthase, although this has not been demonstrated biochemically.

Liang et al. purified the organic acid from isolated *NifV*⁻ dinitrogenase protein from *K. pneumoniae* and identified it as citrate (39). Because citrate was obtained in a relatively low stoichiometric yield, it cannot be concluded that citrate is the only organic acid that substitutes for homocitrate in *nifV* mutants. It is likely that a mixture of organic acids might be obtained and that the composition of the mixture would reflect the relative concentrations of the various acids in the cell and the effectiveness of each in the biosynthesis. It is of interest that *nifV* strains of *A. vinelandii* are less leaky than *nifV* *K. pneumoniae* strains in our hands (40, 41). One explanation for this might be that *nifV* *A. vinelandii* mutants use a different organic acid in place of homocitrate. One might also expect that the predominant organic acid might vary depending on the growth medium employed and the conditions of growth.

Table I presents the accumulated information regarding substitution of organic acids for homocitrate in the in vitro FeMo-co synthesis assay; structures of representative organic acids are shown in Figure 2. Because the data presented here are taken from a number of experiments, values are presented as a percent of the activity observed with homocitrate in the assay. A number of conclusions can be drawn from the accumulated data:

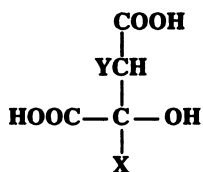
- A hydroxyl group (or in a few cases, a keto group) is required for activity. 1,2,4 tricarboxybutane and its six-carbon analog, tricarallylate, do not replace homocitrate.
- A minimum of two carboxy groups is required for activity.
- The isoacids constitute a group in which proton reduction is not inhibited by CO; proton reduction rate by dinitrogenases containing the isoacids is nearly 100% of homocitrate nitrogenase, but other substrate reductions are greatly reduced.
- The *R* isomers of organic acids are greatly preferred to the *S* acids; the properties of dinitrogenases reconstituted with aberrant FeMo-cofactors containing *R* or *S* forms differ from each other.
- The minimum organic acid that will support synthesis of a functional entity is malate, with *D*-malate the preferred configuration.
- The organic acid component of FeMo-co has a dramatic effect on the substrate specificity and inhibitor susceptibility of the resulting dinitrogenase enzyme.

The accumulated results have been incorporated into a model for the minimum organic moiety required for in vitro FeMo-co synthesis (Figure 3) (42). The primary exceptions to this model are the keto acids, α -ketoglutarate and oxaloacetate, neither of which have hydroxy groups. In neither of these cases has the organic acid been reisolated after incorporation into FeMo-co, so it cannot definitively be concluded that the organic acid has not been chemically changed during the synthesis of FeMo-co. In the case of α -ketoglutarate, it is known that α -hydroxyglutarate is ineffective in the

Table I. Summary of Activities of Dinitrogenase-Containing FeMo-cos with Various Organic Acids

organic acid	concn (mM)	N ₂ reduction activity	C ₂ H ₂ reduction activity	proton reduction activity	
				(-)CO	(+)CO
none	0	1.2	3.3	7	7.1
homocitrate	0.08	100	100	100	100
tricarballylate	16	ND	6.9	6.6	6.6
1,2,4-butanetri-carboxylate	16	1.6	6.7	4.9	5.5
citrate	8	7.3	47.3	49.5	18
chlorocitrate	8	5.8	37	39.3	17.7
1-OH citrate	8	ND	30.5	73.9	60
2-hydroxycitrate	0.8	4	20	58.7	56.4
(<i>R</i>)-citramalate	2	7.3	41.9	52.7	15.6
(<i>S</i>)-citramalate	1.6	2.2	9	11.6	10.6
cis-aconitate	8	7.6	52.2	28.1	9.9
trans-aconitate	16	2.1	14.1	14.1	8.5
3-fluoro-2-oxoglutarate	0.8	ND	13.6	26.3	31.9
<i>D</i> -malate	8	3.8	15.9	30.4	34.9
α -ketoglutarate	1.6	3.4	11.3	32.1	31.5
3-oxoglutarate	1.6	2.3	13.1	24.2	19.5
isocitrate	1.6	3	15.9	71.3	78.2
threo-isocitrate	8	ND	8.9	28.9	13
homoisocitrate	0.3	1.6	5.9	77.7	83.3
<i>L</i> -malate	8	2.3	8.2	28.3	27.9
<i>D</i> -saccharate	8	2.2	8.2	23.3	31.7
oxaloacetate	16	3	12	13.9	12.3
<i>D</i> -2-hydroxyglutarate	16	1.5	7.7	11.1	11.4
3-hydroxy-3-methyl glutarate	16	ND	7.1	8.8	8.7
2-(hydroxymethyl)-butyrate	1.6	ND	4.4	6.4	6.3
glutarate	16	ND	5.7	6.6	5.9
<i>L</i> -2-hydroxyglutarate	16	ND	4.9	7.3	5.9
2-oxocaproate	16	ND	2	4.9	5.5
<i>L</i> -glutamate	16	1.8	6.2	4.9	5.5
erythro-fluorohomocitrate	0.16	27.9	59.3	75	75
threo-fluorohomocitrate	0.16	2.9	51.9	60.7	24.9
fluorohomocitrate (racemic)	0.16	ND	ND	73.9	53.3
(<i>R</i>)-citroylformate	0.16	45.6	62.9	71.4	71.4
(<i>S</i>)-citroylformate	0.16	4.4	10	21.4	9.9
(<i>R,S</i>)-citroylformate	0.16	50	62.9	67.9	67.9
3-hydroxyglutamate	8	2.9	25.2	42.9	42.9
3-carboxyglutamate	8	ND	2	14.3	14.3

(assays performed as described by Madden et al., 44); values are all % of homocitrate.



(R)-isomer

X = H (malate); CH₂COOH (citrate)

CH₂CH₂COOH (homocitrate)

Y = H (homocitrate); OH (isoacids)

Figure 3. Model for structural requirements for organic acid component of FeMo-co.

FeMo-co synthesis assay; thus it seems unlikely that this ketoacid is reduced to its alcohol during the assay.

Because many dinitrogenases containing aberrant FeMo-cofactors exhibit proton-reduction rates nearly as high as the homocitrate enzyme, the effects of the substituted organic acids in FeMo-co on dinitrogenase activity cannot be readily explained as the overall slowing of electron flux through the enzyme. For example, the isocitrate dinitrogenase reduces protons at 75-85% the rate of the homocitrate enzyme, but reduces acetylene at only 16% and N₂ at only 2.9% the homocitrate enzyme rate.

The *R* and *S* isomers of several organic acids were available and have been incorporated into FeMo-co during synthesis (40, 43). For each pair of isomers, both *R* and *S* forms allow enzyme function, but with marked differences. In the case of citroylformate, the *R* analog yields a dinitrogenase with nearly the rate of proton reduction of the homocitrate enzyme and the proton reduction is not inhibited by CO. *S*-citraoylformate yields an enzyme with much lower proton-reduction activity, and that activity is significantly inhibited by CO. The FeMo-co synthesis assay has a strong preference for the *R* isomers of the organic acids and, whenever a mixture of *R* and *S* forms are supplied, the properties of the *R* form predominate in the reconstituted enzyme. A number of models that have been presented for FeMo-co are symmetric, but the binding of the chiral homocitrate must impose asymmetry on the molecule.

The differential effectiveness of organic acids extends to compounds with two chiral centers. Both the *erythro* and *threo* forms of 1-fluoro-homocitrate can be incorporated into FeMo-co, but the resulting enzymes show marked differences in activities (40). Of all analogs tested, the *erythro* form of 1-F-homocitrate is second only to homocitrate and citroylformate in reconstituting an enzyme capable of N₂ reduction, while the *threo* form is essentially inert to N₂. The two forms differ in the sensitivity of proton reduction to CO, with the *erythro* form being insensitive while the *threo* form is strongly inhibited.

The substrate specificity and inhibitor susceptibility of dinitrogenase is dramatically affected by the chain length, stereochemistry and position of the hydroxyl group of the organic acid present in FeMo-co. It is difficult to rationalize these effects if the organic acid is not positioned very near to the reaction site of the enzyme.

The ability of so many organic acids to be incorporated into FeMo-co in the *in vitro* systems raises the question of how the *in vivo* system ensures that homocitrate is specifically incorporated. While the answer no doubt involves the substrate specificity of proteins involved in FeMo-co biosynthesis, it may also reflect the concentration of each organic acid required for optimal activity of the FeMo-co synthesis assay.

Homocitrate is saturating at 80 μM while most other acids must be present at 10-100 fold higher concentrations for optimal FeMo-co synthesis (42, 44). Hoover et al. observed that 0.2 mM homocitrate accumulated in the medium of *nif*-derepressed cells (34), and it appears that the cell makes so much homocitrate that other organic acids are precluded from being incorporated.

Binding of ³H-homocitrate to Proteins of the FeMo-co Synthesis Assay Mixture.

An approach to identifying intermediates in the FeMo-co synthesis pathway is to follow the incorporation of ³H-homocitrate into intermediates. Table II shows preliminary data on the requirements for association of homocitrate with a protein fraction, and it appears that all components of the mixture are necessary. Homocitrate must be involved in an early step of molybdenum incorporation into FeMo-co, as no ⁹⁹Mo accumulates in any fraction in the absence of organic acid (see below and Figure 4).

Spectroscopic Properties of Dinitrogenase Proteins Containing Aberrant FeMo-cofactors. The spectroscopic similarity of the NifV⁻ dinitrogenase to the wild-type enzyme had been established by Hoffman and coworkers (45). We have looked at

Table II. Requirements for the Incorporation of ^3H -Homocitrate in Intermediates of FeMo-co Synthesis

SYSTEM	Extracts/ Gene Products	^3H -HC in Protein Fraction (DPM)	% DPM of Complete System	Relative C_2H_2 Reduction
Complete	UW45;UN1217	27,000	100	100
minus NifB	UW45	3,800	14	0.8
minus NifNE	DJ35;UN1217	1,400	5	0.5
minus Apol	CA12+ NifH	12,300	46	0.6
minus Component II	UW97	3,800	14	0.6
minus Mo	UW45 (W) or UW97 (W)	800	3	0.5
oxidized complete*	UW45;UN1217	14,200	53	N.D.

Complete system contained: 2 ml of desalted UW45 extract (40 mg protein); 0.5 ml partially purified NifB from *K. pneumoniae* strain UN1217; an ATP-regenerating mixture; 1mM (final concentration) sodium dithionite, 10 mM sodium molybdate and 1×10^7 dpm of ^3H -homocitrate (uniformly labelled, 11 mCi/mMole). The reaction mixture was incubated at 30°C for 45 min after which the mixture was loaded onto a G-50 Sephadex column.

*Complete system was incubated for 45 minutes and then exposed to air for 1 hour.

the EPR signals of dinitrogenases containing *in vitro*-synthesized FeMo-cofactors with homocitrate, 1-F-homocitrate and malate to see if any differences could be observed. The spectra in the region of $g = 3.65$ are shown in Figure 1. Although some small shifts in the signals may be present, no dramatic differences can be identified in these spectra.

Inhibitors of FeMo-co Synthesis. A number of organic acids have been tested as inhibitors of FeMo-co synthesis *in vitro*. In general, organic acids that serve as substrates for FeMo-co synthesis also serve to inhibit the incorporation of homocitrate into FeMo-co. It is reasonable to suggest that organic acids inhibit at the step where they are first incorporated, but this has not been demonstrated. Organic acids that fail to allow FeMo-co synthesis also fail to inhibit process; for example, tricarballoylate does not inhibit synthesis. A narrower range of organic acids has been tested for inhibition of synthesis than has been tested for synthesis of FeMo-co, but the observation to date is that the organic acids inhibit the incorporation of homocitrate at much lower concentrations than required for their optimal incorporation into FeMo-co (38).

Isocitrate at 800 μM , for example, inhibits the incorporation of homocitrate by 53%, whereas its optimal concentration for incorporation is approximately 8 mM. The inhibition assay depends on the fact that FeMo-co synthesized with homocitrate is capable of effective acetylene reduction, while the isocitrate form gives very poor acetylene reduction. It is of considerable interest that ^{99}Mo appears to accumulate in a protein-bound form when homocitrate analogs are used in the *in vitro* FeMo-co synthesis assay (Figure 3). Apparently, one or more of the enzymes and binding proteins involved are able to use the analog FeMo-co precursors much less effectively. Homocitrate itself does not inhibit either the synthesis or insertion of FeMo-co (R. Allen and Shah, unpublished).

The molybdate analogs tungstate, vanadate and sulfate have been tested as inhibitors of *in vitro* FeMo-co synthesis (19). While sulfate shows no inhibition at any concentration tested, tungstate and vanadate show 67% and 32% inhibition, respectively, of FeMo-co synthesis when present at 100-fold excess of the 10 μM molybdate in the assay. No tungstate- or vanadate-dependent activity was observed in the absence of molybdate, indicating that the *in vitro* FeMo-co synthesis system discriminates among the compounds as the *in vivo* system does. Because *nifB* and *nifV* are common to the other nitrogenase systems (3, 7), it seems that the discrimination is performed by the *nifNE*, *nifH* gene products or an unknown component of the system. Given the *in vitro* nature of these experiments, the uptake of molybdate and its analogs can be eliminated as the point of discrimination. Because apo-dinitrogenase has been shown to accept the iron-vanadium-cofactor of *A. chroococcum* (4) and the iron-only cofactor of *R. rubrum* (Davis and Ludden, unpublished results), it seems unlikely that the discrimination is at the level of cofactor insertion.

These experiments with tungstate and vanadate were performed before it was realized that homocitrate was a component of the *in vitro* FeMo-co synthesis system. It will be interesting to return to this question and ask if the inhibition of synthesis by tungstate increases if limiting amounts of homocitrate are present. Molybdate, tungstate and vanadate are all known to form complexes with organic acids. However, it is unlikely that 1 mM homocitrate was present in the crude system and thus a model in which the molybdate:homocitrate complex is the real substrate for the first molybdenum-dependent step in synthesis is not attractive.

Tetrathiomolybdate has been shown to inhibit FeMo-co insertion into apo-dinitrogenase and this compound has been shown to be an even more potent inhibitor of FeMo-co synthesis (19). In the presence of excess apo-dinitrogenase, 25 μM tetrathiomolybdate inhibited FeMo-co synthesis by more than 80%. Chloramphenicol, which had been suggested as a possible inhibitor of molybdenum uptake or processing, was found to be ineffective at inhibition of *in vitro* FeMo-co synthesis (19).

A low molecular weight inhibitor of FeMo-co synthesis has been isolated from *K. pneumoniae* (46). The inhibitor is present in both *nif*-repressed as well as *nif*-derepressed cultures and thus is thought to be a normal metabolite of the cell. The compound inhibits NifB in the *in vitro* synthesis of FeMo-co and exogenously-added compound inhibits the accumulation of active nitrogenase *in vivo*, although the NifB specificity of the inhibitor could not be demonstrated *in vivo*. The inhibitory factor copurified with trehalose, but commercial trehalose did not inhibit FeMo-co synthesis and trehalase did not destroy the inhibition by the purified fraction (Downs and Ludden, unpublished results).

In Vivo and In Vitro Incorporation of ^{99}Mo into FeMo-co and Its Precursors.

In spite of its γ -ray emission and short half-life of 60 hr, ^{99}Mo is a useful tool in the study of molybdenum metabolism. Elliot and Mortenson (47, 48) used ^{99}Mo to follow the mechanism and regulation of the uptake of molybdenum in *Clostridium pasteurianum*. They concluded that MoO_4^{2-} uptake is energy-dependent and repressed by fixed sources of nitrogen. Ugalde et al. (25) used ^{99}Mo to follow the accumulation of molybdenum in *nifD* mutants of *K. pneumoniae*. They observed that *K. pneumoniae* did not accumulate molybdenum under *nif*-repressing conditions; this in contrast to *A. vinelandii* which accumulates molybdenum under all conditions in a protein that has been termed the molybdenum storage protein. In mutants that were unable to synthesize the dinitrogenase protein, Ugalde et al. (25) observed the accumulation of ^{99}Mo in the protein fraction in *nif*-derepressed cells. Imperial et al. (38, 49) demonstrated that the protein-bound form of molybdenum that accumulated in *nifKD* mutants of *K. pneumoniae* was capable of activating apo-dinitrogenase and thus satisfied the functional definition of FeMo-co. Hoover et al. (38) showed that ^{99}Mo accumulated on a 65 kD protein in the *in vitro* FeMo-co synthesis assay using *A. vinelandii* strain CA12 (a *nifHDK* deletion) as the source of NifNE and using *K. pneumoniae* strain UN1100 as the source of NifH, apo-dinitrogenase and NifB. Figure 4 shows the accumulation of ^{99}Mo in the *A. vinelandii* Mo-storage protein, in dinitrogenase protein, and in a faster-migrating protein in the *in vitro* FeMo-co synthesis assay. Our working hypothesis is that the accumulation of ^{99}Mo in the faster-migrating band in lane 7 is analogous to the accumulation on the 65 kD protein *in vivo*. The lack of accumulation of ^{99}Mo in any protein band when no organic acid is added to the mixture suggests that homocitrate is involved at an early step in synthesis. Perhaps the most interesting result shown in Figure 4 is that ^{99}Mo accumulates in a band other than dinitrogenase when citrate (lane 7) or α -ketoglutarate (lane 6) is used in place of homocitrate. The use of ^{99}Mo in conjunction with homocitrate analogs will allow accumulation and detection of a number of precursors of FeMo-co.

Synthesis of Homocitrate. A reasonable working hypothesis is that the *nifV* gene product is homocitrate synthase, although the gene product has not been purified and the synthetic reaction has not been performed *in vitro*. The sequence of the *nifV* gene from several organisms is known and there are sequence similarities between it and acetyl-CoA-binding synthases (7, 29). The *nifV* gene from *C. pasteurianum* appears to be split into two segments that are separately transcribed (50).

It would seem most reasonable that the substrates for the synthesis of homocitrate would be acetyl-CoA and α -ketoglutarate by analogy to the citrate synthase reaction. At this point in time, however, no one has reported such an activity in nitrogen-fixing organisms. Homocitrate is found as an intermediate in the lysine biosynthetic pathway of some yeasts and fungi, and there the reaction involves acetyl-CoA and α -ketoglutarate as substrates. While the NifV protein has received little attention and its

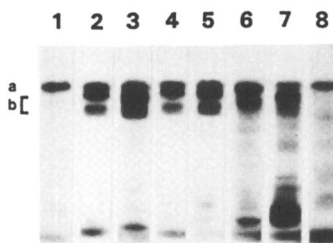


Figure 4. Labelling of proteins by ^{99}Mo during FeMo-co synthesis in vitro. Autoradiography of in vitro FeMo-co synthesis reactions separated by anaerobic native gel electrophoresis. Reactions were carried out with $^{99}\text{MoO}_4^{2-}$ and different analogues of homocitrate. (Lane 1) No homocitrate analogue; (lane 2) homocitrate (0.03 mM); (lane 3) homocitrate (0.3 mM); (lane 4) homoisocitrate (0.15 mM); (lane 5) homoisocitrate (0.75 mM); (lane 6) 2-oxoglutarate (0.75 mM); (lane 7) citrate (7.5 mM); (lane 8) tricarballylate (7.5 mM). (a) Molybdenum-storage protein; (b) dinitrogenase. (Reproduced from reference 38. Copyright 1988 ACS.)

synthetic role has been assumed to be homocitrate synthase, the potential use of a homocitrate synthetic activity to prepare isotopically-labelled homocitrate and its analogs makes the pursuit worthwhile. Furthermore, as the case of NifH has taught us, gene products may have more than a single role.

The accumulation of homocitrate in the medium of nitrogen-fixing organisms suggests an extracellular role for the compound. Perhaps homocitrate is involved in accumulation of molybdenum for FeMo-co synthesis as well as serving as a component of the final cofactor. If so, a role for the *nifQ* product in recognizing homocitrate:molybdate complex might be proposed. Homocitrate has been shown to cure the NifV⁻ phenotype in cultures of both *K. pneumoniae* and *A. vinelandii* (40, 41). [It is important to note that commercial preparations of homocitrate are supplied in the lactone form and must be converted to the open-chain form before use in the biosynthesis of FeMo-co.]

Interestingly, Ramos and Robson (51) observed that lesions in citrate synthase resulted in decreased nitrogenase activity in *Azotobacter chroococcum*, but the relationship of this observation to homocitrate synthesis or FeMo-co assembly is unknown.

The Role of NifH in FeMo-co Synthesis. The role of NifH in FeMo-co synthesis is unknown and it may in fact play several roles. That NifH capable of ATP-dependent electron transfer to dinitrogenase is not required for FeMo-co synthesis is demonstrated by several lines of evidence: i) Filler et al. (18) observed that the truncated NifH encoded by pRD191 was sufficient for in vivo FeMo-co synthesis, although extracts of strains with a single *nifH* gene encoded by pRD191 had no detectable dinitrogenase reductase activity; ii) the *nifH* product from *K. pneumoniae* strain UN1041, which has 100^{arg} replaced by his, supports in vitro FeMo-co synthesis even though the purified protein has no dinitrogenase activity under the ionic strength conditions of the FeMo-co synthesis assay (although it does show 1-3% of the wild-type activity under very low ionic strength conditions) (24); iii) ADP-ribosylated dinitrogenase reductase is able to support in vitro FeMo-co synthesis, but not substrate reduction (24).

In an effort to determine if NifH might serve as donor of part of the iron or sulfur of FeMo-co, ³⁵S-labelled NifH was prepared and used in the in vitro FeMo-co synthesis assay. Although the NifH was highly labelled and at least some of the ³⁵S label was in the FeS center (as judged by the release of ³⁵S by acid), no label was transferred to dinitrogenase (Imperial and Shah, unpublished results). These negative results suggest that NifH does not serve to donate a part of the Fe and S to FeMo-co, but this conclusion can be definitively drawn only when it is possible to donate labelled Fe and S from some source in the assay and demonstrate that it does not come from NifH.

Robinson et al. (52) have proposed a role for NifH in the insertion of FeMo-co into apo-dinitrogenase. This hypothesis is based on the fact that, in their hands, the apo-dinitrogenase that accumulates in *nifH* mutants can be fully activated in vitro in a NifH-dependent process, while the apo-dinitrogenase that accumulates in *nifB* or *N* mutants can be only partially activated. These results are in contrast to those of Paustian et al. (53) who have purified apo-dinitrogenase from *A. vinelandii* strain UW45 (a *nifB* mutant) to homogeneity and demonstrated that the enzyme can be fully activated to a high specific activity of >2200 nmole acetylene reduced per min per mg of dinitrogenase. The biochemical basis for the different observations by these groups will have to be resolved before a complete understanding of the role of NifH in FeMo-co synthesis is achieved.

The Role of Nucleotides and Divalent Metals in FeMo-co Synthesis. FeMo-co synthesis requires MgATP as does substrate reduction by the nitrogenase enzyme complex (19). Table III shows the abilities of various nucleotides and divalent metals to

Table III. Comparison of the Effects of Nucleotides and Divalent Metals on FeMo-co Biosynthesis and Nitrogenase Activity

Nucleotide used in in vitro FeMo-co synthesis	FeMo-co synthesis activity %	Nitrogenase activity %
ATP with regenerating system	100	100
no nucleotide added	7.59	
ATP	38.12	
ADP	5.96	0
GTP	4.20	<50
CTP	5.96	
UTP	5.49	<50
β , γ methylene ATP (nonhydrolysable)	6.37	
ATP/ β , γ methylene ATP = 4/1	75.5	
ATP/ β , γ methylene ATP = 2/1	71.8	
ATP/ β , γ methylene ATP = 1/1	53.9	
ATP/ADP = 9/1	26	33
ATP/ADP = 1/1	20.5	6
ATP/ADP = 1/9	20	
Metal ion used in in vitro FeMo-co synthesis		
Mg	100	100
Mn	93	43
Ni	20	8
Co	5	66
Ca	98	no activity
Fe	77	46
Zn	5	no activity
no metal ion	36	

Final concentration of ATP (with regenerating system) in assay = 1.6 mM.

Final concentration of all other analogs tested in assay = 8.3 mM.

Concentration of M^{2+} ions in synthesis assay = 0.0028 M.

The positive control used contained the following:

100 μ l 0.025 M TrisCl pH 7.5 + 20 μ l 5 mM homocitrate, 10 μ l 1 mM MoO_4^{2-} , 200 μ l Mg ATP, 1 mM dithionite, 200 μ l UW45 extract, 50 μ l NifB

support in vitro FeMo-co synthesis compared to the published data for the ability of the nucleotides to function in substrate reduction by nitrogenase (54-56). In substrate reduction by nitrogenase, dinitrogenase reductase (*nifH*) has been established as the nucleotide-binding protein and it is known that 2 MgATP are hydrolyzed for each electron transferred between dinitrogenase reductase and dinitrogenase (57-61). In Table III, there is data that is inconsistent with the dinitrogenase ATP-binding sites serving as the ATP-binding site involved in FeMo-co synthesis. It is interesting that Georgiadis and Rees isolated a heavy metal derivative of dinitrogenase reductase in which MoO_4^{2-} occupies a site near the putative nucleotide-binding site of the protein (62; Rees et al., Chapter 11, this volume). It has been assumed that the MoO_4^{2-} has bound in place of phosphate in the nucleotide-binding site.

Nucleotide-binding sites have been demonstrated on the dinitrogenase reductase and dinitrogenase proteins and have been inferred for the NifNE protein, based on binding to the nucleotide-mimicking affinity matrix Reactive Red 120 (27); there is no information regarding nucleotide-binding capability of NifB. The nucleotide-binding sites on dinitrogenase are not necessarily involved in FeMo-co synthesis, as FeMo-co is synthesized in their absence. Robinson et al. (52) have presented data in support of the model in which it is the dinitrogenase reductase-MgATP complex that is involved in FeMo-co insertion, but it is also clear that MgATP is not absolutely required for FeMo-co insertion (53). At this point, neither the specific proteins to which MgATP binds nor the role(s) of MgATP in FeMo-co synthesis can be defined unambiguously.

Future Studies on FeMo-co Synthesis. Progress on the biosynthesis of FeMo-co has required isolation, purification and characterization of the protein catalysts for the synthetic pathway. Progress has also been impaired by the lack of precise knowledge of the structure of the product of the pathway, FeMo-co. Studies on the biosynthesis have greatly aided the investigation of the structure by providing the knowledge that homocitrate is a component of the compound. Now studies on the biosynthesis will benefit from a much clearer picture of the product being built. The protein-bound nature of any intermediate may necessitate further protein X-ray crystallography to define the intermediates. The questions to be addressed in the immediate future include:

- Which gene product(s) serve as iron and sulfur donors to FeMo-co; what part of the molecule comes from each donor?
- What is the order of steps in the pathway; is it a linear or branched pathway?
- Which *nif*-specific protein first binds molybdenum; is it MoO_4^{2-} that is bound or is it a homocitrate:molybdate complex?
- Given the similarities of FeMo-co and the cofactors of the alternate systems, how is metal specificity imparted to the biosynthetic system?
- What is the role of nucleotides in FeMo-co synthesis? Is nucleotide hydrolyzed during the synthesis?
- What is the source of reductant for FeMo-co synthesis?
- What are the substrates and requirements for homocitrate synthesis?
- Are any non-*nif*, housekeeping enzymes of FeS-center metabolism involved in FeMo-co synthesis?

Acknowledgments. The authors wish to thank W. J. Brill, L. F. Dahl and R. H. Burris for their encouragement and advice during the course of studies described in this chapter. The assistance of G. Stirr in preparation of this chapter is gratefully acknowledged. Work from the authors' laboratories described here has been supported by the College of Agricultural and Life Sciences at the University of Wisconsin-Madison, the NIH, USDA and NSF.

Literature Cited

1. Bortels, H. *Arch. Mikrobiol.* **1930**, *2*, 333-342.
2. Bishop, P.E.; Jarlenski, D.M.L.; Hetherington, D.R. *Proc. Natl. Acad. Sci. USA.* **1980**, *77*, 7342-7346.
3. Bishop, P.E.; Joerger, R.D. *Annu. Rev. Plant Physiol. Plant Mol. Biol.* **1990**, *41*, 109-125.
4. Eady, R.R.; Richardson, T.H.; Miller, R.W.; Hawkins, M.; Lowe, D.J. *Biochem. J.* **1988**, *256*, 189-196.
5. Eady, R.R. *Polyhedron* **1989**, *8*, 1695-1700.
6. Joerger, R.D.; Wolfinger, E.D.; Bishop, P.E. *J. Bacteriol.* **1991**, *173*, 4440-4446.
7. Kennedy, C.; Dean, D. *Mol. Gen. Genet.* **1992**, *231*, 494-498.
8. Ketchum, P.A.; Cambier, H.Y.; Frazier, W.A.; Madansky, C.H.; Nason, A. *Proc. Natl. Acad. Sci. USA* **1970**, *66*, 1016-1023.
9. Pienkos, P.T.; Shah, V.K.; Brill, W.J. *Proc. Natl. Acad. Sci. USA* **1977**, *74*, 5468-5471.
10. Shah, V.K.; Brill, W.J. *Proc. Natl. Acad. Sci. USA* **1977**, *74*, 3249-3253.
11. Johnson, J.L.; Hainlene, B.E.; Rajagopalan, K.V. *J. Biol. Chem.* **1987**, *255*, 1783-1786.
12. Wink, D.A.; McLean, P.A.; Hickman, A.B.; Orme-Johnson, W. H. *Biochemistry* **1989**, *28*, 9407-9412.
13. Nelson, M.J.; Lindahl, P.; Orme-Johnson, W.H. In *Advances in Inorganic Biochemistry*; Eichhorn, G.L.; Mazilli, L.G., Eds.; Elsevier: New York, 1982; pp. 1-40.
14. Hoover, T.R.; Robertson, A.D.; Cerny, R.L.; Hayes, R.N.; Imperial, J.; Shah, V.K.; Ludden, P.W. *Nature* **1987**, *329*, 855-857.
15. Smith, B.E.; Eady, R.R. *Eur. J. Biochem.* **1992**, *205*, 1-15.
16. Brill, W.J. *Microbiol. Rev.* **1980**, *44*, 449-467.
17. Roberts, G.P.; Brill, W.J.; *J. Bacteriol.* **1980**, *144*, 210-221.
18. Filler, W.A.; Kemp, R.M.; Ng, J.C.; Hawkes, T.R.; Dixon, R.A.; Smith, B.E. *Eur. J. Biochem.* **1986**, *160*, 371-377.
19. Shah, V.K.; Imperial, J.; Ugalde, R.A.; Ludden, P.W.; Brill, W.J. *Proc. Natl. Acad. Sci. USA* **1985**, *83*, 1636-1640.
20. Roberts, G.P.; MacNeil, T.; MacNeil, D.; Brill, W.J. *J. Bacteriol.* **1978**, *136*, 267-79.
21. Imperial, J.; Ugalde, R.A.; Shah, V.K.; Brill, W.J. *J. Bacteriol.* **1984**, *158*, 187-194.
22. Hawkes, T.R.; McLean, P.A.; Smith, B.E. *Biochem. J.* **1984**, *217*, 317-321.
23. Robinson, A.C.; Dean, D.R.; Burgess, B.K. *J. Biol. Chem.* **1987**, *262*, 17327-17332.
24. Shah, V.K.; Hoover, T.R.; Imperial, J.; Paustian, T.D.; Roberts, G.P.; Ludden, P.W. In *Nitrogen Fixation: Hundred Years After*; Bothe, H.; deBruijn, F.J.; Newton, W.E., Eds; Gustav Fischer: New York, 1988; pp. 115-120.
25. Ugalde, R.A.; Imperial, J.; Shah, V.K.; Brill, W.J. *J. Bacteriol.* **1984**, *159*, 888-893.
26. Joerger, R.D.; Bishop, P.E. *J. Bacteriol.* **1988**, *170*, 1475-1487.
27. Paustian, T.D.; Shah, V.K.; Roberts, G.P. *Proc. Natl. Acad. Sci. USA* **1989**, *86*, 6082-6086.
28. Roberts, G.P.; Brill, W.J. *Ann. Rev. Microbiol.* **1981**, *35*, 207-235.
29. Brige, K.E.; Newton, W.E.; Dean, D.R. *Gene* **1985**, *37*, 37-44.
30. Kent, H.M.; Ioannidis, I.; Gormal, C.; Smith, B.E.; Buck, M. *Biochem. J.* **1989**, *264*, 257-264.
31. Dean, D.R.; Brige, K.E.; May, H.D.; Newton, W.E. In *Nitrogen Fixation: Hundred Years After*; Bothe, H.; de Bruijn, F.J.; Newton, W.E., Eds.; Gustav Fischer: New York, 1988; pp. 107-113.

32. Huynh, B.H.; Henzl, M.T.; Christner, J.A.; Zimmerman, R.; Orme-Johnson, W.H.; Münck, E. *Biochim. Biophys. Acta*. **1980**, *623*, 124-138.
33. Hoover, T.R.; Imperial, J.; Ludden, P.W.; Shah, V.K. *Biochemistry* **1989**, *28*, 2768-2771.
34. Hoover, T.R.; Shah, V.K.; Roberts, G.P.; Ludden, P.W. *J. Bacteriol.* **1986**, *167*, 999-1003.
35. McLean, P.A.; Dixon, R.A. *Nature* **1981**, *292*, 655-656.
36. McLean, P.A.; Smith, B.E.; Dixon, R.A. *Biochem. J.* **1983**, *211*, 589-597.
37. True, A.E.; McLean, P.; Nelson, M.J.; Orme-Johnson, W.H.; Hoffman, B.M. *J. Am. Chem. Soc.* **1990**, *112*, 651-657.
38. Hoover, T.R.; Imperial, J.; Liang, J.; Ludden, P.W.; Shah, V.K. *Biochemistry* **1988**, *27*, 3647-3652.
39. Liang, J.; Madden, M.; Shah, V.K.; Burris, R.H. *Biochemistry* **1990**, *29*, 8577-8581.
40. Madden, M.S.; Paustian, T.D.; Ludden, P.W.; Shah, V.K. *J. Bacteriol.* **1991**, *173*, 5403-5405.
41. Hoover, T.R.; Imperial, J.; Ludden, P.W.; Shah, V.K. *J. Bacteriol.* **1988**, *170*, 1978-1979.
42. Imperial, J.; Hoover, T.R.; Madden, M.S.; Ludden, P.W.; Shah, V.K. *Biochemistry* **1989**, *28*, 7796-7799.
43. Madden, M.S.; Krezel, A.M.; Allen, R.M.; Ludden, P.W.; Shah, V.K. *Proc. Natl. Acad. Sci. USA* **1992**, *89*, 6487-6491.
44. Madden, M.S.; Kindon, N.D.; Ludden, P.W.; Shah, V.K. *Proc. Natl. Acad. Sci. USA* **1990**, *87*, 6517-6521.
45. True, A.E.; McLean, P.; Nelson, M.J.; Orme, J.W.; Hoffman, B.M. *J. Am. Chem. Soc.* **1990**, *112*, 651-657.
46. Downs, D.M.; Ludden, P.W.; Shah, V.K. *J. Bacteriol.* **1990**, *172*, 6084-6089.
47. Elliott, B.B.; Mortenson, L.E. *J. Bacteriol.* **1975**, *124*, 1295-1301.
48. Elliott, B.B.; Mortenson, L.E. *J. Bacteriol.* **1976**, *127*, 770-779.
49. Imperial, J.; Shah, V.K.; Ugalde, R.A.; Ludden, P.W.; Brill, W.J. *J. Bacteriol.* **1987**, *169*, 1784-1786.
50. Chen, J.-S.; Wang, S.-Z.; Johnson, J.L. In *Nitrogen Fixation: Achievements and Objectives*; Gresshof, P.M.; Roth, L.E.; Stacey, G.; Newton, W.E., Eds.; Chapman and Hall: New York, 1990; pp. 483-490.
51. Ramos, J.L.; Robson, R.L. *J. Bacteriol.* **1985**, *162*, 746-751.
52. Robinson, A.C.; Chun, T.W.; Li, J.-G.; Burgess, B.K., *J. Biol. Chem.* **1989**, *264*, 10088-10095.
53. Paustian, T.D.; Shah, V.K.; Roberts, G.P. *Biochemistry* **1990**, *29*, 3515-3522.
54. Burns, R.C. *Biochim. Biophys. Acta* **1969**, *171*, 253-259.
55. Lowery, R.G.; Ludden, P.W. *Biochemistry* **1989**, *28*, 4956-4961.
56. Weston, M.F.; Kotake, S.; Davis, L.C. *Arch. Biochem. Biophys.* **1983**, *225*, 809-817.
57. Ljones, T.; Burris, R.H. *Biochim. Biophys. Acta* **1972**, *275*, 93-101.
58. Tso, M.Y.W.; Burris, R.H. *Biochim. Biophys. Acta* **1973**, *309*, 263-270.
59. Upchurch, R.G.; Mortenson, L.E. *J. Bacteriol.* **1980**, *143*, 274-284.
60. Eady, R.R.; Lowe, D.J.; Thorneley, R.N.F. *FEBS Lett.* **1978**, *95*, 211-213.
61. Burns, R.C.; Bulen, W.A. *Biochim Biophys. Acta* **1965**, *105*, 437-445.
62. Georgiadis, M.M.; Komiyama, H.; Chakrabarti, P.; Woo, D.; Kornuc, J.J.; Rees, D.C. *Science* **1992**, *257*, 1653-1659.

Chapter 14

Role of the Iron–Molybdenum Cofactor Polypeptide Environment in *Azotobacter vinelandii* Molybdenum–Nitrogenase Catalysis

William E. Newton¹ and Dennis R. Dean²

¹Department of Biochemistry and Nutrition, Virginia Polytechnic Institute & State University, Blacksburg, VA 24061–0308

²Department of Anaerobic Microbiology, Virginia Polytechnic Institute & State University, Blacksburg, VA 24061–0305

Altered molybdenum-dependent nitrogenases have been constructed with single amino-acid substitutions within targeted regions of the MoFe protein α -subunit. Some of these altered non-N₂-fixing MoFe proteins, particularly with substitutions at α -glutaminy-191 and α -histidiny-195, exhibit concomitantly altered substrate specificity and a changed S=3/2 electron paramagnetic resonance (EPR) signal, confirming an intimate involvement of FeMo-cofactor with a substrate-binding site within the α -subunit. Some substitutions result in catalyzed acetylene reduction that yields both ethylene and ethane, which, although reminiscent of the vanadium-dependent nitrogenase, occurs by a different mechanism. Certain mutant strains having substitutions at either α -Gln-191 or α -His-195 exhibit H⁺-reduction ability that, unlike wild type, is sensitive to either CO or N₂ or both. These results, together with the recent MoFe-protein structural data, suggest that these residues might fine-tune the electronic properties of FeMo-cofactor and so impact its substrate-reduction capabilities. Also, consistent with the recent structural data, all substitutions at those residues that are now known to bind FeMo-cofactor directly, i.e., the Fe-ligating Cys-275 and the Mo-ligating His-442, produce mutant strains, which are Nif⁻ and EPR-silent.

Biological nitrogen fixation is catalyzed by nitrogenase, a two-component metalloprotein comprised of the Fe protein (a homodimer of ca. 63 kDa, encoded by *nifH*) and the MoFe protein (an $\alpha_2\beta_2$ tetramer of ca. 230 kDa, encoded by *nifDK*). The Fe protein is the obligate electron donor to the MoFe protein upon which is located the site of substrate reduction. During catalysis, electrons are delivered one-at-a-time from the Fe protein to the MoFe protein in a process involving the association-dissociation of the component proteins and hydrolysis of two MgATP for each electron transferred.

Major efforts in dissecting the biochemical features of nitrogenase have involved determining the composition and organization of the associated metal cores required for electron transfer and substrate reduction (see, for example, 1-4). These studies have revealed that there are three metal-cluster types contained within the two component proteins. These metalloclusters include: (i) a [4Fe-4S] center, which is symmetrically bridged between the two identical subunits of the Fe protein; (ii) two novel 8Fe clusters, equally distributed among the α - and β -subunits of the MoFe protein; and (iii) two FeMo-cofactors, which are entirely contained within the α -subunits of the MoFe protein. In this brief review, we summarize experiments which established that the FeMo-cofactor is located at the site of substrate binding and reduction and, in addition, describe on-going experiments designed to determine the contribution of the FeMo-cofactor polypeptide environment to substrate binding and reduction.

FeMo-cofactor is involved in Substrate Reduction

As isolated in its semi-reduced state, the MoFe protein exhibits a unique $S=3/2$ electron paramagnetic resonance (EPR) signal. By acid-base denaturation and subsequent extraction by a chaotropic solvent (*N*-methylformamide, NMF), the FeMo-cofactor can be isolated from its polypeptide matrix (5). The semi-reduced form of the extracted entity exhibits an $S=3/2$ EPR signal that resembles the protein-bound species in *g* value but has a considerably broader lineshape (6, see Figure 1). These results indicate that the FeMo-cofactor is responsible for the biologically unique EPR signal in the native protein and that the polypeptide environment of the FeMo-cofactor affects its spectroscopic features. Mutant strains, which fail to synthesize FeMo-cofactor (for example, *nifE*, *nifN* or *nifB* mutants), produce an "apo-MoFe protein" that has neither catalytic activity nor an $S=3/2$ EPR signal (5, 7-10). Extracts from these strains can be reconstituted to full catalytic activity and EPR competence by the addition of FeMo-cofactor extracted from wild type. Thus, the association of the FeMo-cofactor with both catalytic and spectroscopic features of the MoFe protein provided the first evidence that the FeMo-cofactor is located at or is part of the substrate-reduction site.

It is now known that, in addition to its metal-sulfur core, FeMo-cofactor contains homocitrate as an integral organic component (11). An altered FeMo-cofactor is produced in *NifV* mutant strains of *Klebsiella pneumoniae*, where citrate replaces homocitrate as the organic constituent (12). This replacement results in a phenotype of decreased N_2 -fixation capacity and CO-sensitive proton reduction (13,14). Catalytic features (15,16), dissimilar to the Mo-dependent nitrogenase, are also associated with the genetically distinct, but physically similar, vanadium-dependent nitrogenase, which is synthesized in certain *Azotobacter* species when starved for molybdenum but supplemented with vanadium (17,18). Such differences are likely to be accounted for by the substitution of V for Mo in a FeV-cofactor. Other than replacement of V for Mo, FeV-cofactor is likely to be identical to FeMo-cofactor in structure and composition (19). Taken together, all these features point to an essential role for FeMo-cofactor (and its analogues) in substrate reduction.

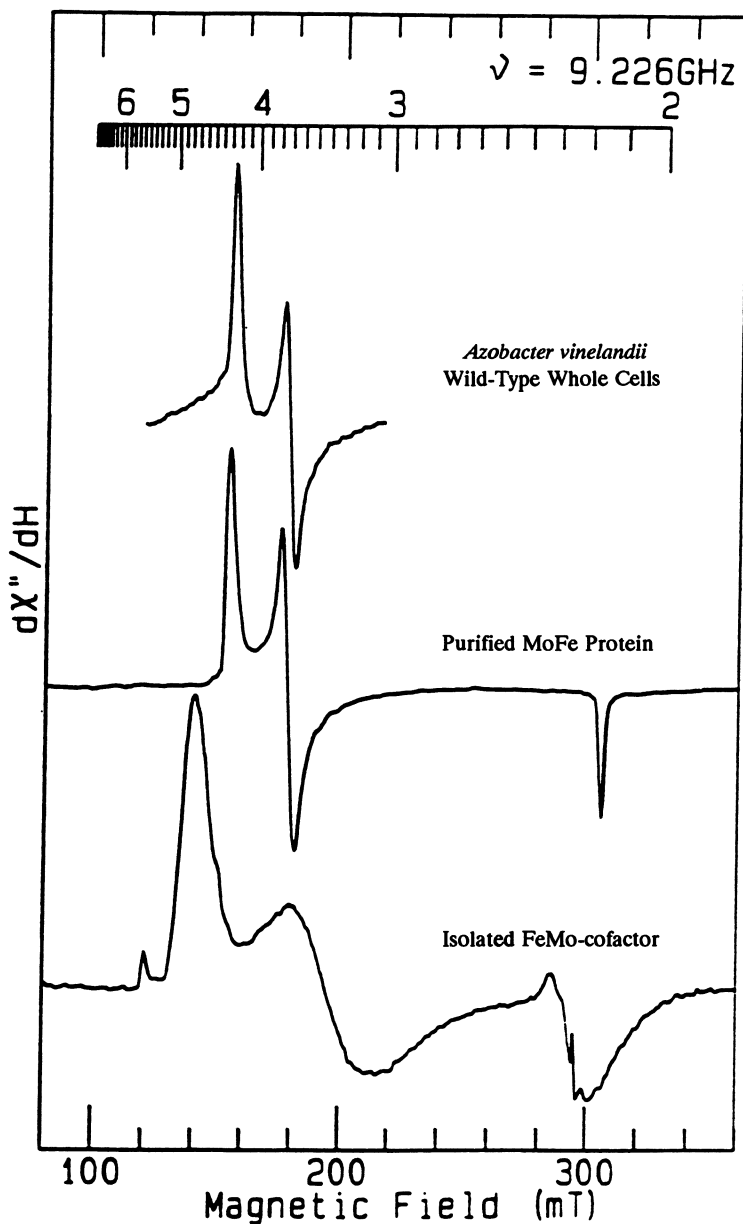


Figure 1. Electron paramagnetic resonance (EPR) spectra of the MoFe protein component of wild-type nitrogenase elicited from *Azotobacter vinelandii* whole cells (top), purified MoFe protein (middle) and isolated FeMo-cofactor in NMF (bottom).

Although FeMo-cofactor is clearly implicated in substrate reduction catalyzed by the MoFe protein, efforts to reduce substrates using the isolated FeMo-cofactor have been either unsuccessful or equivocal (2,3,20,21). Thus, the polypeptide environment of FeMo-cofactor must have one or more critical functions in effecting substrate binding and reduction. Such functions are likely to include the appropriate presentation of FeMo-cofactor to insure productive delivery of protons and reducing equivalents to the substrate-reduction site. Also, the different spectroscopic features of protein-bound *versus* isolated FeMo-cofactor clearly indicate a role for the polypeptide in electronic fine-tuning of the substrate-reduction site.

As an approach to examine the contribution of FeMo-cofactor's polypeptide environment to substrate reduction, two groups have initiated site-directed amino-acid substitution studies (22-26). The basic rationale of this approach has involved specific substitution of amino-acid residues targeted either as direct ligands to or as being located near the FeMo-cofactor. The approach has two goals. First, a description of the catalytic and spectroscopic consequences of such substitutions should provide information concerning the specific functions of individual amino acids located within the FeMo-cofactor environment. For example, such functions could include; (i) provision of proton- or electron-delivery systems, (ii) contributions to the electronic features of the substrate-reduction site, and (iii) proper orientation of FeMo-cofactor within the polypeptide matrix through coordination to particular amino-acid residues. Second, by alteration of the specific ligands which bind FeMo-cofactor to the MoFe protein, solvents more amenable than NMF to analytical techniques might be used for extraction of FeMo-cofactor from its polypeptide matrix.

Because the site-directed amino-acid substitution studies were initiated prior to the availability of structural information, several indirect approaches were used to target amino-acid residues for substitution and to guide choices for substituting amino acids. These approaches included; (i) consideration of the chemical properties of the solvents required for extrusion of FeMo-cofactor from its polypeptide environment (27), (ii) inter-specific comparison of the primary sequences of the MoFe-protein α - and β -subunits (27-33), (iii) comparison of the primary sequences of the MoFe-protein α - and β -subunits to each other (27-33), and (iv) comparison of the MoFe-protein primary sequences to the primary sequences of FeMo-cofactor biosynthetic gene products (in particular, the *nifE* and *nifN* gene products) (9). These considerations led to the conclusions that the FeMo-cofactor is contained entirely within the MoFe-protein α -subunit and that polypeptide domains, which include residues α -Gln-191 through α -His-195 and α -Cys-275, are likely to have dominant roles in providing the FeMo-cofactor polypeptide environment (Figure 2) (23,27,34,35). These predictions turned out to be correct as demonstrated by site-directed amino-acid substitution studies (22-28,35) and the recent elucidation of the MoFe-protein structure (36). However, it should be noted that sequence comparisons and site-directed amino-acid substitution studies fell short of predicting the *entire* FeMo-cofactor polypeptide environment. For example, the close approach of the β -subunit to FeMo-cofactor was not anticipated. Moreover, neither the direct coordination of α -subunit

His-442 to the Mo atom nor the proximity of other residues, such as α -Arg-96, α -Arg-359 and α -Phe-381, was predicted. Below, some features of many of the altered MoFe proteins, which have amino-acid substitutions within FeMo-cofactor domains, are described and considered in the context of the recent report of the MoFe-protein crystal structure (see Figure 3).

Cysteiny-275 of the α -Subunit is the Thiol Ligand to FeMo-cofactor

Shortly after the original extrusion protocol for releasing FeMo-cofactor from the MoFe protein was reported (5), it became clear that isolated FeMo-cofactor was reactive to a variety of chemical reagents, including thiols, EDTA, *o*-phenanthroline, α, α' -bipyridyl and CN^- (6,37-39). Using the interaction of phenylthiol with isolated FeMo-cofactor as an indicator of FeMo-cofactor's situation within the protein, it was found that this thiol binds in a 1:1 stoichiometry (37), which was interpreted as indicating that FeMo-cofactor is bound to its polypeptide matrix by only one cysteinyl residue (27). Using nuclear magnetic resonance (40) and x-ray absorption spectroscopy (41) on isolated FeMo-cofactor, the site of thiol binding was clearly shown to be on Fe and not at the unique Mo. The question then became: which one of the eight (three in the β -subunit and five in the α -subunit) strictly conserved cysteinyl residues was responsible for binding FeMo-cofactor? The most likely candidate was determined to be α -Cys-275 because: (i) it is surrounded by a concentration of conserved residues with amide functions, unmatched elsewhere in the primary sequence, which might be simulated by NMF; and (ii) α -subunit Cys residues 62, 88 and 154 and β -subunit Cys residues 70, 95 and 153 appeared more likely to be Fe-S cluster ligands (22,27).

This prediction was supported by the site-directed mutagenesis results. The initial substitutions at α -Cys-275, by either Ser (22) or Ala (25), result in strains with a *Nif* phenotype that are also unable to reduce acetylene or protons. Other strains that we have constructed since then, for example, with Asp, Glu, Gly, Thr and Val substitutions (Shen, J., Dean, D.R., and Newton, W. E., Virginia Tech, unpublished data), are also inactive in the usual nitrogenase activity assays. Evidence that these substitutions disrupt the FeMo-cofactor-binding domain comes from studies of a crude extract of the α -Cys-275-Ala strain, using EPR spectroscopy, "apo-MoFe protein" reconstitution and non-denaturing gel assays (25,26). The $S=3/2$ EPR spectrum exhibited by this strain is significantly shifted (*g* values of 4.5 and 3.5 versus the wild-type values of 4.3 and 3.7) and broadened and is reminiscent of that of isolated FeMo-cofactor (6,37). The FeMo-cofactor in this extract can also reconstitute the acetylene-reduction activity of the FeMo-cofactor-deficient "apo-MoFe protein" in an extract of a *nifB* strain directly on simply mixing extracts without any pre-acidification to release FeMo-cofactor as required for wild-type extracts (25). Further, non-denaturing gels show that the major form of the MoFe protein in the α -Cys-275-Ala extracts runs as a band that migrates more slowly than does the native MoFe protein in wild-type extracts (26), but similarly to the "apo-MoFe protein" in *nifB* strains (26,42). The interpretation of these data is that the FeMo-cofactor is loosely attached to the MoFe-protein matrix in this mutant. Therefore, the substituted residue, α -Cys-275, must be

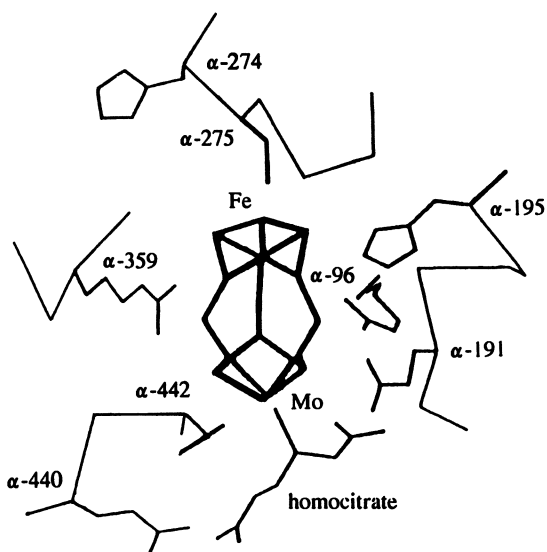


Figure 3. The model of the FeMo-cofactor structure and surrounding α -subunit environment, showing the interacting amino-acid residues that were substituted in this work. (Adapted from reference 36.)

involved in FeMo-cofactor binding in order for its substitution to compromise the FeMo-cofactor polypeptide environment.

A second mutagenesis-based study of the involvement of α -Cys-275 in FeMo-cofactor binding took as its basis the fact that the different properties of the MoFe proteins isolated from a variety of N_2 -fixing organisms could well correlate with constraints placed on their FeMo-cofactors by variations in their respective polypeptide matrices (35). For example, the catalytic properties of the *Clostridium pasteurianum* nitrogenase show subtle differences to those of *A. vinelandii* nitrogenase (43) as do their $S=3/2$ EPR spectra (44). Manifestations of both types of differences indicate some variation at the FeMo-cofactor site. Both MoFe proteins have identical FeMo-cofactors (5), therefore, such differences must arise from the constraints placed on the FeMo-cofactors by their respective polypeptides. Primary sequence comparisons show that the corresponding sequences around α -Cys-275 differ for these two species; for *A. vinelandii*, the sequence is His-Cys-Tyr (27), while for *C. pasteurianum*, the sequence is Gln-Cys-His (31). Thus, by locating the His residue on opposite sides of the Cys residue, different environmental constraints could be placed on the FeMo-cofactors resulting in different catalytic and/or spectroscopic properties. This hypothesis was tested by substituting this small section of the clostridial sequence for the azotobacter sequence (35). The resulting *A. vinelandii* mutant strain, with Gln replacing α -His-274 and His replacing α -Tyr-276, shows good diazotrophic growth as expected, indicating the FeMo-cofactor's ability to function is not seriously impaired. However, the $S=3/2$ EPR signal from this mutant is clearly changed to a more rhombic spectrum with g values at 4.5 and 3.5 (compared with the wild-type values of 4.3 and 3.7). This result indicates a perturbation in the environment of the FeMo-cofactor and, therefore, provides clear evidence for the intimate involvement of this region of the sequence with the FeMo-cofactor.

The recent low-resolution x-ray structure of the MoFe protein (36) has proved all these predictions and interpretations to be correct by showing that α -Cys-275 provides the direct thiol ligand to FeMo-cofactor through its unique terminal Fe atom, one of only two direct anchors holding FeMo-cofactor into its polypeptide matrix.

Effects of Amino-Acid Substitutions at α -Glutamine-191 and α -Histidine-195

The rationale for targeting the domain encompassing α -glutamyl-191 and α -histidinyl-195 is primarily based on our suggestion (9) that the products of the FeMo-cofactor-biosynthetic genes, *nifEN*, form a tetrameric scaffold, analogous to the *nifDK* gene products, upon which FeMo-cofactor is biosynthesized (9,23,32). During maturation of the MoFe protein, the immature FeMo-cofactor must necessarily escape from the NifEN tetramer to the NifDK tetramer to produce the mature MoFe protein. Thus, the sites that interact with the FeMo-cofactor within each of these tetramers are likely to be structurally similar to each other while remaining functionally different. This domain also has the attractive features of a hydrophilic pocket rich in uncharged polar residues and basic residues. These

features are appropriate for a site that must at some point be solvent exposed in order to accept the separately biosynthesized, negatively-charged FeMo-cofactor.

Within this domain of the MoFe protein's α -subunit, certain residues with functionalities that might serve to interact with FeMo-cofactor are not replicated in the corresponding domain of the *nifE*-gene product. Among those not replicated are the highly conserved glutamine (Gln-191) and histidine (His-195) residues of the α -subunit, which are replaced by lysine (Lys) and asparagine (Asn) in NifE. Substitution of either α -Gln-191 by Lys or α -His-195 by Asn should, therefore, alter the functional properties associated with FeMo-cofactor while introducing only minor perturbations on the structural integrity of the resulting altered MoFe protein.

Whole cells of mutant strains with either of these substitutions were unable to grow on N_2 gas as their only nitrogen source, i.e., were Nif⁻. However, both strains exhibit $S=3/2$ EPR signals, which although different both to wild-type and to each other, indicate that the global structure of both altered MoFe proteins is not severely affected. Also, although Nif⁻, the altered MoFe protein in each of these strains remains capable of catalyzing the reduction of both acetylene and H^+ at low rates. Importantly, these strains also show a concomitant change in catalytic specificity by directing a proportion (ca. 15-40%) of their lowered electron flux (ca. 26% of wild type rates) to reduce acetylene by four electrons to ethane, which is not a product of wild-type catalysis (23).

As an aside, vanadium-dependent nitrogenase also catalyzes ethane production from acetylene (15,16), but both ethane and ethylene production from acetylene catalyzed by these altered molybdenum-dependent nitrogenases occur on a common mechanistic pathway, which is not the case for the vanadium nitrogenase. The major differences for our altered molybdenum nitrogenases (24) compared with vanadium nitrogenase (16) are: (i) no lag in catalyzed ethane production, thus, no similar intermediate accumulates; (ii) no temperature dependence of product distribution among ethylene and ethane, indicating that the activation energies for the production of both ethane and ethylene by the altered molybdenum nitrogenase are similar; and (iii) the C_2H_6/C_2H_4 ratio for each mutant strain remains constant as electron flux is varied.

The changed substrate specificity/preference is also manifest in the H_2 -evolution properties of these mutant strains. For the MoFe protein with the α -Gln-191-Lys substitution, for example, 91% of its electron flux produces H_2 under 10% acetylene compared to 14% for wild-type. Most surprisingly, added CO is found to inhibit H_2 evolution by ca. 65% under argon, N_2 or 10% acetylene with this altered MoFe protein, while it has no effect on H_2 evolution by wild type (24). This decrease in overall product formation under CO implies a decrease in total electron flux through the altered MoFe protein; a situation previously encountered only with the Nif^V MoFe protein (13). It is not a characteristic of wild-type molybdenum-dependent nitrogenase (45,46).

Studies of the Nif^V phenotype show that the product of *nifV* is involved in producing the integral FeMo-cofactor component, homocitrate. This organic entity has been shown to play an important role in directing the MoFe protein's substrate-reduction and inhibitor-susceptibility properties (11,47,48). Although homocitrate's

function(s) is still unknown, it has very recently been shown to be coordinated to the Mo atom of FeMo-cofactor in a bidentate manner (36) with one of its uncoordinated terminal carboxylates involved in hydrogen bonding to α -Gln-191. Thus, it appears that the effects of substitution at α -Gln-191 on the properties of FeMo-cofactor are mediated through the homocitrate-Mo linkage and so, not surprisingly, are manifested similarly to changes at the homocitrate itself.

Another unexpected outcome of the low-resolution x-ray crystal structure of the MoFe protein (36) concerns the N-ligation of the FeMo-cofactor (49) as observed *via* electron spin echo envelope modulation (ESEEM) studies. Using mutant strains with many of the strictly conserved histidine residues (mainly in the α -subunit) substituted by a variety of residues, the N-ligation of protein-bound FeMo-cofactor was shown to require the α -subunit residue His-195 (50), which is also absolutely required for N₂ fixation. Surprisingly, α -His-195 does not ligate any constituent atom of FeMo-cofactor, while α -His-442 is directly ligated to the Mo (see later). However, α -His-195 is hydrogen bonded to one of the central bridging sulfides (J.T. Bolin, personal communication, 1992) and, therefore, likely manifests its effects *via* this route.

To investigate the role of α -Gln-191 and α -His-195 further, we have constructed a series of substitutions at each residue. For α -Gln-191, a variety of Nif phenotypes has been found ranging from Nif⁻, as in our original mutant strain with Lys replacing Gln, through Nif[±] (the slow-growers, represented by the Ser substitution), to strains with a diazotrophic growth rate comparable to wild type, e.g., with Ala or, surprisingly, with a Pro substitution (Peters, J. W., Newton, W.E., Dean, D. R., Virginia Tech, unpublished data). In contrast, for α -His-195, all six mutant strains constructed so far (Asn, Gln, Thr, Gly, Leu and Tyr) are strictly Nif⁻.

This group of α -His-195 mutant strains, although Nif⁻, exhibits both changed S=3/2 EPR spectra and a wide range of phenotypes with respect both to acetylene-reduction rates and products and to the characteristics of their catalyzed H⁺ reduction. For example, only the α -His-195-Gln strain reduces acetylene or protons at rates comparable to wild type. The strains with either an Asn or a Leu substituent are the only examples that produce ethane during acetylene reduction. Interestingly, these same two strains show no inhibition of H₂ evolution in the presence of either CO (5%) or N₂ (100%), while the other strains exhibit varying degrees of inhibitor susceptibility. Strains with either a Thr or Gly substituting for α -His-195 catalyze H₂ evolution that is ca. 50% inhibited by the presence of CO and, very surprisingly, approximately 35% inhibited under an 100% N₂ atmosphere.

The third phenotype among these strains is exhibited by the α -His-195-Gln strain, which, unlike its close relative with α -His-195-Asn, does not produce ethane from acetylene and shows no inhibition of H₂ evolution by CO. It does, however, exhibit inhibition of H₂ evolution by N₂. Under 100% N₂, total electron flux is decreased, with only 35% of the H₂ produced under argon evolved, and no nitrogenous (neither ammonia, hydrazine nor hydroxylamine) product detectable (consistent with its Nif⁻ phenotype). Thus, α -His-195 is not absolutely required for N₂ binding but it is essential for N₂ reduction. Further, MgATP hydrolysis is

uncoupled from electron transfer in this strain resulting in ca. 20 ATP hydrolyzed per electron pair transferred *versus* ca. 5 for wild type. This N₂-induced inhibition of H₂ evolution (and total electron flux) can be relieved by adding CO to the gaseous atmosphere (Kim, C., Newton, W. E., Dean, D. R., Virginia Tech, unpublished data). This result, together with the observation that acetylene reduction to ethylene in this strain is also inhibited by N₂ in a competitive manner ($K_i = 0.22$ atm), indicates that all these effects are occurring on a single site, which cannot reach the oxidation-reduction level required to reduce N₂. They also suggest that mutant strains might exist, which bind N₂ irreversibly (unlike α -His-195-Gln which must bind N₂ reversibly), and thus could clearly show where and how N₂ is bound within the MoFe protein. The different reactivity properties exhibited by the α -His-195-Asn strain compared to those of the α -His-195-Gln strain can be explained in terms of the available structural information. The amino-nitrogen atom of Gln can be modeled to occupy a position spatially equivalent to the ϵ -nitrogen of the imidazole ring of α -His-195, while the amino-nitrogen of Asn, which has a side chain one methylene group shorter, can only spatially mimic the δ -nitrogen atom of imidazole in fulfilling its role of hydrogen-bonding to a central bridging sulfide of FeMo-cofactor. Because the α -His-195-Gln strain much more closely resembles wild type in its catalytic and spectroscopic properties, these studies suggest that the ϵ -nitrogen of the imidazole ring is the functionally important donor for the hydrogen-bonding role of α -His-195.

Finally, all of the changes described above in FeMo-cofactor's spectroscopic properties, while bound within the altered MoFe proteins produced by single amino-acid substitutions, are very tightly correlated with its catalytic properties. Therefore, because the S=3/2 EPR spectrum arises in FeMo-cofactor, this correlation strongly supports the intimate involvement of FeMo-cofactor with the catalytic site.

Structure of FeMo-cofactor is not Affected by Substitutions at α -Glutamine-191

As described above, CO-sensitive H⁺ reduction is exhibited by several of the altered MoFe proteins (24) with substitutions in the domain covering residues α -Gln-191 and α -His-195. It also characterizes *K. pneumoniae* nifV⁻ mutants (13), which contain a compromised FeMo-cofactor (12,14). Thus, it is possible that FeMo-cofactor's molecular structure or composition has been changed through the alteration in its polypeptide environment. The MoFe protein with the α -Gln-191-Lys substitution was used as a model for this situation. Using the rationale developed for the analysis of the NifV phenotype of *K. pneumoniae* (14), FeMo-cofactor, which had been extruded from either the wild-type or the α -Gln-191-Lys MoFe protein, was used to reconstitute the "apo-MoFe protein" produced in either a Δ nifEN or a α -Gln-191-Lys/ Δ nifN background. The differences in both substrate-reduction specificity (particularly the formation of ethane from acetylene reduction catalyzed by the holo- α -Gln-191-Lys MoFe protein, but not by wild type) and in the S=3/2 EPR signals exhibited by the wild-type and α -Gln-191-Lys MoFe proteins were used to monitor these experiments. The results showed that, with either source of FeMo-cofactor, no ethane was produced during acetylene reduction

by the reconstituted wild-type "apo-MoFe protein" and that it always exhibited the wild-type $S=3/2$ EPR signal. In contrast, with FeMo-cofactor from either source, ethane was always a product of acetylene reduction catalyzed by the reconstituted altered "apo-MoFe protein" from the α -Gln-191-Lys/ Δ nifN double mutant, which always gave the EPR spectrum characteristic of the holo- α -Gln-191-Lys MoFe protein. Thus, the changed catalytic and spectroscopic properties of the altered MoFe proteins clearly have their origin in the altered environment of their FeMo-cofactor, which itself is unchanged in molecular structure and composition.

Other Residues located within the FeMo-cofactor Environment

Amino-acid sequence comparisons and site-directed mutagenesis strategies were remarkably accurate in predicting some features of the FeMo-cofactor environment. However, the recent structural information has revealed other important regions of the polypeptides whose location within the FeMo-cofactor environment was not anticipated. One such region includes α -subunit His-442, which provides direct N-coordination to the Mo atom, and α -subunit Gln-440 which could be hydrogen-bonded to homocitrate through water. Our current amino-acid substitution studies are in complete agreement with these aspects of the structure at its present stage of refinement. For example, substitution of α -Gln-440 by Glu has no apparent effect on diazotrophic growth or catalytic activity which is an expected result if α -Gln-440 indeed is hydrogen-bonded to the terminal carboxylate group of homocitrate through a water molecule. In contrast, substitution of α -His-442 by Asn results in the complete inactivation of MoFe-protein activity and also eliminates the $S=3/2$ EPR signal characteristic of the protein bound FeMo-cofactor. Thus, α -His-442 appears to play a major role in anchoring FeMo-cofactor to the polypeptide matrix. Such a role for α -His-442 can be contrasted with the thiolate ligand provided by α -Cys-275, which apparently is not essential for FeMo-cofactor binding, but is required for catalytic activity. These observations are consistent with insight from a comparison of the NifE and MoFe-protein α -subunit primary sequences. This comparison reveals that the NifE residues, which correspond to the MoFe-protein α -Cys-275 residue and the α -His-442 residue are Cys and Asn, respectively. Recall that a NifEN tetrameric complex is likely to provide a scaffold for FeMo-cofactor assembly. Thus, the thiolate group on NifE (which corresponds to the MoFe protein α -Cys-275 position) may be involved in the assembly of FeMo-cofactor. In contrast, an Asn residue in NifE is found at the position analogous to the MoFe protein α -His-442 position so that N-coordination to the FeMo-cofactor does not occur. Namely, such coordination within the NifEN complex could prevent donation of the FeMo-cofactor from the biosynthetic complex to an immature form of the MoFe protein. Current genetic approaches, such as those described above, should permit testing of this hypothesis.

Other residues within the FeMo-cofactor environment that are of particular interest include α -subunit Arg-96 and Arg-359. Although, their specific functions are not obvious from the structure, several possibilities can be considered. These include; (i) participation in a proton donor system, (ii) accepting the separately

synthesized FeMo-cofactor, and (iii) orientation of the FeMo-cofactor within the polypeptide pocket. To date, we have substituted both of these residues by Gln. Although, only a limited amount of biochemical data is available concerning these altered MoFe proteins, the growth phenotypes show that α -Arg-96-Gln is capable of slow diazotrophic growth and α -Arg-359-Gln exhibits no diazotrophic growth. Another interesting residue that has emerged from the structure for which phenotypic data is available is α -Phe-381. This residue shows a close approach to a crevice within the FeMo-cofactor formed by the bridging sulfurs of the metal core structure. We have substituted α -Phe-381 by Arg and, not surprisingly, find a strictly Nif phenotype. Although this latter work is obviously at an early stage and has depended on insight gained from the structure, the current ability of investigators to quickly generate a variety of amino-acid substitutions at any position within the nitrogenase structural components points to the importance of developing genetic and biochemical technologies in parallel with structural studies.

Conclusions and Future Directions

In summary, it is clear that single amino-acid substitutions within α -subunit FeMo-cofactor-binding domains, particularly those in the regions α -Gln-191 through α -His-195 and around α -Cys-275, have an enormous effect in fine-tuning the substrate-reduction site, resulting in a plethora of changes in the MoFe protein's substrate-reduction activities, inhibitor susceptibilities and EPR spectroscopic properties with no change in FeMo-cofactor's structure or composition. These results strongly support the concept of FeMo-cofactor as the substrate-reduction site. The recent x-ray solution of the crystal structure of the MoFe protein indicates the features through which these effects are manifested and provides the necessary information to design experiments to determine how electrons enter the MoFe protein, how they are stored and distributed to substrate, and how substrates are bound and reduced.

Acknowledgments

We thank the National Institutes of Health (grant DK-37255) for support.

Literature Cited

1. Eady, R. R.; Smith, B. E. *Eur. J. Biochem.* **1992**, *205*, 1-15.
2. Newton, W. E. In *Biological Nitrogen Fixation*; Stacey, G., Burris, R. H. and Evans, H. J., Eds.; Chapman and Hall: New York, NY, 1992; pp 877-929.
3. Burgess, B. K. *Chem. Rev.* **1990**, *90*, 1377-1406.
4. Burris, R. H. *J. Biol. Chem.* **1991**, *266*, 9339-9342.
5. Shah, V. K.; Brill, W. J. *Proc. Natl. Acad. Sci. U.S.A.* **1977**, *74*, 3249-3253.
6. Rawlings, J.; Shah, V. K.; Chisnell, J. R.; Brill, W. J.; Zimmermann, R.; Munck, E.; Orme-Johnson, W. H. *J. Biol. Chem.* **1978**, *253*, 1001-1004.
7. Shah, V. K.; Davis, L. C.; Gordon, J. K.; Orme-Johnson, W. H.; Brill, W. J. *Biochim. Biophys. Acta* **1973**, *292*, 246-255.

8. Nagatani, H. H.; Shah, V. K.; Brill, W. J. *J. Bacteriol.* **1974**, *120*, 697-7021.
9. Brigle, K. E.; Weiss, M. C.; Newton, W. E.; Dean, D. R. *J. Bacteriol.* **1987**, *169*, 1547-1553.
10. Paustian, T. D.; Shah, V. K.; Roberts, G. P. *Biochemistry* **1990**, *29*, 3515-3522.
11. Hoover, T. R.; Robertson, A. D.; Cerny, R. L.; Hayes, R. N.; Imperial, J.; Shah, V. K.; Ludden, P. W. *Nature* **1987**, *329*, 855-857.
12. Liang, J.; Madden, M.; Shah, V. K.; Burris, R. H. *Biochemistry* **1990**, *29*, 8577-8581.
13. McLean, P. A.; Dixon R. A. *Nature (London)* **1981**, *292*, 655-656.
14. Hawkes, T. R.; McLean, P. A.; Smith, B. E. *Biochem. J.* **1984**, *217*, 317-321.
15. Dilworth, M. J.; Eady, R. R.; Robson, R. L.; Miller, R. W. *Nature (London)* **1987**, *327*, 167-168.
16. Dilworth, M. J.; Eady, R. R.; Eldridge, M. E. *Biochem. J.* **1988**, *249*, 745-751.
17. Robson, R. L.; Eady, R. R.; Richardson, T. H.; Miller, R. W.; Hawkins, M.; Postgate, J. R. *Nature (London)* **1986**, *322*, 388-390.
18. Hales, B. J.; Case, E. E.; Morningstar, J. E.; Dzeda, M. F.; Mauterer, L. A. *Biochemistry* **1986**, *25*, 7251-7255.
19. Smith, B. E.; Eady, R. R.; Lowe, D. J.; Gormal, C. *Biochem. J.* **1988**, *250*, 299-302.
20. Shah, V. K.; Chisnell, J. R.; Brill, W. J. *Biochem. Biophys. Res. Commun.* **1978**, *81*, 232-236.
21. McKenna, C. E.; Jones, J. B.; Eran, H.; Huang, C. W. *Nature (London)* **1979**, *280*, 611-612.
22. Brigle, K. E.; Setterquist, R. A.; Dean, D. R.; Cantwell, J. S.; Weiss, M. C.; Newton, W. E. *Proc. Natl. Acad. Sci. U.S.A.* **1987**, *84*, 7066-7069.
23. Scott, D. J., May, H. D., Newton, W. E., Brigle, K. E. and Dean, D. R. *Nature (London)* **1990**, *343*, 188-190.
24. Scott, D. J.; Dean, D. R.; Newton, W. E. *J. Biol. Chem.* **1992**, *267*, 20002-20010.
25. Kent, H. M.; Ioannidis, I.; Gormal, C.; Smith, B. E.; Buck, M. *Biochem. J.* **1989**, *264*, 257-264.
26. Kent, H. M.; Bainea, M.; Gormal, C.; Smith, B. E.; Buck, M. *Molec. Microbiol.* **1990**, *4*, 1497-1504.
27. Brigle, K.E.; Newton, W.E.; Dean, D. R. *Gene*, **1985**, *37*, 37-44.
28. Dean, D. R.; Setterquist, R. A.; Brigle, K. E.; Scott, D. J.; Laird, N. F.; Newton, W. E. *Molec. Microbiol.* **1990**, *4*, 1505-1512.
29. Lammers, P. J.; Haselkorn, R. *Proc. Natl. Acad. Sci. U.S.A.* **1983**, *80*, 4723-4727.
30. Kaluza, K.; Hennecke, H. *Mol. Gen. Genet.* **1984**, *196*, 35-42.
31. Wang, S.-Z.; Chen, J.-S.; Johnson, J. L. *Biochemistry* **1988**, *27*, 2800-2810.
32. Ioannidis, I.; Buck, M. *Biochem. J.* **1987**, *247*, 287-291.
33. Holland, D.; Zilberstein, A.; Zamir, A.; Sussmann, J. L. *Biochem. J.* **1987**, *247*, 277-286.

34. Dean, D. R.; Jacobson, M. R. In *Biological Nitrogen Fixation*; Stacey, G., Burris, R. H. and Evans, H. J., Eds.; Chapman and Hall, New York, NY, 1992; pp 763-834.
35. Dean, D. R.; Scott, D. J.; Newton, W. E. In *Nitrogen Fixation: Achievements and Objectives*; Gresshoff, P. M., Stacey, G., Roth, L. E. and Newton, W. E., Eds.; Chapman and Hall, New York, NY, 1990; pp 95-102.
36. Kim, J.; Rees, D. C. *Science* **1992**, *257*, 1677-1682.
37. Burgess, B. K.; Stiefel, E. I.; Newton, W. E. *J. Biol. Chem.* **1980**, *355*, 353-356.
38. Yang, S.-S.; Pan, W.-H.; Friesen, G. D.; Burgess, B. K.; Corbin, J. L.; Stiefel, E. I.; Newton, W. E. *J. Biol. Chem.* **1982**, *257*, 8042-8048.
39. Smith, B. E.; Bishop, P. E.; Dixon, R. A.; Eady, R. R.; Filler, W. A.; Lowe, D. J.; Richards, A. J. M.; Thomson, A. J.; Thorneley, R. N. F.; Postgate, J. R. In *Nitrogen Fixation Research Progress*; Evans, H. J., Bottomley, P. J., Newton, W. E., Eds.; Martinus Nijhoff: Dordrecht, The Netherlands, 1985; pp 597-603.
40. Masharak, P.; Smith, M. C.; Armstrong, W. H.; Burgess, B. K.; Holm, R. H. *Proc. Natl. Acad. Sci. U.S.A.* **1982**, *79*, 7056-7060.
41. Newton, W. E.; Gheller, S. F.; Schultz, F. A.; Burgess, B. K.; Conradson, S. D.; McDonald, J. W.; Hedman, B.; Hodgson, K. O. In *Nitrogen Fixation Research Progress*; Evans, H. J., Bottomley, P. J., Newton, W. E., Eds.; Martinus Nijhoff: Dordrecht, The Netherlands, 1985; pp 605-610.
42. Govezensky, D.; Zamir, A. *J. Bacteriol.* **1989**, *171*, 5729-5735.
43. Newton, W. E.; Corbin, J. L.; McDonald, J. W. In *Nitrogen Fixation*; Newton, W. E., Nyman, C. J., Eds.; Washington State University Press: Pullman, WA, 1976, Vol. 1; pp 53-74.
44. Morgan, T. V.; Mortenson, L. E.; McDonald, J. W.; Watt, G. D. *J. Inorg. Biochem.* **1988**, *33*, 111-120.
45. Bulen, W. A.; Burns, R. C.; LeComte, J. R.; Hinkson, J. In *Non-Heme Iron Proteins: Role in Energy Conversion*; San Pietro, A., Ed.; Antioch Press: Yellow Springs, OH, 1965; pp 261-274.
46. Hardy, R. W. F.; Knight, Jr., E.; D'Eustachio, A. J. *Biochem. Biophys. Res. Commun.* **1965**, *20*, 539-544.
47. Hoover, T. R.; Imperial, J.; Liang, J.; Ludden, P. W.; Shah V. K. *Biochemistry* **1988**, *27*, 3647-3652.
48. Imperial, J.; Hoover, T. R.; Madden, M. S.; Ludden, M. S.; Shah V. K. *Biochemistry* **1989**, *28*, 7796-7799.
49. Thomann, H.; Morgan, T. V.; Jin, H.; Burgmayer, S. J. N.; Bare, R. E.; Stiefel, E. I. *J. Am. Chem. Soc.* **1987**, *109*, 7913-7914.
50. Thomann, H.; Bernardo, M.; Newton, W.E.; Dean, D. R. *Proc. Natl. Acad. Sci. U.S.A.* **1991**, *88*, 6620-6623.
51. Joerger, R. D.; Loveless, T. M.; Pau, R. N.; Mitchenall, L. A.; Simon, B. H.; Bishop, P. A. *J. Bacteriol.* **1990**, *172*, 3400-3408.

RECEIVED April 12, 1993

Chapter 15

Extended X-ray Absorption Fine Structure and L-Edge Spectroscopy of Nitrogenase Molybdenum–Iron Protein

J. Chen¹, J. Christiansen², S. J. George², J. van Elp¹, R. Tittsworth³,
B. J. Hales³, S. Al-Ahmad⁴, Dimitri Coucouvanis⁴, Nino Campobasso⁵,
Jeffrey T. Bolin⁵, and S. P. Cramer^{1,2}

¹Energy and Environment Division, Lawrence Berkeley Laboratory,
Berkeley, CA 94720

²Department of Applied Science, University of California, Davis, CA 95616

³Department of Chemistry, Louisiana State University,
Baton Rouge, LA 70803

⁴Department of Chemistry, University of Michigan, Ann Arbor, MI
48109–1055

⁵Department of Biological Sciences, Purdue University,
West Lafayette, IN 47907

Molybdenum *K*-edge EXAFS of lyophilized nitrogenase provided the first spectroscopic evidence for a Mo-Fe-S cluster, and since then experiments have been done on solutions, crystals, and extracted cofactors. The Mo EXAFS data suggest a 4S/2O(N) or 3S/3O(N) Mo site, with 3–4 Fe at ~2.7 Å. Mo *L*-edge spectra are compatible with Mo(III) or Mo(IV). More recent *Av1* Fe EXAFS reveals not only 2.65 and 3.8 Å Fe-Fe interactions, but Fe-S features at 4.3 Å. A second shell Mo-Fe interaction at ~5 Å is also observed in new Mo EXAFS data. The EXAFS distances are consistent with recent crystallographic models for the M-center, and all of the interactions can be assigned. Using new soft x-ray beamlines and detectors, nitrogenase Fe *L*-edge spectra have also been obtained and interpreted as evidence for both Fe(II) and Fe(III). Changes are evident upon dye oxidation. X-ray magnetic circular dichroism offers the prospect of a new generation of nitrogenase experiments.

X-ray absorption spectroscopy has been used to study the metals in nitrogenase since 1977 (1), providing important metal-metal distances to model-builders while the community pined for a crystal structure. Although the x-ray diffraction structures for *Clostridium pasteurianum* (2,3) and *Azotobacter vinelandii* (4,5) Mo-Fe proteins (*Cp1* and *Av1*, respectively) are now progressing rapidly, the information provided by EXAFS remains useful in the model building process. In addition, new approaches using soft x-ray spectroscopy and magnetic circular dichroism can provide additional data about the iron oxidation states and magnetic coupling in the P-clusters and M-centers. This chapter summarizes the latest EXAFS and soft x-ray results, and describes new x-ray spectroscopic techniques made possible by advances in synchrotron radiation sources.

Progress in Solution EXAFS

The first nitrogenase Mo-Fe protein Mo *K*-edge EXAFS (1) found Mo-S and Mo-Fe distances of 2.35 Å and 2.73 Å, respectively, and offered at least two models for the local Mo coordination. Further work by Conradson *et al.* (6) on isolated FeMoco found clear evidence for a shell of oxygen and/or nitrogen ligands around Mo at ~2.1 Å. FeMoco EXAFS from the Fe *K*-edge found an average Fe-S distance of 2.2 Å, and Fe-Fe interactions at both 2.6 and 3.7 Å (7). In contrast to prior work by Antonio *et al.* (8), the Daresbury group found little evidence for Fe-O(N) ligation in FeMoco (7). Until recently, the Fe EXAFS of intact Mo-Fe protein had not been reported, due to the daunting complexity of interpreting overlapping P-cluster and M-center signals. The combination of solid-state fluorescence detectors and dedicated, stable synchrotron radiation sources allows vastly improved EXAFS to be obtained on dilute metalloproteins. Although the interpretation of nitrogenase Fe EXAFS is complicated by the presence of a wide variety of Fe sites, we have recorded the spectra in the hope that symmetry will allow simplification of the analysis. In this regard, nature has been kind; the recent crystal structures reveal approximate 3-fold symmetry for the M-center and high symmetry for the P-clusters as well. The Mo EXAFS of the *Av1* protein has also been recorded, to see if additional features can be distinguished with better signal-to-noise. New long distance interactions, out to ~5 Å, can indeed be observed.

Iron *K*-Edge Results. Previous Fe *K*-edge EXAFS spectra of FeMoco isolated from *Klebsiella pneumoniae* showed numerous distances from the iron point of view that help define the cluster of the FeMo cofactor. The various models consistent with these data have been reviewed frequently (9), but they have all been made largely obsolete by recent crystallographic progress. Still, the crystallography is at a stage where distances from EXAFS can be useful, and there is not complete agreement in the proposed structures (3-5).

Nitrogenase and Model Comparisons. The Fe EXAFS Fourier transforms for resting *Av1* and *Av1'* are compared with the $[\text{Fe}_6\text{S}_6\text{Cl}_6]^{3-}$ prismatic model in Figure 1. For the dithionite-reduced Mo-Fe protein, the EXAFS Fourier transform is dominated by Fe-S and Fe-Fe interactions at 2.32 and 2.64 Å respectively. The Fe-Fe interaction at 3.8 Å, previously seen in isolated FeMoco (7), is also seen in the intact protein spectra. A longer distance feature, assigned as Fe-S at 4.3 Å, is also observed. A similar pattern of Fe interactions is observed for the reduced V-Fe protein. There is even a hint of a very long Fe-Fe component at 4.7 Å.

The features for distances greater than 3 Å are much weaker than the shorter distance interactions, but a noise analysis finds that these features are significant and above Fourier transform ripple level. Because of the wide variety of Fe-X interactions that could lead to distances in the 3-5 Å region, it is useful to summarize how EXAFS can distinguish between different types of neighbors. The combined effect of phase shift and backscattering amplitude on Fe-C, Fe-S, Fe-Fe, and Fe-Mo interactions at an arbitrary distance of 4 Å is illustrated using theoretical curves in Figure 2.

The differences in phases for different Fe-X components allow overlapping components to be resolved, and distant shells to be assigned. This is done by means of a 'search' profile, which portrays the quality of fit as a function of the distance at which an additional component is added. For example, although Fe-Fe and Fe-Mo components overlap in the 2.65 Å region, a search profile clearly resolves the Fe-Mo component (Figure 3). Similarly, a search profile analysis rules out an Fe-C assignment for the 4.3 Å feature, favoring instead a Fe-S assignment (Figure 3). An Fe-Mo assignment might also be plausible, but the matching Mo-Fe component is not observed in the Mo EXAFS.

Distance Summary. The distances observed in the Fe EXAFS are summarized in Table I, along with approximate amplitudes. No attempt is made to

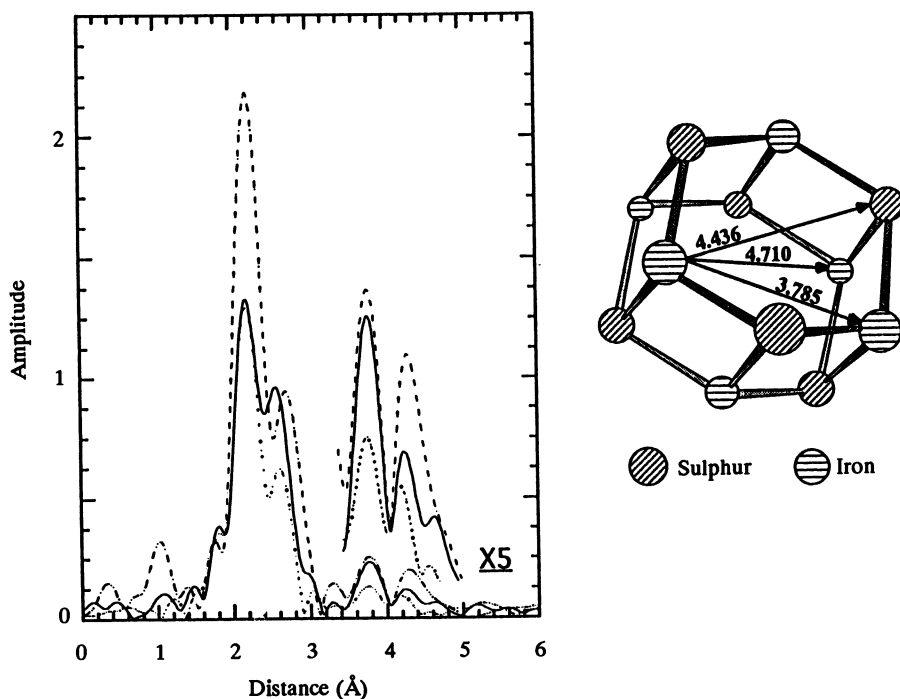


Figure 1. (Left) EXAFS Fourier transforms for $[\text{Fe}_6\text{S}_6\text{Cl}_6]^{3-}$ prismane (---), reduced *AvI* protein (—), and reduced V-Fe protein (*AvI'*) (⋯). Features beyond 3 Å have been multiplied by 5 in insets to enhance visibility. (Right) Structure of $[\text{Fe}_6\text{S}_6\text{Cl}_6]^{3-}$ anion showing long Fe-Fe and Fe-S distances.

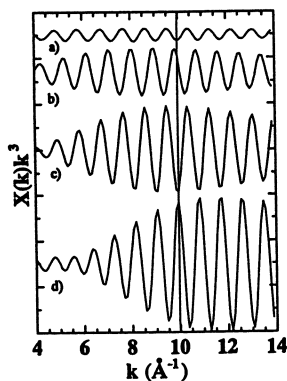


Figure 2. Theoretical EXAFS curves for different types of Fe-X interactions. The curves represent predicted EXAFS for one X atom at 4 Å. Fe-C (a), Fe-S (b), Fe-Fe (c), and Fe-Mo (d). Note that Fe-S and Fe-Mo are relatively in phase with each other and nearly π out of phase with Fe-C and Fe-Fe.

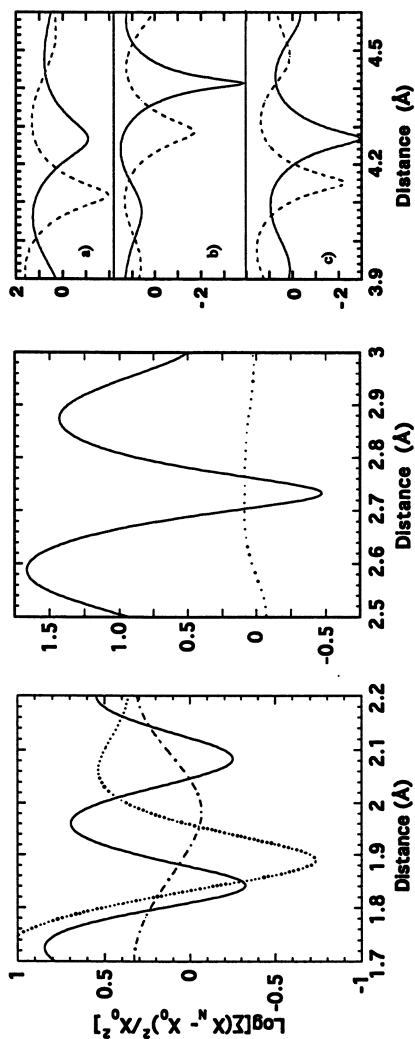


Figure 3. EXAFS search profiles. (Left) Search for Fe-O interaction in $[\text{Fe}_6\text{S}_6(\text{O}^-\text{Ph})_6]^{3-}$ prismatic (\cdots), $[\text{Fe}_6\text{S}_6\text{Cl}_6]^{3-}$ prismatic ($-\cdot-\cdot-$) and reduced *Av1* protein (---). (Middle) Search for Fe-Mo interaction in $[\text{Fe}_6\text{S}_6\text{Cl}_6]^{3-}$ prismatic ($-\cdot-\cdot-$), and reduced *Av1* protein (---). (Right) Search for Fe-C ($-\cdot-\cdot-$) and Fe-S (---) interactions in the (a) $\text{Fe}_2[(\text{O}_2\text{CH})_4(\text{BIPhMe})_2]$, (b) $[\text{Fe}_6\text{S}_6\text{Cl}_6]^{3-}$ prismatic, and (c) reduced *Av1* protein. Note that the zero level corresponds to no improvement in quality of fit. The search profiles were drawn for adding 1 Fe-O (left), 0.3 Fe-Mo (middle), or 4.5 Fe-C (right) interactions.

Table I. Nitrogenase Distances From Fe EXAFS

Component	Amplitude N (N') ^a	Distance R (Å)
Fe-O(N)	0.5 ^b	1.842
Fe-S	3.5 ^b	2.317
Fe-Fe	2 ^b	2.641
Fe-Mo	0.3	2.732
Fe-Fe'	1.3 (2.8)	3.81
Fe-S'	1.2 (1.7) ^c	3.86
Fe-S''	0.8 (1.7)	4.29
Fe-Fe''	0.3 (0.6)	4.7

^aMultiplied by 15/7.^bFixed numbers in refinement.^cMultiplied by 15/7 with consideration that there is one 3.9 Å diagonal Fe-S distance for every Fe atom in the P-cluster.

distinguish between components that are part of P-clusters vs. those from the M-centers.

Molybdenum K-Edge Results. The recent crystallographic models for the M-center show that the clusters are almost symmetrical, and the Mo atom is on one end of a long Mo-Fe-S cluster. These models should have a second set of longer Mo-Fe distances, beyond the 2.7 Å shell. A close look at new Mo EXAFS data (Figure 4) reveals just such a feature, with an amplitude comparable to long Mo-Fe interactions observed in a Mo double-capped prismane complex. However, the distance is significantly longer than in the capped prismane model, showing a fundamental difference between the M-center and prismane geometry. The distances observed in the Mo EXAFS are summarized in Table II.

Table II. Nitrogenase Distances from Mo EXAFS

Component	Amplitude N	Distance R (Å)
Mo-O(N)	1.5	2.15
Mo-S	3.5	2.34
Mo-Fe	3	2.70
Mo-Fe'	3	~5

There are other transform features in the 3-5 Å region, which have not yet been explained. Some of these peaks presumably come from carbons associated with histidine or homocitrate ligands to Mo.

Structure Candidates. On the basis of the new Fe EXAFS distances and previous Mo EXAFS results, a variety of structures remain plausible. Rather than belaboring structures that have been eliminated by recent x-ray diffraction results, it seems more valuable to consider the candidate structures recently proposed by Bolin (Bolin, J. *Chap 12*, this volume), Kim and Rees (4,5), as well as a proposal that came from the Fe EXAFS analysis (Chen, J. *J. Am. Chem. Soc.* in press).

The long 3.8 Å Fe-Fe distances found in the EXAFS could be assigned in different ways. Without further constraints, they could correspond to Fe-Fe interactions in the plane perpendicular to the long FeMoco axis, parallel to that axis (Figure 5c), or at an angle to the long axis. Using the distances provided by the Mo EXAFS, we can put additional constraints on how the FeMoco cluster must be constructed. If we assume two parallel planes of three Fe atoms, capped with Mo on one end and Fe on

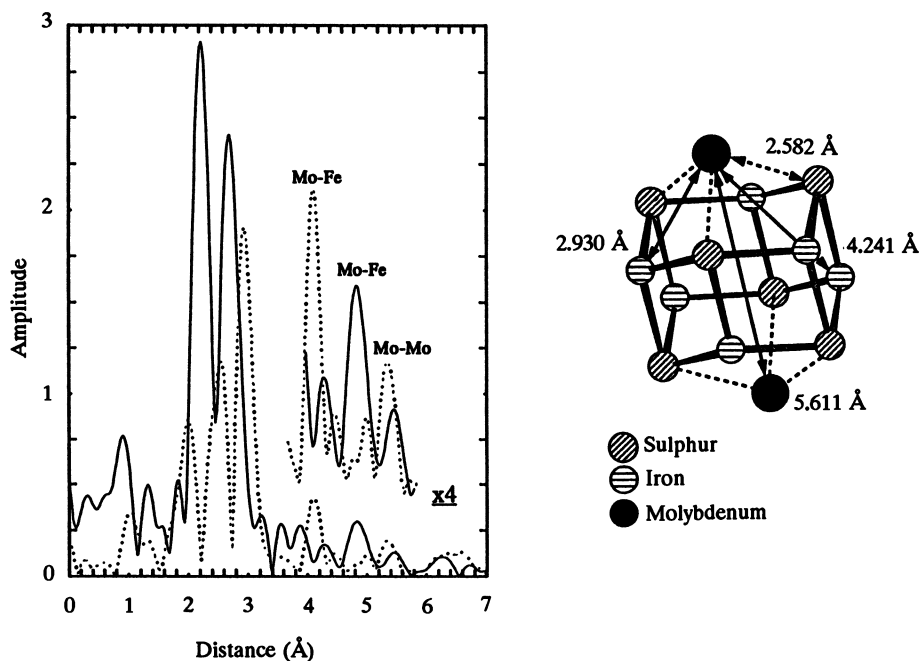


Figure 4. (Left) Comparison of Mo EXAFS data for *Av1* (—) vs. $(\text{CO})_3\text{MoFe}_6\text{S}_6\text{Mo}(\text{CO})_3$ (- - -). Note the shorter Mo-Fe second shell in the model compound vs. the protein spectra, as well as the very long cross-prismane Mo-Mo component in the model. (Right) Structure of $(\text{CO})_3\text{MoFe}_6\text{S}_6\text{Mo}(\text{CO})_3$ showing long Mo-S, Mo-Fe, and Mo-Mo distances.

the other, then the $\sim 5 \text{ \AA}$ Mo-Fe interaction forces us to assign the 3.8 \AA Fe-Fe distance as a diagonal interaction.

In the model recently proposed by Kim and Rees (Figure 5a), there are a significant number of three-coordinate Fe centers. Given the complicating presence of P-cluster interactions, only a small amplitude difference would be expected if the Fe was truly three-coordinate - ~ 3.5 Fe-S interactions averaged over all Fe in the sample. Furthermore, a disordered set of Fe-O(N) would be difficult to detect. For three-coordinate Fe, one might expect a shorter Fe-S bond length. We note that the average Fe-S distance observed for the intact protein was 2.32 \AA . The plausible distance assignments are displayed in Figure 6. If we assume that only 7 of 15 Fe in nitrogenase have longer interactions, the adjusted amplitude for the 3.8 \AA feature found from Fe EXAFS is 2.8 (Table I). The model of Kim and Rees shows an average of 1.7 Fe at $\sim 3.8 \text{ \AA}$ (4).

Oxidation State Changes. Although further analysis remains to be done, we show EXAFS Fourier transforms for Fe and Mo in thionine-oxidized *Av1* in Figure 7. In the dye-oxidized samples, we observe a small change in the average Fe-S distances, from 2.32 to 2.29 \AA . Similar contractions of Fe-S bond lengths are observed for other Fe-S proteins when oxidized. The observed contraction is consistent with removal of an electron from a delocalized iron-sulfur cluster, and is close to that reported for 3-Fe ferredoxin II cluster of *Desulfovibrio gigas* (10). In contrast, the observed Fe-Fe distance in oxidized samples is slightly longer than that in reduced samples. The Fe-Fe distances, averaged over the M-center and P-cluster, expand by 0.016 \AA . Although the change is reproducible, it is near the limit of EXAFS error. Similar results were reported on 3-Fe proteins (10).

From the Mo point of view, the observed Mo-S and Mo-Fe distances for the oxidized protein are 2.34 \AA and 2.71 \AA , while the reduced protein has Mo-S and Mo-Fe distances of 2.34 \AA and 2.70 \AA . The observed Mo-O(N) distances range from 2.09 \AA (oxidized) to 2.15 \AA (reduced).

Some changes in longer interactions are also found. In both Fe and Mo EXAFS spectra, intensities of some longer distance features become smaller in the oxidized sample. This decrease in intensity may implicate long range structural changes upon oxidation. A slight rearrangement of the cofactor would be enough to destroy the long range symmetry needed to see these interactions. However, the low data quality of the oxidized samples and the greater systematic error in long range fittings may also contribute to these changes.

Soft X-Ray Spectra

For x-ray spectroscopy of nitrogenase in the soft x-ray region, where vanadium and iron *L*-edges are found, absorption path lengths are $1 \mu\text{m}$ or less. Extremely thin windows or windowless techniques must be used throughout beamline, sample, and detector paths. The experiments require an efficient detector and frequent sample changes to acquire data before radiation damage becomes significant. Despite these difficulties, we have recently obtained excellent data on the Fe in *A. vinelandii* Mo-Fe proteins, which nicely show both the sharpness of *L*-edge spectra and shifts with oxidation state (Figure 8).

Because of unresolved oxygen, nitrogen and vanadium fluorescence signals, along with the lower V concentration and smaller fluorescence yield, it is at least two orders of magnitude harder to measure the V *L*-edge spectrum compared to the Fe *L*-edge. The spectra measured below and above the V *L*-edge (511 eV), clearly show the presence of a V signal, even though the count rate is low (Figure 8). With newly developed third generation synchrotron radiation sources incident fluxes will be orders of magnitude higher, and the V *L*-edge experiment will become feasible.

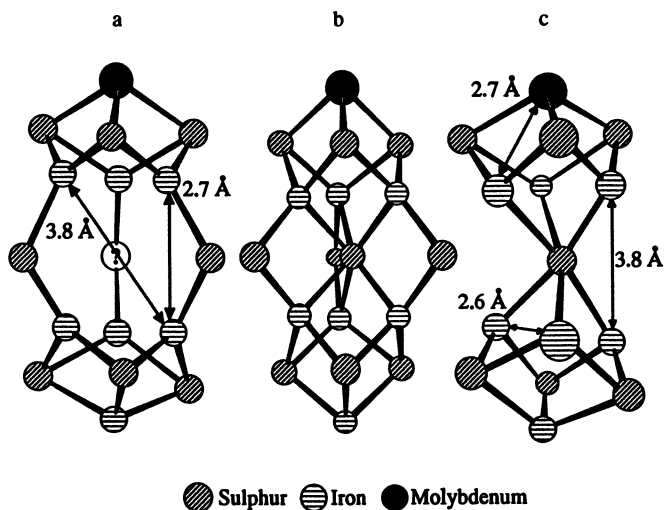


Figure 5. Recent candidate structures for the nitrogenase M-center. (a) proposed by Kim and Rees, (b) proposed by Bolin, and (c) proposed from EXAFS distances.

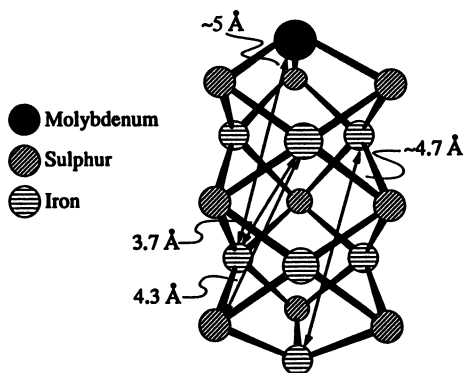


Figure 6. A plausible assignment of long Fe-Fe and Mo-Fe distances in the M-center.

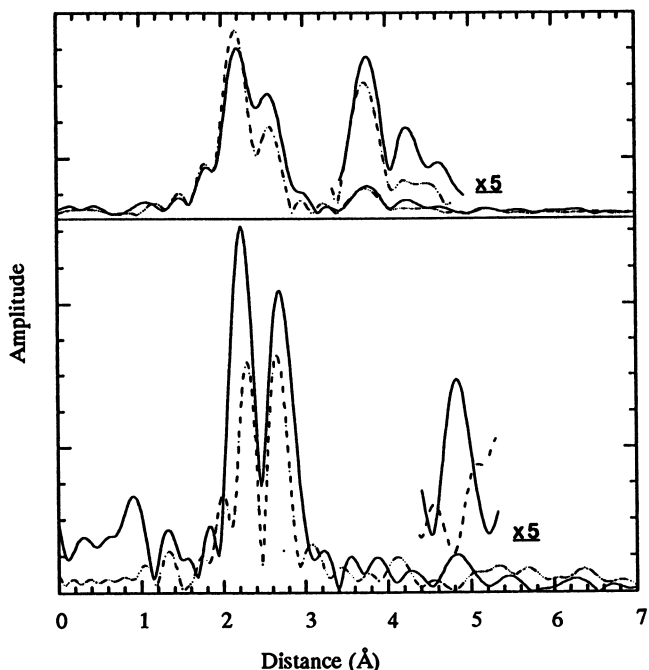


Figure 7. Comparison of (top) Fe and (bottom) Mo EXAFS data for dithionite-reduced (- - -) and thionine-oxidized *AvI* (—). Note the changes in long Fe-S (top) and long Mo-Fe (bottom) features.

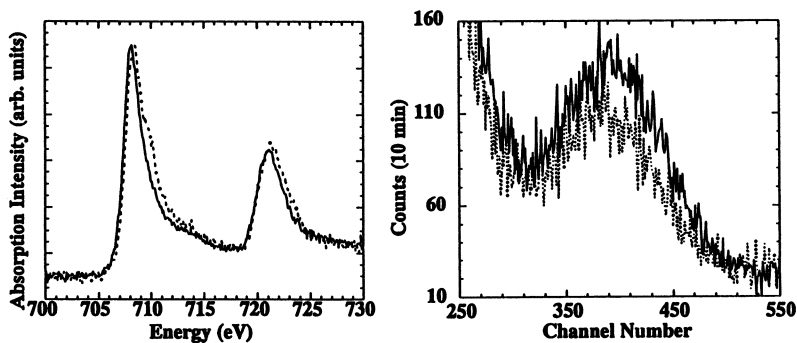


Figure 8. (Left) The Fe $L_{2,3}$ -edges spectra for dithionite-reduced (—) and thionine-oxidized (- - -) Mo-Fe proteins. The shift to higher energies is small but reproducible. (Right) MCA spectra of dithionite-reduced VFe-protein taken on X1B at NSLS. The broken line (- - -) is obtained with 507 eV photon energy (below the $V L$ -edge), and the solid line is measured at 517 eV (above the edge). Note the total measuring time is 10 minutes.

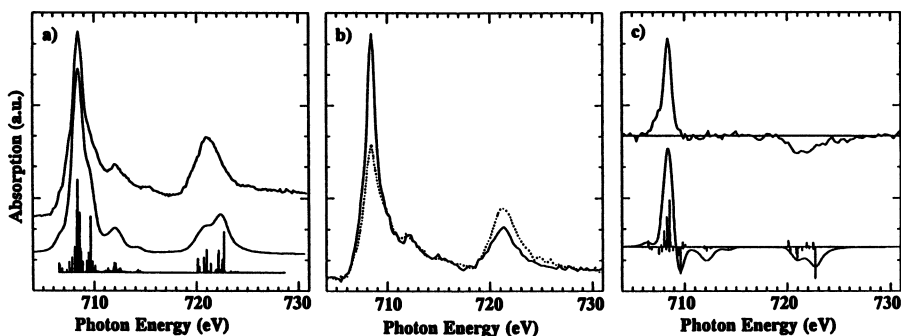


Figure 9. (a) Isotropic oxidized Fe^{3+} spectrum of *Pyrococcus furiosus* rubredoxin, together with the calculation. (b) The left- (—) and right- (---) circular polarized spectra. (c) The experimental MCD spectrum (left-right), and the calculated spectrum. The sticks in (a) and (c) show the strength of the individual calculated transitions before linewidth broadening.

X-Ray Magnetic Circular Dichroism

One limitation for both EXAFS and *L*-edge spectroscopy of iron in nitrogenase is the large number of different irons in the protein. The relatively new technique of soft x-ray magnetic circular dichroism (SXMCD) has the advantage that (a) it is element selective and only sensitive to the paramagnetic metal centers, (b) it can reveal the orientation of the local spin with respect to the bulk spin, as well as the normal ligand field information. SXMCD will be a powerful probe of magnetic coupling in mixed-valence complexes.

Several experiments now permit extending the SXMCD technique to metalloproteins from its conventional UV-visible-NIR domain to the soft x-ray region. First, a simple method for obtaining alternating left- and right-polarized radiation has been demonstrated (11,12). Second, a fluorescence detection system with sufficient sensitivity for protein spectroscopy has been developed (13,14). Finally, a low temperature, high magnetic field system has been developed that allows magnetization of paramagnetic samples.

In preliminary experiments, we have observed a strong SXMCD signal from the high-spin iron in *Pyrococcus furiosus* rubredoxin (Figure 9) (van Elp, J. unpublished data). The ability to determine magnetic structure from x-ray absorption will be an important new tool for metalloprotein studies.

Prospects for the Future

Intense x-ray beams from synchrotron radiation sources have made bioinorganic x-ray spectroscopy feasible. As these sources evolve, the quality of the spectra continues to improve, and more difficult experiments can be conducted. For example, wiggler devices, which increase flux by bending electrons through a tighter radius and a greater number of poles, provided nearly two orders of magnitude more flux for Mo *K*-edge spectroscopy. Undulator sources also use a large number of magnetic poles, but spaced to create constructive interference at certain wavelengths. The resulting radiation is concentrated in space and in frequency, so that the brightness improves quadratically with the number of poles (Figure 10).

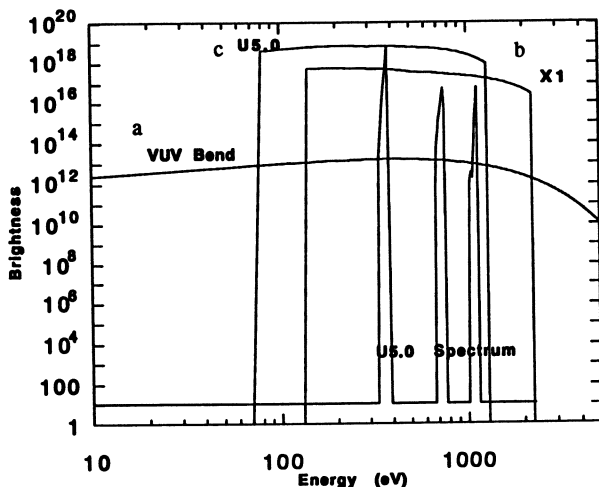
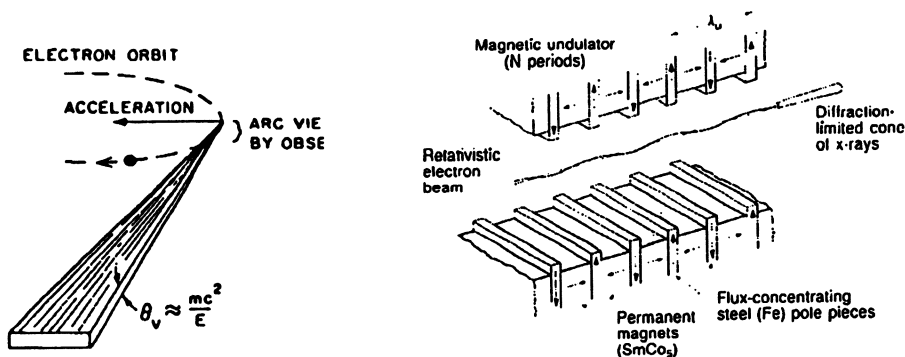


Figure 10. Schematic illustrating differences between bend magnets (left), wigglers and undulators (middle). (Right) The brightness available from a) the Dragon' beamline used for initial studies, b) the newly available X-1B at NSLS, and c) the U5.0 undulator planned for ALS in 1993.

Two new sources in the U.S. (the Advanced Light Source in Berkeley and the Advanced Photon Source at Argonne National Laboratory) will provide undulator beams for soft and hard x-ray spectroscopy.

Special insertion devices are also being built that allow intense beams of circularly polarized x-rays to be produced. For example, if the electrons in the ring are accelerated both horizontally and vertically in an 'elliptical wiggler', the resultant radiation is elliptically polarized. Through control of the trajectory, the relative amounts of circular and linear radiation can be adjusted. The extraordinary control that scientists and engineers now have over the intensity, stability, and polarization of synchrotron radiation promises an entirely new generation of more difficult bioinorganic experiments using x-ray spectroscopy.

Acknowledgments

Support from the Department of Agriculture through grant DOA-91-37305-6514 (to SPC), the National Science Foundation through grant DMB-91073212 (to SPC), and the NIH through GM-44380-2 (to SPC) and GM-33965 (to BJH) are gratefully acknowledged. This work was partially supported by the Department of Energy through Lawrence Berkeley Lab LDRD Exploratory Research Funds. The National Synchrotron Light Source and the Stanford Synchrotron Radiation Lab are supported by the U.S. Department of Energy, Office of Basic Energy Sciences.

Literature Cited

- (1) Cramer, S. P.; Hodgson, K. O.; Gillum, W. O.; Mortenson, L. E. *J. Am. Chem. Soc.* **1978**, *100*, 3398-3407.
- (2) Bolin, J. T.; Ronco, A. E.; Mortenson, L. E.; Morgan, T. V.; Williamson, M.; Xuong, N.-H. *Nitrogen Fixation: Achievements and Objectives*, Gresshoff, P. M.; Roth, L. E.; Stacey, G.; Newton, W. E. eds. Chapman and Hall, New York (1990) 117-124.
- (3) Bolin, J. T.; Ronco, A. E.; Morgan, T. V.; Mortenson, L. E.; Xuong, N.-H. *Proc. Natl. Acad. Sci. USA*, **1993**, *90*, 1078-1082.
- (4) Kim, J.; Rees, D. C. *Science*, **1992**, *257*, 1677-1682.
- (5) Kim, J.; Rees, D. C. *Nature*, **1992**, *360*, 553-560.
- (6) Conradson, S.D.; Burgess, B.K.; Newton, W.E.; Mortenson, L.E.; Hodgson, K.O. *J. Am. Chem. Soc.* **1987**, *109*, 7507.
- (7) Arber, J. M.; Flood, A. C.; Garner, C. D.; Gormal, C. A.; Hasnain, S. S.; Smith, B. E. *Biochem. J.* **1988**, *252*, 421-425.
- (8) Antonio, M. R.; Teo, B. K.; Orme-Johnson, W. H.; Nelson, M. J.; Groh, S. E.; Lindahl, P. A.; Kauzlarich, S. M.; Averill, B. A. *J. Am. Chem. Soc.* **1982**, *104*, 4703-4705.
- (9) Coucouvanis, D. *Accts. Chem. Res.* **1991**, *24*, 1-8.
- (10) Antonio, M. R.; Averill, B. AA.; Moura, I.; Moura, J. J. G.; Orme-Johnson, W. H.; Teo, B. K.; Xavier, AA. *V. J. Biol. Chem.* **1982**, *257*, 6646-6649.
- (11) Chen, C. T.; Sette, F. *Rev. Sci. Instr.* **1989**, *60*, 1616-1621.
- (12) Chen, C. T.; Sette, F.; Ma, Y.; Modesti, S. *Phys. Rev. B*, **1990**, *42*, 7262-7265.
- (13) Cramer, S. P.; Tench, O.; Yocum, M.; Kraner, H.; Rogers, L.; Radeka, V.; Mullins, O.; Rescia, S. *X-ray Absorption Fine Structure - Proc. 6th Intl. XAFS Conf.* Hasnain, S. S.; ed.; Ellis Horwood, Chichester (1991) 640-645.
- (14) Cramer, S. P.; Chen, J.; George, S. J.; van Elp, J.; Moore, J.; Tensch, O.; Colaresi, J.; Yocum, M.; Mullins, O. C.; Chen, C. T. *Nucl. Instr. and Meth.* **1992**, *A319*, 285-289.

RECEIVED April 20, 1993

Chapter 16

Redox Properties of the Nitrogenase Proteins from *Azotobacter vinelandii*

G. D. Watt¹, H. Huang², and K. R. N. Reddy³

¹Department of Chemistry, Brigham Young University, Provo, UT 84602

²Department of Biology, Xiamen University, Xiamen,
People's Republic of China

³Department of Chemistry, University of Maryland, Baltimore, MD 21228

Nitrogenase consists of two dissimilar, metalloproteins (the MoFe protein and the Fe protein) which together catalyze the six-electron reduction of dinitrogen (N₂) to ammonia under mild biological conditions. Both protein components contain metal clusters which are redox active. When the two nitrogenase proteins are combined under turnover conditions, electrons are transferred among the various metal clusters and ultimately to the reducible substrate N₂. We are investigating the spectroscopic and electrochemical properties of various redox states in each protein component to determine their nature, their redox stoichiometry and how they are related to one another. Protein redox intermediates prepared by reaction with artificial redox reagents are being examined. Properties of the isolated FeMoco metal cluster component isolated from the MoFe protein are also being determined. A very low potential redox state of the Fe protein has been prepared which is more reduced than the dithionite-reduced state. This new species has redox reactivity in nitrogenase turnover and may represent an intermediate in the nitrogen reduction process.

Biological nitrogen fixation is a reductive biochemical process (1-3) carried out by the nitrogenase enzyme complex found in several species of microorganisms, which is responsible for the input of ammonia into the earth's nitrogen cycle. The overall reaction, which can be represented as: $N_2 + 8H^+ + 8e = 2NH_3 + H_2$, requires a considerable input of biochemical energy in the form of ATP and low potential reductant and is catalyzed by a protein complex composed (1-3) of the redox active iron protein (Fe protein) and the molybdenum iron protein (MoFe protein). The structure of the smaller and simpler Fe protein is known (4, Rees *et al.* chapter 11, *this volume*) and consists of an α_2 structure (MW = 65,000) containing a single Fe₄S₄ redox cluster bound between two subunits (5). This protein strongly binds ATP in both redox states of the Fe₄S₄ cluster (6) causing the redox potential of the Fe₄S₄ cluster to change in the presence of bound ATP. The iron protein with its ATP dependent redox potential has been proposed (7,8) as the source of low potential electrons for reducing the various clusters in the MoFe protein, which in turn reduce N₂ and other reducible substrates. The MoFe protein is much more complex (1-3) than the iron protein. It consists of an $\alpha_2\beta_2$ structure containing 2 Mo atoms, ≈ 30 iron

atoms, and about 30 S atoms. The large number of metals present suggested that a variety of metal clusters may be present and considerable spectroscopic (2,11,12), biochemical (13,15,16) and electrochemical (6,14,18) effort has gone into elucidating the number and type of clusters present, their redox properties and the protein ligands holding them in the MoFe protein. A total of six redox centers have been identified (2,12), consisting of two molybdenum and iron containing clusters (the FeMo cofactor) responsible for the $S=3/2$ EPR signal observed in reduced MoFe protein and p-clusters first identified (19,20) by Mossbauer spectroscopy. The structure of the MoFe protein has now been determined (9,10, Rees *et al.* chapter 11, Bolin *et al.* chapter 12, *this volume*) and consists of two EPR active, molybdenum containing metal clusters (the FeMoco centers, see below) and two p-clusters, each consisting of two Fe_4S_4 clusters bridged by two cysteine thiol ligands. The six oxidized centers arise from a one-electron oxidation of each of the two FeMoco centers and presumably from a single electron oxidation of each of the four Fe_4S_4 units comprising the two dimeric p-clusters.

The FeMo cofactor (FeMoco) (15) present in the MoFe protein can be isolated from the protein environment and studied (16) in NMF solution. When FeMoco is added to mutant proteins lacking this component, reactivity is restored (15,16). This restoration of reactivity establishes the viability of isolated FeMoco and suggests that its structure, and possibly some of its chemical reactivity (16), can be investigated in this isolated state in the absence of the other metal clusters present in the MoFe protein.

It is clear that a significant part of nitrogenase catalysis is centered around the interaction of MoFe protein and the Fe protein which together require ATP to mediate electron transfer from reductant through the two nitrogenase proteins. Once the MoFe protein is reduced, electrons are then transferred to substrate which is reduced and released. For a thorough understanding of the processes which occur during nitrogenase catalysis, it is necessary to identify the various clusters (12,17), determine their spectroscopic and electrochemical behavior (14,18) so that the electron transfer steps can be identified and followed during the course of substrate reduction. The description of the overall process in terms of which protein first accepts electrons from reductant, how electrons are transferred to other clusters, the role of ATP in these processes and what cluster (or clusters) binds substrate and finally transfers the electrons to the reducible substrates are important steps to be elucidated in understanding the nitrogen reduction process. As part of an ongoing effort (6,14,18) to investigate the steps outlined above, we have studied the electrochemical and spectroscopic properties of a number of redox states of both the Fe protein and the MoFe protein and have begun characterization of isolated FeMoco to aid in this overall process. We discuss here our recent redox and spectroscopic results which have been designed to determine the number and types of clusters present in the nitrogenase proteins and their associated redox properties.

Protein Purification and Physical Measurements.

In order to quantitatively determine the number of redox centers present in the MoFe and Fe proteins, their redox properties, their spectroscopic characteristics and the relationships between redox events and spectroscopic changes, precise electrochemical and spectroscopic measurements must be performed as the redox states of the metal clusters are systematically varied by chemical redox titrations or by electrochemical redox modifications (6,12,14). In conducting such titrations, three major sources of error are encountered (*see ref 11 for further details*), which must be controlled for a proper accounting of the metal clusters present. Imprecision can arise from: 1) inaccurate protein measurements and uncertain metal content of the protein; 2) the inability to precisely standardize the chemical oxidant or reductant used to stepwise vary the redox status of the metal centers in the protein and 3) the inherent error in the spectroscopic and electrochemical measurements. The procedures used here to control each of these variables are briefly outlined.

MoFe protein Purification and characterization. Because bacterial ferritin (typically containing 1000-2500 iron atoms, *ref*, 21) and other metalloproteins are low level contaminants even in crystallized MoFe protein, it is necessary to verify that the MoFe protein used is free of such contaminants. The variability in the reported iron and Mo content (2,11) of MoFe protein preparations and the occasional presence of other metal atoms (22) suggest the presence of such metal containing contaminants. The proposal (17) that apo MoFe protein (i.e. MoFe protein deficient in metal clusters) is present in some MoFe protein preparations requires careful evaluation of protein samples because protein measurements (Biuret, Lowry or amino acid analysis) under these conditions will not reflect the actual molar metal cluster concentration. The addition of standardized oxidant to protein samples deficient in metal clusters will result in oxidation of the remaining MoFe protein redox centers beyond that calculated and consequently, corresponding spectroscopic measurements under such conditions will represent higher oxidation levels than that calculated.

The MoFe protein used in this study has been purified by additional steps consisting of: 1) a second NaCl gradient on DEAE cellulose; 2) multiple crystallization steps (23,24) and 3) additional chromatography on 2.5 cm x 200 cm Ultrogel ACA 54 or Biogel A 1.5. These latter chromatography procedures cleanly separate MoFe protein from contaminating bacterial ferritin, the molybdenum storage protein and other metal containing proteins and yields purified, highly active MoFe protein with a constant metal content and presumably a full compliment of metal clusters present. A value of 5.3 ± 0.1 for the A_{280}/A_{400} ratio for MoFe protein containing 2 Mo and 29 ± 1.0 Fe atoms was found for the purified MoFe protein used in this study. Crystallized MoFe protein often had values as high or higher than 5.6, indicating the presence of other proteins absorbing at 280 nm. The Fe protein was further purified by steps (1) and (3) described above, contained 3.8-4.0 Fe atoms and possessed activities of 2100-2300 nmoles $H_2 \cdot min^{-1} \cdot mg^{-1}$. Protein measurements for both the MoFe and Fe proteins were determined by amino acid analysis and metal content was measured by inductively coupled plasma (ICP) and proton induced x-ray emission (PIXE) spectroscopy calibrated by using carefully prepared analytical standards or analytically pure model compounds. Specific activity measurements of the nitrogenase proteins as isolated and those oxidized by chemical oxidants were routinely determined. Table I summarizes

Table I. Properties of MoFe protein

MoFe Protein ^a	State of oxidation ^b	Specific activity (nMH ₂ /min/mg)	EPR (g=)
as isolated	dithionite	2200	4.3, 3.7, 2.0
IDS ^c	+3	2190	4.3, 3.7, 2.0
methylene blue	+6	2150	_____
[Co(Phen) ₃] ³⁺	+9	2100	2.0
[Co(Phen) ₃] ³⁺	+12	1990	_____

- a) Metal analysis: Mo=2.0; Fe=29±1.0; S=32±2.
 b) Measured by microcoulometry.
 c) IDS is indigodisulfonate.

the specific activities, metal content and other characteristics of purified MoFe protein.

The iron molybdenum cofactor (FeMoco) was isolated by the Shah and Brill method (15) and further purified and characterized as described (25). The EPR silent state was prepared by self oxidation (32) or by anaerobic oxidation by oxidized methyl

viologen. Methylene blue was used as an oxidant to attain even higher states of oxidation.

Oxidants and Reductants. Various organic redox reagents were purified and standardized optically or electrochemically as previously described (18). Stephens (11) reported that $[\text{Co}(\text{phen})_3][\text{ClO}_4]_3$ is an effective oxidant of the metal clusters in the MoFe protein. We have used this reagent to oxidize the clusters in the MoFe protein and also as a precise internal standard for confirming the extent of oxidation of the clusters present in the MoFe protein. This was done by: 1) adding a known amount of standardized $\text{Co}(\text{phen})_3^{3+}$ to the standardized MoFe protein to produce a known level of oxidation; 2) recording the desired electrochemical or spectroscopic information and 3) performing ICP or PIXE analysis on the sample to determine the Co/Mo or Co/Fe ratios and confirm the degree of oxidation. For reductive reactions, specially prepared, reduced methyl viologen (26) free of other redox byproducts was added to MoFe protein previously oxidized by $\text{Co}(\text{phen})_3^{3+}$.

Electrochemical and Spectroscopic Methods. EPR, optical and circular dichroism measurements were carried out as previously described (6,14,18). Quantitation of various redox states of the Fe protein and the MoFe protein was determined by microcoulometry (27). This technique easily measures nanomoles of charge transferred to the oxidized nitrogenase proteins with an uncertainty of less than 2%.

Results and Discussion

The correlation of spectroscopic properties with changes in the redox status has been an important approach (2,12,14,18) in determining the number and type of redox centers present in the MoFe protein. Here, we discuss the electrochemical and corresponding spectroscopic results in three areas of nitrogenase research: the MoFe protein, the FeMo cofactor and the Fe protein.

MoFe Protein Electrochemical and Spectroscopic Results.

Extensive Mossbauer and EPR measurements have been interpreted (2,12,17,28) in terms of two types of centers present in the MoFe protein: 1) two EPR active centers giving rise to the known $S=3/2$ EPR signal of reduced MoFe protein and 2) p-clusters now known (9,10, Rees et al. chapter 11 and Bolin et al., chapter 12, this volume) to consist of two Fe_4S_4 clusters bridged by two cysteine sulfur atoms which are not EPR active but which have distinct Mossbauer spectra. Stepwise oxidation of the MoFe protein combined with spectroscopic monitoring of the metal cluster properties suggested that a four equivalent oxidation of the MoFe protein occurred before the two EPR centers were oxidized by addition of the fifth and sixth oxidation equivalents (2,12). These results established that the metal clusters in the MoFe protein can be oxidized by a total of six electrons. In view of the structural results now reported, this initial four electron oxidation of the MoFe protein likely occurs by a single electron oxidation at each of the four Fe_4S_4 cluster components comprising the two dimeric p-clusters. A single electron oxidation of each of the two remaining EPR centers then accounts for the total of six redox centers present in the MoFe protein.

While the above results are consistent with the reported structural results and are overall intuitively satisfying, there are other reports which suggest that an overall six electron oxidation of the MoFe protein can occur with a different oxidation sequence of the metal clusters. Stephens (11) has stepwise oxidized MoFe protein and has reported that both EPR and circular dichroism measurements which suggest a three electron oxidation occurs before the EPR centers are oxidized. We have also reported (14,40) EPR and optical spectroscopic measurements consistent with a three electron oxidation of MoFe protein before the EPR centers react. Electrochemical reduction measurements of oxidized MoFe protein shown in Figure 1 have confirmed (14) the

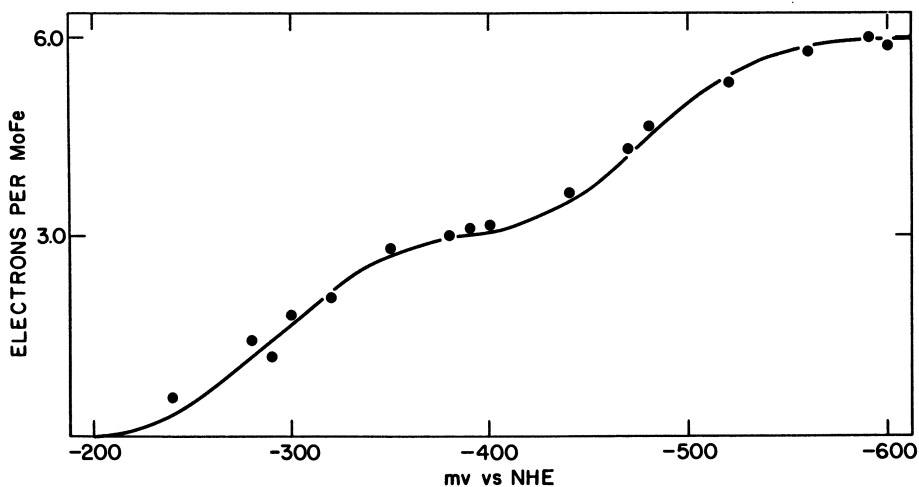


Figure 1. Microcoulometric reduction of six-electron oxidized MoFe protein. The solid line is fit by the Nernst Equation for $E_{1/2}$ values of -290 and -480 mv with $n=1$ for both reactions.

presence of six oxidized clusters but have shown that the reduction of the clusters occurs at two distinct electrochemical potentials, with a three electron reduction occurring at each redox step. The more positive reduction step requires (14) three electrons to fully reduce the two oxidized EPR centers and indicates that another redox center is being coincidentally reduced at the same potential as the FeMo cofactor centers. The two reduction regions in Figure 1 are close together and this third redox center associated with reduction of the EPR centers could be reduction of one of the p-cluster components occurring at a slightly more positive potential than the remaining three. Several possible factors could be responsible for the shifting of this potential. Solution conditions (i.e., salt concentrations) are known (14) to alter the redox properties of the MoFe protein and may shift the potential of this p-cluster component. Another possibility is that the $\alpha_2\beta_2$ MoFe protein could express allosteric behavior (the p-clusters are at the α - β subunit interface) and as oxidation proceeds, the redox potential of the p-cluster components could change more positively with oxidation until the last one is overall more positive than the remaining three. Finally, although the electrochemical measurements just described (18) are very reproducible and appear to conform to Nernstian processes, they have the complication of not being strictly electrochemically reversible. The oxidation potentials for the six reduced metal clusters are well defined but differ (18) by over 200 mv from the reduction potentials of the oxidized metal clusters, indicating that thermodynamic equilibria among the clusters may not be established and that kinetic and not thermodynamic effects may be governing the course of the reaction. Protein structural changes, changes in coordination number or ligand type binding the clusters to the protein or changes in cluster shape upon reduction or oxidation may be factors in causing this irreversibility. Whatever is the cause of this non reversible behavior, one of the four remaining clusters is behaving differently from the other three and it is of interest to understand this aspect of the p-cluster reactivity of the MoFe protein in more detail.

One approach we have used to further investigate the metal cluster behavior of the MoFe protein is to determine if the protein bound FeMoco centers can be further oxidized beyond the EPR silent state and if the p-clusters can attain a higher level of oxidation than already observed. Initial studies (18,30) using this approach have found that at least one more electron can be removed from each of the clusters present in the MoFe protein, suggesting that each cluster type can be oxidized by two electrons. Organic oxidants were initially used (18,30) but here we have utilized Co(phen)_3^{3+} which more conveniently and reproducibly oxidizes the metal clusters to their two-electron oxidized states. Using this oxidant, the MoFe protein can be oxidized by a total of twelve electrons without losing any of its initial activity (Table I). Microcoulometric reduction of twelve-electron oxidized MoFe protein occurs at the same potentials (14,18,30) as shown in Figure 1 but with a total of twelve electrons being required with $n=2$ values instead of the $n=1$ behavior measured for the reduction steps in Figure 1. By controlling the time of reaction and the Co(phen)_3^{3+} /MoFe protein ratio, a redox state can be formed which has undergone a nine-electron oxidation. This oxidation state was previously reported (18,30) using various organic and protein oxidants and is also likely to be that state originally produced by Stephens (11) when describing the Co(phen)_3^{3+} oxidation of MoFe protein. Reduction of this nine-electron oxidized protein proceeds in two reduction steps: one at -290 mv requiring six electrons with $n=2$ and another at -480 mv with $n=1$ requiring a total of three electrons. The $n=2$ values are interpreted as a two electron reduction step of the individual oxidized cluster states.

Table I summarizes the results of these electrochemical measurements and also describes the EPR states observed. An EPR signal at $g=2$ was observed for the nine-electron oxidized MoFe protein, which was also reported by Stephens (11). In neither the nine- or twelve-electron oxidized MoFe protein have we observed the $S=7/2$ spin state reported (31) for thionine oxidized MoFe protein, which was suggested to arise from excited states of the p-clusters. The absence of the $S=7/2$ state in our samples

may be a result of the $S=7/2$ EPR signal arising from a transient state because the formation of the nine- and twelve-electron oxidized MoFe protein reported here were isolated only after at least a 30 min reaction interval.

Taken together, the electrochemical results show that the MoFe protein has a rich redox capacity arising from at least six redox clusters which can undergo either a one or a two electron redox reaction. The redox results show that each of the two FeMoco redox centers present in the MoFe protein can undergo a one- (to the EPR silent state) and a two-electron oxidation and predict that the isolated FeMoco can be oxidized by two electrons, results reported next for the isolated FeMoco. Our results also indicate that each of the two p-clusters can be oxidized by two or four electrons each. If viewed in terms of each of the two Fe_4S_4 clusters comprising the p-cluster, then each Fe_4S_4 component can be oxidized independently by one or two electrons. This extent of oxidation of the p-clusters supports the possibility of all ferrous Fe_4S_4 clusters comprising the p-clusters.

The FeMo Cofactor. The above results on the electrochemical properties of the MoFe protein are a consequence of the oxidation of the individual FeMoco clusters and the p-clusters present in the MoFe protein. The result that each FeMoco cluster in the protein can be oxidized by one or two electrons indicates that the FeMoco can exist in at least two well defined oxidation states. Does the FeMo cofactor in its isolated state in NMF solution undergo the same behavior observed for the FeMoco when bound in the MoFe protein?

In its isolated state in NMF solution, the FeMo cofactor is EPR active in the presence of dithionite, a condition that corresponds to the EPR active reduced state in the protein. Electrochemical studies (32) have shown that oxidized and EPR silent FeMoco in NMF solution undergoes a well defined one-electron reduction, per molybdenum atom, to the EPR active state. Thus, there is an overall one to one correspondence between the redox properties of the isolated FeMoco in NMF solution and that for the same cluster in the protein for a one electron oxidation process.

In view of the results reported above for a two-electron oxidation of the clusters within the MoFe protein, and the correspondence between the FeMo center in the protein and isolated free in solution, it is likely that higher oxidation states of FeMoco exists in NMF solution and that a two-electron oxidized state exists. Direct electrochemical measurements in NMF would be the preferable method to evaluate FeMoco redox properties and to determine the redox stoichiometry, but such electrochemical measurements are only being developed (32) and are quite difficult to carry out on a routine basis. An alternate but less direct approach is to determine the charge for isolated FeMoco species in various oxidation states and then to correlate charge differences of the FeMoco species to infer information about the electrochemical processes relating them.

We have begun characterizing (25,33) FeMoco prepared in the presence of various oxidants and measuring the reduction stoichiometry of these oxidized FeMoco states. One property of FeMoco that is poorly defined but which is relevant to understanding its redox nature is the sign and magnitude of the overall charge of FeMoco. The charge of FeMoco in solution, initially in some well defined redox state (for example, EPR silent or EPR active), should change in magnitude with changes in its redox status. If the overall charge on FeMoco does not change predictably with reduction or oxidation, then charge compensation processes are likely to be occurring which may be associated with the redox event. Charge compensation process could arise from proton equilibria between the two redox states or ion pair formation involving univalent metal ions such as Na^+ and the two redox states of the FeMoco involved in the redox reactions. Therefore, measurements of the FeMoco charge as a function of the redox state of FeMoco could provide information on the reactivity and redox reactions of FeMoco.

The charge of FeMoco in NMF solution was measured (25) conveniently by adding a 10-100-fold excess of a Na, K, Rb or Mg salt to an NMF solution of purified

FeMoco, passing this mixture through an anaerobic 0.5x30 cm Sephadex G-25 column equilibrated in pure NMF and measuring the M/Mo ratio of the emerging FeMoco solution. During passage through the column, the FeMoco separates from the excess salt taking with it the required number of cations equivalent to its overall negative charge. By measuring the M/Mo ratio of the emerging FeMoco, the charge per Mo of FeMoco is determined.

Table II summarizes the charges which we have measured for FeMoco samples in various states of oxidation. Electrochemical

Table II. The charges determined for various FeMoco species by G-25 Sephadex chromatography in NMF solution

oxidation state ^a	M ⁺ /Mo ^b	Species
MV or dithionite	3.0	[MoFe ₆ S ₆] ₂ ⁶⁻
Self-oxidized	2.0	[MoFe ₆ S ₆] ₂ ⁴⁻
MB-oxidized	1.0	[MoFe ₆ S ₆] ₂ ²⁻
Model	1.5	[Mo ₂ Fe ₆ S ₈ (SEt) ₉] ³⁻

a) MV is methyl viologen; MB is methylene blue.

b) M is Na, K, Rb. Mg²⁺ was also used giving Mg/Mo values 1/2 those reported.

reduction of self-oxidized (32) FeMoco was found to undergo a one-electron reduction per molybdenum (32) to form the EPR active state. As seen in Table II, the EPR active FeMoco has a charge exactly one unit more negative per molybdenum atom than the oxidized, EPR silent state. The FeMoco species are shown in Table II as dimer structures consisting of two molybdenum atoms per FeMoco unit, and consequently the overall charges differ by two units per dimeric unit. This dimeric structure of FeMoco was suggested (25) from MW measurements using various molecular sizing columns run in NMF and NMF-DMF mixtures.

Table II further shows that another FeMoco species can be formed by further oxidizing the EPR silent state, producing an oxidized FeMoco species whose overall charge per Mo is two units less than the EPR silent state. This state corresponds to the FeMoco cluster in the MoFe protein oxidized by two electrons, as discussed in the previous section. Thus, a series of FeMoco species is formed, members of which differ by one charge per molybdenum atom and which correspond to the various FeMoco oxidation states observed in the FeMo protein (18,30). The results reported here suggest that the redox reactions interconverting these various states of FeMoco are quite straightforward, and not complicated by charge compensation processes. Direct electrochemical measurements for all of these predicted redox interconversions in Table II are important in fully establishing the correspondence of redox properties between isolated FeMoco in NMF solution and that for FeMoco bound in the protein environment. Such measurements along with corresponding spectroscopic measurements should improve our understanding of the isolated FeMoco in solution.

Fe protein. The iron protein is an Fe₄S₄-containing, redox-active protein whose cluster redox potential is sensitive to the presence of ATP and ADP (1-3,6). The cluster is known to exist in the reduced EPR active Fe₄S₄¹⁺ state and to undergo oxidation to the EPR silent Fe₄S₄²⁺ state. This redox couple is thought to be functional in nitrogenase turnover and a detailed scheme (7,8) for repeated one-electron

cycles of the Fe protein with the MoFe protein has reportedly simulated the nitrogenase substrate reduction behavior.

Although most results of the Fe protein are consistent with it being only a one electron reducing agent, some results have been reported (34,35) which suggest a two electron transfer by the Fe protein may be possible.

The turnover potential of nitrogenase has been measured by two groups (34,35) using independent methods and both find a well defined response of nitrogenase turnover with increasingly negative potentials. Analysis of the variation of specific activity of nitrogenase with potential variation shows that the nitrogenase catalytic reactivity can be fit to a Nernstian process with an $E_{1/2}$ value of -460 mv, but quite interestingly, with an $n = 2$ value. Because the Fe protein is thought to be the electron transfer agent to the MoFe protein, a question arises concerning the relationship of the observed nitrogenase turnover parameters and the actual redox properties of the Fe protein under turnover conditions. Is the Fe protein behaving as a two electron reductant during nitrogenase turnover or are the other two electron requiring clusters observed in the MoFe protein discussed above functioning as two electron centers during nitrogenase turnover? Thorneley and Lowe (7,8) argue that the $n=2$ behavior observed for nitrogenase turnover need not be associated with the Fe protein and still favor a one electron transfer role for the Fe protein.

More direct results have been reported (36), which indicate a two electron transfer ability of the Fe protein, but the valence changes occurring in the cluster to provide two electrons were not specified. Although this observation is of interest with regard to the nitrogenase turnover discussed above, little support for such a two electron transfer step has been forthcoming.

One other interesting, but unusual, property of the Fe protein is that it catalytically destroys any dithionite present in solution and spontaneously oxidizes to its EPR silent state (6,37). This behavior has been confirmed and analysis of the decomposition products has been reported (38). Just how the metal cluster enters into this dithionite decomposition reaction remains to be fully elucidated.

In an attempt to determine if the Fe protein undergoes a one or a two electron transfer reaction and also to determine if the dithionite decomposition reaction is a consequence of an unusual Fe_4S_4 valence state, we examined the reaction of reduced but dithionite free Fe protein ($Fe_4S_4^{1+}$) with reduced MV (26). The results indicate (39) that except for an initial small decrease in MV concentration, this reductant was not decomposed by reduced Fe protein. Thus, the destruction of dithionite ion by the Fe protein is a consequence of some property of dithionite itself and not a general reductant dependent phenomenon. The initial decrease in the concentration of reduced MV indicates that perhaps the Fe protein is further reduced by the MV reductant.

To test this possibility, microcoulometric measurements of reduced Fe protein ($Fe_4S_4^{1+}$) were carried out as shown in Figure 2. These results confirm that a MV-mediated, one-electron reduction of the Fe protein occurs with a midpoint potential of -460 mv, a value coincident with the turnover potential of nitrogenase. Reduction of Fe protein in the $Fe_4S_4^{2+}$ state required a one-electron reduction at -310 mv and a second one electron reduction step at -460 mv, consistent with the prediction of Figure 2. Reduction of the Fe protein in the $Fe_4S_4^{2+}$ state establishes that the result shown in Figure 2 is not a result of inadvertent oxidation.

Figure 3 shows that exhaustive reduction by MV produces reduced Fe protein with no EPR signal in the $g = 2$ region. Stepwise oxidation with indigodisulfonate (IDS) causes the EPR signal to develop with added IDS until at one equivalent, a fully developed EPR signal is observed which corresponds to the Fe protein in the $Fe_4S_4^{1+}$ state. Optical titration of the MV-reduced Fe protein shows that two equivalents of IDS are required to produce Fe protein in the EPR silent, $Fe_4S_4^{2+}$ state. The microcoulometric, EPR and optical results suggest that the MV reduced Fe protein in the absence of dithionite forms the $Fe_4S_4^0$ cluster state. This proposed all ferrous state

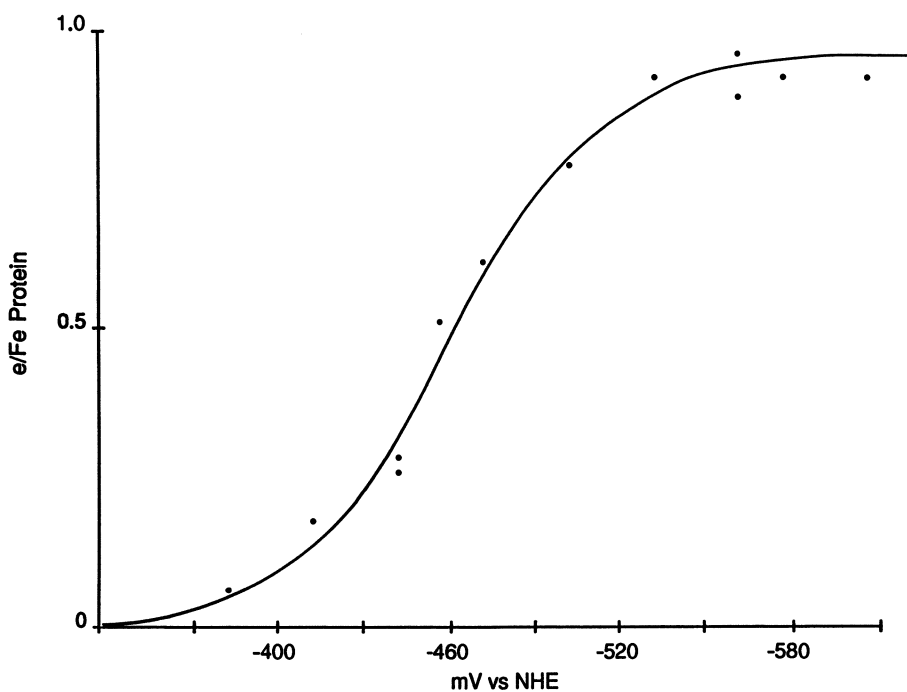


Figure 2. Microcoulometric reduction of Fe protein ($\text{Fe}_4\text{S}_4^{1+}$) at pH 8.0 with MV as mediator. An $E_{1/2}$ value of -460 mV and an $n=1$ value were obtained from fitting the data to the Nernst Equation.

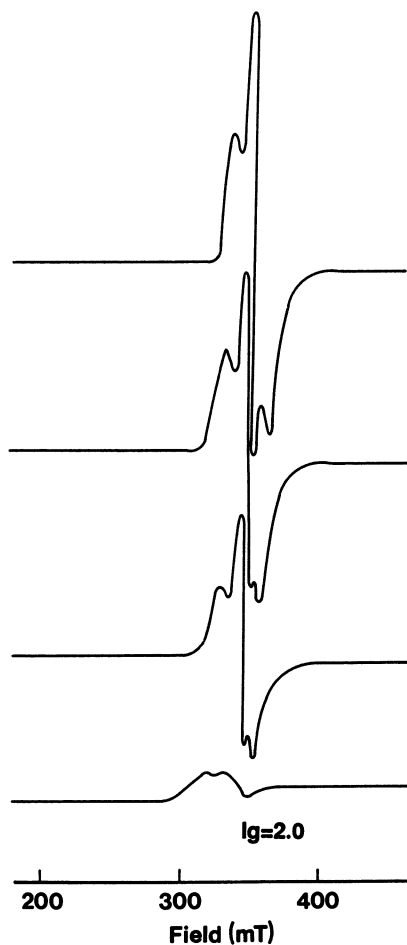


Figure 3. Oxidative EPR titration of MV-reduced Fe protein at 12 K with indigodisulfonate. The bottom spectrum results from the Fe protein reduced with excess MV and separated from the excess reductant by anaerobic G-25 Sephadex chromatography. The ascending spectra result from 0.5, 0.75 and 1.0 equivalents of added oxidant, respectively.

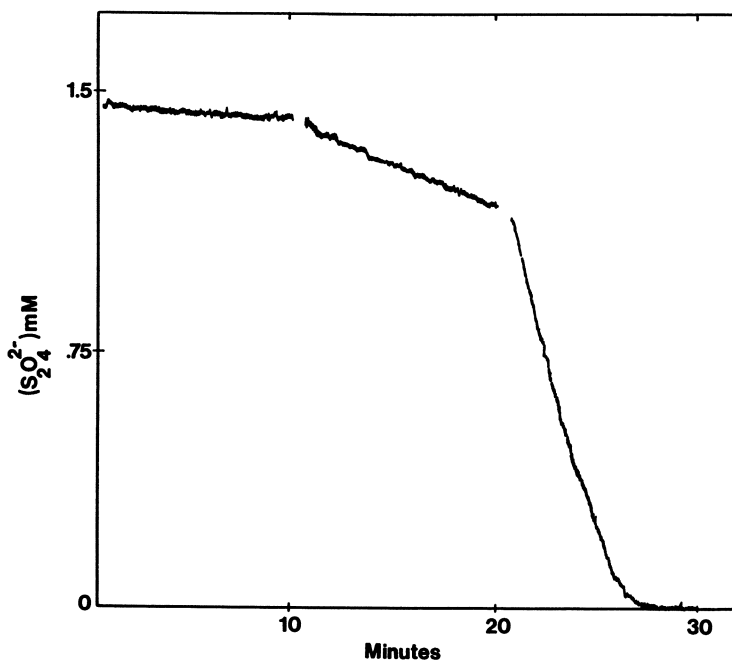


Figure 4. The rate of anaerobic dithionite decomposition. The left curve is 0.45 mM dithionite in 0.025 M Tris pH 8.0 contained in a 1 cm anaerobic quartz cell and monitored at 350 nm. The middle curve results from the same dithionite concentration but in the presence of 0.12 mM Fe protein. The curve on the right results from the same conditions as in the middle curve except 0.1 mM MV is added.

has not been reported before in a biological molecule nor obtained as a crystalline solid from inorganic model compound studies.

Having concluded that an Fe_4S_4^0 cluster can form in the Fe protein, we next consider if this state has any relevance to the dithionite decomposition reaction known (37) to be catalyzed by the Fe protein. Figure 4 summarizes a series of measurements which determine the rate of decomposition of dithionite only, dithionite in the presence of Fe protein and dithionite in the presence of Fe protein and MV. Figure 4 clearly confirms previous (37) results that the Fe protein catalyzes the destruction of dithionite. What is surprising is the dramatic effect that the presence of both MV and Fe protein have on this decomposition process. These results suggest that the Fe_4S_4^0 cluster state plays a significant role in this dithionite destruction process.

We propose that small amounts of Fe_4S_4^0 are formed slowly in dithionite solution by SO_2^- reduction of Fe protein ($\text{Fe}_4\text{S}_4^{1+}$) to form Fe protein in the Fe_4S_4^0 state. The Fe_4S_4^0 then interacts with dithionite directly (or some other oxy sulfur species, i.e. SO_3^{2-}) and disproportionates it into SO_3^{2-} , $\text{S}_2\text{O}_3^{2-}$ and other known decomposition products (38). This process continues until all dithionite is decomposed. The accelerating effect of MV shown in Figure 4 results from the more rapid formation of Fe protein to the Fe_4S_4^0 state in the presence of MV, relative to dithionite alone. Such an explanation is consistent with the observations that only the dithionite reductant promotes its own destruction reaction and that the Fe protein is completely stable in the presence of excess MV in its Fe_4S_4^0 form. The preparation of this proposed all ferrous cluster in reduced Fe protein is important with regard to the various redox reactions that the Fe_4S_4 cluster in the Fe protein can carry out. Preliminary results (39) suggest that the Fe protein in the Fe_4S_4^0 cluster state is functional in nitrogenase catalysis and additional studies are underway (39) to further characterize this redox state.

Acknowledgments. This research was supported by grant number 90-37120-4201 to GDW from The United States Department of Agriculture Competitive Research Grants Program in Nitrogen Fixation.

Literature Cited.

1. Mortenson, L.E.; Thorneley, R. N. F. *Ann. Rev. Biochem.* **1979**, *48*, 387.
2. Orme-Johnson, W. H. *Ann. Rev. Biophys. Biophys. Chem.* **1985**, *419*, 14.
3. Smith, B. E.; Eady, R. *Eur. J. Biochem.* **1992**, *205*, 1
4. Georgiadis, M. M.; Komiya, P.; Chakrabarti, P.; Woo, D.; Kornuc, J.; Rees, D. C. *Science*. **1992**, *257*, 1653.
5. Hausinger, R. D.; Howard, J.B. *J. Biol. Chem.* **1983**, *258*, 13486.
6. Watt, G. D.; Wang, Z. C.; Knotts, R. R. *Biochemistry*, **1986**, *25*, 8156.
7. Lowe, D. J.; Thorneley, R. N. F. *Biochem. J.*, **1984**, *224*, 895.
8. Thorneley, R. N. F.; Lowe, D. J. In *Molybdenum Enzymes*, Spiro, T. G. , Ed., John Wiley: N. Y., N.Y., 1985, p. 221.
9. Bolin, J. T.; Ronco, A. E.; Mortenson, L. E.; Morgan, T. V.; Williamson, M.; Xuong, N.H. In *Nitrogen Fixation: Achievements and Objectives*, Gresshoff, P. M.; Roth, , L. E.; Stacey, G.; Newton, W. E., Eds. Chapman and Hall, N. Y. 1990, p. 117.
10. Kim, J.; Rees, D. C. *Science*, **1992**, *257*, 1677.
11. Stephens, P. J. In *Molybdenum Enzymes*, Spiro, T. G. , Ed., John Wiley: N. Y., N.Y., 1985, p. 221.

12. Orme-Johnson, W. H.; Davis, L. C.; Henzl, M. T.; Averill, B. A.; Orme-Johnson, N. R.; Munck, E.; Zimmerman, R. *In Recent Developments in Nitrogen Fixation*, Newton, W. E.; Postgate, J.R.; Rodriguez-Barrueco, C., Eds., Academic Press, N. Y. 1977, p. 131.
13. Brigle, K. E.; Setterquist, R.A.; Dean, D.R.; Cantwell, J.S.; Weiss, M. C.; Newton, W. E. *Proc Natl. Acad. Sci. USA*. 1987, 84, 7066.
14. Watt, G. D.; Burns, A.; Lough, S.; Tennent, D. L. *Biochemistry*, 1980, 21, 4926.
15. Shah, V. K.; Brill, W. J. *Proc. Natl. Acad. Sci. USA*. 1977, 74, 3249.
16. Burgess, B. K. *Chem. Rev.* 1990, 90, 1377.
17. Zimmerman, R.; Munck, E. Brill, W. J.' Shah, V. K.; Henzl, J. Rawlings, J.; Orme-Johnson, W. H. *Biochim. Biophys. Acta.*, 1978, 537, 185.
18. Watt, G. D.; Wang, Z. C. *Biochemistry*, 1989, 28, 1844.
19. Smith, B. E.; Lang, G. *Biochem. J.*, 1974, 137, 169.
20. Smith, B. E.; O'Donnell, M. J.; Lang, G. *Biochem. J.* 1980, 191, 449 .
21. Watt, G. D.; Frankel, R. B.; Papaefthymiou, G. C.; Spartalian, K.; Stiefel, E. I. *Biochemistry*, 1986, 25, 4330.
22. Lowe, D. J.; Smith, B. E.; Eady R. *In Recent Advances in Biological Nitrogen Fixation*, Subba Rao, N. S., Ed. Oxford & IBH Publishing Co. New Dehli, 1984, 163.
23. Shah, V. K.; Brill, W. J. *Biochim. Biophys. Acta*. 1973, 305, 445.
24. Burgess, B. K.; Jacobs, D. B.; Stiefel, E. I. *Biochim. Biophys. Acta.*, 1980, 614, 196.
25. Huang, H.; Kofford, M.; Simpson, F. B.; Watt, G. D. *Inorg. Biochem.* 1993, in press.
26. Corbin, J. L.; Watt, G. D. *Anal. Biochem.* 1990, 186, 86.
27. Watt, G. D. *Anal. Biochem.* 1979, 99, 399.
28. Orme-Johnson, W. H. Chapter 17, this volume.
29. Watt, G. W. Burns, A; Tennent, D. L. *Biochemistry*, 1981, 20, 7272.
30. Watt, G. D.; Burns, A. Lough, S. in *Nitrogen Fixation, Vol I*, Newton, W. E.; Orme-Johnson, W. H. Eds., University Park Press, Baltimore, MD, 1978, p. 154.
31. Hagen, W. R.; Wassnik, H.; Eady, R. R.; Smith, B. E.; Haaker, H. *Eur. J. Biochem.* 1987, 69, 457.
32. Shultz, F. H.; Gheller, S. F.; Burgess, B. K.; Lough, S.; Newton, W. E. *J. Am. Chem. Soc.*, 1985, 107, 5364.
33. Lough, S. M.; Jacobs, D. L.; Lyons, D. M.; Watt, G. D.; J. W. McDonald, J. W. *Biochem. Biophys. Res. Comm.*, 1986, 139, 740 .
34. Lough, S.; Burns, A.; G. D. Watt, G. D. *Biochemistry*, 1983, 22, 4062 .
35. Hallenbeck, P. *Arch. Biochem. Biophys.* 1983, 220, 657.
36. Braadsma, A.; Haaker, H.; Grande, H. J.; Veeger, C. *Eur. J. Biochem.*, 1982, 121, 483 (1982).
37. Stephens, P. J.; McKenna, C. E.; McKenna, M. C.; Nguyen, H. T.; Morgan, T. V.; Devlin, F. *In Current Perspectives in Nitrogen Fixation*, Gibson, A. H.; Newton, W. E., Eds., Australian Academy of Sciences, Canberra, Australia, 1981, p. 357.
38. McKenna, C. E.; Menard, D.; Dao, C. J.; Stephens, P. J.; McKenna, M. C. *In Nitrogen Fixation: Hundred Years After*, Bothe, H.; deBruijn, F. J.; Newton, W. E., Eds. Gustav Fisher, N. Y. 1988, p. 131.
39. Watt, G. D.; Reddy, K. R. N. *Inorg. Biochem.* 1993, in press.
40. Euler, W. B.; Martinsin, J.; McDonald, J. W.; Watt, G. D. *Biochemistry*, 1984, 23, 3021.

Chapter 17

The Molybdenum–Iron Protein of Nitrogenase

Structural and Functional Features of Metal Cluster Prosthetic Groups

W. H. Orme-Johnson

Department of Chemistry, Massachusetts Institute of Technology,
Cambridge, MA 02139

Current proposals for structures of the two recognized types of metal-sulfur clusters in nitrogenase are compared to chemical and spectroscopic evidence in hand. It appears that the P-clusters are pairs of linked Fe_4S_4 cubes, and the most reasonable interpretation of the oxidation state of the resting enzyme, prior to ATP-coupled injection of electrons from the Fe protein, suggests that the Fe atoms are all *ferrous*, making it appear that electrons added to such clusters would create a strongly reducing entity in the protein, and further suggesting that the P-clusters donate reducing equivalents to the M (cofactor) clusters, the presumed locale of a dinitrogen reduction. The reported trigonal geometry of six of the Fe atoms in the M centers immediately suggests that these have bound hydride unseen in the crystal structure. Enzyme turned over with ATP and reductant, in D_2O , failed in initial experiments to yield EPR evidence for the expected strongly coupled deuterons. If the resting state has a powerful reductant (native P-clusters) and a H^+ -reducing site (M-centers) one has to suppose that ATP facilitates the transfer of e^- *between* these centers, in addition to the already observed binding of ATP to the Fe protein component of nitrogenase.

Nitrogenase, the enzyme responsible for the ATP-driven reduction of N_2 to NH_3 , catalyzes the reaction:



This process is evidently energy-prodigal and involves air-sensitive components (as expected, that which will reduce N_2 will react readily with O_2), as well as being the result of the actions of at least twenty gene

products (Review: 1). Fortunately for the bioinorganic chemist, nitrogenase is a rather languid catalyst, so that rapidly growing nitrogen-fixing bacterial cells must have 1-5% of their cell protein in the form of this enzyme, somewhat making up for the not inconsiderable lack of joy occasioned by the need for anaerobic Schlenk procedures in essentially every phase of nitrogenase research.

The enzyme is composed of two proteins, the Fe Protein (54Kd dimer, containing a single Fe_4S_4 center) and the MoFe protein (240 Kd α_2, β_2 , with 30 Fe and 2 Mo atoms) (1) which act in concert. The process is only derepressed in cells starved of a ready source of fixed nitrogen. The striking requirement for MgATP, in a process that is overall already spontaneous, under typical cellular conditions, is of great current interest. The need for ATP obviously derives from the endoergonic nature (2) of the *initial* step in the reduction of dinitrogen (Figure 1). Early on, we were able to demonstrate (3) that the overall process is as shown in Figure 2.

Mechanisms. Thorneley and Lowe, building on an extensive analysis of steady state and pre-steady state kinetic data, subsequently hypothesized (4) that the molecular mechanism of nitrogenase action involves two interlocking cycles (Figure 3). In this model E_0 through E_7 represent successively reduced states of the MoFe protein, while the triple sets of arrows between the E_n states depict the action of the Fe protein cycle as the ATP-driven electron transfer into the MoFe protein.

Note that a key feature of this diagram is that NH_3 is released prior to the final two electron-transfer cycles, i.e., at least some ATP hydrolysis can have no direct connection to N_2 reduction. This hypothesis further directs attention to the concept of the enzyme nitrogenase as catalyzing the functional reverse of oxidative phosphorylation, i.e. using ATP hydrolysis to create intermediate states, which store low-potential reducing equivalents, rather than a role for direct ATP- N_2 interaction.

Clusters. As referred to below, we made Mössbauer measurements on reversibly oxidized MoFe protein to show that the twenty to thirty iron atoms were disposed into clusters: two M-centers, corresponding (5) to the cofactor originally extracted by Shah and Brill (6), and four P-clusters (7), which were ultimately deduced from the Mössbauer parameters to be organized into two pairs (8) with each half of the pair differing slightly from the other. Using thiophenol to replace the protein thiols, the P-clusters can be extruded from the MoFe protein as individual Fe_4S_4 cubanes. According to their behavior during redox titrations, the pairs of clusters are strongly interacting. In contrast, the unperturbed EPR spectrum of the M-centers suggested that they were far enough apart ($>10\text{\AA}$) so as to give no indications of magnetic interactions. Recently, we observed an integer spin EPR

Energy Profile for N₂ Reduction

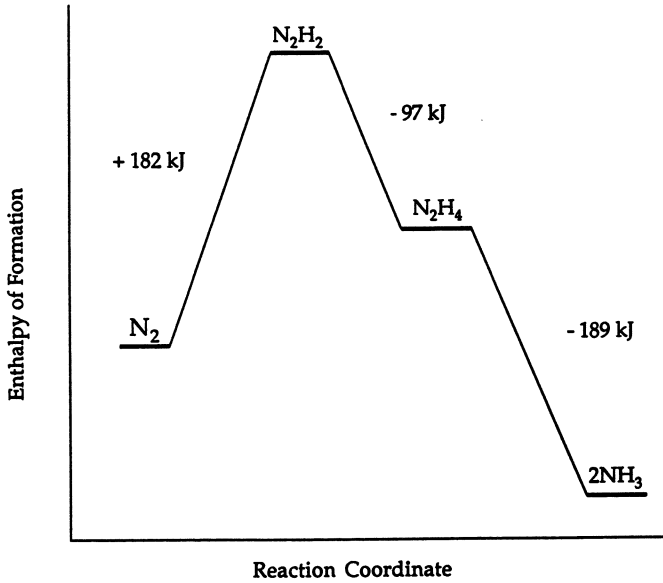


Figure 1 Thermodynamics of dinitrogen reduction. Data from (2). (Courtesy of David Wright).

Overall Nitrogenase Mechanism

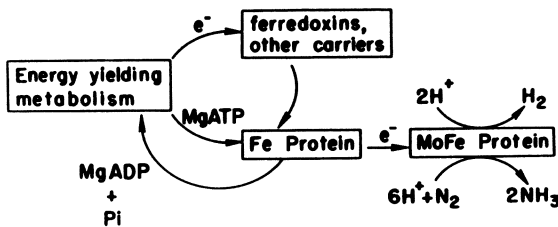


Figure 2 Overall mechanism of nitrogen fixation. (Reproduced with permission from reference 1. Copyright 1985 Annual Reviews, Inc.)

signal originating from a MoFe protein sample from which 2e-/P-cluster pair had been removed, thus proving the presence of 2e-/8Fe electron transfer units (9).

Structures. In an initial crystallographic analysis, an interpretation of 5Å data taken with two x-ray wavelengths allowed Bolin to suggest the following arrangement (Figure 4) of clusters in the MoFe protein from *Clostridium pasteurianum* (*Cp*) (10). Recently, Bolin further proposed that the P-clusters are two Fe₄S₄ centers joined with a common hexavalent corner S atom, some 19Å from FeMoco and 70Å from the symmetrically disposed pair across the two-fold axis (ACS Meeting, Washington, D.C. August 23-25, 1992); see also Chapter 12 for a different interpretation of the data. Our spectroscopic findings referred to above are entirely consistent with the general crystallographic disposition of the clusters, although it is not apparent that the sulfur bridged P-cluster structure of Bolin would yield Fe₄S₄ cubes on treatment with thiophenol.

Our understanding of the intimate structure of the MoFe protein was dramatically enhanced by an atomic-resolution structure proposed by Kim and Rees (11) for the enzyme from *Azotobacter vinelandii* (*Av*). On the basis of sequence homology and spectroscopic parameters, the MoFe proteins of *Cp* and *Av* are identical at the level of the cofactor structure and the chemical mechanism of N₂ reduction. While the two reported structures agree on the general organization of the M-centers and P-cluster pairs, Kim and Rees propose that the P-clusters are Fe₄S₄ cubes bridged in pairs by cysteine thiolate ligands coordinating to two Fe atoms. Such a structure is in agreement with the cluster extrusion experiments.

They also propose the following structure (Figure 5A) for the FeMo cofactor. Figure 5B shows a structure we hypothesize to be the N₂ adduct (c.f. an earlier proposal; 12), based on Kim and Rees' crystallographic data).

Bolin has also proposed a structure of the cofactor which is similar in many features but has in addition a hexavalent S atom within the Fe cage which converts the three-coordinate peripheral Fe atoms to four coordinate (ACS Meeting, Washington, DC, August 23-25, 1992); more recently (AAAS meeting, Boston, February 13, 1993), Bolin stated that newer interpretations of this data agree exactly with Kim and Rees' work; see also Chapter 12.

Previous studies have established that the M-centers yield extractable cofactors when the protein is appropriately unfolded (5,12,13). We have published a highly efficient methodology for such extractions. When the MoFe protein is adsorbed onto DEAE-cellulose and the aqueous buffer is exchanged for DMF or other organic solvents, organic salts (e.g. Et₄N⁺C1⁻) can be used to disrupt the ionic interactions

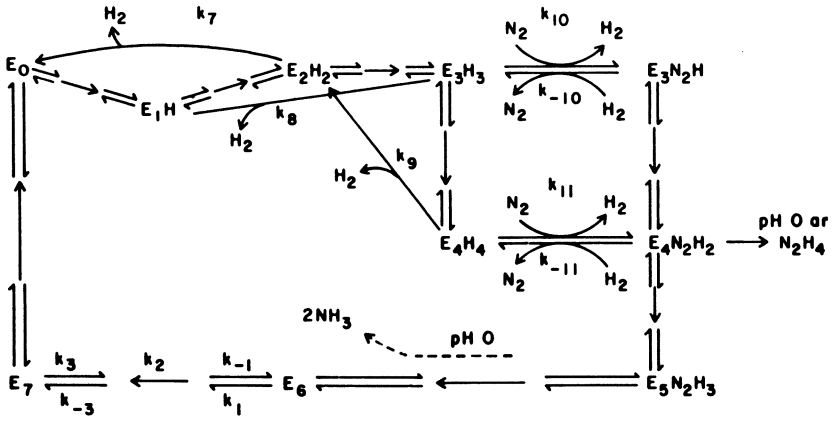


Figure 3 Thorneley-Lowe kinetic mechanism for nitrogenase. (Reproduced with permission from reference 4. Copyright 1984 Biochemical Society Book Depot.)

Organization of the Metal Clusters in MoFe Protein

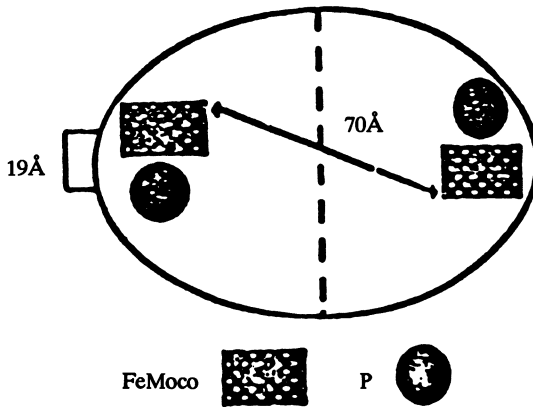


Figure 4 Cluster arrangement in MoFe protein, according to Bolin. (Reproduced with permission from reference 10. Copyright 1990 Chapman and Hall)

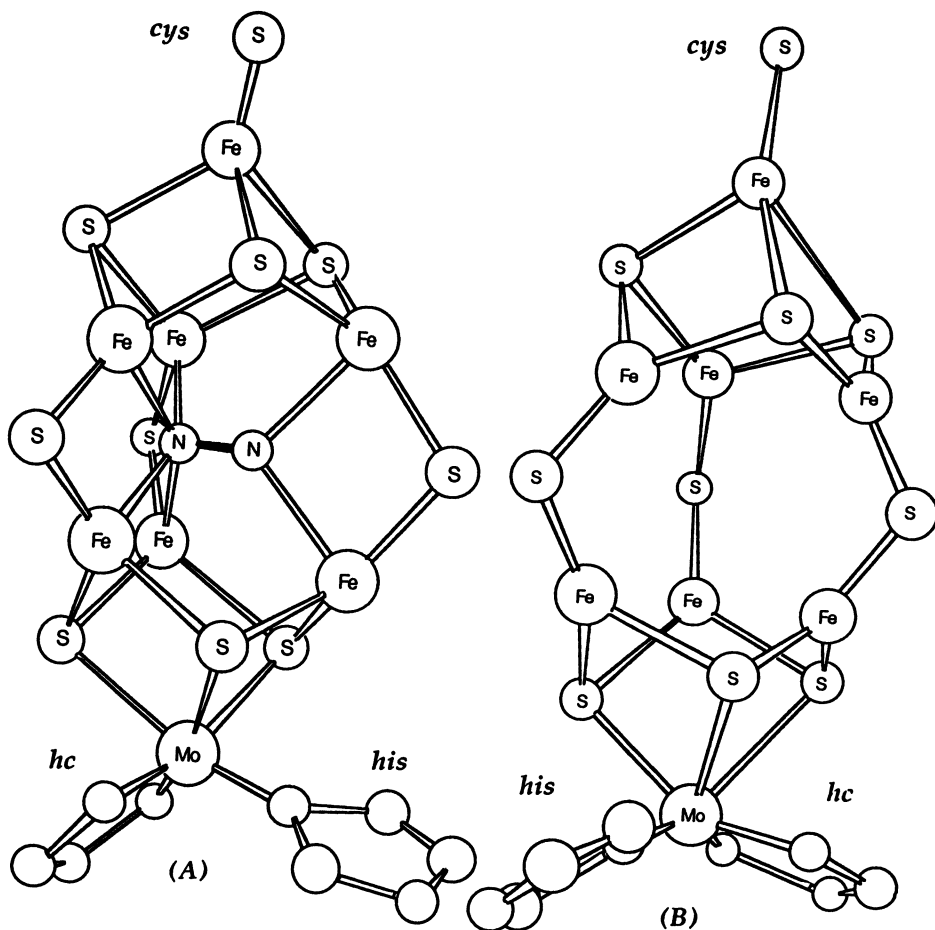


Figure 5 Cofactor model derived from analysis of Kim and Rees (11). (A) speculative model of initial N_2 complex of the cofactor; (B) as in the resting protein; (cf. 11). This is one of many similar possible complexes with N_2 : this choice was made on the basis of minimum compression of the N-N bond. *his* is the imidazole of histidine; *cys* is the cysteine mercaptide S atom; *hc* is homocitrate, coordinated by a carboxyl and a hydroxyl group. (Courtesy of Jeremy Selengut).

between the cofactor and the protein (13,14). Burgess (15) has recently summarized the evidence for these interactions and the nature of FeMoco itself. It has been evident for some time from chemical studies as well as Mössbauer, ENDOR, and EXAFS measurements that the cofactor entity is a sulfur-bridged cluster of approximate composition MoFe_6S_8 -homocitrate (6,16,17). The restoration of wild-type activity, as measured by the substrate reduction catalyzed by cofactorless mutant bacterial strains complemented with isolated FeMoco (6), strongly suggests that the cofactor is a major component of the actual site of substrate reduction. Furthermore, the characteristic signals at g -values of 4.3, 3.7 and 1.9, uniquely associated with the MoFe protein's M-centers, in fact arise from FeMoco bound to the protein. Other experiments on isolated cofactor have shown the existence of a single binding site for aromatic chalcogen ligands such as phenylthiolate or phenylselenolate (5,18). One suspects that this reactivity is analogous to the binding of Cys275 to the capping Fe atoms found in both Rees' and Bolin's structures (10,15). The cofactor also binds the nitrogenase substrate methyl isocyanide, both in the protein (15) and in isolation. Despite intense effort over the last fifteen years that has produced a wealth of spectroscopic, structural, and chemical information, the crystallographic structure of isolated FeMoco has so far eluded researchers.

Fe Protein. On a much firmer footing, the structure of the Fe protein from *Av* has been calculated (19) from 2.8Å data. The current structure is entirely consistent with earlier chemical studies and EPR, Mössbauer and EXAFS measurements, which predicted the presence of a single Fe_4S_4 cubane bound to the two subunits (20). The homology between Fe proteins of various species is so extensive (21) that it is probable that this structure is representative of all nitrogenase Fe proteins. The conformational changes that occur on binding MgATP shatter crystals of the Fe protein, and the MgATP binding site (two per molecule) has not been identified. However, a bound nucleotide, predicted from our earlier observations of bound ADP in Fe protein preparations (22), has been identified at the interface between the subunits. From this crystallographic analysis, it is now possible to direct efforts towards the elucidation of which structural features participate in the MgATP-driven pump that transfers electrons to the MoFe protein.

ATP-driven Electron Transfer. The chemical analysis of the MgATP hydrolysis problem has yielded some interesting results. Based on the evidence of rapid mixing stopped-flow microcalorimetry and stopped-flow spectrophotometry measurements (23), Thorneley has found that MgATP hydrolysis precedes the transfer from the Fe protein to the MoFe protein. He also showed that the cleavage of MgATP to MgADP and P_i was accompanied by the release of a proton into solution, and that the cleavage was endothermic and reversible. With these conclusions in mind, other groups have begun the search for the critical amino acid residues involved in the hydrolysis process.

Focusing on the observation of Lowerey *et al.* (24) that a Arg(101)His substitution produces an Fe protein that catalyzes MgATP hydrolysis in the presence of the MoFe protein but will not transfer electrons to the MoFe protein in a way productive of substrate reductions, Howard and Dean (personal communication) have begun to probe required surface residues by site directed mutagenesis of *Av* Fe protein. ADP ribosylation at Arg-101 produces a similar result (24). The residue Arg-101 is near Cys-94, one of the protein ligands to the Fe₄S₄ center which is the electron-transfer moiety. Such a combination of mechanistic and genetic analysis promises to shed further light on the electron transfer and MgATP hydrolysis processes.

Two Enigmas: M Centers and P Clusters

Building on the foregoing, in the remainder of this paper I will focus on the evidence for two unexpected and indeed questionable features of the prosthetic groups in nitrogenase, namely (A) the apparently extreme state of reduction of the Fe₄S₄ clusters comprising the P-centers in the resting state of nitrogenase and (B) the peculiar coordination of six of the Fe atoms in the M-centers (cofactor cluster) in the state of the enzyme accessible to x-ray crystallography. I will then speculate briefly about the mechanistic significance of these features.

Are the Iron Atoms in P Clusters all Ferrous? The MoFe protein as isolated, anaerobically and in the presence of S₂O₄²⁻, exhibits a unique EPR signal (Figure 6) which arises from the cofactor centers (integrating to two S=3/2 centers per molecule (1)). The MoFe protein may be reversibly oxidized, by e.g., thionin (25), the oxidized form yielding no EPR from the cofactor center. Using the cofactor EPR signal as an indicator, the titration reveals two distinct types of redox centers (Figure 7) which are easily understood to reflect four electrons removed from non-cofactor centers in the initial phases of the oxidation, followed by two electrons being removed from the cofactor centers, which causes the EPR to vanish. Importantly, four electrons are removed from the two P-clusters (two Fe₄S₄ cubes in each cluster); we have recently demonstrated (9) S=1 EPR from the oxidized clusters (i.e. two spins on each pair of Fe₄S₄ cubes); the earlier Mössbauer result proved (26) that all eight Fe atoms in each P-cluster pair experience the oxidation. At the same time (25) we observed that during the oxidation of the P-clusters (plateau in Figure 7) a signal near g=1.94, (Figure 6) reminiscent of reduced ferredoxins, came and went. A fit to potentiometric titration data on this signal (Figure 8) suggested that the P-clusters are coupled in pairs; that the centers are not merely close and therefore magnetically interacting is strongly implied by the recent structural (11) and EPR results (9) cited above; i.e. the EPR results should be interpreted to mean that the pair of Fe₄S₄ cubes are indeed joined covalently. The crux of the matter is that if removal of one

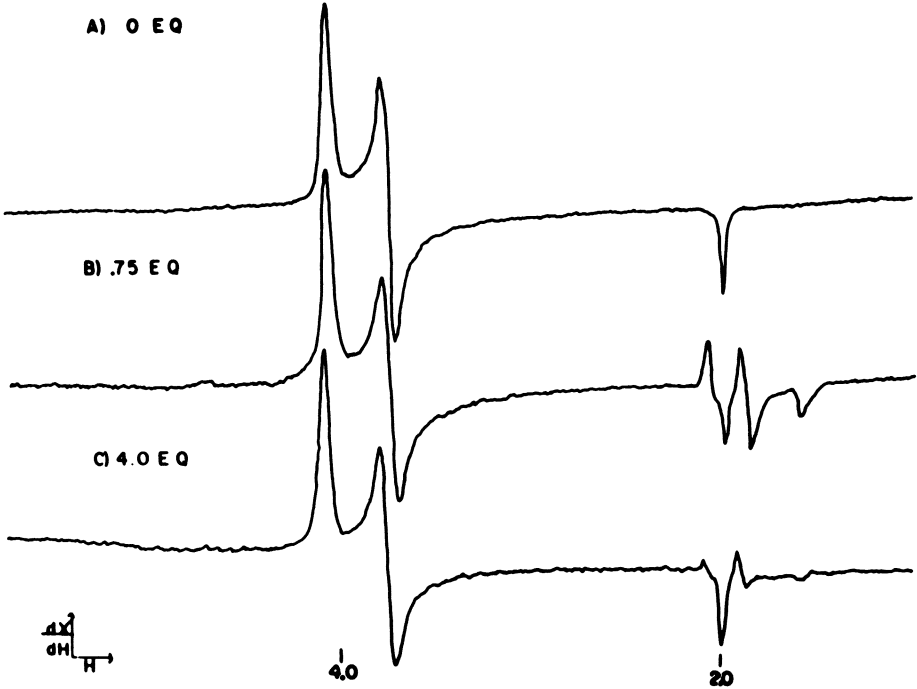


Figure 6 The EPR of MoFe protein, from *A. vinelandii*, as isolated and during oxidation by thionine. Abscissa, magnetic field, gauss; ordinate, first derivative of the microwave absorption. EPR conditions: microwave frequency, 9.5 GHz; modulation frequency 100 KHz; modulation amplitude, 10 gauss; microwave power 0.1 mw; field sweep rate, 100 gauss min⁻¹, time constant, 0.3 sec; sample temperature 10K. (A) Protein as isolated, freed of excess reductant. (B) After oxidation by 0.75 eq thionin per mole MoFe protein. (C) After oxidation by 4 eq thionin per mole MoFe protein. As in (25), samples prepared as previously described (26).

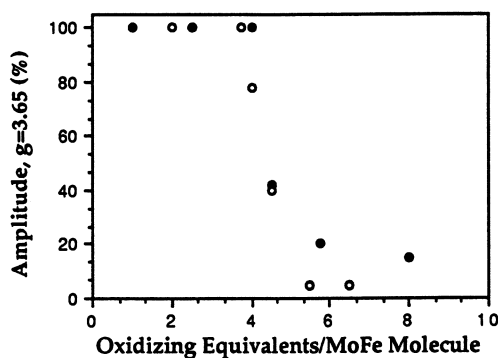


Figure 7 Oxidative titration of MoFe protein with thionin, as in Figure 6. Abscissa, equivalents thionin added (i.e., electrons removed/molecule MoFe); ordinate, amplitude of the EPR signal due to M-centers (i.e. the cofactor). Bear in mind that there are four-Fe₄S₄ clusters present as P-clusters, and two M centers, per MoFe molecule. Open circles, data from (30), closed circles, data from (26). From either experiment one concludes that four equivalents are removed before the cofactor begins to lose electrons; the first four equivalents come from the P-clusters.

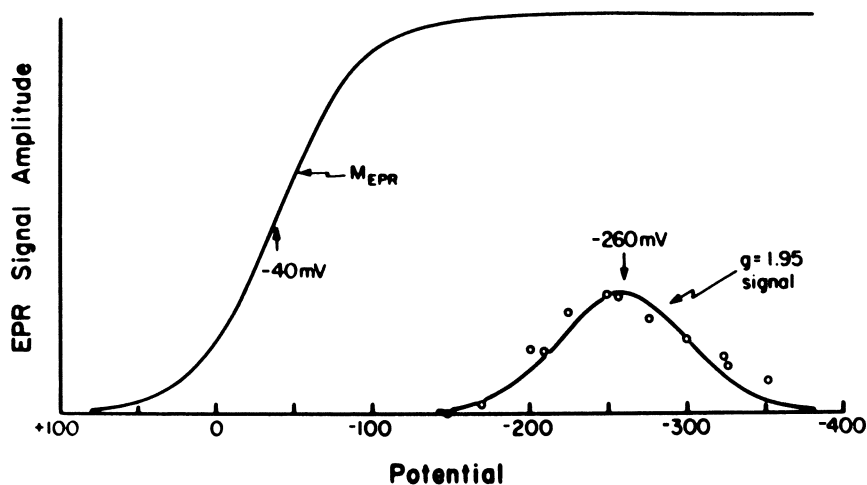


Figure 8. Fits to potentiometric titrations of MoFe protein: the intermediate occurring during oxidation of P clusters can be fit as two successive $1e^-$ processes, producing and then eliminating the EPR species near $g=1.95$ (see Figure 6). ordinate: EPR signal amplitude as in Figure 6; abscissa, redox potential (vs SCE); The samples were prepared as described (26). Unpublished data of Henzl, Rawlings and Orme-Johnson, see also (25).

electron from such a system produces EPR reminiscent of a reduced ferredoxin and removal of two electrons produces an even-spin system (9), then we may legitimately suppose that the native state of the MoFe protein contains P-clusters in a reduced state equivalent to coupling a pair of all-ferrous cubes. Whatever the stability of low mw analogs of Fe_4S_4 systems might be in this oxidation state (27), the interesting aspect would seem to be that putting an additional electron on such a system, by pumping from the Fe protein, might be energetically a very costly affair, or at the least lead to an evanescent state, given that with nothing else to do, nitrogenase simply evolves H_2 in the presence of MgATP. The obverse of this argument might be, that whatever the mechanism of ATP-driven electron-pumping *per se*, the storage of electrons, required ultimately to make energetic H^- in the active site, might well be in a puissant storage location such as hyper-reduced ($\text{Fe}_4\text{S}_4 - \text{Fe}_4\text{S}_4$) pairs. One has wondered for some time (e.g., reference 25) whether this pumping might involve *direct* interaction of ATP, based on the Fe protein, with P-clusters. The recent suggestion, that P-cluster pairs bridge between two protein subunits (11) and that it is plausible that Fe protein docking take place in this neighborhood, makes it of great interest to experimentally test hypotheses about ATP/cluster interactions in nitrogenase during turnovers.

Trigonal Fe Atoms in the Cofactor? The structure proposed by Kim and Rees (Figure 4A) clearly includes planar, three-coordinated Fe atoms at six of the seven positions proposed to be iron sites. One is concerned with the state of bonding that would give rise to such structures; precedent in Fe/S systems (27) clearly favors four-coordinate, essentially tetrahedral Fe site symmetry in known examples, including ferredoxin centers. The cofactor is intriguingly different in this respect, including having at least five Fe sites distinguishable by ENDOR (28). There are two explanations that immediately occur to one: first, that the cofactor is an electron rich, delocalized system and that in the resting state of the enzyme a kind of Faraday cage effect has apparently favored the observed hybridization scheme. Second, the cofactor is really a kind of metal hydride reservoir and therefore the missing Fe ligand is a hydrogen atom in each case. This would not be easily visible in x-ray analyses of proteins, but it certainly would be seen by ENDOR or ESEEM of protein soaked in D_2O under turnover (electron transfer) conditions. Protein passively exposed to D_2O reveals a series of exchangeable protons by these means (29). We have recently done the turnover experiment; in the event, no evidence for electron transfer dependant exchange has been seen up to now (R. Pollock, B. Hoffman, W.H. Orme-Johnson, in progress). Completion of a high resolution structure of isolated cofactor would address this point more effectively. In the meantime, it is useful to note that as a hydrogen evolving system, there must be electron transfer dependent interaction of the MoFe protein with solvent protons. Since the resting state, with the useful $S=3/2$ cofactor signal,

does not evolve H_2 , the lack of evidence for ATP-dependant exchange is disappointing but not surprising. The resting state presumably has no unspent hydride equivalents, according to these preliminary results. Which leaves one exactly where one started: with trigonal Fe atoms, which still invite speculation without at this point producing much certainty as to their significance, and, so far, also leave untouched the question, where *do* the hydride equivalents reside, in H_2^- evolving, N_2^- reducing states of nitrogenase? The smart money would bet on the M-centers, but decisive work remains to be done.

Acknowledgements: This work was supported by the NIH under GM28358. The author thanks his coworkers, particularly Maria G. Mitchell, David Wright, Patricia Christie, Normand Cloutier, Jacquin Niles, Robert Pollock and Jeremy Selengut, for their timely help, as well as acknowledging his extended and profitable collaborations with Eckard Münck and Brian Hoffman and their coworkers, and the work of previous pre- and postdoctoral students, cited in the references and figure legends. The insights and criticisms of Fred Ausubel, Alison Burgess, Jay Hickman, Anne-Francis Miller and Dick Schrock remain valuable resources in the areas of genetics, metal metabolism, and inorganic mechanisms, respectively.

Literature Cited

1. Orme-Johnson, W.H. Molecular Basis of Biological Nitrogen Fixation, *Ann. Rev. Biophys. Chem.*, **1985**, *14*, 419-459.
2. Subcommittee on Ammonia, National Research Council, "Ammonia," *University Park Press*, **1979**. Baltimore, MD.
3. Orme-Johnson, W.H., Hamilton, W.D., Jones, T.L., Tso, M-Y W., Burris, R.H., Shah, V.K., and Brill, W.J. Electron Paramagnetic Resonance of Nitrogenase and Nitrogenase Components from *Clostridium pasteurianum* W5 and *Azotobacter vinelandii* OP, *Proc. Natl. Acad. Sci.*, **1972**, *69*, 3142-3145.
4. Lowe, D.J., Thorneley, R.N.F. The Mechanism of *Klebsiella pneumoniae* Nitrogenase Action. *Biochem J.* **1984**, *224*, 877-886.
5. Rawlings, J., Shah, V.K. Chisnell, J.R., Brill, W.J., Zimmermann, R. Münck, E., Orme-Johnson, W.H. Novel Metal Cluster in the Iron-Molybdenum Cofactor of Nitrogenase, *J. Biol. Chem.*, **1978**, *253*, 1001-1004.
6. Shah, V.K., Brill, W.J. Isolation of an Iron-molybdenum Cofactor from Nitrogenase, *Proc. Natl. Acad. Sci. U.S.A.*, **1977**, *74*, 3249-3256.
7. Huynh, B.W., Münck, E., Orme-Johnson, W.H. Nitrogenase XI: Mössbauer Studies on the Cofactor Centers of the MoFe Protein from *Azotobacter vinelandii* OP, *Biochim. Biophys. Acta*, **1979**, *527*, 192-203.
8. McLean, P.A., Vasilios, P., Orme-Johnson, W.H., Münck, E. Isotopic Hybrids of Nitrogenase Mössbauer Study of MoFe protein with selective ^{57}Fe -Enrichment of the P-Cluster. *J. Biol. Chem.*, **1988**, *262*, 12902-12903.

9. Surerus, K.K., Hendrich, M.P. Christie, P.D., Rottgardt, D., Orme-Johnson, W.H., Münck, E. Mössbauer and Integer-Spin EPR of the Oxidized P-Clusters of Nitrogenase: P^{OX} is a Non-Kramers System with a Nearly Degenerate Ground Doublet. *J. Am. Chem. Soc.*, **1992**, *114*, No. 228579-8590.
10. Bolin, J.T. Ronco, L.E., Mortenson, L.E., Morgan, T.W., Williamson, M. N.-h. Xuong. Structures of the Nitrogenase MoFe Protein: Spatial Distribution of the Intrinsic Metal Atoms Determined by X-ray Anomalous Scattering. Nitrogen Fixation Proc. 8th Int. Congress. Knoxville, Tennessee, Peter M. Gresshoff, L. Evans, Roth, Gary Stacey, William E. Newton, (eds). Chapman and Hall, New York, **1990**, 117-124.
11. Kim, J. , Rees, D.C. Structural Models for the Metal Centers in the Nitrogenase Molybdenum-Iron Protein. *Science*, **1992**, *257*, 1677-1682.
12. Orme-Johnson, W.H. Perspectives: Nitrogenase Structure: Where to Now? *Science*, **1992**, *257*, 1639-40.
13. McLean, P.A., Wink, D.A., Chapman, S.K., Hickman, A.B., McKillop, D.M., Orme-Johnson, W.H. A New Method for Extraction of Iron-Molybdenum Cofactor (FEMOCO) from Nitrogenase Adsorbed to DEAE Cellulose: I. Effects of Anions, Cations, and Preextraction Treatments. *Biochemistry*, **1989**, *28*, 9402-9406
14. Wink, D.A., McLean, P.A., Hickman, A.B., Orme-Johnson, W.H. A New Method for Extraction of Iron-Molybdenum Cofactor (FEMOCO), from Nitrogenase adsorbed on DEAE Cellulose: II. Solubilization of the Iron-Molybdenum Cofactor (FEMOCO) in a Wide Range of Organic Solvents. *Biochemistry*, **1989**, *28*, 9407-9412.
15. Burgess, B. The Iron-Molybdenum Cofactor of Nitrogenase. *Chem. Rev.*, **1990**, *90*, 1377-1406.
16. Nelson, M.J., Levy, M.A., Orme-Johnson, W.H. Metal and Sulfur Composition of Iron-Molybdenum Cofactor of Nitrogenase, *Proc. Natl Acad. Sci.*, **1983**, *80*, 147-150.
17. Hoover, T.R., Imperial, J. , Ludden, P.W., Shah, V.K. Homocitrate Is a Component of the Iron-Molybdenum Cofactor of Nitrogenase. *Biochem.*, **1989**, *28*, 2768-2771.
18. Conradson, S.D., Burgess, B.K., Vaughn, S.A. ,Roe, A.L., Hedman, Britt, Hodgson, K.O., Holm, R.H. Cyanide and Methylisocyanide Binding to the Isolated Iron-Molybdenum Cofactor of Nitrogenase. *J. Biol. Chem.* , **1989**, *264*, 15967-15974.
19. Georgiadis, M.M., Komiyz, H., Chakrabarti, P., Woo, D., Kornuc, J. H., Rees, D.C. Crystallographic Structure of the Nitrogenase Iron Protein from *Azotobacter vinelandii*, *Science*. **1992**, *257*, 1653-1656.
20. Lindahl, P.A., Day, E.P., Kent, T.A., Orme-Johnson, W.H., Münck, E. Mössbauer, EPR and Magnetic Susceptibility of the Iron Protein from *Azotobacter vinelandii* Nitrogenase. *J. Biol. Chem.* ,**1985**, *260*, 11160-73.
21. Pretorius, I.M., Rawlings, D.E., O'Neill, E.G., Jones, W.A., Kirby, R., Woods, D.R. Nucleotide Sequence of the Gene Encoding the Nitrogenase Iron Protein of *Thiobacillus ferrooxidans*. *J. Bact.*, **1987**, *169*, 367-370.

22. Lindahl, P.A., Gorelick, N.J., Münck, E., Orme-Johnson, W.H. EPR and Mössbauer Studies of Nucleotide-bound Nitrogenase Iron Protein from *Azotobacter vinelandii*. *J. Biol. Chem.*, **1987**, *262*, 14945-14953.
23. Thornley, R.N.F. Kinetics and Mechanisms of ATP Hydrolysis, Electron Transfers and Proton Release by *Klebsiella pneumoniae* Nitrogenase. Nitrogen Fixation, Proc. 8th Int. Congress. Knoxville, Tennessee. Peter M. Gresshoff, L. Evans Roth, Gary Stacey, William E. Newton, eds. Chapman and Hall, New York, **1990**, 103-109.
24. Lowery, R.G., Chang, C.L., Davis, L.C., McKenna, M-C., Stephens, P.J., Ludden, P.W. Substitution of Histidine for Arginine-101 of Dinitrogenase Reductase Disrupts Electron Transfer to Dinitrogenase. *Biochem.*, **1989**, *28*, 1206-1212.
25. Orme-Johnson, W.H., Orme-Johnson, N.R., Touton, C., Emptage, M., Henzl, M., Rawlings, J., Jacobson, K., Smith, J.P., Mims, W.B., Huynh, B.H., Münck, E., Jacob, G.S. Spectroscopic and Chemical Evidence for the Nature and Role of Metal Centers in Nitrogenase and Nitrate Reductase in *Molybdenum Chemistry of Biological Significance*, W.E. Newton, S. Otsuka, eds., (International Symposium, held at Lake Biwa, Japan, April 10-13). Plenum, New York City, **1979**, 85-94;
26. Zimmermann, R., Münck, E., Brill, W.J., Shah, V.K., Henzl, M.T., Rawlings, J., Orme-Johnson, W.H. Nitrogenase X: Mössbauer and EPR Studies on Reversibly Oxidized MoFe Protein from *Azotobacter vinelandii* OP, *Biochim. Biophys. Acta.*, **1978**, *537*, 185-207.
27. Averill, B.A., Orme-Johnson, W.H. Iron-Sulfur Proteins and Their Synthetic Analogs, in *Metal Ions in Biological Systems*, **7**, Ch. 4, Helmut Sigel, ed., Marcel Dekker, Inc. Basel, Switzerland, **1978**, 127-183.
28. True, A.E., Nelson, M.J., Venters, R.A., Orme-Johnson, W.H., Hoffman, B.M. Determination of the ^{57}Fe Hyperfine Tensors for Five Distinct Iron Sites of the Iron-Molybdenum Cofactor Within the Molybdenum-Iron Protein of *Azotobacter vinelandii*, *J. Am. Chem. Soc.*, **1988**, *110*, 1935-1943.
29. True, A.E., McLean, Nelson, M.J., Orme-Johnson, W.H., Hoffman, B.M. Comparison of Wild-Type and *nifV* Mutant Molybdenum-Iron Proteins of Nitrogenase from *Klebsiella pneumoniae* by ENDOR Spectroscopy. *J. Am. Chem. Soc.* **1990**, *112*, 651-657.
30. Watt, G.D., Burns, A. Tennent, D.L. Stoichiometry and Spectral Properties of the MoFe Cofactor and Noncofactor Redox Centers in the MoFe Protein of Nitrogenase from *Azotobacter vinelandii*. *Biochemistry* **1981**, *20*, 7272-7277.

RECEIVED May 10, 1993

Chapter 18

Protein Component Complex Formation and Adenosine Triphosphate Hydrolysis in Nitrogenase

James Bryant Howard

Department of Biochemistry, 4-225 Millard Hall, University of Minnesota,
Minneapolis, MN 55455

Substrate reduction by nitrogenase requires efficient electron transfer between the unique donor, Fe-protein, and the site of substrate binding, the MoFe-protein. The unidirectional transfer of electrons between components is accomplished by an elegant switching mechanism which is driven by the hydrolysis of MgATP. Specific ionic interactions at the surface of the two components leads to the formation of a functional complex. The ionic residues involved have been identified by chemical modification and mutagenesis studies. The correlation of the altered properties to the effects on ATP turnover and substrate reduction have been assessed in kinetic experiments. Based upon the recently determined three-dimensional structures of the components, a model for docking and ATP hydrolysis is presented.

Substrate reduction by nitrogenase first requires electron transfer in a complex of the Fe-protein (see end of chapter for list of abbreviations) and the MoFe-protein coordinated with the hydrolysis of 2 MgATP/e⁻. Several years ago Hageman and Burris (1) proposed that the two component complex must dissociate following transfer of individual electrons. Consequently, because all nitrogenase substrates need multiple electrons for reduction, several cycles of complex formation and dissociation occur for each equivalent of product. This redox cycle is presented in Scheme 1. Lowe and Thorneley (2) have determined many of the rate constants for individual steps in the Fe-protein-MoFe-protein redox cycle and have concluded that dissociation of Complex II (see Scheme 1) is the slowest step and is rate determining overall if Fe-protein, MgATP and the electron source (e.g., dithionite) are at saturating concentrations.

A description of the properties and chemistry of these complexes is central to understanding the nitrogenase mechanism. The special nature of the complex is indicated by the requirement for the Fe-protein to serve as the electron donor in substrate reduction; other low potential electron donors such as ferredoxins, flavodoxins, and inorganic complexes are ineffective. Furthermore, although MgATP is bound by free Fe-protein, the nucleotide is hydrolyzed only in the Fe-protein:MoFe-protein complex.

The minimal requirements for an active complex include the following:

1. General recognition of one component by the other,
2. MoFe-protein induced conformational changes in Fe-protein leading to nucleotide hydrolysis,
3. Conformational changes in either or both components leading to the correct alignment of the respective donor/acceptor metallo-centers, and
4. Conformational changes and dissociation after electron transfer to minimize reversal of electron flow.

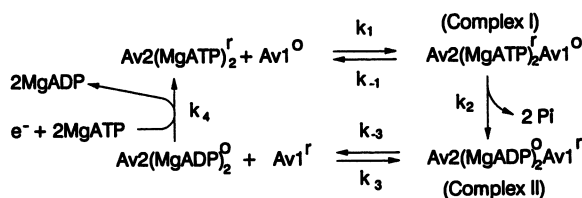
For these properties to be exhibited by the complex, association between components should be tight but not too tight. That is; there must be flexibility in the complex so that conformational changes leading to electron transfer and the subsequent dissociation can occur.

Perhaps the most compelling argument for a conformational change within the complex is the well documented structural change in the Fe-protein leading to exposure of the Fe:S cluster upon binding MgATP (3-6). The nature of the conformational change appears to be dependent upon the oxidation state of the Fe-protein and the nucleotide bound, e.g., MgATP promotes Fe chelation whereas MgADP inhibits chelation; all four Fe atoms are chelated from the reduced state, whereas, in the oxidized state, the first two Fe atoms are much more rapidly chelated than the second two (4,6). Presumably, similar conformational changes occur when the Fe-protein is associated with the MoFe-protein. The need for flexibility once the complex is formed is suggested by the observations on the Cp2-Av1 heterocomplex (7). This is a very tight complex yet ATP is not turned over and substrates are not reduced (7). Likewise, the difference in stabilities of Complex I and II, implicit in the rate data of Lowe and Thorneley (2), is *prima facie* evidence that structural changes have occurred after the electron transfer.

For this report, some recent evidence regarding the properties of the complex recognition site will be discussed. Information gained from enzyme kinetics and chemical modification studies with both wild type and amino acid substituted nitrogenase components will be correlated with the new three dimensional structures (8, -10). Finally, from the structure-function correlation a model for nucleotide binding and hydrolysis will be presented (11)

General Electrostatic Effects

The inhibitory effect of salt on nitrogenase activity has been known for sometime but only more recently have the implications of the effect been recognized (12-14). In Figure 1 are shown representative



Scheme 1. Redox cycle for electron transfer from Fe-protein (Av2) to MoFe-protein (Av1). Superscripts indicate relative oxidation level of individual components. (Adapted from (2)).

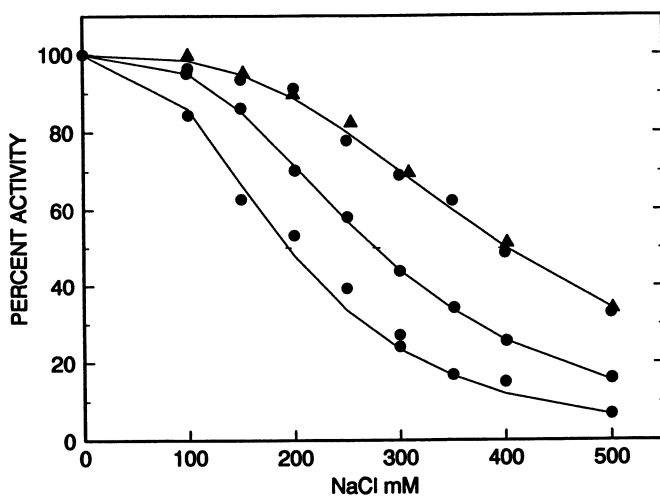


Figure 1. Effect of component ratio on apparent degree of salt inhibition. [Av1] = 1.3 μM. [Av2] = 21.5 μM; 11 μM; and 0.8 μM for highest to lowest curve. Top curve shows both proton and acetylene reduction; other curves are for proton reduction.

data for the inhibition of *A. vinelandii* nitrogenase by NaCl. Several important conclusions can be inferred from these results (12). First, all substrate reduction activities are equally decreased by salt, which suggests a common, general mechanism of inhibition. The inhibition is reversible and is "dead end". The shape of the inhibition curve suggests higher order, cooperative interactions between the proteins and NaCl. Finally, there is a definite competitive relationship between the proteins and NaCl. This can be seen in Figure 1 where a ~10 fold increase in Av2 concentration increases the concentration of NaCl needed for 50% inhibition by ~2 fold. In other experiments not shown here, we found that there was a small increase in the K_m for MgATP, yet even at saturating ATP concentrations, salt was the potent inhibitor shown in Figure 1 (12).

The inhibition could result from salt affecting any one of the four sides of the redox cycle shown in Scheme 1. Electron transfer after complex formation, for example, step k_2 , is first order and would not show competition between salts and a component. Because such competition is observed, it is unlikely that k_2 is the site of inhibition (12). Thorneley and Lowe (15) reported that the dissociation of Complex II (k_3) is rate determining overall yet is increased by Na_2SO_4 ; hence, NaCl should have increased the overall activity. Clearly this is not the case, and salt inhibition is not likely to originate from an altered stability of Complex II. Finally, salts had minimal effect on nucleotide binding or dithionite reduction of Av2 which excludes k_4 as the main site of inhibition (12).

To account for these results, we proposed a simple model in which salts prevent the formation of Complex I (see Scheme 2) (12). In this model, the salt is treated as binding to reduced Fe-protein with bound MgATP. Our assumption is that this dead end form cannot associate with the MoFe-protein. The kinetic expression is equally valid for the salt associated exclusively with the MoFe-protein or partially with both components. The model is best fit if the NaCl is treated as having an inhibitor constant of ~50 mM with effectively 3-4 sites (equivalent to $n = 3-4$ in the Hill equation of cooperative binding) (12). A prediction of the model is that the competitive inhibition of Complex I formation can be partially relieved by increasing the component ratio or by increasing the total protein concentration at a constant component ratio. Both protein effects have been observed and serve as a positive test of the model (see Figure 1).

We favor a simple interpretation of this model where salt ions compete with the protein "docking" ionic residues. Consistent with this interpretation, the effectiveness of the inhibition was dependent on the nature of the salt. Indeed, the K_i for various salts differ by ~15 fold even after correcting for ionic strength, the strongest inhibitors being polycationic amines such as spermine ($K_i \sim 5$ mM) (12). However, the model in Scheme 2 is not limited to any detailed mode of salt interaction. For example, the salt is shown binding to reduced Fe-protein with bound MgATP. However, the interaction could be with any form of the protein in equilibrium with the active state; the only requirement is that nucleotides are not competitive with salt. An alternate mode of salt inhibition could be the effect on an allosteric site such as an internal salt

bridge. In this case, disruption of the salt bridge could lead to a conformational change that decreases the affinity of the components for each other.

Chemical Crosslinking of Components in Complex

The nitrogenase components are readily covalently linked by the water soluble reagent, 1-ethyl-3-dimethylaminopropyl-carbodiimide (EDC) which mediates the formation of an isopeptide bond between the side chain carboxyl of aspartyl or glutamyl residues and the amino of lysyl side chains (16,17). The proximity of carboxyl and amino groups necessary for isopeptide crosslinking is strongly suggestive of ionic bonds at this site in the component interface. Crosslinking of the components was detected by the appearance of an unique $M_r=97,000$ band on denaturing gel electrophoresis of the reaction mixture. This molecular weight is consistent with the crosslinking of one $M_r=58,000$ Av1 subunit and one $M_r=32,000$ Av2 subunit. By repetitive Edman degradation and amino acid analysis, the crosslinked material was found to contain one Av1 β -subunit and one Av2 subunit (16). The degree of crosslinking was dependent upon the component ratio; at -5:1 molar excess of Av2, all of the Av1 β -subunit was consumed concomitant with the appearance of the $M_r=97,000$ band. In contrast only 50% of the Av2 subunits were crosslinked even when Av1 was in large excess. Together these results suggest an asymmetrical association between each β -subunit and the Av2 dimer.

The striking specificity of the reaction was even more evident when the amino acid sequences of the crosslinking site were determined (17). The results are shown in Figure 2. First, all of the crosslinking between components could be accounted for by one isopeptide. Given that there are >100

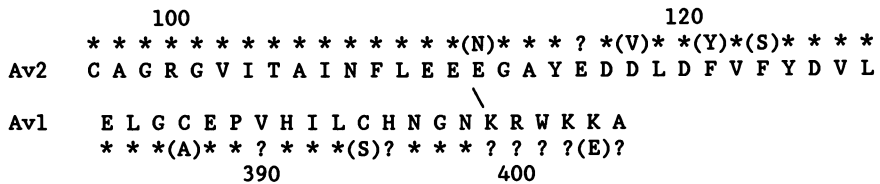


Figure 2. Amino acid sequence of crosslinking site in *A. vinelandii* nitrogenase. *, invariant residue; (), alternate residue found in some species; ?, variable residue.

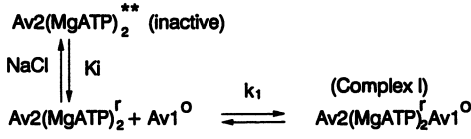
carboxylic acids and >50 lysines in Av1 and Av2, several different peptides might have been expected. Second, selectivity of the site within each subunit is remarkable; there are 7 carboxylic acids in this 11 residue stretch of Av2, yet only one, Glu-112, is crosslinked. Likewise, in Av1 there is a cluster of three lysines, yet only one, Lys-399, is crosslinked.

In part, the specificity arises from the unique reactivity of Glu-112. If Av2 is treated with the same low concentrations of EDC (6-12 mM) as used in the crosslinking reaction, other nucleophiles such as glyNH₂ are readily incorporated and exclusively at Glu-112 (Howard, J. B.; Magnuson, J.; Willing, A. in preparation.). In contrast, no glyNH₂ is incorporated into Av1 unless >100 mM EDC and nucleophile are used with extended reaction times. Furthermore, EDC has the properties of an "active site directed" reagent, namely, the crosslinking reaction rate shows saturation with EDC concentration above ca. 10 mM EDC. One explanation for the specificity of the EDC coupling reaction is that the cationic tertiary amine of EDC associates with an Fe-protein anionic region. The binding of EDC could serve to orient the carbodiimide towards a specific carboxyl side chain. Not only is there a cluster of acidic residues in the primary sequence around Glu-112, but additional carboxylic acids from residues 62-75 are located in this region of the three dimensional structure (8,10). Any one or a group of carboxylic acids might form a pocket for the ionic EDC. To test this hypothesis, two other potential, isopeptide mediating reagents were investigated. Neither anionic Woodward's reagent K (N-ethyl-5-phenyl-isoxazolium-3'-sulfonate) nor a neutral carbodiimide (N,N'-diisopropylcarbodiimide) mediated component crosslinking or glyNH₂ incorporation. Hence, we conclude that Av2 contains a cationic binding site associated with the activation of Glu-112.

Ionic Interactions Near the Fe-Protein Fe:S Cluster

Arginine, residue 100 in Av2, was first recognized as a likely docking site residue because of its proximity to the proposed Fe:S cluster ligands (Cys-97 and Cys-132) (18). Ludden and co-workers (19) strongly implicated Arg-100 as being on the surface and as part of the complex interaction region, with the discovery that, in some species, this residue is reversibly ADP-ribosylated. Furthermore, an inactive form of the *K. pneumoniae* Fe-protein was isolated in which histidine replaced Arg-100 (20). To study the contribution of this residue to complex formation, a series of *A. vinelandii* Fe-proteins substituted at residue 100 was prepared (14). Surprisingly, a wide range of diazotropic growth characteristics were observed for strains harboring these altered Av2. Near wild-type growth was observed for strains with the tyrosyl, phenylalanyl or leucyl substitution while no growth could be detected for strains with the histidyl, alanyl, or glutaminyl substitution. Perhaps, the most surprising result, given the growth patterns of other mutant strains, was that the lysyl substitution (most similar to arginine in charge) resulted in no diazotropic growth.

A more detailed analysis of the activity with purified altered proteins indicated an even more complicated picture. In keeping with the diazotropic growth studies, R100Y-Av2 had high specific activity; however, while the histidine substitution resulted in no growth, the purified R100H-Av2, had low but definite substrate reduction activity. As shown in Figure 3, these altered proteins are considerably more sensitive to salt inhibition than is Av2-WT and, thus, especially for R100H-Av2, the activity was masked by the ionic strength in the usual enzyme assay. (Indeed, the intracellular ionic strength may effectively prevent sufficient nitrogen fixation



Scheme 2. Competition between salts and Av1 for Av2-MgADP. (Adapted from (12)).

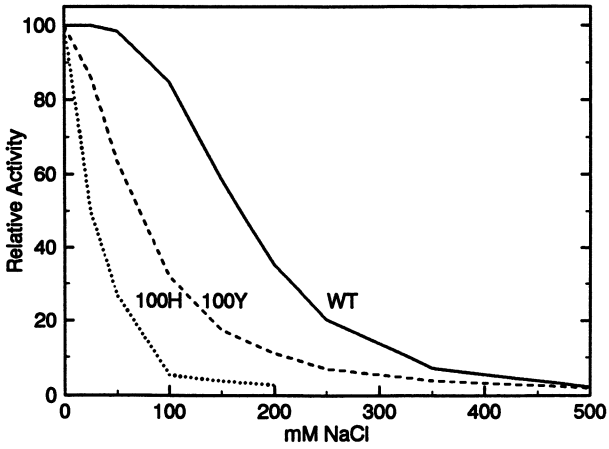


Figure 3. Comparison of salt inhibition of Av2-WT (wild type), Av2-R100Y, and Av2-R100H at the same component ratio with Av1.

for growth by the mutant strain.) Even when the ionic strength of the assay was adjusted to the minimum level necessitated by the ionic substrates of nitrogenase (e.g., 1mM MgATP, 5 mM creatine phosphate, and 10 mM dithionite), R100H-Av2 had only ~3% of Av2-WT activity. On the other hand, no activity or ATP hydrolysis could be detected for R100K-Av2 at any ionic strength tested.

The increased sensitivity of the altered proteins to salt inhibition as shown in Figure 3 is counter-intuitive. One would expect that if a critical ionic interaction has been removed, e. g., Arg --> Tyr, the complex formation and, consequently, the activity would be less sensitive to ionic strength. Clearly, the contrary is the case. The explanation for this apparent contradiction lies in other parameters of the activity measurements. When Av1 (native wild type) is titrated with Av2, a saturation curve is obtained which can be interpreted in terms of an apparent kinetic K_{Av2} for Complex I. The K_{Av2} determined using rapid equilibrium assumptions compared favorably to the value calculated from k_1 and k_{-1} (2). This simplification was adequate to fit the model to the data. Using this approach we found that R100Y-Av2 and R100H-Av2 both have a substantial increase in their apparent K_{Av2} as given in Table 1 (14). If salt inhibits by competing for Av2 with Av1 (Scheme 2), then salt will be more effective when the affinity between Av1 and Av2 is decreased. Indeed, the lines in Figure 3 are those calculated using the same parameters as in Figure 2 for wild-type Av2 and Av1 except for using the appropriate K_{Av2} and decreasing the number of co-operative salt binding sites from ca. 4 to ca. 2. That is; replacing Arg-100 decreases the number of strong ionic interactions and hence decreases the overall affinity. Other, weaker ionic bonds presumably remain as part of the docking interactions and, because they are weaker, they are more sensitive to ionic strength.

Table 1. Properties of purified Fe-protein with substitutions at residue 100. The V_{max} is at saturation of Av1 by Fe-protein except for R100H-Av2 where obtaining saturation is beyond reasonable concentrations of protein. + is the relative rate of crosslinking with Av1

Substitution	Relative V_{max}	K_{Av2}	ATP/e ⁻	Crosslinking
Wild type	100	0.2 μ M	2.1	+++
Tyrosine	35	0.8	2.1	++
Histidine	3	>25	>18	++
Lysine	0	No hydrolysis		++

The second consequence of substitutions at Arg-100 is the change in the apparent V_{max} which is defined by the titration of a constant amount of one component with the second. When Av1 is held constant and titrated by Av2, the altered Av2 have lower V_{max} (see Table 1). Because wild-type Av1 is used, the lower V_{max} cannot be due to a change in the final substrate reduction step but must originate from a smaller concentration of reduced, free Av1, the redox state involved in substrate reduction (2). Rather, the lower overall activity must be a consequence of changes in the redox cycle shown in Scheme 1. For a lower V_{max} , either k_2 or k_{-3} must have been

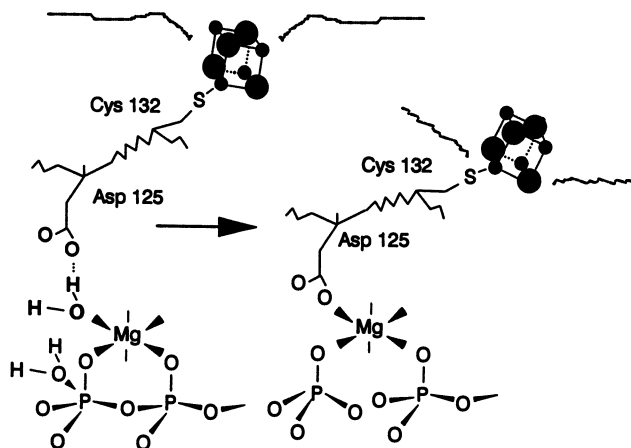
altered. To generate the observed V_{max} for R100Y-Av2, k_2 would need to be decreased ~200x while as little as a ~3x decrease in the rate determining k_{-3} would be sufficient. A significantly larger change in either rate constant is needed for R100H-Av2. There is a profound implication of the simultaneous change in K_{Av2} and V_{max} . Substitutions at residue 100 appear to result in a weaker Complex I (increased K_{Av2}) yet a tighter Complex II (decreased V_{max}). Thus, the bonding interactions in the two complexes must be different and oppositely affected by the substitution. This interpretation implies that there is a critical conformational change in the transition between Complexes I and II. If this is the correct interpretation, then the unique role of arginine is to balance the stability of the two complexes.

Nucleotide Binding and Electron Transfer

Nucleotide hydrolysis in the nitrogenase reaction appears to be the driving force for a conformational switch that ensures essentially unidirectional electron transfer from the Fe-protein to the MoFe-protein. Although the mechanism of conformational change, "gating", is not known, there is ample evidence for different structural forms of nucleotide-bound, Fe-protein in the two oxidation states (for example, 6,3,21-23). Furthermore, the Fe-protein has several regions of amino acid sequence homology to other nucleotide binding proteins including the so-called Walker A and B consensus sequences (24). The primary sequence homology is carried into the three dimensional structure, in particular with the GTPase, p21^{ras} (8,10). In addition to the structural similarity, two important functional similarities between G-proteins and nitrogenase should be noted (11). First, both Fe-protein and G-proteins use nucleotide hydrolysis to switch between states. In the case of nitrogenase, we would propose that the electron transfer occurs from a metastable state when the products of ATP hydrolysis (phosphate and ADP) are still bound; upon release of the phosphate, the Fe-protein proceeds to the ADP bound conformation and the gate is closed. Second, nucleotide hydrolysis occurs in a multiprotein complex; for G-proteins, a GTPase activating protein greatly accelerates the hydrolysis whereas for nitrogenase there is an absolute requirement for both components.

Of the functionally important residues, Av2 Asp-125 appears to be the best candidate for connecting the nucleotide site to the cluster. In p21^{ras}, Asp-57, the analog of Asp-125, is a ligand of the nucleotide-bound Mg (25). Upon hydrolysis of GTP, Asp-57 shifts from indirect coordination of the Mg through an intervening water molecule to direct coordination, with an ensuing adjustment in the conformation. Indeed, in p21^{ras} the largest conformational change is 7-11 residues down from Asp-57 (25), or by extrapolation to Av2, conformational changes transmitted by Asp-125 would include the cluster ligand Cys-132. This hypothesis is shown in Scheme 3.

An altered Av2 (D125E-Av2), generated by site directed mutagenesis of Asp-125 to glutamic acid, was purified and found to be incapable of substrate reduction or ATP hydrolysis (11). However, the longer glutamic acid side chain might still have been able to form a ligand to the nucleotide bound Mg and to induce the conformational changes associated with "exposure" of the cluster to chelators. This, indeed, was found. In striking contrast to Av2-WT



Scheme 3. Proposed role of Asp-125 in MgATP hydrolysis and signal transduction.

where the cluster is accessible to chelation only when MgATP is present, the cluster was readily removed from Av2-D125E in the presence of either MgATP or MgADP. Although there is a slow rate of chelation in the absence of nucleotide, the rate is far slower than the chelation of oxygen, heat or pH inactivated protein. Most importantly, Av2-D125E retained the nucleotide dependence of the chelation reaction, but now both MgATP and MgADP were capable of inducing the conformational change.

Our design rationale anticipated that MgADP might be able to induce a conformational change in Av2-D125E; what was unexpected was the change in Mg requirement (11). Metal free nucleotides were also fully able to induce conformational changes in Av2-D125E. Indeed, the rate of chelation was faster for ADP than for MgADP suggesting that ADP binding more closely mimics MgATP.

The difference between Av2-WT and Av2-D125E was also evident in equilibrium binding measurements (11). For MgADP the apparent K_D 's are similar yet ca. two sites were found for Av2-D125E vs. one site Av2-WT. Two binding sites for Mg-free ADP were also found in Av2-D125E, whereas no ADP binding could be detected for Av2-WT. In the Av2-WT crystal structure, there is a partial occupancy for one ADP (8). It is not clear at present whether there is a metal associated with this ADP or whether it represents a tightly bound ADP (with or without associated metal) that does not readily exchange.

Correlation of the Three Dimensional Structures with Functional Properties

A detailed description of the Fe-protein and MoFe-protein molecular structures is found in Chapter 11 of this Volume by Rees and coworkers. In Figure 4a, the two subunits of Av2 are shown along the two-fold axis with the bridging 4Fe:4S cluster ~ 8-9Å below the top surface as defined by van der Waals contact to the side chains. This top surface contains the two Arg-100 and two Glu-112 that were implicated as potential docking site residues by the chemical and mutational studies described above. The Arg-100 reach above and overlap the cluster while a patch of acidic residues including Glu-110-112 are at the end of an α -helix that extends for ~20Å from Arg-100 to Glu-112. These helices (one helix in each subunit, symmetry related to the cluster) form a rod, bent at the cluster, that spans the length of the top surface. The rod-like structure is more evident when the molecule is rotated 90° about the two-fold axis (Figure 4b). The finding of the cluster, Arg-100, and Glu-112 on the same surface strongly suggests that this is the surface that makes contact with the MoFe-protein. If so, then the residues that are most exposed and most likely to first encounter the other component are Glu-111, Asn-107, and the loop Thr-66, Glu-68, Asp-69; only at the second layer of contact are residues Arg-100 evident. Of the five (10 for the dimer) most exposed residues, three are part of a anionic pocket (Glu-110-112, Glu-63, Glu-68, Asp-69, and Glu-71) which is formed by the termination of the α -helix and a loop from residues 61-75. This pocket probably is responsible for the unique specificity of the EDC reaction with Glu-112.

Most importantly, several unique amino acid differences between Cp2 and other Fe-proteins are also part of the anionic pocket. Namely, Glu-111 is fully conserved except for Cp2 where the residue

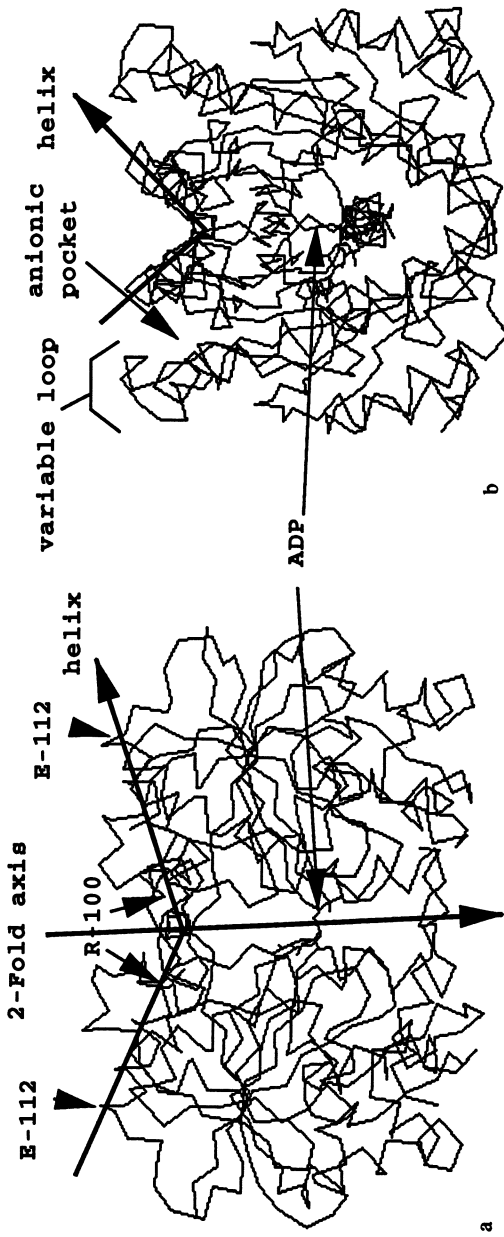


Figure 4. α -Carbon, peptide backbone trace for Av2 (Figure is based upon molecular coordinates provided by D. C. Rees, (8,10)). The two figures are a 90° rotation around the two-fold axis.

is Gln and there is a deletion of two residues, Thr-66 and Val-67 in Cp2 (26). The significance of these changes lies in the fact that Cp2 forms a tight non-productive complex with Av1. Although neutral amino acids are deleted, the orientation of Glu-68 and Asp-69, both of which are conserved, will be different. Thus, the anionic pocket must be somewhat altered. Whether this change leads to a tighter complex is a speculation which can be tested by future site-specific mutagenesis experiments.

The ionic distribution on the Av2 top surface is illustrated in Figure 5a which is a view looking down the two-fold axis. The α -carbons shown are those residues whose side chains extend above the cluster. The distribution of charge is concentrated into an outer ring of negative charges (composed of the acidic residues discussed above) and an inner ring of positive charges (including Arg-100, Arg-140, Lys-143 and Lys-170).

An α - and β -subunit pair of the MoFe-protein containing one P-cluster and one M-cluster is shown in Fig. 6a. Although the degree of amino acid sequence homology between subunits is weak, the three dimensional folds show considerable pseudo-symmetry. Above the P-cluster and leading to it are two α -helices from each subunit (residues ~123-133 and ~157-174 of each subunit). The helices terminate at the subunit interface with the P-cluster buried 15-18 Å below the van der Waals surface. The cleft is more clearly seen with a 90° rotation in Fig. 6b. The residues extending above the helices are hydrophobic and include α -Phe-124 and β -Phe-124, α -Val-123 and β -Val-123, and α -Leu-157 and β -Val-156. It should be noted that Thorneley, et al (27) recently reported that β -Phe-124 was involved in the contact with the Fe-protein and changes at residue 124 resulted in altered electron transfer properties in the complex. At the bottom of the cleft and directly overlaying the P-cluster are two symmetry related, conserved residues α -Phe-185 and β -Phe-188. At the base of the cleft and adjacent to the p-cluster ligands are the acidic residues Asp-120, Asp-159, Asp-160, and Glu-163 of the α -subunit and Asp-119, Asp-159, Asp-160 and Glu-120 of the β -subunit.

The helices and the cleft form a distinct "crown" on the top of the MoFe-protein. Additional surface residues are well below this "crown" yet could make contact with incoming, docking molecules. One surface residue has been identified in our crosslinking experiments as β -Lys-399. When the Av1 surface is observed down the pseudo two-fold axis through the P-cluster (Fig. 5b), the cationic and anionic residues are found in arrays or rings around the Fe:S cluster. What is striking is the distribution of charged residues on the surfaces of the two proteins; namely the two surfaces appear complementary with the outer positive ring on Av1 matching the negative pockets on Av2 while the inner acidic residues on Av1 coinciding with the basic residues on Av2.

The formation of an electron transfer competent complex between Av1 and Av2 requires the closest approximation of the p-cluster and the Av2 4Fe:4S cluster. This is directly accomplished by centering the two clusters on a common two fold axis (7a). Av2 can be rotated such that its surface α -helices (from Glu-112 to the symmetry related Glu-112 on the second subunit) are perpendicular to the α -helices in the "crown" on Av1 and can be inserted into the Av1 cleft. Van der Waals contacts between the Av2 side chains and the cleft limits the inter-cluster distance to ~17-18 Å. Surprisingly,

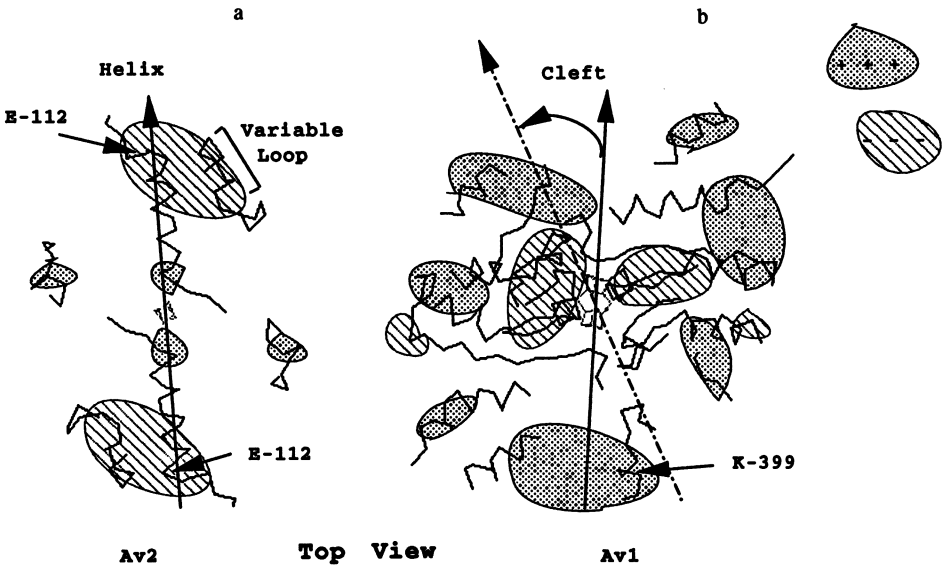


Figure 5. Docking surfaces for Av2 and Av1. Top slice, looking down two-fold axis of Av2 and pseudo two fold axis of Av1. Regions of charged residue clusters indicated by shading.

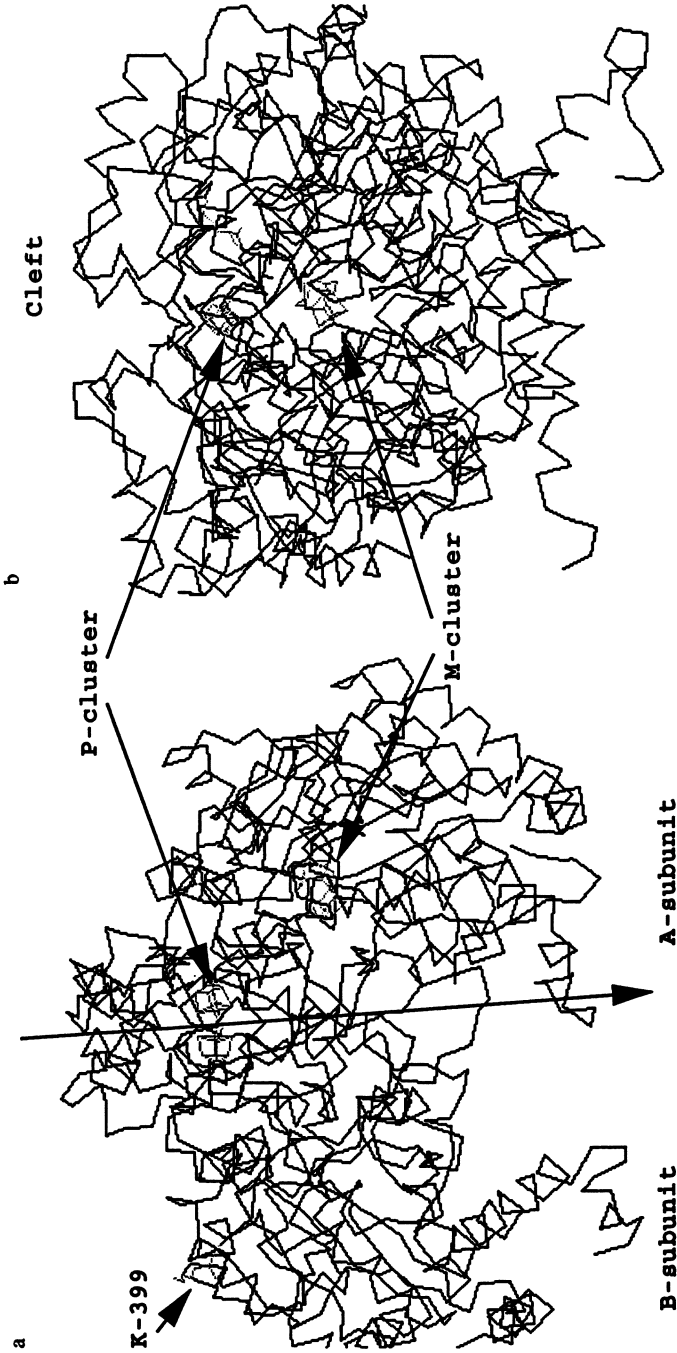


Figure 6. α -Carbon, peptide backbone trace for Av1 (Figure is based upon molecular coordinates provided by D. C. Rees, (9)). The two figures are a 90° rotation around the pseudo two-fold axis.

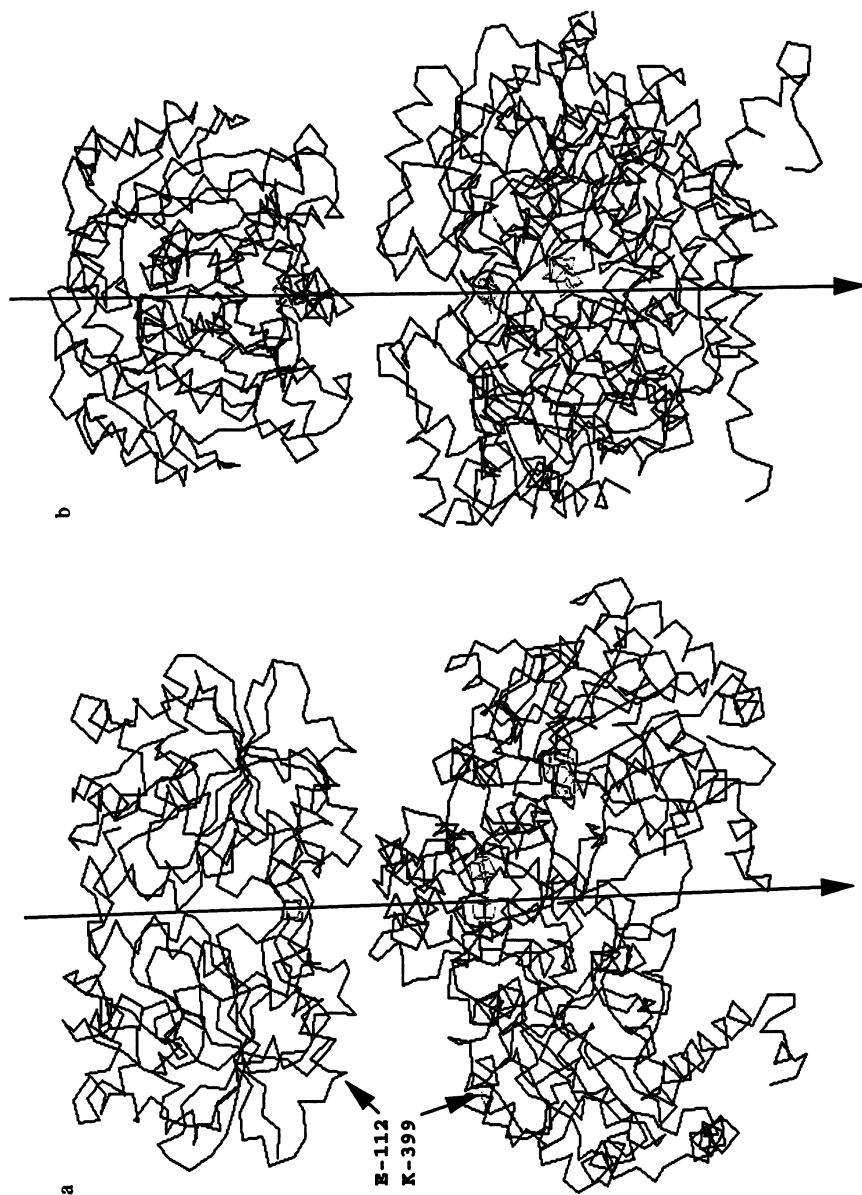


Figure 7. Av1 and Av2 in proposed docking orientation. The two figures are a 90° rotation around the pseudo two-fold axis.

few if any, strong ionic bonds are formed in this docking arrangement although several of the ionic patches are juxtaposed. For example, Lys-399 is positioned below Glu-112 but remains separated by 7-8 Å (Fig. 7b) and none of the acidic residues surrounding the cleft are close enough to make a salt bond with Arg-100. Nevertheless, the chemical and kinetic experiments seem to require such ionic interactions.

Docking Model

The experimental results outlined above and the model building with the new crystal structures lead to the conclusion that several different complexes are likely to be formed during the docking process. To account for these observations, a model is proposed that has several steps (designated cuddle, slide, stick, relax, and release) and is summarized as follows:

The first step in productive docking involves association between the Av2 anionic pocket and the Av1 basic residue clusters. Chemical crosslinking occurs in this complex and, in keeping with our results, the complex can form with inactive as well as active proteins if they retain the active three dimensional structures. This early complex has a minimal contribution to the overall kinetics of substrate reduction because it is stabilized by relatively weak interactions. This complex is, however, highly specific as indicated by the crosslinking studies. It should be noted that this complex is formed exclusively with the β -subunit; no crosslinking between Av2 and the α -subunits was detected even though the crystal structures indicate crosslinking between Glu-112 and α -Lys-49 would be possible for an Av2 approach on the α -subunit side.

The second step in docking could be the sliding from the initial complex to the two-fold symmetry aligned complex shown in Figs. 7a,b. In this state, a conformational change would be induced by Av1 in Av2 such that the hydrolysis of MgATP could be effected. As indicated above, Arg-100 has only minimal ionic bonding potential in this orientation. The amino acid side chain contacts between the hydrophobic residues on the surface of the Av1 cleft (see above) and the two turns of the Av2 α -helixes (residues 102-109) are a likely signal transduction path to the nucleotide binding site (Magneson, J.; Howard, J. B. in preparation.). Residues 103-108 in Av2 interact with a second strand of helix which, in turn, has hydrogen and ionic bonds to Asp-125 and other residues associated with the terminal phosphates of bound nucleotides. Amino acid substitutions in this region lead to altered ATP hydrolysis and turnover (Magneson, J.; Howard, J. B. in preparation.).

The ATP hydrolysis provides the driving force for a conformational change at the Av2 interface. In order to form a strong salt bond with Arg-100, Av2 would need to rotate $\sim 30^\circ$ in the cleft. With the new orientation (Fig 5b), the two Arg-100 could interact with either Asp-159 or Asp-160 in each of the respective α and β Av1 subunits. These ionic bonds are buried in a hydrophobic region around the P-cluster and could serve to orient the clusters in the two proteins for maximal electron transfer efficiency. The rotation of Av2 in the cleft would be a true "work" step in that the cleft is too narrow for the rotation without some parting of the cleft.

The metastable condition of the complex would be relieved with the dissociation of the inorganic phosphate after electron transfer (28). In the new relaxed complex of Av2-Av1-MgADP, electron transfer in the reverse direction (back to Av2) is minimized by the poor overlap of the clusters. This complex (Complex II, Scheme 1) must be structurally different from the earlier complexes since it is a tighter complex (dissociation of the complex is rate limiting).

We have proposed a mechanism for obtaining work derived from MgATP hydrolysis on Av2 (11). In this hypothesis, MgATP is bound along the interface between the two subunits similar to the binding mode in *ras* proteins. Av1 induced nucleotide hydrolysis leads to a unique conformational state in which the electron is transferred. When the inorganic phosphate is released, the MgADP rotates to a binding site, as observed in the crystal structure (8, 10), that bridges the two subunits. The reorientation of the nucleotide would provide the work in a way similar to the mechanism of actin in muscle contraction (28).

Acknowledgments: This work was greatly aided by the generous provision of the protein crystal coordinates from Professor Douglas Rees without which much of our speculation would not be possible. JBH is particularly indebted to Professor Rees and L. Hagerty for hospitality and refreshing, frank discussions during numerous visits. The work of Drs. Deits, Willing, Wolle, and Magnuson provided much of the data presented here and their contribution is gratefully acknowledged.

This work was supported by the National Science Foundation grant 91-20515.

Abbreviations used are: Av1 and Av2, the Fe-protein and MoFe-protein from *Azotobacter vinelandii*; Cp2, the Fe-protein from *Clostridium pasteurianum*; altered proteins are designated by the wild type residue, the residue number, and the substituted residue, e.g., R100H is arginine at residue 100 replaced by histidine; WT is wild type protein; EDC, 1-ethyl-3-dimethylaminopropyl-carbodiimide.

Literature Cited

1. Hageman, R.V.; Burris, R. *Proc. Natl. Acad. Sci., USA* 1978 75 2699.
2. Lowe, D.; Thorneley, R. N. F. in *Molybdenum Enzymes*, T. G. Spiro, ed. (John Wiley and Sons, New York, 1984), pp. 222-284.
3. Walker, G.; Mortenson, L. E. *Biochemistry* 1974 13 1872.
4. Deits, T.; Howard, J. B. *J. Biol. Chem.* 1989 264 6619.
5. Ljones, T.; Burris, R. *Biochemistry* 1978 17 1866.
6. Anderson, G.; Howard, J.B.; *Biochemistry* 1984 23 2118.
7. Emerich, D.; Ljones, T.; Burris, R. *Biochim. Biophys. Acta* 1978 527 359.
8. Georgiadis, M.; Komiya, H.; Chakrabarti, P.; Woo, D.; Kornuc, J.; Rees, D. C. *Science* 1992 257 1653.
9. Kim, J.; Rees, D. C. *Science* 1992 257 1677.
10. Rees et al 1993 Chapter 11, this volume

11. Wolle, D.; Dean, D.; Howard, J. B. *Science* 1992 258 992.
12. Deits, T. L.; Howard, J. B. *J. Biol. Chem.* 1990 265 3859.
13. Burns, A.; Watt, G.; Wang, Z. *Biochem.* 1985 24 3932.
14. Wolle, D.; Kim, C.-H.; Dean, D.; Howard, J. B. *J. Biol. Chem.* 1992 267 3667.
15. Thorneley, R.; Lowe, D. *Biochem. J.* 1983 215 393.
16. Willing, A.; Georgiadis, M., Rees, D.; Howard, J. B. *J. Biol. Chem.* 1989 264 8499.
17. Willing, A.; Howard, J. B. *J. Biol. Chem.* 1990 265 6596.
18. Hausinger, R.; Howard, J. B. *J. Biol. Chem.* 1983 258 13486.
19. Pope, M. R.; Murrell, S. A.; Ludden, P. W. *Proc. Natl. Acad. Sci. U.S.A.* 1985 82 3173.
20. Lowery, R. G.; Chang, C. L.; Davis, L. C.; McKenna, M.-C.; Stevens, P. J.; Ludden, P. W. *Biochemistry* 1989 28 1206.
21. Orme-Johnson, W.; Hamilton, W.; Ljones, T.; Tso, M-Y; Burris, R.; Shah, T.; Brill, W. *Proc. Natl. Acad. Sci. U. S. A.* 1972 69 3142.
22. Stephens, P. J.; McKenna, C. E.; Smith, B. E.; Nguyen, H. T.; McKenna, M_C.; Thomson, A.; Devlin, F.; Jones J. *Proc. Natl. Acad. Sci., U. S. A.* 1979 76 2585.
23. Burgess, B. R. Chapter 10, this vol.
24. Robson, R. *FEBS Lett.* 1984 173 394.
25. Pai, E. F.; Kregel, U.; Petsko, G. A.; Goody, R. S.; Kabsch W.; Wittinghofer, A. *EMBO J.* 1990, 9 2351.
26. Normand P.; Bousquet, J. *J. Mol. Evol.* 1989 29 436.
27. Thorneley, R. N. F. et al; Chapter 19, this vol.
28. Thorneley, R. N. F.; Ashby, G.; Howarth, J.; Millar, N.; and Gutfreund, H. *Biochem. J.* 1989 264 657.

RECEIVED March 8, 1993

Chapter 19

Electron-Transfer Reactions Associated with Nitrogenase from *Klebsiella pneumoniae*

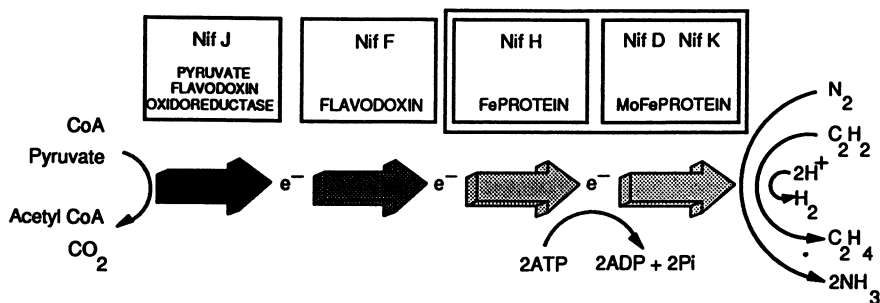
R. N. F. Thorneley, G. A. Ashby, K. Fisher, and D. J. Lowe

Agricultural and Food Research Council, Institute of Plant Science Research, Nitrogen Fixation Laboratory, University of Sussex, Brighton BN1 9RQ, United Kingdom

Pyruvate supported nitrogen fixation in *Klebsiella pneumoniae* principally involves four proteins: a pyruvate-flavodoxin oxidoreductase (*nifJ* protein); a flavodoxin (KpFld); the nitrogenase Fe-protein (Kp2); and the nitrogenase MoFe-protein (Kp1). Recent advances in understanding this electron transfer pathway are reviewed. These include: a novel post-translational modification of KpFld by covalent attachment of coenzyme A that may constitute part of a new regulatory mechanism for nitrogen fixation; the demonstration that the rate constants that define the Fe-protein cycle of nitrogenase are independent of the redox level of Kp1; the effect of changing β -Phe124 of Kp1 to Met or Ile on MgATP-dependent electron transfer from Kp2; and the kinetic analysis of 'slow' absorbance changes and EPR signals associated with Kp1 during substrate reduction that indicate a key role for the 'P'-centers.

This article reviews recent advances made by the Sussex Group and collaborating laboratories in understanding the mechanism of action of the Mo-containing nitrogenase of *Klebsiella pneumoniae* and its associated electron transfer pathway. A detailed description of the structures of the two proteins that comprise Mo-containing nitrogenases is given elsewhere in this volume (Burgess, chapter 10; Rees *et al.*, chapter 11; Bolin, chapter 12) and in the recent reviews by Thorneley (1), Eady (2), Lowe (3), and Smith and Eady (4). Scheme 1 shows the electron transport chain from pyruvate to nitrogenase in *K. pneumoniae*.

The sections below detail sequentially in the direction of electron movement the effects of a novel post-translational modification of the *nifF* gene product, a flavodoxin (KpFld), by coenzyme A (5); the effect the first one-electron reduction of the MoFe-protein has on reactions occurring in the second Fe-protein cycle (6); the involvement of Phe124 on the β -chain of the MoFe-protein in MgATP-dependent electron transfer from the Fe protein (7); and a role for the 'P'-centers in reducing dinitrogen (8).



Scheme 1. Electron Transport Chain to Nitrogenase in *K. pneumoniae*.

Post-translational Modification of *K. pneumoniae* Flavodoxin by Coenzyme A

Flavodoxins are small ($M_r \approx 20$ K) flavin-mononucleotide (FMN)-containing, monomeric proteins that act as low potential (E_m in the range -100 to -520 mV NHE for the physiologically important semiquinone-hydroquinone couple), single electron donors to nitrogenase. The electron transport chain from pyruvate to nitrogenase that involves a flavodoxin (the *nifF* gene product, KpFld) in *K. pneumoniae* is shown in Scheme 1. The expression of the *nifF* gene in diazotrophs is repressed by ammonia (when nitrogenase activity is not required for growth) (9) or in the presence of excess oxygen when nitrogenase is irreversibly inactivated (10). However little is known about the regulation of *K. pneumoniae* nitrogenase activity *in vivo*. There is no evidence for an ADP-ribosylation system in *K. pneumoniae* such as that which operates in *Rhodospirillum rubrum* to render nitrogenase Fe-protein inactive when cultures are exposed to high ammonia concentrations (11). However, chemostat studies have shown that nitrogenase activity of *K. pneumoniae* can be rapidly 'switched off and on' in response to the concentration of dissolved O_2 in the medium (10). The novel post-translational attachment of coenzyme A to KpFld described below may be part of this regulatory mechanism acting as an 'aerobic-anaerobic' switch for nitrogenase activity.

The *nifF* gene product (KpFld) is present at very low concentrations in *K. pneumoniae* even when growth is under N_2 -fixing conditions. Hence for kinetic studies with nitrogenase and crystallization trials it has been over-expressed in *Escherichia coli* so that it comprises $\approx 15\%$ of the soluble protein (5). Two forms of KpFld were separated by f.p.l.c. Since both these proteins had the same N-terminal amino acid sequence (30 residues) that correspond to that predicted from the *nifF* DNA sequence (12), a post-translational modification was suspected.

The ^{31}P NMR spectra in Figure 1 showed that the modified form of KpFld exhibited an additional singlet peak and a multiplet (AB quartet). The assignment of these ^{31}P -resonances to the phosphate groups of coenzyme A was made after highly accurate M_r values were obtained for the two forms of KpFld using the recently developed technique of electrospray mass spectrometry (Table I). The value of 18984 for KpFld is very close to that of 18981 calculated from the DNA-derived

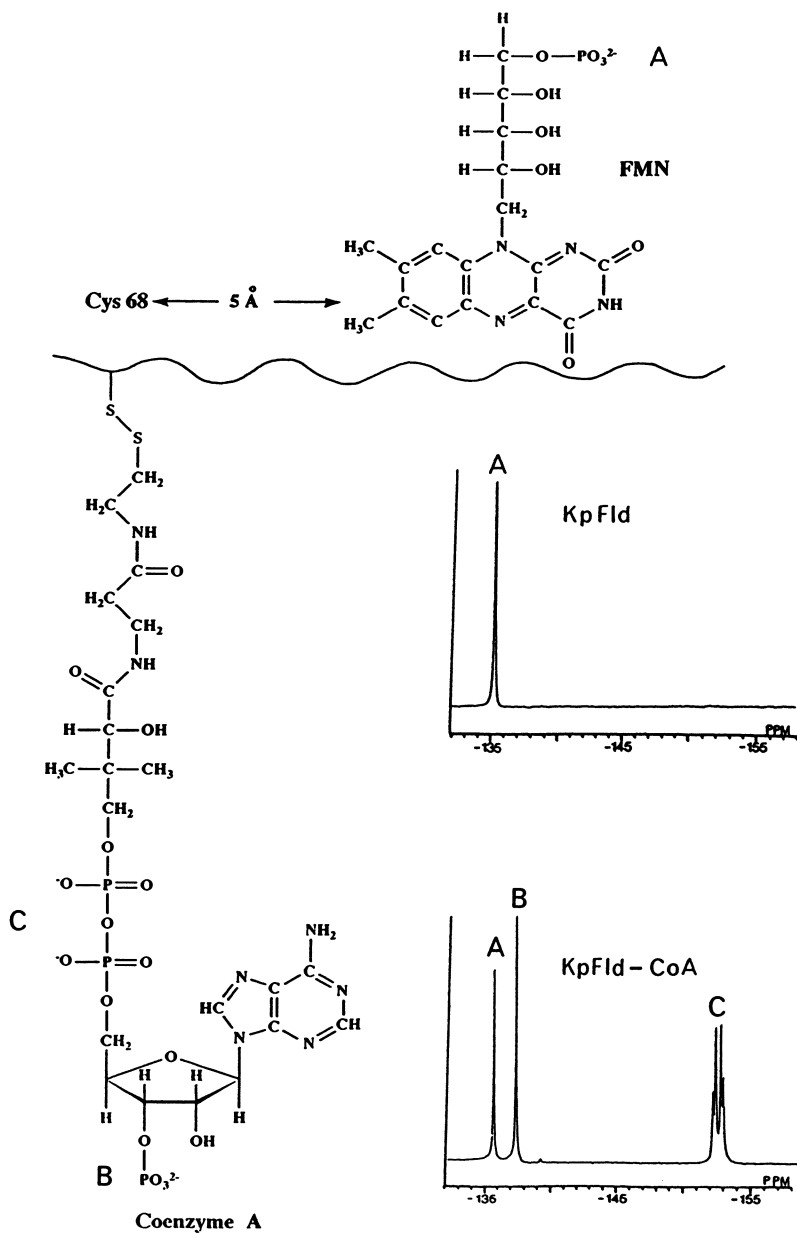


Figure 1. Post-translational modification of *K. pneumoniae* flavodoxin by covalent, mixed disulfide attachment of coenzyme A. Phosphate groups designated A, B and C give rise to the correspondingly labelled ^{31}P NMR peaks.

amino acid sequence assuming the dissociation of non-covalently bound FMN cofactor from the peptide in the electrospray apparatus. The difference in the M_r for the two forms of KpFld allowed us to assign coenzyme A as the most likely modifying group. The measured increase in M_r of 765.6 is remarkably close to the M_r of coenzyme A (767.5 for CoA-SH) and in exact agreement if coenzyme A is attached to KpFld by a mixed disulfide bond formed by the loss of two protons. The linkage was confirmed by thiol group estimations and by 'chemical synthesis' of the modified form by incubation of KpFld with coenzyme A. The modifying group was confirmed as coenzyme A by removing it from KpFld by incubation with dithiothreitol and then assaying this using the coenzyme A specific enzyme, acetylCoA:orthophosphate acetyl transferase.

Table I. Electrospray Mass Spectrometry of Post-translationally Modified *K. pneumoniae* flavodoxin

	<i>Molecular Weight</i>		<i>Observed Average Difference</i>
	<i>Calculated</i>	<i>Observed</i>	
KpFld	18981.4	18984.0 ± 3.8 18984.2 ± 3.5	765.6 ± 3.5
KpFld-CoA	19747.9	19748.7 ± 1.7	
KpFld-CoA*	19747.9	19754.0 ± 7.1	

The data were obtained with 10 μ l, 150 pmol protein samples injected into a VG BIO-Q quadrupole mass spectrometer.

* Synthesized by incubation of KpFld with coenzyme A.

Since KpFld only contains a single cysteine residue (position 68), this must be the site of coenzyme A attachment to the protein. The x-ray structure of homologous flavodoxin from *Azotobacter chroococcum* (AcFldB) shows that this residue is located *ca.* 5Å from the FMN cofactor, Figure 1 (P.M. Harrison, G. Ford and A. Shaw, personal communication). Not surprisingly, the coenzyme A modified flavodoxin is unable to act as an electron carrier between the *nifJ* protein and the nitrogenase Fe-protein, Figure 2 (5). Interestingly, only the electron transfer from the *nifJ* gene product to the flavodoxin semiquinone is prevented by the coenzyme A sited, adjacent to the edge of the FMN, on the surface of the protein. Electron transfer from dithionite-reduced flavodoxin hydroquinone to oxidized nitrogenase Fe-protein does not appear to be affected by the presence of the coenzyme A. An attractive explanation is that the presence of coenzyme A on KpFld stabilizes the protein complex formed with *nifJ*. The coenzyme A attached to KpFld-Cys68 could occupy the site on the *nifJ* protein that is normally involved in the conversion of

coenzyme A to acetyl-coenzyme A during oxidation of pyruvate, i.e., KpFld-CoA is a competitive inhibitor of coenzyme A binding (as a substrate) to *nifJ* protein.

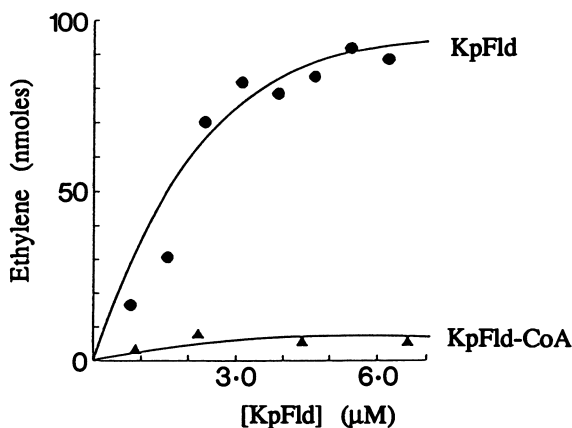


Figure 2. Pyruvate-flavodoxin oxidoreductase-supported acetylene reduction, catalyzed by nitrogenase, is mediated by native KpFld but not by CoA-modified KpFld. See ref. (5) for reaction conditions.

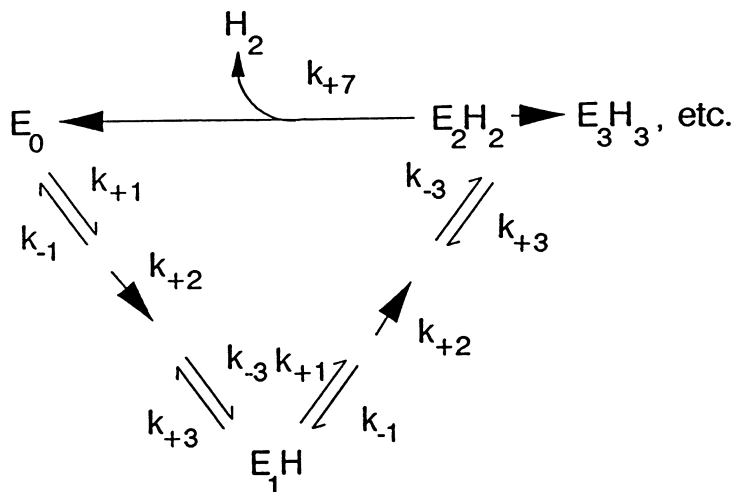
The competent electron transfer to nitrogenase Fe-protein could imply that electrons can leave KpFld-CoA at a site other than the exposed edge of the FMN. Drummond (13) has commented on the pronounced dipole moment of KpFld. He noted five basic residues on helix 1, densely clustered on the surface nearest the FMN and seven basic residues on the surface of helix 2 and the segment immediately before it. The high resolution structures of Nif-specific flavodoxins and nitrogenase Fe proteins that are now becoming available should enable meaningful computer modelling of a physiologically functional electron transfer protein complex. In particular, the effects changes in the redox states of both proteins and of nucleotide-induced conformation changes of the Fe-protein have on the structure/function of the electron transfer protein-complex are intriguing (14).

Coenzyme A levels *in vivo* are likely to be sensitive to the O₂ status of the cell and this novel coenzyme A dependent post-translational modification of flavodoxin must be a strong candidate for the sought after 'aerobic-anaerobic switch' that regulates nitrogenase activity.

Reduction of the MoFe Protein Does Not Change the Kinetics of the Next Fe Protein Cycle

Our current understanding of the complex kinetics and mechanism of nitrogenase is based on five papers that describe the partial reactions that define the Fe-protein cycle (15) and the subsequent combining of eight of these Fe-protein cycles into a single MoFe-protein cycle in which N₂ is reduced and H₂ evolved (16-19). It is possible to restrict the system to the first two cycles only by working at low electron

flux through the MoFe-protein (Fe-protein/MoFe-protein ratio of 1:100). Under these conditions, only H_2 is evolved since the electron flux is not sufficient to generate a significant concentration of the N_2 -binding forms of the MoFe-protein (E_3 and E_4 in Scheme 1 of ref. 16). Thus a subcycle involving only MoFe-protein in states E_0 , E_1 and E_2 can describe the system (Scheme 2).



Scheme 2. MoFe-protein Cycle for H_2 Evolution at Low Electron Flux.

E_0 represents one of two independently functioning halves of the tetrameric ($\alpha_2\beta_2$) structure of the *K. pneumoniae* MoFe-protein. The subscript refers to the number of times the electron transfer Fe-protein cycle has been completed and therefore represents the number of electron equivalents by which the $\alpha\beta$ MoFe-protein moiety has been reduced relative to resting E_0 . Species E_0 has an EPR signal (g -values 4.3, 3.7, 2.01) while species E_1H and E_2H_2 are EPR silent. The rate constants for the Fe-protein cycle are defined in reference (16).

A key assumption of our scheme for the mechanism of nitrogenase action (16) is that the rate constants of the Fe-protein cycle are not dependent on the reduction level of the MoFe-protein. If this assumption is correct, then Scheme 2 predicts that, a) the EPR signal of the MoFe-protein should be 50% bleached when a steady-state has been achieved after a lag phase of several minutes, b) the kinetics of the bleaching of the EPR signal should parallel the lag phase for H_2 evolution and c) stopped-flow absorbance changes associated with MgATP dependent electron transfer from Fe- to MoFe-protein, induced by mixing MoFe-protein with an excess of Fe-protein, should be independent of the redox level of the MoFe-protein. We have verified these predictions and shown that the rates of complex formation ($k_1 = 5 \times 10^7 \text{ M}^{-1} \text{ s}^{-1}$), electron transfer (k_2 with a $k_{\text{obs}} = 140 \text{ s}^{-1}$, Figure 3) and oxidized-complex dissociation ($k_3 = 6.4 \text{ s}^{-1}$) are the same for Kp1 in states E_0 (first Fe-protein cycle) and E_1H (second Fe-protein cycle) (6).

The demonstration that E_0 and E_1 are reduced by the Fe-protein at the same rate suggests that either electron transfer *per se* is not rate limiting or that the site on the MoFe-protein receiving the electron is at the same redox level in E_0 and E_1 . The first possibility is consistent with ATP-hydrolysis or a protein conformation change being rate limiting; the second with electron transfer occurring to a site other than the FeMo-cofactor, the EPR signal of which is ultimately bleached. The 'P' centers are obvious candidates to initially receive the electron from the Fe-protein (see below). The same rate of complex formation for Fe-protein with MoFe-protein in states E_0 and E_1 indicates that reduction of MoFe-protein does not lead to a significant change in protein conformation or charge density at the surface that docks with the Fe-protein. This would be consistent with the neutralization by protonation of the additional negative charge generated on the FeMo-cofactor by reduction to yield metal hydrides as precursors to H_2 evolution and N_2 binding.

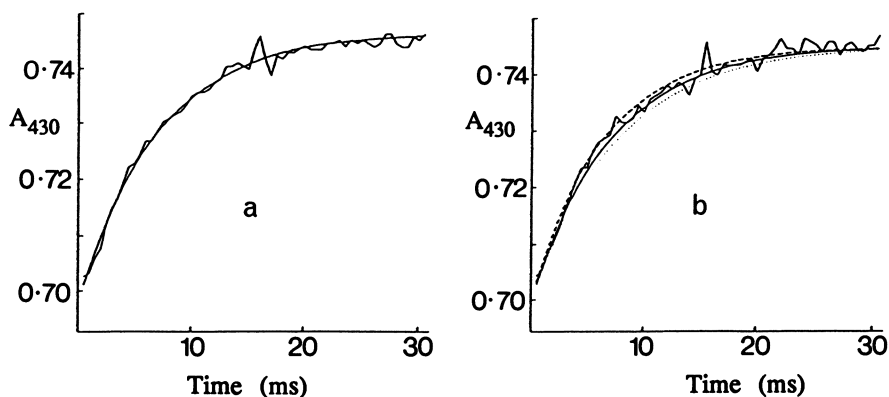


Figure 3. MgATP induced electron transfer from Fe-protein to MoFe-protein at oxidation levels E_0 and E_1 H occurs at the same rate. Trace (a) is for 100% E_0 and trace (b) for 50% E_0 and 50% E_1 H. Traces (a) and (b) are essentially identical and are best fitted by a single exponential function ($k_{obs} = 140 \text{ s}^{-1}$). The dotted and broken lines in trace (b) (which do not fit the data as well as the solid line) were drawn assuming that E_0 and E_1 H are reduced at different rates. See ref. (6) for further details.

β -Phe124 of *K. pneumoniae* MoFe-protein Implicated in MgATP-Dependent Electron Transfer from the Fe-protein

The *K. pneumoniae* MoFe-protein has a single chymotrypsin cleavage site at Phe124 on the β -subunit in a highly conserved region between Cys94 and Cys152 (7). This site must be accessible to chymotrypsin and is therefore on, or close to, the surface of the β -subunit. As such, it could be part of a "docking-site" for binding the Fe-protein. Since MgATP dependent electron transfer only occurs within the Fe-MoFe-protein complex, kinetic parameters associated with these partial reactions might be expected to change if Phe124 is changed to another residue by site specific mutagenesis. Subsequent to the results described below being obtained, it has been

confirmed that Phe124 is on the surface and that the adjacent Cys94 provides a thiolate ligand to bridge the two 4Fe-4S clusters that comprise each 'P'-center (assuming structural homology between Kp1 and Av1, Rees *et al.*, Chapter 11).

Two recombinant Kp1 proteins, β -Phe124Ile and β -Phe124Met, have been purified with similar Mo and Fe contents to native Kp1. As expected, both proteins were totally resistant to proteolysis by chymotrypsin. The β -Phe124Ile protein had a lower specific activity than either β -Phe124Met or native Kp1, Table II.

Table II. Kinetic Effects of Changing β -Phe124 to Met and Ile

	β -Phe124	β -Phe124Met	β -Phe124Ile
Electron transfer $k_{\text{obs}}(\text{s}^{-1})$	140	130	40
MgATP binding $K_{\text{D}}(\mu\text{M})$	400	320	110
Spec. activity per ng atom Mo	283	259	107

Stopped-flow spectrophotometry showed that MgATP dependent electron transfer from Fe-protein (Kp2) to β -Phe124Ile was much slower ($k_{\text{obs}} = 40 \text{ s}^{-1}$) than to β -Phe124Met ($k_{\text{obs}} = 130 \text{ s}^{-1}$) or native Kp1 ($k_{\text{obs}} = 140 \text{ s}^{-1}$), Figure 4 traces (a) and (c). The dependences of k_{obs} on MgATP concentration showed that the β -Phe124Ile-Kp2 protein complex binds MgATP ($K_{\text{D}} = 110 \mu\text{M}$) significantly tighter than do the β -Phe124Met- and native Kp1-Kp2 protein complexes ($K_{\text{D}} = 320 \mu\text{M}$ and $400 \mu\text{M}$ respectively). Stopped-flow absorbance changes at times between 0.1 and 1.0 s (Figure 4 traces (b) and (c)) were quite different for the β -Phe124Ile than for β -Phe124Met or native protein. Instead of the characteristic "slow-effects" shown in trace (b) (discussed in detail below), the absorbance in trace (d) decreases essentially to the initial value. This means that in the steady state a much higher percentage of the Fe-protein is in the reduced state. If complex dissociation (k_3 in the Fe-protein cycle) remains as the rate-limiting step, then k_3 must decrease from 6.4 s^{-1} to *ca.* 2.4 s^{-1} to be consistent with the lower specific activity of β -Phe124Ile (Table II). However a decrease in k_3 should result in a higher steady-state concentration of oxidised Fe-protein, not the observed decrease. We conclude therefore that with Phe124Ile another reaction has become rate limiting and that this effectively slows down the oxidation of the Fe-protein in the second cycle. Since the Phe124Ile mutation effects MgATP binding to the protein complex, we speculate that this may involve energy transduction and electron transfer occurring within the MoFe-protein involving a 'P'-center that is now known to be adjacent to Phe124 (Rees *et al.*, Chapter 11).

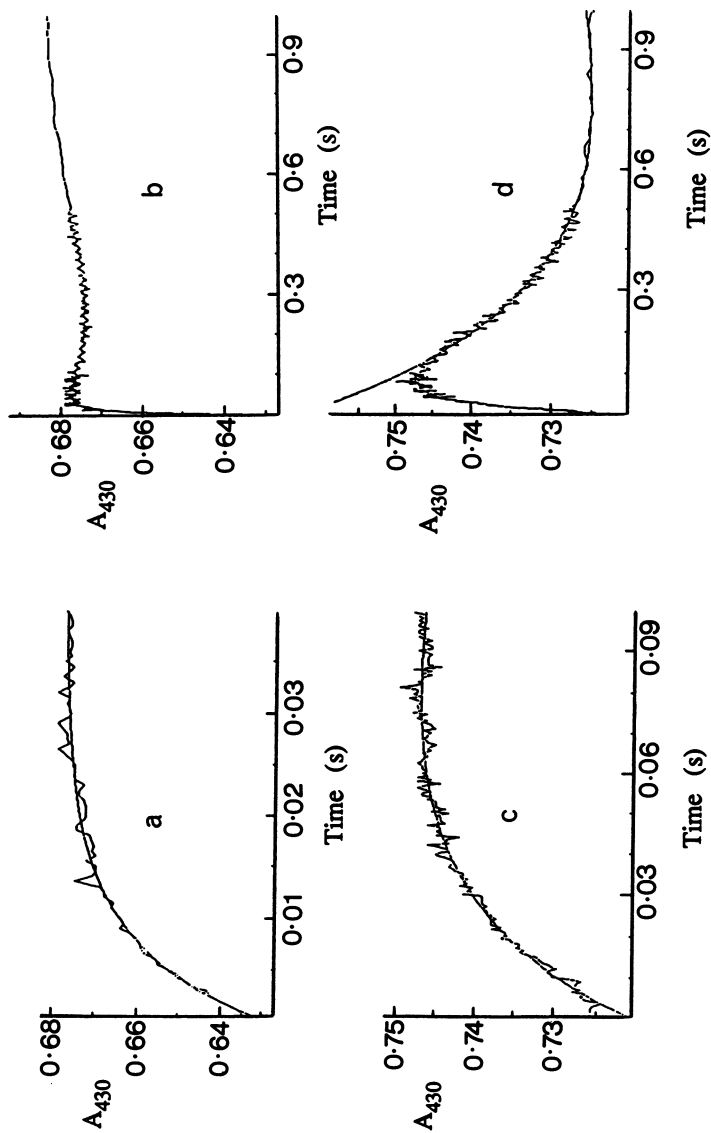


Figure 4. MgATP induced electron transfer from *K. pneumoniae* Fe-protein to β -Phe124Met and β -Phe124Ile. The traces were obtained by stopped-flow spectrophotometry at 430 nm when pre-equilibrated nitrogenase component proteins Kp2 (80 μ M) with β -Phe124Met (traces a and b) or β -Phe124Ile (20 μ M) (traces c and d) were mixed with MgATP in the presence of sodium dithionite. The single exponentials drawn through traces (a) and (c) give the first order rate constants shown in table II. Trace (d) shows a single exponential absorbance decrease ($k_{obs} = 3 \text{ s}^{-1}$) occurring after primary electron transfer.

A Role for 'P'-Centers in Nitrogen Reduction

Previous stopped-flow spectrophotometric studies of the pre-steady-state phases of nitrogenase have utilised absorbance changes associated with the oxidation/reduction of the Fe-protein and have not considered, in any detail, changes due to the MoFe-protein (6, 15, 20, 21). This is because the technique has been used to determine the rate constants that describe the partial reactions of the first (15) and second (6) Fe-protein cycles. We have previously not attempted to explain or simulate the small, kinetically complex absorbance changes, occurring at times up to 1 s (the so called 'slow effects'), simply because we did not understand them. Recently (8), by combining 'slow effect' data, obtained with stopped-flow spectrophotometry under different gaseous, reducible substrates ($\text{Ar}(\text{H}^+)$, N_2 , and C_2H_2) with EPR data obtained under the same conditions, we have been able to rationalize and simulate these effects, Figure 5. These simulations used the Lowe-Thorneley model for H^+ (16), N_2 (17) and C_2H_2 (22) reduction, the published rate constants for the partial reactions (18), and assigned $\Delta\epsilon_{430\text{nm}}$ values to the MoFe-protein as it is reduced sequentially from state E_0 through E_1 and E_2 to the N_2 binding states E_3 and E_4 , Table III. The most significant conclusion is that the reductive formation of E_4 is associated with the oxidation of a cluster within the MoFe-protein, and furthermore, by EPR, that the centers oxidized are the 'P'-centers, Figure 6. Thus, at E_4 electron transfer from the 'P'-centers to FeMoco is triggered resulting in increased reducing power at the N_2 -binding/reduction site. We have previously shown that an irreversible step at E_4 , after N_2 has bound, is necessary in order to simulate the dependence of the K_m for N_2 on $[\text{Kp2}]:[\text{Kp1}]$ and suggested that this step was a protonation of bound N_2 to yield a hydrazido(2) intermediate.

Table III. Extinction Coefficient Changes Associated with MoFe-protein (Kp1) During the Pre-steady-state Phase of Substrate Reduction

$\Delta\epsilon_{430}$ ($\text{mM}^{-1}\text{cm}^{-1}$)	Reaction	Comment
<0.5	$\text{E}_0 \rightarrow \text{E}_1$	FeMoco reduced to EPR silent state
-2.2	$\text{E}_1 \rightarrow \text{E}_2$	Negative $\Delta\epsilon_{430}$ assumed to be due to 'P'-center or FeMoco reduction
<0.5	$\text{E}_2 \rightarrow \text{E}_3$	
+6.7	$\text{E}_3 \rightarrow \text{E}_4$	'P'-center oxidation shown by EPR under Ar and N_2 but not C_2H_2 when E_4 state is not achieved

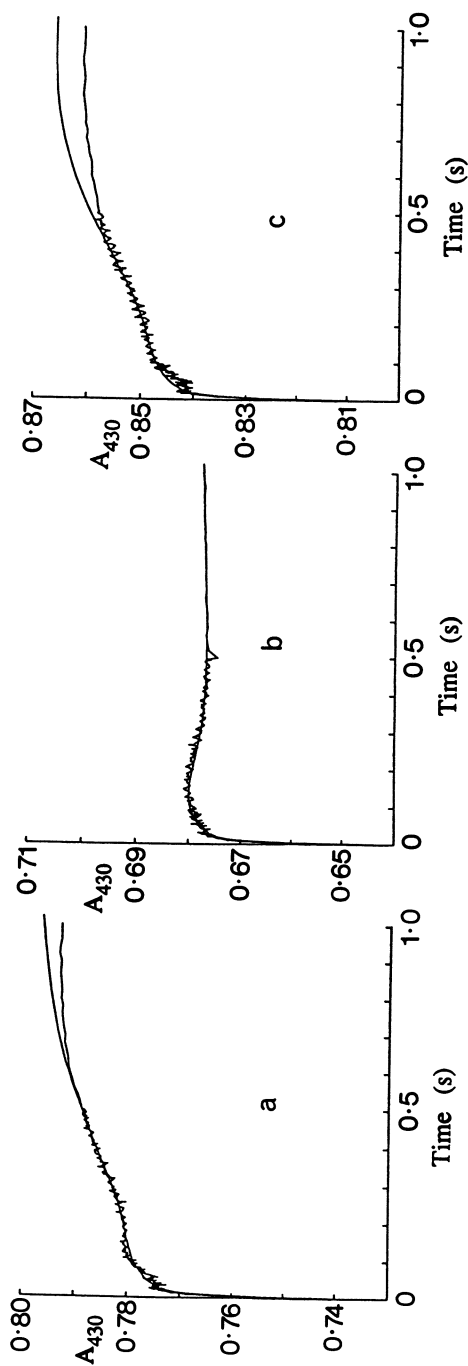


Figure 5. Stopped-flow traces for *K. pneumoniae* nitrogenase functioning under an atmosphere of a) Ar, b) C_2H_2 and c) N_2 . The solid lines are simulations using the Lowe-Thorneley model together with the extinction coefficient changes associated with the various reduced states of Kp1 shown in Table III and $\Delta\epsilon_{430} = 4 \text{ mM}^{-1} \text{ cm}^{-1}$ for oxidation of Kp2. The increase in absorbance after ca. 0.2 s for traces (a) and (c) is thought to be due to the oxidation of the 'P'-centers of Kp1 as it is reduced from state E_3 to E_4 . Under C_2H_2 , trace (b), state E_4 is not reached and oxidation of the 'P'-centers is not triggered.

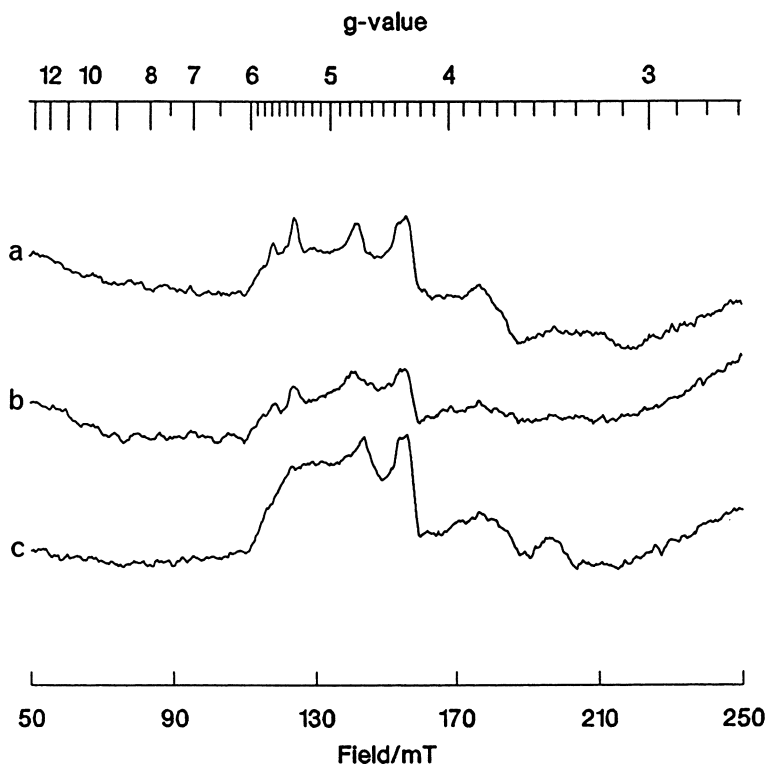


Figure 6. EPR spectra from *K. pneumoniae* nitrogenase functioning under an atmosphere of Ar, N₂ or C₂H₂. The sharp signals at $g=5.4$ and 5.7 are characteristic of oxidized 'P'-centers (23, 24) and they are only seen in the presence of Ar (a) or N₂ (b) and not C₂H₂ (c). These spectra, together with the simulations shown in Figure 5 allow the conclusion that the 'P'-centers become oxidized when Kp1 in state E₃ is reduced to state E₄ (8).

Thorneley *et al.* (25) had earlier identified an intermediate during N₂ reduction that produces hydrazine on acid or alkali quenching and assigned a hydrazido(2⁻) structure to it. This intermediate is the dominant form of E₄ when nitrogenase is reducing N₂. We now propose that oxidation of 'P'-centers, with a consequent increase in electron density on N₂ bound to FeMoco, induces protonation of the β -nitrogen atom. This is a crucial step in the catalytic cycle of nitrogenase that irreversibly couples electron transfer to the protonation of bound N₂.

Literature Cited

- 1 Thorneley, R.N.F. *Phil. Trans. R. Soc., Lond. B.* **1992**, *336*, 73-82.
- 2 Eady, R.R. *Adv. Inorg. Chem.* **1991**, *36*, 77-102.
- 3 Lowe, D.J. *Prog. in Biophys & Mol. Biol.* **1992**, *57*, 1-22.
- 4 Smith, B.E.; Eady, R.R. *Eur. J. Biochem.* **1992**, *205*, 1-15.
- 5 Thorneley, R.N.F.; Abell, C.; Ashby, G.A.; Drummond, M.H.; Eady, R.R.; Huff, S.; Macdonald, C.J.; Shneier, A. *Biochemistry.* **1992**, *31*, 1216-1224.
- 6 Fisher, K.; Lowe, D.J.; Thorneley, R.N.F. *Biochem. J.* **1991**, *279*, 81-85.
- 7 Fisher, K.; Lowe, D.J.; Pau, R.N. *Biochem. J.* **1993**, in press.
- 8 Lowe, D.J.; Fisher, K.; Thorneley, R.N.F. *Biochem. J.* **1993**, in press.
- 9 Dixon, R.A. In *The Nitrogen and Sulphur cycles*; Cole, C.D.; Ferguson, S., Ed.; Cambridge University Press, Cambridge, U.K. 1988, pp 417-438.
- 10 Hill, S. *FEMS Microbiol. Rev.* **1988**, *54*, 111-130.
- 11 Ludden, P.W.; Roberts, G.P. *Curr. Top. Cell Regul.* **1989**, *30*, 23-56.
- 12 Drummond, M.H. *Biochem. J.* **1985**, *232*, 891-896.
- 13 Drummond, M.H. *Eur. J. Biochem.* **1986**, *159*, 549-553.
- 14 Thorneley, R.N.F.; Deistung, J. *Biochem. J.* **1988**, *253*, 587-595.
- 15 Thorneley, R.N.F.; Lowe, D.J. *Biochem. J.* **1983**, *215*, 393-403.
- 16 Lowe, D.J.; Thorneley, R.N.F. *Biochem. J.* **1984**, *224*, 877-886.
- 17 Thorneley, R.N.F.; Lowe, D.J. *Biochem. J.* **1984**, *224*, 887-894.
- 18 Lowe, D.J.; Thorneley, R.N.F. *Biochem. J.* **1984**, *224*, 895-901.
- 19 Thorneley, R.N.F.; Lowe, D.J. *Biochem. J.* **1984**, *224*, 902-909.
- 20 Thorneley, R.N.F. *Biochem. J.* **1975**, *145*, 391-396.
- 21 Ashby, G.A.; Thorneley, R.N.F. *Biochem. J.* **1987**, *246*, 455-465.
- 22 Lowe, D.J.; Fisher, K.; Thorneley, R.N.F. *Biochem. J.* **1990**, *272*, 621-625.
- 23 Lowe, D.J.; Eady, R.R.; Thorneley, R.N.F. *Biochem. J.* **1978**, *173*, 277-290.
- 24 Hagen, W.R.; Wassink, H.; Eady, R.R.; Smith, B.E.; Haaker, H. *Eur. J. Biochem.* **1987**, *169*, 457-465.
- 25 Thorneley, R.N.F.; Eady, R.R.; Lowe, D.J. *Nature.* **1978**, *272*, 557-558.

RECEIVED March 8, 1993

Chapter 20

Recent Structure Determinations of the Molybdenum–Iron Protein of Nitrogenase

Impact on Design of Synthetic Analogs for the Iron–Molybdenum–Sulfur Active Site and the Iron–Molybdenum Cofactor

Dimitri Coucouvanis

Department of Chemistry, University of Michigan,
Ann Arbor, MI 48109–1055

Independent structure determinations of the MoFe proteins from *C. pasteurianum* and *A. vinelandii* by Bolin et al. and by Kim and Rees et al., respectively, have revealed for the first time the structures of the “P” clusters and the Fe/Mo/S center in nitrogenase. These studies are of extraordinary fundamental significance and are expected to be very important in our understanding of nitrogenase function. In this overview, an account is presented of outstanding questions that have been answered as a result of the recent structure determinations. The latter also have introduced a number of new questions with respect to structure-function relationships and the reduction of substrate molecules in nitrogenase. A brief review of previous studies directed toward the synthesis of Fe/Mo/S clusters as analogs for the nitrogenase active site is put into perspective and various “model” compounds are critically evaluated.

Nitrogenase. The reduction of N_2 to ammonia at ambient temperature and pressure is catalyzed in nature by nitrogenase (1). Nitrogenase contains two proteins of which the Fe protein (M_r , 60,000 D) binds two molecules of MgATP and serves as a specific activator and source of electrons for the FeMo protein (M_r , 220,000 D) where N_2 reduction takes place. The transfer of electrons from the Fe protein to the FeMo protein is coupled strongly to MgATP hydrolysis and, under optimum conditions, one electron is transferred for every two molecules of ATP that undergo hydrolysis. The crystal structure of the Fe protein has been determined (2) and contains an Fe_4S_4 cluster that bridges two identical subunits. The MoFe protein contains 30 Fe and two Mo atoms that are distributed in two $Fe_7MoS_{8.9}$ clusters, (“M” clusters), and two $Fe_8S_{7.8}$ clusters, (“P” clusters), (3-4). The FeMoS cluster can be reversibly removed from the protein as an inorganic cofactor, (FeMo-cofactor) (5) of as yet unknown structure, but with spectroscopic properties very similar to those of the FeMoS center in nitrogenase. Numerous excellent reviews contain detailed information on mechanistic and genetic aspects of nitrogenase function and biosynthesis (1). Similar comprehensive reviews are available for the nitrogenase cofactor (6-7).

In the last decade, two alternate nitrogenase systems have been discovered. These systems are synthesized in the absence of Mo (8-10) and are not as effective in N_2 reduction. In one of the alternative nitrogenases, V has replaced Mo and the FeV-cofactor (11) is structurally similar to the FeMo-cofactor (12-13). An alternative nitrogenase that contains neither Mo nor V also has been reported (14). In the latter, the partially purified protein, analogous to the MoFe and VFe proteins, reduces substrates with comparatively low activity (15).

The Metal Clusters In the FeMo Protein of Nitrogenase. A determination of the structure and a detailed understanding of the function of the dinitrogen-reducing Fe/Mo/S center in nitrogenase are problems that have received considerable attention in the last two decades. In addition to extensive studies that have placed emphasis mainly on the biology, biochemistry and biophysics of nitrogenase, a significant effort has been expended in attempts to obtain synthetic Fe/Mo/S complexes of possible utility as analogs for the enzyme active site (16-17).

In the past, the synthetic biomimetic Fe/Mo/S chemistry, relevant to the nitrogenase problem, was conducted only in a speculative manner. This was due to the lack of a clear definition of the problem which, in turn, had its origin mainly in: a) the lack of an x-ray crystallographic structure of the MoFe protein or of the isolated FeMo-cofactor of nitrogenase; b) the lack of angular information in the structural, x-ray absorption derived data available for the FeMo-cofactor and for the Fe/Mo/S center in the MoFe protein; c) difficulties in obtaining sufficiently accurate analytical results to firmly establish stoichiometry and a uniformly acceptable Mo:Fe:S ratio, and; d) difficulties in associating the integrated spectroscopic data with a unique cluster. These problems notwithstanding, there exist a number of well established criteria that must be met in the synthesis and evaluation of synthetic analogs. These criteria are based on the judicious appraisal of the available stoichiometric, structural, spectroscopic and reactivity data. Attempts to obtain synthetic analogs for the "P" clusters of the FeMo protein (18) have been infrequent and until recently, were based on the widely held hypothesis that the "P" clusters are variants of the Fe_4S_4 ferredoxin-type clusters (19).

Recent Developments. In a recent single-crystal x-ray diffraction study, Bolin and coworkers determined the basic cell architecture of crystalline MoFe protein from *Clostridium Pasteurianum* and established the relative positions of the two "P" clusters and the two Fe/Mo/S centers (3a). The latter were unequivocally identified on the basis of anomalous x-ray scattering effects. More recently Kim and Rees (4) reported on the x-ray crystal and molecular structure of the MoFe protein from *A. vinelandii* and at 2.7Å resolution. This study not only verified the original unit cell organization (3a) but also gave the first glimpse of the "P" clusters and the Fe/Mo/S centers at a molecular level. At the present level of resolution, the electron density maps can be interpreted in terms of models for the "P" clusters and the Fe/Mo/S centers that, on the whole, agree quite well with most of the available spectroscopic and analytical data. The recent crystallographic results are of historical significance in the chemistry of nitrogenase. They mark the beginning of a new era for biomimetic inorganic chemistry and herald the transition from speculative to corroborative chemistry.

In this review we will: a) present brief composite pictures of the "P" clusters and the Fe/Mo/S centers in nitrogenase as revealed previously by spectroscopic studies; b) describe and analyze the crystallographic results in terms of the spectroscopic data; c) briefly review and place in perspective the presently available synthetic Fe/Mo/S clusters, and; d) identify important unanswered questions and new challenges in synthetic metal sulfur chemistry relevant to the nitrogenase problem.

The Metal Centers in Nitrogenase as Outlined in Terms of Analytical and Spectroscopic Data

The P Clusters. The presence in the FeMo protein of two types of metal centers was suggested originally by detailed Mössbauer spectra analyses (20). The ~30 iron atoms in the protein were roughly assigned to two M centers, each containing a molybdenum and ~7 iron atoms, and to four unusual Fe₄S₄ centers, "P-clusters" that, in the reduced state, "P^N", were diamagnetic and contained four Fe⁺² atoms. Within these reduced clusters, three different iron sites were identified by Mössbauer spectral analyses and labeled as Fe⁺², D and S (20).

The quantitative extrusion (3.4 to 4.0 Fe₄S₄ clusters per α₂β₂ subunit complex) of the "P" clusters from the FeMo proteins of *C. pasteurianum*, or *A. vinelandii* (21) further reinforced the suggestion that the "P" clusters were, in fact, of the Fe₄S₄ type. The oxidation of the "P^N" clusters by 1e⁻ (per Fe₄S₄ center) initially was thought to give a non-integer spin "P^{ox}" state for each of the clusters (20). This non-integer spin nature of the "P^{ox}" clusters also was suggested (22) on the basis of magnetic circular dichroism, MCD, spectroscopic data. Paradoxically the non-integer spin "P^{ox}" state, although paramagnetic, did not show an electron paramagnetic resonance EPR spectrum. The "P^{ox}" clusters were reported to undergo reduction with a E_{1/2} value of -0.47V (23). The tetranuclear nature of the "P" clusters was challenged by Hagen and coworkers who, on the basis of EPR spectroscopy on thionine-oxidized "P" clusters, suggested that the "P" centers were octanuclear rather than tetranuclear clusters (24) that could undergo a 2e⁻ oxidation to an integer spin (and EPR silent) state and a further 1e⁻ oxidation to a S = 7/2 state. This view is presently accepted as the correct one and is in apparent agreement with a reevaluation of the original Mössbauer data (25). The octanuclear nature for the "P" clusters now has been unequivocally established (3c, 4) and two possible structures have been proposed on the basis of the crystal-structure determinations (vide infra).

Specific Characteristics of the Fe/Mo/S Clusters. Prior to the structure determination of the MoFe protein of nitrogenase, a composite picture of the Fe/Mo/S center had emerged that was defined by the following six specific characteristics:

A Fe:Mo:S stoichiometry of 6±1:1:8±1, and a cationic [MoFe₆S_{8,9}]⁺ⁿ core (n ~ +4) that likely contains Mo(IV). Various determinations of the stoichiometry of the Fe/Mo/S site have been reported over the years. The reported Fe:Mo ratios are found in the range from 10:1 (26) to 5.5±0.5:1 (27) with most of the determinations between 6:1 and 8:1 (5a, 26, 28-32). These values are slightly higher than the 5±1:1 ratio deduced by a quantitation of the Mössbauer spectra of the cofactor (33). The determinations of the S:Mo ratio show a similar scatter. Reported ratios include 4:1 (34) 8.7±1:1 (28) and 8.8±0.6:1 (34). Evaluations of the analytical data reported to date have reached the conclusion that the minimum Fe:Mo stoichiometry very likely is 6:1 (6) or 6.5±1.5:1 (7). The most likely S:Mo ratio is accepted as 8-9:1 (6) or 9±1:1 (7).

Spectroscopic evidence regarding the oxidation state of the Mo atom has become available from ⁹⁵Mo-electron nuclear double resonance ENDOR (35) studies on the Fe-Mo protein from *A. vinelandii* in the semireduced S = 3/2 state. On the basis of the small ⁹⁵Mo hyperfine couplings observed, it has been argued that the Mo atom is an even-electron ion. This would exclude Mo(III) and Mo(V) but not Mo(IV). The overall charge of the FeMoS core can be calculated for the most likely stoichiometry and oxidation states of the component atoms. If one assumes that the Mo atom is indeed Mo(IV), and the average oxidation state of the iron atoms is ~+2.66 as indicated by the isomer shift of the cofactor in the S = 3/2 semireduced state (0.37 mm/s) (33), the overall core charge would be ~+4 for either a Fe₆MoS₈ or

a Fe_7MoS_9 core. This type of calculation of the overall charge assumes that the Fe atoms in the nitrogenase cofactor are mainly S^{2-} -ligated, tetrahedrally-coordinated ions. If this assumption is valid, one may use the oxidation state-Mössbauer isomer shift empirical relationship to assign formal oxidation states to the iron atoms. This relationship has been found reliable in studies of the Fe/S centers in the ferredoxins and synthetic analogs (36).

A core structure that contains MoS_2Fe and FeS_2Fe rhombic units with Mo-Fe distances of $2.70(2)\text{\AA}$ and two shells of Fe-Fe distances of $2.65\pm 0.1\text{\AA}$ and 3.8\AA . The presence of a $\text{S}_3\text{Mo}(\text{X})_3$ structural unit ($\text{X} = \text{O}$ or N) with Mo-S and Mo-X distances of $2.37(2)\text{\AA}$ and $2.10(2)\text{\AA}$, respectively. The structural data available for the Fe/Mo/S center in nitrogenase, prior to the single crystal x-ray diffraction studies, have been obtained from x-ray absorption spectroscopic studies and particularly from extended x-ray absorption fine structure EXAFS analyses. The Mo-K-edge EXAFS results for the MoFe protein and for the FeMo-cofactor in NMF solution (37-39) show that the first Mo coordination sphere contains 2-3 light atoms (O, N?) at $2.11\pm 0.01\text{\AA}$ and 3-4 sulfur atoms at $2.37\pm 0.02\text{\AA}$. The second coordination sphere shows ~3 Fe atoms at $2.70\pm 0.01\text{\AA}$. A comparison of EXAFS results for the semireduced MoFe protein, the "as isolated cofactor," and the cofactor following the addition of $\text{C}_6\text{H}_5\text{SH}$ (37), shows that the Mo atom is attached to more light atoms in the isolated cofactor than in the protein bound Fe/Mo/S center (3.1 vs 1.7). Furthermore, the number of sulfur atoms attached to the Mo atom in the isolated cofactor (3.1) is less than that in the protein bound cluster (4.5). No other neighboring atoms have been reported at distances $> 2.8\text{\AA}$ from the Mo atom.

Two early reports on the Fe-EXAFS of the FeMo-cofactor showed the average environment per Fe atom to contain ~2.2 Fe or 2.3 Fe atoms at 2.64\AA or 2.66\AA , respectively, and 3 S or 3.4 S atoms at 2.20\AA or 2.25\AA , respectively (40-41). The average number of light atoms around the Fe atoms has been uncertain. While one EXAFS analysis places 1.2 light atoms per iron atom at a distance of 1.81\AA (40), the other simply does not "see" any light atom neighbors (41). The latter study also reports a second shell of Fe atoms (1.3 Fe per Fe) at a distance of 3.68\AA that was not detected previously (40). The results of a very recent Fe-EXAFS study (42) on the MoFe protein from *A. vinelandii* indicate light donor atoms coordinated to at least some of the Fe atoms. In this latest study, an average of 0.5 light atoms (O, N) per iron atom at a distance of 1.842\AA was reported. The previously detected (41) Fe shell at 3.76\AA was verified, and a new iron shell (0.3 Fe per Fe) at 4.70\AA was discovered. These results are not inconsistent with cores such as MoFe_5S_6 (Figure 1A) or MoFe_6S_6 (Figure 1B).

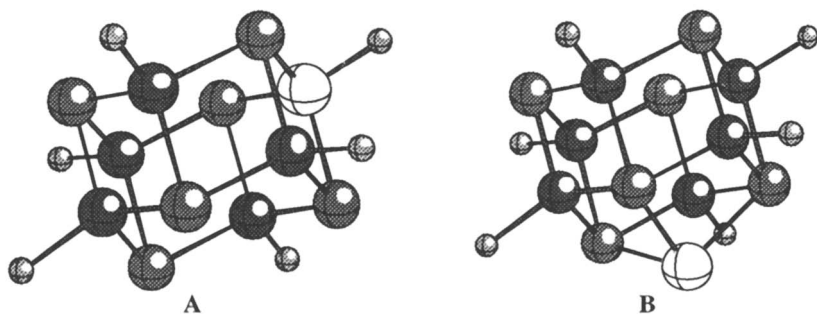


Figure 1. The $[\text{Fe}_5\text{MoS}_6(\text{L})_6]^{n-}$ and $[\text{Fe}_6\text{MoS}_6(\text{L})_6]^{n-}$ clusters. Earlier Speculative Models for the Fe/Mo/S Center in Nitrogenase. Both of these structures having their origin in the Fe_6S_6 prismanes (43).

An overall asymmetric structure with approximately one half of the iron atoms farther than 2.7Å away from the Mo atom. This conclusion is based on the Fe-EXAFS results. These results show that the average number of Mo atoms "seen" by the Fe atoms are 0.4 at 2.76Å (40, 42) or 0.8 at 2.7Å (41) and suggest that some Fe atoms are close to the Mo at 2.76Å, while others (perhaps a similar number) are too far to be influenced by the Mo atom. An asymmetry in the structure of the "M" centers also is suggested from ENDOR spectroscopic studies on the MoFe protein. These studies show five distinct iron sites that can be grouped into two subgroups on the basis of hyperfine parameter values (35b).

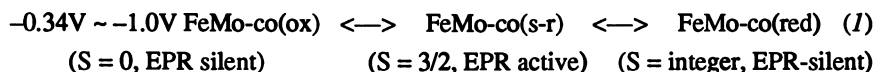
The MoFe₅S₆ or MoFe₆S₆ clusters (Figure 1) satisfy the requirements set forth by the Fe-EXAFS analyses (42) and, with an appropriate mixed-ligand environment, could give rise to a multitude of Fe sites as required by the ENDOR data (35).

A number of terminal ligands most likely less than the number of Fe atoms. Of these ligands one may contain a sulfur donor atom and another a nitrogen donor atom. The analysis of the Fe-EXAFS of the MoFe protein shows an average of 3.5 S atoms for each of the Fe atoms at 2.317Å (42) and 0.5 light atoms per iron. These results suggest that there is an insufficient number of ligands to satisfy the coordination requirements of a full set of four-coordinate iron atoms and may indicate that some of the iron atoms are coordinated by only three sulfur atoms. The same conclusion can be reached from the analysis of one of the two Fe-EXAFS studies of the cofactor (41) that shows no light atoms at all. The earliest study (40), however, detects a light atom neighbor near each of the iron atoms in the FeMo-cofactor and does not indicate coordinatively unsaturated Fe atoms. It is apparent that another Fe-EXAFS study of the cofactor is needed to resolve the controversy regarding the number of light ligands on the Fe atoms. The sharpening of the $S = 3/2$ EPR spectrum of the FeMo-cofactor upon addition of one equivalent of thiophenol (44) has been quantitated by ¹⁹F NMR spectroscopy (45) using p-CF₃C₆H₄S⁻, and is attributed to Fe-thiophenol coordination (45). This result establishes the presence of an exocluster sulfur ligand for one of the iron atoms. The binding of the thiol ligand to an iron atom rather than to the Mo atom is supported further by the observation that the Mo-K XANES and Mo-K EXAFS of the cofactor (46) are unaffected by the addition of either thiophenol or selenophenol (38). A similar conclusion is reached by the Se-edge EXAFS analysis of the selenophenol-treated FeMo-cofactor. This analysis shows a Fe atom in the first coordination shell of the Se atom at 2.42Å (39). Evidence for the coordination of an N ligand to the FeMo-cofactor within the protein has been obtained by a comparison of electron spin echo results for the MoFe protein to that of the isolated FeMo-cofactor (47).

The presence of an $S = 3/2$ EPR ground state with accessible one electron oxidation and one-electron reduction levels and EPR silent, $S = 0$ or $S = \text{integer}$ electronic ground states. The early classic studies by Münck, Orme-Johnson and coworkers, on the EPR spectra (44, 48) of the MoFe protein and the nitrogenase FeMo-cofactor attributed the $S = 3/2$ center in the MoFe protein to the FeMo-cofactor. A similar conclusion was reached on the basis of the very similar magnetic properties of the protein-bound Fe/Mo/S centers and the isolated FeMo-cofactor obtained by low temperature MCD spectroscopic studies (49). Extensive analyses of the Mössbauer spectra (50-51) indicated that most of the Fe atoms in the FeMo-cofactor were part of a $S = 3/2$ spin-coupled system.

The changes observed between the Mössbauer spectra of the MoFe protein and the FeMo-cofactor after extrusion from the protein have been interpreted (32) as indicative of increased symmetry in the isolated FeMo-cofactor.

The oxidation reduction properties of the FeMo-cofactor (29, 52-54) and the MoFe protein have been reviewed in detail (6-7). A summary of these properties as it appeared in (7) is shown in Equation 1 (ox = oxidized, s-r = semireduced, red = reduced).



Have the ability to accommodate a homocitrate or other structurally similar polycarboxylate anions. Damaging mutation in *nifV*, one of the six nitrogen fixation genes involved in the biosynthesis of the FeMo-cofactor, results in a MoFe protein severely hindered in its ability to reduce N_2 (55). This drastic change in the function of the MoFe protein was traced to a defective FeMo-cofactor (56) that apparently lacked a specific low molecular weight species (V-factor). This V-factor that was produced in the presence of the *nifV* gene product is essential for activity (57) and has been identified as (R)-homocitrate (58). The Fe/Mo/S center is associated with (R)-homocitrate in a 1:1 ratio (59) and (R)-homocitrate is retained on the FeMo-cofactor when the latter is extracted from the MoFe protein. The presence of light atom ligands (O,N) on the Mo atom as revealed by Mo-EXAFS analyses (37-39) and the probable absence of similar ligands on the Fe atoms marginally favor coordination of the (R)-homocitrate ligand to the Mo atom. Other polycarboxylate ions that seem to substitute for the (R)-homocitrate ligand in the Fe/Mo/S centers fail to be effective in N_2 reduction (60).

The Structures of the Metal Centers as Revealed by X-ray Crystallography

The Fe-Mo Cofactor. in the unit cell of the FeMo protein from *C. pasteurianum* nitrogenase (3a), there exist four well-separated metal clusters in the $\alpha_2\beta_2$ protein tetramer. Two of these clusters are identical Fe/Mo/S units ("M" centers) and the other two are identical Fe/S units ("P" clusters). In the structure of the MoFe protein from *A. vinelandii* (4), the Fe/Mo/S center is a heterometallic cluster that contains two isostructural, cuboidal subunits. The M/S cores in the two subunits are chemically different, one being Fe_4S_3 and the other $MoFe_3S_3$. Both subunits lack one S^{2-} ligand from having the well known Fe_4S_4 and $MoFe_3S_4$ "cubane" core structures. According to Kim and Rees (4), the subunits are linked by two $Fe-\mu_2-S-Fe$ and one $Fe-\mu_2-X-Fe$ bridges ($X = \text{a light atom, N, O?}$). This arrangement results in six, very unusual, iron atoms that are three-coordinate and nearly planar (Figure 2A). At the present stage of refinement, no other ligands are apparent near the coordinatively unsaturated Fe atoms in the $Fe_3(\mu-S)_2(\mu-X)Fe_3$ unit and the $Fe-\mu_2-X-Fe$ bridge has been tentatively proposed as a possible site for substrate activation.

In the structure of the Fe/Mo/S cluster, the Mo atom is found at the end corner of the molecule and is octahedrally coordinated by three $\mu_3.S^{2-}$ ligands, two donor atoms from what is proposed to be a homocitrate molecule (possibly an OH group and a carboxylate group), and a histidine imidazole nitrogen (His α 442). It seems likely that the Mo atom is not directly involved in substrate activation. Other than the Mo-bound histidine residue, the only other ligand anchoring the cofactor to the protein backbone is a cysteine ligand (Cys α 275). This residue is coordinated to the outermost corner iron atom in the Fe_4S_3 subunit.

The six, coordinatively-unsaturated Fe atoms in the structure (Figure 2A) are rather unsettling and nearly unprecedented. Only one example of trigonally coordinated Fe complex is known and this forms only because of severely, sterically encumbered ligands (61).

Coordination saturation, and a more conventional trigonal pyramidal or distorted tetrahedral geometry for the three-coordinate iron atoms could be achieved either by addition of one terminal ligand to each iron atom (Figure 2B) or by the addition of a $\mu_6\text{-S}^{2-}$ ligand in the center of the Fe_6 prism (Figure 2C). Similar overall structural features for the "M" centers have been observed in an independent structure determination of the *C. pasteurianum* MoFe protein by Bolin and coworkers (3*b-c*). In this study, three sites of nearly equal electron density have been found around the middle of the Fe/Mo/S cluster and have been assigned to three $\mu_2\text{-S}$ ligands. The three bridges in the structure span the edges of the trigonal prism defined by two triangular Fe_3 arrays supplied, one each, from the two M_4S_3 subunits. In the latter structure (3C), that also does not show exocluster ligand coordination to the meridial iron atoms, the presence of a $\mu_6\text{-L}^{2-}$ central ligand (L = O, S) (Figure 2C) is not proposed as a structural feature, however it cannot be entirely ruled out.

The "P" Clusters. Two ellipsoidal high electron density areas in the unit cell have been assigned to the "P", Fe/S, centers on the basis of anomalous scattering observations (3*a*). Two types of Fe_8 clusters, with somewhat different structures have been proposed as models for these centers. Both contain two cuboidal subunits and are anchored to the protein matrix by four terminal and two bridging cysteinyl residues. Of these models, the one suggested by Rees (4) consists of a doubly-bridged double-cubane and contains two Fe_4S_4 ferredoxin-like cubes bridged by two cysteinyl residues (Figure 3A). The model suggested by Bolin (3*b*) consisted of two Fe_4S_3 subunits bridged by two cysteinyl residues and sharing a $\mu_6\text{-S}^{2-}$ (or perhaps a $\mu_6\text{-S}_2^{2-}$ ligand) (Figure 3B). Both of these initial models for the cofactor have now evolved to a consensus model. In the latter, the two cuboidal subunits are bridged by two cysteinyl residues, and also by a $\mu_6\text{-S}_2^{2-}$ ligand that appears to have formed by oxidation of two $\mu_3\text{-S}^{2-}$ ligands (one from each of the two Fe_4S_4 subunits) (Figure 3C). At present, a $\mu_6\text{-S}^{2-}$ ligand between the two subunits

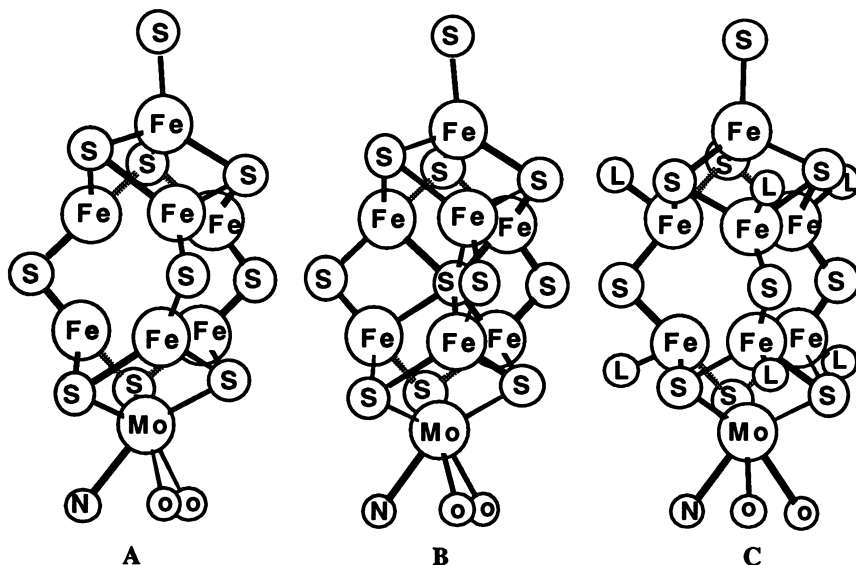


Figure 2. The structure of the Fe/Mo/S center in the MoFe protein of nitrogenase, A (3*c*, 4); and possible structure for the nitrogenase cofactor B, C.

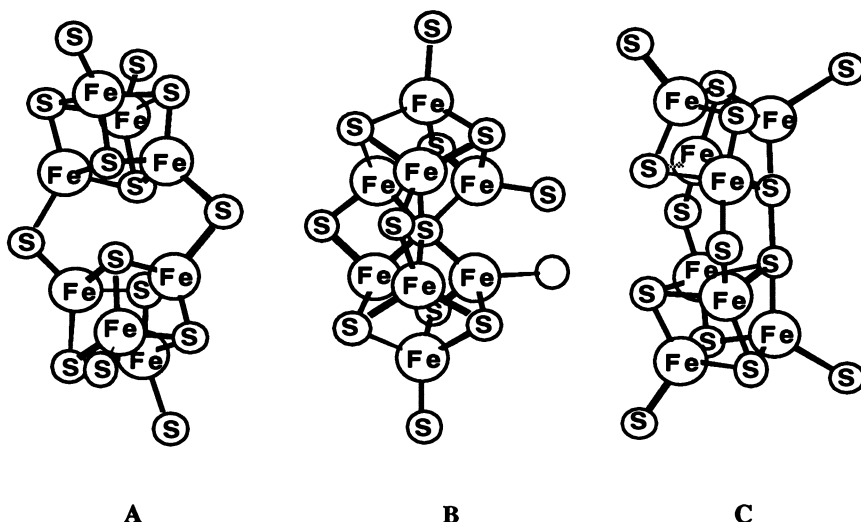


Figure 3. Suggested structures for the “P” clusters in the MoFe protein of nitrogenase, A (4a); B (3b) and C (4b).

although not preferred as a structural feature, still cannot be ruled out (3c). It is tempting to speculate that the $\mu_6\text{-S}_2^{2-}$ ligand is a site used for the storage of two additional electrons.

Alternatively, it could be the oxidation product of two $\mu_3\text{-SH}$ moieties as two protons are reduced to H_2 . This would place the site of H^+ reduction at the “P” clusters rather than the M centers. The presence of two rather than four “P” clusters in the FeMo protein vindicated an earlier proposal that, based on EPR studies, suggested the existence of octanuclear rather than tetranuclear “P” clusters (24).

An Analysis of the Proposed Structures In Terms of the Analytical and Spectroscopic Data. A reexamination of the unanswered questions regarding the metal centers in the MoFe protein of nitrogenase, in the light of the recent crystallographic results, reveals some answers and offers many new insights.

The Fe/Mo/S center. The Fe:Mo:S stoichiometry appears now settled at 7:1:8-9. This ratio is not unexpected in view of the average analytical data that previously indicated a similar stoichiometry (see section II-B-1). The ligation of the cofactor to the protein also has been settled and two anchor points are revealed in the structure, of the *A. vinelandii* protein (4). A cysteinyl residue (Cys α 275) as was predicted on the basis of site directed mutagenesis studies (62-63) and a histidine residue (His α 442). The His α 195 residue, previously suggested to bind to the cofactor on the basis of site directed mutagenesis studies (47, 64), is close to the cofactor ($\sim 5\text{\AA}$ from an iron atom) but is not involved in covalently binding the cofactor to the protein.

The “gross” structure of the FeMo-cofactor can be described in terms of two cuboidal M_4S_3 subunits. The presence or absence of a central $\mu_6\text{-S}_2^{2-}$ in this structure (Figure 2C) will determine whether it resembles qualitatively some of the models proposed earlier (vide infra). The M_4S_3 structural subunits in the new structural model (Figure 2A) have only one precedent. This is the Fe_4S_3 core in the long known $[\text{Fe}_4\text{S}_3(\text{NO})_7]^-$ Roussin anion (65). The structure of this cluster (Figure 4) (66) shows a pyramidal Fe_4 frame, with short Fe-Fe distances from the

unique apical to the three equatorial iron atoms (2.70Å) and long Fe-Fe distances between the equatorial iron atoms (3.55Å). The monoanion contains seven NO⁺ ligands that require low *formal* oxidation states for the Fe atoms (3Fe(0) and 1Fe(-1)).

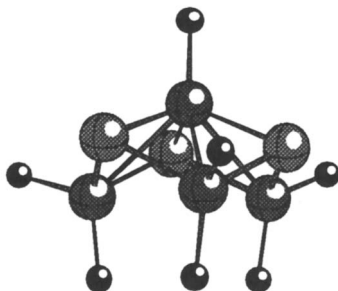


Figure 4. The structure of the $[\text{Fe}_4\text{S}_3(\text{NO})_7]^-$, Roussin's anion (65-66).

The structure of the Fe/Mo/S core, as revealed in the protein structure, is compatible with the EXAFS results, but different from the structures of other cores in previously proposed models (16). Nearly all of the latter contain Fe- μS -Fe and Mo- μS -Fe rhombic units and, consequently, are in some agreement with the EXAFS-derived structural data. The core structures of proposed models that also contain long Fe-Fe distances of $\sim 3.7\text{\AA}$ (as dictated by the Fe-EXAFS of the cofactor) are either based on the prismane structure (Figure 1) or are derivatives (67) of the Fe_6S_9 cluster (68). In the prismane derivative clusters, Fe-Fe distances of 3.8\AA are found in the hexagonal Fe_3S_3 prismane subunits (43).

In the new model based on x-ray crystallographic results (3-4), the long Fe-Fe distances are found within a new core structure that contains a central Fe_6 trigonal prism (Figure 2). The square faces of this prism have sides with Fe-Fe distances of $\sim 2.6\text{\AA}$ and diagonal Fe-Fe distances of 3.7\AA .

The protein structure shows the Mo atom on the periphery of the molecule close to three Fe atoms and outside the "reach" of the other four in the distant subunit. This structure is in agreement with the Fe-EXAFS analyses results that show only a small number of Mo atoms attached to the average Fe atom (~ 0.5 Mo atoms per Fe). The coordinative saturation of the Mo atom with six ligand atoms in its coordinative sphere would seem to preclude the direct involvement of Mo in substrate reduction (*vide infra*). This being the case, other sites within the Fe/Mo/S clusters will have to be identified as functionally important in the activation and reduction of substrate molecules. The model suggested by Kim and Rees (Figure 2A) has six, coordinatively unsaturated Fe sites that could get involved in substrate binding and activation. In contrast, the model shown in Figure 2C, although more acceptable from a coordination chemist's point of view, does not contain a site obviously suited for substrate activation. A mode has been suggested (4b) (Figure 5).

The position of the homocitrate molecule as a bidentate ligand on the Mo atom and distant from the core of the molecule, also raises questions regarding its function in nitrogen fixation. It has been suggested (4) that the homocitrate molecule may be involved in the "modulation of the redox properties of the coordinated FeMo-cofactor," and may play a role in the protonation of intermediates, or even participate in the electron transfer pathway between the "P" cluster and the FeMo-cofactor (4).

The "P" clusters. The octanuclear nature of the "P" clusters appears now to be an indisputable fact. Equally indisputable is the position of these clusters

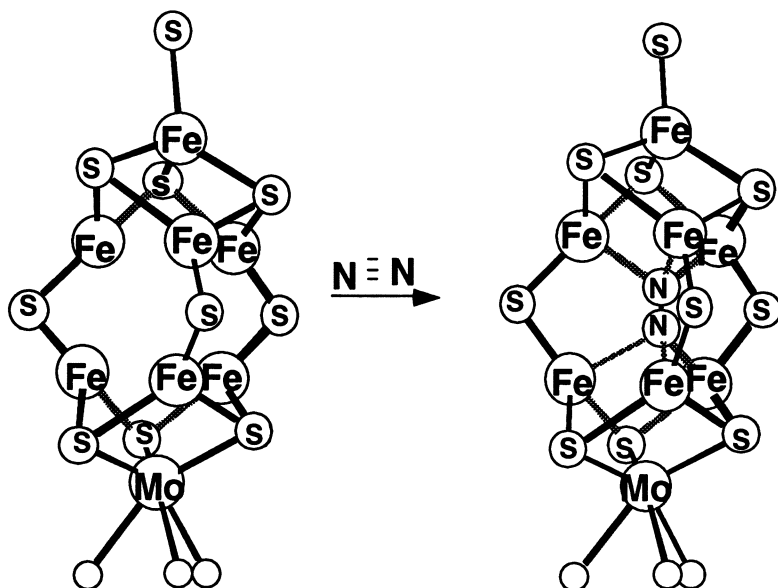


Figure 5. A proposed mode of N_2 activation by the Fe/Mo/S center in nitrogenase (4b).

between the α and β subunits attached to the protein matrix by six cysteinyl residues (Cys β 95, Cys β 153, Cys β 70, Cys α 88, Cys α 62 and Cys α 154). Of these, Cys β 95 and Cys α 88 serve as bridging ligands between the two subunits (3b, 4). In the earlier Kim-Rees structure, the bridging cysteinyl residues are related centrosymmetrically and bridge two Fe_4S_4 clusters (Figure 3A). In the earlier Bolin structure, the "P" clusters are appreciably different. They consist of two fused Fe_4S_4 clusters sharing a six-coordinate S^{2-} ligand and having the two bridging cysteinyl residues in a non-centrosymmetric arrangement (Figure 3B). A possible advantage of the structure shown in Figure 3A over that shown in Figure 3B is that the former can easily account for the quantitative extrusion of four Fe_4S_4 centers from the FeMo protein. From a structural point of view, however, the structure shown in Figure 3A may be subject to some strain brought about by the repulsions between the μ_3 - S^{2-} ligands in adjacent Fe_4S_4 units (vide infra). In the "consensus" latest structure (3c, 4b), the two Fe_4S_4 cores are linked by a common μ_6 - S^{2-} unit. Such a unit is unprecedented in model Fe/S cluster chemistry although, as indicated above, it may be an ideal site to reversibly deposit two electrons. Such a site may be effective in the catalytic reduction of two H^+ to H_2 . In one of the two protein structures (4), the proximity (within bonding distance) of a serine residue (Ser β 188) to one of the iron atoms in the "P" cluster may result in a five-coordinate site. The Mössbauer spectrum of the "P^N" clusters has been analyzed (20a) in terms of four quadrupole doublets with isomer shifts and quadrupole splittings of: 0.55mm/s, 3.03 mm/s, ("Fe²⁺"); 0.51mm/s, 1.33 mm/s, ("S"); 0.51mm/s, 0.87 mm/s, ("D(a)"), and; 0.52mm/s, 0.68 mm/s, ("D(b)"). A five-coordinate Fe site has previously been suggested as the origin of the "Fe²⁺" component based on a study of model Fe_4S_4 clusters with mixed-ligand, mixed-coordination geometry (69).

Synthetic Analogs for the Fe/Mo/S and Fe/S Sites of the Fe/Mo Protein of Nitrogenase

A plethora of clusters with structures partially conforming to, or anticipated to satisfy the requirements outlined above, have been proposed as models for the nitrogenase Fe/Mo/S center. For each of these models, the stoichiometry and structure were based on the information available at the time of their intellectual conception. A nearly complete tabulation of the models that had been proposed prior to 1985 can be found in a comprehensive review (16). Interestingly, few of the proposed models have been synthesized to date. This lack of synthetic analogs for the various suggested models emphasizes an important fact: the synthesis of a particular target Fe/Mo/S cluster is far from trivial due to the considerable difficulty associated with the rational synthesis of inorganic clusters, particularly if the latter are kinetically labile and do not possess appreciable inherent thermodynamic stability. Indeed, the vast majority of the soluble Fe/Mo/S inorganic clusters known have been obtained serendipitously and usually represent thermodynamically stable molecules that assemble spontaneously from mixtures of appropriate reagents in the absence of significant kinetic barriers.

Of the chemically relevant clusters that have been synthesized and structurally characterized thus far, no one possesses a Fe:Mo:S ratio close to the commonly accepted $6 \pm 1:1:8 \pm 1$, and the synthesis of at least a stoichiometrically acceptable model still remains an unfulfilled goal. Nearly all of the various Fe/Mo/S clusters that have been obtained thus far which have been structurally characterized contain as a common feature, either the MoS_2Fe , or both the MoS_2Fe and FeS_2Fe structural units. These units in synthetic analog complexes give rise to Mo and Fe EXAFS that are similar in various degrees to those obtained for the nitrogenase center (37-42).

Thus far, the failure to obtain acceptable synthetic analogs for the Fe/Mo/S center and the "P" clusters of nitrogenase by spontaneous self assembly, SSA, may indicate that such centers are intrinsically metastable and owe their stability within a protein to a specific stabilizing environment.

Oligonuclear Fe/M/S Complexes. The syntheses, structures, and electronic properties of the oligonuclear Fe/M/S ($M = \text{Mo}, \text{W}$) complexes have been described and reviewed in detail (16, 70). These compounds are derivatives of the MS_4^{2-} thioanions and include complexes such as: $[\text{L}_2\text{FeS}_2\text{MS}_2]^{2-}$ ($L = \text{PhS}^-$ (71); $L = \text{Cl}^-$ (72); PhO^- (73) NO^+ (74); $L_2 = \text{S}_5^{2-}$, (75), $[\text{Cl}_2\text{FeS}_2\text{MS}_2\text{FeCl}_2]^{2-}$, (72a-b), $[\text{Fe}(\text{MoS}_4)_2]^{3-}$ (76), $[\text{Fe}(\text{WS}_4)_2(\text{DMF})_2]^{2-}$ (77), $[(\text{S}_2)\text{OMoS}_2\text{FeCl}_2]^{2-}$ (78), $[\text{S}_2\text{MoS}_2\text{FeS}_2\text{Fe}(\text{S-p-C}_6\text{H}_4\text{Me})_2]^{3-}$ (73, 79), $[\text{Mo}_2\text{FeS}_6(\text{edt})_2]^{3-}$ (80), and $[(\text{S}_2\text{WS}_2)_3\text{Fe}_3\text{S}_2]^{4-}$ (81). On an elementary level these complexes have been useful in understanding structural aspects of the Fe/Mo/S center in nitrogenase. All of them contain FeS_2M rhombic units with Fe-M distances (2.73Å-2.84Å) similar to those determined by EXAFS for the Fe-Mo distances in the nitrogenase center. In the oligonuclear Fe-Mo-S complexes, the bridging Mo-S distances range from 2.25Å to 2.26Å and the terminal Mo-S from 2.15Å to 2.18Å. These distances are much shorter than those found (by EXAFS analyses) in nitrogenase (37-42) and can be attributed to the high oxidation state of the Mo atom (+6) in the oligonuclear complexes. The anticipated utility of the oligonuclear Fe-M-S complexes, as building blocks for high nuclearity Fe/Mo/S clusters has not been realized.

Polynuclear Fe/M/S Complexes. The synthesis of polynuclear, Fe-M-S clusters (16) is readily accomplished by SSA procedures using $[\text{MS}_4]^{2-}$ anions as a soluble source of Mo or W. These clusters contain as a common structural feature the MFe_3S_4 cubane type units ($M = \text{Mo}, \text{W}$), and are represented by two general structural types: the double-cubanes that contain two bridged MFe_3S_4 cubane units (82) and the single cubanes that contain the MFe_3S_4 cores. The former include

$[\text{M}_2\text{Fe}_6\text{S}_9(\text{SR})_8]^{3-}$ (82-83), $[\text{M}_2\text{Fe}_6\text{S}_8(\text{SR})_9]^{3-, 4-}$ (84), $[\text{M}_2\text{Fe}_6\text{S}_8(\text{OMe})_3(\text{SR})_6]^{3-}$ (83), $[\text{M}_2\text{Fe}_7\text{S}_8(\text{SR})_{12}]^{3-, 4-}$ (84) and $[\text{M}_2\text{Fe}_6\text{S}_8(\text{SR})_6(3,6\text{-R}'_2\text{cat})_2]^{4-}$ (85). The reactivity of some of the double-cubanes, in bridge cleavage reactions, has led to the synthesis of the $[\text{MoFe}_3\text{S}_4(\text{L})_3(3,6\text{-R}'_2\text{cat})(\text{L}')]^{2-, 3-}$ single cubanes (L = RS⁻, Cl⁻; R' = allyl, n-Pr; L' = DMSO, DMF, CH₃CN, PR₃, RS⁻, CN⁻, RO⁻) (16, 86) and the pentanuclear $[\text{MoFe}_3(\text{S})_4(\text{SEt})_3\text{Fe}(\text{cat})_3]^{3-}$ (87).

The solvated forms of the very important single-cubane clusters (L = DMSO, DMF, CH₃CN) are obtained by the dissociation of the $[\text{Mo}_2\text{Fe}_6\text{S}_8(\mu\text{-SR})_2(\text{SR})_4(3,6\text{-R}'_2\text{cat})_2]^{4-}$ (85), weakly bridged cubane dimers in coordinating solvents and are characterized by S = 3/2 ground states. The ligated single cubes (Figure 6) are obtained readily by substitution of the solvent ligands by other ligands (L = PR₃, RS⁻, CN⁻, RO⁻). The core within the MFe_3S_4 cubanes represents the first synthetic structural unit that shows Mo-EXAFS (at least for the first and second Mo coordination shells) very similar to the Mo-EXAFS of nitrogenase. A comprehensive review of the MFe_3S_4 cubanes is available (16).

The $[\text{Fe}_6\text{S}_6\text{L}_6(\text{M}(\text{CO})_3)_2]^{3-, 4-}$ Octanuclear Clusters. The $[\text{Fe}_6\text{S}_6\text{L}_6]^{n-}$ clusters (43) with hexagonal prismatic Fe_6S_6 cores (Figure 7A) were the first hexanuclear Fe/S clusters that proved useful as “building-blocks” for the synthesis of

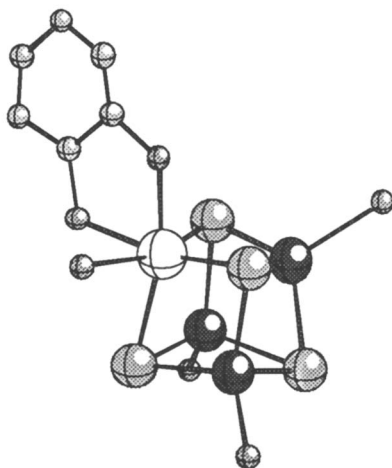


Figure 6. The $[\text{MoFe}_3\text{S}_4(\text{L})_3(\text{R}_n\text{-cat})(\text{L}')]^{2-, 3-}$ cubanes (16).

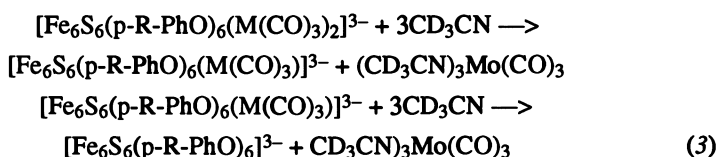
polynuclear Fe/Mo/S clusters. The hexagonal Fe_3S_3 faces in the $[\text{Fe}_6\text{S}_6\text{L}_6]^{n-}$ “prismanes” with a “chair” conformation and S_3 arrays sterically poised for coordination could readily serve as ligands in ligand substitution reactions with the $(\text{CH}_3\text{CN})_3\text{M}(\text{CO})_3$ complexes, (M = Mo, W), (Equation 2).



The $[\text{Fe}_6\text{S}_6(\text{L})_6(\text{M}(\text{CO})_3)_2]^{3-}$ clusters (Figure 7B) (88) show two one-electron reversible waves in cyclic voltammetry that correspond to the 3-/4- and 4-/5-redox couples ($E_{1/2}$ values range from +0.08V to -0.31V for the 3-/4- couples and from -0.50V to -0.91V for the 4-/5- couples). For the clusters with L = p-R-C₆H₄O, the redox potentials are affected predictably by the nature of the para substituents in a manner similar to that observed for the parent prismane clusters (43). Chemical oxidation by $[\text{Fe}(\text{Cp})_2]^+$ or reduction by BH_4^- can be used for the

synthesis of the trianionic and tetraanionic clusters from their one electron redox counterparts, respectively. The C = O stretching frequencies in the tetraanionic clusters are significantly lower than those in the trianionic clusters (by ca 50 cm⁻¹) and suggest that the reductions of the trianions are centered on the M(CO)₃ units.

The ¹H-NMR spectra of the aryloxy prismane adducts resemble the isotropically shifted spectra of the [Fe₂S₂(ArO)₄]²⁻ dimers (89), the [Fe₄S₄(ArO)₄]²⁻ cubanes (90), and the "parent" prismane clusters (43), but the isotropic shifts of the prismane adducts are greater in magnitude. The tetraanionic adducts (with an integer spin ground state) show even larger isotropic shifts than the trianionic adducts. A solution ¹H-NMR study of the [Fe₆S₆(p-CH₃C₆H₄O)₆(Mo(CO)₃)₂]³⁻ cluster shows two sets of isotropically shifted resonances for the o-, m- and p-CH₃ protons. One set (all singlets) is due to the [Fe₆S₆(p-CH₃C₆H₄O)₆(Mo(CO)₃)₂]³⁻ cluster where all phenyl rings are equivalent. The other set (all doublets) is tentatively assigned to the [Fe₆S₆(p-CH₃C₆H₄O)₆(Mo(CO)₃)₃]³⁻, 1:1 adduct that contains two sets of phenyl rings (88c). The relative intensities of the two sets of resonances change upon addition of an excess of (CH₃CN)₃Mo(CO)₃ or [Fe₆S₆(p-R-PhO)₆]³⁻ as expected for the equilibria shown in Equation 3. The [Fe₆S₆(p-R-PhO)₆(M(CO)₃)₃]³⁻ clusters thus far have not been obtained in pure form.



The electronic spectra of the [Fe₆S₆(ArO)₆(Mo(CO)₃)₂]ⁿ⁻ adducts are dominated by intense L-Fe (ε ~ 1x10⁴) charge transfer absorptions between 400nm and 500nm. These absorptions are bathochromically shifted (by ca 30-50nm) when compared to the same absorptions in the "parent" prismanes. The antiferromagnetically coupled [Fe₆S₆(L)₆(M(CO)₃)₂]ⁿ⁻ clusters are characterized by a S = 1/2 ground state and their EPR spectra (obtained at temperatures < 15K) resemble those of the parent prismanes (43). The tetraanionic clusters are EPR silent.

The crystal structures of the centrosymmetric [Fe₆S₆(L)₆(M(CO)₃)₂]ⁿ⁻ anions (L = Cl⁻, M = Mo (88a-b), n = 4; L = p-CH₃(CO)-C₆H₄O⁻, M = Mo (88c) n = 4; L = Cl⁻, Br⁻, M = Mo (88), n = 3; L = PhO⁻, M = W (92), n = 3) have been determined. All of these clusters show very similar rhombic [Fe₆M₂S₆]^{2+, 3+} cores (Figure 7B). In comparison to the structures of the [Fe₆S₆Cl₆]ⁿ⁻ clusters, the [Fe₆S₆] subunits in the [Fe₆M₂S₆]^{2+, 3+} cores are slightly elongated along the idealized 6 axis and show slightly shorter Fe-Fe distances and Fe-S bond lengths. The Fe-Mo and Mo-S distances in the [Fe₆S₆(L)₆(M(CO)₃)₂]ⁿ⁻ clusters are significantly longer than those determined by EXAFS analyses for the Fe/Mo/S center in nitrogenase. These differences are not unexpected in view of the low formal oxidation state of the Mo atoms in the [Fe₆S₆L₆(M(CO)₃)₂]ⁿ⁻ clusters. Furthermore, they argue in favor of a higher oxidation state for the Mo atom in nitrogenase. A significant shortening of the Mo-Fe and the Mo-S distances is found in the trianions. The crystallographic and Mössbauer data (vide infra) suggest that the highest occupied MO in the tetraanions consists mainly of Mo and S atomic functions and is antibonding in character.

The ⁵⁷Fe Mössbauer spectra of the [Fe₆S₆L₆(Mo(CO)₃)₂]ⁿ⁻ clusters at two different oxidation levels are similar and consistent with the structural data which indicate that the Fe₆S₆ cores are not significantly perturbed as a result of a change in the oxidation level. These results further reinforce the conclusion that the oxidation of the tetraanionic Mo(CO)₃ adducts is centered primarily on the Mo atoms.

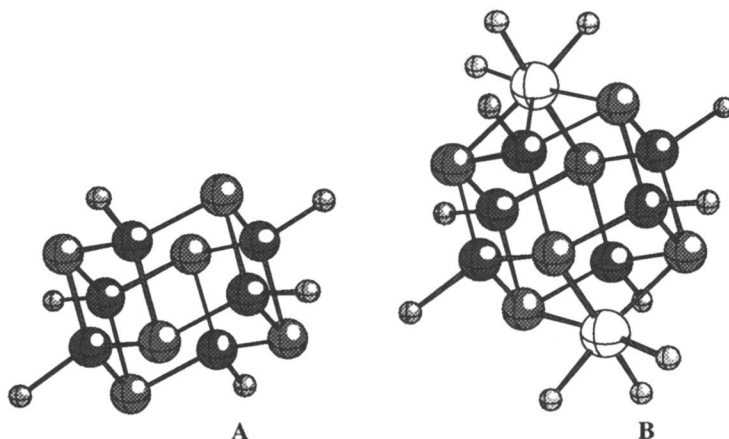


Figure 7. Structures of A, the $[\text{Fe}_6\text{S}_6(\text{L})_6]^{2-, 3-}$ prismanes, and B, the $[\text{Fe}_6\text{S}_6(\text{L})_6(\text{M}(\text{CO})_3)_2]^{3-, 4-}$ derivatives.

Attempts to oxidatively decarbonylate the prismane adducts with orthoquinones have not resulted in the formation of decarbonylated Fe_6Mo_2 prismanes containing oxidized Mo atoms. Instead, following decarbonylation and oxidation of the Mo atoms, the prismane clusters collapsed and formed the known $[\text{MoFe}_3\text{S}_4\text{L}_3(\text{R}_n\text{-cat})\text{L}]^{3-}$ cubanes. Apparently, the Fe_3S_3 prismane faces are not as well suited to accommodate the smaller Mo(III) ions as are the Fe_3S_4 cubane-type “ligands.” The effects of “ligand-pocket” size in stabilizing Fe/Mo/S clusters with Mo in different oxidation states also is apparent in the chemistry of the $[(\text{CO})_3\text{MoFe}_3\text{S}_4(\text{SEt})_3]^{3-}$ cluster (93a). The latter, in the presence of a stoichiometric amount of phenol at ambient temperature, affords the $[\text{Fe}_6\text{S}_6(\text{OPh})_6(\text{Mo}(\text{CO})_3)_2]^{3-}$ cluster in 40% yield (93b).

Singly and Doubly Bridged Double Cubanes. A very recent proposed model for the Fe/Mo/S site in nitrogenase (94) was inspired by an earlier suggestion that N_2 reduction in nitrogenase may occur at a coordinatively unsaturated, heterodinuclear Fe- μ_2 -S-Mo site (95). This model (Figure 8A) contains the $[\text{MoFe}_3\text{S}_4]\text{S}[\text{Fe}_4\text{S}_4]^{3+}$ frame and, in principle, should be accessible by coupling reactions of known clusters that contain the $[\text{MoFe}_3\text{S}_4]^{3+}$ and $[\text{Fe}_4\text{S}_4]^{2+}$ cores.

Attractive features of this model (Figure 8A) are: a) an acceptable Fe/Mo/S stoichiometry of 7:1:9; b) a site for the bimetallic activation of molecular nitrogen; c) the presence of at least four distinct iron sites as indicated by ENDOR studies for the Fe/Mo/S site in nitrogenase; d) a flexible (M) site capable of accommodating Mo, V (or Fe); e) the presence of redox active subunits for the storage and delivery of electrons, and; f) predicted Mo-EXAFS features very similar to those obtained for the FeMo protein and the nitrogenase cofactor.

The feasibility of coupling cubane clusters was demonstrated initially by the synthesis of the singly-bridged double-cubane, SBDC, $[(\text{Fe}_4\text{S}_4\text{Cl}_3)_2\text{S}]^{4-}$ (Figure 8B). A crystal structure determination shows (96) the tetraanion (Figure 8B) located on a crystallographic two-fold axis that passes through the $\mu_2\text{-S}^{2-}$ ligand. Intercluster S-S repulsions in the anion are relieved by a twist of one cubane subunit relative to the other by 38.3° . The Fe-Fe, Fe-S and Fe-Cl bond lengths are

unexceptional and very similar to those reported (97) for the $[\text{Fe}_4\text{S}_4\text{Cl}_4]^{2-}$ cluster. The Fe-S bridge bonds at 2.206(4)Å are similar to those found (97) in $[\text{Fe}_2\text{S}_2\text{Cl}_4]^{2-}$ (2.200(1)Å) and the Fe-Fe distance across the Fe- μ_2 -S-Fe bridge at 3.433(4)Å is a direct consequence of the oblique Fe- μ_2 -S-Fe angle of 102.2°. The electronic spectrum of the product shows absorptions at 670nm ($\epsilon \sim 10,700$), at ~480nm (sh, $\epsilon \sim 17,700$), and at 240nm ($\epsilon \sim 57,500$). The spectrum is, indeed, very similar to that of $[\text{Fe}_4\text{S}_4\text{Cl}_4]^{2-}$ (97). The cyclic voltammetry, in CH_3CN solution vs SCE, shows two quasireversible waves at -0.80V and -1.10V. The two waves arise as a result of the $1e^-$ reduction of each of the two subclusters and the 300mV separation between these waves indicates that intracuster, intercube interactions are substantial. The Mössbauer spectrum consists of a broad asymmetric quadrupole doublet with average IS and ΔE_{q} values of 0.48 and 0.98 mm/sec, respectively.

The structure of the $[(\text{Fe}_4\text{S}_4\text{Cl}_3)_2\text{S}]^{4-}$ cluster (Figure 8B) has some relevance to one of the proposed structures for the "P" clusters (Figure 3A). In the former intracuster, intercube S-S repulsions prevent the introduction of a second μ_2 -S ligand and a doubly-bridged, double-cubane, DBDC, cannot be synthesized. One may attribute the failure in obtaining the $[(\text{Fe}_4\text{S}_4\text{Cl}_2)_2(\text{S})_2]^{4-}$ DBDC to the short Fe- μ_2 -S²⁻ bonds (and acute Fe-S-Fe angles). Longer Fe- μ_2 -SR bonds and less acute Fe- μ_2 -SR-Fe angles may be possible for a cluster such as the one shown in Figure 3A. Geometric considerations indicate that with Fe- μ_2 SR distances of 2.30Å and Fe- μ_2 SR-Fe angles of 122° the shortest S-S intracuster, intercube distances in a doubly-bridged double-cubane are ~3.4Å. These distances are similar to those found in the structure of the doubly-bridged $[(\text{MoFe}_3\text{S}_4\text{Cl}_2(\text{Cl}_4\text{cat}))_2(\mu_2\text{-S})(\mu_2\text{-OH})]^{5-}$ cluster (vide infra). The parameters used in the above calculation for the S-S distances have been taken from $[\text{Mo}_2\text{Fe}_6\text{S}_8(\text{SEt})_6(\text{Pr}_2\text{cat})_2]^{4-}$, the only doubly-bridged double-cubane with bridging thiolate ligands that has been characterized structurally (85). In this cluster, two intramolecular, intercube Mo- μ_2 SEt-Fe bridges exist with Fe-SEt bonds of 2.305(3)Å, Mo-S bonds of 2.689(2)Å, Mo- μ_2 SEt-Fe angles of 122.2(1)° and intercube S-S distances of 3.831(5)Å. The longer S-S distances in this cluster are due to the rather long Mo-S bonds.

The self coupling of the $[\text{MoFe}_3\text{S}_4\text{Cl}_3(\text{Cl}_4\text{cat})(\text{CH}_3\text{CN})]^{2-}$ cluster with $(\text{Et}_4\text{N})_2\text{S}$ in CH_3CN solution yields the $[(\text{MoFe}_3\text{S}_4\text{Cl}_2(\text{Cl}_4\text{cat}))_2(\mu_2\text{-S})]^{6-}$ DBDC cluster (94). In good yield, a similar reaction in the presence of Et_4NOH affords the $[(\text{MoFe}_3\text{S}_4\text{Cl}_2(\text{Cl}_4\text{cat}))_2(\mu_2\text{-S})(\mu_2\text{-OH})]^{5-}$ cluster (94). The OH- bridge in this cluster is a site of reactivity that has been exploited for the synthesis of several derivatives in reactions with the oxophilic $(\text{R}_3\text{Si})_n\text{X}$ reagents or with $\text{N}_2\text{H}_4 \cdot \text{HCl}$ (98). The structure of the $(\mu_2\text{-N}_2\text{H}_4)$ derivative (98) is shown in Figure 9.

The electronic spectra of the DBDC clusters are essentially featureless and show a steadily increasing absorption from 750nm to the UV region of the spectrum. The DBDC clusters show quasireversible reduction waves between -1.0V and -1.3V (in 1,2-dichloroethane solution vs Ag/AgCl) and two oxidation waves between -0.10 and +0.04V. By comparison the $[\text{MoFe}_3\text{S}_4\text{Cl}_3(\text{Cl}_4\text{cat})(\text{CH}_3\text{CN})]^{2-}$ single cube, shows a quasireversible reduction at -0.8V and irreversible oxidation at ~+0.4V.

The Mössbauer spectra for the DBDC can be fitted with two doublets in a 2:1 intensity ratio. The major components show IS values that range from 0.50 to 0.53 mm/sec and ΔE_{q} values that range from 1.10 to 1.19 mm/sec. The minor components have IS values in the range from 0.30 to 0.34 mm/sec and ΔE_{q} values between 1.05 and 1.13 mm/sec.

Common structural features in the DBDC anions (99) are the Fe- μ_2 -S-Fe and Mo- μ_2 -L-Mo bridges (L = OH-, S²⁻ (94); CN- and N₂H₄) (98). Other structural features in these clusters are short Fe-S bonds in the Fe- μ_2 -S-Fe bridges (~2.20Å), and oblique Mo- μ_2 -L-Mo angles of 137.2(7)° (L = S²⁻), 158(2)° (L = OH-), 161° (L = CN-), and 162° (L = N₂H₄). The DBDC show a remarkable steric flexibility in accepting widely different Mo-Mo distances. A decrease in the Mo-Mo distance is

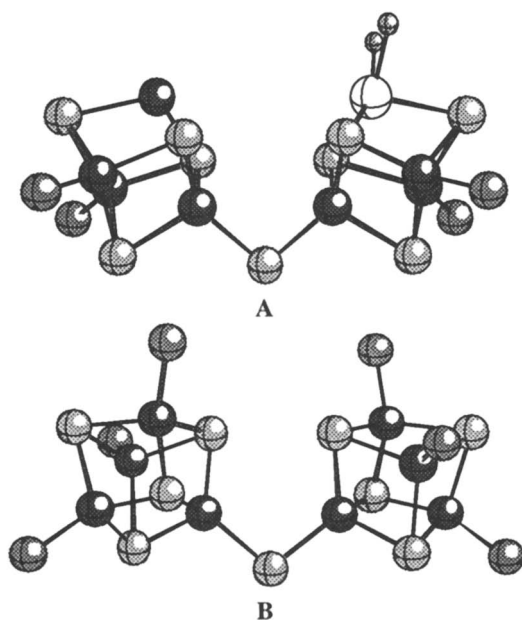


Figure 8. A, $[(\text{MoFe}_3\text{S}_4)(\mu_2\text{-S})(\text{Fe}_4\text{S}_4)]^{3+}$, a proposed model for the Fe/Mo/S site in nitrogenase (94); and B, the $[(\text{Fe}_4\text{S}_4\text{Cl}_3)_2\text{S}]^{4-}$ singly-bridged, double-cubane (96).

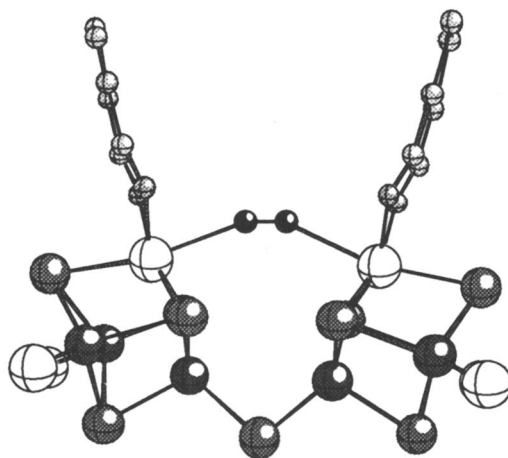


Figure 9. The $[\text{MoFe}_3\text{S}_4\text{Cl}_2(\text{C}_{14}\text{cat})]_2(\mu_2\text{-S})(\mu_2\text{-N}_2\text{H}_4)]^{4-}$ double-bridged, double cubane (98).

observed from 5.221(8)Å ($L = \text{CN}^-$) and 5.22(1)Å ($L = \text{N}_2\text{H}_4$) to 4.926(8), ($L = \text{S}^{2-}$) to 4.248(9)Å ($L = \text{OH}^-$) as the steric demands of the bridging ligand change. The intracuster intercube S-S distances vary from the very short distances of 3.19Å and 3.50Å found in the $L = \text{OH}^-$ DBDC to the longer distances of 3.87Å and 3.77Å found in the $L = \text{N}_2\text{H}_4$ derivative. The Fe- μ_2 -S-Fe angles and the Fe-Fe distances within the intercube bridges do not show as pronounced a variation and are found at 101.1(9)° and 3.47(1), ($L = \text{CN}^-$), 98.7(8)° and 3.33(1)Å, ($L = \text{S}^{2-}$) and 97.8(8)°, and 3.35(2)Å ($L = \text{OH}^-$).

The reaction of the $[[\text{MoFe}_3\text{S}_4\text{Cl}_2(\text{Cl}_4\text{cat})]_2(\mu_2\text{-S})(\mu_2\text{-OH})]^{5-}$ cluster with $\text{NH}_3\text{OH} + \text{Cl}^-$ affords the short-lived DBDC ($L = \text{NH}_2\text{OH}$, $n = 4$) analogous to the N_2H_4 bridged cluster. Upon standing, CH_3CN solutions of this cluster decompose and upon dilution with diethyl-ether deposit crystals of $(\text{Et}_4\text{N})_2[(\text{Cl}_4\text{cat})\text{Mo}(\text{O})(\mu\text{-S})_2\text{FeCl}_2]$, and $(\text{Et}_4\text{N})_4\{[(\text{S})\text{Mo}(\text{O})(\mu\text{-S})_2\text{FeCl}_2] [\text{FeCl}_4]\}$ (Figure 10) (100). The source of the molybdenyl oxygen in these by-products is the bridging hydroxylamine molecule that apparently has undergone a N-O bond cleavage reaction as the oxygen atom is transferred oxidatively to one of the Mo atoms in the $L = \text{NH}_2\text{OH}$, DBDC.

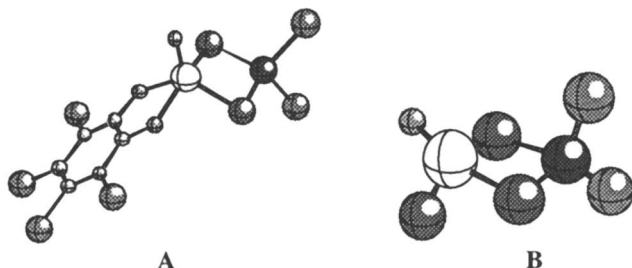


Figure 10. Oxidative decomposition products of the $[\text{MoFe}_3\text{S}_4\text{Cl}_2(\text{Cl}_4\text{cat})]_2(\mu_2\text{-S})(\mu_2\text{NH}_2\text{OH})^{4-}$ cluster. A, $[(\text{Cl}_4\text{cat})\text{Mo}(\text{O})(\mu\text{-S})_2\text{FeCl}_2]^{2-}$; and B, $[(\text{S})\text{Mo}(\text{O})(\mu\text{-S})_2\text{FeCl}_2]^{2-}$.

The electronic spectra of the dimeric, oxidative degradation products with major absorptions 470 nm for $[(\text{Cl}_4\text{cat})\text{Mo}(\text{O})(\mu\text{-S})_2\text{FeCl}_2]^{2-}$ and 422 nm for $[(\text{S})\text{Mo}(\text{O})(\mu\text{-S})_2\text{FeCl}_2]^{2-}$ are characteristic of the perturbed thiomolybdate chromophores and resemble the electronic spectra obtained from oxidized solutions of the nitrogenase cofactor. The presence of the $[\text{OMoS}_3]^{2-}$ unit in such solutions has been reported previously (101-103).

The absence of 3.8Å Fe-Fe distances in the x-ray structures of the bridged cubanes is a major weakness of the bridged cubane model. Such distances are required by the Fe-EXAFS results obtained for nitrogenase (41-42) and must be present in an acceptable synthetic analog. In the proposed model shown in Figure 8A the proximity of the Mo atom to the center of the cluster and the implied importance of the Mo atom in substrate activation are at variance with the proposed x-ray structural model (Figure 2). These shortcomings notwithstanding, the doubly-bridged, double cubanes still can answer basic questions regarding the nitrogenase Fe/Mo/S aggregate. As is the case with the cofactor, the double cubanes have a multibridged structure and consists of cluster subunits that may carry out the bimetallic activation of bridging substrate molecules prior to multielectron redox reactions.

Other Clusters. Other Fe/Mo/S clusters obtained from preassembled Fe/S units have been reported. The syntheses of these clusters employ reactions of the $[\text{Fe}_2\text{S}_2(\text{CO})_6]^{2-}$ dianion with various Mo sources and have afforded the $[[\text{Fe}_2\text{S}_2(\text{CO})_6]\text{Fe}(\text{MoS}_4)]^{2-}$, $[\text{MoOFe}_5\text{S}_6(\text{CO})_{12}]^{2-}$ (104) and $[\text{MoFe}_6\text{S}_6(\text{CO})_{16}]^{2-}$

(105) clusters. The oxidative decarbonylation of the $[[\text{Fe}_2\text{S}_2(\text{CO})_6]\text{Fe}(\text{MoS}_4)]^{2-}$ cluster with $(p\text{-Cl-C}_6\text{H}_4\text{S})_2$ gives the $[\text{Mo}_2\text{Fe}_6\text{S}_{12}(\text{SR})_6]^{4-}$ cluster (106). The latter consists of two $[\text{Mo}(\text{S}_2)\text{Fe}_3\text{S}_4]^{2-}$ single cubanes asymmetrically bridged by the two $\mu_2\text{-}\eta^3$ -persulfide ligands. The same cluster may also be obtained in low yield by a SSA reaction. The $[\text{MoFe}_6\text{S}_6(\text{CO})_{16}]^{2-}$ cluster (105) is very asymmetric and shows three Mo-Fe distances at 2.7 Å and three at 3.0 Å to 3.6 Å. It undergoes oxidative decarbonylation with I_2 to give the $[\text{MoFe}_5\text{S}_6(\text{CO})_6\text{I}_3]^{2-}$ cluster (107) that reacts further with PET_3 to give $[\text{MoFe}_5\text{S}_6(\text{CO})_6(\text{PET}_3)_3]^{2-}$. The structure of the latter has been determined and consists of a MoFe_3S_4 cubane with terminal, Fe-bound PET_3 ligands and a $[\text{Fe}_2\text{S}_2(\text{CO})_6]^{2-}$ “ligand” bound to the Mo atom in bidentate fashion. The Fe-Fe distances in this cluster vary from 2.605(4) Å to 2.611(5) Å and the Mo-Fe distances vary from 2.655(3) Å to 2.677(3) Å.

The $[\text{MoFe}_5\text{S}_6(\text{CO})_{12}]^{2-}$ (104) cluster consists of a $[\text{Fe}(\text{III})(\mu\text{-S})_2\text{Mo}(\text{V}) = \text{O}]^{2+}$ central unit with two $[\text{Fe}_2\text{S}_2(\text{CO})_6]^{2-}$ “ligands” bound in bidentate fashion to the Fe(III) and $\text{Mo}^{\text{V}} = \text{O}$ sites. The $[\text{Fe}(\text{III})(\mu\text{-S})_2\text{Mo}(\text{V}) = \text{O}]^{2+}$ unit in this cluster metrically is very similar to essentially the same unit in $[(\text{Cl}_4\text{cat})\text{Mo}(\text{O})(\mu\text{-S})_2\text{FeCl}_2]$, (100) (Figure 10A) and the $[\text{Fe}(\text{III})(\mu\text{-S})_2\text{Mo}(\text{V}) = \text{S}]^{2+}$ unit in $[\text{Mo}_2\text{FeS}_6(\text{edt})_2]^{3-}$ (80).

A few of the $[\text{Fe}_2\text{S}_2(\text{CO})_6]^{2-}$ derived clusters closely approach the Fe/Mo cofactor stoichiometry. Prior to the structure determination of the MoFe protein of nitrogenase, these could be considered as reasonable models provided that they retained their integrity upon replacement of the carbonyl or phosphine ligands with biologically relevant ligands. At present, they represent the few FeMoS clusters known that display short Fe-Fe distances. These distances are different than those observed with the majority of the known FeMoS clusters, and resemble more closely the Fe-Fe distances determined by Fe-EXAFS for the nitrogenase cofactor and the somewhat short Fe-Fe distances in the Roussin's black salt (66).

Questions That Remain Unanswered and New Challenges In Synthetic Metal Sulfur Chemistry Relevant to the Nitrogenase Problem

The Role of the Mo and V Atoms in Nitrogenase Function. The role of the Mo atom (and of the V atom in alternate nitrogenase) in the function of the “M” centers in nitrogenase at present is an unsolved problem. The location of the Mo atom on the periphery of the $\text{MoFe}_7\text{S}_{8-9}$ cluster would support the argument that the Mo atom is not directly involved in N_2 fixation, particularly if the activation and reduction of N_2 involves a bimetallic site.

Evidence for the indirect involvement of the M atoms in substrate reduction is ambiguous. In support of the indirect involvement of Mo in nitrogenase function are the latest EPR and ENDOR data and the relative activities of the presumably isostructural alternate nitrogenases, where various other metal atoms have replaced Mo. The integration of the Mo atom in the S-3/2 spin system has been demonstrated by EPR spectroscopic studies on $^{95,96}\text{Mo}$ -labeled centers (108) and is apparent in the ENDOR spectra of ^{95}Mo labeled protein (35b). The inability of the V (12-13) and Fe (15) containing alternate nitrogenases to reduce substrates with the efficiency of the Mo nitrogenase demonstrates that the atom M plays a role in the reduction process. A similar conclusion can be reached from experiments involving WO_4^{2-} . Thus, an inactive form of the MoFe protein was produced by *A. vinelandii* cells when MoO_4^{2-} was replaced by WO_4^{2-} as a nutrient in the growth media (109-110). These and other observations suggest that WO_4^{2-} is a competitive antagonist relative to MoO_4^{2-} in N_2 fixation (7).

Spectroscopic results that do not appear to support the involvement of Mo in nitrogenase action are available from x-ray absorption spectroscopy, Mössbauer spectroscopy, and the earlier EPR studies (111-112).

The Mo-L-edge x-ray absorption near edge structure, XANES, for FeMo-cofactor(ox) and FeMo-cofactor(s-r), show that the Mo-L-edge is essentially unperturbed in the two different redox levels (113). This lack of significant changes in the Mo-L-edge may indicate an insensitivity of the technique, and is not in conflict with results obtained from Mössbauer spectroscopy (32). The change in the ^{57}Fe isomer shift (IS) values from 0.32 mm/s for the FeMo-cofactor(ox) to 0.37 mm/s for the FeMo-cofactor(s-r) demonstrates that the contribution of Fe atomic orbitals to the LUMO of FeMo-cofactor(ox) is high and the reduction is not affecting the Mo atom to a significant extent. The $\Delta(\text{IS})$ of 0.05 mm/s can be placed in perspective by comparison to $\Delta(\text{IS})$ values obtained with synthetic Fe/S compounds. The difference in IS values between Fe^{2+} and Fe^{3+} ions with tetrahedral sulfur coordination is ~ 0.45 mm/s. In Fe_nS_m clusters with completely delocalized electronic structures, a change in the IS by $0.45/n$ mm/s may be expected for a cluster valence change of 1. In the case of the FeMo-cofactor with $n = 7$, a valence change of 1 would require a $\Delta(\text{IS})$ of ~ 0.06 mm/s. In the $[\text{Fe}_6\text{S}_6(\text{Cl})_6(\text{Mo}(\text{CO})_3)_2]^n$ clusters ($n = 2,3$), the $\Delta(\text{IS})$ of 0.05 mm/s was smaller than the expected 0.075 mm/s and was attributed to the involvement of the Mo centers in the redox process (91). This contention is supported by the large bathochromic shifts of the CO stretching vibrations of the $\text{Mo}(\text{CO})_3$ fragments as the clusters undergo reduction. Such shifts are expected if the reduction involves a LUMO with appreciable Mo character (88c). The early EPR studies with ^{57}Fe labeled (111) and ^{95}Mo labeled (112) MoFe protein showed changes in the EPR ($S = 3/2$) signal only with the ^{57}Fe labeled protein. These results were interpreted to imply that the Mo is not a significant participant in the EPR chromophore (7).

A reasonable "guess" regarding the function of the Mo atom (or of the V and Fe structurally equivalent counterparts in the alternative nitrogenases) would be one that assigns a "potential-tuning" role to these atoms. Such a role would be consistent with the known inability of W substituted centers to reduce nitrogenase substrates (109-110) and the differing catalytic effectiveness and product distribution of the V (12-13) and Fe (15) substituted centers in the alternative nitrogenases.

How Does the Substrate Interaction/Activation Take Place at the Fe/Mo/S Center? In one of the crystallographic models of the Fe/Mo/S center in nitrogenase (4) (Figure 2), the Fe-Fe distances of 2.7Å and 3.7Å between coordinatively unsaturated Fe atoms appear well suited for some type of bimetallic activation of substrate molecules. With an atom of a first row element, X, in an Fe-X-Fe bridge ($X = \text{O}, \text{N}$) and Fe-X distances of $\sim 1.9\text{Å}$, an Fe-Fe distance of 2.7Å would require a reasonable Fe-X-Fe angle of $\sim 90^\circ$. These metric considerations suggest that a diatomic substrate molecule can only bridge "side-on" (Figure 11A) across two Fe atoms separated by 3.8Å. A substrate molecule, however, can coordinate either "end-on" (Figure 11B) or most likely "edge-on" (Figure 11C) across Fe atoms separated by 2.7Å. Substrate binding of any type is difficult to visualize with a model that does not contain coordinatively unsaturated Fe sites.

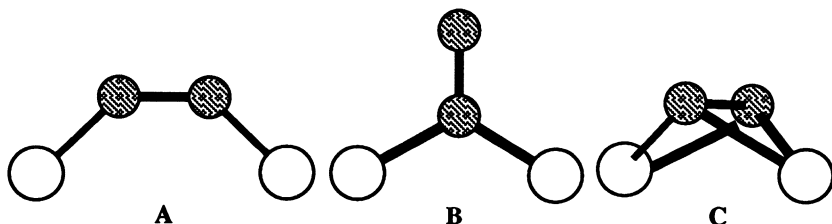


Figure 11. Possible N_2 -substrate bridging modes between metal atoms in the Fe/Mo/S center of nitrogenase.

In the models shown in Figure 2B, 2C coordination unsaturation may be achieved either by ligand (L) dissociation (Figure 2B) or by a shift of the central μ_6 -S²⁻ ligand (Figure 2C) towards one of the cuboidal subunits and its conversion to a μ_3 -bridging mode. The previously discussed doubly-bridged double-cubanes, do not structurally qualify as analogs for the Fe/Mo/S site in nitrogenase; however, basic structural details are of interest. Of particular importance are the intermetallic distances in the bridging units. The Fe-Fe distances in the Fe- μ_2 -S-Fe bridges vary from 3.33 Å to 3.47 Å, and the Mo-Mo distances in the Mo- μ_2 -X-Mo bridges with “side-on” bridging diatomic ligands (X = CN⁻, H₂N-NH₂) are 5.22 Å.

What Is the Electronic Structure of the Cuboidal Subunits? Are the Trigonal FeS₃ Subunits Realistic? Do They Exist Outside the Protein? At present, the only cluster that contains a pyramidal M₄S₃ core is the Roussin’s black salt [Fe₄S₃(NO)₇]⁻ (65) with Fe-Fe bonds linking an apical Fe(NO) fragment to three basal Fe(NO)₂ units (Figure 4). These bonds range from 2.683(2) Å to 2.708 Å (66) and are shorter than the Fe-Fe distances in the Fe₆S₆ prismanes (2.76 Å), but longer than the Fe-Fe distances (bonds?) in the Fe/Mo/S center of nitrogenase (2.64 Å). The Fe-Fe distances within the basal plane in Roussin’s salt range from 3.519(2) Å to 3.628(2) Å and are shorter than the longer Fe-Fe distances in the Fe₆S₆ prismanes (3.80 Å) and the FeMo-cofactor (3.68 Å). It appears likely that the Fe-EXAFS of the Roussin’s salt would be quite similar to that of the FeMo-cofactor. The apparent structural similarities of the two Fe₄S₃ subunits in Roussin’s salt and in the FeMo-cofactor, however, are not the result of similar electronic structures and do not give rise to similar chemical properties. The Roussin’s salt contains tetrahedrally coordinated Fe atoms in three [(NO)₂Fe(S)₂] and one [(NO)Fe(S)₃] moieties and is a very robust, air stable molecule. Furthermore, the formal oxidation state of the Fe atoms in the Roussin’s salt is quite low. The ⁵⁷Fe Mössbauer of Roussin’s salt (114) consists of two quadrupole doublets with IS and ΔE_Q values (vs Fe), of 0.78 mm/s and 0.802 mm/s for the major doublet (3Fe), and 0.64 mm/s and 0.895 mm/s for the minor doublet (1Fe). At this time, it is unclear whether the Mössbauer IS data for the Fe/Mo/S site in nitrogenase and for the FeMo-cofactor can be used to ascertain an approximate oxidation state for the iron atoms. The six Fe atoms in the Fe/Mo/S cluster (Figure 2A) that are coordinatively unsaturated and very likely are involved in strong Fe-Fe bonding do not belong in the same class as the tetrahedral, S-coordinated Fe atoms used in IS-oxidation state correlations.

The trigonal FeS₃ subunits in the structure of the Fe/Mo/S center (4) (Figure 2A) are intriguing, considering that such units are very rare in the coordination chemistry of iron. At this stage, it may still be possible that water molecules or protein appendices interact with the trigonally coordinated irons. If this were the case, the trigonal-pyramidal Fe sites would be structurally similar to the (R₃P)Fe(S)₃ sites encountered previously in the structures of the [Fe₆S₆(PET)₄L₂] (115), [Fe₆S₆(PET)₆]⁺ (116) and [Fe₇S₆(PET)₃Cl₃] (117) clusters.

As indicated previously (III-A), another way to partially alleviate the coordination unsaturation of the 6 Fe atoms in the Kim-Rees structure (Figure 2A) would be to place a S²⁻ ion in the center of the Fe₆ trigonal prism (Figure 2C). This type of trigonal prismatic coordination for a sulfide ion surrounded by Fe atoms has a precedent in the NiAs structural form of FeS (118). The presence of a central S²⁻ ion in the Fe/Mo/S center of nitrogenase cannot be ruled out on the basis of at least one of the crystallographic data sets (3b).

If the Fe/Mo/S centers indeed contain trigonally coordinated Fe sites, the latter must owe their existence to extreme steric constraints imposed by the protein matrix, and they should rapidly coordinate to available ligands as the Fe/Mo/S center is extruded from the protein. This being the case, the target for a synthetic analog cluster should not be a coordinatively unsaturated species (Figure 2A) but rather a

coordinatively saturated one (Figure 2B, C) that will hopefully be competent to reconstitute the apo-MoFe protein.

Is the Structure of the Isolated Cofactor the Same as That of the Fe/Mo/S Center in Nitrogenase? A preponderance of data indicates that the Fe/Mo/S center undergoes significant changes when extruded from the MoFe protein, even though the gross features of the center in the protein and the isolated cofactor are similar. These similarities are apparent in magnetic circular dichroism data (49). In the EPR spectra of the FeMo-cofactor, g -value shifts indicate greater rhombicity for the $S = 3/2$ center outside the protein environment (44, 119).

The extraction of the FeMo-cofactor is possible only with basic *N*-methyl formamide, NMF, whereas acidic NMF appears ineffective (28). This observation supports the suggestion that deprotonated NMF may serve as a terminal ligand for some of the iron atoms (31). The addition of uninegative terminal ligands to the Fe/Mo/S centers would impart the expected (120) overall negative charge to the FeMo-cofactor. The cations associated with such an ionic cofactor would greatly influence its solubility properties. With alkali metal cations (K^+ , Na^+), the FeMo-cofactor would be soluble only in very polar (high dielectric) solvents such as NMF. Cation exchange with softer, hydrophobic cations such as Et_4N^+ , Ph_4As^+ or $n-Bu_4N^+$ would be expected to change the solubility characteristics to the FeMo-cofactor and make it soluble in "conventional" organic solvents. This is indeed the case and the $(Et_4N^+)_x$ FeMo-cofactor is soluble in dimethylformamide, DMF, whereas the $(n-Bu_4N^+)_x$ FeMo-cofactor is soluble in CH_3CN or even CH_2Cl_2 (121-122). In the absence of NMF, the counterions (Cl^- , Br^-) that accompany the tetraalkyl or tetraaryl ammonium, phosphonium, or arsonium salts may serve as terminal ligands for the Fe atoms. The presence of Cl^- in the FeMo-cofactor, obtained by a NMF-based isolation procedure, has been tested by a Cl-K-edge XANES study. The absence of any chlorine in the sample has led to the conclusion that Cl^- plays no part as a ligand on intact cofactor (123). These results may reflect the inability of Cl^- to replace other ligands ($NMF^-?$) from the coordination spheres of the Fe atoms. A Cl-K-edge XANES study on DMF-isolated FeMo-cofactor (121-122) may be necessary before Cl^- can be ruled out as a possible ligand. The extraction of the FeMo-cofactor in a DMF solution of $n-Bu_4NCl$ occurs readily and the solution displays an EPR signal centered around $g = 2$ indicating a $S = 1/2$ ground state (121). This change in the spin ground state could be due to the introduction of Cl^- ions as terminal ligands to the metal atoms in the cofactor.

The conclusion one may reach is that the isolated cofactor has a different structure than the protein-bound Fe/Mo/S center. The most likely differences would involve the coordination of the Fe atoms. The latter in the isolated FeMo-cofactor may be coordinated by deprotonated NMF. In the absence of NMF, halide ions may be coordinated to the Fe atoms as terminal ligands.

A systematic evaluation of Fe-EXAFS of samples of the FeMo-cofactor obtained by different isolation procedures, and if possible, a single-crystal structure determination of the FeMo-cofactor would obviously be very desirable.

Specific Aspects of FeMo-Cofactor Chemistry That Must Be Assessed In Light of the MoFe Protein Structure Determination. The interactions of the FeMo-cofactor with excess EDTA (124) or *o*-phenanthroline (*o*-phen) (28) result in a complete loss of the $S = 3/2$ EPR signal. The signal is recovered when Zn^{+2} or Fe^{+2} ions are added to the solutions that contain EDTA or *o*-phen, respectively. It appears that addition of EDTA or *o*-phen causes aggregation of the FeMo-cofactor and possibly spin-coupling. These effects are reversed when the perturbing ligand are removed by coordination to Zn^{+2} or Fe^{+2} ions. An examination of Figure 2 does not offer an obvious mechanism for this chemistry. The fact that 2-2'-bipyridyl, 2-2'-bipy does not show a similar effect is also very peculiar.

The reconstitution of the apo-MoFe protein by FeMo-cofactor is inhibited by MoS_4^{2-} but is not affected by WS_4^{2-} , $\text{MoO}_2\text{S}_2^{2-}$ or $\text{MoO}_3\text{S}^{2-}$ (125-126). The mutual exclusivity in binding to the MoFe protein between the FeMo-cofactor and MoS_4^{2-} is difficult to explain. The indirect effect of MoS_4^{2-} binding at a distant site from the Fe/Mo/S site has been offered as a possible explanation (7).

The Fe/Mo/S cluster isolated by acidification (HCl) of the MoFe protein and extraction with methyl ethyl ketone, MEK, (127) appears to be a derivative of the FeMo-cofactor with a $S = 1/2$ ground state. It is likely that the two clusters are structurally similar and that the MEK extracted cluster does not contain homocitrate. A possible candidate for terminal ligation to the Mo atom in this case would be Cl-ligands. This Fe/Mo/S cluster is a potent inhibitor of FeMo-cofactor binding to the apo-MoFe protein (126). It would be interesting if acidification (HCl) of the FeMo-cofactor leads to the $S = 1/2$ Fe/Mo/S cluster.

The treatment of the FeMo-cofactor in NMF with excess thiol (21) does not give Fe_4S_4 or Fe_2S_2 fragments. Furthermore, the FeMo-cofactor does not "release" its Fe atoms to either 2-2'-bipy or o-phen (28). An examination of the most recently proposed structure (Figure 2A) suggests that such a molecule may break up into Fe_4S_4 or Fe_3MoS_4 clusters in reactions with S^{2-} . The unusual robustness of the FeMo-cofactor toward nitrogenous ligands contrasts with the easy anaerobic hydrolysis. It has been reported (5a) that the cofactor loses 50% of its activity in two hrs at $^{\circ}\text{C}$.

Concluding Remarks

It is perhaps appropriate that the extraordinary reduction of N_2 to NH_3 at ambient temperature and pressure is carried out by an extraordinarily unusual molecule. It is now apparent that an extraordinary effort will be needed to obtain a synthetic analog for the Fe/Mo/S center or the FeMo-cofactor of nitrogenase.

Acknowledgments. The generous support of our research by the National Institutes of Health (GM33080) is gratefully acknowledged. The invaluable contributions to our research by a dedicated group of graduate students and research collaborators made the work that originated in our laboratory possible. Particularly, I wish to acknowledge the immense contributions of my students, M.G. Kanatzidis, A. Salifoglou, S. Al-Ahmad, P.R. Challen, K. Demadis and P. Mosier. The solid state physics group (A. Kostikas, A. Simopoulos and V. Papaefthymiou) in the Nuclear Research Center Demokritos in Athens, Greece, and Dr. W.R. Dunham in the University of Michigan biophysics department have been instrumental in conducting Mössbauer and EPR studies, which are very important for an in-depth understanding of the electronic structure of the Fe/Mo/S clusters.

References

1. a. Orme-Johnson, W.H. *Ann. Rev. Biophys. Biophys. Chem.* **1985**, *14*, 419.
- b. Burgess, B.K. In *Advances in Nitrogen Fixation Research*; Veeger, C.; Newton, W.E.; Eds.; Martinus-Nijhoff: The Hague, 1983; pp 103.
- c. Burris, R.H. *J. Biol. Chem.* **1991**, *266*, 9339.
- d. Smith B.E.; Eady, R.R. *Eur. J. Biochem.* **1992**, *205*, 1.
2. Georgiadis, M.M.; Chakrabarti, P.; Woo, D.; Kornuc, J.J.; Rees, D.C. *Science* **1992**, *257*, 1653.
3. a. Bolin, J.T.; Ronco, A.E.; Mortenson, L.E.; Morgan, T.V.; Williamson, M.; Xuong, N.-H. In *Nitrogen Fixation: Achievements and Objectives*;

- Gresshoff, P.M.; Stacey, G.; Roth, L.E.; Newton, W.E.; Eds.; Chapman and Hall: New York, 1990; pp 117.
- b. Bolin, J.T.; Ronco, A.E.; Morgan, T.V.; Mortenson, L.E.; Xuong, N.-H. *Proc. Natl. Acad. Sci. U.S.A.*, in press.
 - c. Bolin, J.T.; Campobasso, N.; Muchmore, S.W.; Morgan, T.V.; Mortenson, L.E. Chapter 12 in this volume.
 - d. Bolin, J.T., personal communication, 1992.
4. a. Kim, J.; Rees, D.C. *Science* **1992**, *257*, 1677.
 - b. Rees, D.C.; Kim, J.; Georgiadis, M.M.; Komiya, H.; Chirino, A.J.; Woo, D.; Schlessman, J.; Chan, M.K.; J-Tor, L.; Santillan, B.; Chakrabarti, P.; Chu, B.T. Chapter 11, this volume.
5. a. Shah, V.K.; Brill, W.J. *Proc. Natl. Acad. Sci. USA* **1977**, *74*, 3249.
 - b. Shah, V.K. *Methods Enzymol.* **1980**, *69*, 792.
6. Burgess, B.K. *Chem. Rev.* **1990**, *90*, 1377.
7. Newton, W.E. In *Biological Nitrogen Fixation*; Stacey, G.; Burris, R.H.; Evans, H.J.; Eds; Chapman and Hall: New York, 1992; pp 877.
8. Bishop, P.E.; Hawkins, M.E.; Eady, R.R. *Biochem. J.* **1986**, *238*, 437.
9. Bishop, P.E.; Premakumar, R.; Dean, D.R.; Jacobson, M.R.; Chisnell, J.R.; Rizzo, T.M.; Kopczynski, J. *Science* **1986**, *232*, 92.
10. Robson, R.L. *Arch. Microbiol.* **1986**, *146*, 74.
11. Bishop, P.E. *Trends Biol. Sci.* **1986**, *11*, 225.
12. Arber, J.M.; Dobson, B.R.; Eady, R.R.; Hasnain, S.S.; Garner, C.D.; Matsushita, T.; Nomura, M.; Smith, B.E. *Biochem. J.* **1989**, *258*, 733.
13. a. Garner, C.D.; Arber, J.M.; Harvey, L.; Hasnain, S.S.; Eady, R.R.; Smith, B.E.; deBoer, E.; Wever, R. *Polyhedron* **1989**, *8*, 1649.
 - b. Garner, C.D.; Arber, J.M.; Hasnain, S.S.; Dobson, B.R.; Eady, R.R.; Smith, B.E. *Physica* **1989**, *158*, 74.
14. Bishop, P.E.; Jarlenski, D.M.L.; Hetherington, D.R. *Proc. Natl. Acad. Sci USA* **1980**, *77*, 7342.
15. Chisnell, J.R.; Premakumar, R.; Bishop, P.E. *J. Bacteriol.* **1988**, *170*, 27.
16. Holm, R.H.; Simhon, E.D. In *Molybdenum Enzymes*; Spiro, T.G., Ed.; John Wiley and Sons: New York, 1985; p 1.
17. Coucouvanis, D. *Acc. Chem. Res.* **1991**, *24*, 1.
18. Kanatzidis, M.G.; Baenziger, N.C.; Coucouvanis, D.; Simopoulos, A.; Kostikas, A. *J. Am. Chem. Soc.* **1984**, *106*, 4500.
19. Holm, R.H.; Ciurli, S.; Weigel, J.A. In *Progress In Inorganic Chemistry: Bioinorganic Chemistry*; Lippard, S.J., Ed.; John Wiley and Sons: New York, 1990; pp 1.
20. a. McLean, P.A.; Papaefthymiou, V.; Orme-Johnson, W.H.; Munck, E. *J. Biol. Chem.* **1975**, *262*, 12900.
 - b. Zimmermann, R.; Trautwein, A.X. In *Nitrogen Fixation: The Chemical, Biochemical Genetic Interface*; Muller, A.; Newton, W.E.; Eds.; Plenum Press: New York, 1983; pp 63.
21. Kurtz, Jr., D.M.; McMillan, R.S.; Burgess, B.K.; Mortenson, L.E.; Holm, R.H. *Proc. Natl. Acad. Sci. USA* **1979**, *76*, 4986.
22. a. Johnson, M.K.; Thomson, A.J.; Robinson, A.E.; Smith, B.E. *Biochim. Biophys. Acta* **1981**, *671*, 61.
 - b. Morningstar, J.E.; Johnson, M.K.; Case, E.E.; Hales, B.J. *Biochemistry* **1987**, *26*, 1795.
23. a. Watt, G.D.; Burns, A.; Tennent, D.L. *Biochemistry* **1981**, *20*, 7272.
 - b. Watt, G.D.; Burns, A.; Lough, S.; Tennent, D.L. *Biochemistry* **1980**, *19*, 4926.
 - c. Watt, G.D.; Wang, Z. *Biochemistry* **1986**, *25*, 5196.
24. Hagen, W.R.; Wassink, H.; Eady, R.R.; Smith, B.E.; Haaker, H. *Eur. J. Biochem.* **1987**, *169*, 457.

25. Surerus, K.K.; Hendrich, M.P.; Christie, P.D.; Rottgardt, P.; Orme-Johnson, W.E.; Munck, E. *J. Am. Chem. Soc.* **1992**, *114*, 8579.
26. Orme-Johnson, W.H.; Wink, D.A.; McLean, P.A.; Harris, G.S.; True, A.E.; Hoffman, B.; Munck, E. *Rec. Trav. Chim. Pays-Bas* **1987**, *106*, 299.
27. Nelson, M.J.; Levy, M.A.; Orme-Johnson, W.H. *Proc. Natl. Acad. Sci. USA* **1983**, *80*, 147.
28. Yang, S.-S.; Pan, W.-H.; Friesen, G.D.; Burgess, B.K.; Corbin, J.L.; Stiefel, E.I.; Newton, W.E. *J. Biol. Chem.* **1982**, *257*, 8042.
29. Schultz, F.A.; Gheller, S.F.; Burgess, B.K.; Lough, S.; Newton, W.E. *J. Am. Chem. Soc.* **1985**, *107*, 5364.
30. Stiefel, E.I. *Prog. Inorg. Chem.* **1977**, *22*, 1.
31. Walters, M.A.; Chapman, S.K.; Orme-Johnson, W.H. *Polyhedron* **1986**, *5*, 561.
32. Newton, W.E.; Gheller, S.F.; Sands, R.H.; Dunham, W.R. *Biochem. Biophys. Res. Commun.* **1989**, *162*, 882.
33. Eady, R.R.; Imam, S.; Lowe, D.J.; Miller, R.W.; Smith, B.E.; Thorneley, R.N.F. In *Nitrogen Fixation*; Stewart, W.D.P.; Gallon, J.R.; Eds.; Academic Press: New York, 1980; p 19.
34. Smith, B.E.; Bishop, P.E.; Dixon, R.A.; Eady, R.R.; Filler, W.A.; Lowe, D.J.; Richards, A.J.M.; Thomson, A.J.; Thornley, R.N.F.; Postgate, J.R. In *Nitrogen Fixation Research Progress*; Evans, H.J.; Bottomley, P.J.; Newton, W.E.; Eds.; Martinus Nijhoff: Dordrecht, 1985; pp 597.
35. a. Hoffman, B.M.; Roberts, J.E.; Orme-Johnson, W.H. *J. Am. Chem. Soc.* **1982**, *104*, 860.
 b. Venters, R.A.; Nelson, M.J.; McLean, P.A. *J. Am. Chem. Soc.* **1986**, *108*, 3487.
 c. Hoffman, B.M.; Venters, R.A.; Roberts, J.E.; Nelson, M.J.; Orme-Johnson, W.H. *J. Am. Chem. Soc.* **1982**, *104*, 4711.
36. Christou, G.; Mascharak, P.K.; Armstrong, W.H.; Papaefthymiou, G.C.; Frankel, R.B.; Holm, R.H. *J. Am. Chem. Soc.* **1982**, *104*, 2820.
37. Conradson, S.D.; Burgess, B.K.; Newton, W.E.; Mortenson, L.E.; Hodgson, K.O. *J. Am. Chem. Soc.* **1987**, *109*, 7507.
38. Cramer, S.P.; Hodgson, K.O.; Gillum, W.O.; Mortenson, L.E. *J. Am. Chem. Soc.* **1978**, *100*, 3398.
39. Flank, A.M.; Weininger, M.; Mortenson, L.E.; Cramer, S.P. *J. Am. Chem. Soc.* **1986**, *108*, 1050.
40. Antonio, M.R.; Teo, B.K.; Orme-Johnson, W.H.; Nelson, M.J.; Groh, S.E.; Lindahl, P.A.; Kauzlarich, S.M.; Averill, B.A. *J. Am. Chem. Soc.* **1982**, *104*, 4703.
41. Arber, J.M.; Flood, A.C.; Garner, C.D.; Gormall, C.A.; Hasnain, S.S.; Smith, B.E. *Biochem. J.* **1988**, *252*, 421.
42. a. Chen, J.; George, S.J.; Tittsworth, R.C.; Hales, B.J.; Christiansen, J.; Coucouvanis, D.; Cramer, S.P. *J. Am. Chem. Soc.*, submitted.
 b. See also Chapter 15, this volume.
43. a. Kanatzidis, M.G.; Dunham, W.R.; Hagen, W.R.; Coucouvanis, D. *J. Chem. Soc. Chem. Comm.* **1984**, 356.
 b. Coucouvanis, D.; Kanatzidis, M. G.; Dunham, W.R.; Hagen, W.R. *J. Am. Chem. Soc.* **1984**, *106*, 7998.
 c. Kanatzidis, M.G.; Hagen, W.R.; Dunham, W.R.; Lester, R.K.; Coucouvanis, D. *J. Am. Chem. Soc.* **1985**, *107*, 953.
 d. Kanatzidis, M.G.; Salifoglou, A.; Coucouvanis, D. *J. Am. Chem. Soc.* **1985**, *107*, 3358.
 e. Kanatzidis, M.G.; Salifoglou, A.; Coucouvanis, D. *Inorg. Chem.* **1986**, *25*, 2460.

- f. Coucouvanis, D.; Kanatzidis, M.G.; Salifoglou, A.; Dunham, W.R.; Simopoulos, A.; Sams, J.R.; Papaefthymiou, V.; Kostikas, A.; Strouse, C.E. *J. Am. Chem. Soc.* **1987**, *22*, 6863.
44. Rawlings, J.; Shah, V.K.; Chisnell, J.R.; Brill, W.J.; Zimmerman, R.; Munck, E.; Orme-Johnson, W.H. *J. Biol. Chem.* **1978**, *253*, 1001.
45. a. Mascharak, P.K.; Smith, M.C.; Armstrong, W.H.; Burgess, B.K.; Holm, R.H. *Proc. Natl. Acad. Sci.* **1982**, *79*, 7056.
b. Conradson, S.D.; Burgess, B.K.; Holm, R.H. *J. Biol. Chem.* **1988**, *263*, 13743.
46. Newton, W.E.; Gheller, S.F.; Schultz, F.A.; Burgess, B.K.; Conradson, S.D.; McDonald, J.W.; Hedman, B.; Hodgson, K.O. In *Nitrogen Fixation Research Progress*; Evans, H.J.; Bottomley, P.J.; Newton, W.E.; Eds.; Martinus Nijhoff: Dordrecht, 1985, pp 605.
47. Thomann, H.; Morgan, T.V.; Jin, H.; Burgmayer, S.J.N.; Bare, R.E.; Stiefel, E.I. *J. Am. Chem. Soc.* **1987**, *109*, 7913.
48. Shah, V.K.; Davis, L.C.; Gordon, J.K.; Orme-Johnson, W.H.; Brill, W.J. *Biochim. Biophys. Acta* **1973**, *292*, 246.
49. Robinson, A.C.; Richards, A.J.M.; Thomson, A.J.; Hawkes, T.R.; Smith, B.E. *Biochem. J.* **1984**, *219*, 495.
50. Zimmermann, R.; Munck, E.; Brill, W.J.; Shah, V.K.; Henzl, M.T.; Rawlings, J.; Orme-Johnson, W.H. *Biochim. Biophys. Acta* **1978**, *537*, 185.
51. Huynh, B.H.; Henzl, M.T.; Christner, J.A.; Zimmermann, R.; Orme-Johnson, W.H.; Munck, E. *Biochim. Biophys. Acta* **1980**, *623*, 124.
52. Schultz, F.A.; Gheller, S.F.; Newton, W.E. *Biochem. Biophys. Res. Commun.* **1988**, *152*, 629.
53. Newton, W.E.; Gheller, S.F.; Feldman, B.J.; Dunham, W.R.; Schultz, F.A. *J. Biol. Chem.* **1989**, *264*, 1924.
54. Schultz, F.A.; Gheller, S.F.; Feldman, B.J.; Newton, W.E. In *Nitrogen Fixation: Hundred Years After*; Bothe, H.; DeBruijn, F.J.; Newton, W.E.; Eds.; Fischer: Stuttgart, 1988, pp 121.
55. McLean, P.A.; Dixon, R.A. *Nature* **1981**, *292*, 655.
56. Hawkes, T.R.; McLean, P.A.; Smith, B.E. *Biochem. J.* **1984**, *217*, 317.
57. Hoover, T.R.; Shah, V.K.; Roberts, G.P.; Ludden, P.W. *J. Bacteriol.* **1986**, *167*, 999.
58. Hoover, T.R.; Robertson, A.D.; Cerny, R.L.; Hayes, R.N.; Imperial, J.; Shah, V.K.; Ludden, P.W. *Nature* **1987**, *329*, 855.
59. a. Hoover, T.R.; Imperial, J.; Ludden, P.W.; Shah, V.K. *Biofactors* **1988**, *1*, 199.
b. Hoover, T.R.; Imperial, J.; Ludden, P.W.; Shah, V.K. *Biochemistry* **1989**, *28*, 2768.
60. Hoover, T.R.; Imperial, J.; Liang, P.; Ludden, P.W.; Shah, V.K. *Biochemistry* **1988**, *27*, 3647.
61. Powers, P.P.; Shoner, S.C. *Angew. Chem. Int. Ed. Engl.* **1991**, *30*, 330.
62. Kent, H.M.; Ioannidis, I.; Gormal, C.; Smith, B.E.; Buck, M. *Biochem. J.* **1989**, *264*, 257.
63. Dean, D.R.; Scott, D.J.; Newton, W.E. In *Nitrogen Fixation: Achievements and Objectives*; Gresshoff, P.M.; Stacey, G.; Roth, L.E.; Newton, W.E.; Eds.; Chapman and Hall: New York, 1990, pp 95.
64. Scott, D.J.; May, H.D.; Newton, W.H.; Brigle, K.E.; Dean, D.R. *Nature* **1990**, *343*, 188.
65. Roussin, M.L. *Ann. Chim. Phys.* **1858**, *52*, 285.
66. Chu, C.-W.; Dahl, L.F. *Inorg. Chem.* **1977**, *16*, 3245.
67. Coucouvanis, D. In *Advances in Nitrogen Fixation Research*; Veeger, C.; Newton, W.E.; Eds.; Nijhoff/Junk: The Hague, 1984, pp 81.

68. a. Christou, G.; Sabat, M.; Ibers, J.A.; Holm, R.H. *Inorg. Chem.* **1982**, *21*, 3518.
b. Hagen, K.S.; Watson, A.D.; Holm, R.H. *J. Am. Chem. Soc.* **1983**, *105*, 3905.
69. Kanatzidis, M.G.; Coucouvanis, D.; Simopoulos, A.; Kostikas, A.; Papaefthymiou, V. *J. Am. Chem. Soc.* **1985**, *107*, 4925.
70. Coucouvanis, D. *Acc. Chem. Res.* **1981**, *14*, 201.
71. a. Coucouvanis, D.; Simhon, E.D.; Swenson, D.; Baenziger, N.C. *J. Chem. Soc. Chem. Commun.* **1979**, 361.
b. Tieckelmann, R.H.; Silvis, H.C.; Kent, T.A.; Huynh, B.H.; Waszczak, J.V.; Teo, B.-K.; Averill, B.A. *J. Am. Chem. Soc.* **1980**, *102*, 5550.
72. a. Coucouvanis, D.; Baenziger, N.C.; Simhon, E.D.; Stremple, P.; Swenson, D.; Simopoulos, A.; Kostikas, A.; Petrouleas, V.; Papaefthymiou, V. *J. Am. Chem. Soc.* **1980**, *102*, 1732.
b. Coucouvanis, D.; Simhon, E.D.; Stremple, P.; Ryan, M.; Swenson, D.; Baenziger, N.C.; Simopoulos, A.; Papaefthymiou, V.; Kostikas, A.; Petrouleas, V. *Inorg. Chem.* **1984**, *23*, 741.
73. Silvis, H.C.; Averill, B.A. *Inorg. Chem. Acta* **1981**, *54*, L57.
74. Coucouvanis, D.; Simhon, E.D.; Stremple, P.; Baenziger, N.C. *Inorg. Chem. Acta* **1981**, *53*, L135.
75. Coucouvanis, D.; Baenziger, N.C.; Simhon, E.D.; Stremple, P.; Swenson, D.; Kostikas, A.; Simopoulos, A.; Petrouleas, V.; Papaefthymiou, V. *J. Am. Chem. Soc.* **1980**, *102*, 1730.
76. a. Coucouvanis, D.; Simhon, E. D.; Baenziger, N.C. *J. Am. Chem. Soc.* **1980**, *102*, 6644.
b. McDonald, J.W.; Friesen, G.D.; Newton, W.E. *Inorg. Chim. Acta* **1980**, *46*, L79.
c. Müller, A.; Hellmann, W.; Schneider, J.; Schimanski, U.; Demmer, U.; Trautwein, A.; Bender, V. *Inorg. Chim. Acta* **1982**, *65*, L41.
77. Stremple, P.; Baenziger, N.C.; Coucouvanis, D. *J. Am. Chem. Soc.* **1981**, *103*, 4601.
78. Miller, A.; Sarkar, S.; Bögge, H.R.; Jostes, R.; Trautwein, A.; Lauer, U. *Angew. Chem. Int. Ed. Engl.* **1983**, *22*, 561.
79. a. Tieckelmann, R.H.; Averill, B.A. *Inorg. Chim. Acta* **1980**, *46*, L35.
b. Teo, B.K.; Antonio, M.R.; Tieckelmann, R.H.; Silvis, H.C.; Averill, B.A. *J. Am. Chem. Soc.* **1982**, *104*, 6126.
80. Dahlstrom, P.L.; Kumar, S.; Zubieta, J. *J. Chem. Soc. Chem. Commun.* **1981**, 411.
81. Müller, A.; Hellmann, W.; Bögge, H.; Jostes, R.; Romer, M.; Schimanski, U. *Angew. Chem. Int. Ed. Engl.* **1982**, *21*, 860.
82. Wolff, T.E.; Berg, J.M.; Warrick, C.; Hodgson, K.O.; Holm, R.H.; Frankel, R.B. *J. Am. Chem. Soc.* **1978**, *100*, 4630.
83. Acott, S.R.; Christou, G.; Garner, C.D.; King, T.J.; Mabbs, F.E.; Miller, R.F. *Inorg. Chem. Acta* **1979**, *35*, L337.
84. Christou, G.; Garner, C.D.; Mabbs, F.E.; King, T.J. *J. Chem. Soc. Chem Commun.* **1978**, 740.
85. Armstrong, W.H.; Holm, R.H. *J. Am. Chem. Soc.* **1981**, *103*, 6246.
86. Palermo, R.E.; Single, R.; Bashkin, J.K.; Holm, R.H. *J. Am. Chem. Soc.* **1984**, *106*, 2600.
87. Ubeff, T.E.; Berg, J.M.; Holm, R.H. *Inorg. Chem.* **1981**, *20*, 174.
88. a. Kanatzidis, M.G.; Coucouvanis, D. *J. Am. Chem. Soc.* **1986**, *108*, 337.
b. Coucouvanis, D.; Salifoglou, A.; Kanatzidis, M.G.; Dunham, W.R.; Simopoulos, A.; Kostikas, A. *Inorg. Chem.* **1988**, *27*, 4066.
c. Al-Ahmad, S.A.; Salifoglou, A.; Kanatzidis, M.G.; Dunham, W.R.; Coucouvanis, D. *Inorg. Chem.* **1990**, *29*, 927.

89. a. Coucouvanis, D.; Salifoglou, A.; Kanatzidis, M.G.; Simopoulos, A.; Papaefthymiou, V. *J. Amer. Chem. Soc.* **1984**, *106*, 6081.
b. Cleland, W.E.; Averill, B.A. *Inorg. Chem.* **1984**, *23*, 4192.
90. Cleland, W.E.; Holtman, D.A.; Sabat, M.; Ibers, J.A.; Defotis, G.C.; Averill, B.A. *J. Am. Chem. Soc.* **1983**, *105*, 6021.
91. Coucouvanis, D. In *Metal Clusters in Proteins*; Que, Jr., L.; Ed.; ACS Symposium Series 372; 1988; pp 390.
92. Salifoglou, A.; Kanatzidis, M.G.; Coucouvanis, D. *J. Chem. Soc. Chem. Commun.* **1986**, 559.
93. a. Coucouvanis, D.; Al-Ahmad, S.; Salifoglou, A.; Dunham, W.R.; Sands, R.H. *Angew. Chem. Int. Ed. Engl.* **1988**, *27*, 1353.
b. Coucouvanis, D.; Al-Ahmad, S.; Salifoglou, A.; Papaefthymiou, V.; Kostikas, A.; Simopoulos, A. *J. Amer. Chem. Soc.* **1992**, *114*, 2472.
94. Coucouvanis, D.; Challen, P.R.; Koo, S.-M.; Davis, W.M.; Butler, W.; Dunham, W.R. *Inorg. Chem.* **1989**, *28*, 4181.
95. Hardy, R.W.F.; Burns, R.C.; Parshall, G.W. In *Inorganic Biochemistry*; Eichhorn, G.L.; Ed.; Elsevier: Amsterdam, 1973, pp 745 and references therein.
96. Challen, P.R.; Koo, S.-M.; Dunham, W.R.; Coucouvanis, D. *J. Amer. Chem. Soc.* **1990**, *112*, 2455.
97. Bobrik, M.A.; Hodgson, K.O.; Holm, R.H. *Inorg. Chem.* **1977**, *16*, 1851.
98. Challen, P.R.; Koo, S.-M.; Kim, C.G.; Dunham, W.R.; Coucouvanis, D. *J. Am. Chem. Soc.* **1990**, *112*, 8606.
99. Challen, P.R., University of Michigan, Ph.D. thesis, 1990.
100. Coucouvanis, D.; Al-Ahmad, S.; Kim, C.G.; Mosier, P.E.; Kampf, J.W. *Inorg. Chem.*, submitted for publication.
101. Zumft, W.G. *Eur. J. Biochem.* **1978**, *91*, 345.
102. Newton, W.E.; Schultz, F.A.; Gheller, S.F.; Lough, S.; McDonald, W.J.; Conradson, S.D.; Hedman, B.; Hodgson, K.O. *Polyhedron* **1986**, *5*, 567.
103. Newton, W.E.; Gheller, S.F.; Hedman, B.; Hodgson, K.O.; Lough, J.; McDonald, J.W. *Eur. J. Biochem.* **1986**, *159*, 111.
104. Bose, K.S.; Lamberty, P.E.; Kovacs, J.E.; Sinn, E.; Averill, B.A. *Polyhedron* **1986**, *5*, 393.
105. Eldredge, P.A.; Bryan, R.F.; Sinn, E.; Averill, B.A. *J. Am. Chem. Soc.* **1988**, *110*, 5573.
106. Kovacs, J.A.; Bashkin, J.K.; Holm, R.H. *J. Am. Chem. Soc.* **1985**, *107*, 1784.
107. Bose, K.S.; Chmielewski, S.A.; Eldredge, P.A.; Sinn, E.; Averill, B.A. *J. Amer. Chem. Soc.* **1989**, *111*, 8953.
108. George, G.N.; Bare, R.E.; Stiefel, E.I.; Prince, R.C. *Biochem. J.* **1989**, *262*, 349.
109. Bulen, W.A. *J. Bacteriol.* **1965**, *82*, 130.
110. Keeler, R.F.; Varner, J.E. *Arch. Biochem. Biophys.* **1957**, *70*, 585.
111. Munck, E.; Rhodes, H.; Orme-Johnson, W.H.; Davis, L.C.; Brill, W.J.; Shah, V.K. *Biochim. Biophys. Acta* **1975**, *400*, 32.
112. Palmer, G.; Multani, J.S.; Cretney, W.C.; Zumft, W.G.; Mortenson, L.E. *Arch. Biochem. Biophys.* **1972**, *153*, 325.
113. Newton, W.E.; Cantwell, J.S.; Feldman, B.J.; Gheller, S.F.; Schultz, F.A.; Frank, P.; Hedman, B.; Hodgson, K.O. In *Nitrogen Fixation: Achievements and Objectives*; Gresshoff, P.M.; Stacey, G.; Roth, L.E.; Newton, W.E.; Eds.; Chapman and Hall: New York, 1990, p 165.
114. Kostiner, E.; Steger, J.; Rea, J.R. *Inorg. Chem.* **1970**, *9*, 1939.
115. a. Snyder, B.S.; Reynolds, M.S.; Noda, I.; Holm, R.H. *Inorg. Chem.* **1988**, *27*, 595.
b. Snyder, B.S.; Holm, R.H. *Inorg. Chem.* **1988**, *27*, 2339.

116. Snyder, B.S.; Holm, R.H. *Inorg. Chem.* **1990**, *29*, 274 and references therein.
117. Noda, I.; Snyder, B.S.; Holm, R.H. *Inorg. Chem.* **1988**, *27*, 3851.
118. West, A.R. In *Solid State Chemistry and its Applications*; John Wiley and Sons: New York, 1984, p 249.
119. George, G.N.; Bare, R.E.; Jin, H.; Stiefel, E.I.; Prince, R.C. *Biochem. J.* **1989**, *262*, 349.
120. Newton, W.E.; Burgess, B.K.; Stiefel, E.I. In *Molybdenum Chemistry of Biological Significance*; Newton, W.E.; Otsuka, S.; Eds.; Plenum Press: New York, 1980, pp 191.
121. Lough, S.; Jacobs, D.J.; Lyons, D.M.; Watt, G.D.; McDonald, J.W. *Biochem. Biophys. Res. Commun.* **1986**, *139*, 740.
122. McLean, P.A.; Wink, D.A.; Chapman, S.K.; Hickman, A.B.; McKillop, D.M.; Orme-Johnson, W.H. *Biochemistry* **1989**, *28*, 9402.
123. Hedman, B.; Frank, P.; Gheller, S.F.; Roe, A.L.; Newton, W.E.; Hodgson, K.O. *J. Am. Chem. Soc.* **1988**, *110*, 3798.
124. Burgess, B.K.; Stiefel, E.I.; Newton, W.E. *J. Biol. Chem.* **1980**, *255*, 353.
125. Hawks, T.R.; Smith, B.E. *Biochem. J.* **1984**, *223*, 783.
126. Shah, V.K.; Ugalde, R.A.; Imperial, J.; Brill, W.J. *J. Biol. Chem.* **1985**, *260*, 3891.
127. Shah, V.K.; Brill, W.J. *Proc. Natl. Acad. Sci. USA* **1981**, *78*, 3438.

RECEIVED March 8, 1993

Chapter 21

Bonding, Activation, and Stabilization of Small Molecules by Molybdenum–Sulfur and Iron–Sulfur Systems

Dieter Sellmann

Institut für Anorganische Chemie der Universität Erlangen-Nuernberg,
Egerlandstrasse 1, W-8520 Erlangen, Germany

In quest for model compounds for oxidoreductases with [MoS] and/or [FeS] centers, coordination, activation, and stabilization of CO, NO, N₂, N₂H₂, N₂H₃, N₂H₄, NH₃, NH₂O, and NH₂ by Mo and Fe sulfur ligand complexes was investigated. Reduction of NO to NH₂OH was achieved at [Mo(NO)(S₄')] centers. [Mo(η²-N₂H₃)(NO)(S₄')] and [Mo^{IV}(CO)₂(^{bu}S₂'₂)] model structure and, potentially, function of the Mo centers in [Fe/Mo] nitrogenases. [Fe(L)(N_HS₄')] complexes (L = CO, N₂H₂, N₂H₄, NH₃) yield a new model for the active centers of [Fe/Fe] and possibly also [Fe/Mo] nitrogenases. (N_HS₄'²⁻ = 2,2'-bis(2-mercaptophenylthio)diethylamine(2-); S₄'²⁻ = 1,2-bis(2-mercaptophenylthio)ethane(2-); ^{bu}S₂'²⁻ = 3,5-di(tertiarybutyl)-benzene-1,2-dithiolate(2-)).

Activation of stable and stabilization of unstable molecules has been a long standing challenge for chemists. When [MoS] enzymes are the topic, inevitably nitrogenases and molecules such as the inert N₂ and the elusive nitrogen hydrides N₂H, N₂H₂ or N₂H₃ come into mind (1).

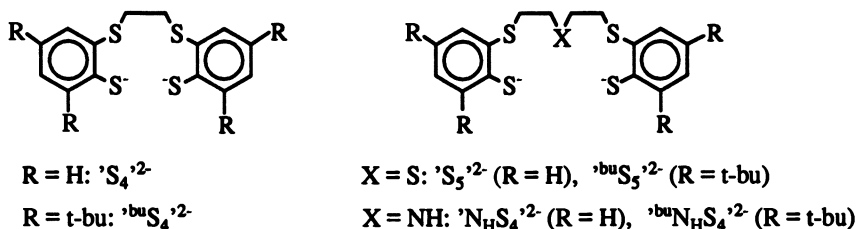
All nitrogenases, however, contain by far more iron, and one nitrogenase contains exclusively iron (2). Thus, if chemists want to design systems that are either equally efficient as nitrogenases or allow deeper insights into the mechanisms and elementary steps of N₂ fixation, iron-sulfur complexes are at least equally important.

[MS] centers also occur in other oxidoreductases that catalyze reactions that are extremely difficult in chemical terms. What makes [MS] centers particularly suited to catalyze these reactions which require not only activation and stabilization of molecules, but also addition and release of substrates and transfer of electrons and protons? Answers to these questions may be obtained from model complexes, which may be mononuclear even though the [MS] centers of native proteins are polynuclear.

Ligands and complexes

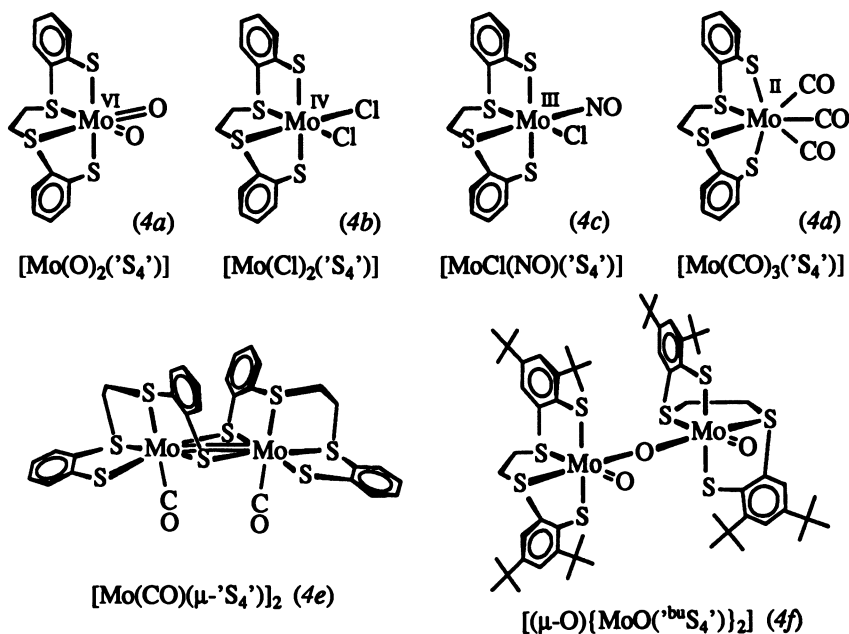
Suitable model compounds should have a relatively robust [MS] core and vacant sites for the coordination of substrates. For this purpose polydentate thioetherthiolate ligands were designed (scheme I) (3).

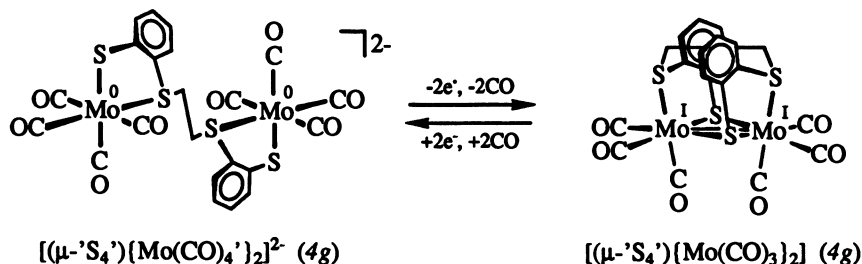
Scheme I



The $'XS_4'^{2-}$ ligands allow variation of the coordination sphere of a given complex in a defined way by substituting thioether S for amine N or ether O donors.

These ligands coordinate high-valent as well as low-valent molybdenum. The resulting complex fragments prefer either hard or soft coligands as is shown for a series of $'S_4'$ complexes in scheme II.

Scheme II: Molybdenum complexes with $'S_4'^{2-}$ ligands



In binuclear complexes, the metal centers are bridged via coligands ($[(\mu\text{-O}\{\text{Mo}(\text{O})(\text{bu}'S_4')\}_2)]$) or via thiolate donors of the sulfur ligand ($[(\mu\text{-}'S_4')\{\text{Mo}(\text{CO})_4\}_2]$). The complexes form when suitable precursor complexes, e. g., $[\text{Mo}(\text{O})_2(\text{acac})_2]$, $[\text{Mo}(\text{Cl})_4(\text{THF})_2]$, $[\text{Mo}(\text{NO})(\text{Cl})_3(\text{CH}_3\text{CN})_2]$, $[\text{Mo}(\text{CO})_4(\text{Cl})_2]$ or $[\text{Mo}(\text{CO})_4(\text{norbornadiene})]$ are reacted with the neutral or dianionic ligands $'S_4\text{-H}_2$ or $'S_4^{2-}$. Dinuclear complexes usually are obtained from mononuclear ones.

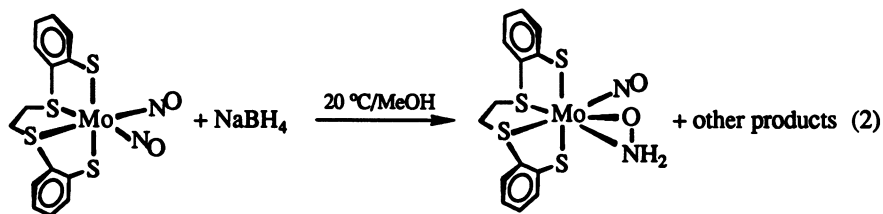
When the metal centers are in low to medium oxidation states, the 18-electron rule is obeyed. The $[(\mu\text{-}'S_4')\{\text{Mo}(\text{CO})_4\}_2]^{2-}/[(\mu\text{-}'S_4')\{\text{Mo}(\text{CO})_3\}_2]^0$ pair of complexes provides a model for a bimetallic enzyme center that may close or generate vacant sites of coordination by reversible transfer of electrons.

Reactions of Small Molecules in the Coordination Sphere of [MoS] Complexes

Reduction of NO. NO occurs as an intermediate in the $\text{NO}_2^- \rightarrow \text{NH}_3$ reduction, which is catalyzed by nitrite reductases (5). Equation 1 shows that this reduction potentially comprises many steps.

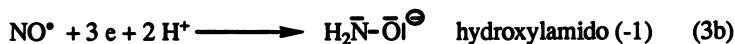
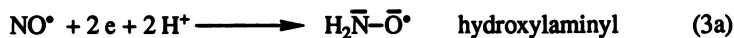


Irrespective of the question whether nitrogen monoxide is bound to a metal as NO^+ , NO^\bullet or NO^- (6), a key step in the sequence of equation 1 is the transformation of NO into NH_2OH , because this step allows the bypass of the energetically and kinetically favoured N_2 molecule. This stability and inertness of N_2 may also be the reason why such reductions of NO ligands in fully characterized complexes were not known until recently and observed for the first time in $[\text{Mo}(\text{NO})_2('S_4')]$ (6). Its $\nu(\text{NO})$ frequencies ($1765, 1660 \text{ cm}^{-1}$) and linear Mo NO bonds indicate that the NO ligands function as neutral $3e^-$ donors such that molybdenum has the oxidation state +II. Upon reaction with NaBH_4 in MeOH (equation 2),

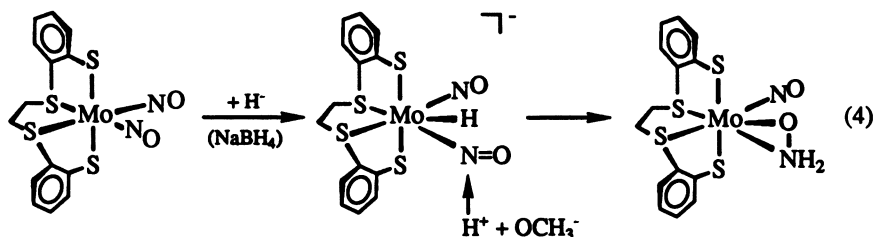


$[\text{Mo}(\text{NO})_2('S_4')]$ rapidly yields $[\text{Mo}(\text{NH}_2\text{O})(\text{NO})('S_4')]$ (7). The addition of 2 [H] is equivalent to the addition of $2 \text{H}^+ + 2 e^-$, but only if the metal oxidation state is not changed. This is indeed the case as follows from the ^{95}Mo -NMR spectra. The ^{95}Mo shifts of $[\text{Mo}(\text{NO})_2('S_4')]$ (-512 ppm) and $[\text{Mo}(\text{NH}_2\text{O})(\text{NO})('S_4')]$ (-395 ppm) differ only by 117 ppm , which is negligible if the total shift range of Mo complexes

(ca. 10,000 ppm) is taken into account. Thus, the $[2\text{H}^+, 2\text{e}^-]$ reduction of neutral NO in $[\text{Mo}(\text{NO})_2(\text{S}_4)]$ must have led to a neutral (side-on bound) hydroxylaminylligand (equation 3a), and not to a hydroxylamido(1-) ligand (equation 3b), which would result if the Mo center would contribute one electron by becoming oxidized to Mo(III) (equation 3c).



The facile change of the molybdenum coordination number between six and seven allows suggestion of a reaction mechanism for the reduction. Nitrosyl complexes with low $\nu(\text{NO})$ frequencies are not expected to be susceptible to nucleophilic addition reactions at the N atoms (6). Thus, the reduction of $[\text{Mo}(\text{NO})_2(\text{S}_4)]$ by NaBH_4 might rather occur according to equation 4.



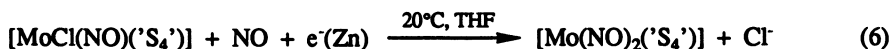
In the primary step, the nucleophilic hydride adds to the Mo center yielding a seven-coordinate species with a bent MoNO entity. Via the Mo center, two electrons are transferred to the NO, one H^+ (resulting from the hydride) and one H^+ from the solvent methanol add to the N atom, and the site that had been occupied by the hydride is closed by the oxygen atom of the resulting NH_2O ligand.

$[\text{Mo}(\text{NH}_2\text{O})(\text{NO})(\text{S}_4)]$ is not the first NH_2O complex ever described (8), but it appears to be the first example obtained by reduction of a nitrosyl complex. Previously, NH_2O complexes were also obtained from NO complexes, but in contrast to $[\text{Mo}(\text{NH}_2\text{O})(\text{NO})(\text{S}_4)]$, by addition of protons only which initiated an intramolecular electron transfer from metal to NO ligand (8). Consequently, these complexes are relatively stable towards acids and differ from $[\text{Mo}(\text{NH}_2\text{O})(\text{NO})(\text{S}_4)]$ which rapidly reacts with protons according to equation 5,



to yield free hydroxylamine and the Mo(III) complex $[\text{Mo}(\text{Cl})(\text{NO})(\text{S}_4)]$ (9). In this step, one electron is transferred from the Mo center to the $[\text{NH}_2\text{O}]$ ligand such that the complete reduction from NO to NH_2OH is achieved which requires a total of three electrons plus three protons ($\text{NO}^\bullet + 3\text{e}^- + 3\text{H}^+ \rightarrow \text{NH}_2\text{OH}$).

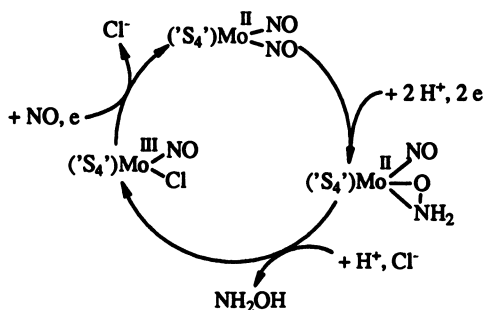
$[\text{Mo}(\text{Cl})(\text{NO})(\text{S}_4)]$ can be reductively nitrosylated according to equation 6,



when treated with gaseous NO in the presence of zinc (9). Thus, combination of equations 2, 5, and 6 yields a reduction of NO to NH_2OH , which takes place in the

coordination sphere of the $[\text{Mo}(\text{NO})(\text{S}_4)]$ fragment and is, in principle, catalytic. This is summarized in scheme III.

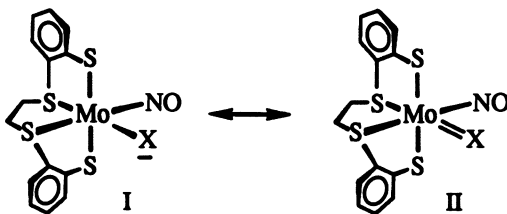
Scheme III



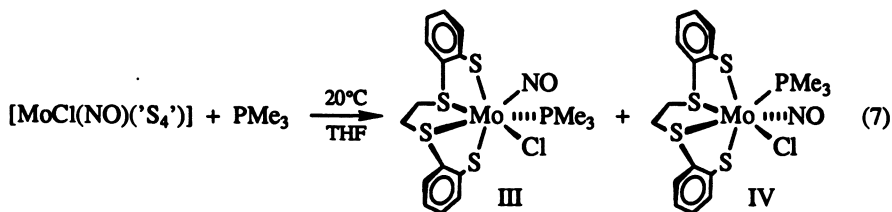
$[\text{MoS}]$ centers have been shown to be present in nitrate reductases, but not yet in nitrite reductases (5). Scheme III shows that the $\text{NO} \rightarrow \text{NH}_2\text{OH}$ reduction is facilitated at $[\text{MoS}]$ centers whose Mo atoms readily increase their coordination numbers, and this may be considered an incentive to search for nitrite reductases having such centers.

Coordination and Stabilization of N_2H_3 and NH_2 . $[\text{Mo}(\text{Cl})(\text{NO})(\text{S}_4)]$ with its Mo(III) center demonstrated the importance of the 18-electron rule and readily accessible sites of coordination.

$[\text{Mo}(\text{NO})(\text{S}_4)]^+$ has a 14-electron Mo(III) center which is stabilized by anionic X^- ligands that must act as 4 electron σ - π donors according to the mesomeric structures I and II,



if the Mo center is to achieve an 18-electron configuration. I has a 16-electron Mo center and can be expected to exhibit a vacant site of coordination. This is proved by addition of PMe_3 to $[\text{Mo}(\text{Cl})(\text{NO})(\text{S}_4)]$, which yields $[\text{Mo}(\text{Cl})(\text{PMe}_3)(\text{NO})(\text{S}_4)]$ according to equation 7.



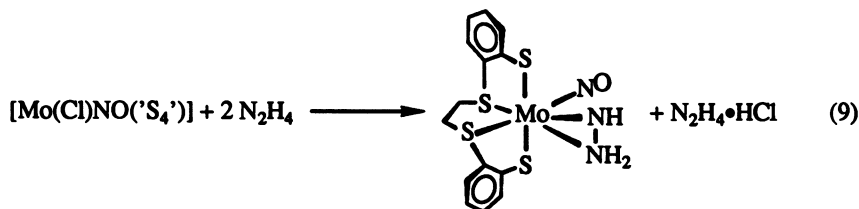
Due to the chirality of the $[\text{Mo}(\text{S}_4)]$ fragment and the prostereogenicity of the Mo center in $[\text{Mo}(\text{Cl})(\text{NO})(\text{S}_4)]$, the two diastereomers III and IV form (10).

The partial double bond character of the Mo-X bond in II follows from the Mo-X bond lengths in $[\text{Mo}(\text{X})(\text{NO})(\text{S}_4)]$, X = Cl (4c), S(t-bu) (10b), and NMe₂ (4c), which are short in comparison with typical MoX single bonds. It further follows from the hindered rotations of the X ligands around the Mo-X axis, when X = NMe₂ or S(t-bu). The $[\text{Mo}(\text{X})(\text{NO})(\text{S}_4)]$ complexes with X = NMe₂, NH₂ or SR form according to equation 8:



When A^+X^- is liquid ammonia, $[\text{Mo}(\text{NH}_2)(\text{NO})(\text{S}_4)]$ (4c) is obtained, which is of interest as a structural and functional model of nitrogenases, if N₂ fixation occurs at the [MoS] centers of Fe/Mo nitrogenases.

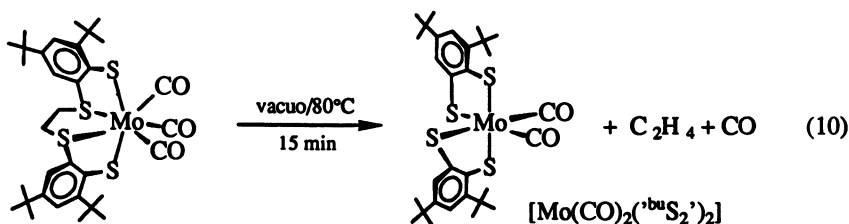
In the substitutions according to equation 8, the oxidation state +III of the Mo centers remains unchanged. This is not the case in the reaction according to equation 9,



which yields the N₂H₃ complex $[\text{Mo}(\text{N}_2\text{H}_3)(\text{NO})(\text{S}_4)]$ (11). It is also a structural and functional model compound in the above mentioned sense. The η^2 -bonding of the N₂H₃ ligand was deduced from the spectroscopic properties of $[\text{Mo}(\text{N}_2\text{H}_3)(\text{NO})(\text{S}_4)]$ and further corroborated by the X-ray structure analysis of the analogous complex $[\text{Mo}(\text{NHNMe}_2)(\text{NO})(\text{S}_4)]$. The ⁹⁵Mo NMR shift of $[\text{Mo}(\text{N}_2\text{H}_3)(\text{NO})(\text{S}_4)]$ (-445 ppm) indicates a molybdenum oxidation state of +II (see above) and shows that substitution according to equation 9 includes a redox step in which Mo(III) is reduced to Mo(II) and N₂H₄ oxidized to give the hydrazinyl ligand N₂H₃, which acts as three-electron donor.

$[\text{Mo}(\text{N}_2\text{H}_3)\text{NO}(\text{S}_4)]$ is a rare example of a N₂H₃ complex, and the first example of N₂H₃ coordination at a [MoS] site. In previously described N₂H₃ complexes, the metal centers (Co, W) carry cyclopentadienyl or triphosphine coligands and exhibit no resemblance to the active sites of nitrogenases with respect to metals and donors (12).

Binding of CO to High-Valent [MoS] Centers: $[\text{Mo}(\text{CO})_2(\text{t-buS}_2)_2]$, $\text{t-buS}_2^{2-} = \text{S}_2\text{C}_6\text{H}_2\text{Me}_2^{2-}$. For many years, the molybdenum center of Fe/Mo nitrogenase has been postulated to be the binding sites of N₂ or the strong nitrogenase inhibitor CO. The molybdenum centers, however, probably are in the high-oxidation state +IV (13), and the question arises whether such centers can bind N₂ or CO. High-valent N₂ complexes with [MoS] cores are unknown. Even high-valent metal carbonyl complexes are extremely rare (14), usually unstable, and have never been obtained with exclusively sulfur coligands until recently. The first example is formed in the unusual redox elimination according to equation 10 (15),



The Mo(II) complex $[\text{Mo(CO)}_3\text{('buS}_4\text{')}]$ loses C_2H_4 and CO to give the Mo(IV) complex $[\text{Mo(CO)}_2\text{('buS}_2\text{')}_2]$. The PPh_3 derivative $[\text{Mo(CO)(PPh}_3\text{)('buS}_2\text{')}_2]$ formed by an analogous redox elimination from $[\text{Mo(CO)}_2\text{(PPh}_3\text{)('buS}_4\text{')}]$ and could be characterized by X-ray structure determination.

Bright-blue $[\text{Mo(CO)}_2\text{('buS}_2\text{')}_2]$ proves that CO can bind to Mo(IV) centers which carry no stabilizing phosphines or cyclopentadienyl ligands and are coordinated exclusively by CO and four thiolate donors. Its Mo(IV) character follows from spectroscopic data and the structural data of $[\text{Mo(CO)(PPh}_3\text{)('buS}_2\text{')}_2]$, which show that it is not necessary to invoke any 'non-innocent' properties (16) of benzene dithiolate ligands in order to explain the stability of these complexes.

$[\text{Mo(CO)}_2\text{('buS}_2\text{')}_2]$ exhibits two intense high-frequency $\nu(\text{CO})$ bands at 2041 and 2006 cm^{-1} . The absolute position of these bands and their significant shift to higher frequency relative to the bands of the starting complex $[\text{Mo(CO)}_3\text{('buS}_4\text{')}]$ ($\nu(\text{CO})$: 2028, 1951 cm^{-1}) indicate that CO binds to an electron-deficient high-valent [MoS] center. The same argument applies to $[\text{Mo(CO)(PPh}_3\text{)('buS}_2\text{')}_2]$ ($\nu(\text{CO})$: 1978 cm^{-1}) and $[\text{Mo(CO)}_2\text{(PPh}_3\text{)('buS}_4\text{')}]$ ($\nu(\text{CO})$: 1930, 1864 cm^{-1}).

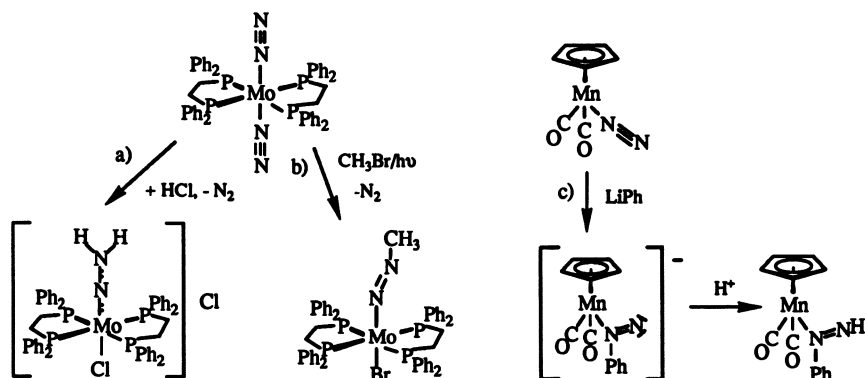
The stabilization of the Mo(IV) centers in the 14-electron complexes $[\text{Mo(CO)}_2\text{('buS}_2\text{')}_2]$ and $[\text{Mo(CO)(PPh}_3\text{)('buS}_2\text{')}_2]$ can be traced back to $\text{S} \rightarrow \text{Mo} \pi$ -donor bonds. Such bonds are suggested by the average Mo-S distances of $[\text{Mo(CO)(PPh}_3\text{)('buS}_2\text{')}_2]$ (235.5 pm), which are considerably shorter than those in $[\text{Mo(CO)}_2\text{(PMe}_3\text{)(S}_4\text{')}]$ (250.6 pm) or related Mo(II) complexes (15).

Do these results prove that the Mo(IV) centers in Fe/Mo nitrogenases are the binding sites for N_2 or CO? Even after the discovery of 'Fe-only' nitrogenases (2), this possibility cannot be entirely ruled out. It is, however, also possible that N_2 binds to iron and CO to molybdenum. Such an arrangement could impede the electron transport within the Fe-Mo clusters and cut off the N_2 molecule from electrons, even if it is already bound. Thus, speculation on the role of molybdenum can continue.

Fe Complexes with Sulfur dominated Coordination Spheres

Molybdenum versus Iron in N_2 Fixation. The metal which occurs most frequently in all nitrogenases is iron. In Fe/Mo as well as Fe/V nitrogenases, the number of iron centers considerably exceeds the number of Mo or V centers (1), and the Fe/Mo cofactor exhibits a Fe:Mo ratio of ca. 6-8 Fe:1Mo. Thus, it is hard to understand why so much stress has been put on molybdenum as the binding site of N_2 , even if the long known molybdenum dependence of many nitrogen fixing plants (and microorganisms) is taken into account, and the fact that it was a dinitrogen molybdenum complex, $[\text{Mo(N}_2\text{)}_2\text{(dppe)}_2]$, which yielded the first conversion of N_2 into nitrogen hydride ligands in fully characterized complexes (17). Scheme IV displays the three types of N_2 ligand reactions which lead to a reduction of the N_2 triple bond and allow a characterization of starting and resulting complexes.

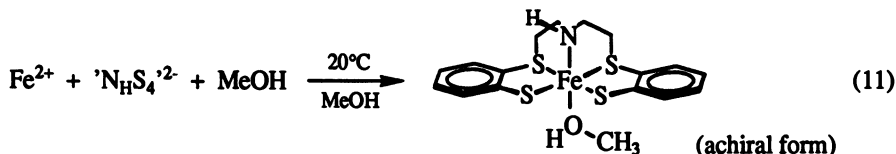
Scheme IV



The reactions can be classified as reduction of N_2 ligands by (a) electrophilic, (b) radical and (c) nucleophilic attack. The first two types involve intramolecular electron transfer reactions from the $Mo(0)$ center to one N_2 ligand yielding hydrazido(2-) (four-electron transfer) or diazenido(1-) ligands (two-electron transfer). In the third type, the oxidation state of the metal center stays unchanged, because the electrons that reduce the triple bond stem from the attacking nucleophile (18).

These model systems face the problem that either the metals or their ligand sphere or both are incompatible with the enzyme centers. In addition, unphysiologically strong reducing agents such as metallic sodium or lithium are necessary, if not for the transformation of the N_2 ligand, then in one of the preceding steps for the synthesis of the N_2 complex. This requirement holds also for $[Mo(N_2)_2(L)]$, (L = octamethyl-tetrathiacyclohexadecane) which is the first metal N_2 complex having only sulfur coligands (19). Finally, the discovery of the 'Fe-only' nitrogenases (2) could signify that even in Mo-Fe nitrogenases the iron centers represent the binding site for N_2 . This is the reason why iron sulfur ligand complexes such as $[Fe(L)(NHS_4)]$ may be of interest.

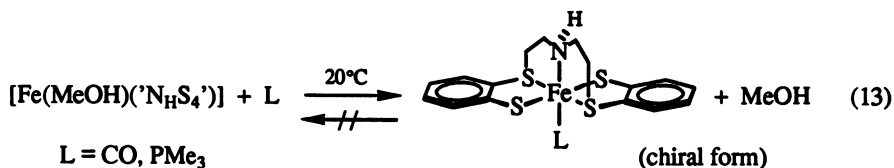
Synthesis and Properties of $[Fe(L)(NHS_4)]$ Complexes. The most convenient access to $[Fe(L)(NHS_4)]$ complexes is the reaction according to equation 11.



It yields $[Fe(MeOH)(NHS_4)]$ which has a highly labile $MeOH$ ligand that readily and reversibly exchanges for other hard σ ligands such as THF, N_2H_4 or NH_3 according to equation 12 (20).



It also exchanges for soft σ - π ligands such as CO or PMe_3 , but these substitutions are irreversible (equation 13).



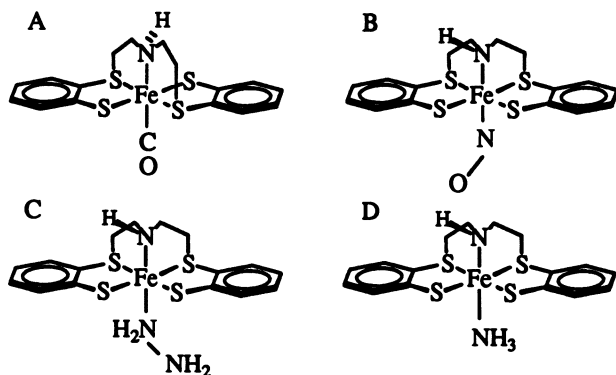
All complexes have Fe(II) centers and 18-electron configurations. The complexes with hard σ -donors, however, have high-spin Fe(II) centers with four unpaired electrons, are highly reactive, extremely O₂-sensitive and exhibit the achiral structure with C_{2v} symmetry depicted in equation 12. In contrast, the diamagnetic complexes with σ - π donors have low-spin Fe(II) centers, are practically inert towards substitutions and O₂, and exhibit the chiral structure with C₁ symmetry shown in equation 13. An intermediate position is taken by the 19 electron complex [Fe(NO)(N_HS₄')] which forms according to equation 14.



It is also a low-spin complex, but due to its one unpaired electron it is paramagnetic. [Fe(NO)(N_HS₄')] exhibits the achiral structure, and is relatively reactive (21). This complex exchanges NO for CO to give [Fe(CO)(N_HS₄')] which is quite unusual for NO complexes.

Magnetic, structural and reactive properties of [Fe(L)(N_HS₄')] complexes are evidently coupled strongly. These properties appear to be determined by the coligand L, and the [Fe(N_HS₄')] fragment must be in a borderline electronic situation where small changes, such as the substitution of only one ligand, lead to spin crossovers, or perhaps vice versa, the structure and spin-state of the [Fe(N_HS₄')] fragment determine which type of coligand L is to be bound. A clue to understand the different properties of [Fe(L)(N_HS₄')] complexes is yielded by X-ray structure determinations, the results of which are summarized in scheme V.

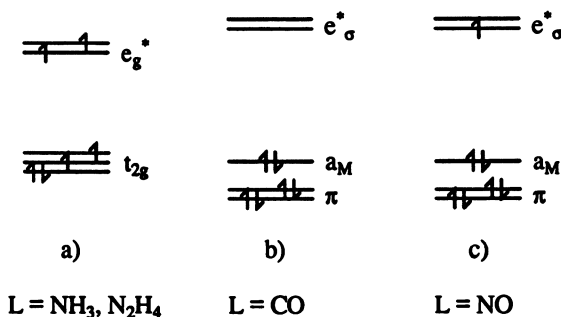
Scheme V: Distances (pm) in low-spin and high-spin [Fe(L)(N_HS₄')] complexes



	A	B	C	D
d(FeN _H)	207.2(8)	225.8(7)	225.5(6)	224.4(3)
d(FeS) _{av}	226.8	230.6	249.7	249.1

A dramatic increase of the Fe-N_H distances of more than 18 pm occurs when going from the low-spin diamagnetic 18-electron CO complex to the low-spin, but paramagnetic 19-electron NO complex. Simultaneously, also the average Fe-S bond distances increase 4 pm. In the paramagnetic 18-electron N₂H₄ and NH₃ complexes, the Fe-N_H bond distances remain as long as in the NO complex. The average Fe-S bond distances, however, make a further jump to about 249 pm. These results can be explained in terms of molecular orbital theory for octahedral complexes (Scheme VI) (22).

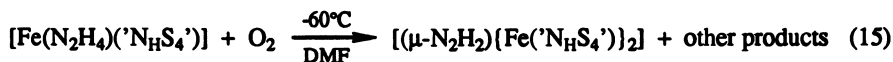
Scheme VI: Splitting and occupancy of frontier orbitals in [Fe(L)(N_HS₄')] complexes.



In the high-spin 18-electron complexes with the σ ligands N₂H₄ and NH₃, the frontier orbitals exhibit the splitting and occupancy according to a). The t_{2g} orbitals have pure metal character and are nonbonding, the e_g* orbitals are antibonding with respect to the metal-ligand σ bonds. The energy gap between e_g* and t_{2g} orbitals is so small that Hund's rule is valid, and two electrons must become antibonding. Substitution of the σ ligands N₂H₄ or NH₃ by the σ - π ligand CO leads to the splitting of b) such that all electrons can become paired. The σ - π three-electron donor NO in [Fe(NO)(N_HS₄')] causes the identical splitting, but the nineteenth electron is forced to occupy one of the antibonding e_g* orbitals.

Thus, the different bond distances, magnetic properties, and reactivities of [Fe(L)(N_HS₄')] complexes can be traced back to the number of antibonding electrons. The structural change from the racemic to the meso structure, which is connected with the change from diamagnetic to paramagnetic behavior is due to conformational effects in the N(C₂H₄)₂ bridge, which are discussed in more detail elsewhere (23).

Stabilization of Diazene, HN=NH, by [Fe(N_HS₄')] Fragments. The properties of [Fe(L)(N_HS₄')] complexes gain relevance with regard to N₂ fixation, because diazene can also be coordinated. Diazene, HN=NH, is considered the product of the first 2e⁻, 2H⁺ reduction step. In the free state, however, diazene is extremely unstable ($\Delta H_{298}^\circ = +212$ kJ/mol) (24), and the question arises how such an unstable molecule could be stabilized in nitrogenases. The diamagnetic and centrosymmetric diazene complex $[\mu\text{-N}_2\text{H}_2\{\text{Fe}(\text{N}_\text{H}\text{S}_4')\}_2]$ may yield answers. It forms according to equation 15, and its molecular structure is shown in figure 1. (25).



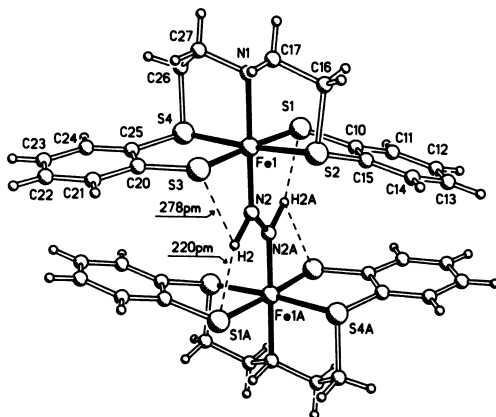


Figure 1: Molecular structure of $[\mu\text{-N}_2\text{H}_2\{\text{Fe}(\text{NHS}_4')\}]_2$ (Reproduced with permission from ref. 25. Copyright 1989 V.C.H. Publishers, Inc.)

Three factors which stabilize the diazene ligand can be recognized. N_2H_2 bridges two enantiomeric $[\text{Fe}(\text{NHS}_4')]$ fragments such that the Fe-NH-NH-Fe system can form a four-center- $6e^-$ - π bond. It is indicated by the distances and an intense absorption in the visible region of the UV-Vis spectrum ($\lambda_{\text{max}} = 573 \text{ nm}$). Steric shielding hinders access of small molecules or ions such as OH^- which can induce disproportionation of the N_2H_2 ligand (26). Very strong tricentric $\text{S}\cdots\text{H-N}$ bridges between thiolate donors and diazene protons provide a stabilization energy that can be tentatively estimated to reach ca. 70 kJ/mole. This stabilization 'neutralizes' one third of the positive ΔH^\ddagger of free N_2H_2 , which could have particular significance for the mechanism of N_2 fixation, because hydrogen bridges are not to be expected in potential precursor N_2 complexes. Thus, even the first step of N_2 reduction may become exoenergetic.

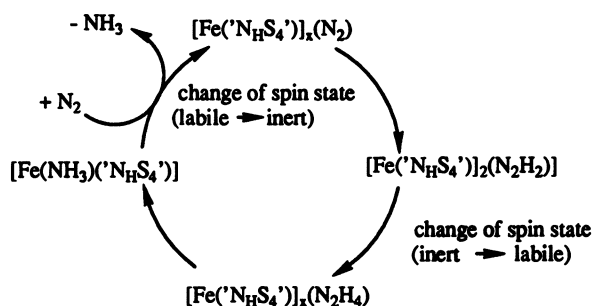
Conclusion and Outlook

The $[\text{Fe}(\text{NHS}_4')]$ fragment allows the coordination of three key stages of N_2 fixation: N_2H_2 , N_2H_4 and NH_3 . Although the corresponding N_2 complex is still missing, and the reduction $\text{N}_2\text{H}_2 \rightarrow \text{N}_2\text{H}_4 \rightarrow \text{NH}_3$ has not yet been achieved, the results suggest possible features and functions of the active centers of Fe/Fe and possibly also Fe/heterometal nitrogenases. Without change of the Fe oxidation state, coordination of either the σ - π ligand N_2H_2 or the σ ligands N_2H_4 and NH_3 leads to complexes that are chemically extremely different due to the Fe(II) spin-state change. Such spin-state changes influence the reduction steps and definitely should favour the final step, the substitution of NH_3 by N_2 . This is summarized in the cycle of scheme VII.

It is further noted that this cycle comprises only Fe(II) complexes and no extraordinary oxidation states such as Fe(O) or Fe(I).

What could make the $[\text{Fe}(\text{NHS}_4')]$ fragment ready to accept the σ - π ligand N_2 after the release of NH_3 ? Perhaps it is deprotonation of the N_H donor converting it into a strong amido σ - π donor such that the high-spin $[\text{Fe}(\text{NHS}_4')]$ core becomes

Scheme VII



a low-spin $[\text{Fe}(\text{'NS}_4)]^-$ entity. Protonation-deprotonation reactions in protein environments are not unusual, and if they could cause such spin-state changes of Fe centers, the iron centers would indeed become strong candidates for binding N_2 in all types of nitrogenases. In contrast, complexes with the 4d metal molybdenum always exhibit low-spin configurations. It is ironic that in a book that focuses on molybdenum we propose the importance of iron. However, the predominance of iron at the active site makes this an idea which might be worthwhile to pursue, particularly in the light of the X-ray structural model of the FeMo cofactor (D. C. Rees et al., Chapter 11) reported briefly after this article had been completed.

Acknowledgment

I thank my coworkers who are cited in the references for their dedication, hard work, and willingness to share my hopes and disappointments. Support of our investigations by the Deutsche Forschungsgemeinschaft, Fonds der Chemischen Industrie and Bundesministerium für Forschung und Technologie is gratefully acknowledged.

Literature Cited

- (1) a) Lowe, D. J.; Thorneley, R. N. F.; Smith, B. E. In *Metalloproteins Part 1, Metal Proteins with Redox Roles*; Harrison P., Ed.; Verlag Chemie, Weinheim, 1985. b) Eady, R. R. In *Perspectives on Bioinorganic Chemistry*; Hay, R. W.; Dilworth, J. R.; Nolan, K. B. Eds.; JAI Press, London, 1991, 225.
- (2) Chiswell, J. R.; Premakumar, R.; Bishop, P. E.; *J. Bacteriol.* **1988**, *170*, 27.
- (3) a) Sellmann, D.; Jonk, H. E.; Pfeil, H. R.; Huttner, G.; v. Seyerl, J. *J. Organomet. Chem.* **1980**, *191*, 171. b) Sellmann, D.; Reisser, W. *Z. Naturforsch.* **1984**, *39b*, 1268. c) Sellmann, D.; Freyberger, G.; Eberlein, R.; Böhlen, E.; Huttner, G.; Zsolnai, L. *J. Organomet. Chem.* **1987**, *323*, 21. d) Sellmann, D.; Kleinkleffmann, U. *J. Organomet. Chem.* **1983**, *258*, 315. e) Sellmann, D.; Kunstmann, H.; Knoch, F.; Moll, M. *Inorg. Chem.* **1988**, *27*, 4183. f) Sellmann, D.; Binker, G.; Moll, M.; Hardtweck, E. *J. Organomet. Chem.* **1987**, *327*, 403. g) Sellmann, D.; Soglowek, W.; Moll, M. *Z. Naturforsch.*, **1992**, *47b*, 1105.

- (4) a) Sellmann, D.; Zapf, L. *Z. Naturforsch.* **1985**, *40b*, 368. b) Sellmann, D.; Kaul, B. B. *Z. Naturforsch.* **1983**, *38b*, 562. c) Sellmann, D.; Pöhlmann, G.; Knoch, F.; Moll, M. *Z. Naturforsch.* **1988**, *44b*, 312. d) Sellmann, D.; Schwarz, J. *J. Organomet. Chem.* **1983**, *241*, 343. e) Sellmann, D.; Weiss, R.; Knoch, F. *Inorg. Chim. Acta* **1990**, *175*, 65. f) Sellmann, D.; Seubert, B.; Knoch, F.; Moll, M. *Z. Allg. Anorg. Chem.* **1991**, *600*, 95. g) Sellmann, D.; Binker, G.; Schwarz, J.; Knoch, F.; Boese, R.; Huttner, G.; Zsolnai, L. *J. Organomet. Chem.* **1987**, *323*, 323.
- (5) Cole, J. A.: Assimilatory and Dissimilatory Reduction of Nitrate to Ammonia. In 'The Nitrogen and Sulphur Cycles'. Cole, J. A.; Ferguson, S. J.; Eds. Cambridge University Press, **1988**, 281.
- (6) a) McCleverty, J. A. *Chem. Rev.* **1979**, *79*, 53. b) The metal mediated electrochemical NO reduction to give various products ranging from N₂O, N₂ and NH₂OH to NH₃ has been described by other groups. (T. J. Meyer et al., *Inorg. Chem.* **1991**, *30*, 629 and references cited therein.)
- (7) a) Sellmann, D.; Seubert, B.; Moll, M.; Knoch, F. *Angew. Chem.* **1988**, *100*, 1221; *Angew. Chem. Int. Ed. Engl.* **1988**, *27*, 1164. b) Sellmann, D.; Seubert, B.; Knoch, F.; Moll, M. *Z. Naturforsch.* **1991**, *46b*, 1449.
- (8) a) Wieghardt, K.; Quilitzsch, U. *Z. Naturforsch.* **1991**, *36b*, 683. b) Wieghardt, K. *Adv. Inorg. Bioinorg. Mech.* **1984**, *3*, 213.
- (9) Sellmann, D.; Seubert, B. *Angew. Chem.* **1992**, *104*, 200; *Angew. Chem. Int. Ed. Engl.* **1992**, *31*, 205.
- (10) a) Sellmann, D.; Kern, W.; Holzmeier, A.; Pöhlmann, G.; Moll, M. *Z. Naturforsch.* **1991**, *46b*, 1349. b) Hannakam, M. Thesis University of Erlangen, **1992**.
- (11) Sellmann, D.; Kern, W.; Pöhlmann, G.; Knoch, F.; Moll, M. *Inorg. Chim. Acta* **1991**, *185*, 155.
- (12) a) Schrock, R. R.; Liu, A. H.; O'Regan, M. B.; Finch, W. C.; Payack, J. P. *Inorg. Chem.* **1988**, *27*, 3574. b) Vogel, F.; Barth, A.; Huttner, G.; Klein, T.; Zsolnai, L.; Kremer, R. *Angew. Chem.* **1991**, *103*, 325; *Angew. Chem. Int. Ed. Engl.* **1991**, *30*, 303.
- (13) Burgess, B. K. *Chem. Rev.* **1990**, *90*, 1377.
- (14) a) Erler, B. S.; Dewan, J. C.; Lippard, S. J. *Inorg. Chem.* **1981**, *20*, 2719. b) Crayston, J. A.; Almond, H. J.; Downs, A. J.; Poliakov, M.; Turner, J. J. *Inorg. Chem.* **1984**, *23*, 3051. c) Lazarowych, N. J.; Morris, R. H. *Can. J. Chem.* **1990**, *68*, 558.
- (15) a) Sellmann, D.; Grasser, F.; Knoch, F.; Moll, M. *Angew. Chem.* **1991**, *103*, 1346; *Angew. Chem. Int. Ed. Engl.* **1991**, *30*, 1311; b) *Inorg. Chim. Acta* **1992**, in press.
- (16) Mueller-Westerhoff, U. T.; Vance, B. In *Compr. Coord. Chem.*; Wilkinson, G.; Gillard, R. D.; McCleverty, J. A.; Eds.; Pergamon, Oxford, **1987**, *Vol.2*, 595.
- (17) a) Chatt, J.; Dilworth, J. R.; Richards, R. L. *Chem. Rev.* **1977**, *78*, 589. b) Henderson, R. A. Leigh, G. J. Pickett, Ch. *J. Adv. Inorg. Chem. Radiochem.* **1983**, *27*, 198.
- (18) a) Sellmann, D.; Weiss, W. *Angew. Chem.* **1977**, *89*, 918; *Angew. Chem. Int. Ed. Engl.* **1977**, *16*, 880; *ibid.* **1978**, *90*, 295; **1978**, *17*, 269; b) *J. Organomet. Chem.* **1978**, *160*, 183.
- (19) Yoshida, T.; Adachi, T.; Kaminaka, M.; Ueda, T. *J. Am. Chem. Soc.* **1988**, *110*, 4872.
- (20) Sellmann, D.; Soglowek, W.; Knoch, F.; Ritter, G.; Dengler, J. *Inorg. Chem.* **1992**, *31*, 3711.
- (21) Sellmann, D.; Kunstmann, H.; Moll, M.; Knoch, F. *Inorg. Chim. Acta* **1988**, *154*, 157.
- (22) Albright, T. A.; Burdett, J. K.; Whangbo, M. H. *Orbital Interactions in Chemistry*; Wiley, New York, **1985**.

- (23) Sellmann, D.; Fünfgelder, S.; Pöhlmann, G.; Knoch, F.; Moll, M. *Inorg. Chem.* **1990**, *29*, 4772.
- (24) Foner, S. N.; Hudson, R. L. *J. Chem. Phys.* **1978**, *68*, 3162.
- (25) Sellmann, D.; Soglowek, W.; Knoch, F.; Moll, M. *Angew. Chem.* **1989**, *101*, 1244; *Angew. Chem. Int. Ed. Engl.* **1989**, *28*, 1271.
- (26) Sellmann, D.; Brandl, A.; Endell, R. *J. Organomet. Chem.* **1975**, *90*, 309.

RECEIVED April 12, 1993

Chapter 22

Chemical Transformations of Coordinated Dinitrogen in Molybdenum and Tungsten Phosphine Complexes

Masanobu Hidai and Yasushi Mizobe

Department of Synthetic Chemistry, University of Tokyo, Hongo,
Bunkyo-ku, Tokyo 113, Japan

Diazoalkane complexes of Mo and W *trans*-[MF(NN=CRR')(dppe)₂]⁺ and *cis, mer*-[MX₂(NN=CRR')(PMe₂Ph)₃] readily derived from *trans*-[M(N₂)₂(dppe)₂] (**1**) and *cis*-[M(N₂)₂(PMe₂Ph)₄] (**2**) undergo various unique reactions leading to formation of new organodiazenido and diazoalkane complexes with monomeric and dimeric structures. Silylation of **1** and **2** affords a series of silylated dinitrogen complexes, while silylamines are produced catalytically from the reaction of Me₃SiCl and Na under N₂ in the presence of **1** or **2**. A bimetallic approach towards new reactions of N₂ is also described, involving silylation and arylation of coordinated dinitrogen in Mo and W complexes using silylcobalt and chromium arene complexes.

Dinitrogen complexes of Mo have been attracting much attention in relation to the biological N₂-fixing system, the catalytic component of which commonly involves Mo as an essential element. Following our discovery of the first well-defined Mo complex containing dinitrogen *trans*-[Mo(N₂)₂(dppe)₂] (dppe = Ph₂PCH₂CH₂PPh₂) in 1969 (1–3), complexes of the type [Mo(N₂)₂(P)₄] (P = tertiary phosphine) and their W analogs have been prepared and their reactivities have been extensively investigated. Since the N–N bond in the N₂ molecule is significantly weakened and polarized upon coordination to the low-valent Mo or W center, the ligated dinitrogen in these complexes shows various reactivities under ambient conditions. In this account our recent findings are summarized on reactions of the dinitrogen ligand in *trans*-[M(N₂)₂(dppe)₂] (**1a**: M = Mo; **1b**: M = W) and *cis*-[M(N₂)₂(PMe₂Ph)₄] (**2a**: M = Mo; **2b**: M = W) to form organo-nitrogen ligands as well as nitrogen-containing organic compounds. It should be emphasized that no other dinitrogen complexes isolated to date exhibit such intriguing reactivities. Previous reviews by us (4,5) and by others (6–8) present a wider view of the chemistry of dinitrogen complexes.

Reactions of coordinated dinitrogen in **1** and **2** to form organo-nitrogen ligands

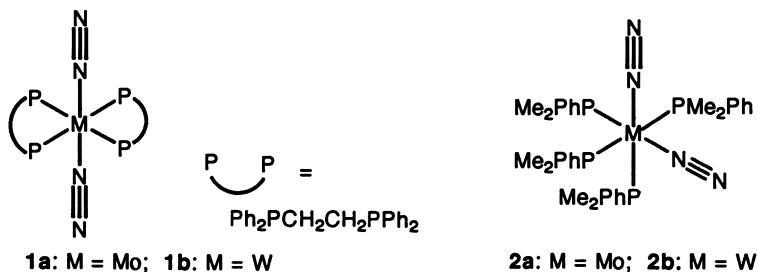
are depicted in Scheme I. Direct acylation or alkylation of the N_2 ligand by $RCOCl$ or RX provides a route to form a C–N bond. However, this reaction has only been applied to the diphosphine complexes **1**. Alternative more versatile methods to make C–N bonds involve the initial conversion of **1** and **2** into hydrazido(2–) complexes *trans*-[MF(NNH₂)(dppe)₂][BF₄] (**3**) and *cis, mer*-[MX₂(NNH₂)(PMe₂Ph)₃] (**4**; X = halogen) by treatment with acids. Since these hydrazido(2–) complexes are susceptible to electrophilic attack at the terminal nitrogen atom, they can serve as key intermediates in the preparation of NH₃ and N₂H₄ upon further protonation, and organo–nitrogen complexes by subsequent reactions with organic carbonyl compounds. Thus condensation with aldehydes or ketones gives the diazoalkane complexes *trans*-[MF(NN=CRR')(dppe)₂][BF₄] (**5**) (**9**) and *cis, mer*-[MX₂(NN=CRR')(PMe₂Ph)₃] (**6**) (**10,11**), while both substitution reactions with acid chlorides (**12**) and addition reactions with heterocumulenes (**12,13**) result in the formation of organohydrazido(2–) complexes. Reaction of **2b** with MeCOCH₂COMe (acac–H) giving an alkenyldiazenido complex *mer*-[W(acac)(N=NCMe=CHCOMe)(PMe₂Ph)₃] also demonstrates an example of C–N bond formation at the dinitrogen ligand, which presumably proceeds via a hydrazido(2–) or diazenido (M≡N=NH) intermediate (**14**). Another important reaction of coordinated dinitrogen is the silylation of **1** and **2**, giving a series of silyldiazenido and silylhydrazido(2–) complexes (**15–18**). Among the organo–nitrogen complexes derived from **1** and **2**, diazoalkane complexes and silylated dinitrogen complexes are of particular interest because these are readily obtained. More intensive work has therefore been carried out on these complexes, which has led to the discovery of their unique reactivities described below.

Reactivities of Diazoalkane Complexes Derived from Dinitrogen Complexes

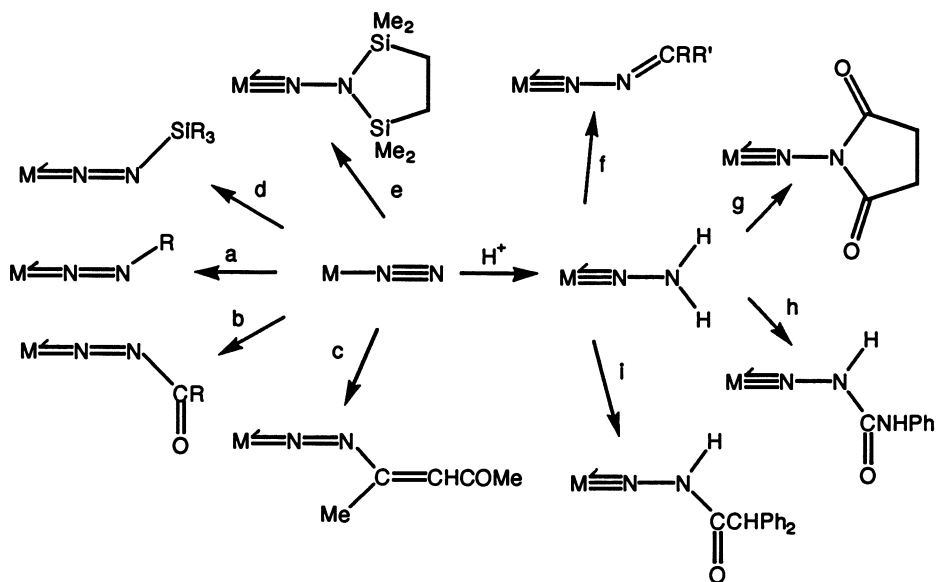
Diazoalkanes are reactive compounds having a wide range of synthetic utility in organic synthesis. The novel method to prepare diazoalkane complexes of the type **5** and **6** developed by us is of importance because it provides a general route to obtain stable diazoalkane complexes with a variety of substituents under mild conditions. It is quite interesting to elucidate the metal–assisted reactions of these diazoalkane ligands, which are not observed for free diazoalkanes.

Reactions of Alkenyldiazenido Complexes *trans*-[MF(N=NCR¹=CR²R³)(dppe)₂] (7**) Derived from Diazoalkane Complexes **5**.** Previously we have reported that alkenyldiazenido complexes *trans*-[MF(N=NCMe=CHCOMe)(dppe)₂] can be isolated from the reaction of diazoalkane complexes **5** (R = Me, R¹ = CH₂COMe) with NaOMe (**14**). Now we have found that treatment of **5** formulated as *trans*-[MF(NN=CR¹CHR²R³)(dppe)₂]⁺ with LDA or NaN(SiMe₃)₂ in benzene at room temperature gives alkenyldiazenido complexes *trans*-[MF(N=NCR¹=CR²R³)(dppe)₂] (**7**) (eq 1). Since formation of **7** is quantitative for various R¹ R³ from ¹H NMR criteria, this reaction provides a potential route to prepare a series of alkenyldiazenido complexes (**19,20**). In the reactions of **5** (R¹ = R² = H, R³ = Me) with NaN(SiMe₃)₂, *Z* isomers are produced preferentially to the corresponding *E* isomers with the ratio of 6 : 1 (M = W) and 10 : 1 (M = Mo) in C₆D₆ at room temperature.

X–ray analysis of **7** (R¹ = H, R² = R³ = Me) has disclosed that the dimethylvinylidiazido ligand is planar with essentially linear W–N–N and bent N–



Scheme I



- a) RX. b) RCOCl . c) acac-H . d) Me_3SiI or $\text{R}_3\text{SiCl/NaI}$. e) $\text{ClSiMe}_2\text{CH}_2\text{CH}_2\text{SiMe}_2\text{Cl/NaI}$.
 f) $\text{RR}'\text{C=O/H}^+$. g) $\text{ClCOCH}_2\text{CH}_2\text{COCl}$. h) PhNCO . i) Ph_2CCO .

N–C linkages of 171(1) and 120(2)°, respectively. The bond lengths observed in this diazenido ligand are noteworthy; the N–N bond distance of 1.29(3) Å is significantly elongated from that of the typical N–N double bond (1.24 Å in MeN=NMe), while the C–N bond (1.26(3) Å) is much shorter than common C–N single bond (1.47 Å). These structural features as well as the long C–C double bond (1.38 (4) Å) can be explained by the presence of substantial contribution of resonance structure $[M^{\dagger}\equiv N-N=CR^1-C^{\ominus}R^2R^3]$ (i) compared with $[M\equiv N=N-CR^1=CR^2R^3]$ in this diazenido complex, which may also account for the low $\nu(N=N)$ and $\nu(C=C)$ values observed in the IR spectra of 7.

As suggested by resonance structure i, 7 undergo electrophilic reactions at the terminal carbon to give new diazoalkane complexes as shown in Scheme II. Reactions of 7 with excess alkyl halides RX readily afford *trans*- $[MF(NN=CR^1CR^2R^3R)-(dppe)_2]^{\dagger}$, presenting a sharp contrast to the alkyl diazenido complexes that are susceptible to electrophilic attack at the outer nitrogen atom. Complexes 7 also react with isocyanates to give C-acylated diazoalkane complexes after aqueous workup (20, 21); treatment of 7 ($R^1 = Me, R^2 = R^3 = H$) with almost equimolar PhNCO results in the formation of a monoacylated complex *trans*- $[MF(NN=CMeCH_2CONHPh)-(dppe)_2]^{\dagger}$, while reaction with excess PhNCO affords a diacylated complex *trans*- $[MF\{NN=CMeCH(CONHPh)_2\}(dppe)_2]^{\dagger}$. The structure of the latter has been unequivocally determined by X-ray analysis. Analogous reactions of 7 with PhNCS and Ph₂CCO also lead to the formation of the diazoalkane complexes, but diacylated products are not obtained. For 7 ($M = W, R^1 = R^2 = R^3 = H$), aldol-type condensation also proceeds by treatment with RCHO ($R = Bu^t, Ph$). The products are α, β -unsaturated diazoalkane complexes *trans*- $[WF(NN=CHCH=CHR)(dppe)_2]^{\dagger}$. It is to be noted that reaction of 7 ($R^1 = Me, R^2 = R^3 = H$) with MeCOMe or EtCHO results in the recovery of 5 by deprotonation of this enolizable ketone or aldehyde with 7.

Electrochemical study has been carried out on these complexes of type 7 that were isolated in pure and stable crystalline form ($M = W; R^1 = H, R^2 = R^3 = Me; R^1 = H, R^2 = R^3 = Ph$). This has revealed that the complexes are susceptible to irreversible or reversible one-electron oxidation in THF under cyclic voltammetric conditions. Attempts to oxidize 7 ($R^1 = R^2 = H, R^3 = Me; R^1 = Me, R^2 = R^3 = H$) by I₂ or CuCl₂ resulted in the isolation of the dinuclear complexes *trans, trans*- $[(dppe)_2MF(NN=CR^1CR^2R^3CR^2R^3CR^1=NN)MF(dppe)_2]^{2\dagger}$, which contain the μ -bis(diazo)alkane ligand. The X-ray analysis of the W complex with $R^1 = R^2 = H$ and $R^3 = Me$ has confirmed the structure of the bridging bis(diazo)alkane ligand. Moreover, it has also been clarified that among the two stereoisomers observed in the ¹H NMR spectra of this complex and its Mo analog the major product is assignable to the *threo* isomer with respect to the two carbon atoms in the N–C–C–N units (eq 2) (20).

The reactions described here provide several potential routes to synthesize new diazoalkane complexes and related species. Further investigation is now continuing to find a convenient method to liberate these organo-nitrogen ligands as nitrogen-containing organic compounds.

Syntheses and Some Reactions of Diazoalkane Complexes with π -Acceptor Ligands Derived from 6. In contrast to considerable difficulty in cleaving M–N

and N–N bonds of diazoalkane complexes **5** with dppe ligands, diazoalkane ligands in monophosphine complexes **6** are readily converted into nitrogenous compounds. Thus, treatment of **6** ($M = W$, $R = R' = Me$, $X = Br$) with excess HBr gas affords $Me_2C=NN=CMe_2$ and N_2H_4 , while treatment with excess $LiAlH_4$ gives Pr^iNH_2 and NH_3 (10). The acidolysis of **6** by HBr gas was extended later to the reaction of **2b** with a MeOH/MeCOMe mixture at 50 °C, in which one dinitrogen ligand in **2b** is quantitatively converted into $Me_2C=NN=CMe_2$ (eq 3) (22). Although the detailed mechanism of this reaction is still uncertain due to the lack of information about intermediate stages, this may also involve the diazoalkane intermediate generated by protonation of **2b** with MeOH and subsequent condensation of the resultant hydrazido(2-) species with MeCOMe.

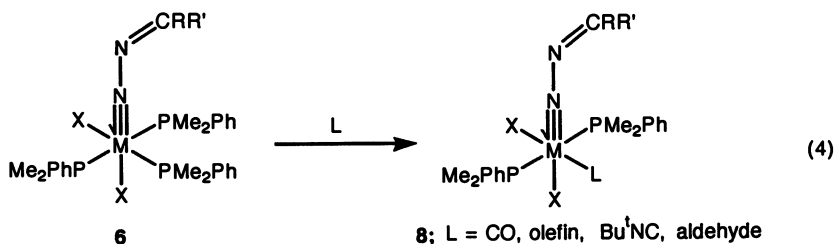
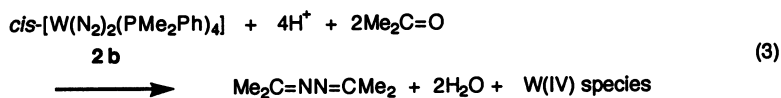
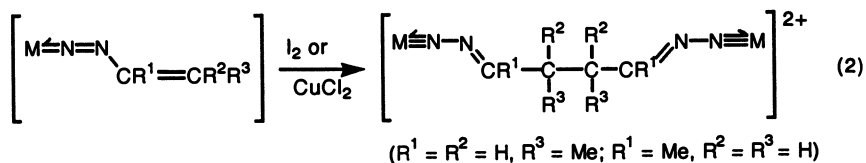
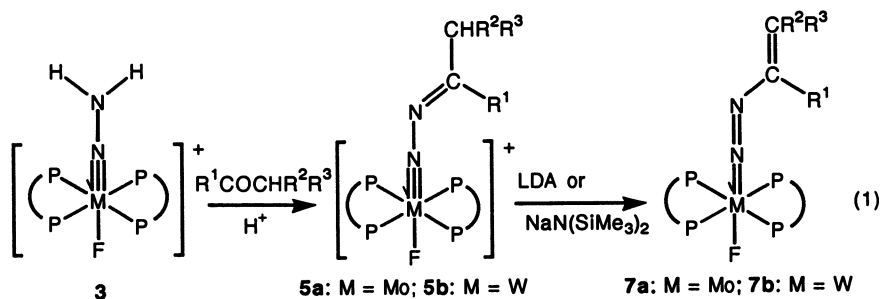
Stimulated by these remarkable reactions observed for monophosphine complexes, further intensive study has been carried out to disclose new reactivities of **6**. Now we have found that various diazoalkane complexes with π -acceptor ligands, *cis*, *trans*- $[MX_2(NN=CRR')(PMe_2Ph)_2(L)]$ (**8**), can be derived from **6** upon replacement of one PMe_2Ph ligand by L such as CO, olefins, isonitriles, and aldehydes (eq 4) (23). In these reactions, one PMe_2Ph ligand *cis* to the diazoalkane ligand and *trans* to the halide is selectively substituted by π -acceptor ligands L. This finding is consistent with the result of EHMO calculations on model compounds *cis*, *mer*- $[WCl_2(NN=CH_2)(PH_3)_3]$ and *cis*, *trans*- $[WCl_2(NN=CH_2)(PH_3)_2(CH_2=CH_2)]$, indicating that donation of *d* electron density from the W center predominantly occurs to the ligand *cis* to the $W=N$ bond in these d^2 complexes. X-ray structures of *cis*, *trans*- $[WCl_2(NN=CMe_2)(PMe_2Ph)_2(CH_2=CH_2)]$ and *cis*, *trans*- $[WCl_2(NN=CMePh)(PMe_2Ph)_2(\eta^2-p-MeC_6H_4CHO)]$, disclosing long C=C and C=O bond lengths in coordinated ethylene and aldehyde, also confirm this feature.

Although the diazoalkane ligand in **6** remains intact during its conversion into **8**, this reaction is of importance because it provides a convenient method to bind various reactive molecules on the *cis* site of the diazoalkane ligand. A preliminary study on the reaction of *cis*, *trans*- $[WCl_2(NN=CMePh)(PMe_2Ph)_2(Bu^iNC)]$ with $AlMe_3$ followed by hydrolysis has shown the formation of a diazoalkane-carbene complex *cis*, *trans*- $[WCl_2(NN=CMePh)(PMe_2Ph)_2(=CMeNHBu^i)]$. Exploration of such reactivities of **8** might lead to novel transformation of the diazoalkane ligand into organo-nitrogen compounds.

When **6** ($M = W$, $R = R' = Me$, $X = Cl$) is allowed to react with CO in the presence of $ZnCl_2$ (dioxane), a cationic diazoalkane complex *mer*- $[WCl(NN=CMe_2)(PMe_2Ph)_3(CO)]^+$ has been isolated instead of **8**. Interestingly, this cationic complex is reduced by Mg in THF under CO to give a dinuclear complex with a bridging diazenido ligand $[(Me_2PhP)_2(CO)_2WCl(N=NCMe_2CMe_2N=N)WCl(PMe_2Ph)_2(CO)_2]$ (eq 5) (24). X-ray analysis has been undertaken to clarify the structure of this intriguing diazenido complex derived from **2**, for which the atom connecting scheme is shown in eq 5.

Silylation and Germylation of Dinitrogen

Reactions of **1** and **2** with numerous acids including hydrogen halides have been extensively investigated due to their potential relevance to biological nitrogen fixation. However, those with silyl halides remained unexplored until recently. We have found



previously that although R_3SiCl does not react with coordinated dinitrogen in **1** and **2** at room temperature or under more forcing conditions, treatment with Me_3SiI produces silyldiazenido complexes in moderate yields. It is to be noted that corresponding diazenido (MNNH) complexes cannot be isolated upon protonation of **1** and **2** by acids. Results of the detailed study on the silylation and related germylation of coordinated dinitrogen are summarized below.

Silylation and Germylation of Dinitrogen Complexes 1 and 2. Treatment of **1** or **2** with Me_3SiI in benzene under rigorously dry conditions gives silyldiazenido complexes $[MI(N=NSiMe_3)(dppe)_2]$ or *trans*- $[MI(N=NSiMe_3)(PMe_2Ph)_4]$ (**9**) (eq 6). In the presence of HI, silylhydrazido(2-) complexes $[MI(NNHSiMe_3)(dppe)_2]I$ and *cis*, *mer*- $[MI_2(NNHSiMe_3)(PMe_2Ph)_3]$ are obtained as the major products. Analogous treatment with $CF_3SO_3SiMe_3$ also gives silylated dinitrogen complexes (15,16).

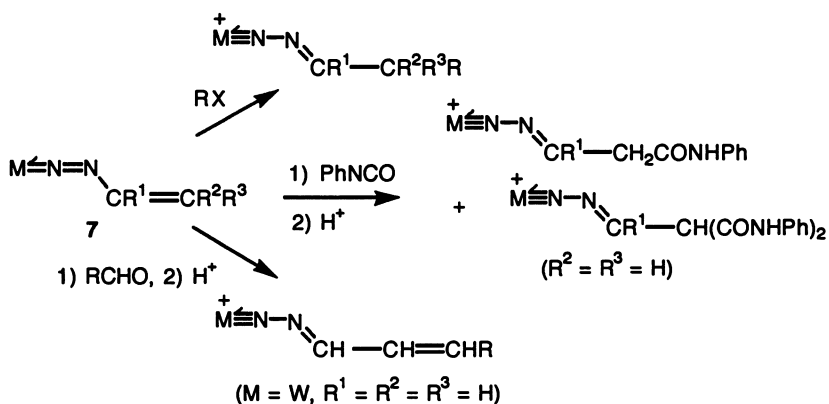
A mixture of R_3SiCl and excess NaI serves as a more convenient silylating reagent and thus **2b** can be converted into a variety of silyldiazenido complexes *trans*- $[WI(N=NSiR_3)(PMe_2Ph)_4]$ by using a wide range of easily available R_3SiCl . In the reaction of $ClSiMe_2CH_2CH_2SiMe_2Cl/NaI$ with **2**, disilylation of the terminal nitrogen atom takes place to give *cis*, *mer*- $[MI_2(NNSiMe_2CH_2CH_2SiMe_2)(PMe_2Ph)_3]$ (**10**) (17,18). This versatile method has been further extended to the germylation of dinitrogen ligand and *trans*- $[WI(N=NGeR_3)(PMe_2Ph)_4]$ ($R = Me, Ph$) can be isolated from the reaction of **2b** with R_3GeCl/NaI (Scheme III).

X-ray analyses of **9b** ($M = W$) and *trans*- $[WI(N=NGePh_3)(PMe_2Ph)_4]$ have shown that the N-N bond distances in the essentially linear W-N-N units of these diazenido ligands (1.24(3) and 1.25(2) Å, respectively) correspond well to that of a typical N-N double bond, while the N-Si and N-Ge bond lengths of 1.68(3) and 1.86(1) Å are slightly shorter than a common N-Si single bond and in the range of N-Ge single bond lengths, respectively. The N-N-Si and N-N-Ge angles are 152(2) and 133(1)°, respectively. The much wider N-N-Si angle than the expected 120° might be ascribed to steric repulsion between the silyl group and phosphine ligands.

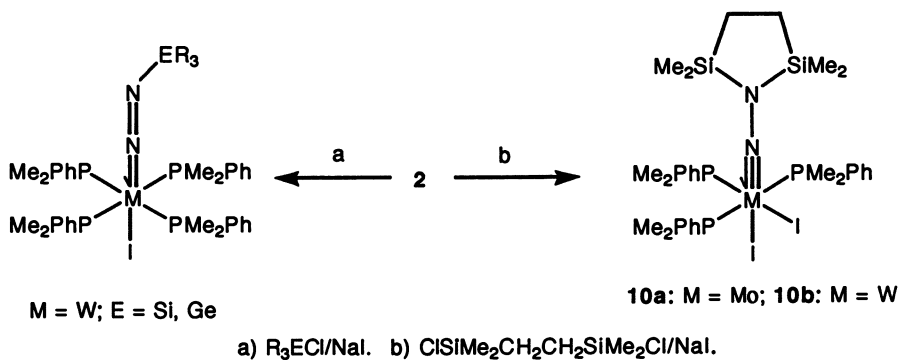
The structures of *cis*, *mer*- $[WI_2(NNHSiMe_3)(PMe_2Ph)_3]$ and **10b** ($M = W$) have also been determined by X-ray crystallography. The W-N-N linkages are almost linear and the N-N bond lengths in these complexes are 1.33(3) and 1.36(1) Å, respectively, indicating the bond order between one and two. The N-Si bond orders are estimated to be essentially unity and the N-N-Si angles of 127(2)° for the former and 120(1) and 126(1)° for the latter are close to 120°. These may be explained by the considerable contribution of the resonance structure $[M^{\ominus} \equiv N=N^{\oplus}(X)-SiR_3]$ compared to $[M \equiv N-N(X)SiR_3]$ ($X = H, SiR_3$) in silylhydrazido(2-) complexes as evidenced by the planar structure of the WNNSiCCSi fragment in **10b**.

Reactions of Silylated Dinitrogen Complexes 9 and 10. Some reactions of these silylated dinitrogen complexes with neutral ligands and *gem*-dihalides have been investigated. Thus, treatment of disilylhydrazido(2-) complex **10b** with $CH_2=CH_2$, CO_2 , and RCN results in the formation of *cis*, *trans*- $[WI_2(NNSiMe_2CH_2CH_2SiMe_2)(PMe_2Ph)_2(L)]$ (eq 7) as observed in **6** described above, while analogous reaction with $Bu^{\oplus}NC$ gives *cis*, *mer*- $[WI(NNSiMe_2CH_2CH_2SiMe_2)(PMe_2Ph)_3(Bu^{\oplus}NC)]I$. In addition, **10b** shows interesting reactivity towards CH_2X_2 ($X = Cl, I$). When dissolved in CH_2Cl_2 or a CH_2I_2/C_6H_6 mixture and stirred at room

Scheme II



Scheme III

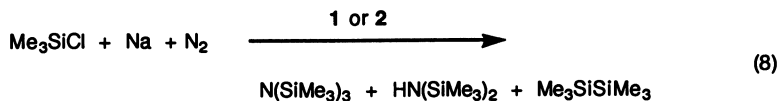
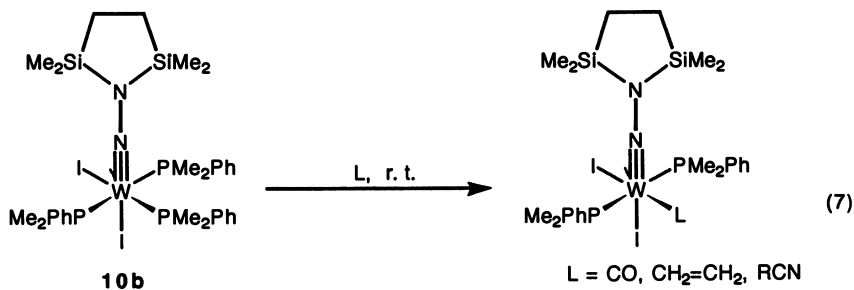
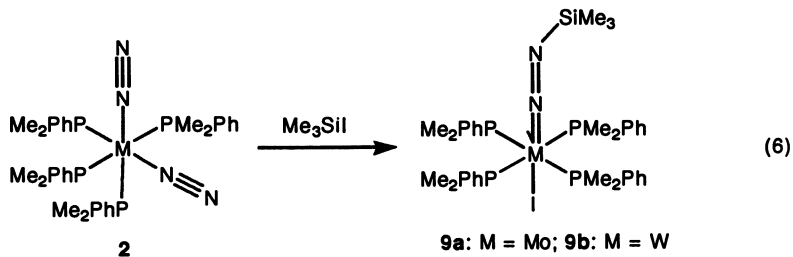
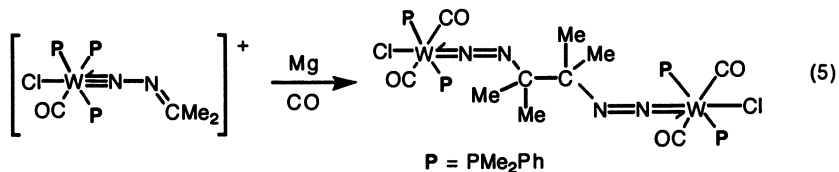


temperature in the dark, **10b** is converted into paramagnetic W(V) complexes *mer*, *trans*-[WX₃(NNSiMe₂CH₂CH₂SiMe₂)(PMe₂Ph)₂] (X = Cl, I). In the reaction with CH₂Cl₂, this oxidation reaction is accompanied by the halogen exchange, giving the trichloride complex, exclusively. It is to be noted that the C-Cl bond cleavage of CH₂Cl₂ has been rarely observed on such high-valent metal sites. X-ray analyses of *cis*, *trans*-[Wl₂(NNSiMe₂CH₂CH₂SiMe₂)(PMe₂Ph)₂(*p*-MeCOC₆H₄CN)] and *mer*, *trans*-[WCl₃(NNSiMe₂CH₂CH₂SiMe₂)(PMe₂Ph)₂] have shown that bond lengths and angles in disilylhydrazido(2-) ligands in these complexes are quite analogous to those in **10b** (**18**).

In contrast to the substantial stability of disilylhydrazido(2-) ligand in **10b** during substitution and oxidation reactions shown above, the silyldiazenido ligand in **9b** rapidly decomposes under analogous reaction conditions. Details are still uncertain and now under investigation. On the other hand, reactions of **9** with Na metal have been well elucidated. Reduction of **9** by excess Na in THF under Ar produces HN(SiMe₃)₂ and NH₃ in substantial yields. Additional amounts of NH₃ are obtained after hydrolysis of the evaporated residue of the reaction mixture, which includes sodium salts such as NaNH₂, NaNHSiMe₃, and NaN(SiMe₃)₂. Quantitative analysis of the nitrogenous products has proven that about half of the nitrogen atoms in **9** are converted into N₁ products, with the remainder forming molecular N₂. In the presence of excess Me₃SiCl, the major N₁ product becomes N(SiMe₃)₃. Importantly, when the reduction of **9** was carried out under N₂, parent dinitrogen complex **2** was recovered in moderate yields. These results are summarized in Scheme IV (**16,25**).

These observations led to further investigation of the reactions of Me₃SiX and Na promoted by dinitrogen complexes **1** and **2** under N₂, and eventually to discovery that silylamines such as N(SiMe₃)₃ and HN(SiMe₃)₂ are produced catalytically from equimolar mixture of Me₃SiCl and Na microdispersion under N₂ (1 atm) in THF in the presence of **1** or **2** (eq 8) (**25**). In a typical run using 1 mol% of **2a** at 30 °C, all charged Me₃SiCl was consumed in 4 h and silylamines N(SiMe₃)₃ and HN(SiMe₃)₂ are produced in 24% (7.5 mol/Mo atom) and 1.2% (0.6 mol/Mo atom) yields, respectively, accompanied by the formation of the major by-product Me₃SiSiMe₃ (45%) from the Wurtz-type coupling reaction. As shown in Table I, **2a** showed the highest activity for forming the silylamines among dinitrogen complexes **1** and **2**, and, when the reaction using **2a** was carried out in a solution diluted 5 times by THF, the yield of the silylamines increased to 38% (25 mol/Mo atom). Although the silylation of coordinated dinitrogen in **1** and **2** proceeds cleanly with Me₃SiI in benzene, it is highly reactive toward THF and cannot be used in the present system. From the reaction using Me₃SiBr, the silylamines are obtained catalytically but the yield is much lower than that using Me₃SiCl.

Reactions of **1** with alkyl bromides and iodides giving alkylidiazenido complexes have been shown to involve the homolysis of the carbon-halogen bond in the intermediate stage [M(N₂)(RX)(dppe)₂] and the subsequent attack of the free radical R on the coordinated dinitrogen (**26**). This mechanism may closely relate to the initiation step of the present system; the first step is probably the attack at the terminal nitrogen atom by a Me₃Si· radical generated from Me₃SiCl and Na in the presence of Mo or W species. Involvement of the reaction at coordinated dinitrogen has been confirmed by the fact that treatment of **2a** with a Me₃SiCl/Na mixture under Ar results in the formation of N(SiMe₃)₃ and HN(SiMe₃)₂ in 1.24 and 0.06 mol per



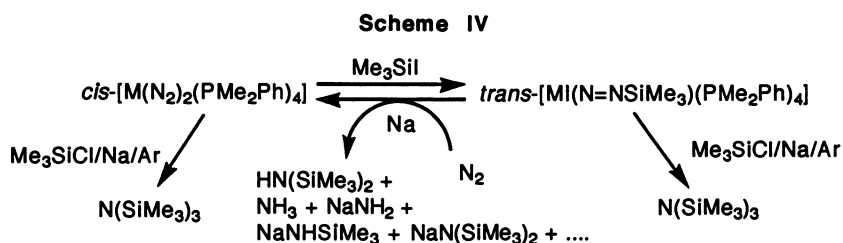


Table I. Catalytic Conversion of Molecular Nitrogen into Silylamines^a

Complex	Time/h	Conv. /%	Yield/% ^b (turnover number) ^c		
			<i>N</i> (SiMe ₃) ₃	<i>HN</i> (SiMe ₃) ₂	<i>Me</i> ₃ SiSiMe ₃
none	4	10	0	0	2.7
2a	4	>95	23.7(7.5)	1.2(0.6)	45.1
2a^d	15	>99	36.6(24.3)	1.1(1.1)	39.0
1a	4	>99	9.7(3.2)	0.8(0.4)	53.9
2b	4	>99	2.9(0.9)	1.6(0.8)	71.8
1b	4	>95	3.3(1.1)	1.4(0.7)	50.7

^aMe₃SiCl, 10 mmol; Na microdispersion, 10 mmol; THF, 6.5 ml; catalyst, 0.1 mmol; N₂, 1 atm; 30 °C. ^b(Me₃SiCl converted into the compound)/(Me₃SiCl charged) × 100. ^cMol per M atom. ^dTHF, 32.5 ml; **2a**, 0.5 mmol.

Mo atom, respectively. Although the details of the whole reaction mechanism are not yet clear, the present reaction system is one of the rare examples in which N_2 gas is catalytically converted into nitrogen compounds and the involvement of the reaction at coordinated dinitrogen has been clarified.

Silylation and Arylation of Dinitrogen Using Bimetallic Systems

Although the reactions of dinitrogen complexes **1** and **2** with inorganic and organic substrates have been studied extensively, few are reported about those with organometallic compounds except for the reactions with metal hydrides containing transition metals such as Fe, Co, Ru, and Zr (27–29). In this section, we will describe our recent findings on the Si–N and C–N bond formation at coordinated dinitrogen using organometallic reagents. These results may lead to development of new catalytic reactions effectively promoted by bimetallic systems containing metals with different reactivities.

Silylation of Dinitrogen Ligand in **1** and **2** with Silylcobalt Complexes.

Silylcobalt complexes $[R_3SiCo(CO)_4]$ ($R_3 = Ph_2Me, Me_2Ph$) prepared from the reactions of $[Co_2(CO)_8]$ with R_3SiH readily react with **1** and **2b** to give silyldiazenido complexes *trans*- $[M(N=NSiR_3)(P)_4][(\mu-OC)Co(CO)_3]$ (**11**; $P = 1/2dppe, PMe_2Ph$) (eq 9). X-ray crystallography has been carried out for *trans*- $[Mo(N=NSiPh_2Me)(dppe)_2][(\mu-OC)Co(CO)_3]$, which demonstrates that the silyldiazenido ligand has essentially the same bonding parameters as those in **9** and the *trans* site of this ligand is occupied by the weakly bound oxygen atom of one carbonyl ligand in $Co(CO)_4$ anion (**30**). Protonation of its W analog by H_2O , MeOH, and HBr results in the formation of silylhydrazido(2-) complexes *trans*- $[WX(NNHSiPh_2Me)(dppe)_2]-[Co(CO)_4]$ ($X = OH, OMe, Br$) and the X-ray structure of the silylhydrazido(2-) complex with $X = OH$ corresponds well to that of *cis, mer*- $[Wl_2(NNHSiMe_3)(PMe_2Ph)_3]$ as well as to that of **10b**.

Reduction of **11** ($M = W$) by Na or $Na[Co(CO)_4]$ in THF under Ar and successive hydrolysis of the reaction mixture produces NH_3 in yields of 0.3–0.8 mol/W atom, accompanied by liberation of some N_2 . Interestingly, a significant amount of N_2H_4 (0.1–0.2 mol/W atom) is also obtained from the reaction of the PMe_2Ph complex. Regeneration of the parent dinitrogen complex is evidenced by IR spectroscopy in the case of the diphosphine complex **1b**. These observations might provide a clue to design an alternative catalytic silylation of N_2 gas using R_3SiH in place of R_3SiCl , i.e., hydrosilylation of dinitrogen.

Arylation of Coordinated Dinitrogen in Anionic W Complexes $[WX(N_2)(dppe)_2]^-$ ($X = SCN, F$) and Related Reactions.

As already described, coordinated dinitrogen in **1** is alkylated or acylated directly by treatment with RX or $RCOCl$ to give alkyl- and acyldiazenido complexes. However, arylation of the dinitrogen ligand in **1** and related phosphine complexes by aryl halides does not proceed under analogous conditions despite interest in such reactions from both fundamental and industrial points of view. Reaction of a Mo dinitrogen complex with a cyclic tetrathioether ligand with bromo- and iodoarenes giving aryldiazenido complexes demonstrates the only precedent for the arylation of dinitrogen ligand (**31**).

Recently attempts have been made to effect arylation of dinitrogen via bimetallic activation, involving reactions of coordinated dinitrogen with coordinated haloarenes. Although the reaction of $[\text{Cr}(p\text{-FC}_6\text{H}_4\text{COOMe})(\text{CO})_3]$ with **1b** is unsuccessful, an anionic complex $\text{trans-}[\text{W}(\text{NCS})(\text{N}_2)(\text{dppe})_2]^-$ smoothly reacts with the haloarene complex at room temperature in THF to afford a bimetallic complex with a bridging aryldiazenido ligand $[\text{W}(\text{NCS})(\text{dppe})_2\{\text{N}=\text{N}[(\eta^6\text{-C}_6\text{H}_4\text{COOMe-}p)\text{Cr}(\text{CO})_3]\}]$ (eq 10) (32). Experimental data suggest that the present arylation proceeds not by a radical mechanism but by direct nucleophilic substitution at the coordinated haloarene.

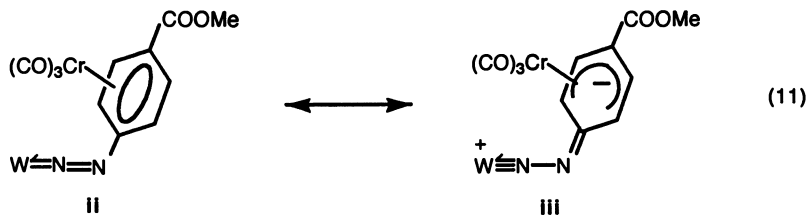
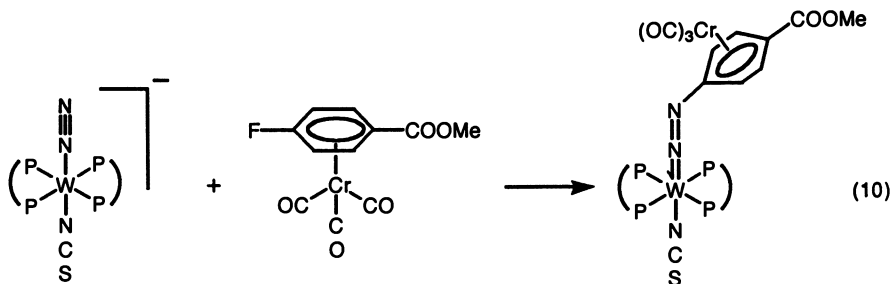
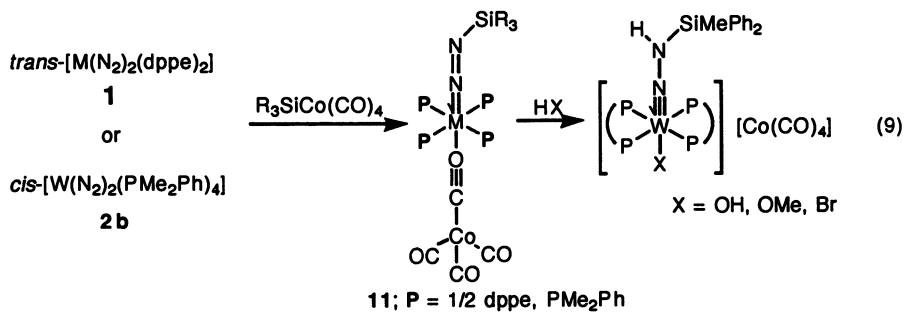
The structure of the μ -aryldiazenido ligand has been unequivocally determined by X-ray analysis, revealing a substantially elongated N=N bond (1.314(5) Å) as well as a relatively short N-C bond (1.366(6) Å) compared with related singly bent diazenido complexes. Further, the bond distance between Cr and the carbon atom attached to the outer nitrogen atom (2.431(5) Å) is longer than the other Cr-arene carbon bonds (2.174(5)-2.301(5) Å). These data indicate the large contribution of resonance structure iii, whose zwitterionic structure is stabilized by the electron-withdrawing $\text{Cr}(\text{CO})_3$ moiety (eq 11).

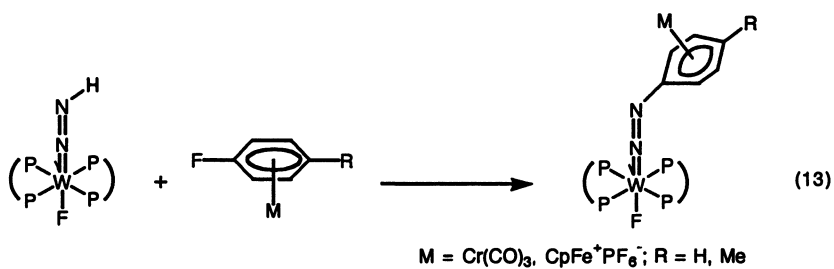
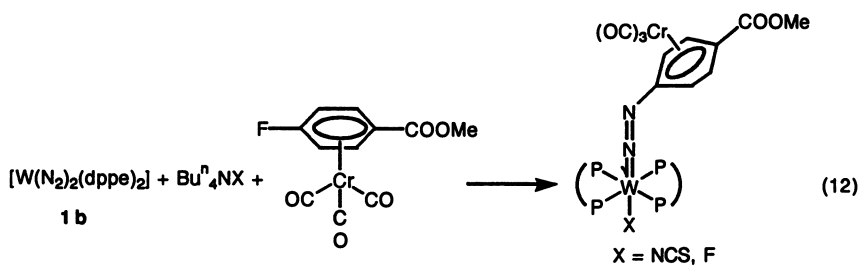
This bimetallic aryldiazenido complex and its F analog can be isolated by reaction of **1b** with the Cr complex in the presence of Bu_4NX ($X = \text{SCN}, \text{F}$) in THF. In these reactions, irradiation with a W-filament lamp is required for generating reactive anionic dinitrogen complexes $[\text{WX}(\text{N}_2)(\text{dppe})_2]^-$ (eq 12).

It is to be noted that the reaction of the diazenido complex $[\text{WF}(\text{NNH})(\text{dppe})_2]$ with $[(\eta^6\text{-}p\text{-RC}_5\text{H}_5\text{F})\text{Cr}(\text{CO})_3]$ ($R = \text{COOMe}, \text{H}$) provides another route to prepare analogous μ -aryldiazenido complexes. As shown in eq 13, coordinated $\text{C}_6\text{H}_5\text{F}$ and $p\text{-MeC}_6\text{H}_4\text{F}$ in cationic Fe(II) complexes also react with this diazenido complex, affording μ -aryldiazenido complexes. Although the diazenido complexes $[\text{MX}(\text{NNH})(\text{dppe})_2]$ are well known to undergo electrophilic reactions at the terminal nitrogen atoms, arylation of the diazenido ligand has been poorly explored; the examples reported until now are limited to the reactions of $[\text{WX}(\text{NNH})(\text{dppe})_2]$ with the strongly electrophilic arene 2,4-(NO_2) $\text{C}_6\text{H}_3\text{F}$, which give $[\text{WX}\{\text{NNC}_6\text{H}_3(\text{NO}_2)_2\text{-}2,4\}(\text{dppe})_2]$ ($X = \text{Br}, \text{F}, \text{CF}_3\text{COO}$) characterized only spectroscopically (33).

Concluding Remarks

Reactivities demonstrated to date for dinitrogen ligands in Mo and W phosphine complexes **1** and **2** are extensive. Reactions of **1** and **2** with acids to give NH_3 and N_2H_4 as well as several protonated dinitrogen complexes have already been studied in detail, showing these complexes to be attractive model compounds for considering the N_2 -fixation mechanism in biological systems. Furthermore, as summarized in this account, it has also been shown that by treatment with various organic substrates dinitrogen complexes **1** and **2** can be converted into a wide range of organo-nitrogen complexes and, under certain conditions, into organo-nitrogen compounds. These general C-N and Si-N bond forming reactions observed for Mo and W dinitrogen complexes are particularly interesting, since they might lead to direct synthesis of organo-nitrogen compounds from N_2 gas and a cheap organic feedstock. Our continuing research in this field is now directed toward the unattained goal of the development of novel catalytic systems producing organo-nitrogen compounds with high efficiencies.





Literature Cited

- (1) Hidai, M.; Tominari, K.; Uchida, Y.; Misono, A. *Chem. Commun.* **1969**, 1392.
- (2) Hidai, M.; Tominari, K.; Uchida, Y. *J. Am. Chem. Soc.* **1972**, *94*, 110.
- (3) Uchida, T.; Uchida, Y.; Hidai, M.; Kodama, T. *Acta Cryst.* **1975**, *B31*, 1197.
- (4) Hidai, M. In *Molybdenum Enzymes*; Spiro, T. G., Ed.; Metal Ions in Biology, Vol. 7; Wiley-Interscience: New York, NY, 1985; pp 285–341.
- (5) Hidai, M.; Mizobe, Y. In *Reactions of Coordinated Ligands*; Braterman, P. S., Ed.; Plenum: New York, NY, 1989, Vol. 2; pp 53–114.
- (6) Chatt, J.; Dilworth, J. R.; Richards, R. L. *Chem. Rev.* **1978**, *78*, 589.
- (7) Dilworth, J. R.; Richards, R. L. In *Comprehensive Organometallic Chemistry*; Wilkinson, G.; Stone, F. G. A.; Abel, E. W., Eds.; Pergamon: Oxford, 1982, Vol. 8; pp 1073–1106.
- (8) Colquhoun, H. M. *Acc. Chem. Res.* **1984**, *17*, 23.
- (9) Hidai, M.; Mizobe, Y.; Sato, M.; Kodama, T.; Uchida, Y. *J. Am. Chem. Soc.* **1978**, *100*, 5740.
- (10) Bevan, P. C.; Chatt, J.; Hidai, M.; Leigh, G. J. *J. Organomet. Chem.* **1978**, *160*, 165.
- (11) Mizobe, Y.; Uchida, Y.; Hidai, M. *Bull. Chem. Soc. Jpn.* **1980**, *53*, 1781.
- (12) Iwanami, K.; Mizobe, Y.; Takahashi, T.; Kodama, T.; Uchida, Y.; Hidai, M. *Bull. Chem. Soc. Jpn.* **1981**, *54*, 1773.
- (13) Aoshima, T.; Mizobe, Y.; Hidai, M.; Tsuchiya, J. *J. Organomet. Chem.* **1992**, *423*, 39.
- (14) Hidai, M.; Aramaki, S.; Yoshida, K.; Kodama, T.; Takahashi, T.; Uchida, Y.; Mizobe, Y. *J. Am. Chem. Soc.* **1986**, *108*, 1562.
- (15) Hidai, M.; Komori, K.; Kodama, T.; Jin, D.-M.; Takahashi, T.; Sugiura, S.; Uchida, Y.; Mizobe, Y. *J. Organomet. Chem.* **1984**, *272*, 155.
- (16) Komori, K.; Sugiura, S.; Mizobe, Y.; Yamada, M.; Hidai, M. *Bull. Chem. Soc. Jpn.* **1989**, *62*, 2953.
- (17) Oshita, H.; Mizobe, Y.; Hidai, M. *Chem. Lett.* **1990**, 1303.
- (18) Oshita, H.; Mizobe, Y.; Hidai, M. *Organometallics* **1992**, *11*, 4116.
- (19) Ishii, Y.; Miyagi, H.; Hidai, M. *J. Chem. Soc., Chem. Commun.* **1990**, 1570.
- (20) Ishii, Y.; Miyagi, H.; Jitsukuni, S.; Seino, H.; Harkness, B. S.; Hidai, M. *J. Am. Chem. Soc.* **1992**, *114*, 9890.
- (21) Miyagi, H.; Ishii, Y.; Aoshima, T.; Mizobe, Y.; Hidai, M. *Chem. Lett.* **1991**, 611.
- (22) Watakabe, A.; Takahashi, T.; Jin, D.-M.; Yokotake, I.; Uchida, Y.; Hidai, M. *J. Organomet. Chem.* **1983**, *254*, 75.
- (23) Aoshima, T.; Tamura, T.; Mizobe, Y.; Hidai, M. *J. Organomet. Chem.* **1992**, *435*, 85.
- (24) Aoshima, T.; Tanase, T.; Mizobe, Y.; Yamamoto, Y.; Hidai, M. *J. Chem. Soc., Chem. Commun.* **1992**, 586.
- (25) Komori, K.; Oshita, H.; Mizobe, Y.; Hidai, M. *J. Am. Chem. Soc.* **1989**, *111*, 1939.
- (26) Chatt, J.; Head, R. A.; Leigh, G. J.; Pickett, C. J. *J. Chem. Soc., Dalton Trans.* **1978**, 1638.
- (27) Hidai, M.; Takahashi, T.; Yokotake, I.; Uchida, Y. *Chem. Lett.* **1980**, 645.

- (28) Nishihara, H.; Mori, T.; Tsurita, Y.; Nakano, K.; Saito, T.; Sasaki, Y. *J. Am. Chem. Soc.* **1982**, *104*, 4367.
- (29) Jia, G.; Morris, R. H.; Schweitzer, C. T. *Inorg. Chem.* **1991**, *30*, 593.
- (30) Street, A. C.; Mizobe, Y.; Gotoh, F.; Mega, I.; Oshita, H.; Hidai, M. *Chem. Lett.* **1991**, 383.
- (31) Yoshida, T.; Adachi, T.; Ueda, T.; Kaminaka, M.; Sasaki, N.; Higuchi, T.; Aoshima, T.; Mega, I.; Mizobe, Y.; Hidai, M. *Angew. Chem. Int. Ed. Engl.* **1989**, *28*, 1040.
- (32) Ishii, Y.; Ishino, M.; Aoki, T.; Hidai, M. *J. Am. Chem. Soc.* **1992**, *114*, 5429.
- (33) Colquhoun, H. M. *J. Chem. Res., Synop.* **1979**, 325.

RECEIVED March 8, 1993

Chapter 23

Modeling the N–N Bond-Cleavage Step in the Reduction of Molecular Nitrogen to Ammonia

Protonation and Electron-Transfer Reactions of Dinitrogen, Nitrogen Hydride, and Organonitrogen Complexes of Molybdenum and Tungsten

T. Adrian George and Jeffery R. D. DeBord

Department of Chemistry, University of Nebraska,
Lincoln, NE 68588–0304

Organic-substituted hydrazido(2-) complexes of molybdenum and tungsten are investigated as possible reaction analogues of the nitrogen-nitrogen bond cleavage step during the reduction of molecular nitrogen to ammonia. The reactions of $[\text{WCl}_2(\text{NNR}_2)(\text{PMe}_2\text{Ph})_3]$, **1** ($\text{R} = \text{Ph}$) and **2** ($\text{R} = \text{Me}$) with HCl in CH_2Cl_2 produce a secondary amine (ca. 0.62 mol/mol W) and ammonia (ca. 0.20 mol/mol W). The reaction of **1** with water in CH_2Cl_2 produces 0.98 mol of Ph_2NH and 0.30 mol of ammonia, respectively. These nitrogen balances approach those obtained in the form of ammonia from reactions of unsubstituted hydrazido(2-) complexes that are prepared directly from dinitrogen complexes. The crystal structures of **1** and **2** have been determined. Although the relative positions of the atoms and orientations of the phenyl rings are the same in **1** and **2** there are significant differences in the W–N, W–Cl and W–P bond distances.

Nitrogenase catalyzes the reduction of molecular nitrogen to ammonia together with the production of dihydrogen (eq. 1). Efforts to understand the mechanism by which



the N_2 molecule is transformed into ammonia have focused upon reactions of N_2 complexes of transition metals. From these studies it is expected that reactivity and structural analogues of the natural system will be forthcoming. Very recent x-ray diffraction studies of the MoFe protein (*1,2*), one of the two-component proteins of nitrogenase, confirm the earlier interpretation of the x-ray absorption data (*3*) that iron and molybdenum in the FeMo-cofactor (*4*) are located in a sulfur-rich environment with molybdenum bonded to three sulfur atoms and three lighter atoms. On the basis of current structural data iron or a combination of iron atoms look to be a more likely binding site for N_2 than molybdenum. However, there remain valuable

mechanistic lessons to be learned at the molecular level about N_2 reduction from studies of N_2 complexes of transition metals that afford nitrogen hydride intermediates and ammonia.

The transformation of N_2 to ammonia can be viewed as taking place in a series of steps that should be identifiable. These include: (i) N_2 binding, (ii) protonation of N_2 , (iii) electron transfer, and (iv) nitrogen-nitrogen bond cleavage leading to ammonia release. Regeneration of the original binding site completes the catalytic cycle.

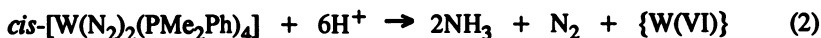
Nitrogen Binding

There are many N_2 complexes known that have been prepared from N_2 and a selection is shown below together with the N-N bond distance (dppe = $Ph_2PCH_2CH_2PPh_2$, dmpe = $Me_2PCH_2CH_2PMe_2$, py = pyridine, $C_{10}H_8 = \eta^5:\eta^5$ -fulvalenyl). It is evident that N_2 is able to bind to one or more metals with a wide variety of coligands and in very different geometric arrangements. There are simple end-on N_2 complexes (I-VII) that resemble carbonyl complexes. Bonding between N_2 and the metal has been proposed to involve N_2 -to-metal σ -bonding and metal-to- N_2 π -backbonding. In these complexes the N-N bond length is very similar to that of gaseous N_2 (1.09758 (10) Å).

Dinitrogen displays unique bonding arrangements in a number of different bridging modes. These include: (a) linear end-on bridging between (i) identical metal units

[Ru(N_2)(NH_3) $_5$] $^{2+}$ (5) I Ru(II), d^6 (N-N = 1.12 (9) Å)	[CoH(N_2)(PPh_3) $_3$] (6) II Co(I), d^8 (N-N = 1.123 (13) Å)	[FeH(N_2)(dmpe) $_2$] $^+$ (7) III Fe(II), d^6 (N-N = 1.13 (3) Å)
[ReCl(N_2)(PMe_2Ph) $_4$] (8) IV Re(I), d^6 (N-N = 1.055 (30) Å)	[Mo(N_2) $_2$ (dppe) $_2$] (9) V Mo(0), d^6 (N-N = 1.10 (2) Å)	[W(N_2) $_2$ (PMe_2Ph) $_4$] (10) VI W(0), d^6
[V(N_2) $_2$ (dppe) $_2$] $^-$ (11) VII V(-I), d^6 (N-N = 1.130 (16) Å)	[($PhMe_2P$) $_4$ ClRe- N_2 -MoCl $_4$ (OMe)] (12) VIII Re(I), d^6 ; Mo(IV), d^2 (N-N = 1.18 (3) Å)	
[(C_5Me_5) $_2$ (N_2)Zr] $_2$ (μ - N_2) (13) IX Zr(II), d^2 (N-N = 1.182 (5) Å)	[(η^6 - $C_6H_3Me_3$)(dmpe)Mo] $_2$ (μ - N_2) (14) X Mo(0), d^6 (N-N = 1.145 (7) Å)	
[(o - $Me_2NCH_2C_6H_4$) $_2$ (py)V] $_2$ (μ - N_2) (15) XI V(II), d^3 (N-N = 1.228 (4) Å)	[(C_5Me_5) Me_3W] $_2$ (μ - N_2) (16) XII W(IV), d^2 (N-N = 1.334 (26) Å)	

is no crystal structure) is the only complex known in which all six electrons come from a single metal center in the formation of ammonia (eq. 2; $\text{H}_2\text{SO}_4/\text{MeOH}$) (22).

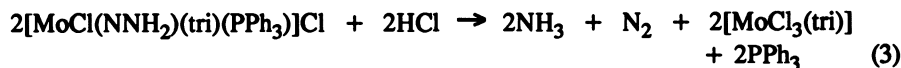


Complex V and its tungsten analogue react with strong acids to form a complex containing the diprotonated hydrazido(2-) (NNH_2) ligand (23). Although these complexes do not react further to yield ammonia, complexes containing the hydrazido(2) ligand have been identified and characterized in ammonia-forming reactions of VI (24).

Other complexes that afford ammonia upon treatment with acid do so in a disproportionation reaction. These complexes include the molybdenum analogue of VI, and VII, XI, and XII, and the novel iron(0) complex $[\text{Fe}(\text{N}_2)(\text{dmpe})_2]$ (25). Complex XV reacts with HCl in diglyme with loss of N_2 . However, aqueous hydrolysis of XV yields mostly ammonia (ca. 2 mol per mol of XV). The metal complex with the longest N-N bond, XIV, yields one equiv. of hydrazine upon treatment with excess acid.

Two proposed mechanisms for the reduction of N_2 to ammonia are shown in Figure 1 and Scheme I. The first mechanism, attributed to Hardy, Burns and Parshall (26), espouses two metals working together. The second mechanism proposed by Chatt, Richards et al (22) and further elaborated on on the basis of kinetic data by Thorneley and Lowe (27) details the reduction of N_2 at a single metal center following along from the behavior of VI. In both mechanisms electrons and protons are provided from an external source as required. The hydrazido(2-) intermediate is highlighted in Scheme I because (i) so far the ligand is unique to the chemistry of N_2 complexes of molybdenum and tungsten, (ii) on the basis of experimental data it has been proposed as an intermediate in the reduction of N_2 to ammonia by nitrogenase, and (iii) disproportionation occurs at or following the formation of this intermediate (28).

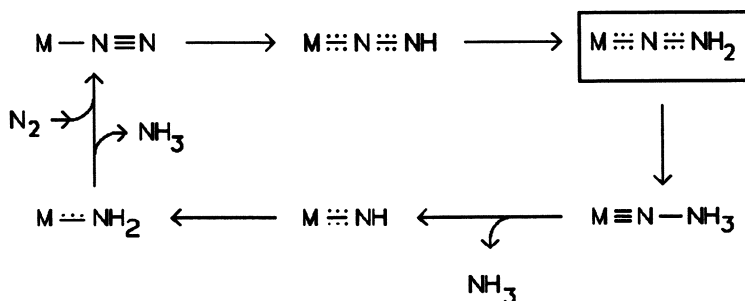
Disproportionation. Why is disproportionation bad? First, as shown in equation 3 for the molybdenum hydrazido(2-) complex $[\text{tri} = \text{PhP}(\text{CH}_2\text{CH}_2\text{PPh}_2)_2]$ disproportionation leads to the loss of one mole of N_2 for every two moles of



ammonia formed. Thus, one complex acts as a reducing agent for a second complex, yielding two moles of ammonia and one of N_2 . Therefore, beginning with the bis(N_2)-molybdenum(0) complex each molybdenum atom provides three electrons for a maximum yield of one mol of ammonia per mol of Mo; $2\{\text{Mo}^0(\text{N}_2)_2\} + 6\text{H}^+ \rightarrow 2\{\text{Mo}^{\text{III}}\} + 3\text{N}_2 + 2\text{NH}_3$. The same stoichiometry appears to arise in the reaction of the vanadium(-I) complex VII with excess HBr. However, identification of $[\text{FeCl}_2(\text{dmpe})_2]$ as the end product of the reaction of $[\text{Fe}(\text{N}_2)(\text{dmpe})_2]$ with HCl suggests an even more complex stoichiometry; $3\{\text{Fe}^0(\text{N}_2)\} + 6\text{H}^+ \rightarrow 3\{\text{Fe}^{\text{II}}\} + 2\text{NH}_3 + 2\text{N}_2$. No intermediates have been detected in these reactions of N_2 complexes of vanadium and iron.

Second, disproportionation is unlikely to occur in the enzyme and therefore reactions in which disproportionation occurs are unsatisfactory reaction analogues of the enzyme. That such reactions are unlikely in the protein suggested the technique of site-isolation of a molybdenum N_2 complex on a polymer (*vide infra*) in order to prevent disproportionation.

SCHEME I



Electron transfer

In order to circumvent disproportionation another source of electrons is required. We discovered a suitable reducing agent while investigating the disproportionation of $[\text{MoBr}(\text{NNH}_2)(\text{dppe})(\text{PPh}_2\text{Me})_2]\text{Br}$ attached to a polymer (see Scheme II) (29). The complex *trans*- $[\text{Mo}(\text{N}_2)_2(\text{dppe})(\text{PPh}_2\text{Me})_2]$ reacts with HBr in THF to afford ammonia, and in CH_2Cl_2 to afford ammonia and hydrazine. However, *trans*- $[\text{Mo}(\text{N}_2)_2(\text{PS-diphos})(\text{PPh}_2\text{Me})_2]$ (XVII), where PS-diphos is $[-\text{P}(\text{Ph})\text{CH}_2-\text{CH}_2\text{PPh}_2]$ covalently bonded to a polystyrene-2% divinylbenzene copolymer (PS), reacts with HBr in THF to produce the corresponding hydrazido(2-) complex $[\text{MoBr}(\text{NNH}_2)(\text{PS-diphos})(\text{PPh}_2\text{Me})_2]\text{Br}$ (XVIII) but no ammonia. In CH_2Cl_2 , hydrazine is produced but no ammonia. Thus, a single molybdenum center is able to provide the four electrons required for the formation of hydrazine but there are not sufficient electrons available for the formation of ammonia since disproportionation is prevented by site-isolation of the metal centers. Addition of a soluble N_2 -complex of molybdenum or tungsten to a $^{15}\text{N}_2$ -labelled sample of XVIII yielded $^{15}\text{NH}_3$ upon treatment with HBr in CH_2Cl_2 . Thus, in this case disproportionation involves reaction between an anchored nitrogen hydride and one that is in solution (30). A complex such as *trans*- $[\text{Mo}(\text{N}_2)_2(\text{dppe})_2]$ which does not afford ammonia, similarly does not cause ammonia formation from XVIII.

Of most interest is the discovery that two-electron reducing agents such as SnX_2 ($\text{X} = \text{Br}, \text{Cl}$), $[\text{SnX}_3]^-$, and GeI_2 are able in the presence of acid to (i) reduce the polymer-supported hydrazido(2-) complex XVIII to ammonia (see Scheme II) and (ii) increase the yield of ammonia by 300% in a reaction involving a non-anchored N_2 complex (31). The four-coordinate tin(II) complex $\text{Sn}(\text{acac})_2$, where acac = acetylacetonate, is ineffectual as a reducing agent in these reactions.

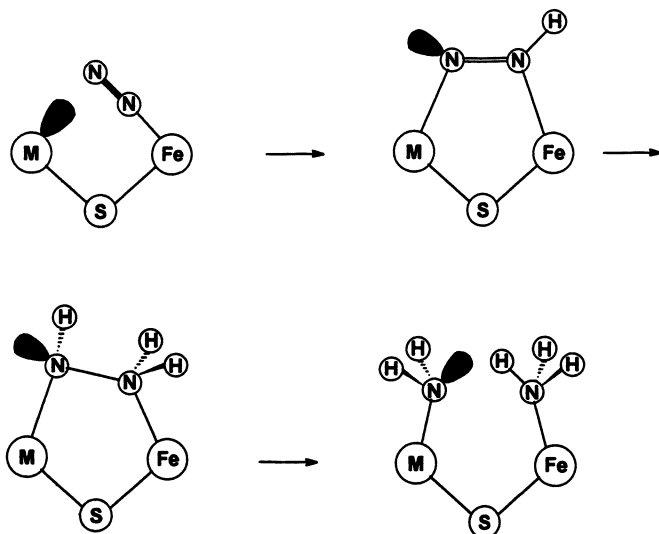
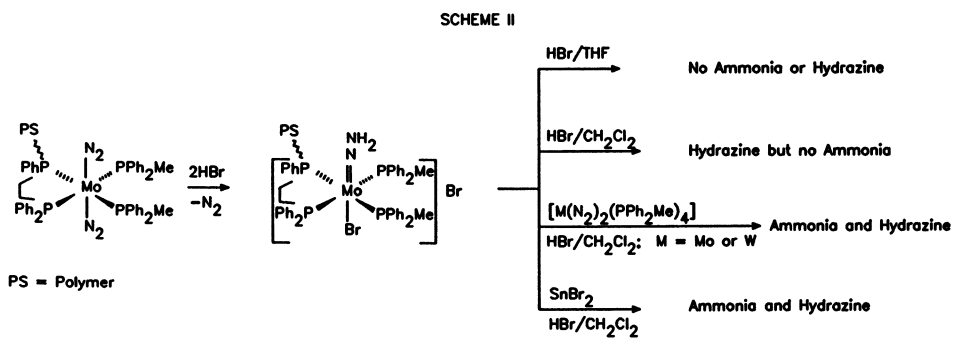


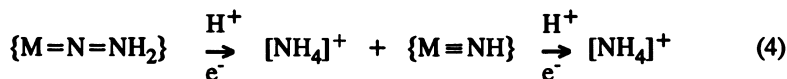
Figure 1. Proposed model for active site and reduction of N_2 to ammonia. Adapted from reference 26.



Schrock et al (15) have found that the yields of ammonia formed from **XII** and $[(C_5Me_5)Me_3W(NNH_2)]$ are dramatically increased using zinc amalgam as the reducing agent and lutidine·HCl as the acid. Under similar reaction conditions $[(C_5Me_5)Me_3W](\mu-N_2)[MoMe_3(C_5Me_5)]$ produced an almost 90% yield of ammonia.

Nitrogen-Nitrogen Bond Cleavage.

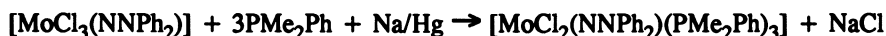
If nitrogen-nitrogen bond cleavage occurs at a single metal center with the elimination of one mol of ammonia then it should be possible to identify the remaining nitrogen-containing ligand as well as monitor spectroscopically the events preceding nitrogen-



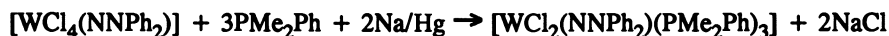
nitrogen bond cleavage. However, the detection and characterization of intermediates beyond the hydrazido(2-) stage are complicated by (i) the difficulty of monitoring the formation of N-H bonds in acidic solution, (ii) the problems in distinguishing between ammonia formed from each of the two nitrogen atoms, and (iii) the generation of paramagnetic species. In an effort to differentiate between the two nitrogen atoms and provide better monitoring capabilities alkyl- and aryl-substituted hydrazido(2-) complexes have been prepared and their reactions with acid studied. Two resonance forms of the complexes in question are shown below. Complexes of this type where $R' = H$ are known and yield ammonia (22). Although alkyl- and aryl-substituted hydrazido(2-) complexes are well known, only recently have complexes that also contain monodentate phosphines (PMe_3) been reported although no reactions with acid have been described (32).

Synthesis of Complexes. Examples of the synthesis of a molybdenum and a tungsten complex are shown in Schemes III and IV. At this time neither $[MoCl_3(NNPh_2)]$ nor $[WCl_4(NNPh_2)]$ have been characterized. Extended reduction times result in significantly diminished yields for both molybdenum and tungsten complexes. The new organohydrazido(2-) complexes are air-stable. We have also prepared complexes

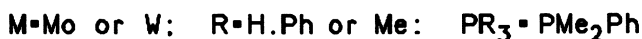
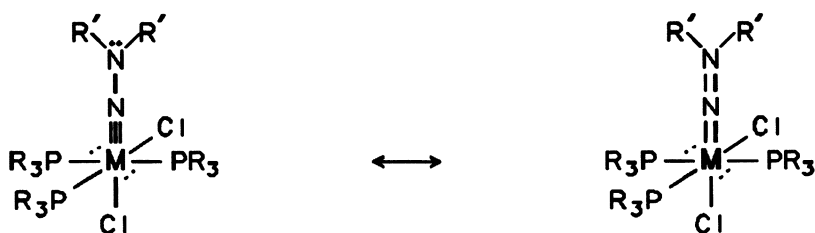
Scheme III



Scheme IV



containing the methylphenylhydrazido(2-) ligand and complexes having dppe and one PMe_2Ph coligands.



Synthesis of [WCl₂(NNPh₂)(PMe₂Ph)₃] (1). Dichloromethane (40 mL) was added to a mixture of WCl₆ (2.5 g, 6.3 mmol) and Ph₂NNH₂·HCl (1.4 g, 6.3 mmol) cooled at -78°C. After stirring for 5 min, solvent was removed in vacuo. The solid was redissolved in CH₂Cl₂ (5 mL), and [WCl₄(NNPh₂)] precipitated by adding pentane (40 mL), collected by filtration and dried in vacuo. To a mixture of [WCl₄(NNPh₂)] (2.0 g, 3.9 mmol), PMe₂Ph (1.66 g, 12 mmol) and THF (50 mL) was added 1% Na/Hg (1.1 g, 47 mmol of Na). The mixture was stirred for 0.75 h. The solution was decanted and filtered through Celite. The solvent was removed and the solid dissolved in CH₂Cl₂ (10 mL). After filtration, the product was precipitated by adding pentane (40 mL), collected by filtration, washed with pentane (3 x 10 mL) and dried in vacuo. The yield of product was 68%. Anal. Calcd. for C₃₆H₄₃Cl₂N₂P₃: C, 50.79; H, 5.09; N, 3.29. Found: C, 50.68; H, 5.17; N, 3.31. ³¹P NMR [C₆D₆]: -15.7 (s, 2, J_{PW} = 244 Hz), -16.2 (s, 1, J_{PW} = 305 Hz).

Synthesis of [MoCl₂(NNPh₂)(PMe₂Ph)₃] (3). This complex was prepared similarly to the tungsten analogue beginning with MoCl₅. The first step was complete within 2-3 min. In the second step only one equiv. of sodium amalgam is necessary and the reaction took only 12 min. Yield of product was 52%. ³¹P NMR [C₆D₆]: 11.47 (t, 1, J_{PP} = 14.88 Hz), 2.88 (d, 2).

Reactions with Acid. In a typical acid reaction, the metal complex was dissolved in CH₂Cl₂ and treated with excess HCl (1M in Et₂O). The solution was allowed to stir for 48 h. After this time water was added and the mixture stirred for 1 h. The aqueous phase was analyzed for ammonia and the organic phase for amine and organohydrazine. In parallel experiments, excess water was added in place of HCl and the mixture stirred for 48 h before analysis. Yields of ammonia were determined by the indophenol method (33), yields of Ph₂NH by HPLC, and yields of Me₂NH by the pyrocatechol/silver oxide method (34).

Results are shown in Table I. The following points are particularly worthy of note. First, no organohydrazine was formed. Considering the ancestry of the hydrazido(2-) ligand in these specific complexes, simple cleavage of the metal-nitrogen bond might have been expected. Clearly, the reduction step results in a weakening of the N-N bond and a strengthening of the M-N bond, respectively.

Table I. Yields^a of Nitrogen-Containing Products

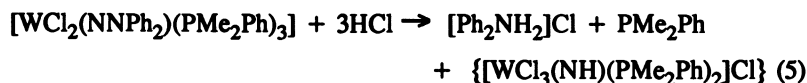
compd	M	R	Acid (mol)	mol of product	
				R ₂ NH	NH ₃
1		W	Ph HCl (20)	0.62	0.20
1		W	Ph H ₂ O (excess)	0.98	0.30
2		W	Me HCl (20)	0.62	0.25
2		W	Me H ₂ O (excess)	0	trace
3		Mo	Ph HCl (20)	trace	0.21
3		Mo	Ph H ₂ O (excess)	trace	0.19

^aMol per mol of metal complex

Second, reactions of **1** and **2** with HCl produced both an amine and ammonia. We believe that this is the first example of the generation of both an amine and ammonia from organohydrazido(2-) metal complexes that are strict analogues of the corresponding unsubstituted hydrazido(2-) complexes, which afford ammonia.

Third, when water was used in place of HCl for reaction with **1** the yield of Ph₂NH was essentially quantitative. Although the yield of ammonia also increased, more than half of the remaining nitrogen was unaccounted for. Two electrons are required in order to cleave the N-N bond and produce one mol of Ph₂NH. Thus, tungsten is oxidized from W(IV) to W(VI) with a tungsten(VI) amide as a *possible* intermediate (eq. 6). No further redox chemistry is necessary for the formation of ammonia. It is interesting but perhaps not surprising that more Ph₂NH and ammonia were formed when water was used in place of HCl.

In the presence of water, coordination of water and subsequent formation of a



W=O bond will result in a more stable tungsten(VI) complex, hence facilitating oxidation of tungsten, than if only chloride ions are available.

Fourth, although yields of amine and ammonia were similar for **1** and **2** when HCl was used, this was not true for reactions with water. In fact no ammonia or Me₂NH were formed when the dimethylhydrazido(2-) complex was treated with water.

Fifth, the molybdenum complex **3** reacts with both either HCl and water to afford a low yield of ammonia but no Ph₂NH. This is surprising since ammonia would be formed after the generation of Ph₂NH if the Ph₂NN group remains bonded in a linear arrangement.

Structures of 1 and 2. We were able to grow crystals of [WCl₂(NRR₂)(PMe₂Ph)₃] (R₂ = Me₂ and Ph₂) (see Figures 2 and 3) and some of the important bond lengths and angles are listed in Table II. The complexes are essentially isostructural with similar atom positions and orientations of the PMe₂Ph groups. However, some of the key bond lengths are significantly different. Although the N-N bond lengths are

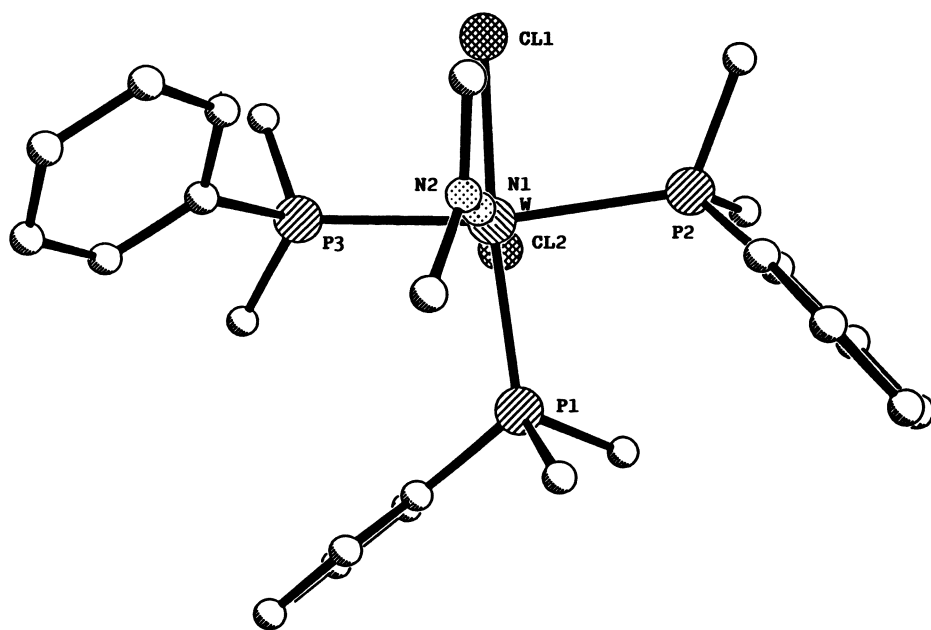


Figure 2. ORTEP view of the structure of $[\text{WCl}_2(\text{NNMe}_2)(\text{PMe}_2\text{Ph})_3]$.

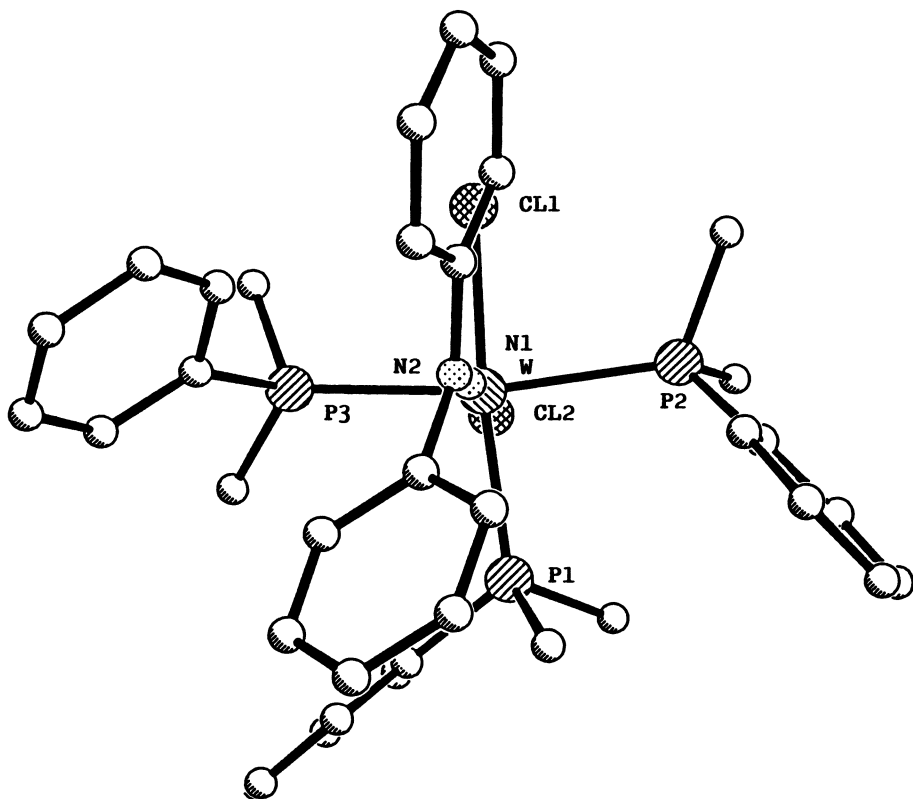


Figure 3. ORTEP view of the structure of $[\text{WCl}_2(\text{NNPh}_2)(\text{PMe}_2\text{Ph})_3]$.

not statistically different and are at the long end of the range for hydrazido(2-) complexes, the W-N distance in the diphenylhydrazido(2-) complex is significantly shorter than that of the dimethylhydrazido(2-) complex. The corresponding trans W-Cl distance is also dramatically shorter in the diphenylhydrazido(2-) complex. This is counter-intuitive since a shorter W-N multiple bond would be expected to cause a correspondingly longer trans W-Cl bond; the opposite is observed. The cis W-Cl

Table II. Comparison of Structural Data for Hydrazido(2-) Complexes

	$[WCl_2(NNMe_2)(PMe_2Ph)_3]$	$[WCl_2(NNPh_2)(PMe_2Ph)_3]$
Bond lengths (Å)		
N-N	1.385 (8)	1.36 (1)
W-N	1.851 (5)	1.761 (8)
W-Cl2	2.625 (2)	2.486 (3)
W-Cl1	2.481 (2)	2.497 (3)
W-P1	2.391 (2)	2.481 (5)
W-P2	2.422 (2)	2.517 (3)
W-P3	2.442 (2)	2.506 (3)
Bond angles (°)		
N-N-W	173.8 (4)	178.0 (6)
N-W-Cl2	175.2 (2)	174.9 (3)
N-N-C	112.4 (5)	119.4 (7)
N-N-C	121.1 (5)	118.8 (8)
C-N-C	114.4 (6)	121.3 (8)

distances are the same. The W-P distances also show considerable variation. All W-P distances are shorter in the dimethylhydrazido(2-) complex than the diphenylhydrazido(2-) complex. Thus, in the dimethylhydrazido(2-) complex the three phosphine ligands are pulled in towards the metal and the axial chlorine and nitrogen atoms pushed away from the metal compared with the diphenylhydrazido(2-) complex where the phosphine ligands are pushed away from the metal and the axial chlorine and nitrogen atoms drawn towards the metal.

Until we know the fate of the nitrogen-containing ligand in the reaction of $[WCl_2(NNMe_2)(PMe_2Ph)_3]$ with water, we cannot tell whether these structural differences are contributing to the differences in chemistry. Certainly there is no difference in reactivity with HCl in CH_2Cl_2 .

Conclusion

The most difficult phase of the reduction of coordinated N_2 is protonation of N_2 to form N-H bonds. Dinitrogen has been shown to bind to many different metals and in many different ligand environments. However, very few of these complexes produce ammonia upon the simple addition of acid because electrons are not readily available for the formation of the N-H bonds. The recent structural data on the FeMo-cofactor suggests the presence of a void between two interconnected metal clusters; an $[Fe_4S_3]$ and an $[Fe_3MoS_3]$ cluster. Enzymatic studies indicate that N_2 does not bind to the protein until after the addition of three low-potential electrons per

cofactor. Addition of a fourth low-potential electron is required for N_2 to bind irreversibly to the protein. Thus, efforts to develop reaction analogues of the cofactor using metal clusters may require strongly reducing conditions for N_2 to bind. However, under these conditions bound N_2 is likely to be susceptible to protonation. Those clusters containing three or more metals that are known to contain N_2 were all synthesized under reducing conditions.

Acknowledgments

We thank the National Institutes of Health (Grant GM-38613) for support of this work. Additional funding was provided by the University of Nebraska-Lincoln Research Council and NIH Biomedical Research Support Grant RR-07055. We thank Professor Zubieta for providing the two crystal structures.

Literature Cited

1. (a) Rees, D. C.; Kim, J.; Georgiadis, M. M.; Komiya, H.; Chirino, A. J.; Woo, D.; Schlessman, J.; Chan, M. K.; Joshua-Tor, L.; Santillan, B.; Chakrabarti, P.; Chu, B. T. *This Vol.* Chapter 11. (b) Kim, J.; Rees, D. C. *Science* **1992**, *257*, 1677-1682. (c) Kim, J.; Rees, D. C. *Nature* **1992**, *553*-560.
2. Bolin, J.; Campobasso, N.; Muchmore, S. W.; Morgan, T. V.; Mortenson, L. E. *This Vol.* Chapter 12.
3. Conradson, S. D.; Burgess, B. K.; Newton, W. E.; Mortenson, L. E.; Hodgson, K. O. *J. Am. Chem. Soc.* **1987**, *109*, 7507.
4. Burgess, B. K. *Chem. Rev.* **1990**, *90*, 1377.
5. Harrison, D. E.; Taube, H. *J. Am. Chem. Soc.* **1967**, *89*, 5706.
6. Sacco, A.; Rossi, M. *Inorg. Chim. Acta*, **1968**, *2*, 127.
7. Hills, A.; Hughes, D. L.; Jimenez-Tenorio, M.; Leigh, G. J. *J. Organometal. Chem.* **1990**, *391*, C41.
8. Chatt, J.; Dilworth, J. R.; Leigh, G. J. *J. Chem. Soc. Dalton Trans.* **1973**, 612.
9. Hidai, M.; Tominari, K.; Uchida, U.; Misono, A. *J. Chem. Soc. Chem. Commun.* **1969**, 1392.
10. Bell, B.; Chatt, J.; Leigh, G. J. *J. Chem. Soc. Dalton Trans.* **1972**, 2492.
11. Rehder, D.; Woitha, C.; Pribsch, W.; Gailus, H. *J. Chem. Soc. Chem. Commun.* **1992**, 364.
12. Chatt, J.; Richards, R. L. *J. Less Common Metals*, **1977**, *54*, 477.
13. Manriquez, J. M.; Bercaw, J. E. *J. Am. Chem. Soc.* **1974**, *96*, 6229.
14. Green, M. L. H.; Silverthorn, W. E. *J. Chem. Soc. Dalton Trans.* **1974**, 2164.
15. Edema, J. J. H.; Meetsma, A.; Gambarotta, S. *J. Am. Chem. Soc.* **1989**, *111*, 6878.
16. O'Regan, M. B.; Liu, A. H.; Finch, W. C.; Schrock, R. R.; Davis, W. M. *J. Am. Chem. Soc.* **1990**, *112*, 4331.
17. Evans, W. J.; Ulibarri, T. A.; Ziller, J. W. *J. Am. Chem. Soc.* **1988**, *110*, 6877.
18. Fryzuk, M. D.; Haddad, T. S.; Rettig, S. J. *J. Am. Chem. Soc.* **1990**, *112*, 8185.
19. Pez, G. P.; Apgar, P.; Crissey, R. K. *J. Am. Chem. Soc.* **1982**, *104*, 482.

20. Jonas, K.; Brauer, D. J.; Kruger, C.; Roberts, P. J.; Tsay, Y. -H. *J. Am. Chem. Soc.* **1976**, *98*, 74.
21. Chatt, J.; Kan, C. T.; Leigh, G. J.; Pickett, C. J.; Stanley, D. R. *J. Chem Soc. Dalton Trans.* **1980**, 2032.
22. Chatt, J.; Pearman, A. J.; Richards, R. L. *J. Chem Soc. Dalton Trans.* **1977**, 1852.
23. Chatt, J.; Pearman, A. J.; Richards, R. L. *J. Chem Soc. Dalton Trans.* **1978**, 1766.
24. Anderson, S. N.; Fakley, M. E.; Richards, R. L.; Chatt, J. *J. Chem Soc. Dalton Trans.* **1981**, 1973.
25. Leigh, G. J.; Jimenez-Tenorio, M. *J. Am. Chem. Soc.* **1991**, *113*, 5862.
26. Hardy, R. W. F.; Burns, R. C.; Parshall, G. W. *ACS Symposium Series* **1971**, *100*, 219.
27. Thorneley, R. N. F.; Lowe, D. *J. Isr. J. Bot.* **1982**, *31*, 61.
28. Baumann, J. A.; Bossard, G. E.; George, T. A.; Howell, D. B.; Koczon, L. M.; Lester, R. K.; Noddings, C. M. *Inorg. Chem.* **1985**, *24*, 3568.
29. Kaul, B. B.; Hayes, R. K.; George, T. A. *J. Am. Chem. Soc.* **1990**, *112*, 2002.
30. George, T. A.; Kaul, B. B. *Inorg. Chem.* **1990**, *29*, 4969.
31. George, T. A.; Kaul, B. B. *Inorg. Chem.* **1991**, *30*, 882.
32. Dilworth, J. R.; Morton, S. *Transition Met. Chem.* **1987**, *12*, 41.
33. Weatherburn, M. W. *Anal. Chem.* **1967**, *39*, 971.
34. Pesez, M.; Bartos, J. *Colorimetric and Fluorimetric Analysis of Organic Compounds and Drugs*; Clinical and Biochemical Analysis; Marcel Dekker: New York, NY, 1974; Vol 1, 159.

RECEIVED March 8, 1993

Author Index

- Al-Ahmad, S., 231
Allen, Jeff, 196
Allen, Ronda, 196
Armstrong, E. M., 98
Ashby, G. A., 290
Ashcroft, M. J., 98
Austerberry, M. S., 98
Birks, J. H., 98
Bolin, Jeffrey T., 186,231
Bostick, Laura, 114
Burgess, Barbara K., 144
Burgmayer, Sharon J. Nieter, 114
Campobasso, Nino, 186,231
Chakrabarti, P., 170
Chan, M. K., 170
Chatterjee, Ranjini, 196
Chen, J., 231
Chirino, A. J., 170
Christiansen, J., 231
Collison, D., 98
Coucovanis, Dimitri, 231,304
Cramer, S. P., 231
Dean, Dennis R., 216
DeBord, Jeffrey R. D., 363
Enemark, John H., 130
Eriksen, K., 83
Everett, Kristin, 114
Fisher, K., 290
Frunzke, K., 50
Garner, C. D., 98
Gea, Y., 83
George, S. J., 231
George, T. Adrian, 363
Georgiadis, M. M., 170
Goodwin, A. J., 98
Goswami, S., 83
Greaney, M. A., 83
Hales, B. J., 231
Hidai, Masanobu, 346
Hille, Russ, 22
Homer, Mary, 196
Howard, James Bryant, 271
Hsu, B. T., 170
Huang, H., 243
Joshua-Tor, L., 170
Kilpatrick, L., 83
Kim, J., 170
Komiya, H., 170
LaBarre, Michael J., 130
Larsen, L., 98
Lowe, D. J., 290
Ludden, Paul W., 196
Madden, Mark, 196
Meyer, O., 50
Mizobe, Yasushi, 346
Morgan, T. Vance, 186
Mortenson, Leonard E., 186
Muchmore, Steven W., 186
Newton, William E., 216
Orme-Johnson, W. H., 257
Paustian, Tim, 196
Pilato, Robert S., 83
Raitsimring, Arnold, 130
Rajagopalan, K. V., 38
Reddy, K. R. N., 243
Rees, D. C., 170
Rheingold, A. L., 83
Roberts, Gary P., 196
Roll, Jon, 196
Rowe, D. J., 98
Russell, J. R., 98
Santillan, G., 170
Schlessman, J., 170
Sellmann, Dieter, 332
Shah, Vinod K., 196
Spiro, T. G., 83
Stiefel, Edward I., 1,83
Tachil, J., 50
Taylor, E. C., 83
Thomeley, R. N. F., 290
Tittsworth, R., 231
van Elp, J., 231
Volk, M., 50
Watt, G. D., 243
Wedd, Anthony G., 70
Woo, D., 170
Young, Charles G., 70

Affiliation Index

- Brigham Young University, 243
 Bryn Mawr College, 114
 California Institute of Technology, 170
 California State University—Los Angeles, 170
 Duke University Medical Center, 38
 Exxon Research and Engineering Company, 1,83
 Lawrence Berkeley Laboratory, 231
 Louisiana State University, 231
 Massachusetts Institute of Technology, 257
 Ohio State University, 22
 Princeton University, 83
 Purdue University, 186,231
 Universität Bayreuth, 50
 Universität Erlangen-Nuernberg, 332
 University of Arizona, 130
 University of California—Davis, 231
 University of California—Irvine, 144
 University of Delaware, 83
 University of Georgia, 186
 University of Manchester, 98
 University of Maryland, 243
 University of Melbourne, 70
 University of Michigan, 231,304
 University of Minnesota, 271
 University of Nebraska—Lincoln, 363
 University of Sussex, 290
 University of Tokyo, 346
 University of Wisconsin, 196
 Virginia Polytechnic Institute and State University, 216
 Xiamen University, 243

Subject Index

A

- Acquisition of molybdenum, role of molybdenum enzymes, 2
 Activation, MoS and FeS systems, 332–343
 Adenosine 5'-triphosphate (ATP) driven electron transfer, nitrogenase, 263–264
 Adenosine 5'-triphosphate (ATP) hydrolysis in nitrogenase
 electron transfer, 279–281
 experimental description, 272
 nucleotide binding, 279–281
 role in docking model, 287–288
 Aldehyde oxidases, function, 2,6
 Alkenyldiazenido complexes, reactions, 347,349,351,353
 Amino acid substitutions at α -Gln-191 and α -His-195 of MoFe protein, role in nitrogenase catalysis, 223–226
Azotobacter A. vinelandii, redox properties of nitrogenase proteins, 243–255
Azotobacter A. vinelandii molybdenum nitrogenase catalysis, FeMo cofactor polypeptide environment, 216–228

B

- Bacterial molybdenum cofactor, 51
 Bacterial pterins
 chemical structures, 51–53f
 occurrence in molybdenum enzymes, 52,54f
 Bacteropterin, description, 51
 Bimetallic systems, silylation and arylation of dinitrogen, 357–360
 Biochemistry, molybdenum cofactors, 38–48
 Biogeochemical cycles, role of molybdenum enzymes, 2,5f–7
 Biological nitrogen fixation
 models, 12–15
 process, 243
 Biosynthesis, molybdenum cofactor, 46–48f
 Biosynthesis of iron–molybdenum cofactor of nitrogenase
 discovery as homocitrate component, 197
 divalent metals, 211–213
 future studies, 213
 [^3H]homocitrate binding to proteins, 206–208f
 homocitrate synthesis, 210–211
 in vitro synthetic assay, 198,199f
 incorporation of ^{99}Mo , 208f,210

Affiliation Index

- Brigham Young University, 243
 Bryn Mawr College, 114
 California Institute of Technology, 170
 California State University—Los Angeles, 170
 Duke University Medical Center, 38
 Exxon Research and Engineering Company, 1,83
 Lawrence Berkeley Laboratory, 231
 Louisiana State University, 231
 Massachusetts Institute of Technology, 257
 Ohio State University, 22
 Princeton University, 83
 Purdue University, 186,231
 Universität Bayreuth, 50
 Universität Erlangen-Nuernberg, 332
 University of Arizona, 130
 University of California—Davis, 231
 University of California—Irvine, 144
 University of Delaware, 83
 University of Georgia, 186
 University of Manchester, 98
 University of Maryland, 243
 University of Melbourne, 70
 University of Michigan, 231,304
 University of Minnesota, 271
 University of Nebraska—Lincoln, 363
 University of Sussex, 290
 University of Tokyo, 346
 University of Wisconsin, 196
 Virginia Polytechnic Institute and State University, 216
 Xiamen University, 243

Subject Index

A

- Acquisition of molybdenum, role of molybdenum enzymes, 2
 Activation, MoS and FeS systems, 332–343
 Adenosine 5'-triphosphate (ATP) driven electron transfer, nitrogenase, 263–264
 Adenosine 5'-triphosphate (ATP) hydrolysis in nitrogenase
 electron transfer, 279–281
 experimental description, 272
 nucleotide binding, 279–281
 role in docking model, 287–288
 Aldehyde oxidases, function, 2,6
 Alkenyldiazenido complexes, reactions, 347,349,351,353
 Amino acid substitutions at α -Gln-191 and α -His-195 of MoFe protein, role in nitrogenase catalysis, 223–226
Azotobacter A. vinelandii, redox properties of nitrogenase proteins, 243–255
Azotobacter A. vinelandii molybdenum nitrogenase catalysis, FeMo cofactor polypeptide environment, 216–228

B

- Bacterial molybdenum cofactor, 51
 Bacterial pterins
 chemical structures, 51–53f
 occurrence in molybdenum enzymes, 52,54f
 Bacteropterin, description, 51
 Bimetallic systems, silylation and arylation of dinitrogen, 357–360
 Biochemistry, molybdenum cofactors, 38–48
 Biogeochemical cycles, role of molybdenum enzymes, 2,5f–7
 Biological nitrogen fixation
 models, 12–15
 process, 243
 Biosynthesis, molybdenum cofactor, 46–48f
 Biosynthesis of iron–molybdenum cofactor of nitrogenase
 discovery as homocitrate component, 197
 divalent metals, 211–213
 future studies, 213
 [^3H]homocitrate binding to proteins, 206–208f
 homocitrate synthesis, 210–211
 in vitro synthetic assay, 198,199f
 incorporation of ^{99}Mo , 208f,210

Biosynthesis of iron–molybdenum cofactor
 of nitrogenase—*Continued*
 inhibitors, 209–210
nif gene products required, 197–198
nifH, 211
 nucleotides, 211–213
 organic acids as component, 201–206
 pathway determination approach, 197
 purification and characterization
nifB, 200–201
nifNE gene products, 198,200
 Biotin sulfoxide reductase, function, 6
 Bonding, MoS and FeS systems, 332–343

C

Carbon metabolism, role of molybdenum
 enzymes, 6–7
 Catalytic cycle, xanthine oxidase, 77,79–80
 Chemical transformations, coordinated
 dinitrogen in Mo and W phosphine
 complexes, 346–360
 Citrate, FeMo cofactor synthesis, 202,203†
Clostridium pasteurianum, structure and
 environment of metal clusters in
 nitrogenase MoFe protein, 186–194
 CO, binding to high-valent [MoS] centers,
 337–338
 CO dehydrogenase(s), specificities of
 molybdopterin dinucleotides for target
 proteins, 56,60†
 CO dehydrogenase molybdenum cofactor,
 metabolic relationship with urothione,
 62–65†
 CO dehydrogenase pterin, characteristics, 51
 Coenzyme A, posttranslational modification
 of *Klebsiella pneumoniae* flavodoxin,
 291–294†
 Cofactor of oxomolybdoenzymes, 98–111
 Compound Z, structure, 47†
 Coordinated dinitrogen in Mo and W
 phosphine complexes, chemical
 transformations, 346–360
 Copper–molybdenum antagonism, role of
 molybdenum enzymes, 2
 Coupled electron–proton transfer reactions
 molybdenum cofactor, 105
 pterin-containing molybdenum
 enzymes, 75,77
 (CpCo[S₂C₂H(quinoxalin-2-yl)])
 coupled proton–electron transfer, 107–111
 structure, 107,108†
 Crystal structures of iron protein and molyb-
 denum–iron protein, nitrogenase, 170–183
 Cuboidal subunits of nitrogenase, electronic
 structure, 323–324
 Cysteiny-275 of a subunit, thiol ligand to
 FeMo cofactor, 221,223

D

Desmethylurothione, structure, 39†
 Diazene, stabilization using FeS systems,
 341–342
 Diazoalkane complexes derived from
 dinitrogen complexes, reactivities,
 347,349–357
 Diazoalkane complexes with π -acceptor
 ligands
 reactions, 350–351,355
 syntheses, 349–351
 Di(carboxamidomethyl)molybdopterin, 39†
 Di(carboxamidomethyl)molybdopterin
 cytosine dinucleotide
¹³C-NMR spectrum, 56,57†
 chemical structure, 52
¹H-NMR spectrum, 52,55†,56
 high-performance LC, 52,54†
 Dimethyl sulfoxide reductase, function, 6
 Dinitrogen
 arylation using bimetallic systems,
 357–360
 gemylation, 352–353
 protonation, 365–368†
 silylation, 352,355
 silylation using bimetallic systems,
 357,359
 Dinitrogen complexes of Mo, 346–348
 Dinitrogenase proteins containing aberrant
 FeMo cofactors, spectroscopic properties,
 199†,206,209
 Disproportionation, problem, 366–367
 Divalent metals, role in FeMo cofactor
 synthesis, 211–213
 Docking model, nitrogenase, 287–288
 Doubly bridged double cubanes, structure,
 317–320†

E

- Eight-Fe cluster in nitrogenase MoFe protein, environment and structure, 191–194
- Electrochemical organization, molybdenum cofactor enzymes, 7,8f
- Electrochemical studies, molybdenum cofactor, 92
- Electrochemistry, $\text{Mo}_2\text{O}_4(\text{H}_4\text{-6,7-dimethylpterin})_2\text{Cl}_2$, 124,125f
- Electron transfer, N_2 reduction, 367–369
- Electron-transfer reactions associated with nitrogenase from *Klebsiella pneumoniae* electron-transport chain, 290–291
- MgATP-dependent electron transfer, role of β -Phe-124 of MoFe protein, 296–298f
- MoFe protein reduction vs. kinetics of Fe protein cycle, 294–296f
- P center role in nitrogen reduction, 299t–301f
- posttranslational modification of flavodoxin by coenzyme A, 291–294f
- Electrostatic effects, protein component complexes in nitrogenase, 272–275,279

F

- Fe–Mo–S center
structure from analytical and spectroscopic data, 311–313
substrate interaction–activation mechanism, 322f,323
- Fe–Mo–S clusters, characteristics, 306–309
- Fe protein, assembly, 161
- Fe protein of nitrogenase
binding of MgATP and MgADP, 147–148
binding to MoFe protein, 148
composition, 171,186,243,304
consensus sequence, 145,146f
interaction with MoFe protein, 178,180–182
metal clusters, 305
redox properties, 145,147,250–255
reduction of MoFe protein vs. kinetics of cycle, 294–296f
schematic representation, 144,146f
structural description, 176,178,179f,183
structural determination, 171–172
structure, 263

- Fe protein of nitrogenase—*Continued*
structure of metal center, 172
three-dimensional structure–property relationship, 281
- Fe protein of nitrogenase Fe:S cluster, ionic interactions, 276–279
- FeMo cofactor
binding, 189,191
composition, 186
ligands, 152–153
metal composition and organization, 152
protein-bound structure, 153
restoration of reactivity, 244
structure, 189–192f
structure from X-ray crystallography, 309,311f
substitutions at α -Gln-191 vs. structure, 226–227
substrate reduction, 217–222
vnf and *anf* metal clusters, 153–154
- FeMo cofactor biosynthesis, 161–163
- FeMo cofactor-deficient MoFe protein, assembly, 163–164
- FeMo cofactor of nitrogenase
redox properties, 249,250t
structure of metal center, 173–177
- FeMo cofactor of nitrogenase MoFe protein
structure, 260,262f,263
trigonal Fe atoms, 267–268
- FeMo cofactor polypeptide environment role in *A. vinelandii* molybdenum–nitrogenase catalysis, 217–228
- $\{\text{Fe}_6\text{S}_6\text{L}_6[\text{M}(\text{CO})_3]_2\}^{3-4}$ octanuclear clusters, structure, 315–317f
- Formate dehydrogenase, 6
- Formylmethanofuran dehydrogenase, 6
- Function, nitrogenase, 144–164

G

- Genetics, nitrogenase, 144–164

H

- [^3H]Homocitrate, binding to proteins of FeMo cofactor synthetic assay mixture, 206–208f

Homocitrate

- FeMo cofactor component, 201
- synthesis, 210–211
- Hydrogenophaga pseudoflava*, identification of urothione as excretion product, 58–62
- Hydrogenophaga pseudoflava* CO dehydrogenase pterin
 - ¹³C-NMR spectrum, 56,57f
 - chemical structure, 52
 - ¹H-NMR spectrum, 52,55f,56
 - high-performance LC, 52,54f
- 2-Hydroxy-6-methylpurine, reaction with xanthine oxidase, 27–29

I

- Inhibitors, FeMo cofactor synthesis, 209–210
- Ionic interactions, Fe protein of nitrogenase Fe:S cluster, 276–279
- Iron–molybdenum cofactor, 12–15
- Iron–molybdenum cofactor of nitrogenase, 196–213
- Iron–molybdenum sulfide clusters, models for biological nitrogen fixation, 13
- Iron porphyrin–oxomolybdenum center coupling, *See* Oxomolybdenum center–iron porphyrin coupling
- Iron protein, schematic representation, 144,146f
- Iron sulfide clusters, models for biological nitrogen fixation, 13
- Iron–sulfur systems
 - comparison to Mo in N₂ fixation, 338–339
 - complexes, 333–334,339–341
 - coordination of N₂ fixation stages, 342–343
 - diazene stabilization, 341,342f
 - ligands, 333

K

- Klebsiella pneumoniae* flavodoxin, posttranslational modification by coenzyme A, 291–294f

L

- L*-edge spectroscopy nitrogenase MoFe protein, 231–241f

M

- Metal centers in nitrogenase
 - Fe–Mo–S clusters, 306–309
 - P clusters, 306
 - structures from analytical and spectroscopic data, 311–313f
 - structures from X-ray crystallography, 309–311f
- Metal centers in nitrogenase proteins
 - Fe protein, 172
 - FeMo cofactor, 173–177
 - MoFe protein, 172–173
 - P cluster pair, 176,177f
- Metal cluster(s), Fe protein of nitrogenase, 305
- Metal cluster(s) in nitrogenase MoFe protein from *Clostridium pasteurianum*
 - α and β subunits, tertiary structure, 188,190f
 - experimental procedure, 187
 - 8-Fe cluster
 - environment, 191,193f,194
 - structure, 191,192f
 - FeMo cofactor
 - binding, 189,191
 - structure, 189–192f
 - quaternary structure of protein, 188
 - status of model, 187–188
- Metal cluster prosthetic groups, MoFe protein of nitrogenase, 257–268
- 1-Methylxanthine, reaction with xanthine oxidase, 29–31f
- MgATP, FeMo cofactor biosynthesis, 163
- MgATP-dependent electron transfer, role of β-Phe-124 of *K. pneumoniae* MoFe protein, 296–298f
- ⁹⁹Mo, in vivo and in vitro incorporation into FeMo cofactor and precursors, 208f,210
- Mo phosphine complexes, chemical transformation of coordinated dinitrogen, 346–360
- Mo₂O₄(H₄-6,7-dimethylpterin)₂Cl₂, 124,125f
- Models, pterin-containing molybdenum enzymes, 70–81
- MoFe protein
 - EXAFS and *L*-edge spectroscopy, 231–241
 - quaternary structure, 188
- MoFe protein of nitrogenase
 - ATP-driven electron transfer, 263–264

- MoFe protein of nitrogenase—*Continued*
 comparison to photosynthetic reaction center, 182
 composition, 148–149,171,186,243–244,304
 EXAFS and *L*-edge spectroscopy, 231–241
 Fe protein cycle, reduction vs. kinetics, 294–296*f*
 FeMo cofactor, 152–154
 FeMo cofactor structure, 260–263
 Fe₄S₄ clusters, reduction state, 264–267
 interactions with Fe protein, 178–182
 kinetic mechanism for nitrogenase, 257
 P cluster(s), 149–152,258
 P cluster structures, 260,261*f*
 properties, 245*t*
 purification and characterization procedure, 245–246
 redox properties, 246–249
 structural description, 178,179*f*,183
 structural determination, 171–172,305
 structure and environment of metal clusters in *Clostridium pasteurianum*, 186–194
 structure of metal center, 172–173
 three-dimensional structure–property relationship, 281
 trigonal Fe atoms in FeMo cofactor, 267–268
- Molybdenum
 component of enzymes, 38
 exploitation by nature, 79,81
 ligand field in Mo enzymes, 44–46*f*
 W, use by thermophilic organisms, 15–16
- Molybdenum active sites, 71–74,76*f*
- Molybdenum-based hydroxylation, chemical mechanism, 33–36
- Molybdenum center
 nature in oxomolybdoenzymes, 100–102,106*f*
 structure in xanthine oxidase, 23–25*f*
- Molybdenum cofactor
 bacterial, 51
 biosynthesis, 46–48*f*
 catalytic center, 99
 coupled proton–electron transfer, 105–111
 discovery, 98
 distribution of variant forms, 40,41*t*
 electrochemical studies, 92
 evidence, 38
 isolation, 98–99
 ligand field of molybdenum, 44–46*f*
- Molybdenum cofactor—*Continued*
 oxidation state of pterin ring, 43–44*f*
 oxidative decomposition products, 83–85
 proposed structure, 83,84*f*
 pterin–ene–dithiolate and quinoxaline–ene–dithiolate synthesis, 89–92
 redox and acid–base reactivity, 92,94–96
 release from enzymes, 39–40
 spectroscopic studies, 92
 stability, 39
 stereochemistry of pteridine 6-position, 98
 structure, 39*f*,99
 structure(s) of derivatives, 39–40*f*
 structure–spectra correlations, 41,42*f*
 synthetic strategy, 85,87–89
 theoretical studies, 92
- Molybdenum cofactor deficiency, 48
- Molybdenum cofactor enzymes
 bacterial cofactor, 50–65
 biochemistry, 38–48
 composition, 7
 electrochemical organization, 7,8*f*
 model systems, 9–10
 reaction mechanisms, 7,9
 site of action, 7
 xanthine oxidase reaction mechanism, 22–36
- Molybdenum cofactor models
 chemical and physical coupling of oxomolybdenum centers and iron porphyrin, 130–141
 molybdenum complexes of reduced pterins, 114–127
 oxomolybdoenzyme cofactor, synthesis, 98–111
 pterin-containing molybdenum enzymes, 69
 synthesis using pterins, quinoxalines, and metallo–ene–dithiolates, 83–96
- Molybdenum(VI) complexes,
 tetrahydropterin reactions, 118–121*f*
- Molybdenum complexes of reduced pterins,
See Molybdenum(VI)–tetrahydropterin complexes
- Molybdenum-containing hydroxylases, 22
- Molybdenum–copper antagonism, role of molybdenum enzymes, 2
- Molybdenum-dependent nitrogenase catalysis, role of FeMo cofactor polypeptide environment, 216–228

- Molybdenum dioxobis(dithiocarbamate) complexes, tetrahydropterin reactions, 115–118
- Molybdenum–ene–dithiolate complexes
electrochemical studies, 92
redox and acid–base reactivity, 92,94–96
side-chain reduction, 94–95
spectroscopic studies, 92
theoretical studies, 92
transmetallation of ligand, 94,96
- Molybdenum enzymes
carbon metabolism, 6–7
categories and functions, 1–2
composition, 2–4†
hydroxylation function, 38
ligand field of molybdenum, 44–46†
molybdenum acquisition effect, 2
molybdenum–copper antagonism effect, 2
nitrogen cycle effect, 2,5†,6
occurrence and distribution, 1
study techniques, 38
sulfur metabolism effect, 6
- Molybdenum hydroxylases, chemical mechanism, 33–36
- Molybdenum–iron protein, schematic representation, 144,146†
- Molybdenum–sulfur systems
CO binding to center, 337–338
comparison to Fe in N_2 fixation, 338–339
complexes, 333–334
coordination and stabilization of N_2H_3 and NH_2 , 336–337
ligands, 333
NO reduction, 334–336
occurrence, 332
- Molybdenum(VI)–tetrahydropterin complexes
occurrence of redox, 126
oxidation reactions, 126,127†
spectral properties, 122–124
- Molybdopterin
distribution, 40,41†
function, 99,114
pathway of S incorporation, 47,48†
structure, 39–40†
synthetic strategy, 102–105
- Molybdopterin cytosine dinucleotide
 ^{13}C -NMR spectrum, 56,57†
chemical structure, 52
distribution, 40,41†
- Molybdopterin cytosine dinucleotide—
Continued
 1H -NMR spectrum, 52,55†,56
high-performance LC, 52,54†
structure, 40†
- Molybdopterin derivatives, structures and synthesis, 83–86
- Molybdopterin dinucleotides, specificities for target proteins, 56,60†
- Molybdopterin guanine dinucleotide, 40–41
- Mononuclear oxomolybdenum complexes, 130–132
- N
- N_2 complexes, 364–365
- N_2 fixation, coordination of stages by iron–sulfur systems, 342–343
- N_2 reduction
electron transfer, 367–369
mechanism, 258,259†,363–364
N–N bond cleavage, 369
nitrogen binding, 364–365
protonation of dinitrogen, 365–368†
reaction, 363
reaction stoichiometry, 170
steps, 364
thermodynamics, 258,259†
- N_2H_3 and NH_2 , coordination and stabilization using MoS systems, 336–337
- nif* gene products, role in FeMo cofactor synthesis, 197–198
- nifB*
FeMo cofactor biosynthesis, 162
purification and characterization, 200–201
- nifE*, FeMo cofactor biosynthesis, 162–163
- nifH*
FeMo cofactor biosynthesis, 163
role in FeMo cofactor synthesis, 211
- nifN*, FeMo cofactor biosynthesis, 162–163
- nifNE* gene products, purification and characterization, 198,200
- nifQ*, FeMo cofactor biosynthesis, 162
- nifV*, FeMo cofactor biosynthesis, 161
- Nitrate assimilation and dissimilation, 2
- Nitrate reductase
coupled electron–proton transfer, 75,77
function, 2

- Nitrate reductase—*Continued*
 half-reaction, 70
 model, 75,77–78
 molybdenum active site, 71–74,76f
 oxygen atom transfer reactions, 74–76
- Nitrate respiration, description, 2
- Nitrite oxidase, function, 2
- Nitrogen binding, examples, 364–365
- Nitrogen cycle
 role of molybdenum enzymes, 2,5f,6
 schematic representation, 2,5f
- Nitrogen fixation
 biological models, 12–15
 mechanism, 258,259f
- Nitrogen fixing systems, models for
 biological nitrogen fixation, 15
- Nitrogen–nitrogen bond cleavage
 complex synthesis, 369–370
 [MoCl₂(NNPh₂)(PMe₂Ph)₃] synthesis, 370
 reaction, 369
 reactions with acid, 370,371t
 [WCl₂(NNPh₂)(PMe₂Ph)₃] synthesis, 370
 [WCl₂(NNR₂)(PMe₂Ph)₃] structure,
 371–374t
- Nitrogen reduction, role of P centers,
 299t–301f
- Nitrogenase
 ATP-driven electron transfer, 263–264
 biosynthesis of iron–molybdenum cofactor,
 196–213
 catalysis of N₂ reduction, 304
 catalytic reaction, 257–258
 component proteins, 170
 composition, 216
 crystal structures of iron protein and
 molybdenum–iron protein, 170–183
 description of system, 10,11f
 docking model, 287–288
 Fe protein, 145–148
 function, 6
 kinetic mechanism, 258,261f
 metalloclusters, 217
 models, 12–15
 MoFe protein, 258–268
 nucleotide hydrolysis, 272,279–281
 protein component(s), 186,304–305
 protein component complexes, 272–287
 protein composition, 144–146f,257
 redox cycle, 271,273
 requirements for substrate reduction, 271
- Nitrogenase assembly
 Fe protein assembly, 161
 FeMo cofactor biosynthesis, 161
 FeMo cofactor deficient MoFe protein
 assembly, 163–164
- Nitrogenase catalysis
 requirements for understanding, 244
 role of FeMo cofactor polypeptide
 environment, 216–228
- Nitrogenase MoFe protein, *See* MoFe protein
 of nitrogenase
- Nitrogenase proteins from *Azotobacter*
A. vinelandii, redox properties, 244
- Nitrogenase turnover
 electron flux vs. substrate reactivity,
 157,159
 electron transfer in MoFe protein, 155
 homocitrate alteration vs. substrate
 reactivity, 160–161
 MoFe protein changes vs. substrate
 reactivity, 160
 oxidized Fe protein, 154
 reactivity, comparison to those for V and
 Fe-only nitrogenases, 158–160
 steps, 154–155
 substrate reactivity, changes, 157–161
 substrate reduction by wild-type MoFe
 protein, 155–157,159f
- NO reduction, use of MoS systems, 334–336
- Nucleotide(s), role in FeMo cofactor
 synthesis, 211–213
- Nucleotide hydrolysis in nitrogenase
 docking model, 287–288
 electron transfer, 279–281
 experimental description, 272
 nucleotide binding, 279–281
- O
- Oligonuclear Fe–M–S complexes,
 structure, 314
- Organic acids
 in vitro FeMo cofactor synthesis, 201–206
 structures, 202,204f
- Oxidation reactions, molybdenum(VI)–tetra-
 hydropterin complexes, 126,127f
- Oxomolybdenum center(s), reaction cycle,
 130–131

Oxomolybdenum center–iron porphyrin coupling
 cyclic voltammograms, 138,140f,141
 electron paramagnetic resonance spectroscopy, 132,136–139
 experimental description, 132
 fragments, calculated conformation, 132,135f
 half-wave reduction potentials, 138t
 porphyrins, synthesis, 132–134
 Oxomolybdoenzymes, nature of molybdenum center, 100–102,106f
 Oxygen atom transfer reactions, pterin-containing molybdenum enzymes, 74–76

P

P centers, role in nitrogen reduction, 299t–301f
 P clusters
 composition, 186
 concept, 149
 description, 10–12,186
 Fe atoms, 149–150
 ligands, 150–152
 MoFe protein of nitrogenase
 reduction state, 264–267
 structures, 258,260,261f
 structure(s), 152,306
 from analytical and spectroscopic data, 313
 from X-ray crystallography, 310,311f
 β -Phe–124 of *Klebsiella pneumoniae* MoFe protein, role in MgATP-dependent electron transfer, 296–298f
 Picolinic acid dehydrogenase, function, 2
 Polynuclear Fe–M–S complexes, structure, 314,315f
 Protein component complexes in nitrogenase conformational change within complex, 272
 docking model, 287–288
 electrostatic effects, 272–275,279
 experimental description, 272
 ionic interactions near Fe protein Fe:S cluster, 276–279
 minimal requirements, 272
 three-dimensional structure–function property relationship, 281–287
 Protonation, dinitrogen, 365–368f

Pterin-containing molybdenum enzymes
 catalytic cycle, 77,79–80
 coupled electron–protein-transfer reactions, 75,77
 half-reactions, 70–71
 model, 75,77–78
 molecular electrochemical cells, 70
 molybdenum
 active sites, 71–74,76f
 reasons for use, 79,81
 oxygen atom transfer reactions, 74–76
 redox processes, 70
 Pterin–ene–dithiolate, molybdenum cofactor synthesis, 89–92
 Pyridoxal oxidase, function, 6
 Pyrimidine oxidases, function, 2,6

Q

Quinoline oxidase, function, 2
 Quinoxaline-2,3-dithiolates, coupled proton–electron transfer, 105–108f
 Quinoxaline–ene–dithiolate, molybdenum cofactor synthesis, 89–92

R

Reaction mechanism, xanthine oxidase, 22–36
 Reactivities, diazoalkane complexes derived from dinitrogen complexes, 347,349–357
 Redox properties of nitrogenase proteins
 from *Azotobacter A. vinelandii*
 electrochemical procedure, 246
 Fe protein, 250–255
 FeMo cofactor, 249,250t
 MoFe protein, 246–249
 MoFe protein purification and characterization procedure, 245t,246
 oxidant preparation procedure, 246
 redox titration, sources of error, 244
 reductant preparation procedure, 246
 spectroscopic procedure, 246
 Redox reactions, tetrahydropterins, 115f
 Reduced pterin–molybdenum complexes, *See* Molybdenum(VI)–tetrahydropterin complexes
 Rhodanese, function, 6

S

Silylated dinitrogen complexes, reactions, 352,354–357

Singly bridged double cubanes, structure, 317–320*f*

Solution X-ray absorption fine structure spectroscopy of nitrogenase MoFe protein distances, 232,237–238*f*

dithionite-reduced and thionine-oxidized proteins, 237,239*f*

Fe K-edge results, 232–235*t*

Mo results, 235,236*f*

studies, 231–232

Spectral properties, molybdenum(VI)–tetrahydropterin complexes, 122–124

Spectroscopic studies, molybdenum cofactor, 92

Stabilization, MoS and FeS systems, 332–343

Structure, nitrogenase, 144–164

Substrate reduction, role of FeMo cofactor, 217–222

Substrate reduction by nitrogenase, requirements, 271

Substrate reduction by wild-type MoFe protein characteristics, 156–157

substrate binding, 155–156,159*f*

Sulfite oxidase chemical transformations at molybdenum center, 130–131

coupled electron–proton-transfer reactions, 75,77

function, 6

half-reaction, 70

importance, 130

model, 75,77–78

molybdenum active site, 71–74,76*f*

molybdenum center, nature, 100–101

oxomolybdenum center–iron porphyrin coupling, 130–141

oxygen atom transfer reactions, 74–76

reaction mechanisms, 7,9

Sulfur metabolism, role of molybdenum enzymes, 6

Synthetic analogs for Fe–Mo–S and Fe–S sites of FeMo protein of nitrogenase ($\text{Fe}_6\text{S}_6\text{L}_6\{\text{M}(\text{CO})_3\}_2\}^{3-4}$ octanuclear clusters, 315–317*f*

oligonuclear Fe–M–S complexes, 314

Synthetic analogs for Fe–Mo–S and Fe–S sites of FeMo protein of nitrogenase—*Continued*

polynuclear Fe–M–S complexes, 314,315*f*

singly and doubly bridged double cubanes, 317–320*f*

Synthetic metal sulfur chemistry electronic structure of cuboidal subunits, 323–324

ethylenediaminetetraacetic acid effect, 324

methyl ethyl ketone effect, 325

Mo and V atoms, role in nitrogenase function, 321–322

structure of isolated cofactor vs. that of Fe–Mo–S center, 324

substrate interaction–activation at Fe–Mo–S center, 322*f*,323

T

Target proteins, specificities of molybdopterin dinucleotides, 56,60*t*

Tetrahydropterin(s) catalytic substrate reduction, 114

redox reactions, 115*f*

Tetrahydropterin complexes of molybdenum(VI), evidence, 122,123*f*

Tetrahydropterin–molybdenum(VI) complexes, *See* Molybdenum(VI)–tetrahydropterin complexes

Tetrahydropterin reactions, molybdenum dioxobis(dithiocarbamate) complexes, 115–118

Tetrathionate reductase, function, 6

Theoretical studies, molybdenum cofactor, 92

Transition metal–sulfur complexes, models for biological nitrogen fixation, 13,14*f*

Tungsten, use by thermophilic organisms instead of Mo, 15–16

U

Urothione excretion product of *Hydrogenophaga pseudoflava*, identification, 58–62

metabolic relationship with CO dehydrogenase molybdenum cofactor, 62–65*f*

W

W phosphine complexes, chemical transformation of coordinated dinitrogen, 346–360

Wild-types MoFe protein, substrate reduction, 155–157, 159*f*

X

Xanthine, reaction with xanthine oxidase, 29–31*f*

Xanthine oxidase

catalytic cycle, 77, 79–80

composition, 23

description, 22

electron paramagnetic spectroscopy of reaction with substrate, 24–26

function, 2, 22–23

half-reaction, 71

hydroxylation, chemical mechanism, 33–36

2-hydroxy-6-methylpurine, reaction, 27–29

kinetic mechanism, 32–33

model, 75, 77–78

molybdenum active site, 71–74, 76*f*

molybdenum center

nature, 101–102

Xanthine oxidase—*Continued*

molybdenum center—*Continued*

structure, 23–25*f*

oxygen atom transfer reactions, 74–76

reductive half-reaction, UV–visible spectroscopy, 26

resonance Raman spectroscopy of reductive half-reaction, 26

species giving rise to rapid type 1 Mo(V)

electron paramagnetic resonance

spectroscopic signal, 30–32

stoichiometric concentrations of substrate, reaction, 26–30

xanthine and methylxanthine, reaction, 29–31*f*

X-ray absorption fine structure spectroscopy

(EXAFS) of nitrogenase MoFe protein

future work, 240, 241*f*

progress, 231–239

X-ray absorption spectroscopy

metals in nitrogenase, study, 231

molybdenum center in

oxomolybdoenzymes,

nature, 100–102

X-ray magnetic circular dichroism,

nitrogenase MoFe protein, 240*f*